# AN INVESTIGATION INTO FLOW AND ACOUSTIC COUPLING OF TUBES IN GAS HEAT EXCHANGER TUBE BANKS

by Robin Graeme Arak, B.Sc.(Hons.)

A thesis submitted for the degree of

Doctor of Philosophy in the

UNIVERSITY OF SOUTHAMPTON

Institute of Sound and Vibration Research
Faculty of Engineering and Applied Science
University of Southampton
U.K.

December 1982

One aim of the physical sciences has been to give an exact picture of the material world.

One achievement of physics in the twentieth century has been to prove that that aim is unattainable.

— J. Bronowski

CONTENTS


| | Page |
|---|---|
| ABSTRACT | x |
| ACKNOWLEDGEMENTS | xi |
| LIST OF SYMBOLS | xii |
| LIST OF ABBREVIATIONS | xv |
| KEY TO FIGURE SYMBOLS | xvi |
| CHAPTER 1. INTRODUCTION | 1 |
| 1.1 Motivation for Research | 1 |
| 1.2 Brief Review of Major Tube Excitation Mechanisms in Staggered Tube Banks | 2 |
| 1.2.1 Vortex shedding | 2 |
| 1.2.2 Turbulent buffeting | 3 |
| 1.2.3 Fluid-elastic instabilities | 4 |
| 1.2.4 Acoustic excitations | 4 |
| 1.3 Aims of the Present Research Project | 5 |
| 1.4 References | 7 |
| Figure 1.1 | 10 |
| CHAPTER 2. THE WIND TUNNEL | 11 |
| 2.1 Introduction | 11 |
| 2.2 Modelling Considerations | 11 |
| 2.3 Wind Tunnel Design Considerations | 12 |
| 2.4 Design of the Wind Tunnel | 15 |
| 2.5 Bellmouth Inlet | 15 |
| 2.6 Settling Section | 16 |
| 2.7 Inlet Contraction | 16 |
| 2.8 Sound Injection Box | 17 |
| 2.9 Working Section | 18 |
| 2.10 High Speed Contraction | 19 |
| 2.11 Variable Sonic Throat | 20 |
| 2.12 Injector Box | 20 |
| 2.13 Diffuser | 21 |
| 2.14 Compressed Air System | 22 |
| 2.15 Theoretical Estimation of Wind Tunnel Speed | 22 |
| 2.16 Wind Tunnel Calibration | 23 |

| | | Page |
|---|---|---|
| 2.17 | Conclusion | 25 |
| 2.18 | References | 25 |
| | Tables 2.1 - 2.3 | 27 |
| | Figures 2.1 - 2.6 | 29 |
| | Plates 2.1 - 2.4 | 34 |
| CHAPTER 3. | THE MODEL TUBE BANK AND INSTRUMENTATION | 37 |
| 3.1 | Introduction | 37 |
| 3.2 | The Support Structure for the Flexibly Supported Tubes | 37 |
| 3.3 | The Fixed Tubes | 37 |
| 3.4 | The Flexibly Supported Tubes | 38 |
| 3.5 | The Pressure Measuring Tube | 40 |
| 3.6 | The Electret Microphone Power Supply | 41 |
| 3.7 | The Microphone Amplifiers and Power Supply | 42 |
| 3.8 | The r.m.s.-to-d.c. Converter | 42 |
| 3.9 | Calibration of the Pressure Measuring Tube Microphones | 43 |
| 3.10 | Description and Calibration of the Pressure Transducer | 43 |
| 3.11 | The Pressure Transducer Strain Gauge Amplifier | 45 |
| 3.12 | The Hot Wire Probe and Traversing Mechanism | 46 |
| 3.13 | Measurement of the Pressure Distribution round a Tube | 46 |
| 3.14 | Design of an Automatic Data Acquisition and Control System | 47 |
| 3.15 | Specifications of the Nascom 2 Microprocessor System | 47 |
| 3.16 | Measurement Procedure | 48 |
| 3.17 | Interface Requirements | 48 |
| 3.18 | Measuring Tube Drive and Control Interface | 49 |
| 3.19 | Analogue-to-Digital Converter and Sampling Circuit | 50 |
| 3.20 | Analogue Multiplexer | 51 |
| 3.21 | Digital-to-Analogue Converter | 51 |
| 3.22 | Paper Tape Punch Interface | 52 |
| 3.23 | Paper Tape Reader Interface | 52 |
| 3.24 | Acquisition and Control System Software | 53 |
| 3.25 | Conclusion | 54 |
| 3.26 | References | 54 |
| | Table 3.1 | 56 |

| | | Page |
|---|---|---|
| | Figures 3.1 - 3.24 | 57 |
| | Plates 3.1 - 3.6 | 82 |
| CHAPTER 4. | INVESTIGATION OF A SINGLE ROW OF TUBES | 86 |
| 4.1 | Introduction | 86 |
| 4.2 | General Description of the Experiments | 86 |
| 4.3 | Average and Fluctuating Pressure Measurements round the Circumference of a Tube | 87 |
| 4.3.1 | Experimental method | 87 |
| 4.3.2 | Aims of the experiments | 88 |
| 4.3.3 | General description of the results for a row of fixed tubes | 88 |
| 4.3.4 | Summary of results for a fixed row of tubes | 89 |
| 4.3.5 | Summary of results for a flexible tube mounted next to the pressure measuring tube | 91 |
| 4.3.6 | The effects of the presence of a flexible vibrating tube | 92 |
| 4.3.7 | Three dimensional flow effects | 94 |
| 4.3.8 | Comparison of results with previous investigations and current theories | 94 |
| 4.4 | P.S.D. Measurements of Pressure round the Circumference of a Tube | 97 |
| 4.4.1 | Experimental method | 97 |
| 4.4.2 | Aims of the experiment | 97 |
| 4.4.3 | Presentation of P.S.D. measurements of pressure | 98 |
| 4.4.4 | P.S.D. of pressure round a tube in a uniformly spaced fixed tube row | 98 |
| 4.4.5 | P.S.D. of pressure round a tube displaced by 0.1 diameter in a fixed tube row | 99 |
| 4.4.6 | P.S.D. of pressure round a tube next to a flexible tube in a uniformly spaced fixed tube row | 99 |
| 4.4.7 | Discussion of the acoustic interaction | 100 |
| 4.4.8 | Interaction of a vibrating flexible tube with the pressure field round a neighbouring tube | 101 |
| 4.4.9 | Interaction of a vibrating flexible tube with the wake of a neighbouring tube | 102 |

| | | Page |
|---|---|---|
| 4.5 | P.S.D. Measurements of Pressure as a Function of Static Tube Displacement | 103 |
| 4.5.1 | Experimental method | 103 |
| 4.5.2 | Aims of the experiments | 103 |
| 4.5.3 | Variation of P.S.D. of pressure on the measuring tube with static displacement of the measuring tube | 103 |
| 4.5.4 | Variation of the amplitude probability distribution of pressure with static displacement of the measuring tube | 104 |
| 4.5.5 | Variation of the P.S.D. of the flexible tube displacement with pressure measuring tube static displacement | 105 |
| 4.5.6 | Variation of the amplitude probability distribution of flexible tube displacement with static tube displacement | 106 |
| 4.5.7 | Interaction of a vibrating flexible tube with the pressure field round a neighbouring tube | 106 |
| 4.6 | P.S.D. Measurement of Pressure and Coherency along the Spanwise Axis of a Tube | 107 |
| 4.6.1 | Experimental method | 107 |
| 4.6.2 | Aims of the experiment | 107 |
| 4.6.3 | Experimental results | 107 |
| 4.6.4 | Comparison with previous results | 109 |
| 4.7 | P.S.D. Measurements of Pressure and Displacement as a Function of Flow Velocity | 109 |
| 4.7.1 | Experimental method | 109 |
| 4.7.2 | Aims of the experiment | 110 |
| 4.7.3 | Variation in the pressure fluctuations with flow velocity | 110 |
| 4.7.4 | Variation in the flexible tube displacement with flow velocity | 111 |
| 4.7.5 | Variation of r.m.s. pressure and r.m.s. displacement with flow velocity | 112 |
| 4.7.6 | Comparison with other investigations | 112 |
| 4.8 | Measurement of the Effect of Sound on the Pressure round a Tube and the Vibration Response of a Flexible Tube | 113 |
| 4.8.1 | Experimental method | 113 |
| 4.8.2 | Aims of the experiment | 113 |

| | | Page |
|---|---|---|
| 4.8.3 | Variation of the static and r.m.s. pressure distribution round a tube with superimposed sound | 114 |
| 4.8.4 | The effect of sound on the fluctuating pressure and displacement signals | 114 |
| 4.8.5 | Comparison with other investigations | 116 |
| 4.9 | Measurement of the Relative Phase of the Vortex Shedding Mode as a Function of Angle round the Tube | 117 |
| 4.9.1 | Experimental method | 117 |
| 4.9.2 | Aims of the experiment | 117 |
| 4.9.3 | Experimental results and discussion | 117 |
| 4.9.4 | Comparison with other investigations | 118 |
| 4.10 | Measurement of the Velocity and Turbulence Intensity in the Wake of a Row of Tubes | 119 |
| 4.10.1 | Experimental method | 119 |
| 4.10.2 | Aims of the experiment | 119 |
| 4.10.3 | Experimental results and discussion | 119 |
| 4.10.4 | Comparison with other investigations | 120 |
| 4.11 | Measurement of the Time History of the Displacement of a Vibrating Tube | 121 |
| 4.11.1 | Experimental method | 121 |
| 4.11.2 | Aims of the experiment | 121 |
| 4.11.3 | Results and discussion | 121 |
| 4.12 | Conclusions | 122 |
| 4.12.1 | Conclusions from section 4.3 | 122 |
| 4.12.2 | Conclusions from section 4.4 | 122 |
| 4.12.3 | Conclusions from section 4.5 | 123 |
| 4.12.4 | Conclusions from section 4.6 | 124 |
| 4.12.5 | Conclusions from section 4.7 | 125 |
| 4.12.6 | Conclusions from section 4.8 | 125 |
| 4.12.7 | Conclusions from section 4.9 | 126 |
| 4.12.8 | Conclusions from section 4.10 | 126 |
| 4.12.9 | Conclusions from section 4.11 | 126 |
| 4.13 | References | 127 |
| | Figures 4.1 - 4.47 | 131 |

| | | Page |
|---|---|---|
| CHAPTER 5. | INVESTIGATION INTO THE VIBRATION OF A DYNAMICALLY MODELLED TUBE BANK | 218 |
| 5.1 | Introduction | 218 |
| 5.2 | General Experimental Technique | 218 |
| 5.3 | Interaction of Two Vibrating Tubes in the Same Row | 220 |
| 5.3.1 | Experimental measurements | 220 |
| 5.3.2 | Results and discussion | 220 |
| 5.4 | Interaction of Two Vibrating Flexible Tubes in a Staggered Arrangement and the Investigation of Wake Velocity and Pressure Fluctuations | 222 |
| 5.4.1 | Experimental measurements | 222 |
| 5.4.2 | Results and discussion | 223 |
| 5.4.3 | Comparison with other work | 225 |
| 5.5 | Variation of Tube Vibration with Flow Velocity | 227 |
| 5.5.1 | Experimental measurements | 227 |
| 5.5.2 | Results and discussion | 228 |
| 5.5.3 | Comparison with other work | 230 |
| 5.6 | Variation of Static Pressure Distributions with Tube Spanwise Axial Position and Tube Position in the Tube Bank | 231 |
| 5.6.1 | Experimental measurements | 231 |
| 5.6.2 | Results and discussion | 231 |
| 5.6.3 | Comparison with other work | 232 |
| 5.7 | The Effects of Sound on Tube Vibration and Static Pressure Distribution round a Tube | 233 |
| 5.7.1 | Experimental measurements | 233 |
| 5.7.2 | Results and discussion for 333 Hz sound excitation | 233 |
| 5.7.3 | Results and discussion for 256 Hz sound excitation | 234 |
| 5.7.4 | Results and discussion for 293 Hz sound excitation | 235 |
| 5.7.5 | General discussion of the effects of superimposed sound and comparison with other results | 235 |

| | | Page |
|---|---|---|
| 5.8 | Conclusions | 236 |
| 5.8.1 | Conclusions from sections 5.3 and 5.4 | 236 |
| 5.8.2 | Conclusions from section 5.5 | 237 |
| 5.8.3 | Conclusions from section 5.6 | 238 |
| 5.8.4 | Conclusions from section 5.7 | 238 |
| 5.9 | References | 239 |
| | Tables 5.1 - 5.2 | 242 |
| | Figures 5.1 - 5.16 | 243 |
| CHAPTER 6. | MODELLING OF TUBE COUPLING VIA THE FLOW IN TUBE ROWS AND TUBE BANKS | 270 |
| 6.1 | Introduction | 270 |
| 6.2 | Review of Tube Row and Tube Bank Models | 270 |
| 6.2.1 | Prediction of the onset of fluid-elastic instabilities in single tube rows by Connors and modification of Connors' prediction equation by other researchers | 270 |
| 6.2.2 | Blevins' model | 272 |
| 6.2.3 | Goyder's model | 274 |
| 6.2.4 | Models of Whiston and Thomas | 274 |
| 6.2.5 | Balsa's model | 276 |
| 6.2.6 | S.S. Chen's model | 277 |
| 6.2.7 | Lengendre's model | 278 |
| 6.2.8 | Robert's model | 278 |
| 6.2.9 | Y.N. Chen's model | 279 |
| 6.2.10 | Model of Tanaka and Takahara | 280 |
| 6.3 | Discussion of the Modelling of Flow in Tube Rows and Tube Banks | 281 |
| 6.4 | Solution of Potential Problems using the Boundary Element Technique | 284 |
| 6.4.1 | Formulation of the method | 284 |
| 6.4.2 | Discretization of the equations | 285 |
| 6.4.3 | Evaluation of the integrals | 286 |
| 6.4.4 | Representation and solution of the integral equations on the computer | 286 |
| 6.4.5 | Brief description of the program | 287 |
| 6.4.6 | Verification and checking of the program | 288 |

| | | Page |
|---|---|---|
| 6.5 | The Tube Models | 290 |
| 6.6 | Single Tube Row Model (One tube with a wake model) | 292 |
| 6.6.1 | Description of model and investigation | 292 |
| 6.6.2 | Results for a tube displaced in the cross-flow direction | 292 |
| 6.6.3 | Results for a tube displaced in the streamwise direction | 293 |
| 6.7 | Single Tube Row Model (Three tubes with wake models) | 294 |
| 6.7.1 | Description of model and investigation | 294 |
| 6.7.2 | Results for a tube displaced in the cross-flow direction | 294 |
| 6.8 | Discussion of Results for a Single Tube Row | 295 |
| 6.9 | Equilateral Triangular Pitched Tube Bank Model | 296 |
| 6.9.1 | Description of model and investigation | 296 |
| 6.9.2 | Results and discussion | 296 |
| 6.10 | Staggered Tube Bank Model (transverse pitch ratio, 1.043; longitudinal pitch ratio, 1.023) | 297 |
| 6.10.1 | Description of the model | 297 |
| 6.10.2 | Results and discussion | 297 |
| 6.11 | Conclusions for Sections 6.6 to 6.10 | 298 |
| 6.12 | Summary | 299 |
| 6.13 | References | 300 |
| | Figures 6.1 - 6.34 | 304 |
| CHAPTER 7. | SUMMARY AND CONCLUSIONS | 351 |
| CHAPTER 8. | SUGGESTIONS FOR FURTHER WORK | 355 |
| APPENDIX 1. | CIRCUIT DIAGRAMS | 357 |
| | Figures A4.1 - A4.6 | 357 |

| | | Page |
|---|---|---|
| APPENDIX 2. | LISTINGS OF COMPUTER PROGRAMMES | 362 |
| LISTING 1. | MICROPROCESSOR DATA ACQUISITION AND CONTROL PROGRAMME | 362 |
| LISTING 2. | EXPERIMENTAL RESULTS ANALYSIS AND PLOTTING PROGRAMME | 372 |
| LISTING 3. | BOUNDARY ELEMENT POTENTIAL FLOW PROGRAMME | 378 |
| APPENDIX 3. | CALIBRATION OF THE PRESSURE MEASURING TUBE ELECTRET MICROPHONES | 391 |
| APPENDIX 4. | TABLES OF CO-ORDINATES OF THE WIND TUNNEL SECTIONS | 393 |

UNIVERSITY OF SOUTHAMPTON

ABSTRACT

FACULTY OF ENGINEERING AND APPLIED SCIENCE

INSTITUTE OF SOUND AND VIBRATION RESEARCH

Doctor of Philosophy

# AN INVESTIGATION INTO FLOW AND ACOUSTIC COUPLING OF TUBES IN GAS HEAT EXCHANGER TUBE BANKS

by Robin Graeme Arak

The design, construction and commissioning of a wind tunnel and associated instrumentation for the investigation of flow and acoustic coupling phenomena in tube rows and tube banks is described. Dynamically similar models of a typical AGR heat exchanger tube bank were constructed and tested at representative Reynolds numbers in the range $3 \times 10^4$ to $1{\cdot}2 \times 10^5$.

It is found that tubes vibrating with small amplitudes have a non-linear effect on the pressure fields round neighbouring tubes, and that sound also has a non-linear effect on the pressure distribution round the tubes. It is also shown that sound below SPL's of approximately 140 dB does not significantly increase the level of tube vibrations in tube banks unless its frequency, or the frequencies generated by the non-linear interaction in the tubes' boundary layers, are coincident with the tube resonance frequencies.

Current methods for predicting the onset of large amplitude vibrations in tube banks are critically discussed. It is shown, both experimentally and theoretically, using a boundary element potential flow model, that current methods for predicting the forces on tubes which are statically displaced from their mean positions in tube rows and tube banks are in error. Hence, present schemes for predicting the onset of large amplitude fluid-elastic vibrations in heat exchanger tube banks are not necessarily reliable.

Suggestions for further experimental work are made and a scheme for the prediction of the onset of large amplitude tube vibrations based on the boundary element model is suggested.

## ACKNOWLEDGEMENTS

The author wishes to thank all persons who gave their advice, time and effort during the research project. In particular, thanks go to Dr. F.J. Fahy, who has given constant encouragement and advice in his capacity as project supervisor. Thanks also go to all the technicians involved with the construction of the experimental apparatus. In particular to Mr. A. Sanger and Mr. D. Edwards, who devoted much of their time to the construction of the wind tunnel and the model tube bank respectively. Thanks go also to the departmental secretaries who typed the thesis and to Miss S.M. Greenfield who assisted in the proof reading.

The author acknowledges financial support from the Central Electricity Research Laboratories, Leatherhead, U.K., as part of the contract "Interaction of externally applied acoustic fields and vortex shedding in tube banks".

# LIST OF SYMBOLS

## List of Symbols for Chapters 1 to 5

| | |
|---|---|
| $A$ | blocked cross-sectional area of working section |
| $A_t$ | cross-sectional area of variable throat |
| $A_w$ | cross-sectional area of working section |
| $a$ | internal radius of tube |
| $b$ | external radius of tube |
| $C$ | capacity of compressed air storage tanks |
| $C_a$ | velocity of sound in air |
| $c$ | velocity of sound in gas |
| $D_L$ | longitudinal spacing of tubes in the tube bank |
| $D_T$ | transverse spacing of tubes in the tube bank |
| $d$ | tube diameter |
| $E$ | Young's modulus for flexible tube material |
| $f$ | tube resonance frequency |
| $I$ | second moment of area of flexible tube |
| $L$ | tube length |
| $\ell$ | length from boundary layer tripping point |
| $M_w$ | Mach number in working section |
| $ME$ | air mass efficiency of wind tunnel |
| $m$ | tube mass per unit length |
| $P_e$ | minimum allowable air storage tank pressure |
| $P_s$ | maximum air storage tank pressure |
| $P_w$ | air pressure in working section |
| $Re_\ell$ | Reynolds number in unblocked working section |
| $s$ | sound pressure |
| $t$ | run time of wind tunnel |
| $u$ | velocity of gas |
| $V_w$ | air velocity in working section |
| $x$ | cross-stream tube displacement |
| $y$ | streamwise tube displacement |
| $z$ | displacement along tube spanwise axis |
| $\gamma$ | ratio of principal specific heats of air |
| $\delta$ | boundary layer thickness |
| $\zeta$ | tube damping ratio |
| $\eta$ | dynamic viscosity of gas |
| $\lambda$ | sound wavelength |

List of Symbols for Chapters 1 to 5 (continued)

| | |
|---|---|
| $\lambda_i$ | parameter for tube vibrational mode shape |
| $\rho$ | gas density |
| $\rho_T$ | density of flexible tube material |

List of Symbols Not Defined in the Text of Chapter 6

| | |
|---|---|
| a | tube radius |
| $C_x$ | fluid force constant in streamwise direction due to tube displacement in the cross-flow direction |
| D | tube diameter |
| d | tube diameter |
| f | tube vibration frequency |
| $f_o$ | tube vibration frequency in still fluid |
| $K_y$ | fluid force constant in cross-flow direction due to tube displacement in the streamwise direction |
| m | tube mass per unit length |
| $m_o$ | tube mass per unit length in still fluid |
| $P_R$ | mode number of tube bank vibration |
| Re | Reynolds number |
| St | Strouhal number |
| U | fluid velocity |
| $U_c$ | critical flow velocity for large amplitude tube vibrations |
| $U_\infty$ | free stream velocity |
| u | flow velocity in tube bank |
| $V_{c\ det}$ | critical flow velocity for large amplitude tube vibrations when the tube resonance frequencies are different |
| $V_{c\ tun}$ | critical flow velocity for large amplitude tube vibrations when the tube resonance frequencies are the same |
| $X_T$ | transverse tube spacing ratio in tube bank |
| $\beta$ | fluid-elastic 'Whirling' constant |
| $\delta_o$ | tube damping ratio in still fluid |
| $\delta_{det}$ | damping ratio of tubes when tube resonance frequencies are different |
| $\delta_{tun}$ | damping ratio of tubes when tube resonance frequencies are the same |

List of Symbols Not Defined in the Text of Chapter 6 (continued)

| | |
|---|---|
| $\lambda_{TM}$ | tube bank vibration mode wavelength |
| $\rho$ | fluid density |
| $\phi$ | velocity potential |

## LIST OF ABBREVIATIONS

| | |
|---|---|
| A.G.R. | advanced gas reactor |
| a.c. | alternating current |
| a.d.c. | analogue-to-digital converter |
| Bsp | British standard pipe |
| B & K | Bruel and Kjaer |
| C.E.G.B. | Central Electricity Generating Board |
| C.E.R.L. | Central Electricity Research Laboratories |
| C.M.O.S. | complementary metal oxide semiconductor |
| C.P.U. | central processor unit |
| C.S.D. | cross spectral density |
| D.A.C. | Data Analysis Centre |
| d.a.c. | digital-to-analogue converter |
| d.c. | direct current |
| disp. | displacement |
| F.E.T. | field effect transistor |
| F.S.K. | frequency shift keying |
| I.C. | integrated circuit |
| ICL 2970 | International Computers 2970 series computer |
| I.D. | internal diameter |
| ISVR | Institute of Sound and Vibration Research |
| I/O | input/output |
| L.S.B. | least significant bit |
| M.S.B. | most significant bit |
| NAG | Numerical Algorithms Group |
| O.D. | outside diameter |
| P.I.O. | parallel input output (port) |
| P.S.D. | power spectral density |
| prob. | probability |
| p.s.i. | pounds per square inch |
| R.A.M. | random access memory |
| R.O.M. | read only memory |
| SPL | sound pressure level |
| U.S.R. | user subroutine |

## KEY TO FIGURE SYMBOLS

The graphs in Chapters 4,5 and 6 which show the variation of static pressure and the components of lift and drag with angle round the pressure measuring tube, use the following symbols.

* Static pressure.

▲ Lift component of static pressure.

◆ Drag component of static pressure.

## Definition of Pressure Coefficients

The static pressure coefficient $C_p(\theta)$ round a tube in a single tube row is defined by:

$$C_p(\theta) = \frac{P_\theta - P_s}{\frac{1}{2}\rho u^2}$$

and round a tube in a tube bank is defined by:

$$C_p(\theta) = \frac{P_\theta - P_o + \frac{1}{2}\rho u^2}{\frac{1}{2}\rho u^2} \quad .$$

The r.m.s. pressure coefficient $C_p(\theta)_{rms}$ round a tube is defined by:

$$C_p(\theta)_{rms} = \frac{P(\theta)_{rms}}{\frac{1}{2}\rho u^2} \quad .$$

$\theta$ is the angle from the front of the tube,
$P_\theta$ is the pressure on the tube at angle $\theta$,
$P_s$ is the free stream static pressure,
$P_o$ is the pressure on the front of the tube (i.e. $\theta = 0^o$),
$P(\theta)_{rms}$ is the r.m.s. pressure fluctuations measured on the tube at angle $\theta$,
$\rho$ is the free stream air density,
and u is the free stream flow velocity.

# CHAPTER 1

# INTRODUCTION

## 1.1 Motivation for Research

All electricity generating plant powered by burning gas, coal or oil, or by heat from nuclear fission, incorporates one or more heat exchangers. The heat exchangers can be very varied in design but all contain banks of tubes over which fluid is passed. The thermal energy in the primary fluid passing over the tubes is transferred through the tube walls (by conduction) to a secondary fluid (water or steam) which is circulated through the tubes and then passes into a steam turbine generator set which is used to produce electricity.

The kinetic energy of the primary fluid circulating through the heat exchanger is sometimes sufficient to cause severe vibrations of the tubes in the tube bank which leads to rapid tube fatigue resulting in cracked tubes. When the tubes crack the secondary fluid passes into the primary fluid circuit, and so either a section of the tube bank has to be shut down, or the whole heat exchanger has to be shut down for repair which is extremely time consuming and costly.

One well documented example of a serious failure of a heat exchanger caused by excessive tube vibrations leading to cracks developing in the tubes is given in reference [1.6]. In this case the problem with the heat exchanger at the Wylfa nuclear power station in Anglesey, U.K., cost £54 million in lost electricity generation (which had to be replaced by a generating plant which was more expensive to run) and £2 million in labour for repairing the heat exchanger. Further case histories of failures in heat exchangers are given in [1.5, 1.16, 1.19, 1.21].

The current tendency is to make modern heat exchangers more compact in order to reduce the production costs. However this means that the velocity of the fluid flowing over the tubes has to be increased to achieve the same total heat transfer as that in a larger heat exchanger. These increased fluid velocities produce larger excitation forces on the tubes leading to higher levels of tube vibrations. This can be a serious problem, particularly in compact Advanced Gas Reactor heat exchangers where gas velocities and pressures are high. In liquid heat exchangers (where fluid densities are high) the tube vibration can be even more severe.

The large capital cost of a new heat exchanger (which is typically £200 million for a nuclear reactor heat exchanger) and the large cost of repairing a badly designed heat exchanger which is prone to excessive tube vibrations, is a strong motivation for carrying out research into the mechanisms which cause tube vibrations in heat exchangers.

Since the 1960's many investigations have been carried out on the various aspects of vibrations in heat exchangers which are too numerous to list and discuss in detail here. Some good review papers which list and discuss much of the important work are given in [1.5, 1.7, 1.19, 1.20, 1.24].

The work carried out by the author is restricted to the study of certain phenomena in staggered tube bank models of gas heat exchangers which are used in nuclear powered electricity generating plant in the U.K.

## 1.2 Brief Review of the Major Tube Excitation Mechanisms in Staggered Tube Banks

The major tube excitation mechanisms which have been found to occur in staggered tube banks subjected to gas cross-flow are:

(i) vortex shedding,

(ii) turbulent buffeting,

(iii) fluid-elastic instabilities,

(iv) acoustic excitations.

In sections 1.2.1 to 1.2.4 the four different tube excitation mechanisms are briefly discussed.

### 1.2.1 Vortex shedding

The process of vortex shedding from isolated bodies is well known and is described in many standard texts, e.g. [1.15].

When a fluid flows over a tube, boundary layers form on the surface. Towards the rear of the tube the flow slows down producing an adverse pressure gradient which causes the boundary layers to separate from the tube surface. Between Reynolds numbers of approximately 300 and $2 \times 10^5$ the separated boundary layers (named shear layers) roll up to form vortices which are shed into the wake of the tube and convected

downstream. The vortices are shed alternately from each side of the tube producing a fluctuating pressure force which acts on the tube with its major component in a direction perpendicular to the oncoming flow and the tube spanwise axis. This fluctuating pressure force excites tube vibrations and when the vortex shedding frequency is nearly coincident with the tube mechanical resonance frequency, large amplitude tube vibrations are produced.

The pattern of vortex shedding from tubes mounted in a tube bank is considerably different from that observed from a single tube. Of the numerous researchers who have studied vortex shedding in tube banks, one of the most prolific is Y.N. Chen [1.8, 1.9, 1.10] who uses shedding processes to explain most observable phenomena occurring in tube banks, where often an alternative explanation using a buffeting or fluid-elastic model might be more appropriate.

Several investigators have failed to observe vortex shedding inside closely packed staggered tube banks in gas cross-flow, e.g. [1.1, 1.2, 1.12]. Hence it is apparent that although vortex shedding does occur in some tube banks, it is not always present in closely packed tube banks and therefore is not always the most important tube excitation mechanism.

### 1.2.2 Turbulent buffeting

Owen [1.18] developed a theory to explain the broadband variation of the velocity spectrum measured behind the last row of a tube bank. This led to the explanation of the excitation of tubes by broadband turbulent velocity fluctuations produced by turbulent eddies which are generated by turbulence (produced near the separation points on the tubes) convecting downstream through the tube bank. This excitation mechanism is known as turbulent buffeting. The measurements of Owen [1.18] and the theory of Blevins [1.3] have been used by Blevins [1.4] to predict vibration levels in model and full scale tube banks, without much success (see section 5.4.3). However, turbulent buffeting is undoubtedly one of the most important excitation mechanisms in tube banks where the vibration levels are small.

### 1.2.3 Fluid-elastic instabilities

Fluid-elastic instabilities in a single tube row were first observed by Connors [1.11]. In some cases when a tube is displaced from a uniformly spaced position in a tube row the force on the tube acts in a direction so as to increase the displacement of the tube further. When this occurs and the energy transferred to the tube by the fluid is greater than the energy dissipated by mechanical and fluid damping, a fluid-elastic instability occurs producing large amplitude tube vibrations. Connors analysed this excitation process using a quasi-static approach, and derived an empirical formula (based on experimental data) to predict the onset of large amplitude vibrations in a single tube row. Since the original investigation by Connors many researchers have measured vibrations in tube banks and compared their measured values of the onset of fluid-elastic instabilities with Connors' formula. However the formula was not designed to predict the onset of fluid-elastic instabilities inside tube banks, and several modifications to the original formula, and to the empirically derived constants in it, have been made to produce correlations with the results of existing experimental measurements in tube banks. These modifications are reviewed by Païdoussis [1.20].

Several researchers have developed theories for predicting the onset of fluid-elastic instabilities in tube banks, and these are critically discussed in Chapter 6.

Jet switching originally observed by Roberts [1.23] is another mechanism which causes instabilities in single tube rows but there are no reports in the literature of the jet switching mechanism occurring in closely packed staggered tube bundles, so it is not discussed here.

### 1.2.4 Acoustic excitations

One of the first researchers to discuss the presence of acoustic oscillations in heat exchangers was Putnam [1.22]. An acoustic resonance in a heat exchanger is produced when there is a sufficiently high fluctuating pressure at the frequency of one of the acoustic modes of the heat exchanger vessel. An acoustic mode is then excited at one or more of the vessel modal frequencies and produces an increase

in the pressure fluctuations in the flow which in turn drives the acoustic modes to a higher amplitude. The initial excitation of the acoustic mode can be either by vortex shedding, when the vortex shedding frequency is nearly coincident with the acoustic modal frequency, or by broadband turbulence which has sufficient energy at the acoustic modal frequency to excite the mode to a high enough amplitude to sustain a positive feedback loop.

Another type of acoustic excitation is produced by acoustic pressure fluctuations generated in the heat exchanger gas circulator system by, for example, the circulator fan. The sound propagates upstream or downstream from the source until it reaches the tubes in the heat exchanger. If the sound pressure levels are high enough, significant tube vibration can be produced. The influence of externally applied sound has been investigated in [1.13, 1.14, 1.17] and the important results are discussed and compared with the results of the present investigation in Chapter 4.

## 1.3 Aims of the Present Research Project

The aim of the experiments carried out during the present research project was to investigate the fluid coupling between adjacent vibrating tubes, and the effect of sound on tube vibrations in a model of a staggered tube bank typical of those used in nuclear powered electricity generating plant.

Many of the investigations into heat exchanger tube vibrations have been previously carried out using arbitrary flow and tube parameters. Very few investigators have seriously attempted to use dynamically modelled tube banks having the important non-dimensional parameters similar to those measured in full scale heat exchangers. In the current investigation a dynamically modelled tube bank was designed and constructed so that the non-dimensional parameters were similar to those measured in full scale heat exchangers found in nuclear powered generating plant in the U.K. An investigation into the coupling of tubes via the flow in the dynamically modelled tube bank was then carried out, and the effect of externally imposed sound was also studied. In the experimental investigation the onset of fluid-elastic instabilities was not studied, since the tube and flow parameters were such that this phenomenon did not occur. The investigation was mainly concerned

with small amplitude vibrations which do not catastrophically damage the tubes, but may over a period of years cause fatigue and eventual failure of some of the tubes. It is important to know the levels of vibration and the statistics of the tubes' vibration responses so that reliable failure predictions can be made in order to estimate the service lifetime of heat exchangers.

Figure 1.1 shows an idealised r.m.s. response of a tube to varying flow velocity and also shows the general form of a tube's response due to the different excitation mechanisms discussed in sections 1.2.1 to 1.2.3. In the present investigation only the different types of tube responses below the flow velocity required to produce fluid-elastic instability are studied. The descriptions of the experiments carried out on the dynamically modelled tube bank together with the results, discussions, comparisons with other work and conclusions are presented in Chapter 5.

In Chapter 4 investigations into the mechanisms by which vibrating tubes and the presence of sound affects the pressure distributions and hence exciting forces on a neighbouring tube in a single tube row are reported. Although a tube in a single tube row is not representative of a tube inside a tube bank, it was thought that the flow coupling mechanism between tubes executing small amplitude vibrations would be similar in both situations.

An investigation into the variation of the pressure distributions on a tube in a single row as the tube was displaced from a uniformly spaced position between its neighbours was also carried out. The results were compared with the results of Connors [1.11] to discover if his conclusions are generally applicable to arbitrary tube rows subjected to gas cross-flow at Reynolds numbers typical of those in Advanced Gas Reactor heat exchangers. A description of the experiments performed, the results, discussions, comparisons with previous work and the conclusions, for the investigations using a single tube row, are given in Chapter 4.

Several researchers have developed models of the fluid dynamic coupling between tubes in tube rows and tube arrays. These models are critically discussed in Chapter 6 and a potential flow model which includes a facility for a simple wake model using free streamlines is developed to investigate tube coupling via the mean flow in tube rows and tube banks.

In Chapters 4, 5 and 6 relevant work previously carried out by other researchers is discussed and compared with the present results.

Chapter 2 discusses the design of a wind tunnel which was constructed in order to carry out the experimental investigations and Chapter 3 discusses the design of the model tube bank and the associated instrumentation used in conducting the experiments.

The major conclusions from the research project are given in Chapter 7 and in Chapter 8 suggestions for further work are made.

## 1.4 References


1.1 J.P. BATHAM 1973 Proceedings of the International Symposium on Vibration Problems in Industry held at Keswick, U.K., 10-12 April 1973. Paper 411. "Pressure distribution on in-line tube arrays in cross flow".

1.2 G. BAYLAC, D. BAI and J.P. GREGOIRE 1973 Proceedings of the International Symposium on Vibration Problems in Industry held at Keswick, U.K., 10-12 April 1973. Paper 219. "Study of flow and acoustic phenomena in a tube bank".

1.3 R.D. BLEVINS 1977 "Flow-Induced Vibration". London: Van Nostrand Reinhold.

1.4 R.D. BLEVINS 1978 Proceedings of the International Conference on Vibration in Nuclear Plant held at Keswick, U.K., 9-12 May 1978. Paper 3:4. "Buffeting of heat exchanger tube arrays in a cross flow".

1.5 R.D. BLEVINS 1979 Progress in Nuclear Energy, Vol. 4, No. 1, pp. 25-49. "Flow-Induced Vibrations in Nuclear Reactors - A Review".

1.6 C.E.G.B. 1977 C.E.G.B. publication G823. "Wylfa nuclear boiler repair".

1.7 S.S. CHEN 1980 Shock and Vibration Digest Vol. 12, pp. 21-34. "Cross-flow-induced instabilities of circular cylinders".

1.8 Y.N. CHEN 1967 Journal of Royal Aeronautical Society Vol. 7., pp. 211-214. "Frequency of the Karman vortex streets in tube banks".

1.9 Y.N. CHEN 1968 Journal of Engineering for Industry, Trans. A.S.M.E. Series B, Vol. 90, pp. 134-136. "Flow induced

vibration and noise in tube bank heat exchangers due to Von Karman streets".

1.10 Y.N. CHEN 1972 Journal of Engineering for Industry, Trans. of A.S.M.E. Series B, Vol. 94, pp. 603-628. "Fluctuating lift forces of the Karman vortex streets on single circular cylinders and in tube bundles".

1.11 H.J. CONNORS, Jr. 1970 Proceedings of the A.S.M.E. Winter Annual Meeting held in New York, 1 December 1970. Flow-induced vibration in heat exchangers, pp. 42-56. "Fluid-elastic vibrations of tube arrays excited by cross flow".

1.12 R.E. FRANKLIN 1974 U.K. Atomic Energy Authority, A.E.R.E. Harwell Report RS 117. "Fluid dynamic forces on tubes in a typical heat exchanger array".

1.13 R.S. HILL 1976 Transactions of the North East Coast Institution of Engineers and Shipbuilders, Vol. 92. "Tube vibration in boiler and other heat exchangers".

1.14 S.C. KACKER and R.S. HILL 1974 University of Newcastle upon Tyne, Department of Mechanical Engineering Report No. Tb 30A. "Flow over a circular cylinder in the presence of standing sound waves".

1.15 B.S. MASSEY 1975 "Mechanics of Fluids". New York: Van Nostrand.

1.16 H.A. NELMS 1970 Proceedings of the A.S.M.E. Winter Annual Meeting, held in New York, 1 December 1970. Flow-induced vibration in heat exchangers, pp. 8-17. "Flow-induced vibrations: A problem in the design of heat exchangers for nuclear service".

1.17 S. OKAMOTO, T. HIROSE and T. ADACHI 1981 Bulletin of J.S.M.E., Vol. 24, No. 187, pp. 45-53. "The effect of sound on the vortex-shedding from a circular cylinder (acoustical vibrations directed along axis of cylinder)".

1.18 P.R. OWEN 1965 Journal of Mechanical Engineering Science, Vol. 7, No. 4, pp. 431-439. "Buffeting excitation of boiler tube vibration".

1.19 M.P. PAIDOUSSIS 1979 Proceedings of IAHR/IUTAM Symposium on Practical Experiences with Flow-Induced Vibrations, held at Karlsruhe, Germany, September 1979. "Flow-induced vibration in nuclear reactors and heat exchangers: practical experiences and state of knowledge".

1.20 M.P. PAIDOUSSIS 1981 Journal of Sound and Vibration 76(3), pp. 329-360. "Fluidelastic vibration of circular cylinder arrays in axial and cross flow: state of the art".

1.21 H.R. PEARCE 1973 University of Oxford D.Phil. Thesis. "Noise and Vibration in Heat Exchangers".

1.22 A.A. PUTNAM 1959 Journal of Engineering Power, Vol. 81, A(4), pp. 417-422. "Flow induced noise in heat exchangers".

1.23 B.W. ROBERTS 1966 Mechanical Engineering Science Monograph No. 4. "Low Frequency Aeroelastic Vibrations in a Cascade of Circular Cylinders".

1.24 S.D. SAVKAR 1977 Journal of Fluids Engineering, Trans. A.S.M.E. Series I, Vol. 99, pp. 517-519. "Brief review of flow induced vibrations of tube arrays in cross-flow".

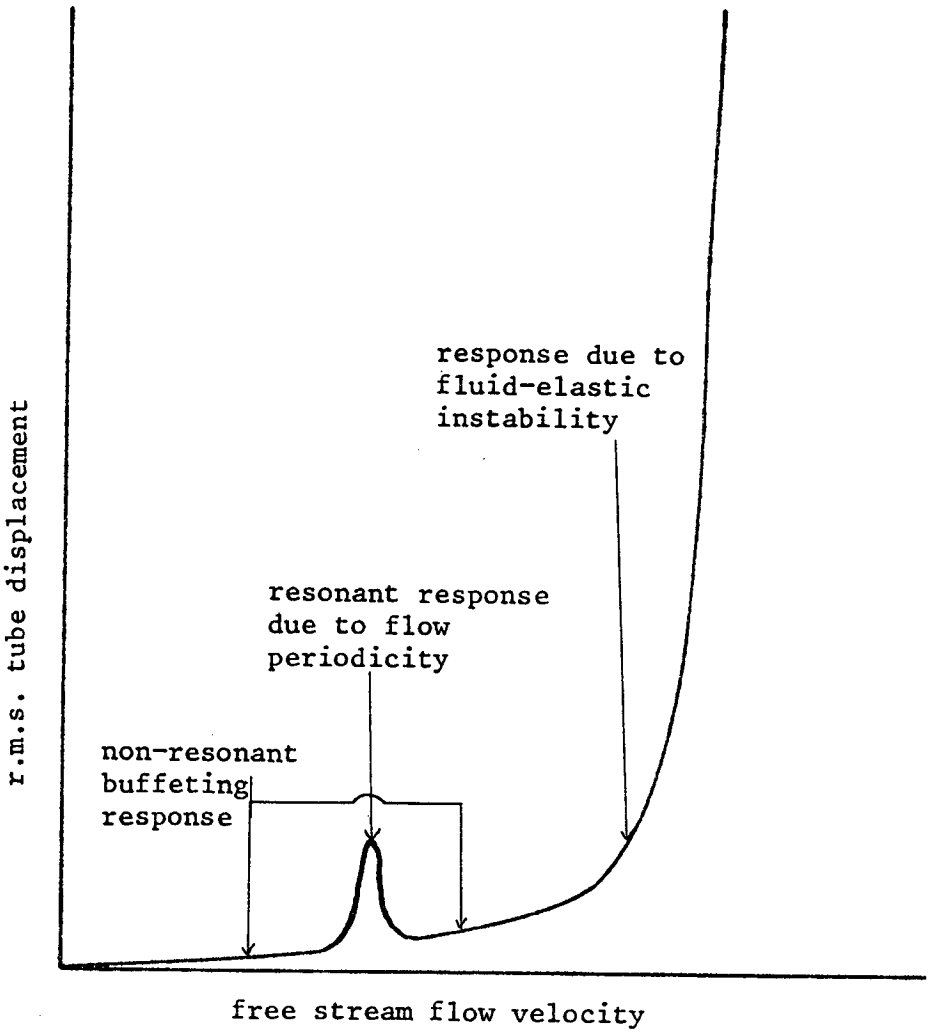


FIGURE 1.1. Idealized response of a tube in a tube bank subjected to cross-flow (from Païdoussis [1.20]).

# CHAPTER 2

# THE WIND TUNNEL

## 2.1 Introduction

The investigation of tube, flow and acoustic coupling in heat exchanger tube banks was to be carried out with a dynamically modelled tube bank. The important non-dimensional parameters were to be kept approximately the same in the model as in full scale advanced gas-cooled nuclear reactor (A.G.R.) heat exchanger tube bank. The flow regime and coupling mechanisms observed in the scale model tube bank mounted in the wind tunnel and in the full scale A.G.R. heat exchanger would then be similar. The design of the wind tunnel was therefore governed by the magnitudes of the non-dimensional parameters calculated from measured parameters in full scale A.G.R. heat exchangers.

In this chapter the important parameters used in modelling a heat exchanger tube bank are discussed, and the design, construction and calibration of the wind tunnel is described in detail because they formed a substantial and vital component of the project effort.

## 2.2 Modelling Considerations

Table 2.1 lists the important measurable parameters which effect the vibrations of tubes in a heat exchanger tube bank. The fluid dynamic forces acting in the tubes are taken into account by the inclusion of the variables $\rho$, u, $\eta$ and d. The stagnation pressure of the fluid was not included in the dynamically scaled flow because it only effects the static fluid forces on the tubes. The effect of gravity on the fluid forces acting on the tubes is negligible since there are no free surfaces and buoyancy effects are small. The non-dimensional groups were determined from these parameters using the Buckingham method [2.7] and are shown in Table 2.2. It was unnecessary to keep all the non-dimensional groups in Table 2.2 exactly the same in the model and the full scale heat exchanger. This was because the influence on the fluid and tube dynamics is small when the magnitudes of some of the non-dimensional groups are changed. The Mach number (u/c) has very little effect on the fluid dynamics provided that it is much smaller than unity. When this condition is satisfied the fluid in the tube bank can be considered to be

incompressible. In the model and full scale tube bank the Mach number is less than 0.2, so the effects of gas compressibility can be neglected. The ratio $(d/\lambda)$ effects the magnitude of the direct acoustic exciting force on the tube. However, the effects of interaction of the sound with the flow and the flow interaction with the tubes are to be investigated and it is not expected that the variation of $(d/\lambda)$ will effect the flow/tube interaction mechanisms. Therefore the non-dimensional groups $(u/c)$ and $(d/\lambda)$ did not have to have exactly the same magnitude in the scale model and the full scale tube bank. A list of the magnitudes of the important non-dimensional groups in a full scale A.G.R. heat exchanger tube bank is given in Table 2.3. Throughout the design of the wind tunnel and dynamically modelled tube bank the non-dimensional groups were kept within the limits given in Table 2.3.

In tube banks the flow conditions between the first three rows of tubes varies considerable from row to row[2.18]. In order to investigate the vibrations of a tube in the middle of a large tube bank it has been shown that at least six rows are required, [2.9,2.18, 2.21]. It was therefore decided to use a ten row tube bank consisting of six rows of dynamically modelled tubes with two rows of fixed tubes at each end. This arrangement would permit the flow conditions deep inside a large tube bank to be modelled in the sixth and seventh rows of the model tube bank. All other calculations in the design of the wind tunnel were based on a ten row staggered tube bank consisting of alternate rows of five and six tubes.

An investigation into the fluid dynamic tube coupling and the influence of sound on a single row of tubes was to be carried out. It was decided that in order to reduce the complexity of the investigation the oncoming flow to the row of tubes should be well defined and of low turbulence intensity. The wind tunnel was therefore designed to have a low flow turbulence intensity and the magnitudes of the non-dimensional parameters in Table 2.3 were to be achieved in the wind tunnel working section when a ten row tube bank was installed.

## 2.3 Wind Tunnel Design Considerations

The diameter of the tubes in the model tube bank and the dimensions of the wind tunnel working section were decided by

considering several factors as follows:-

(i) The maximum allowable pressure drop across the model tube bank.

(ii) The Reynolds number (based on tube diameter and gap velocity) which had to be achieved.

(iii) The mass rate at which air could be drawn through the wind tunnel.

(iv) The total running time required to carry out an experiment.

The pressure drop across a ten row tube bank is difficult to predict because of the lack of reliable information. Several different sources of information were used to estimate the pressure drop [2.3,2.8, 2.13,2.18]; these gave considerably different results. It was found that to achieve a Reynolds number of $1.5 \times 10^5$ with the appropriate geometrical tube spacings, and very little by-pass round the edges of the tube bank, the largest estimate gave a pressure drop of approximately 15kPa across the tube bank. The power required to achieve this pressure drop with an appropriate mass flow rate (6.5 $kgs^{-1}$) to achieve a Reynolds number of $1.5 \times 10^5$ is approximately 80kW. If a d.c. motor with a semi-conductor rectifier and control system were used to drive the wind tunnel the a.c. input power would be approximately 200 kW. This system was impractical to build with the facilities and funds available. It was therefore decided that the wind tunnel should be an intermittent test facility which is driven by the compressed air system available in the ISVR.

The 1.7 GPa (250 p.s.i.), $85m^3$ compressed air supply system permits two different types of compressed air driven wind tunnel to be driven, the direct blowdown system and the injected air boundary layer suckdown system. In the direct blowdown system the compressed air driving the wind tunnel is reduced to a suitable driving pressure, to produce the desired flow rate, using an automatic control valve. As the air in the storage tanks is used up the pressure drops and the automatic control valve opens to maintain the correct driving pressure to keep the flow rate constant. There are three main disadvantages of this system:

(i) The large pressure drop in the valve introduces a lot of turbulence and noise into the air supply to the wind tunnel.

(ii) The pressure control valve has a finite response time and hysteresis, so the supply pressure to the wind tunnel is not constant, which produces a variation in the wind tunnel flow rate.

(iii) The run time before the minimum allowable storage tank pressure is reached with the system available in ISVR, is approximately 200 seconds which gives very little time for taking measurements.

The injected air suckdown wind tunnel uses compressed air which is injected through slots in an injector box so that air is directed downstream parallel to the axis of the wind tunnel. The injected air which expands rapidly entrains the air upstream of the injection nozzles to produce a flow of air through the wind tunnel. The advantages of the injected air suckdown system over the blowdown system are:-

(i) More air is entrained than injected so for a given mass of compressed air used the wind tunnel run time is greater than in the blowdown system. Run times are generally increased by a factor of 3 to 5.

(ii) If a sonic throat is established upstream of the injection nozzles the flow rate through the wind tunnel is determined by the speed of sound at the throat and the ratio of working section to throat areas. Hence the flow rate can be controlled very precisely by varying the throat area.

(iii) The air is injected downstream of the working section so turbulence and noise produced in the injection process does not propagate upstream into the working section, except through the boundary layer.

It was therefore decided to design an injected air suckdown wind tunnel. In the ISVR there was an injector box and diffuser which were built as part of a supersonic wind tunnel constructed several years ago [2.1]. It was decided to use these facilities, but several points had to be considered when using a fixed size injector box in the wind tunnel design:

(i) The maximum velocity of air through the working section is determined by the ratio of the working section to maximum sonic throat area and the speed of sound at the sonic throat. Since the maximum sonic throat area is fixed by the injector box size the maximum attainable velocity in the working section is governed by the working section area.

(ii) The maximum and minimum velocities of the wind tunnel with a fixed working section is governed by the maximum and minimum sonic throat areas.

(iii) The maximum pressure drop obtainable across the tube bank is the working section without the wind tunnel stalling is governed by the maximum pressure drop that can be achieved between the

inlet and sonic throat.

The points outlined above were very important in the design of the working section and variable throat described in sections 2.9 and 2.11 respectively. The maximum pressure drop that could be maintained across the tube bank was calculated to be 30 k Pa using pressure data from an existing injection wind tunnel which used a similar injector box [2.10,2.16]. In order to decide on the working section size and model tube diamter the pressure drops, mass flow rates and Reynolds numbers for different 10 row staggered tube banks with different size tubes and working sections were calculated, keeping the geometrical tube spacing ratios constant, [2.8,2.13]. It was found that the optimum solution (i.e. highest Reynolds number for the lowest pressure drop) was to design a working section of cross-section 400 mm x 400 mm and to use 30 mm diameter tubes.

## 2.4 Design of the Wind Tunnel

A diagram of the wind tunnel is shown in Figure 2.1. A general view of the completed wind tunnel is shown in Plate 2.1. The wind tunnel has an overall length of approximately 15.8 metres and consists of a bellmouth inlet, settling section, contraction, sound injection box,working section, high speed contraction, variable throat, air injector box and diffuser. The wind tunnel was designed to be of a modular construction so that the relatively large low speed working section could be replaced by a smaller high speed working section suitable for use in other projects.

## 2.5 Bellmouth Inlet

The bellmouth inlet was designed to give a smooth inlet flow and was constructed on a wooden frame overlaid with two layers of 1.5 mm plywood. The bellmouth shape is a modified version of a design used previously in the Aeronautics department which has given a smooth inlet flow to many different wind tunnels used in Southampton University. It is a modified shape derived from the streamlines of a flow into a pipe calculated using the hodograph transformation [2.21]. Figure 2.2 shows the shape of the bellmouth and Table A4.1 gives the co-ordinates of the bellmouth inlet section.

## 2.6 Settling Section

The settling section is approximately 2.2 metres long and 1.6 metres x 1.6 metres in cross-section. The large scale turbulence of the flow into the wind tunnel is reduced by two aluminium alloy honeycomb screens of 50 mm thickness with 6 mm hexagonal cells. The honeycomb screens reduce the transverse turbulence to a scale of the same order as the hexagonal cell size. There is a 300 mm gap between the two honeycomb screens to allow the small scale turbulence generated by the first screen to decay before the second honeycomb screen is reached. Another 300 mm settling length between the last honeycomb screen and the first wire mesh screen allows small scale turbulence generated by the honeycomb screen to decay before the wire mesh screens are reached. There is provision for putting up to four wire mesh screens, each separated by 150 mm, into the settling section. In the current design two wire mesh screens separated by a 450 mm settling length are used to reduce the turbulence in the settling section. The first screen is made from stainless steel 0.51 mm diameter wires woven at 787 mesh per metre (24 s.w.g. 20 mesh per inch) and has a pressure drop coefficient of approximately 9 at the highest flow speed in the settling section. The pressure drop coefficient is well above 2.5 which is the magnitude required to satisfy the Batchelor criteria for reducing longitudinal turbulence to zero [2.19]. The last screen, also made from stainless steel, has 0.11 mm diameter wires woven at 3937 mesh per metre (41 s.w.g. 100 mesh per inch) and a pressure drop coefficient of approximately 12. The Reynolds number based on the screen wire diameter is approximately 17 which is well below the value of 40 required as a condition for no eddy shedding from the wire [2.19]. All the screens are supported in wooden frames which slide into the settling section. The frames are secured in the settling section by wood screws. After the last wire mesh screen there is a settling length of 1 metre to allow any small scale turbulence to die down.

## 2.7 Inlet Contraction

The inlet contraction is made from two layers of 3 mm plywood mounted on a wooden frame. The shape of the two dimensional contraction was designed by the method due to Cheers [2.4] which gives a long low speed section suitable for settling and a short high speed section. The theoretically designed contraction has an infinite length so the

contraction dimensions were calculated using a larger inlet area and a smaller outlet area than required and truncating the contraction. This produced an inlet cross-section of 1.6 metres x 1.6 metres and an outlet cross-section of 400 mm x 400 mm with a contraction length of 2.3 metres. The co-ordinates of the contraction are given in Table A4.2. The large 16:1 contraction ratio reduces the turbulence in the settling section by a factor of 16 giving a turbulence intensity of less than 0.1% in the working section.

## 2.8 Sound Injection Box

The sound injection box was constructed from a dense 12 mm thick laminated wood in order to reduce the vibrations of the walls when high intensity sound is being introduced into the wind tunnel. The internal dimensions of the sound injector box are 400 mm x 400 mm x 400 mm and 350 mm diameter holes cut on the top and bottom panels of the box enable two exponential horns from the loudspeaker driver system to be connected to the box. The exponential horns are both 850 mm long giving a cut-off frequency of approximately 230 Hz. The large end of each horn is covered with a fine wire mesh screen which is mounted flush with the wall of the sound injection box, to reduce the flow disturbance through the box. The wire mesh was chosen to have a small flow resistance so that very little sound is absorbed or reflected back up the horns. The wire mesh was also chosen to be very fine to reduce boundary layer thickening. Brass wire mesh screens with wire diameters of 0.17 mm woven at 2362 mesh per metre (37 s.w.g. 60 mesh per inch) are used since they have a flow resistance of less than $9 Nsm^{-3}$ and give a sound transmission loss of less than 0.1 dB. Two 100 watt electrodynamic pressure driver loudspeaker units are connected to the small end of each exponential horn by means of a T piece adapter. When the wind tunnel is running the static pressure inside the sound injector box is less than atmospheric pressure. Each loudspeaker was therefore modified to produce static pressure equalisation between the front and back of the diaphragm. This was done so that the diaphragms were not operated in a non-linear regime, or damaged due to a static pressure differential across them. The pressure relief hole at the back of each loudspeaker was covered with an adapter connected via a piece of plastic tubing to a tube inserted near the large end of each exponential horn. The two loudspeakers at the end of each horn are connected in series and each pair of loudspeakers is driven by one channel of a two channel 300 watt audio amplifier. Each loudspeaker is approximately 10% to 15% efficient

when radiating into free space so that when the loudspeakers are driven at full power 40 to 60 acoustic watts are produced in the sound injector box. Approximately half of this power is radiated out through the inlet and half is transmitted into the working section. The maximum sound pressure level generated in the working section is therefore approximately 140 dB.

The bellmouth inlet, settling section, inlet contraction and sound injector box are all supported on a movable frame constructed from 25 mm steel angled sections. The frame, when in position, is supported on six antivibration mounts so that vibrations transmitted from the floor to the flow in the inlet sections are reduced.

## 2.9 Working Section

The working section has a cross-section of 400 mm x 400 mm and a length of 1.2 metres. It was designed to use a steel framework to which panels made from 12.7 mm bright mild steel plate could be bolted. This method is construction enables panels to be changed easily permitting the use of different panels with windows, pressure probes, hot wire anemometers, etc., depending on the investigation being carried out. During the investigation of the fluid tube coupling, it was desirable to eliminate the coupling of the tubes to each other, or to other parts of the wind tunnel structure via the working section. To effect this, several methods of reducing the transmission of vibrations to the working section were adopted.

(i) The working section was made very massive (approximately 400 kg) so that when mounted on four antivibration mounts, vibration transmitted from the supporting structure to the working section is isolated above 40 Hz. This ensures that vibration coupling between the wind tunnel structure and the dynamically modelled tubes is reduced.

(ii) The vibration produced in the injector box and variable sonic throat is also isolated by the antivibration mounts which provide effective isolation in all three mutually perpendicular directions.

(iii) The working section was isolated from the vibrations produced in the sound injection box by using a foam rubber seal to connect the two sections together.

(iv) Vibrations transmitted to the working section through the high speed contraction were reduced by manufacturing the high speed contraction from a low density material (fibre-glass) so that

there was an impedance mismatch between the working section and high speed contraction.

(v) The tube to tube coupling via the supporting structure was reduced at frequencies near the resonant frequencies of the tubes by mounting the tubes on two massive 12.7 mm thick steel plates which were bolted on opposite sides of the working section. The steel plates were drilled with holes in the appropriate places for mounting the tubes.

Plates 2.2 and 3.3 show the measures taken to reduce vibration coupling in the model tube bank.

Two different side plate sizes were constructed from 12.7 mm bright mild steel with internal dimensions 400 mm x 400 mm and 400 mm x 200 mm. Two side plates with 400 mm x 400 mm x 3 mm thick perspex windows were constructed so that the tubes could be visually monitored when mounted in the working section. The side plates which bolted on to the skeleton frame of the working section were all manufactured to high tolerance (0.1 mm) so that a tight fit was produced when all the side plates are mounted. When the working section side plates were mounted a sealing compound (hermetite) was used to produce an air tight seal between all the plates.

Throughout the investigation holes were drilled and tapped in the side plates to permit the insertion of different types of probes used to monitor flow and acoustic conditions in the working section.

## 2.10 High Speed Contraction

The high speed contraction contracts from the working section cross-section of 400 mm x 400 mm to the variable sonic throat cross-section of 240.5 mm x 152.4 mm. The contraction was designed by the method due to Cheers [2.4] and has a length of 800 mm. The co-ordinates of the high speed contraction are given in Table A4.3. The contraction was required to withstand a static pressure difference of approximately 59 kPa across the walls at the exit end without becoming significantly distorted. It was therefore constructed using fibre-glass reinforced by circumferential and longitudinal steel wires. The fibre-glass contraction was constructed on a mould made from 3 mm marine plywood (to give a smooth finish) mounted on a wooden batten frame. The fibre-glass was laid up until the contraction was 9 mm thick. Four sets of circumferential wooden reinforcing battens were spaced along the length of the contraction, and fibre-glass was laid over them to further strengthen the structure. A 140 mm long box section of

cross-section 240.5 mm x 152.4 mm constructed from 6 mm steel plate is used to connect the high speed contraction to the variable sonic throat.

## 2.11 Variable Sonic Throat

The variable sonic throat has an internal cross-section of 240.5 mm x 152.4 mm. Figure 2.3 shows the principle of operation of the throat. The outer box section was constructed from 12.7 mm steel plates and two pairs of 6 mm steel plates hinged together form the throat. The leading and trailing edges of the throat plates are attached to spigots which run in slots milled into the two vertical side plates of the box section. This arrangement prevents the aerodynamic forces acting on the plates from lifting their edges. The leading edges of the plates are attached to 1 mm thick spring steel plates which are mounted flush with the 6 mm throat plates and provide a metal-to-metal seal between the top and bottom box section plates. The edges of the throat plates have a rubber seal so that there are no gaps between the throat plates and the box section side plates. The width of the throat is varied by means of two 200 mm long threaded rods (connected to control knobs) which pass through opposite sides of the box section wall and attach on to the hinges which connect the throat plates together. When the rods are screwed in, both sets of steel plates are moved closer together, and the edges of the plates slide towards the centre of the box section. Mechanical counters which are driven by gears on the control knobs allow the throat area to be calculated for any setting of the throat. The maximum opening of the throat is 186 mm giving a maximum throat area of approximately 0.283 $m^2$.

The variable sonic throat allows the air velocity in the working section to be controlled very precisely and provides an almost anechoic termination at the throat where the air is travelling at the local speed of sound. A 100 mm long expansion section constructed from 12.7 mm steel plate was used to connect the 240.5 mm x 152.4 mm variable throat cross-section with the 247.6 mm x 152.4 mm injector box cross-section.

## 2.12 Injector Box

The injector box was designed for a wind tunnel constructed in 1960 in the Aeronautics department [2.1]. It consists of a rectangular pressure chamber (cross-section 247.6 mm x 152.4 mm) made of cast iron with four separate exit slots, one for each side of the injector box.

Compressed air is fed from the control valve to the injector box by means of a 75 mm diameter pipe which splits into four 37 mm pipes. Each of these pipes feed one corner of the injector pressure chamber. Air passes from the pressure chamber to the exit slots down convergent passages formed by a 'nozzle' and 'antinozzle' [2.10]. The slot width can be adjusted by varying the position of the adjustable 'antinozzle' which is set by changing a set of packing pieces in the pressure chamber. Air is injected into the wind tunnel through the slots in a direction parallel to the wind tunnel axis which was found to be the most efficient direction for entraining air upstream of the slots [2.10]. The velocity of the air immediately upstream of the injector box is always supersonic when sonic velocity is established at the variable throat. Experiments with a similar injector box [2.10,2.12] have shown that for a supersonic air velocity upstream of the injector box and a low injector box pressure the maximum tunnel running time is achieved when the slot to injector box area ratio is approximately 0.06. This gives an optimum slot width of approximately 2.8 mm which was set using appropriate packing pieces. The pressure chamber was designed to operate up to pressures of 2.5 MPa and was therefore sufficiently strong to operate using the 1.7 MPa compressed air supply.

## 2.13 Diffuser

The diffuser is rectangular in cross-section throughout its length and comprises two horizontal diverging sections and one vertical diverging section joined by two corner sections fitted with turning vanes. The diffuser is made from 22 mm wood block board and 16 mm plywood and has a divergence angle of less than 4 degrees throughout its length to maintain a high pressure recovery efficiency. The total length of the diffuser is approximately 5.6 metres and has an exit cross-section of 1049 mm x 457 mm giving an expansion ratio of approximately 13:1. The diffuser is sound proofed by using an outer blockboard wall with an inner plywood wall with a 75 mm sand filled cavity, separating them. The outer and inner walls are bolted together at intervals using cavity spacers with layers of felt in between to reduce transmission of vibration from the inner to the outer walls. This type of construction gives a sound attenuation of approximately 40 dB through the walls so that the transmission of sound generated in the sonic throat and injector box into the laboratory and back into the wind tunnel inlet, is reduced. The exit of the diffuser is outside the laboratory to prevent feedback of sound into the inlet.

## 2.14 Compressed Air System

The compressed air system in the ISVR comprises four electrically driven reciprocating compressors which in total supply compressed air to the storage tanks via a drier at a rate of 36.8 $m^3$ of free air per minute. There are three large cylindrical storage tanks which have a combined capacity of 85 $m^3$. The system is normally operated at a pressure of 1.7 MPa so the total time to pump up the system is approximately 2400 seconds (40 minutes) when no air is being drained from the system. The air supply from the compressors is dried to a specific humidity of $10^{-4}$ kg water/kg air before passing it to the storage tanks. The laboratory is supplied with dry air from the storage tanks via a 150 mm internal diameter pipe. The wind tunnel air supply is from a 75 mm pipe which passes through a gate valve before entering the automatic control valve. The output of the control valve is connected to the injector box system via a 75 mm pipe. A block diagram of the compressed air system and wind tunnel control mechanism is shown in Figure 2.4. The pneumatic servo mechanism which controls the 75 mm automatic control valve operates with a 272 kPa air supply derived from the 1.7 MPa air line using a pressure reducer. The control box supply pressure of 136 kPa is obtained from the servo supply using another pressure reducer. When the wind tunnel is switched on using the control box the desired input pressure to the injector box is set and the control box maintains this pressure by monitoring the main line pressure. When the line pressure drops the control box sends a pneumatic signal to the servo mechanism which opens the automatic control valve to maintain a constant pressure in the injector box. For the most efficient use of air the pressure in the injector box is set for the minimum required to maintain sonic velocity at the variable throat. Any increase in pressure to the injector box once sonic velocity at the throat is established wastes air, decreasing the total running time of the wind tunnel.

## 2.15 Theoretical Estimation of the Wind Tunnel Speed

The Mach number can be calculated by solving equation (2.1) iteratively [2.2]

$$\frac{A_w}{A_t} = \frac{1}{M_w}\left[\frac{2(1+((\gamma-1)/2)M_w^2)}{\gamma+1}\right]^{\frac{\gamma+1}{2(\gamma-1)}} \qquad (2.1)$$

Using equation (2.2) the velocity in the working section can be

calculated since

$$M_w = \frac{V_w}{C_a} \quad . \qquad (2.2)$$

The boundary layer displacement thickness in the working section can be approximated by equation (2.3) [2.17]

$$\delta = 4.62 \times 10^{-2} \ell Re_\ell^{-0.2} \quad . \qquad (2.3)$$

The maximum velocity in the working section was estimated by first assuming there was no boundary layer and solving equations (2.1) and (2.2) for the maximum variable throat area. The velocity obtained was then used to estimate the displacement thickness of the boundary layer in the working section using equation (2.3). The boundary layer thickness in the variable throat was assumed to be negligible since the flow is contracting towards the variable throat which produces a very thin boundary layer [2.14,2.17]. Using the modified working section area corrected for a 1.8 mm boundary layer thickness calculated from equation (2.3), assuming $\ell$ = 600 mm. The maximum velocity in the working section was calculated to be 35.7 $ms^{-1}$ using equations (2.1) and (2.2), assuming standard atmospheric conditions. When the atmospheric pressure changes the maximum pressure drop between the inlet and sonic throat changes. The maximum wind tunnel flow speed for a given throat area is therefore a function of atmospheric pressure. When the atmospheric temperature changes the speed of sound at the sonic throat changes so the maximum wind tunnel flow velocity is also a function of atmospheric temperature.

## 2.16 Wind Tunnel Calibration

Fifteen holes separated by 25 mm were drilled and tapped into one of the horizontal working section side plates so as to permit the insertion of the pitot static tube. When not being used the holes were blanked off by screwing in brass plugs. The flow velocities (at the maximum wind tunnel speed) in a plane of the working section approximately 600 mm downstream of the end of the contraction were measured at 25 mm intervals using a pitot static tube connected to a Betz manometer with a resolution of ±0.1 mm column height of water. The percentage velocity variations in the working section cross-section taking the centre of the cross-section as the reference velocity, were then calculated and are shown

plotted in Figure 2.5. It can be seen that, providing the pitot static tube is not too near the working section walls (where the measurements become very inaccurate due to boundary layer disturbance by the probe) the maximum variation in velocity is 0.5%. The velocity in the centre of the working section was 35.6 $ms^{-1}$ when the atmospheric pressure and temperature were 99.2 kPa and 294.2 K respectively. This result agrees with the theoretically predicted maximum working section flow velocity. The turbulent spectrum in the centre of the working section was then measured using a hot wire anemometer bridge and amplifier system. It was found that the longitudinal and transverse combined r.m.s. turbulence intensity was less than 0.3%. The spectrum of the turbulence intensity in the working section is shown in Figure 2.6.

The efficiency of the wind tunnel at full speed was measured as follows:

(i) The compressor system was allowed to reach its maximum working pressure of 1.7 MPa and the compressors were then switched off.

(ii) The variable sonic throat was fully opened.

(iii) The wind tunnel was then started setting the injector box pressure to the minimum required to produce choking at the variable throat and noting the time.

(iv) The dynamic pressure in the centre of the working section was then monitored using a pitot static tube and Betz manometer, checking that sonic velocity was maintained at the variable throat. When the pressure in the system had dropped to the minimum permitted working pressure of 680 kPa the time was noted.

The mass ratio efficiency of the tunnel is given by equation (2.4).

$$ME = \frac{100\ A\ V_w P_w t}{(P_s - P_e)\ C} \quad \% \qquad (2.4)$$

It was found that the run time was 660 seconds which gives a mass ratio efficiency of approximately 430% when the injector box pressure is a minimum of 200 kPa. When the compressors were operating the run time was increased to 900 seconds (15 minutes) which was sufficient to carry out the experiments in the investigation. The variation in the flow speed throughout a run was not detectable using the pitot static tube and an accurate Betz manometer. The flow speed was therefore constant to within 0.1%.

## 2.17 Conclusion

The preliminary project design investigations and the design of the wind tunnel was completed in 6 months and the construction of the wind tunnel was completed in 18 months: this latter period was much greater than planned, but was largely outside the control of the author. The wind tunnel performs to the original design specifications. A well defined flow speed constant to within 0.1% was achieved with a flow speed variation of less than 0.5% across the working section. The r.m.s. turbulence level was less than 0.3%. The wind tunnel run time was approximately 15 minutes but could be increased to over 20 minutes if the pressure in the compressed air system was permitted to drop to 350 kPa.

## 2.18 References


2.1 M.K. BULL 1963 University of Southampton Ph.D.Thesis. "Wall pressure fluctuations associated with subsonic turbulent boundary layer flow".

2.2 BUREAU OF ORDNANCE 1950 Naval Report 1488 (volume 2) "Handbook of Supersonic Aerodynamics", published by U.S. Government Printing Office.

2.3 D. BROWN and T.A. FALLOW 1966 Babcock and Wilcox (Operations) Report No. 1/66/280 811/306. "Effect of noise on heat exchanger pressure loss in a cross-flow heat exchanger".

2.4 F. CHEERS 1945 A.R.C. Report R&M 2137. "Note on wind tunnel contractions".

2.5 H.L. DRYDEN and I. ABBOT 1949 N.A.C.A. Report No. 940. "Design of low turbulence wind tunnels".

2.6 H.L. DRYDEN and G.B. SCHUBAUER 1947 Journal of Aeronautical Science, vol.14, 4 pp 221-228. "The use of damping screens for the reduction of wind tunnel turbulence".

2.7 W.J. DUNCAN 1953 "Physical Similarity and Dimensional Analysis". London: Edward Arnold.

2.8 ENGINEERING SCIENCES DATA 1974 Fluid mechanics, internal flow sub-series, volume 3, item number 74040. "Pressure loss during cross-flow of fluids with heat transfer over plain tube banks without baffles". London: Engineering Sciences Data Unit L.T.D..

2.9 J.A. FITZPATRICK and I.S. DONALSON 1980 J.S.V. 73(2) pp 225-237. "Row Depth Effects on Turbulence Spectra and Acoustic Vibrations in Tube Banks".

2.10 D.W. HOLDER 1946 A.R.C. monograph R & M. 2560. "The high speed laboratory of the Aerodynamics Division, N.P.L.".

2.11 M. JUDD 1960 University of Southampton Ph.D. Thesis."Some Aspects of Separated Flow".

2.12 A.E. KNOWLER and D.W. HOLDER 1948 A.R.C. Report R & M 2448. "The efficiency of high speed wind tunnels of the induction type".

2.13 J.G. KNUDSEN and D.L. KATZ 1958 "Fluid Dynamics and Heat Transfer". New York: Mc Graw-Hill.

2.14 L.D. LANDAU and E.M. LIFSHITZ 1959 "Fluid Mechanics". London: Pergamon Press.

2.15 H.L. LANGHAAR 1967 "Dimensional Analysis and Theory of Models". New York: Wiley and Sons.

2.16 W.F. LINDSEY and W.L. CHEW 1950 N.A.C.A. Report TN2189. "The development and performance of two small tunnels capable of intermittent operation at Mach numbers between 0.4 and 4.0".

2.17 B.S. MASSEY 1975 "Mechanics of Fluids". New York: Van Nostrand.

2.18 M.G. MORSY 1975 Proceedings of the Institute of Mechanical Engineers 189, pp 519-532. "Skin friction and form pressure loss in tube bank condensers".

2.19 R.C. PANKHURST and D.W. HOLDER 1952 "Wind Tunnel Technique". London: Pittman.

2.20 A. Y. POPE and J.J. HARPER 1966 "Low Speed Wind Tunnel Testing". London: Wiley.

2.21 O.G. TIETJENS 1957 "Fundamentals of Hydro and Aeromechanics". New York: Dover.

2.22 D.S. WEAVER and M.EL-KASHLAN 1981 J.S.V. 75(2), pp 265-273. "On the number of tube rows required to study cross-flow induced vibrations in tube banks".

2.23 J. ARMITT C.E.R.L. Leatherhead, England, June 1979 Personal Communication.

TABLE 2.1. Important variables affecting the flow and vibration in tube banks in the presence of intense acoustic fields.

| Symbol | Parameter | Dimensions |
|---|---|---|
| $u$ | velocity of gas | $LT^{-1}$ |
| $\rho$ | density of gas | $ML^{-3}$ |
| $\eta$ | dynamic viscosity of gas | $ML^{-1}\ T^{-1}$ |
| $d$ | diameter of tubes | $L$ |
| $D_L$ | geometric longitudinal spacing of tubes | $L$ |
| $D_T$ | geometric transverse spacing of tubes | $L$ |
| $m$ | mass per unit length of tubes | $ML^{-1}$ |
| $f$ | resonant frequency of tubes | $T^{-1}$ |
| $\zeta$ | damping ratio of tubes | Dimensionless |
| $x$ | displacement of tube | $L$ |
| $c$ | velocity of sound | $LT^{-1}$ |
| $s$ | sound pressure | $ML^{-1}\ T^{-2}$ |
| $\lambda$ | wavelength of sound | $L$ |

TABLE 2.2. Non-dimensional groups obtained by Buckingham analysis of the important parameters in Table 2.1.

| Non-dimensional group | Physical meaning and name |
|---|---|
| $\rho ud/\eta$ | inertia force/viscous force - Reynolds number |
| $D_L/d$ | longitudinal tube spacing/diameter of tube |
| $D_T/d$ | transverse tube spacing/diameter of tube |
| $m/\rho d^2$ | tube mass/effective mass of fluid displaced by tube |
| $fd/u$ | non-dimensional structural vibration frequency |
| $\zeta$ | damping ratio of tube |
| $x/d$ | non-dimensional tube displacement |
| $u/c$ | velocity of gas/velocity of sound in gas = Mach number |
| $s/\rho d^2$ | non-dimensional sound pressure |
| $d/\lambda$ | tube scale/sound wavelength scale |

TABLE 2.3. Important measured non-dimensional groups for a typical nuclear reactor heat exchanger

| Non-dimensional group | Magnitude |
|---|---|
| $\rho ud/\eta$ | $5 \times 10^4 - 1.5 \times 10^5$ |
| $m/\rho d^2$ | 80 - 180 |
| $D_L/d$ | 1.02 - 1.42 |
| $D_T/d$ | 1.02 - 1.42 |
| $fd/u$ | 0.12 - 0.5 |
| $\zeta$ | $1.5 \times 10^{-3} - 5 \times 10^{-3}$ |
| $x/d$ | $2 \times 10^{-3} - 4 \times 10^{-3}$ |
| $u/c$ | $< 0.12$ |
| $s/\rho u^2$ | $2.5 \times 10^{-2} - 2.5 \times 10^{-1}$ |
| $d/\lambda$ | $< 0.05$ |

Plan view

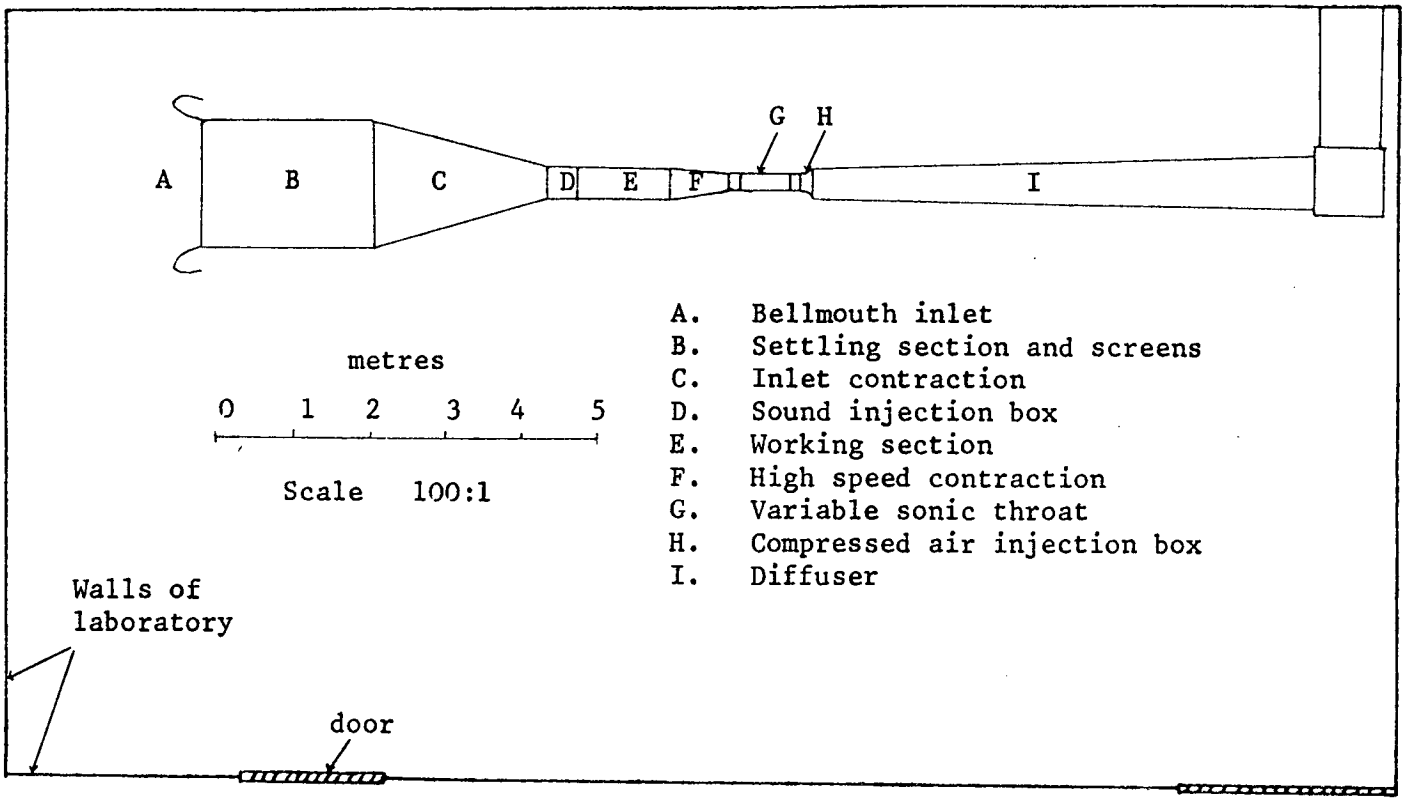


Side view

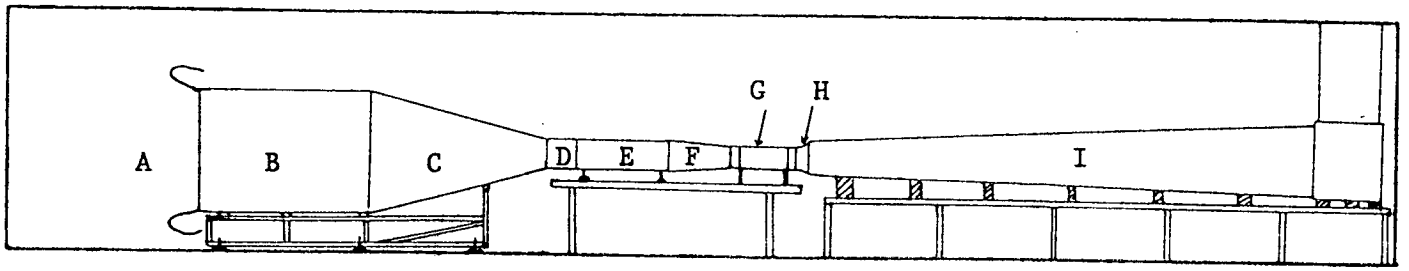


FIGURE 2.1. General assembly of wind tunnel.

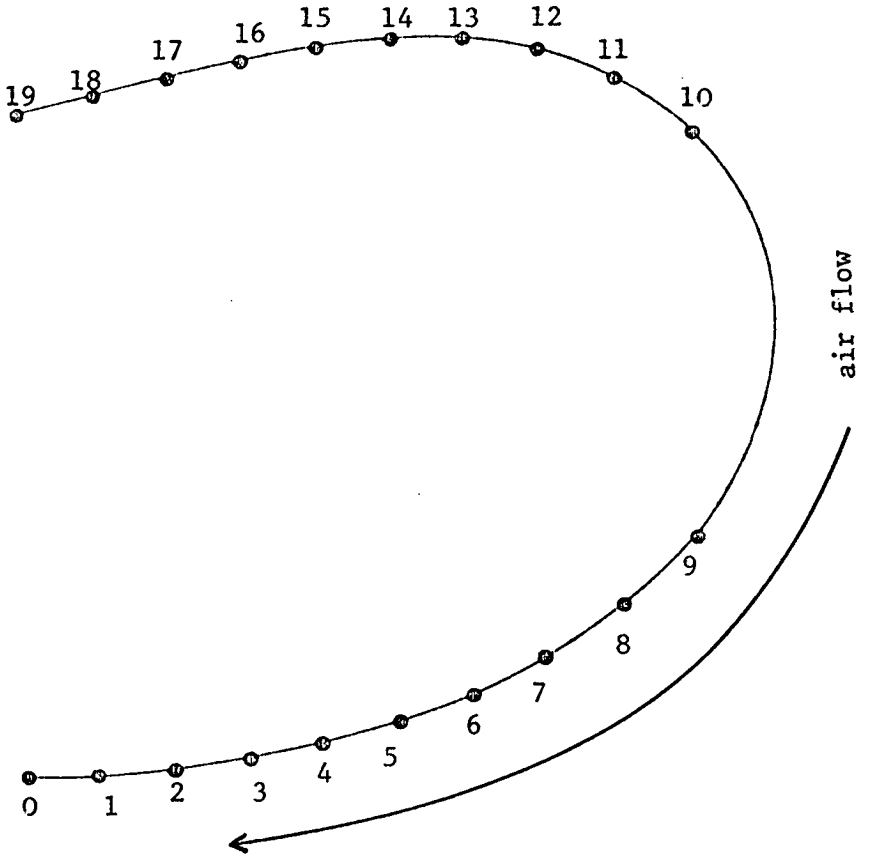


FIGURE 2.2. Shape of the bellmouth inlet sections (co-ordinates are given in Table A4.1.)

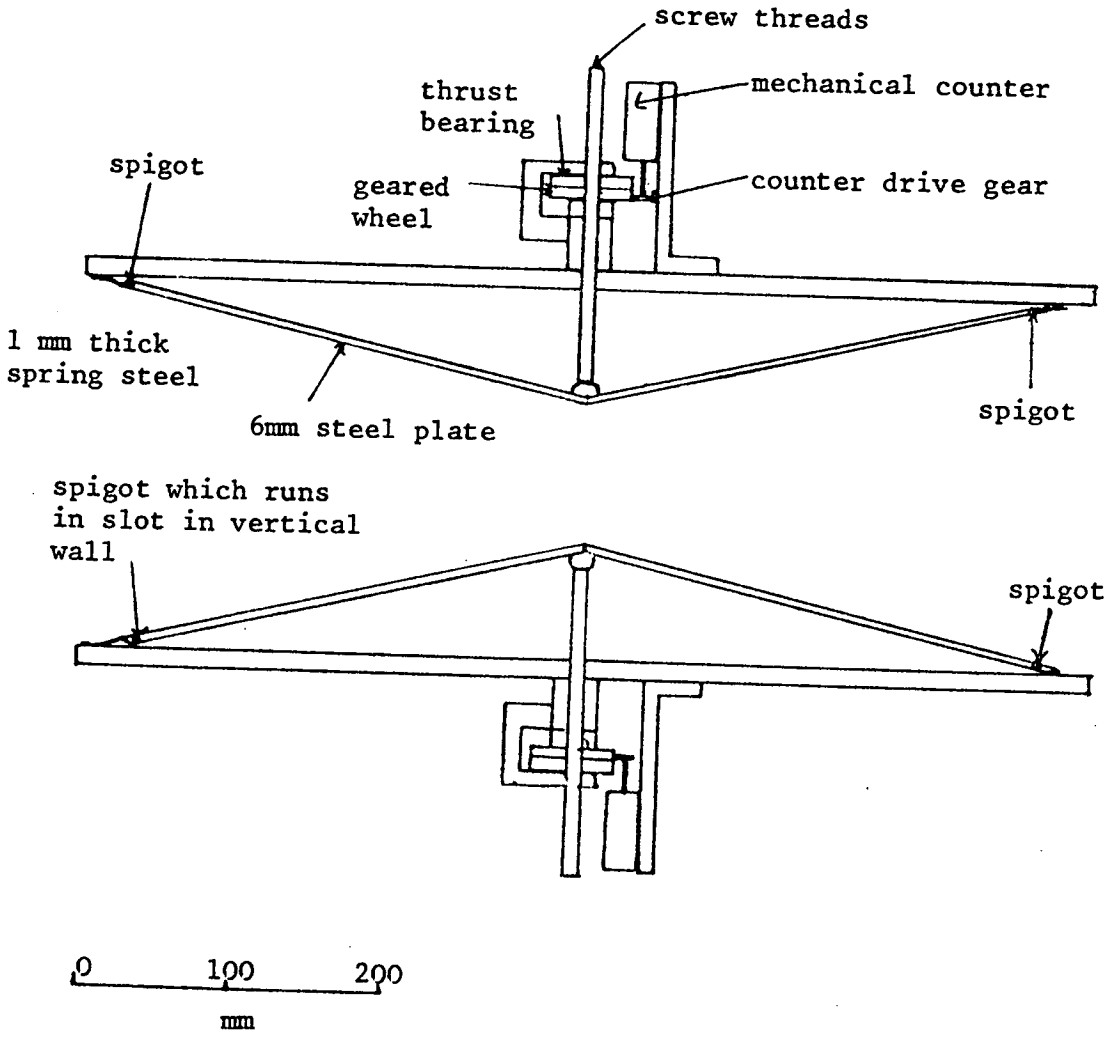


FIGURE 2.3. Side view of variable sonic throat showing principle of operation.

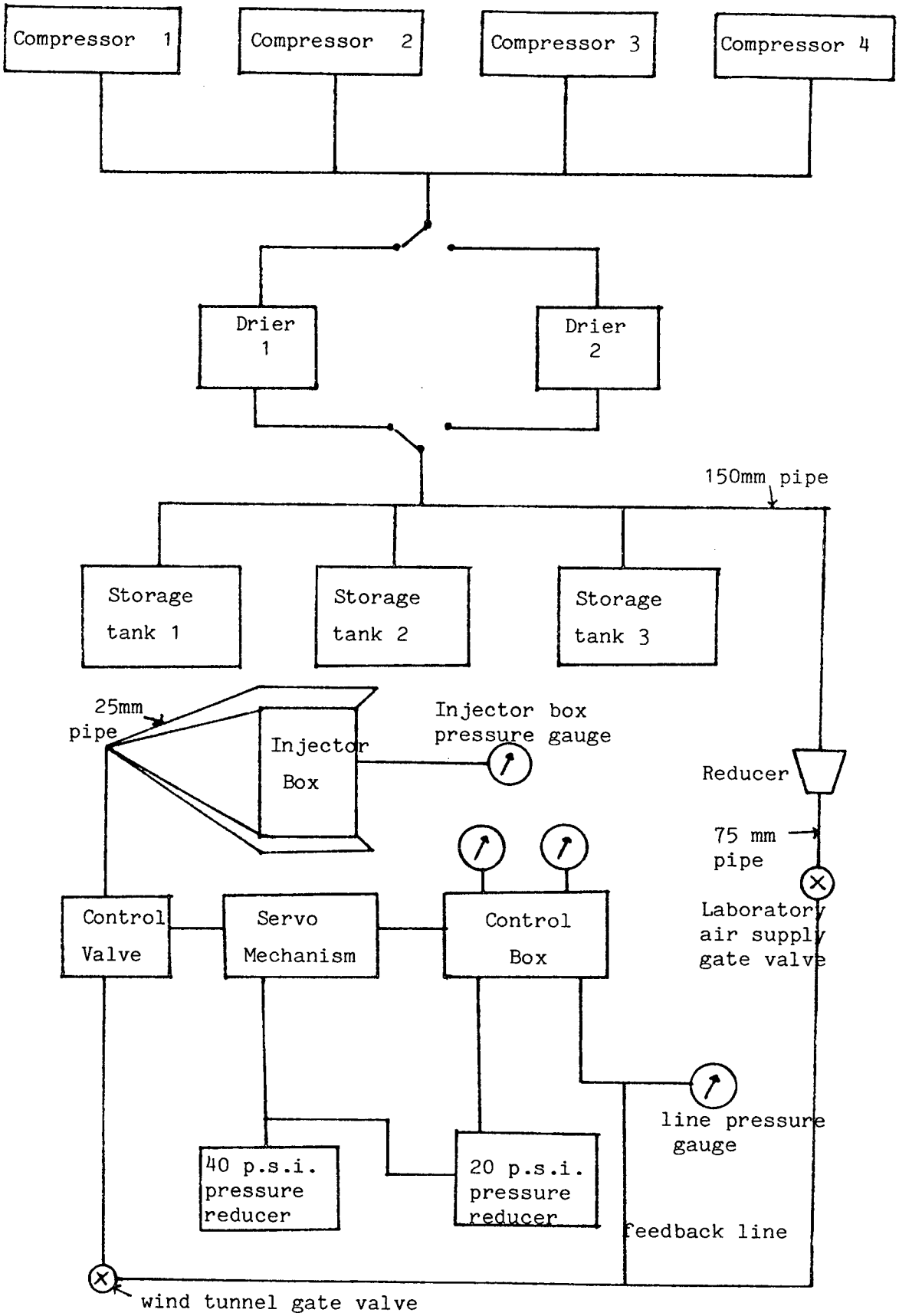


FIGURE 2.4. Block diagram of the compressed air supply system and the wind tunnel control mechanism.

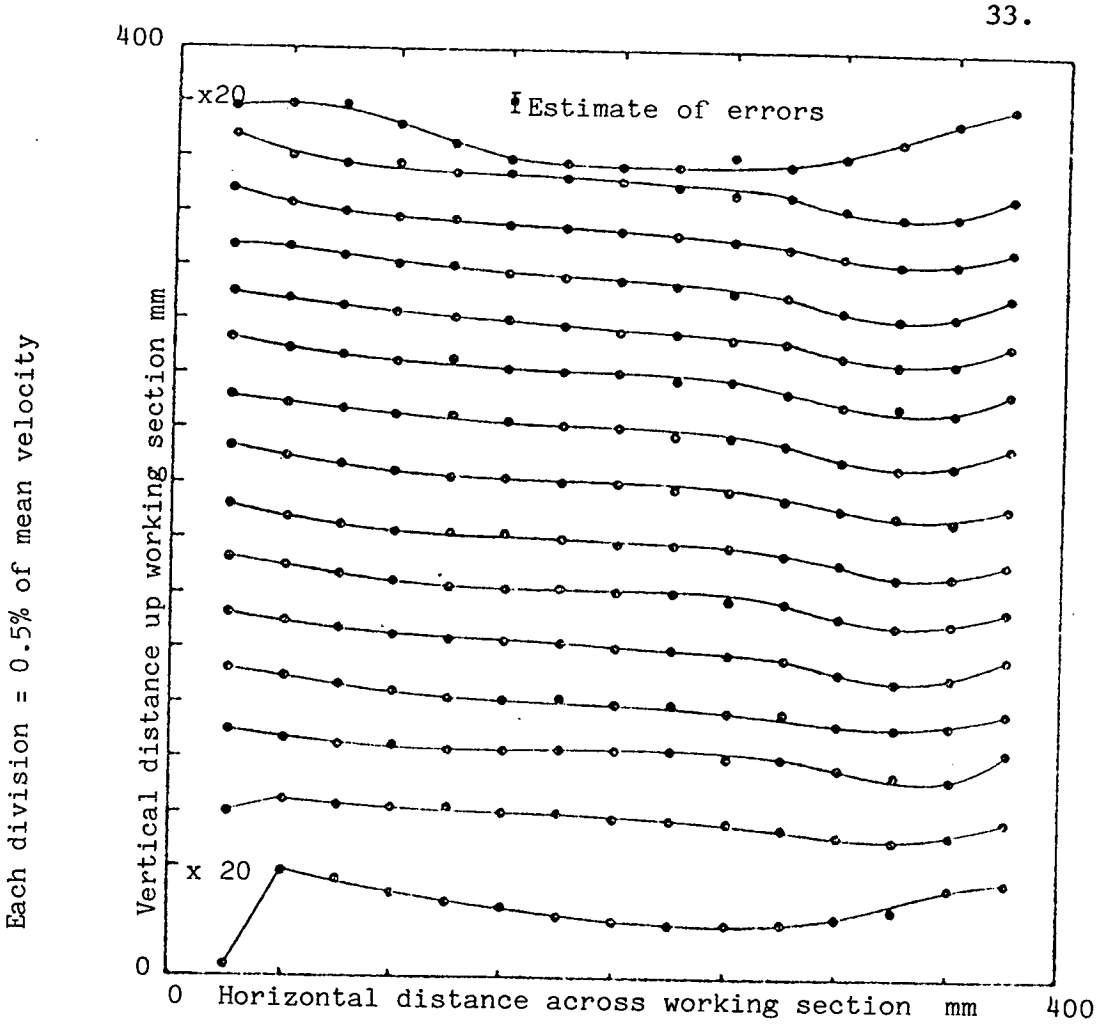


FIGURE 2.5. Percentage variation of flow velocity in the wind tunnel working section. (mean flow velocity = 35.3 $ms^{-1}$)

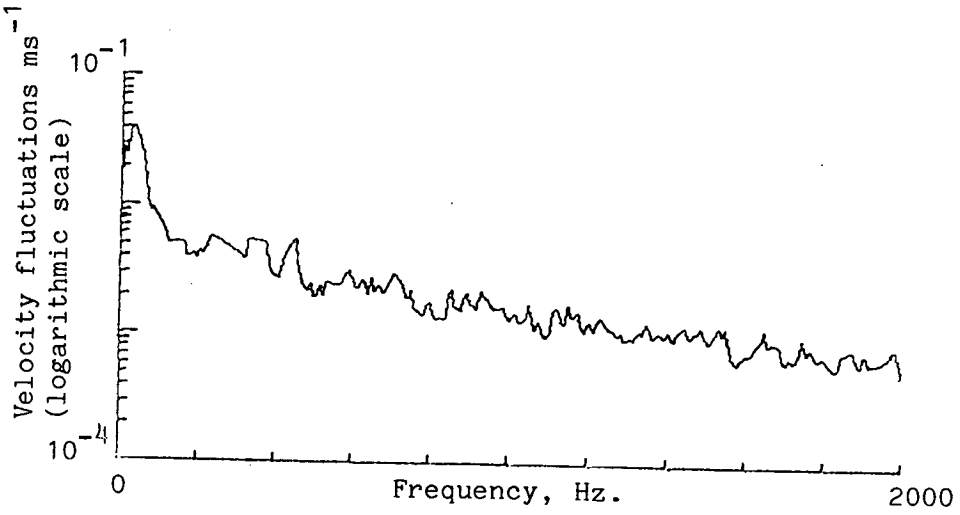


FIGURE 2.6. Turbulent velocity level in the centre of the working section. (mean flow velocity = 35.3 $ms^{-1}$)

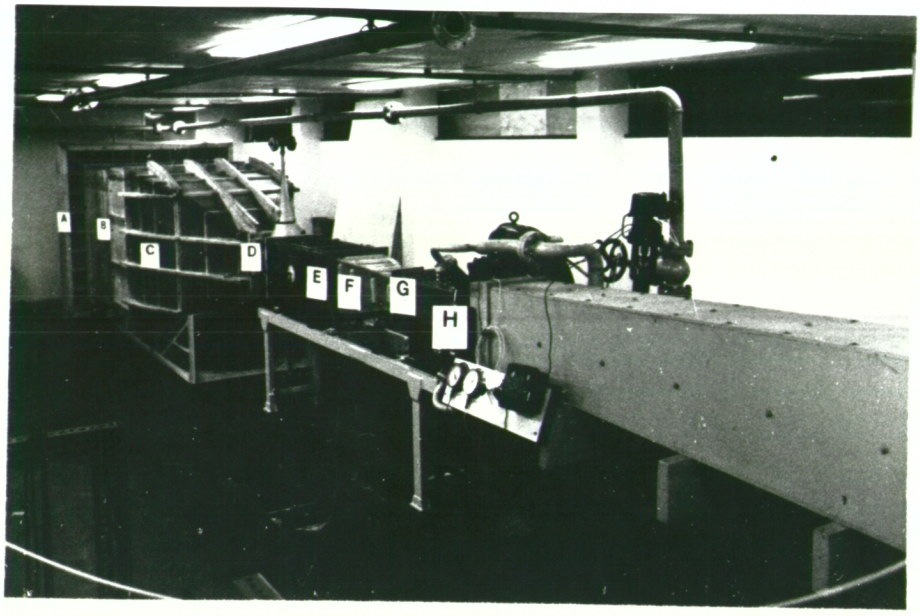


A. Bellmouth inlet.

B. Settling section and screens.

C. Inlet contraction.

D. Sound injection box.

E. Working section.

F. High speed contraction.

G. Variable sonic throat.

H. Compressed air injector box.

Plate 2.1 Overall View of the Wind Tunnel

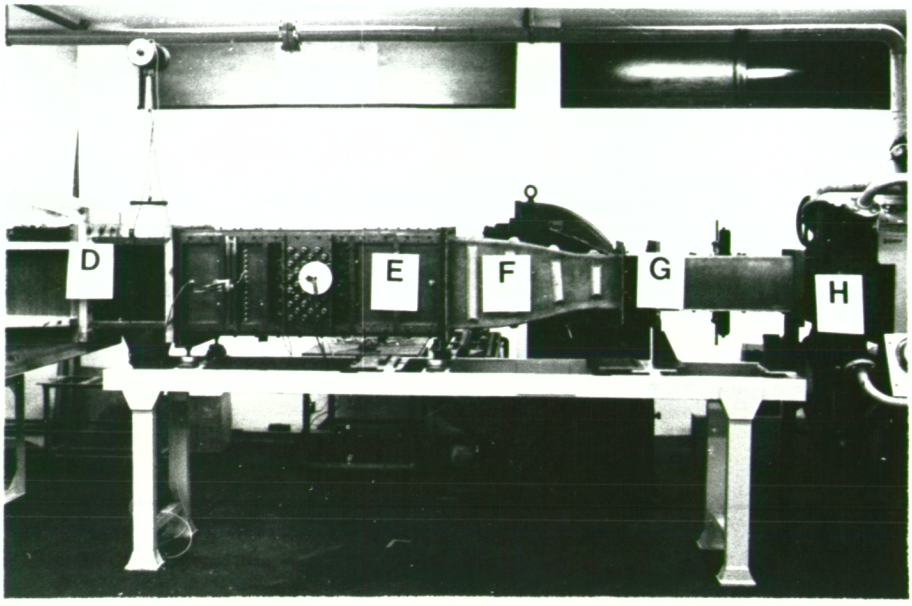


Plate 2.2 Side view of the wind tunnel high speed sections

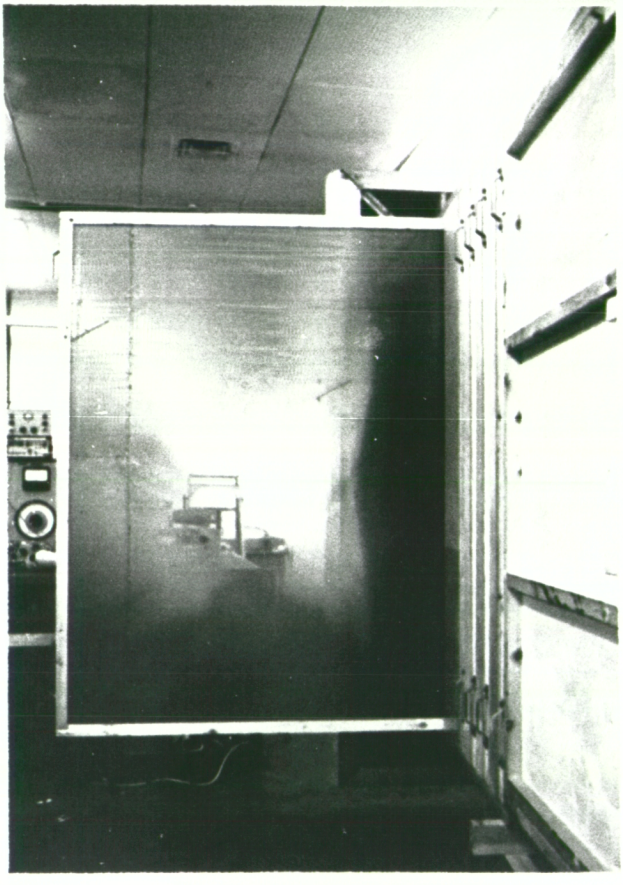

Plate 2.3 Screen mounting arrangements

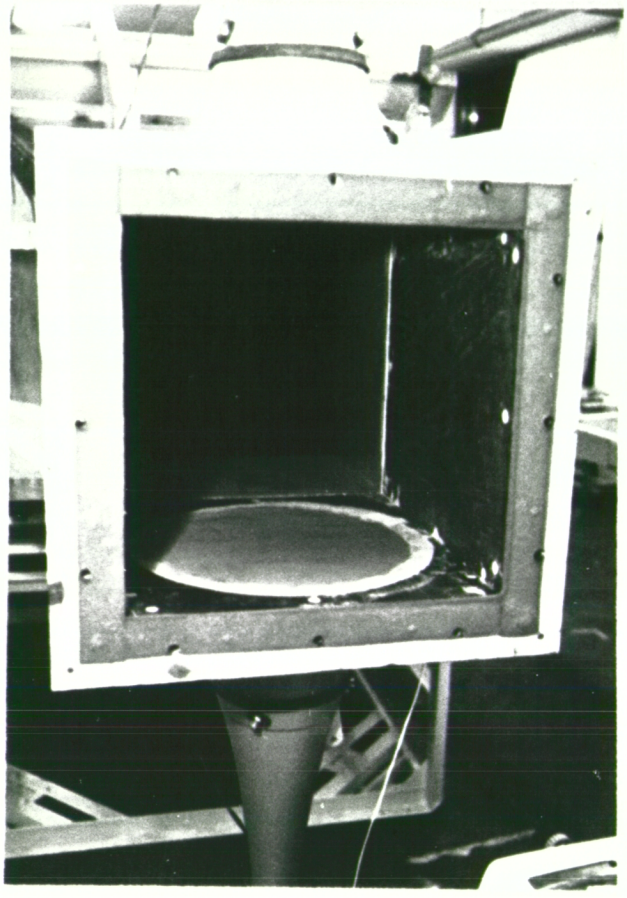

Plate 2.4 Inside view of the sound injection box

# CHAPTER 3

# THE MODEL TUBE BANK AND INSTRUMENTATION

## 3.1 Introduction

The experiments which were to be carried out on a single row of tubes, and on a flexible array of tubes, required several transducers and items of signal processing equipment which was not available within the ISVR. Some of the transducers, signal processing and control equipment was purchased but when the equipment was either unobtainable or too costly, it had to be designed and constructed in the ISVR.

This chapter describes the design, construction and calibration of the model tube bank, and the major items of equipment designed specifically for use in the investigation of fluid, tube and acoustic coupling in heat exchanger tube banks.

## 3.2 The Support Structure for the Flexibly Supported Tubes

The support structure for the flexibly supported tubes was constructed from two 455 mm x 228 mm x 12.7 mm mild steel plates which were bolted securely to the working section. The plates were further stiffened by bolting 20 mm x 25 mm x 455 mm pieces of steel to each 455 mm edge of the plates. The rods used to connect the tubes to the supporting structure on the working sections were required to be very rigid and massive so that the vibration of the supporting structure and rods was minimized. $\frac{3}{4}$ inch Bsp steel threaded rods of diameter 26.4 mm were used since they were cost effective and easily obtainable. Clearance holes for the $\frac{3}{4}$ inch Bsp rods were drilled to 0.2 mm tolerance in the steel supporting plates and the perspex windows so that the tubes would be aligned with their axes exactly at right angles to the flow direction. The array of holes was designed with transverse and longitudinal spacing ratios ($D_T/d$ and $D_L/d$ respectively) of 1.043 and 1.023 respectively. These ratios are the same as those of a full scale heat exchanger at present under consideration for construction, [3.15].

## 3.3 The Fixed Tubes

The fixed tubes were required to be very rigid so that any flow induced tube movement was negligible. The tubes were therefore made from 395 mm lengths of 30 mm outside diameter steel rod. A

hole approximately 25 mm deep was drilled and tapped with a $\frac{3}{4}$ inch Bsp thread down the axis at each end of the rod. The fixed tubes are fastened into holes drilled in the perspex windows by screwing the $\frac{3}{4}$ inch Bsp rod through the holes into the tubes and then screwing a $\frac{3}{4}$ inch Bsp nut on to the rod until a tight fit is achieved.

## 3.4 The Flexibly Supported Tubes

The design of the "flexibly supported tubes" (hence forward called flexible tubes) was governed by the non-dimensional parameters $(m/\rho d^2)$, $(fd/u)$ and $(\zeta)$ as explained in section 2.2. When the length of the tube is fixed by the dimensions of the working section cross-section the magnitudes of these three parameters specify the ranges of the tube resonant frequency, mass and damping. It has been observed that the major tube vibrations in some nuclear reactor heat exchangers are limited to a direction transverse to the flow [3.3]. It was decided to reduce the complexity of the investigation by using tubes which could only vibrate in a direction transverse to the flow and by keeping the various vibrational modes of the tubes well separated in frequency. It would have been preferable to investigate the effect of the flow and sound on just one vibrational mode of the tube structure. Constraining significant tube motion to just one vibrational mode is very difficult when the constraints imposed by the magnitudes of the non-dimensional groups are considered. The group $(m/\rho d^2)$ required the tube mass per unit length to be 87 $gm^{-1}$ to 196 $gm^{-1}$ which is a very low value. This can only be achieved with a low density material and a thin walled tube. The use of tubes constructed from carbon fibres was considered but the problems of manufacture and expense were too great. The thin walled tubes were therefore made from aluminium alloy tubing. The aluminium tube was treated as a rigid body and the correct vibration frequency of the tube, as governed by $(fd/u)$, was obtained by mounting the tube on pairs of carbon fibre flexures at each end of the tube. The frequency of the tube could be set to the desired value by varying the lengths of the flexures. At an average flow velocity in tube gap of 60 $ms^{-1}$ (assuming a free stream velocity of 33 $ms^{-1}$ flowing into a 10 row tube bank of 30 mm diameter tubes as described in sections 2.2 and 2.3) and a non-dimensional tube structural vibration frequency of 0.14, the tube resonant frequency is 260 Hz. The approximate frequency of the first bending mode of the thin walled aluminium was calculated using equation (3.1) (see [3.2]).

$$f = \frac{\lambda_i^2}{2\pi L^2} \left[\frac{E\,I}{m}\right]^{\frac{1}{2}} , \qquad (3.1)$$

where $\lambda_i = \pi$ for the first sliding-sliding or pinned-pinned mode shape. Substituting I and m for a thin walled cylinder into equation (3.1) gives equation (3.2) from which the resonant frequency of the first sliding-sliding mode of the aluminium cylinder can be calculated.

$$f = \frac{\pi}{4L^2} \left[\frac{E(a^2 + b^2)}{\rho_T}\right]^{\frac{1}{2}} , \qquad (3.2)$$

For the aluminium tube E=70.3 $GNm^{-2}$, a=15mm, b=14.66mm, $\rho_T$=2710$kgm^{-3}$ and L=300mm. Substituting these values into equation (3.2) gives a first bending mode frequency of 932 Hz. The first bending mode is therefore well separated from the rigid body mode of the tube and flexures (260 Hz). The rigid body frequency of the tube with flexures could not be calculated exactly since the end clamping conditions were not very well defined. A prototype tube was constructed and the flexure lengths were adjusted to produce the desired resonance frequency. The tube at its supports were clamped in a jig and an accelerometer was temporarily mounted on the outside of the prototype tube using bee's wax. The tube was released from a displaced position while acquiring the output from the accelerometer charge amplifier on the Data Analysis Centre (D.A.C.) computer. The damping ratio of the tube was determined to check that it was within the desired value of $1.5 \times 10^{-3}$ to $5 \times 10^{-3}$. It was found that the damping ratio was $2.2 \pm 0.1 \times 10^{-3}$ so it was unnecessary to modify the tube mounting arrangements to change the damping.

The flexible tube design was finalised and 33 flexible tubes were constructed as shown in Figure 3.1. The aluminium tubes were made from lengths of 31.75mm O.D., 1.22mm wall thickness aluminium tubes ($1\frac{1}{4}$ inch 18 s.w.g.) which were turned down in a lathe to produce a 30mm O.D., 0.34mm thickness tubes. The carbon fibre flexures were made from 1mm thick 60% volume fraction carbon fibre. The lengths of the carbon fibre flexures were adjusted to obtain a tube rigid body resonance frequency above 260 Hz. The tubes could then be individually tuned to approximately 260 Hz by sticking plasticine inside them. The tube flexures were covered over by cylindrical jackets (as shown in Plate 3.3), which were fastened to the flexure supports. The jackets prevent the air flow from interacting directly with the flexures. The jackets also prevent the tube from executing very large amplitude vibrations by acting as stops so that the flexures

hit the inside of the jackets if the vibration amplitude exceeds 3mm peak to peak. Two of the tubes were to be instrumented with accelerometers, so holes were drilled through the flexure supports to permit the accelerometer cable to pass through. The accelerometers (attached to their cables) were then guided down the inside of the tubes and glued in position with an epoxy resin glue. The sensitive axis of the accelerometers was fixed parallel to the flexure vibration axis, for each of the instrumented flexible tubes.

Each tube was mounted in a jig and a very small accelerometer temporarily attached to the outside of the tube. A small loudspeaker was suspended above the tube as in Plate 3.5 and excited with a 260 Hz sinewave. Plasticine was added to the tube until the tube vibration response was a maximum. Once the tube had been tuned the plasticine was taken off the tube and securely fixed inside the tube so that it would not come loose.

The instrumentation system that was used with the two instrumented flexible tubes consisted of a dual channel charge amplifier, high pass filter and double integrator, so that a signal proportional to the tube displacement could be obtained.

## 3.5 The Pressure Measuring Tube

Some of the experiments in the investigation involved the measurement of average and fluctuating pressure distributions round the circumference of a tube. A pressure measuring tube of diameter 30 mm and length 395 mm was constructed, as shown in the drawings in Figure 3.2. Correlation measurements along the axis of the tube were to be carried out so three separate fluctuating pressure tappings and transducers were required. Funds were limited so three relatively inexpensive electret microphones were used as fluctuating pressure transducers. The disadvantage of these devices over the more expensive small semiconductor strain gauge type pressure transducers is that the frequency response is not flat from 0 Hz to 2 kHz. The devices therefore have to be calibrated and have the disadvantage that the output starts to clip above fluctuation pressure levels of 2 kPa. (SPL level of 168 dB). An advantage is that the output of the electret microphones is not very sensitive to temperature changes whereas semiconductor strain gauge pressure transducers are very sensitive to small temperature changes and require constant recalibration. The microphones are mounted on a 0.4 mm I.D. hypodermic tube which

passes through the wall of the 30 mm diameter tube and is cut-off flush with the tube surface. The angular resolution of the pressure measuring tube is therefore approximately 1.5 degrees. Each electret microphone is mounted diametrically opposite a static pressure tapping, constructed from 0.4 mm I.D. hypodermic tube, mounted in an interchangeable 30 mm tube section. The tube sections,when assembled are held together by brass pins and steel dollies which are pushed inside the end of each section and fastened by grub screws which pass through the wall of the tube. 150 mm long 19 mm diameter steel drive rods were pushed into the ends of the tube and secured with grub screws. The drive rods each pass through a 40 mm long section of $\frac{3}{4}$ inch Bsp rod drilled with a clearance hole and fitted with lubricated brass sleeve bearings. One drive rod is connected to the stepping motor drive shaft by means of a notch and pin and is secured with grub screws. The other drive rod is connected to a protractor pointer mechanism which indicates the angle the tube has rotated through. A spirit level fastened to the protractor and a long silver steel rod screwed into a hole with its centre on the same line as the pressure tappings are used to set up the protractor system. The pointer is set so that it reads zero degrees when the average pressure tapping is pointing towards the flow parallel to the axis of the wind tunnel. The microphone wires and pressure tapping tubes run through the centre of the tube and pass through the drive rod connected to the protractor.

## 3.6 The Electret Microphone Power Supply

The electret microphones (Knowles Electronics Ltd, type EA1843) contain an internal F.E.T. amplifier stage which can be operated with a d.c. supply of 0.9 to 20 volts. In the normal mode of operation the biasing arrangements are such that the d.c. output level is approximately 1.0 volts. The maximum a.c. signal that can be output is therefore approximately 1.8 volts peak to peak, which corresponds to a maximum SPL of 140 dB. The dynamic range of the microphone was increased by changing the d.c. power supply system to bias the F.E.T. amplifier to that a d.c. output level of half the supply voltage was achieved. The circuit of the microphone power supply is given in Appendix 1. The modified biasing arrangement increases the maximum SPL output to 160 dB before clipping.

## 3.7 The Microphone Amplifiers and Power Supply

The microphones have an output impedance of 2kΩ to 6kΩ and therefore need a high input impedance, low output impedance amplifier. For most of the time the microphones were to be used in experiments where high output levels would be produced, so no amplification was required. However, for the purposes of microphone calibration an amplifier with a voltage gain of up to 60 dB was required. It was therefore decided to construct a general purpose four channel switchable gain amplifier. All four channels of the amplifier are identical. The circuit diagrams of one channel of the amplifier and the power supply are given in Appendix 1.

The amplifier consists of three a.c. coupled non-inverting operational amplifiers. Each amplifier has a maximum gain of 20 dB which gives the complete amplifier an upper 3 dB cut-off frequency of 100 kHz. The lower 3 dB cut-off frequency is approximately 3 Hz. The non-inverting inputs are biased to earth potential with 3.3 MΩ resistors which gives an input impedance of greater than 1 MΩ for each amplifier. Two of the amplifier stages have gains of 20 dB each and are switched in circuit when required. The third amplifier stage is always in circuit and has switchable 1,2,5,10 gain ranges with an optional continuously variable gain control which can be switched in when required. The gains of each stage were set up precisely by means of variable resistors in the amplifier feedback circuit. Once the variable resistors were adjusted they were not altered except for a complete recalibration of the amplifier. The amplifier power supply is a general purpose ±15 volts 1 amp dual rail d.c. regulated power supply.

## 3.8 The r.m.s. - to - d.c. Converter

Preliminary investigations of the measurement of the r.m.s. pressure distribution round the circumference of a tube showed that there was a considerable low frequency variation in the value obtained. This variation could not be averaged out and displayed as a d.c. voltage using any of the equipment currently available in the ISVR. An r.m.s -to- d.c. converter, with a variable averaging time, was therefore constructed. The circuit diagram is shown in Appendix 1. The active part of the circuit is the AD536A true r.m.s. -to- d.c. converter integrated circuit whose time constant is controlled by switchable capacitors. Two LM741 operational amplifiers provide

additional gain and buffering so that the system can be easily calibrated. The r.m.s. -to- d.c. converter has a conversion accuracy of 0.1% for signals of frequency above the switchable ranges of 0.2 Hz to 4 Hz. The ±15 volt power supply was supplied from the general purpose microphone amplifier power supply. Details of the operation and calibration of the r.m.s. to d.c. converter are given in [3.11].

## 3.9 Calibration of the Pressure Measuring Tube Microphones

The pressure measuring tube microphones were calibrated in the anechoic chamber in the ISVR. The tube was held in a clamp so that the port of the microphone to be calibrated was pointing along the axis of a 305 mm diameter loudspeaker which was positioned 5 metres from the tube. The tube was then moved slightly to reposition the microphone port 15 mm off the loudspeaker axis in a horizontal plane. The diaphragm of a clibrated $\frac{1}{4}$ inch B & K free-field microphone type 4135 was then positioned 15 mm of the axis of the loudspeaker in the same horizontal plane as the electret microphone port. The apparatus was then connected as shown in Figure 3.3. The loudspeaker was excited with white noise while acquiring the amplified signals from the pressure measuring tube electret microphone and the $\frac{1}{4}$ inch B & K microphone on two analogue channels of the D.A.C. computer. The sample rate was 8 kHz and 30,000 samples of each signal were taken so that a statistically reliable estimate of the power spectra of the signals could be calculated. This procedure was repeated for each of the three electret microphones in the pressure measuring tube. Details of the calibration calculations are given in Appendix 3, and the calibration curves for the microphones are shown in Figures 3.4a, 3.4b and 3.4c.

## 3.10 Description and Calibration of the Pressure Transducer

The pressure transducer was to be used for measuring the distribution of time averaged pressure round the circumference of a tube. The pressures were to be measured relative to atmosphere. In the various experiments, full scale pressure readings would vary from approximately 2940 Pa to 9810 Pa (i.e. 300 mm to 1000 mm column height of water). A differential pressure transducer with a linearity

and hysteresis of better than 1% for a full scale reading of approximately 3kPa was therefore required. Pressure transducers which were designed to operate at full scale pressures of 3kPa were very expensive, but transducers designed to operate with full scale pressures of 100 kPa were relatively inexpensive. However, the linearity of these transducers was typically quoted as ±0.25% of full scale with a hysteresis of less than 0.1% of full scale. If the transducers were operated with a 3 kPa full scale the linearity would therefore be ±8.3% which is not sufficiently accurate to carry out the investigations. It was decided that the pressure transducer would be calibrated so that deviations from linearity would not matter. A strain gauge pressure transducer type P102 fitted with a differential reference tube was purchased from Maywood Instruments Ltd. Full details of the specifications of the transducer are given in Table 3.1.

The pressure transducer was calibrated using the arrangement shown in Figure 3.5. The gain of the strain gauge amplifier described in section 3.11 was set to 20 dB. Air was evacuated from the pressure transducer by sucking on the mouthpiece and tightening the clamp when the desired pressure, as registered on the manometer, was reached. The reading on the digital voltmeter was then taken. Initially the output of the strain gauge amplifier and the Betz manometer were zeroed for zero pressure differential across the pressure transducer. Strain gauge amplifier voltage outputs were then taken at 16 evenly spaced pressure readings between 0 Pa and 2.943 kPa (i.e. 0 mm and 300 mm column height of water). When the highest reading was reached the air was allowed to enter the pressure transducer and readings were taken at the same pressure intervals for increasing and decreasing pressures. The linearity and hysteresis as a percentage of the 2.943 kPa full scale reading were then calculated and are shown plotted against pressure in Figure 3.6. It was found that the linearity was better than ±0.5% of full scale and hysteresis better than 0.4% of full scale. These values were within the desired accuracy for the experiments, so it was only necessary to calibrate the pressure transducer system at the zero, and full scale pressure values desired for the experiment. All readings were then assumed to lie on a straight line passing between the full scale and zero values. When a full scale reading of approximately 3 kPa was used thermal sensitivity shift was less than ±0.7% of full scale per Kelvin. The temperature of the pressure transducer was therefore required to be kept nearly constant if drift due to temperature change was to be kept below 0.5%. This was

achieved by clamping the pressure transducer to the drive rod which directly couples to the main structure of the working section. The working section has a large thermal capacity so temperature changes during the course of the experiment were minimised. In practice, before any experiments were carried out, the wind tunnel was run for 15 minutes so that the working section reached its working temperature, before any measurements were taken. In order to check that these measures were effective in reducing thermal drift in the pressure transducer, the wind tunnel was run for 15 minutes with zero pressure differential across the pressure transducer and the output of the pressure transducer strain gauge amplifier was recorded at 30 second intervals. A graph of percentage drift compared to the full scale value of approximately 3 kPa was then plotted against time and is shown in Figure 3.7. It can be seen from the graph that thermal drift effects were less than 0.2% of full scale over a 15 minute period on the most sensitive measurement. The drift due to thermal effects was therefore acceptable in the experiments for the measurement of pressure distributions round the tubes in a tube bank.

## 3.11 The Pressure Transducer Strain Gauge Amplifier

The strain gauge amplifier was required to amplify a 1.741 mV full scale signal (corresponding to 3 kPa) to produce a 5 volt output signal. The resolution must be 1 part in 256 so noise and drift levels must therefore be less than 3 μV. A high gain low noise and low drift strain gauge amplifier system was therefore required. An encapsulated strain gauge amplifier module type SGA100 was purchased. The details of its specifications and operation are given in [3.10]. The circuit diagram of the strain gauge amplifier system is given in Appendix 1. The noise in the amplifier was reduced by the use of low noise metal film resistors throughout the circuit and by de-coupling the power supply rails. Noise was further reduced by reducing the amplifier bandwidth by the addition of $C_1$ and $C_2$. Noise pickup from the input and output leads was reduced by the use of $R_6, C_5$ and $R_5$, $C_2$ respectively. Power supply interference and drift were reduced by using a ±12 volt stabilised power supply with a noise voltage of less than 1 mV and stabilisation better than 0.5%. The circuit diagram of the power supply is given in Appendix 1. The use of fixed metal film resistor and cermet trimmer resistors reduces drift due to

temperature changes. The temperature of the amplifier was always allowed to stabilise by switching it on at least half an hour before any measurements were taken.

## 3.12 The Hot Wire Probe and Traversing Mechanism

A hot wire anemometer probe to measure fluctuating velocities in the wind tunnel working section was required. It was constructed from a 915 mm length of 8 mm stainless steel tubing which was bent at right angles 55 mm from the end. A microdot connector was fastened in the end of the short section after the bend so that 15 mm length 5 mm O.D. hot wire probes could be plugged in. A wire was connected to the microdot socket and passed down the inside of the probe tube and terminated in a B.N.C. plug. Several 15 mm long hot wire probes were constructed so that when hot wires were damaged they could easily be replaced. Plate 3.6 shows the hot wire probe and details of the construction, calibration and operation of the hote wire equipment are given in [3.4,3.5].

A traversing mechanism was also designed and constructed for use with the hot wire and pitot static probes. A scale marked on a steel bar enables the position of the probe in the working section to be determined with am accuracy of ±1 mm. The traversing mechanism and hot wire probe are shown in Plate 3.6.

## 3.13 Measurement of the Pressure Distribution Round a Tube

During the investigation, the pressure distribution round the circumference of a tube had to be measured many times. The wind tunnel had a limited run time and the storage tank pump up time between runs is approximately 40 minutes. If measurements of pressure were to be carried out manually at 5 degree intervals round the tube circumference several runs of the wind tunnel would be required. It would also be necessary for more than one person to operate the wind tunnel and to carry out the experiments. It was therefore necessary to design the experiment which measures pressure distribution round a tube to be controlled and carried out automatically. The description of the design of a general purpose system for carrying out experiments automatically is given in Section 3.14.

## 3.14 Design of an Automatic Data Acquisition and Control System

A general purpose flexible system for acquiring data and controlling experiments was required so that if the experiment was changed it could be carried out with the minimum change in hardware. The most cost effective and flexible system for achieving this was a microprocessor system with appropriately designed peripherals and software. A microprocessor system offers the following advantages over a complicated hard-wired system.

(i) When a different experiment is to be carried out, it is necessary to change only the software provided the necessary control peripherals for the experiment remain the same; this gives a very high degree of flexibility.

(ii) The microprocessor system can be used to process the raw data to produce and display results almost immediately after the experiment has been carried out. This is very useful since a check on the validity of the results can be carried out immediately after the experiment.

(iii) A general purpose microprocessor system is less expensive than a complicated hard-wired system.

A 'Nascom 2' microprocessor system was available so the experimental control and data acquisition peripherals were designed to be interfaced to this system.

## 3.15 Specifications of the Nascom 2 Microprocessor System

The detailed specifications for the Nascom 2 microprocessor system are given in [3.6]. A summary of the main features of the system are given below.

(i) C.P.U. Zilog 4 MHz Z80 8 bit microprocessor

(ii) Memory

(a) R.O.M.

2 k bytes system monitor
8 k bytes 'microsoft' BASIC
(2 k bytes of character generator)
(2 k bytes of graphics generator)

(b) R.A.M.

1 k bytes (Static) Monitor Scratchpad
1 k bytes (Static) Video Display
48 k bytes (Dynamic) Main User Memory

(iii) Video Display — 48 character x 16 lines upper and lower case

(iv) Keyboard — Scanning 'typewriter' type keyboard

(v) Non volatile storage
- (a) 110-2400 baud F.S.K. cassette interface
- (b) Teletype output with RS232 and current loop interface.

(vi) Interface ports — 2 8 bit I/O ports.

## 3.16 Measurement Procedure

The control and measurements carried out during the experiments govern the interface design. A detailed specification of the steps carried out during the experiment is as follows:-

(i) The time-averaged pressure and r.m.s. fluctuating pressure are measured using the calibrated pressure transducer and electret microphone respectively.

(ii) The data is input into the microprocessor system and stored in the memory.

(iii) The measuring tube is rotated through a preset angle and the measurement procedure repeated until measurements have been taken round the circumference of the tube.

(iv) The input data is displayed on an oscilloscope for a 'quick check'.

(v) Further parameters measured manually in the experiment are input using the microprocessor system keyboard.

(vi) The data is formatted in memory ready to be processed and output.

(vii) The results are calculated from the raw data and output on a teletype.

(viii) The formatted data is output to paper tape so that it can be transferred to the main frame computer for processing and plotting.

(ix) A provision for inputing data from paper tape is required so that previously acquired data can be viewed on the oscilloscope and the results printed.

## 3.17 Interface Requirements

Several different interfaces listed below, were required to carry out the experiment detailed in section 3.16.

(i) An interface to drive and control the measuring tube.

(ii) An analogue-to-digital converter and sampling circuit to digitize measurements and input them into the microprocessor system.

(iii) An analogue multiplexer to permit the acquisition of data from more than one channel.

(iv) A digital-to-analogue converter to output data sequentially on to an oscilloscope to produce a display of the acquired data.

(v) A paper tape punch interface and driver to enable the formatted data to be output.

(vi) A paper tape reader interface and driver to permit data to be read into the microprocessor system.

## 3.18 Measuring Tube Drive and Control Interface

The measuring tube was driven by a motor and clutch mechanism, constructed from a surplus paper tape punch. When the tube is to be rotated the motor is switched on and the clutch is released by means of a solenoid. The drive shaft starts to rotate and the solenoid is then switched off so that the clutch disengages the drive mechanism. When it has rotated through exactly one revolution, the main drive shaft from the clutch drives a set of reduction gears and a reduction gear box which gives a reduction ratio of 360:1. This permits the tube to be rotated through one degree every time the clutch is engaged by the solenoid. The direction of the motor can be reversed using a relay to enable the tube to be rotated both clockwise and anticlockwise. The motor is a reversible d.c. motor and is driven from a variable voltage d.c. power supply. The voltage required to drive the motor is governed by the speed at which the solenoids operate and the loading on the final drive shaft. The circuit diagram of the motor power supply is given in Appendix 1. A block diagram of the motor control interface is given in Figure 3.8. The relays which switch the motor on and reverse its direction are driven by darlington transistors controlled from two bistables. The bistables are toggled from two output lines of a 4 to 16 line demultiplexer which is driven from the 4 most significant bits of P.I.O. port B, on the Nascom microprocessor board. The clutch solenoid is controlled using a similar method except that the darlington transistor is driven directly from an output line of the demultiplexer. By use of the appropriate software which sends different output words to P.I.O. port B to activate demultiplexer lines

4,5 and 14, the rotation of the measuring tube can be controlled.

## 3.19 Analogue-to-Digital Converter and Sampling Circuit

The block diagram of the analogue-to-digital converter (a.d.c.) and sampling circuit is given in Figure 3.9. The circuit was designed to be a general purpose data acquisition interface which would operate at the maximum possible sampling rate.

The Least Significant Bit +1 (L.S.B.+1) of P.I.O. port B starts the conversion cycle when its level goes to logic '0'.
Clock signals derived from a divider (driven from the microprocessor 4 MHz clock) are used to drive a programmable counter. The cycle time of the free running multiple sampling circuit is set up on eight binary switches which programme the number at which the programmable counter starts counting down from. Each time the counter reaches zero a new sampling cycle is initiated. The circuit can be operated in two modes. The first mode is where the L.S.B.+1 of P.I.O. port B is switched to '0' and a single sample taken, digitized and the result held in the P.I.O. latch. The result can then be input via P.I.O. port A at any time after the sample sequence has ended. The second mode of operation is where the sample sequence, once initiated by toggling L.S.B.+1 of P.I.O. port B from '1' to '0' and back to '1', continues taking samples and latching the result each time the programmable counter counts down to zero. In this mode the software loop which reads in the data via the P.I.O. port A has to be synchronized with the cycle time of the programmable counter. This mode of operation gives a higher sampling rate and can operate at up to 80000 samples per second. The sample timing circuit derives the timing pulses to control the sample and hold circuit and the a.d.c. The a.d.c. was designed from standard combinational and sequential logic circuits. The circuit is controlled by the sample timing circuit which produces the following switching pulses.

(i) On initiation of the sample sequence the sample and hold circuit is switched from the sample mode to the hold mode.

(ii) 1.25 µs after the hold mode has started and the output of the sample and hold circuit has settled a 625 ns negative start conversion pulse coincident with a negative clock pulse is produced which is used to start the conversion of the analogue to digital converter.

(iii) When an end of conversion pulse is produced by the a.d.c. the sample and hold circuit is switched to the sample mode so that its output follows the analogue input signal.

(iv) When L.S.B.+1 of P.I.O. port B is at logic '0' the sample timing circuit is inhibited after one operation so that only one sample is taken, digitized and latched on to the input of P.I.O. port A.

The analogue input signal is fed through a level shifter so that the system can be adjusted to give a zero result for any d.c. input voltage between ±12 volts. The sample and hold circuit was designed using an LF 398H sample and hold I.C. The hold capacitor was chosen to be 100 pF to give an acquisition time of approximately 9 μs. The hold step is reduced as explained in [3.9]. The output from the LF398H is input into a ZN427E bipolar successive approximation A-to-D converter I.C. The details of its operation are given in [3.12]. The full scale range and zero level of the a.d.c. can be adjusted but for normal operation are set to 5 volts and 0 volts respectively. A tristate latch connected to the digital outputs of the ZN427E permits data to be read into the P.I.O. port A whilst a conversion is being carried out in the a.d.c.

In the experiment to measure the pressure distribution round a tube the a.d.c. and sampling circuit is used in its single sample mode of operation.

## 3.20 Analogue Multiplexer

The analogue multiplexer uses a DG508 C.M.O.S. analogue switch I.C. The block diagram of the multiplexer and drive circuits is given in Figure 3.10. The three data select lines are driven from the outputs of three J.K. bistables. The bistables are connected so that they 'toggle' and the clocks are driven from the outputs of lines 6,7 and 8 of the 4 to 16 line demultiplexer connected to the 4 M.S.B. of P.I.O. port B. A maximum of eight channels can be used and channel selection is achieved by addressing the data select lines.

## 3.21 Digital-to-Analogue Converter

The block diagram of the digital-to-analogue converter (d.a.c.) interface is given in Figure 3.11. The digital data on P.I.O. port A is latched on to the input of the D to A converter I.C. (type DAC800)

when the L.S.B. of P.I.O. port B changes from logic '1' to '0'. The d.a.c. uses a 5 volt Zener diode as a voltage reference and produces a 5 volt output for a full scale input word. An inverting operational amplifier buffers the d.a.c. and permits the full scale output voltage to be adjusted.

During the experiments the output of the d.a.c. is connected to the Y input of an oscilloscope. A signal from output 12 of the 4 to 16 line demultiplexer is connected to the trigger input of the oscilloscope. An appropriate time base is selected and the software drives the circuits to transfer stored data in the microprocessor system memory to the d.a.c. so that a display of the stored data is obtained on the oscilloscope screen.

## 3.22 Paper Tape Punch Interface

The block diagram of the paper tape punch interface is given in Figure 3.12. The 8 bit character to be punched is set up on P.I.O. port A. The output of the bistable connected to line 2 of the 4 to 16 line demultiplexer enables a buffer which drives the 8 darlington transistors connected to the 8 punch solenoids. A darlington transistor connected to the guide hole punch solenoid is driven by the punch enable line. The paper tape punch motor is switched on by control line 3 which drives a J.K. bistable, darlington transistor and a relay. The punch clutch (which when released punches the character) is enabled by control line 11 which drives a darlington transistor connected to the clutch release solenoid. The timing and operation of the solenoids is controlled by a software routine which outputs the appropriate bytes to P.I.O. ports A and B to ensure the correct mechanical operation of the punch.

## 3.23 Paper Tape Reader Interface

The block diagram of the paper tape reader interface is given in Figure 3.13. The output from line 1 of the 4 to 16 line demultiplexer switches a bistable which enables a buffer.
The buffer transmits data from the paper tape hole sensing wires to P.I.O. port A. Line 10 is the input to a darlington transistor which drives the tape advance solenoid to move the tape forward ready for reading the next character. Software controls the timing of the paper tape reader advance solenoid and the reading of data from

## 3.24 Acquisition and Control System Software

The major part of the microprocessor system software was written in BASIC. The operations which were required to run very quickly were written in Z80 neumonic assembler language and assembled using a general purpose Z80 assembler programme to obtain the machine code routines. The machine code routines were all accessed from BASIC, by using a user machine code subroutine call (U.S.R.). The machine code routines were stored in memory by inputting the decimal machine code numbers from DATA statements in the BASIC programme. This method of storing the machine code routines was used so that when the software was loaded it was only necessary to load one large BASIC programme.

The different functions performed by the system are all called from a 'menu' routine which asks the user which function is required and then accesses the appropriate subroutine. On completion of the function control is returned to the 'menu' routine. The major BASIC routines in the programme are as follows:-

(i) Initialization and menu.
(ii) Transducer calibration.
(iii) Data acquisition and tube rotation control.
(iv) Data display.
(v) Data formatting.
(vi) Results printing.
(vii) Paper tape output.
(viii) Paper tape input.
(ix) Input formatter.
(x) Change of serial I/O speed.
(xi) Rotation of tube.

The subroutines written in Z80 assembler language and accessed from one of the BASIC subroutines are:-

(i) Paper tape punch timing control.
(ii) Oscilloscope data display.
(iii) Teletype output.
(iv) Transference of a character input from machine code keyboard scan routine to the BASIC subroutine as an argument in a U.S.R. call.

Flow charts giving details of the different software subroutines

are given in Figures 3.14 to 3.24. The complete listings of the BASIC programme and machine code subroutines are given in Appendix 2.

## 3.25 Conclusion

The microprocessor data acquisition and experimental control system and other electronic instrumentation was designed, constructed, calibrated and tested before the wind tunnel was completed. The automatic data acquisition system saved much experimental time which was limited by the time required to construct the model tube bank. All the equipment constructed was used successfully in obtaining the results discussed in Chapters 4 and 5.

## 3.26 References


3.1 R.G. ARAK 1981 Proceedings of the Institute of Acoustics "A microprocessor based control and data acquisition system for pressure measurements in an acoustic wind tunnel".

3.2 R.D. BLEVINS 1979 "Formulas for natural frequency and mode shape". New York: Van Nostrand Reinhold.

3.3 C.E.G.B. 1977 C.E.G.B. publication G823 "Wylfa Nuclear Boiler Repair".

3.4 P.O.A.L. DAVIES and M.R. DAVIS 1966 University of Southampton ISAV Report No. 155. "The hot wire anemometer".

3.5 P.O.A.L. DAVIES and J. MASON 1974 University of Southampton I.S.V.R., Technical Report No. 66. "The ISVR constant temperature hot wire anemometer".

3.6 NASCOM "Nascom Microprocessor Systems Documentation", Chesham, U.K.: Nascom Microcomputers L.T.D..

3.7 NATIONAL 1976 "National Semiconductor T.T.L. data book". Santa Clara, U.S.A.: National Semiconductor Corporation.

3.8 R.S. COMPONENTS 1981 RS components data sheet No. R/1873 "78/79 Series Regulator data sheet".

3.9 R.S. COMPONENTS 1977 RS Components data sheet No. R/2999 "LF398H sample and hold data sheet".

3.10 R.S. COMPONENTS 1980 RS Components data sheet No. R/3605 "SGA100 strain gauge amplifier data sheet".

3.11 R.S. COMPONENTS 1980 RS Components data sheet No. R/4002 "AD536A r.m.s. to dc converter data sheet".

3.12 R.S. COMPONENTS 1980 RS Components data sheet No. R/4052 "ZN4275 A-to-D converter data sheet".

3.13 R.S. COMPONENTS 1980 RS Components data sheet No. R/4068 "DAC0800 D-to-A converter data sheet".

3.14 R.S. COMPONENTS 1981 RS Components data sheet No. R/4175 "DG508 analogue switch data sheet".

3.15 J. ARMITT C.E.R.L. Leatherhead, England, June 1979. Personal Communication.

TABLE 3.1. Technical specification of Maywood Instruments P102 pressure transducer

| Parameter | Magnitude | Units |
|---|---|---|
| Model Number | P102 | |
| Serial Number | 3103 | |
| Range | 0-15 | P.S.I.(differential) |
| Test temperature | 24 | $^{o}C$ |
| Voltage supply | 10 | Volts D.C. |
| Non-linearity | ±0.23 | % full scale |
| Hysteresis & Non Repeatability | <0.10 | % full scale |
| Full range output | 60.20 | mV |
| Input Resistance | 1130 | ohms |
| Output Resistance | 470 | ohms |
| Compensated temperature range | -18 to +65 | $^{o}C$ |
| Thermal Zero Shift | <±0.62 | % full scale $^{o}C^{-1}$ |
| Thermal Sensitivity Shift | <±0.02 | % full scale $^{o}C^{-1}$ |
| Natural frequency | 17 | kHz |
| Volumetric Displacement | 0.22 | $mm^3$ |
| Weight | 110 | grammes |
| Overpressure | x4 | |

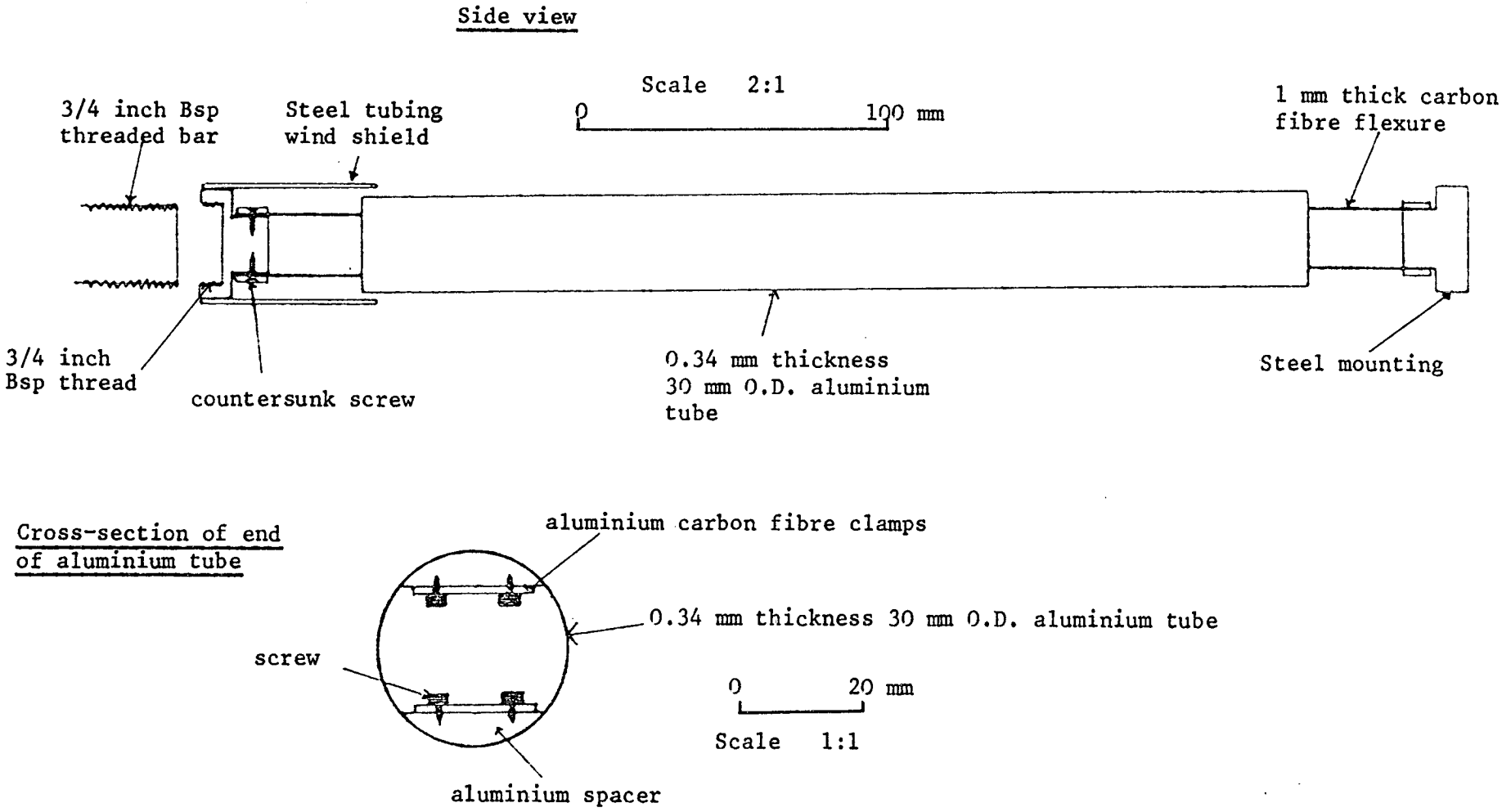


FIGURE 3.1. Sketch diagrams of the flexibly mounted tubes.

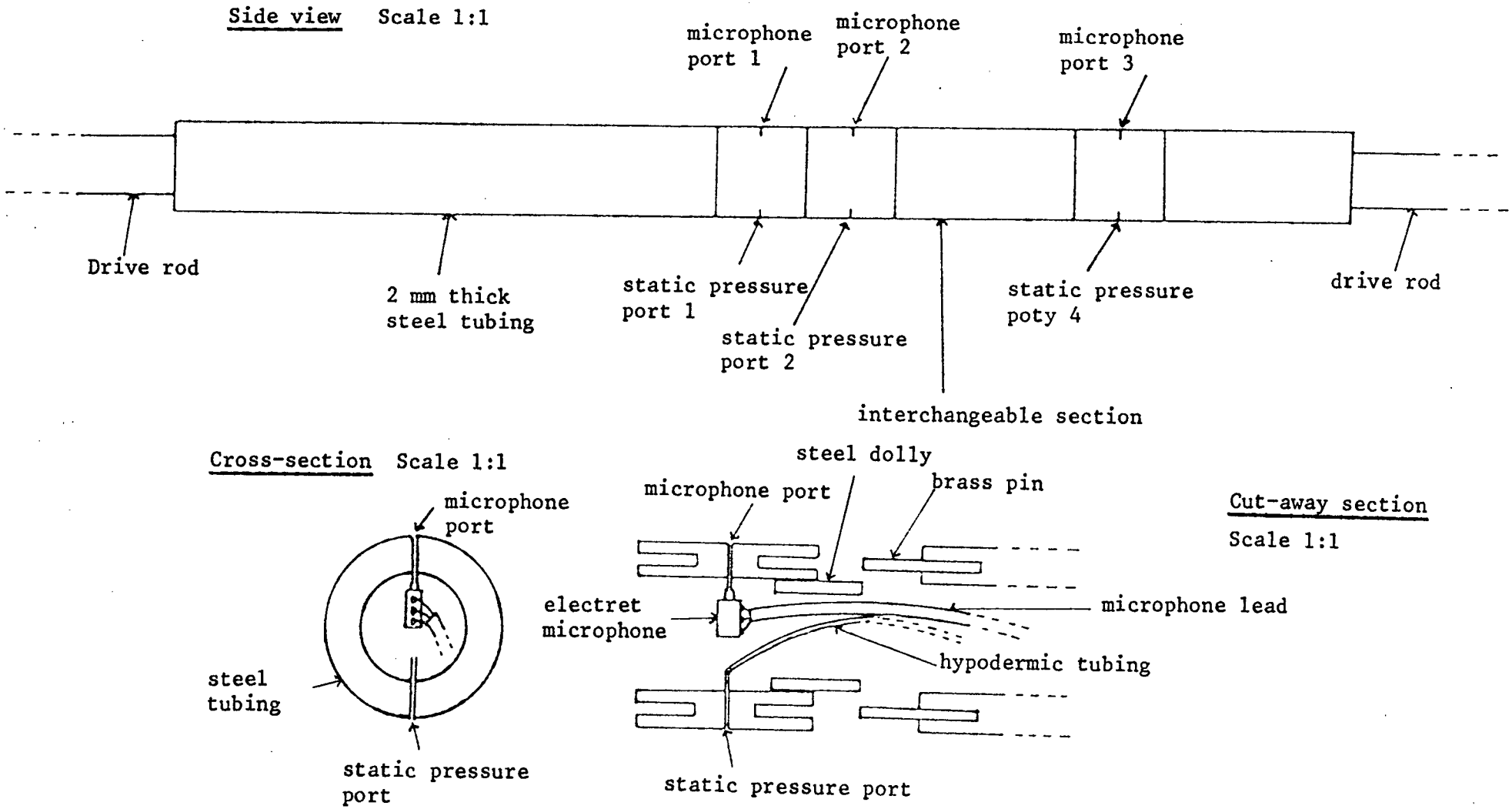


FIGURE 3.2. Sketch diagrams of the pressure measuring tube.

Apparatus set up in anechoic chamber

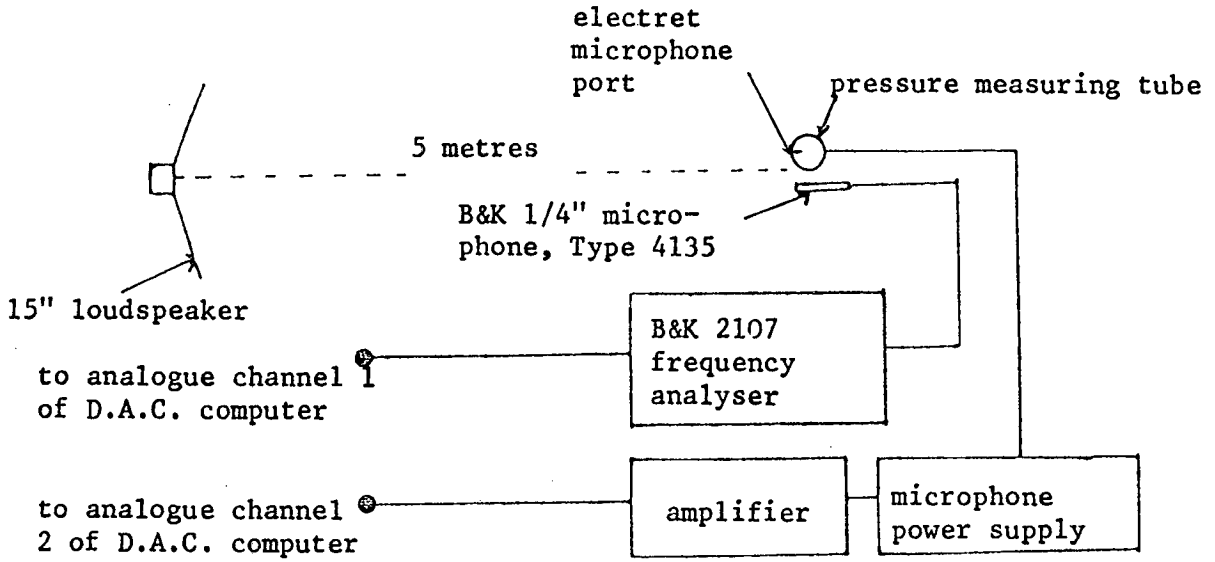


FIGURE 3.3. Block diagram of apparatus for calibration of electret microphones mounted inside the pressure measuring tube.

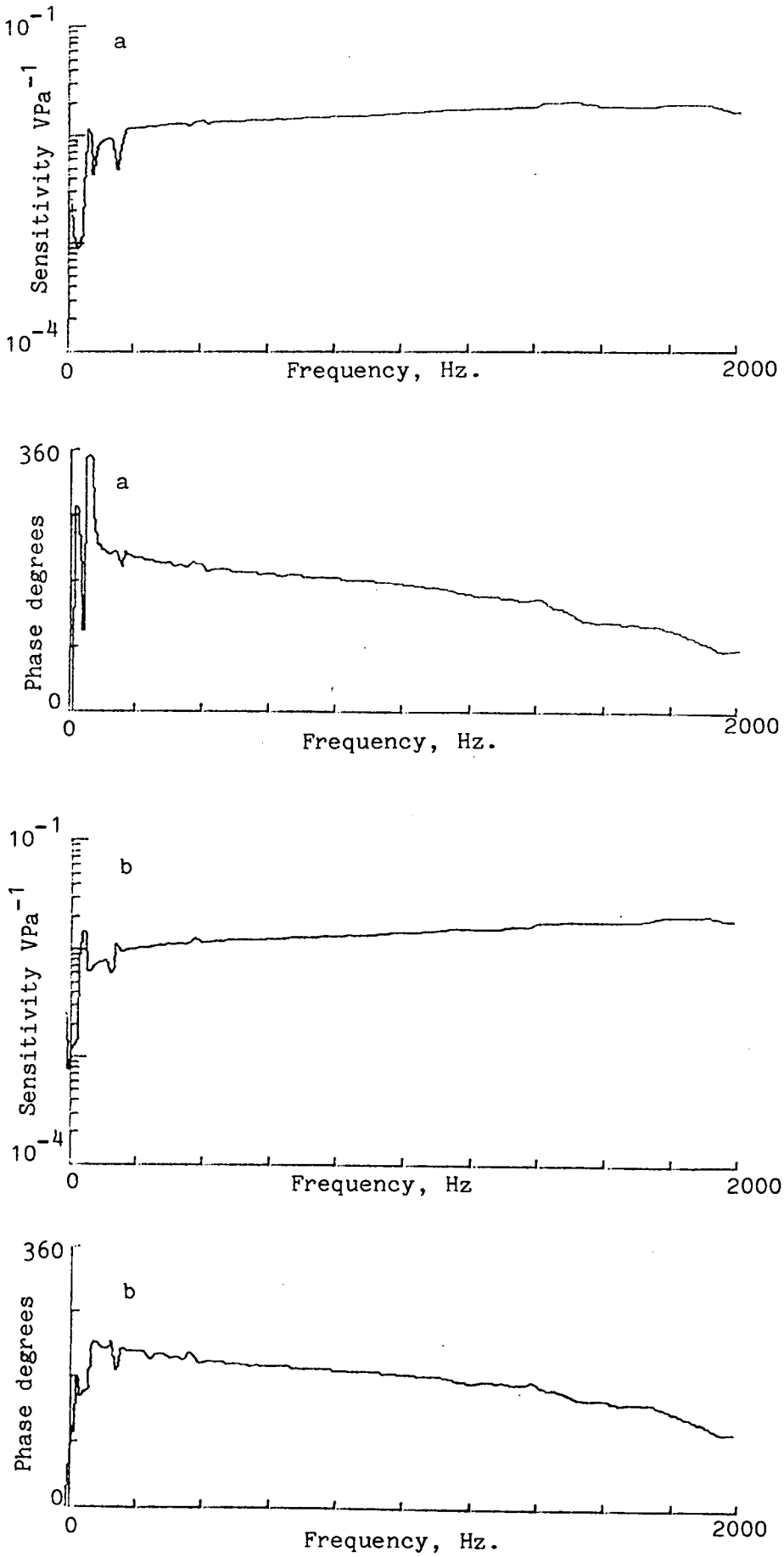


FIGURE 3.4. Microphone calibration curves. a = microphone 1.
b = microphone 2.

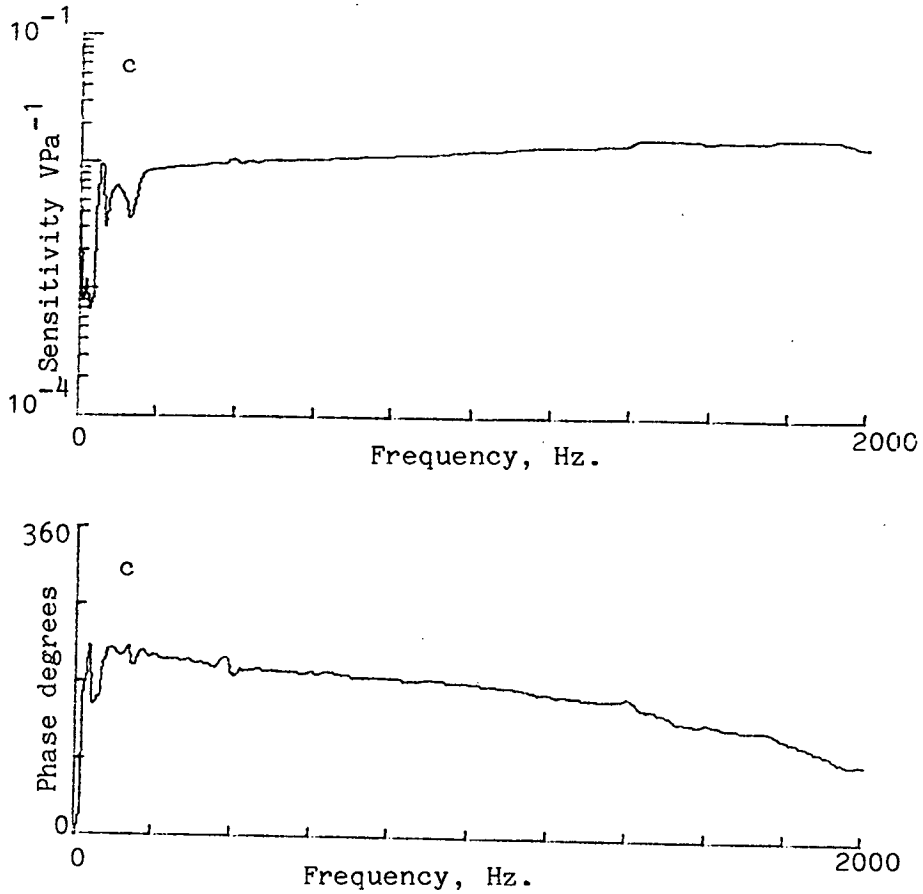


FIGURE 3.4.(continued)

Microphone calibration curves. c = microphone 3.

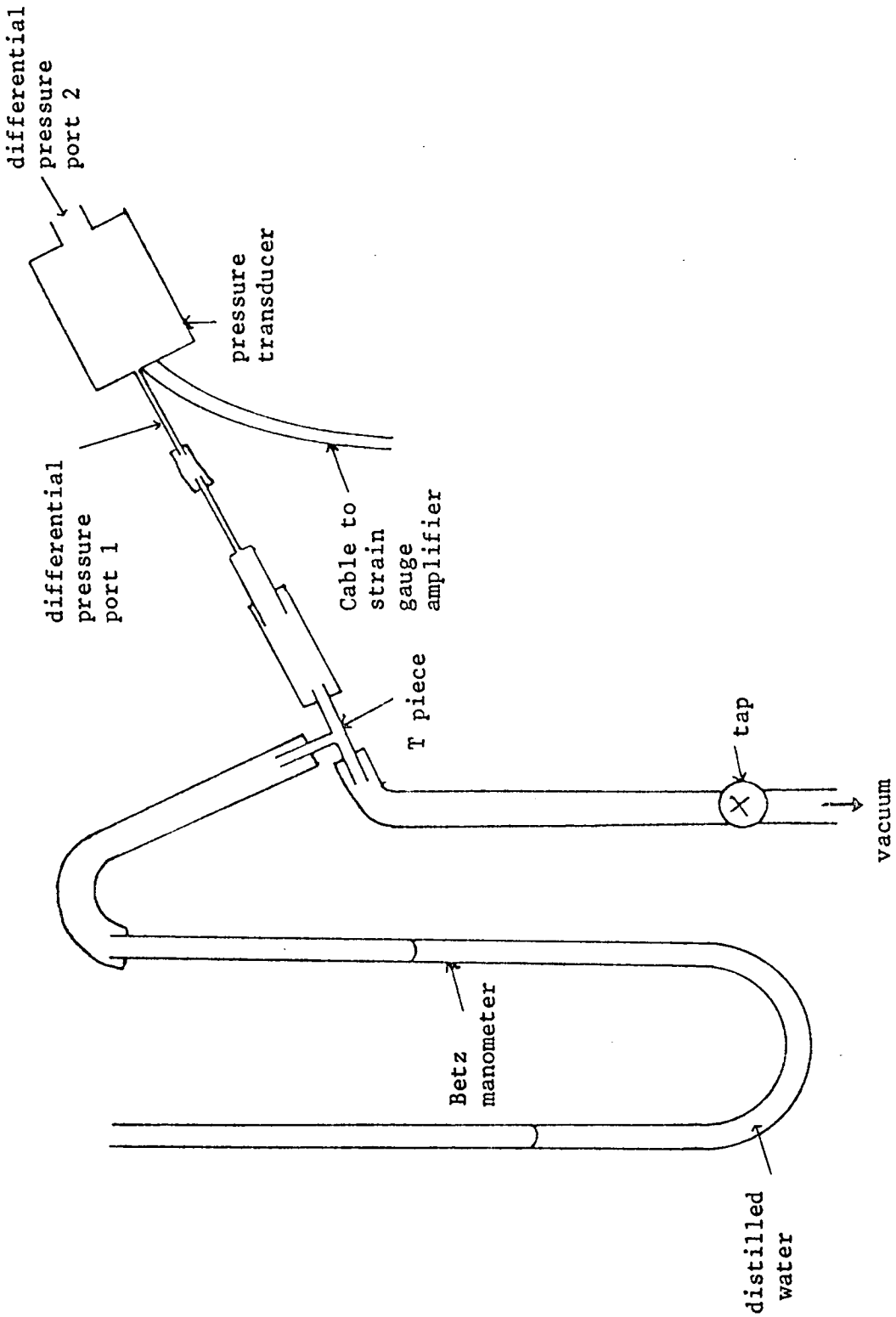


FIGURE 3.5. Schematic diagram of apparatus used to calibrate pressure transducer.

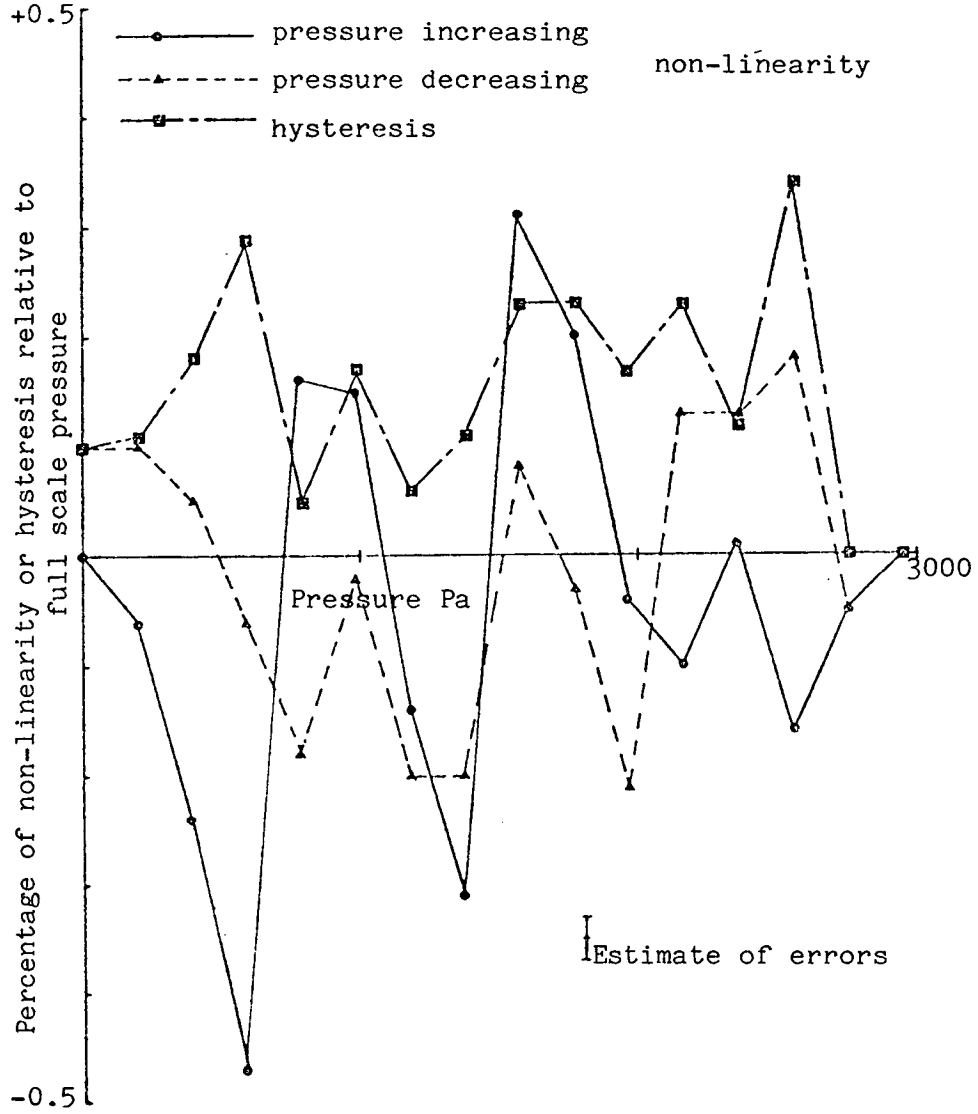


FIGURE 3.6. Non-linearity and hysteresis of pressure transducer versus pressure.

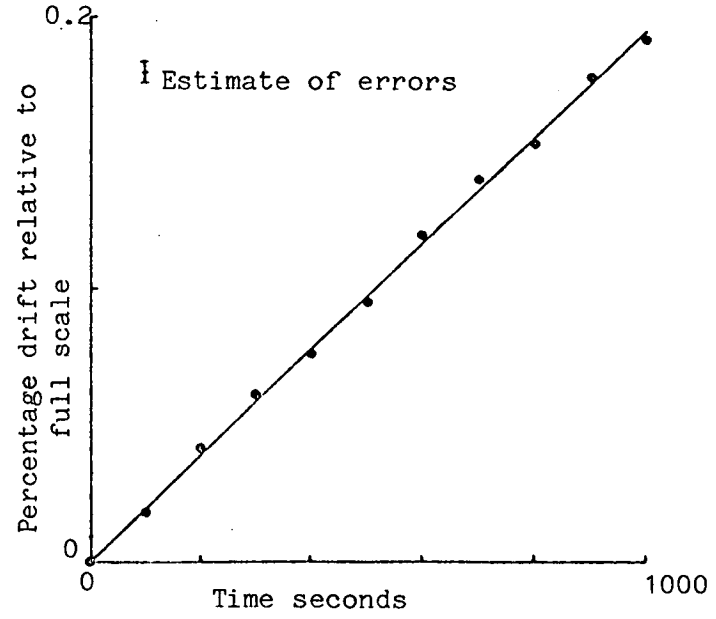


FIGURE 3.7. Drift of pressure transducer versus time.

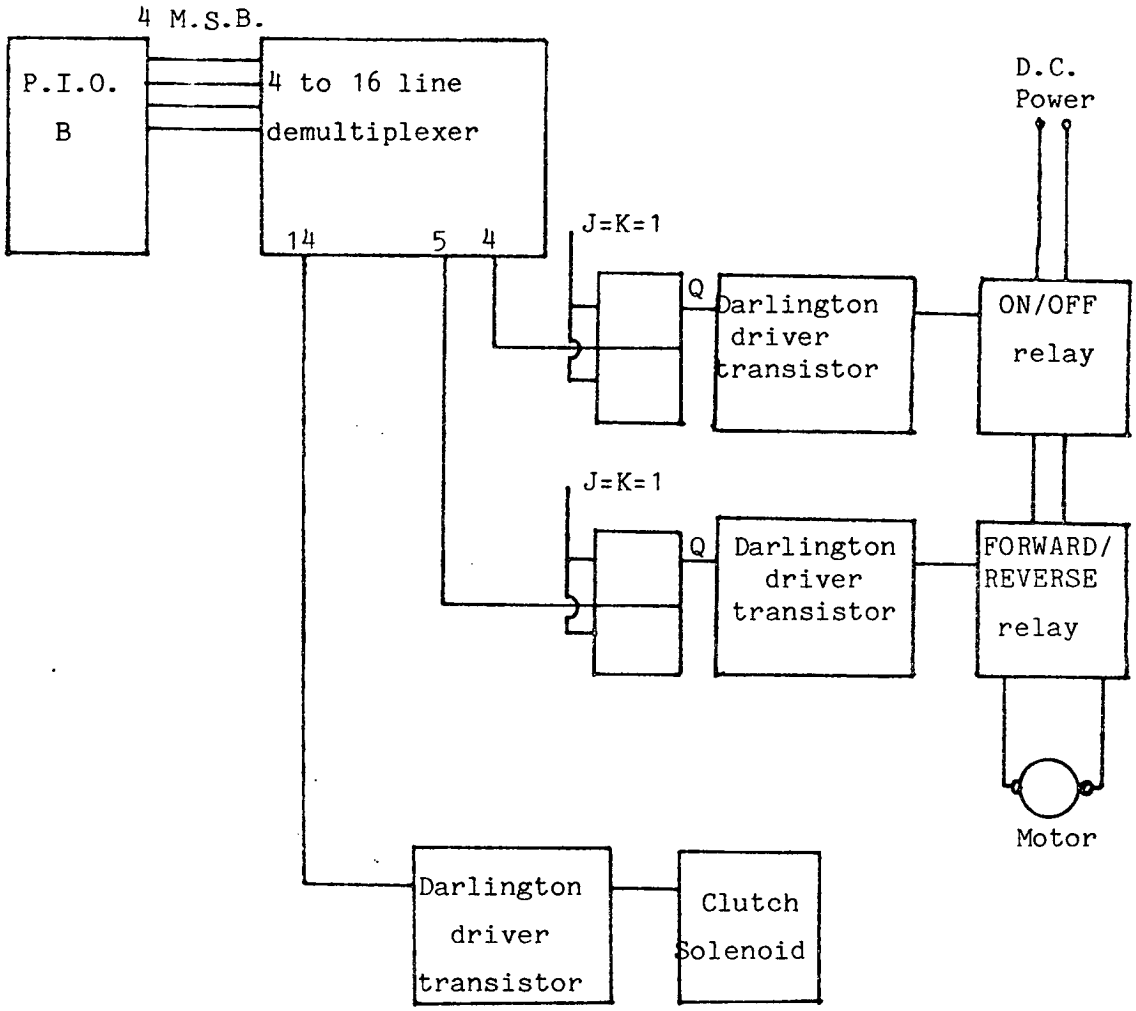


FIGURE 3.8. Block diagram of pressure measuring tube drive interface.

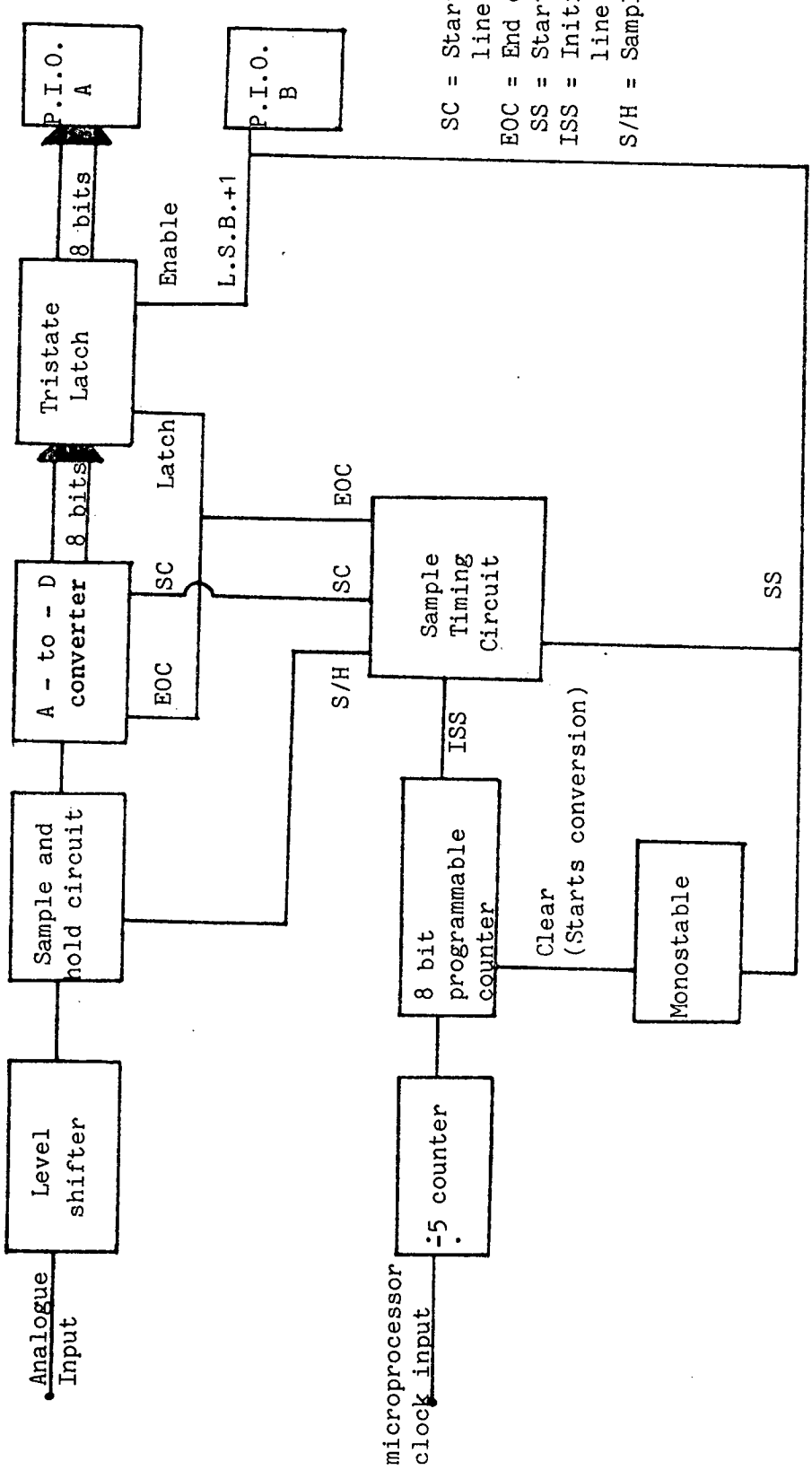


FIGURE 3.9. Block diagram of analogue to digital converter and sampling circuit.

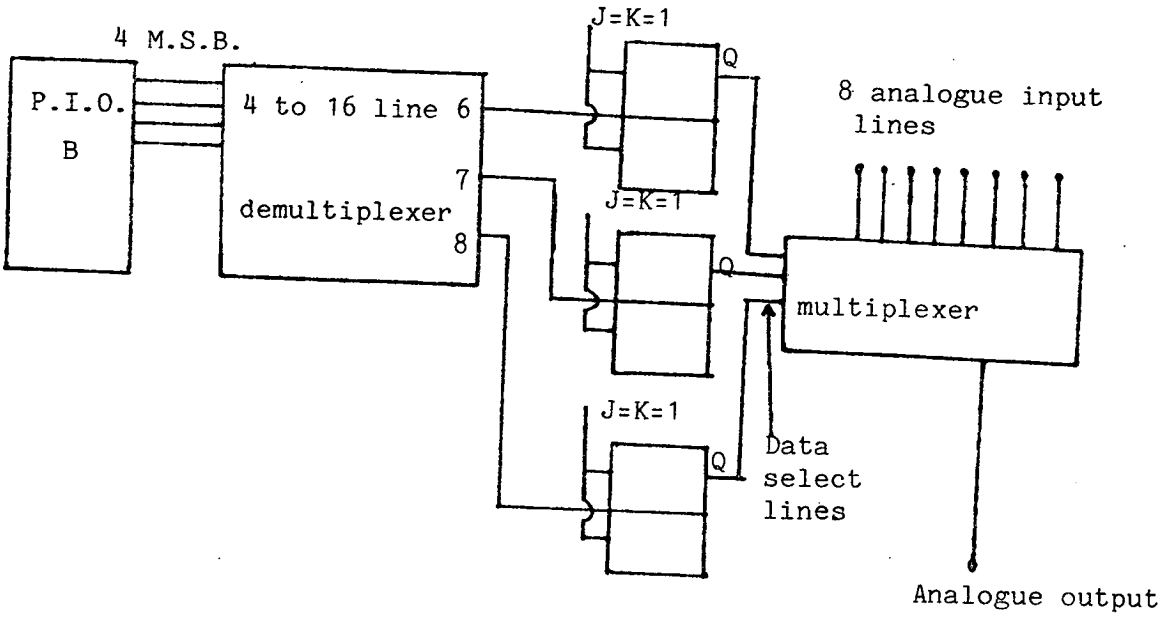


FIGURE 3.10. Block diagram of the analogue multiplexer.

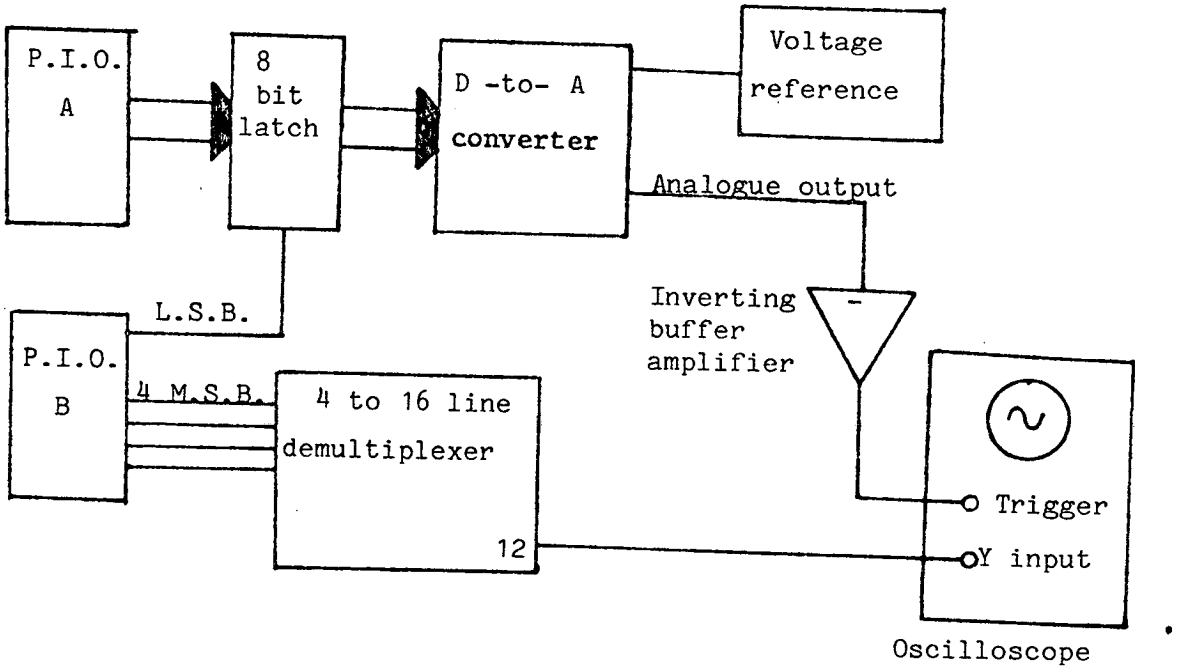


FIGURE 3.11. Block diagram of digital-to-analogue converter.

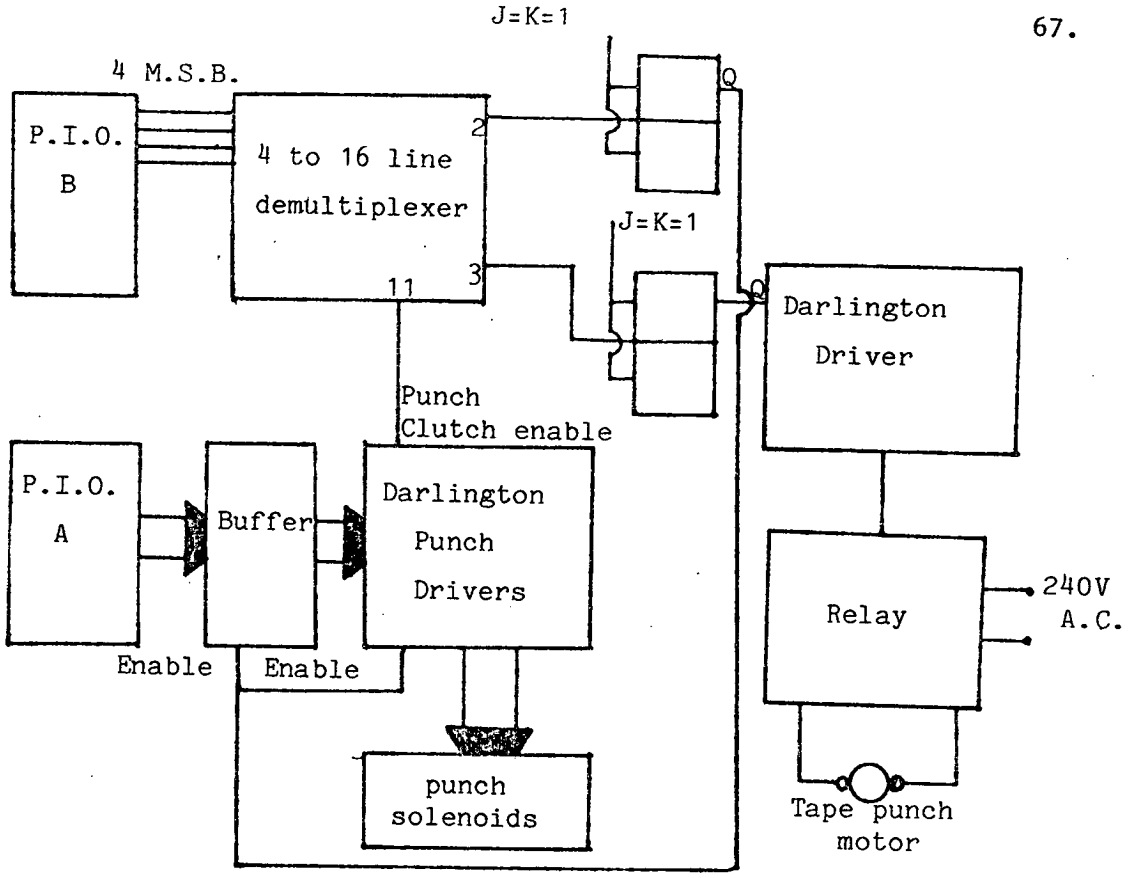


FIGURE 3.12. Block diagram of paper tape punch interface.

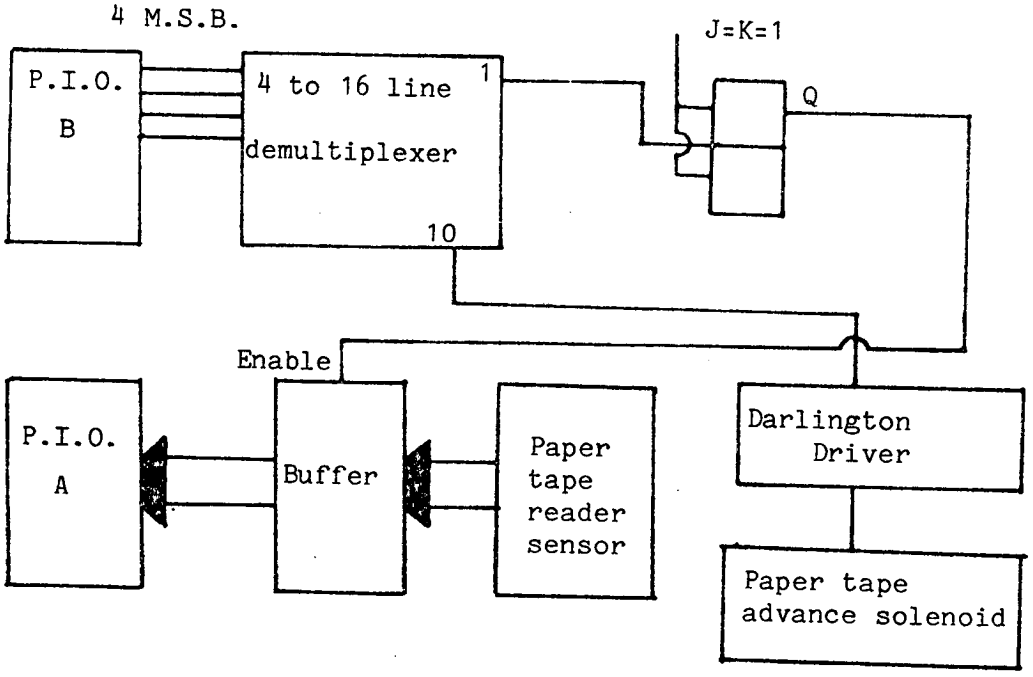


FIGURE 3.13. Block diagram of paper tape reader interface.

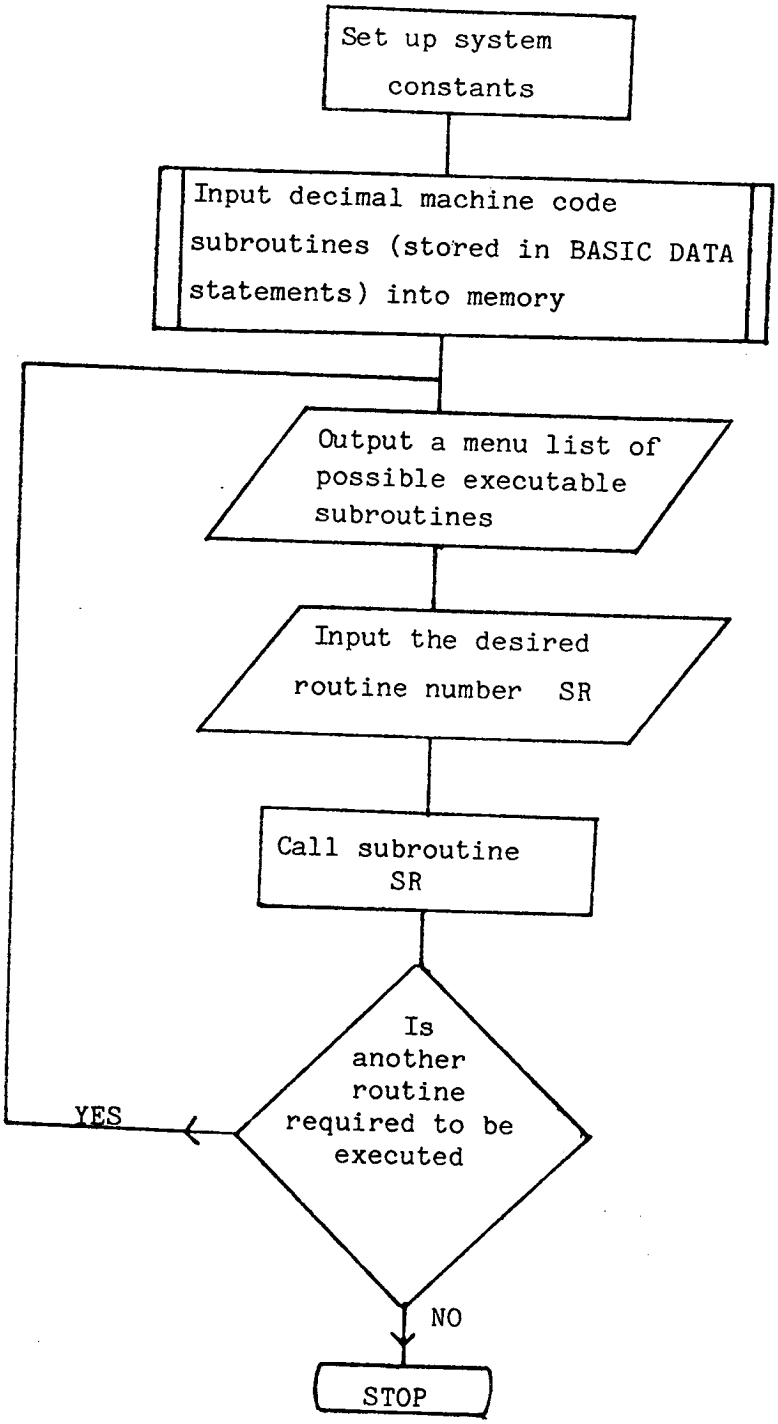


FIGURE 3.14. Flow diagram of variable declaration and menu routine.

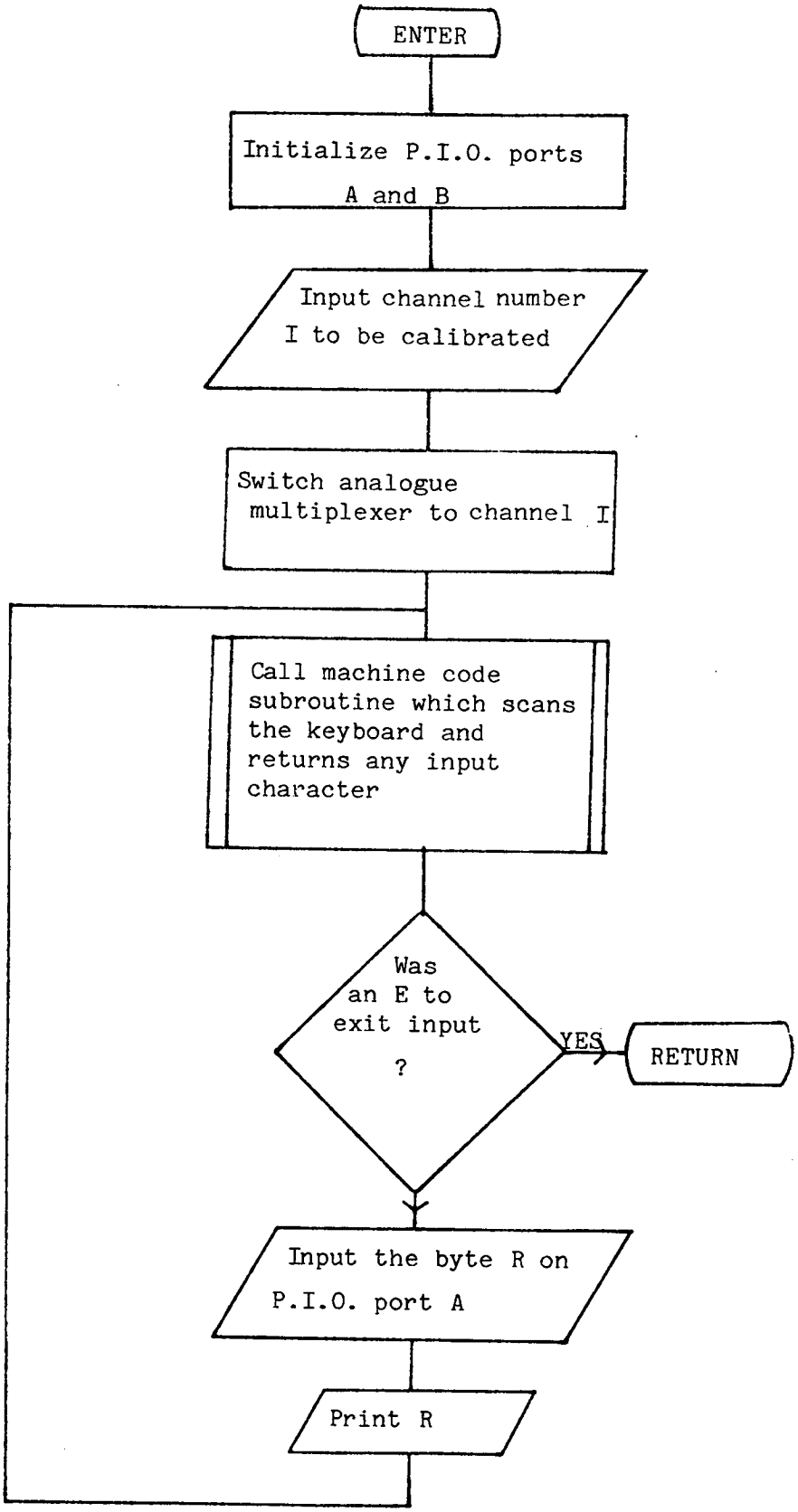


FIGURE 3.15. Flow diagram of instrumentation calibration routine.

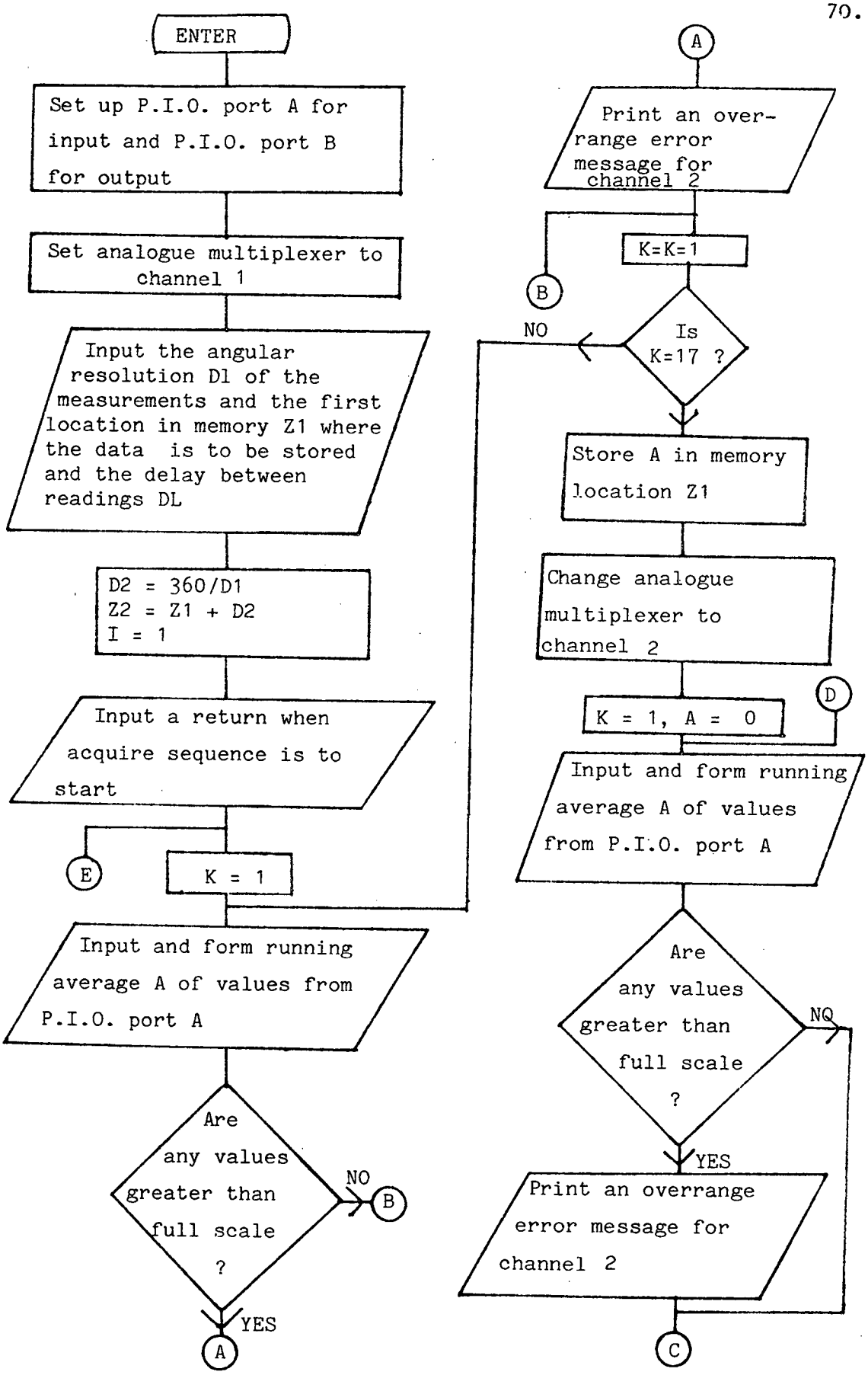


FIGURE 3.16. Flow diagram of data acquisition and tube control routine.

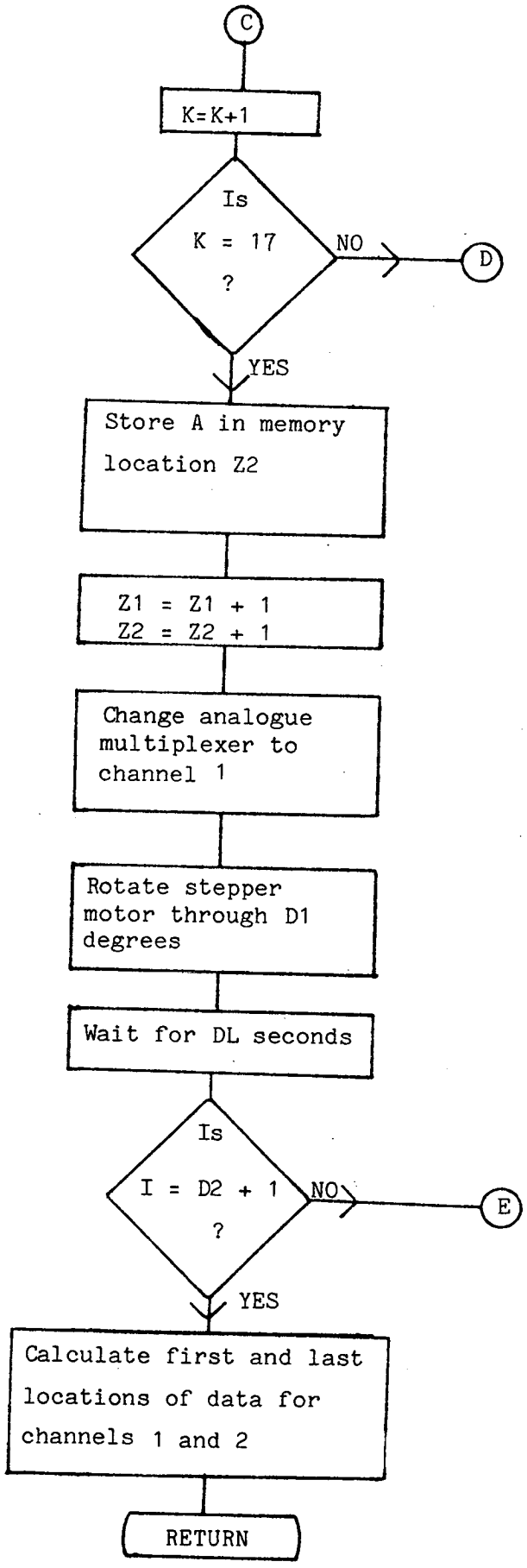


FIGURE 3.16. (continued)

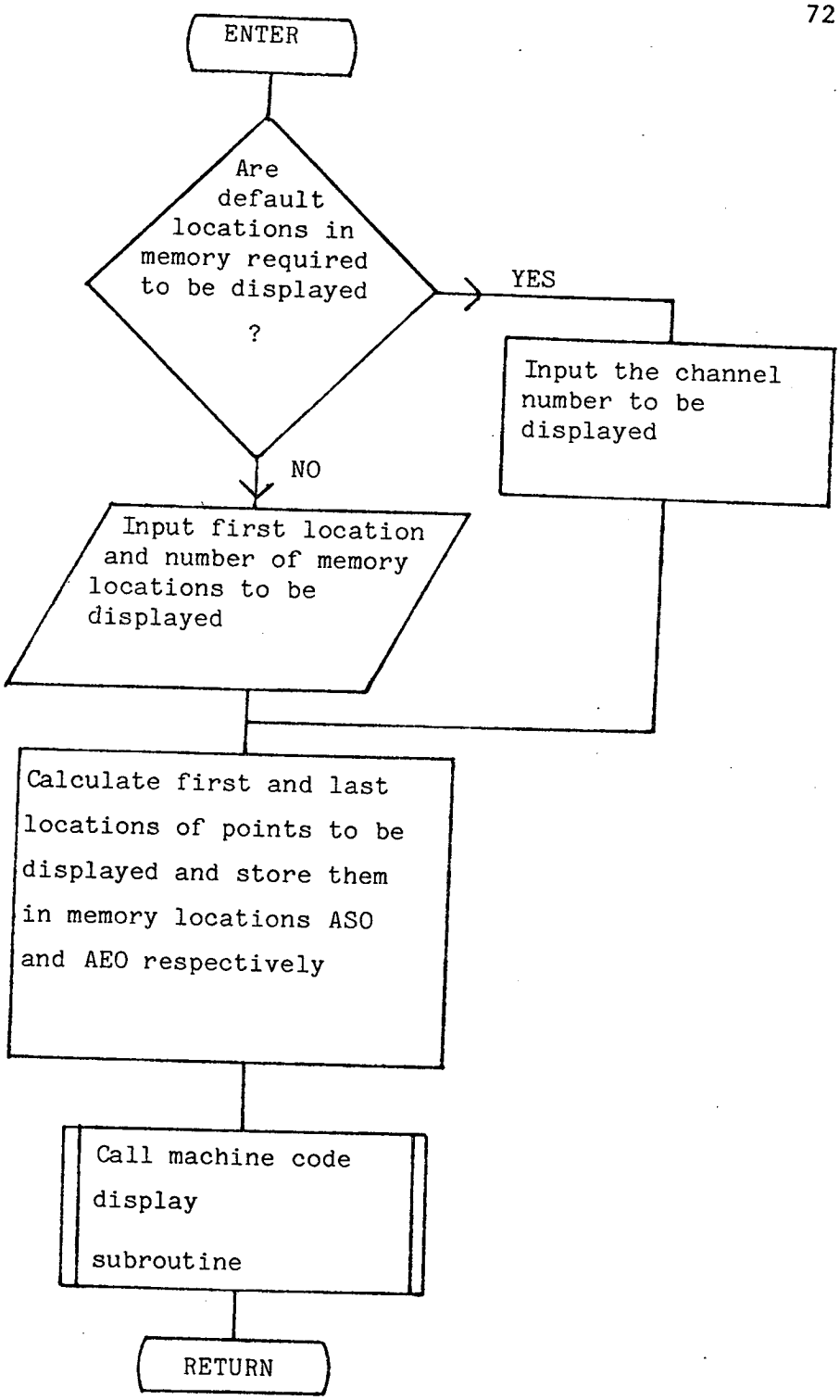


FIGURE 3.17a. Flow diagram of data display routine.

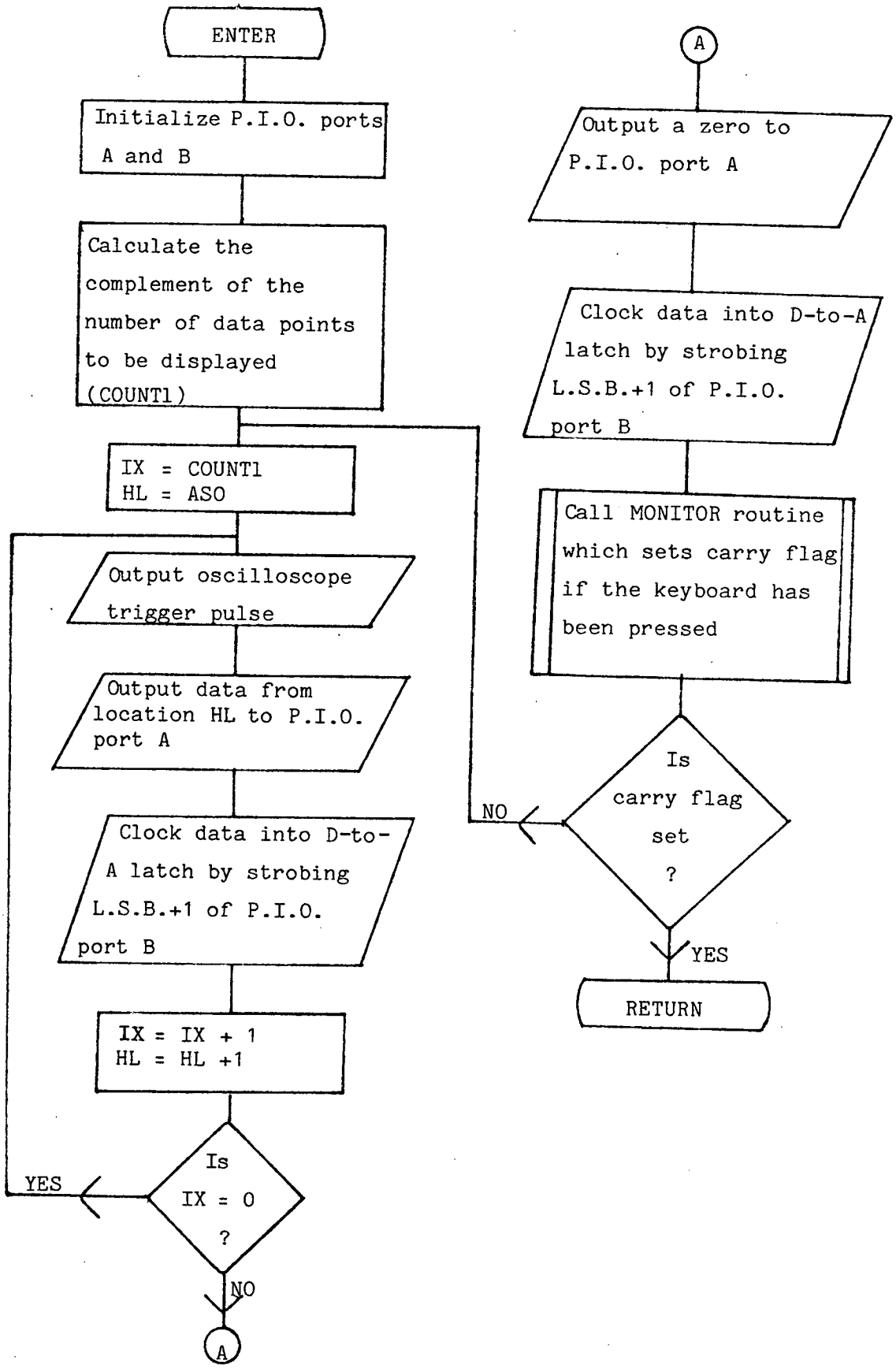


FIGURE 3.17b. Flow diagram of machine code data display routine.

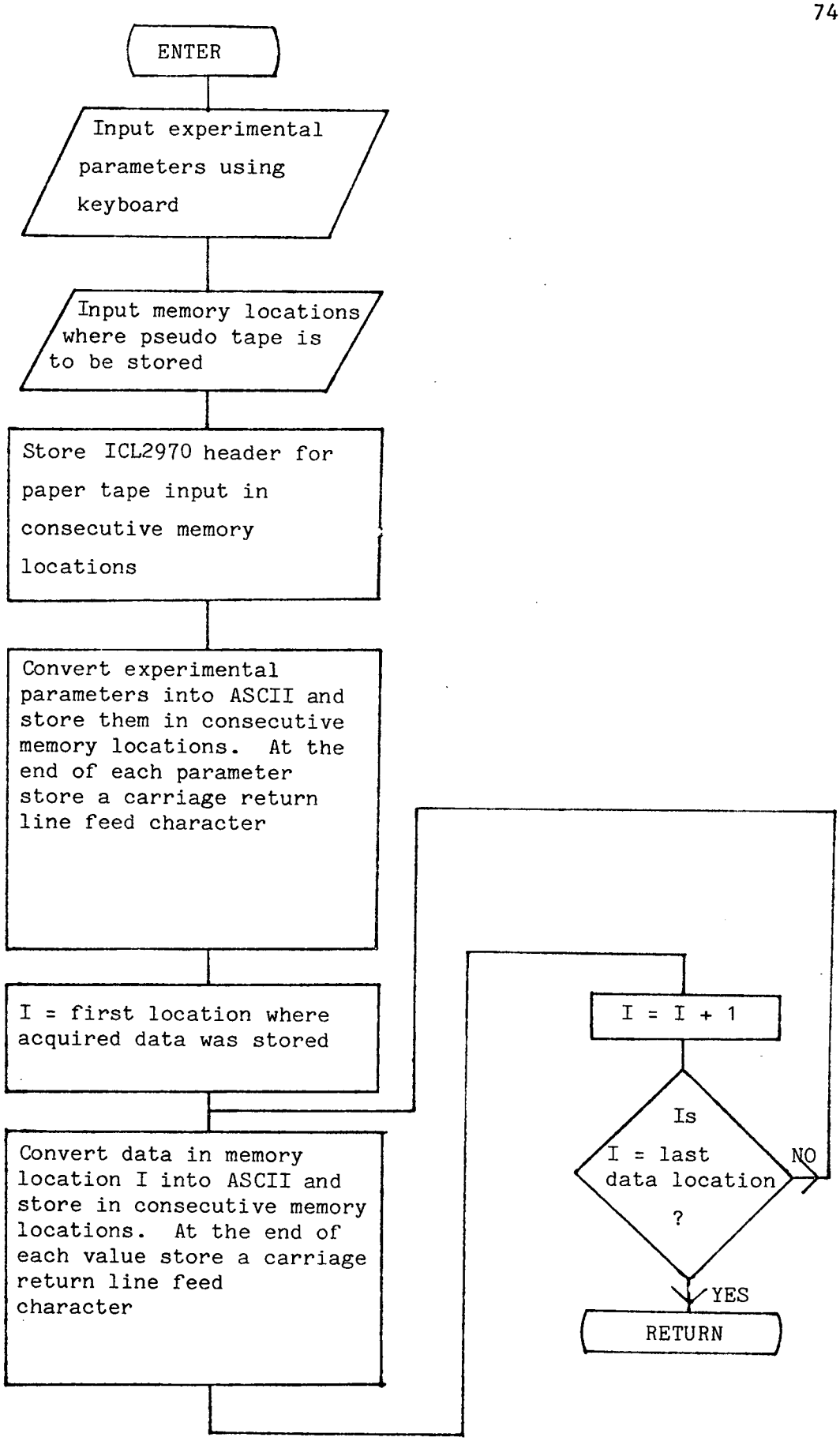


FIGURE 3.18. Flow diagram of data formatting routine.

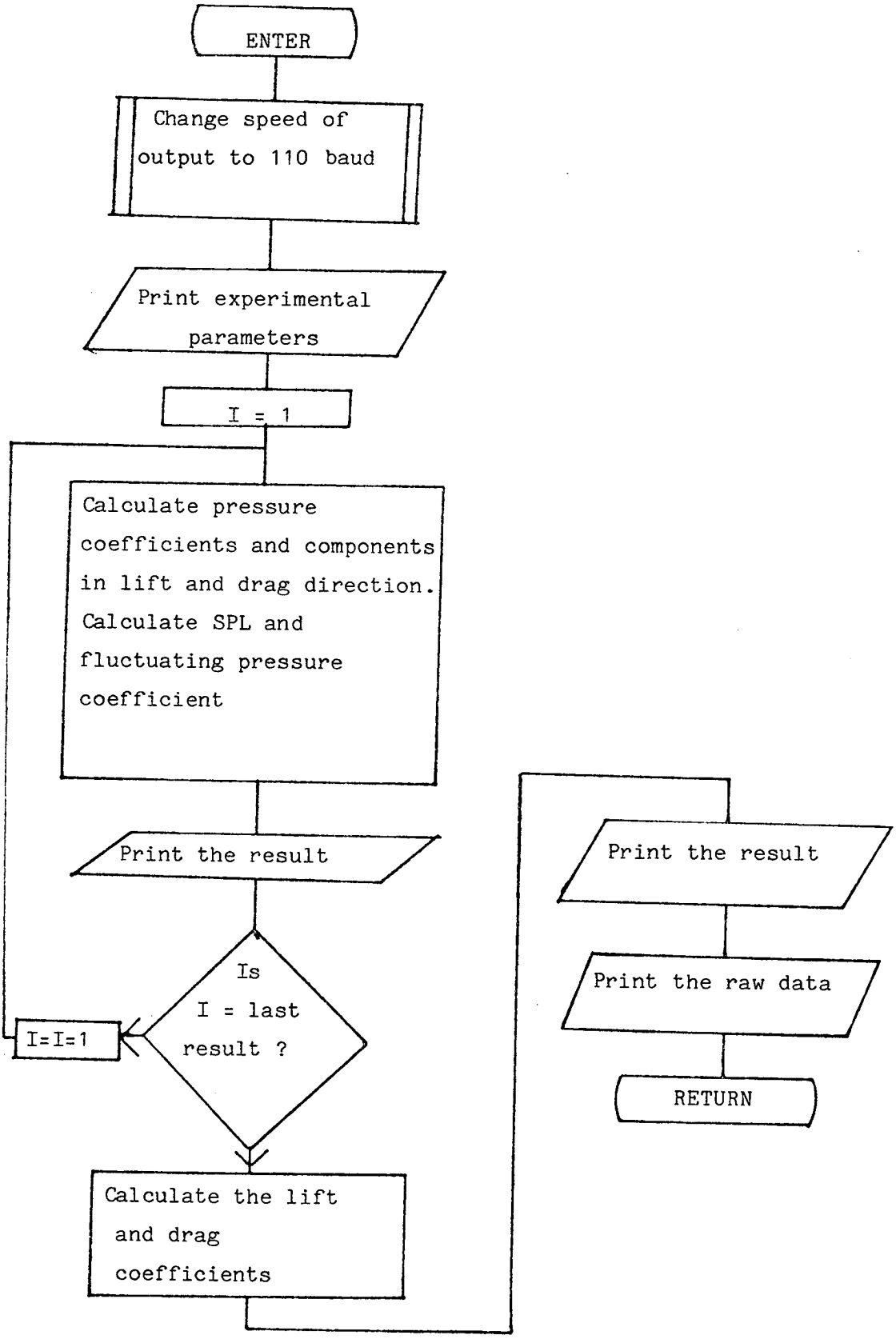


FIGURE 3.19. Flow diagram of results printing routine.

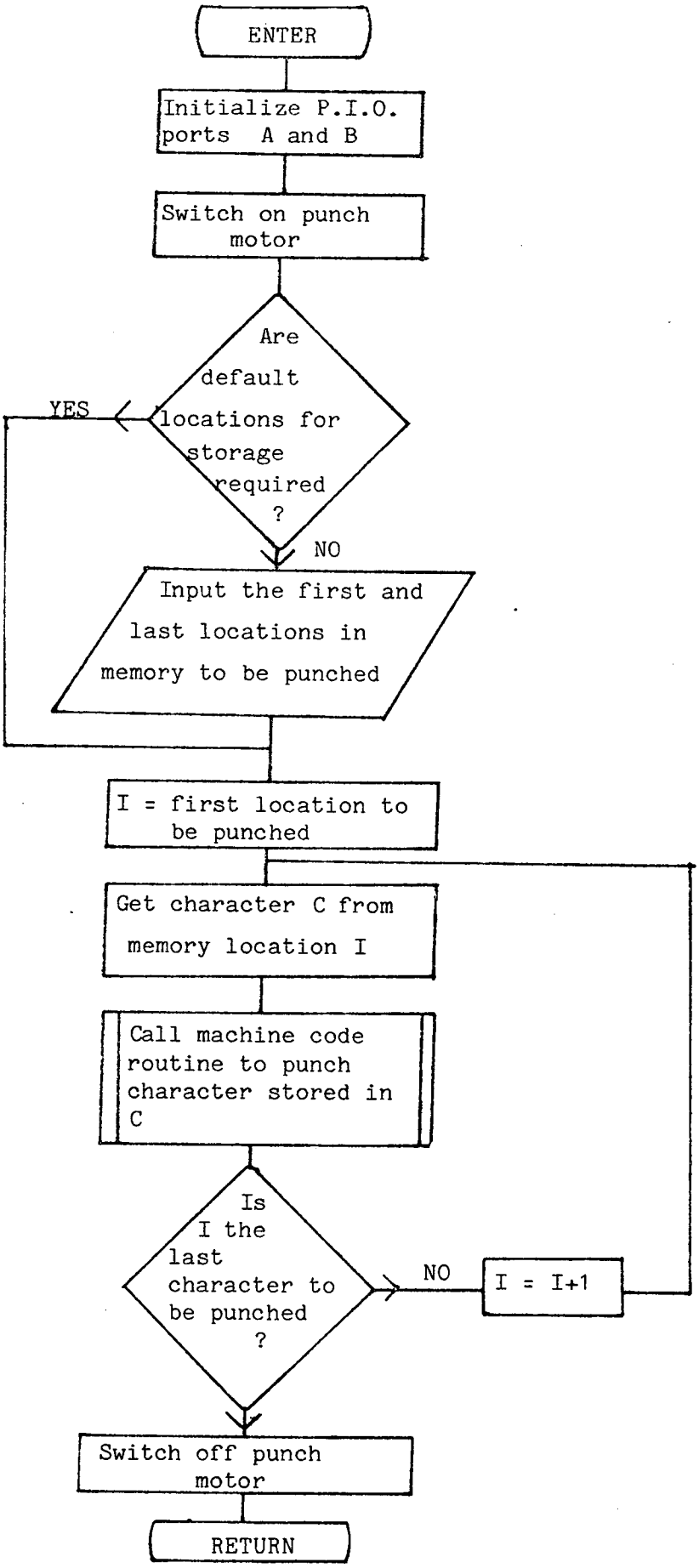


FIGURE 3.20a. Flow diagram of paper tape punch routine.

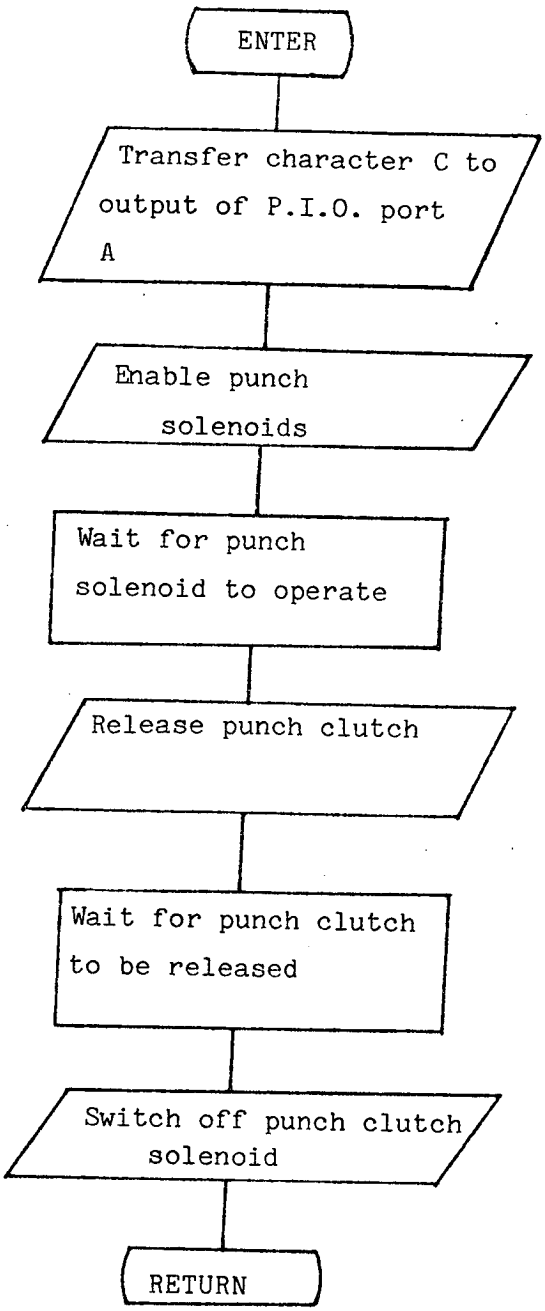


FIGURE 3.20b. Flow diagram of machine code punch routine.

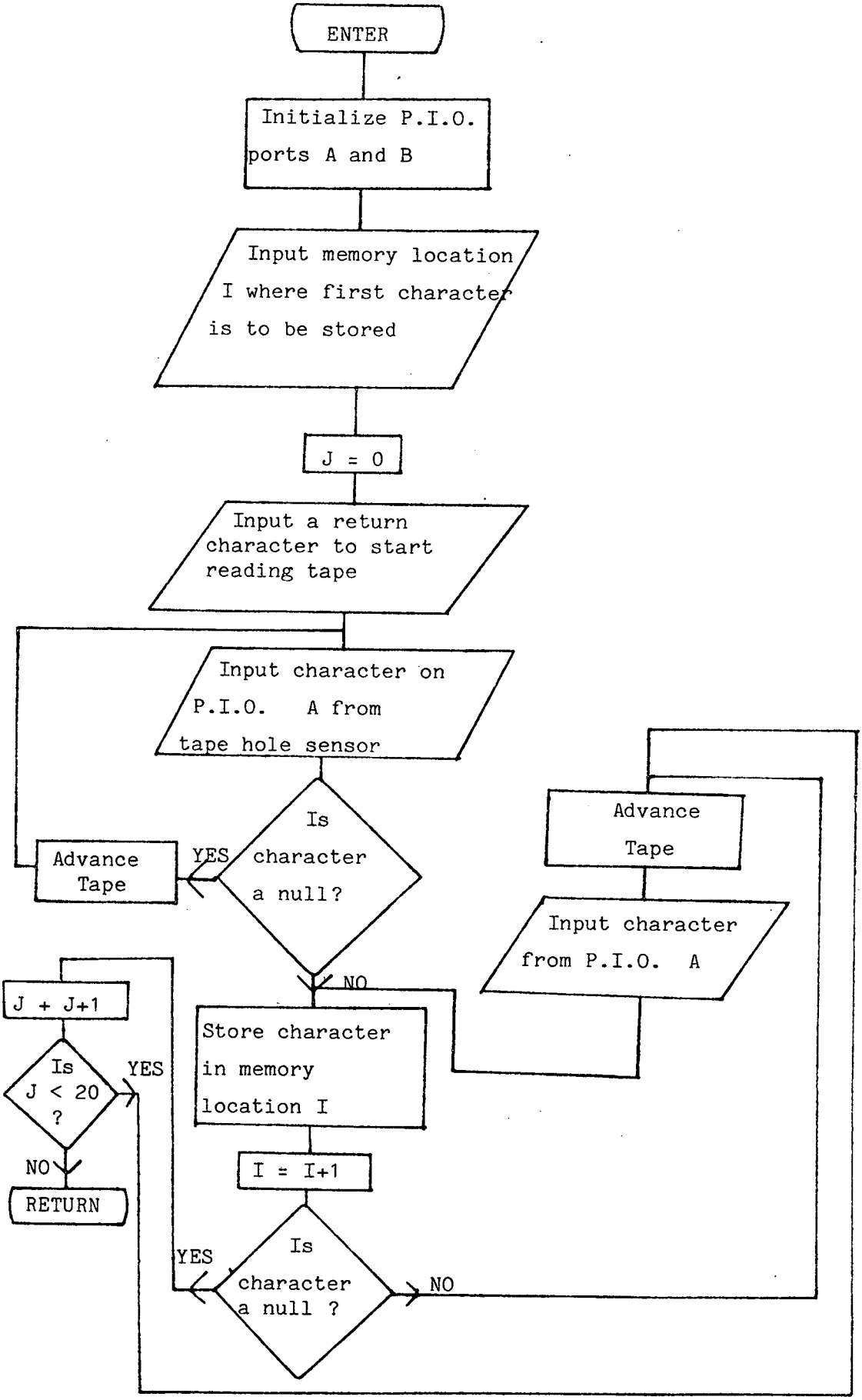


FIGURE 3.21. Flow diagram of paper tape input routine.

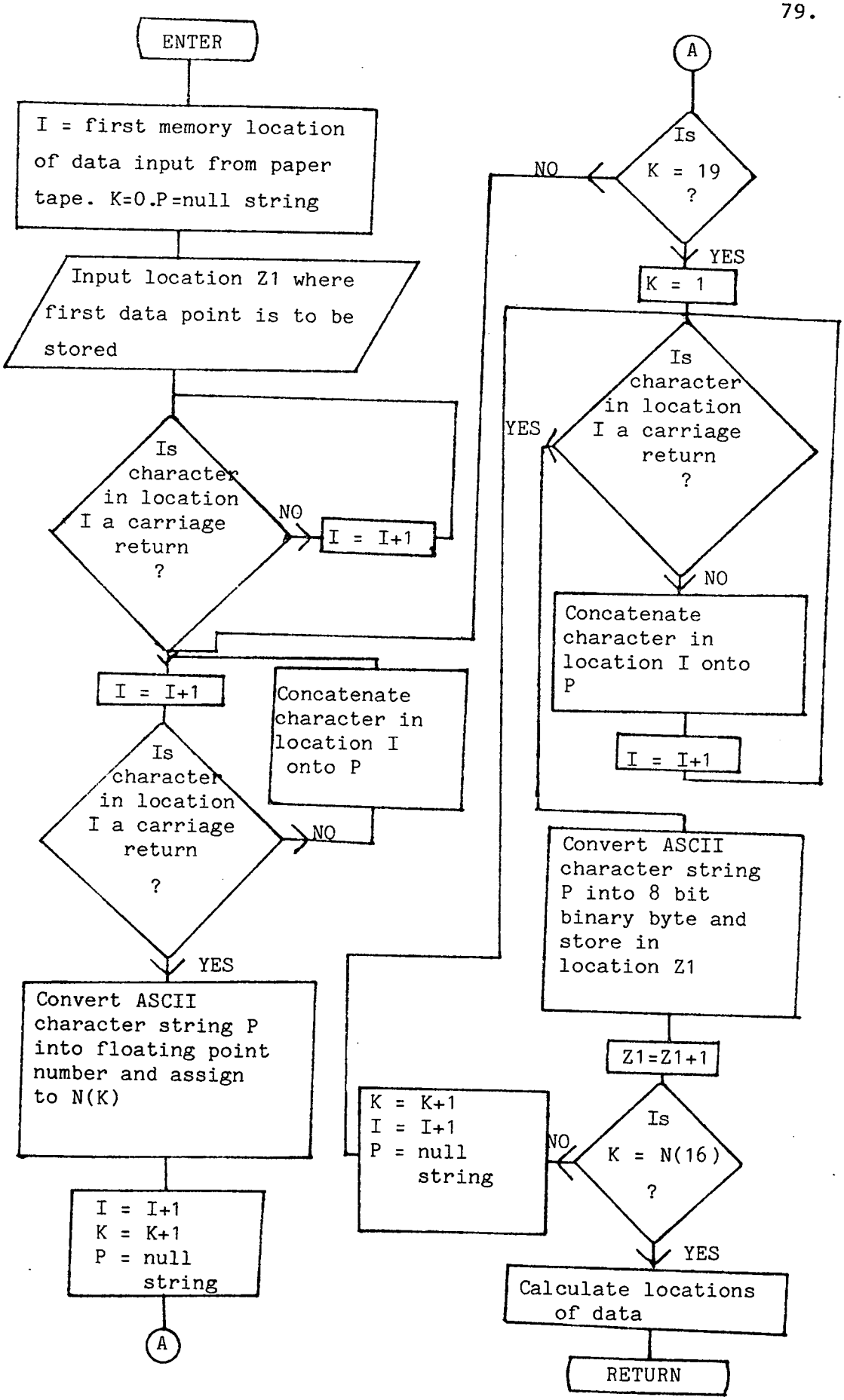


FIGURE 3.22. Flow diagram of paper tape input formatting routine.

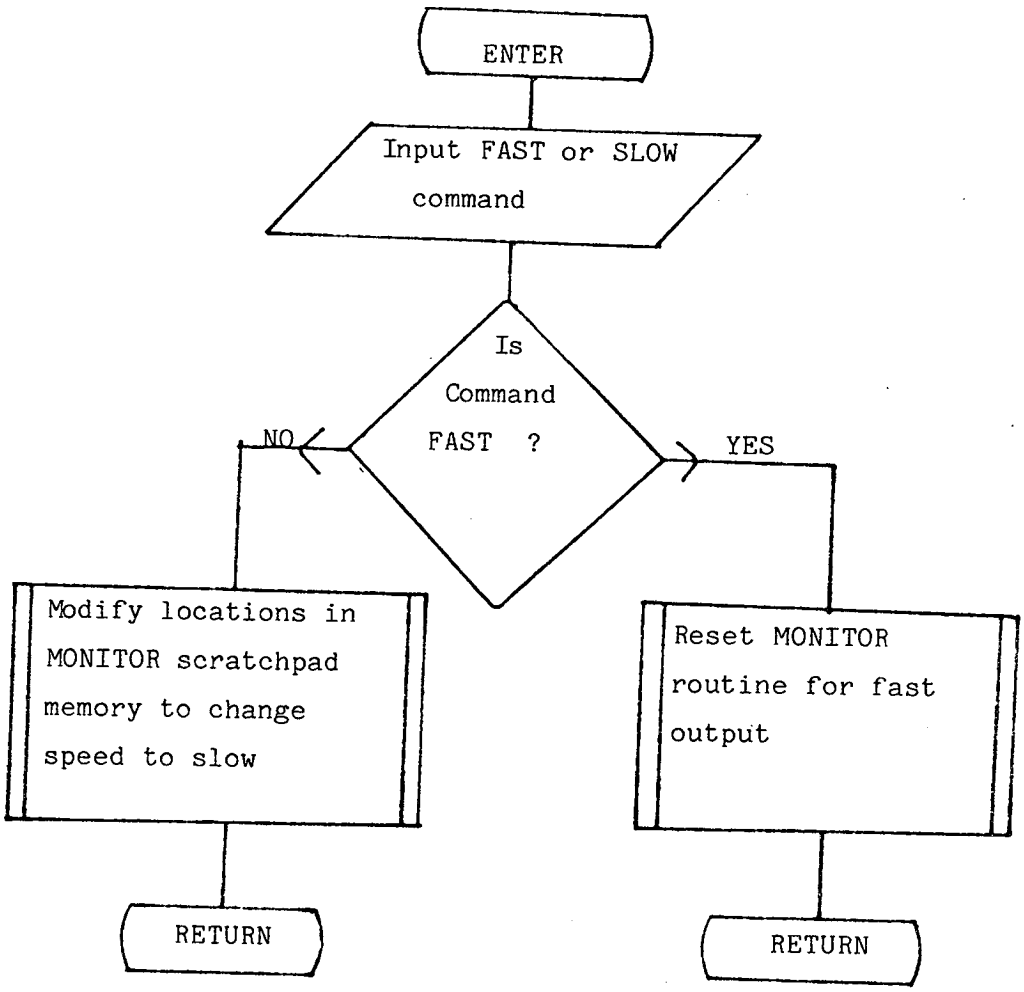


FIGURE 3.23. Flow diagram of routine to change output speed.

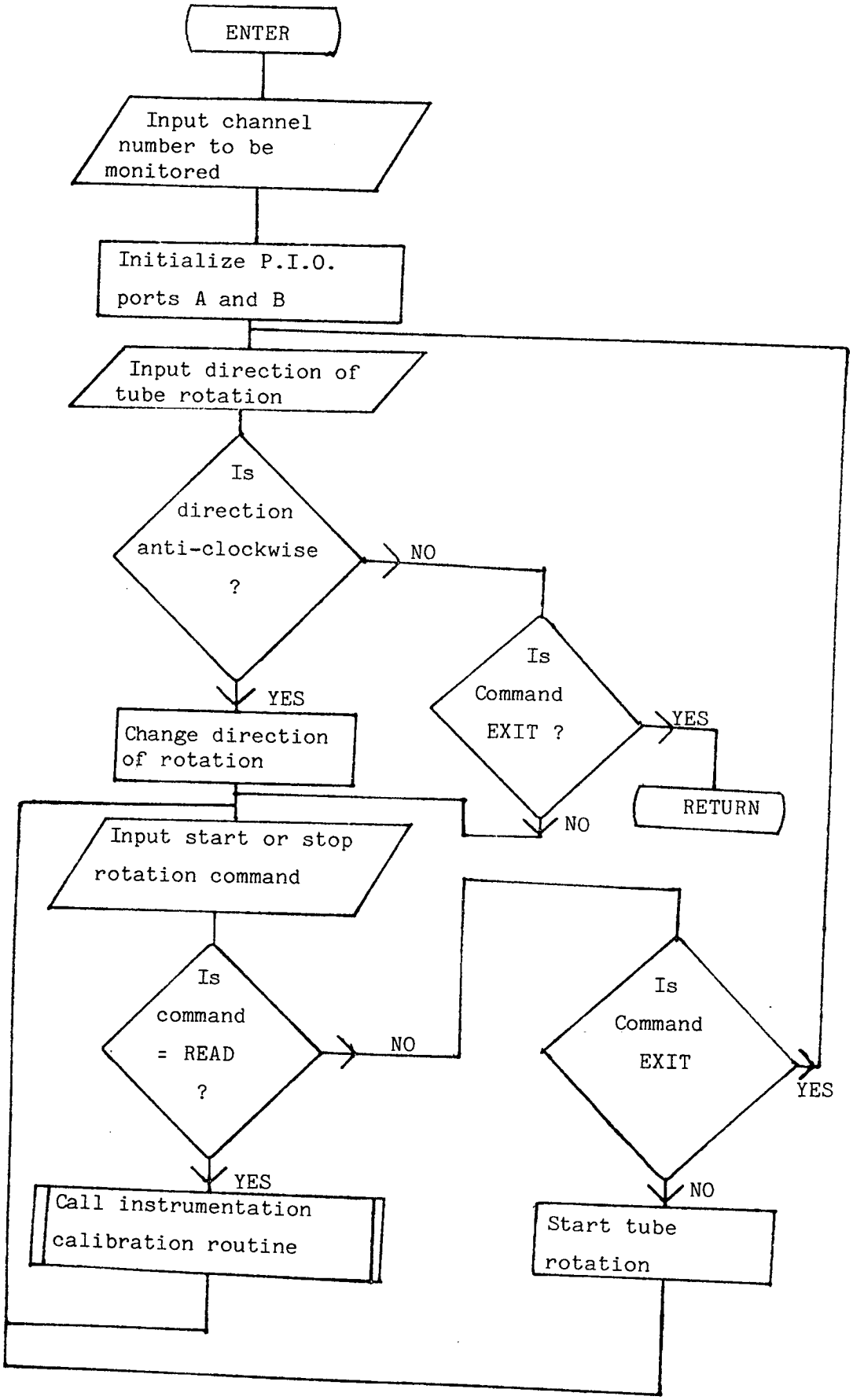


FIGURE 3.24. Flow diagram of tube rotation routine.


Plate 3.1 The instrumentation systems used for experimental measurements

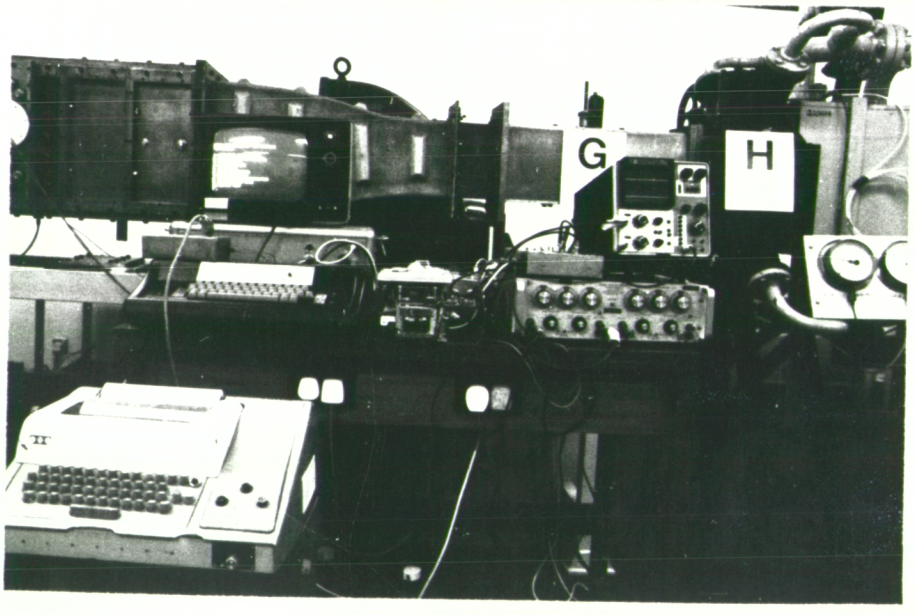


Plate 3.2 The microprocessor data acquisition and control system

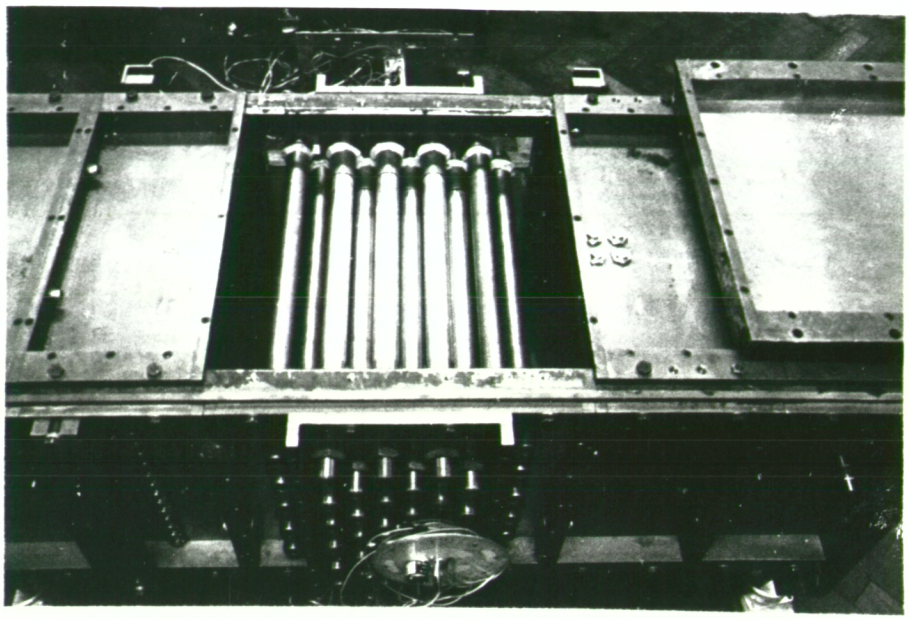

Plate 3.3a View looking down on working section with the top panel removed

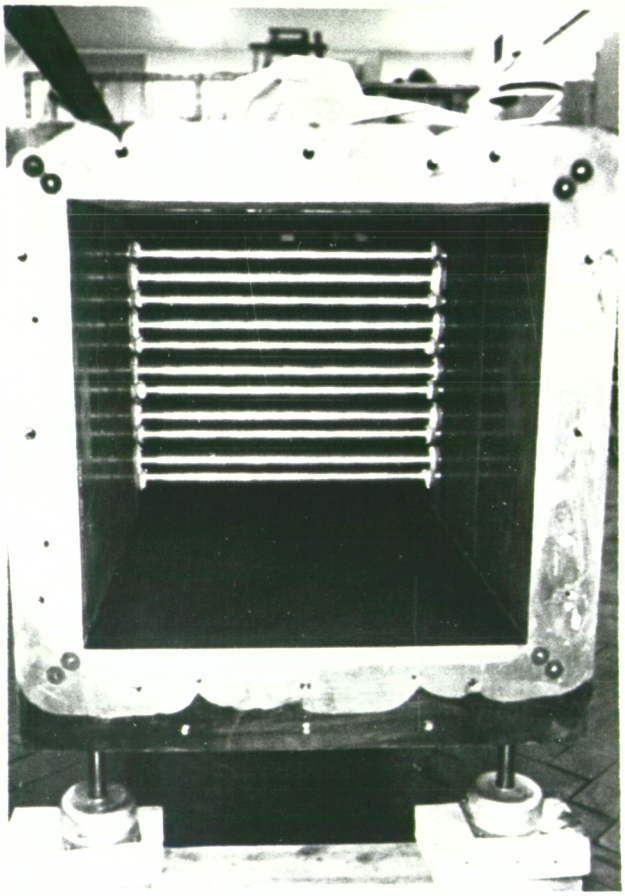

Plate 3.3b View down working section cross-section

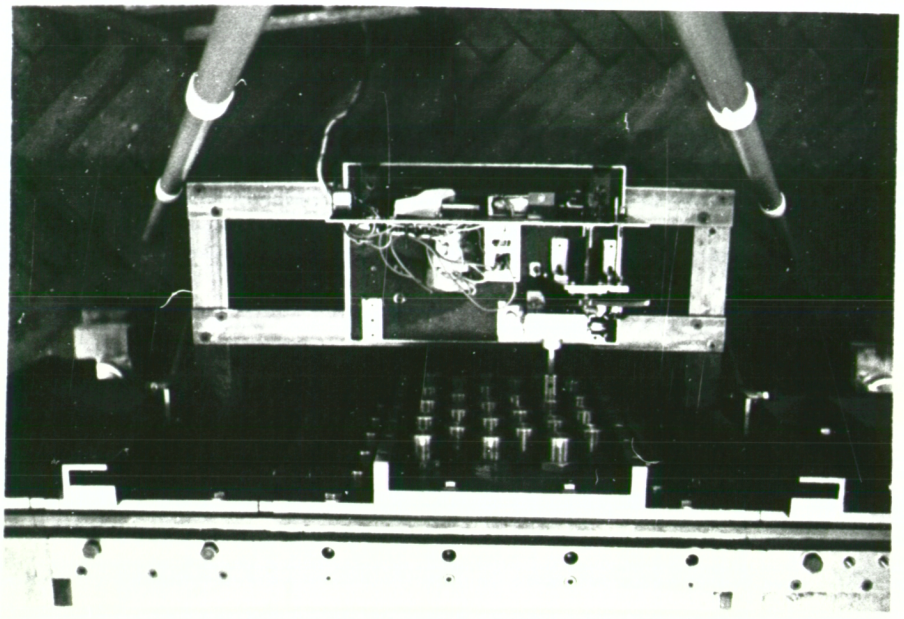

Plate 3.4 The drive mechanism for the rotating tube and the tube support structure

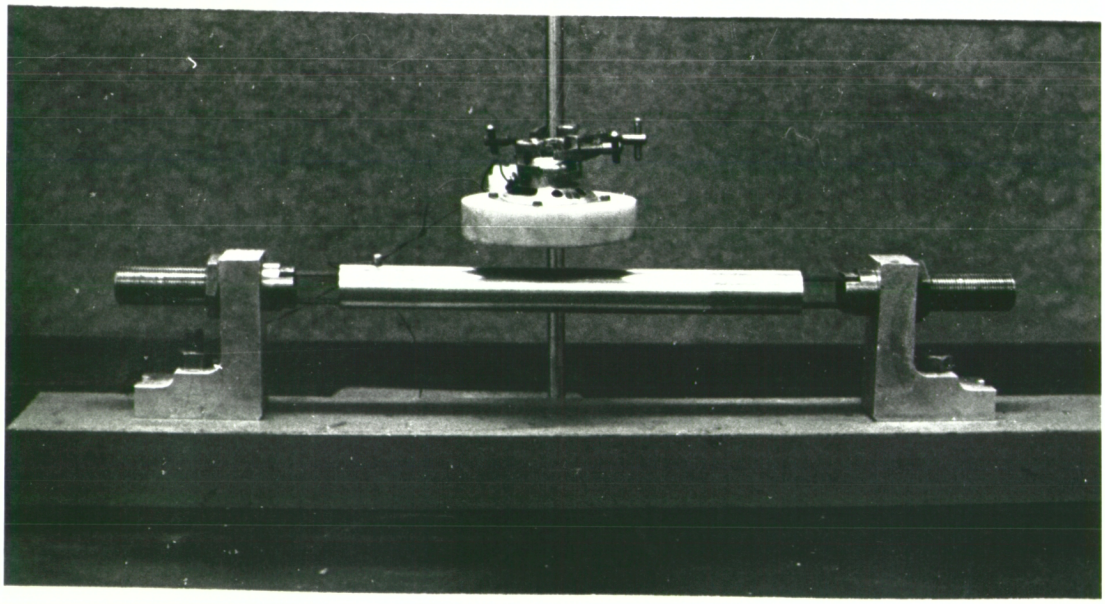

Plate 3.5 Experimental arrangement showing the measurement of resonance frequency and damping of a flexible tube

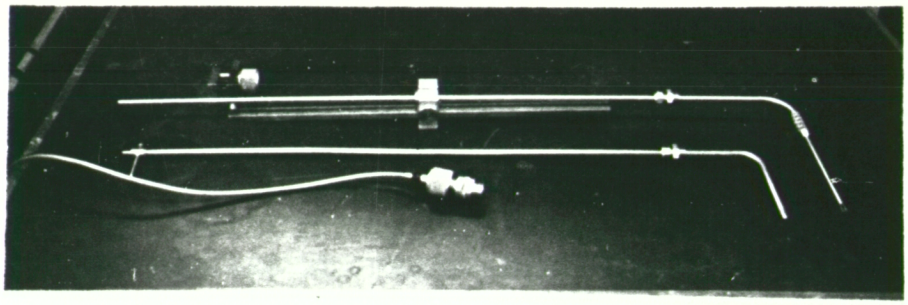

Plate 3.6 The hot wire, pitot static tube and microphone mountings

# CHAPTER 4

# INVESTIGATION OF A SINGLE ROW OF TUBES

## 4.1 Introduction

A series of experiments was carried out on a single row of fixed tubes, and on a row of fixed tubes with one flexibly mounted tube next to an instrumented, pressure measuring tube.

These experiments were performed in order to investigate the mechanisms by which the presence of a single vibrating tube, and also sound, affects the pressure distributions, and hence the forces, on a neighbouring tube. Although a tube in a single row of tubes is not representative of a tube in the middle of a large tube bank, it was thought that some of the mechanisms by which a vibrating tube interacts with a neighbouring tube would be similar in both situations.

## 4.2 General Description of the Experiments

The experiments were carried out in the wind tunnel described in Chapter 2, using the apparatus described in Chapter 3. Throughout the experiments great care was taken in calibrating transducers before each test run, and after each test run; the calibration was checked to make sure that there had been no change in the calibration factors of the instruments during the experiments. Many of the experiments were repeated several times to check the repeatability of the results and where this was impractical (during the measurement of pressure spectra) sufficiently long time histories of the signals were acquired so that statistically valid results could be obtained.

All the measurements of the fluctuating pressure and tube displacement signals, from which the pressure and displacement power spectra were calculated, were recorded on a calibrated four channel F.M. tape recorder. The tapes were then played back and the time histories of the signals acquired on the D.A.C. computer. The subsequent analysis of the data was carried out using the standard programme packages available on the system [4.15]. All the pressure power spectra were corrected by the appropriate microphone calibration factors so that power spectra density curves in $Pa^2\ Hz^{-1}$ were obtained.

During several of the experiments the pressure measuring tube was displaced from a uniformly spaced position between its two neigh-

bouring tubes. This was achieved by unscrewing the nuts of the pressure measuring tube and moving the tube to its new position in the slots in the supporting structure. Two precisely adjusted jacks which were placed between the measuring tube and the lower neighbouring tube defined the new position which was fixed by re-tightening the nuts. The jacks were then removed, and the relative displacements of the tubes checked using vernier calipers before proceeding with the experiments. The accuracy to which the pressure measuring tube could be defined was approximately $5 \times 10^{-3}$ of the tube diameter.

Block diagrams showing the configuration of the experimental apparatus are given in Figures 4.1a and 4.1b and the arrangement of uniformly spaced tubes in the working section is shown in Figure 4.2. Descriptions of the experiments carried out and the results and discussions are given in sections 4.3 to 4.11.

## 4.3 Average and Fluctuating Pressure Measurements Round the Circumference of a Tube

### 4.3.1 Experimental method

The time-averaged (referred to as static) and r.m.s. fluctuating pressure distributions round a tube were measured for different displacements of the pressure measuring tube from a uniformly spaced arrangement of tubes. A block diagram showing the configuration of the experimental apparatus is given in Figures 4.1a, and the details of the measurement procedure are given in section 3.16. These measurements were all carried out at a Reynolds number of approximately $1.2 \times 10^5$. (The Reynolds number was based on the maximum tube gap velocity for a symmetrical arrangement of tubes.) When the pressure measuring tube was displaced from its mean position it was always displaced towards the top of the working section.

The static and r.m.s. pressure coefficients were calculated and plotted as a function of angle from the direction of the oncoming flow. The components of average and fluctuating lift and drag were also calculated and plotted as a function of angle. The average lift and drag coefficients for the measuring tube were calculated by integrating the components of average lift and drag round the circumference of the tube. Estimates of the fluctuating lift and drag coefficients were made by integrating the components of fluctuating lift and drag round the tube assuming that the pressure fluctuations

round the circumference of the tube were uncorrelated.

The pressure coefficients were also measured at three different positions along the tube spanwise axis.

### 4.3.2 Aims of the experiments

The aim of this set of experiments was to investigate the effect of static tube displacement on the static and fluctuating pressure distributions round a tube. The form of variation of the lift and drag coefficients with static tube displacement was also to be investigated.

In some current theories for predicting the onset of fluid elastic instabilities in a single row of tubes it is assumed that the lift and drag on a tube are linear functions of static tube displacement [4.6]. The experiments were designed to verify whether these assumptions are valid when used in a quasi-static analysis for predicting the onset of fluid-elastic instabilities.

The variation of the pressure distribution along the axis of the tube was to be investigated to discover how important three dimensional effects are in influencing the forces on the tubes.

### 4.3.3 General description of the results for a row of fixed tubes

The static and r.m.s. pressure coefficient curves obtained by measuring the pressure round the circumference of the measuring tube in a row of fixed tubes vary considerably as the displacement of the pressure measuring tube from its mean position is changed. The general description and explanation of a typical result obtained at a measuring tube displacement of $x/d=0.1$ (Figure 4.3c) is given below.

From $0^{\circ}$ to $75^{\circ}$ the flow is accelerated through the gap between the tubes which causes the static pressure round the tube to drop with increasing angle. Near $80^{\circ}$ the laminar boundary layer on the tube separates which causes the static pressure to increase. Large fluctuating pressures associated with vortex shedding at the separation point produce a peak in the r.m.s. pressure curve indicating the approximate position of separation. After laminar separation has occurred the pressure on the surface of the tube increases up to an angle of $90^{\circ}$. The turbulent shear layer then re-attaches itself on the tube because of a favourable pressure gradient produced by the converging flow between the two separation shear layers in the gap

between the two tubes. The exact position of the re-attachment of the separated shear layer is not very well defined and probably fluctuates due to the movement of the separation point in the vortex shedding process. The turbulent boundary layer then separates between $130^{o}$ and $140^{o}$ and the static pressure rises. The turbulent separation point is indicated by a peak in the r.m.s. pressure curve. The pressure in the wake of the tube remains almost constant until the position of the turbulent separation point is reached on the other side of the tube. The turbulent and laminar separation points are at approximately $240^{o}$ and $280^{o}$ respectively. Before laminar separation the pressure coefficient drops as the fluid is accelerated through the gap between the tubes.

The Reynolds number at which the measurements were taken is approximately $1.2 \times 10^{5}$ which is in the critical flow regime, where the exact flow pattern and separation positions are influenced by the roughness of the tubes, gap geometry and turbulence through the gaps of the tubes. The r.m.s. pressure measurements give an indication of the position of separation and in the wake region the position of the peaks and their widths show whether the wake flow re-circulation regions are similar for different test runs.

### 4.3.4 Summary of results for a row of fixed tubes

Figures 4.3a-k show the static and r.m.s. pressure coefficients for a tube displaced in an entirely fixed row of tubes. Figures 4.6, 4.7 and 4.10, 4.11 show the average and r.m.s. lift and drag coefficients plotted against the non-dimensional displacement of the pressure measuring tube from a uniformly spaced position.

The major observations from the results are as follows:-

(i) As the tube displacement increases from x/d=0 to x/d=0.1 the change in pressure between laminar separation and turbulent re-attachment becomes larger.

(ii) The wake structure is almost symmetrical about a diametric line parallel to the oncoming flow when the measuring tube is not displaced. When the tube is displaced the wake structure loses its symmetry and becomes increasingly asymmetrical as the tube displacement is increased.

(iii) As the tube displacement is increased (i.e. the tube is moved towards the top of the working section) the stagnation point on the measuring tube moves round the tube towards the position

of the minimum gap. At a maximum displacement of x/d=0.7 the stagnation point moved 15° towards the minimum gap. The movement of the stagnation point causes the separation points to move round the tube. The movement of the separation points in general causes the negative average lift coefficient to increase with increasing tube displacement.

(iv) Above tube displacements of x/d=0.15 there is no evidence of the re-attachment of the turbulent boundary layer on the side of the tube in the smaller gap. Turbulent re-attachment occurs in the larger gap for all tube displacements and can be seen to reduce the wake pressure at the point of re-attachment.

(v) As the tube displacement is increased the pressures just before separation are decreased. There is also a decrease in the wake pressure which increases the drag at higher tube displacements.

(vi) Between displacements of x/d=0.3 and x/d=0.4 the position of the laminar separation point in the larger gap shifts towards the front of the tube. The turbulent re-attachment and separation points also change and the wake pressure at x/d=0.4 is lower than at x/d=0.3. The reduction in wake pressure is opposite to the general trend for the wake pressure to increase with increasing displacement. The change in the flow situation reduces the magnitude of the average lift coefficient from approximately 0.32 to 0.12 and the average drag coefficient from 1.62 to 1.50 as the displacement is increased from x/d=0.3 to x/d=0.4.

(vii) The average negative lift coefficient is not a linear function of tube displacement, and at displacements of less than x/d=0.25 its magnitude is less than 0.14. There is a change in flow regime between x/d=0.3 and x/d=0.4 so at x/d=0.4 the magnitude of the average lift coefficient decreases, but then increases above x/d=0.4 with increasing displacement.

(viii) The average drag coefficient is not a linear function of tube displacement and does not monotonically increase or decrease with tube displacement. At low tube displacements the drag decreases with increasing tube displacement but after x/d=0.4 the drag increases with increasing tube displacement.

(ix) The fluctuating lift coefficient decreases from approximately 0.374 at x/d=0 to a minimum of approximately 0.214 at x/d=0.6. The decrease in fluctuating lift with increasing tube displacement is approximately linear over the range x/d=0 to x/d=0.6. (The correlation coefficient for a least squares

fit is approximately 0.95)

(x) The fluctuating drag coefficient decreases with increasing tube displacement and can be approximated to a linear decrease with tube displacement from x/d=0 to x/d=0.6. (The correlation coefficient for a least squares fit is 0.90.)

### 4.3.5 Summary of results for a flexible tube mounted next to the pressure measuring tube

Figures 4.4a-h show the static and r.m.s. pressure coefficients for a tube displaced towards a vibrating flexible tube mounted in a fixed row of tubes. Figures 4.8,4.9,4.12 and 4.13 show the average and r.m.s. lift and drag coefficients plotted against the non-dimensional displacement of the pressure measuring tube from a uniformly spaced position.

The major observations are as follows:-

(i) At all tube displacements except x/d=0.7 there is evidence of laminar separation and turbulent re-attachment occurring on the side of the tube with the larger gap. There is no evidence of laminar separation and turbulent re-attachment on the side of the tube nearest the flexible tube (i.e. in the smaller gap) except at x/d=0.

(ii) The r.m.s. pressure coefficient curves for x/d=0 and 0.1 are very similar which implies that the wake structure is similar. There is a change in wake structure at x/d=0.2 which then remains similar up to displacements of x/d=0.4. The wake structure then changes significantly but looks similar for displacements between x/d=0.5 and x/d=0.7.

(iii) As the displacement is increased the stagnation point shifts round the tube towards the smaller gap. (At a displacement of x/d=0.7 the shift is $15^{o}$ from the front of the tube.) As the stagnation point moves the separation points on both sides of the tube shift so that the separation angles are decreased for increasing tube displacement.

(iv) The minimum pressures attained before laminar separation are very similar for all tube displacements and the static wake pressure does not change significantly for any of the tube displacements investigated.

(v) The static pressure coefficient curves are very similar for all the tube displacements investigated except that the

minimum pressure trough (associated with laminar separation on the side of the tube nearest the flexible tube) becomes narrower above x/d=0.3.

(vi) The average negative lift coefficient shows no obvious trend as the tube displacement is increased. The magnitude of the lift coefficient is always greater than 0.22 except at x/d=0 where it is approximately 0.12.

(vii) The variation in the drag coefficient with tube displacement is almost linear between x/d=0 and x/d=0.3. (The correlation coefficient for a least squares fit is 0.97.) There is a change in the trend at x/d=0.4 and at x/d=0.5 the drag increases almost linearly with increasing tube displacement.

(viii) The fluctuating lift coefficient in general decreases with increasing tube displacement. The change in fluctuating lift with tube displacement is not linear throughout the range and decreases most rapidly between x/d=0 and x/d=0.2.

(ix) The fluctuating drag coefficient decreases with increasing tube displacement from x/d=0 to x/d=0.2 and then remains almost constant till x/d=0.6.

### 4.3.6 The effects of the presence of a flexible vibrating tube

The differences between the pressure, lift and drag coefficients when a fixed tube next to the pressure measuring tube is replaced by a vibrating flexible tube are presented below.

(i) The presence of the flexible tube shifts the laminar separation points on both sides of the tube towards the rear of the tube (i.e. away from the stagnation point) for tube displacements between x/d=0 and x/d=0.4. Above displacements of x/d=0.4 the positions of the laminar separation points are the same when either a flexible or fixed tube is next to the pressure measuring tube.

(ii) The wake pressure is generally lower when a flexible tube is mounted next to the pressure measuring tube. This implies that the average drag on a tube mounted next to a flexible tube is generally higher than the average drag on a tube mounted next to a fixed tube, which is verified by reference to Figures 4.7 and 4.9.

(iii) The ratios of the minimum pressures at the separation points on different sides of the tube is greater when the tube is

mounted next to a flexible tube for displacements up to x/d=0.25. The magnitude of the average negative lift coefficient is therefore greater for a tube mounted next to a single flexible tube.

(iv) For tube displacements x/d=0 to x/d=0.5 the r.m.s. pressure coefficient has three major peaks in it after $180^{o}$ when the tube is mounted next to a flexible tube, whereas the r.m.s. pressure coefficient has only two major peaks when mounted next to a fixed tube. The wake structure on the side of the tube nearest the flexible tube is therefore different for x/d=0 to x/d=0.5 when a tube is mounted next to a flexible tube. The r.m.s. pressure coefficient curves for angles smaller than $180^{o}$ are very similar in shape when the pressure measuring tube is mounted next to a fixed or flexible tube. (Although the absolute magnitudes are not the same.) This implies that the wake structure on the side of the tube furthest away from the flexible tube is not greatly affected by the presence of a vibrating flexible tube. However the position of the separation points can be changed by the presence of a vibrating flexible tube which affects the boundary layers round its neighbouring tubes.

(v) The average lift coefficient for the pressure measuring tube next to the fixed tube varies from approximately 0 to -0.4 and its magnitude generally increases with increasing tube displacement except at x/d=0.4. The variation of the average lift coefficient when the tube is next to a flexible tube is not as great and varies from approximately -0.22 to -0.4. There is no general trend for the magnitude of the lift to increase with increasing tube displacement except between x/d=0 and x/d=0.1.

(vi) The variation in the average drag coefficient as the tube is displaced next to a flexible tube is from 1.58 to 1.70. When the tube is next to a fixed tube the average drag coefficient varies from approximately 1.42 to 1.66. The general trend of the variation of drag coefficient with tube displacement is similar for a tube mounted next to a fixed or flexible tube except between displacements of x/d=0.25 and x/d=0.4.

(vii) The fluctuating lift coefficient when the pressure measuring tube is next to a fixed tube is generally higher than when mounted next to a flexible tube. The variation of fluctuating

lift with tube displacement is more linear when the pressure measuring tube is mounted next to a fixed tube.

(viii) The fluctuating drag coefficient when the pressure measuring tube is next to a fixed tube is generally higher than when the tube is mounted next to a flexible tube. The largest decrease in fluctuating drag is between displacements of x/d=0 and x/d=0.2 when the tube is mounted next to a flexible tube, and the variation of fluctuating drag with displacement is linear. When the pressure measuring tube is mounted next to a fixed tube the variation of fluctuating drag is almost linear with displacement between x/d=0 and x/d=0.6.

### 4.3.7 Three dimensional flow effects

Figures 4.5a-c show the pressure coefficients measured round the measuring tube in a uniformly spaced row of tubes next to a flexible tube for positions at distances of 0d, 1d and 4d from the centre of the tube along its axis.

The static and r.m.s. pressure coefficients vary considerably along the axis of the tube. The position of the separation points, wake pressures and wake structure are different in all three cases. This shows that the flow varies considerably along the axis of a tube at a Reynolds number of approximately $1.2 \times 10^5$. In this flow regime, if the flow is to be correctly modelled in a theory, three dimensional effects have to be taken into account.

### 4.3.8 Comparison of results with previous investigations and current theories

Several investigators have measured the static pressure distribution round a tube in a tube bank. e.g. [4.1,4.2,4.3,4.18,4.22,4.23, 4.27]. However, none have measured the variation in static and r.m.s. pressure distribution as a tube is displaced in a tube row or tube bank. The results of Morsey [4.22] and Namork [4.23] are similar to the present investigation for a tube in the first row when the tubes are not displaced. However, no direct comparison of results can be made since the Reynolds numbers of their investigations were approximately $7 \times 10^4$ and the row geometry was different. Namork [4.23] observed double troughs in the static pressure coefficient curves near separation. These troughs are associated with laminar separation

and turbulent re-attachment and were observed in the present investigation.

Connors [4.13] measured the steady lift and drag on a tube in a single row of tubes when the measuring tube was effectively displaced in a direction both transverse and parallel to the oncoming flow. He found that the steady lift and drag forces varied linearly with tube displacements in the parallel and transverse flow directions respectively. He also found that a tube displacement in one direction only changes the force coefficient in the direction perpendicular to the displacement direction. Connors investigations were conducted with a tube spacing ratio of $D_T/d=1.41$ at a Reynolds number of approximately $8.8\times10^4$. The present investigations were carried out with a tube spacing ratio of $D_T/d=2.09$ at a Reynolds number of approximately $1.2\times10^5$. In the present investigation the steady or average lift and drag coefficients of the measuring tube were calculated by integrating the appropriate components of the pressure coefficient round the circumference of the tube. This does not give to total lift and drag forces on the whole length of the tube because the flow would have to be perfectly two dimensional which is not true. However the lift and drag coefficients of the centre of the tube were calculated and compared with Connors' results.

It was found that the variation of tube displacement in the direction transverse to the flow caused both the lift and drag coefficients to change. The changes in lift and drag were not linearly related to the displacement over the full ranges of displacement investigated. However, the drag varied nearly linearly for displacements $x/d=0$ to $x/d=0.15$ (least squares correlation coefficient $=0.83$) when the pressure measuring tube was next to a fixed tube. When the pressure measuring tube was mounted next to a vibrating flexible tube the drag varied almost linearly for displacements between $x/d=0$ and $x/d=0.3$ (least squares correlation coefficient $=0.97$). The slope of the drag versus displacement curves were approximately 0.28 and 0.34 for the fixed and flexible tube arrangement respectively which is higher than the 0.202 slope obtained by Connors. Connors uses his results to predict the onset of high amplitude tube vibrations due to a fluid-elastic instability. It is suggested that great care has to be taken in using the results of Connors to predict the onset of high amplitude tube vibrations since the experimental results of Connors which are used to fit the parameters in his theory are specific to the tube geometry and Reynolds numbers which he investigated.

Blevins [4.5] developed a theory for predicting the onset of fluid elastic instabilities in a single tube row when the fluid force coefficients and the variables characterising the tubes' vibration properties are known. Another analysis by Blevins [4.6] uses the Bernoulli equation (assuming flow separation occurs in the minimum gap between the tubes) to predict the fluid force coefficients on the tubes in a single row of tubes. In this analysis Blevins assumes that the force on a displaced tube is linearly related to the displacement. Using the experimental results of Connors [4.13] he assumes that the lift and drag forces are only related to tube displacements in the parallel and transverse flow directions respectively.

The theory developed by Blevins was compared against the lift and drag measurements carried out in the present investigation. The results are shown in Figures 4.7 and 4.9. It can be seen that there is very little agreement between the results of the present investigation and Blevins' theory. For fixed and flexible tubes the variation of drag coefficient in the present investigation does not agree with the variation in drag as predicted by Blevins' theory. The prediction of the variation of lift and drag coefficients with tube displacement by Blevins' theory for Connors' arrangement of tubes is compared with the experimental results of Connors in Figures 4.14 and 4.15 respectively. The slopes of the lift coefficient curves vary by 30% for the worst case, and the slope of the drag coefficient curve agrees to within 5% but the prediction of the absolute magnitude of the drag coefficient has a discrepancy greater than 10%.

It is therefore suggested that some of the assumptions made by Blevins in deriving his force coefficients on the tubes displaced in a single row are not valid, particularly at the Reynolds numbers investigated by the author. The assumption by Blevins that the position of separation occurs at a position in the minimum gap has been shown to be invalid for the present investigation since laminar separation occurs before the minimum gap and its position shifts with increasing tube displacement. The assumption that the lift and drag coefficients are only functions of tube displacements in the streamwise and transverse flow directions respectively is invalid for the situation investigated by the author.

## 4.4 P.S.D. Measurements of Pressure Round the Circumference of a Tube

### 4.4.1 Experimental method

The P.S.D. of the pressure was measured round the circumference of the pressure measuring tube using the signals from the electret microphones mounted in the measuring tube. This was carried out in a uniformly spaced arrangement of fixed tubes, and in an arrangement where the pressure measuring tube was displaced by 0.1 diameter from a uniformly spaced position. The experiment was also repeated in a uniformly spaced arrangement when one fixed tube next to the pressure measuring tube was replaced by a flexible tube instrumented for vibration measurement. The fluctuating displacement signal from the flexible tube was recorded simultaneously with the fluctuating pressure signal and the cross power spectral density and coherence between the pressure and displacement signals were calculated. Signals from a hot wire anemometer in the wake of pressure measuring tube and the flexible tube displacement signal were also recorded and the C.S.D. and coherence between wake velocity and tube displacement were calculated.

### 4.4.2 Aims of the experiment

The aim of these experiments was to investigate the nature of the pressure excitation spectrum to which the tube was subjected at different angles. The proportion of the aerodynamic pressures generated by vortex shedding fed back to the front of the tube could also be deduced.

When the flexible tube was placed next to the measuring tube the effect of a vibrating tube on the pressure excitation frequencies on a neighbouring tube could be investigated. The C.S.D. and coherence between the pressure displacement signals would show if there was any linear interaction between the vibrating tube and the pressure round its nearest neighbour.

The C.S.D. and coherence between the wake velocity signal and flexible tube displacement signal would show whether the vibration of the tube produces a fluctuating velocity at the maximum response frequency of the flexible tube in the wake of the neighbouring tube.

### 4.4.3 Presentation of P.S.D. measurements of pressure

Figures 4.16 to 4.18 show the variation of the P.S.D. of the pressure with angle round the tube for a fixed tube in a uniformly spaced fixed row, a fixed tube displaced by 0.1 tube diameter in a fixed row, and for a fixed tube mounted next to a flexible tube in a uniformly spaced fixed tube row, respectively. In the linear scaled figures the low frequency turbulence signals below 80 Hz were filtered out in order to 'highlight' the signals near the vortex shedding frequency, the first transverse duct cut on frequency, and the flexible tube resonant frequency, when presented on linear scales.

### 4.4.4 P.S.D. of pressure round a tube in a uniformly spaced fixed tube row

There are two main peaks in the pressure power spectra which correspond to the broad band vortex shedding peak at approximately 360 Hz and the 'sharp' first transverse hard-walled duct mode frequency peak at 425 Hz. At some angles there is a low amplitude peak at 414 Hz which may correspond to the first acoustic transverse duct mode in the region of the duct occupied by the tube row. The amplitude of the first transverse duct mode frequency peak is higher than the vortex shedding frequency peak at angles near the front of the tube. As the separation point is approached the vortex shedding peak increases in amplitude and becomes narrower until it becomes the largest peak at $80^{\circ}$ (near the separation point). After laminar separation at $100^{\circ}$ the vortex shedding peak is reduced in amplitude and broadened in frequency and the duct mode frequency peak increases in amplitude to become the largest peak. At $120^{\circ}$ the turbulent shear layer re-attaches and the vortex shedding peak increases in amplitude. Between $120^{\circ}$ and $140^{\circ}$ the turbulent boundary layer separates and at $140^{\circ}$ the vortex shedding peak and duct mode peak are both reduced in amplitude. In the wake the vortex shedding and duct mode peaks are both reduced and similar in amplitude. On the other side of the tube (i.e. at high angles) the vortex shedding peak again increases as the separation point is approached and becomes the dominant peak near the separation point between $260^{\circ}$ and $280^{\circ}$. The low frequency turbulence level increases from $0^{\circ}$ to $80^{\circ}$ and there is a peak in the turbulence at 180 Hz. This peak corresponds to half the vortex shedding frequency and is present in the spectra at all angles. The low

frequency turbulence reaches a maximum at separation and remains high in the wake where there is a turbulent recirculation region. Near the front of the tube (i.e. at low angles) there are peaks in the pressure power spectra which correspond to higher duct modal frequencies. These cannot be seen at higher angles because the level of the turbulence increases to a value greater than the amplitudes of the higher duct modes.

### 4.4.5 P.S.D. of pressure round a tube displaced by 0.1 diameter in a fixed tube row

When the tube is displaced by 0.1 diameter the behaviour of the pressure power spectra is the larger gap between the tubes (i.e. at low angles) is very similar to the undisplaced case. In the smaller gap at $280^{o}$ the vortex shedding frequency peak is present and two very closely spaced duct modes at 414 Hz and 425 Hz are also present. The power in the duct modal frequency peaks at the laminar separation point in the smaller gap is greater than the power at the vortex shedding frequency and only at the point of turbulent separation (near $140^{o}$) does the vortex shedding peak dominate. At the point of laminar separation the sub-harmonic vortex shedding peak at 180 Hz is three times the amplitude of the peak for the undisplaced tube.

### 4.4.6 P.S.D. of pressure round a tube next to a flexible tube in a uniformly spaced fixed tube row

In the gap further from the flexible tube the first transverse duct modal frequency dominates the spectra. The vortex shedding frequency peak increases as separation is approached but does not become the dominant peak as in the case of an entirely fixed row of tubes. In the gap nearest the flexible tube the vortex shedding peak is considerably broader than the peak when the tube is next to a fixed tube. The duct modal frequency peak in the smaller gap is broader in frequency but this is probably due to the merging of the 414 Hz and 425 Hz duct modal frequency peaks described previously in sections 4.4.4 and 4.4.5. The amplitudes of the vortex shedding peaks round the circumference of the tube are almost the same as when the tube is next to a fixed tube but the presence of the vibrating flexible tube increases the amplitudes of the duct mode pressures round the tube by factors of up to four.

### 4.4.7 Discussion of the acoustic interaction

The ratios of the mean square pressure at different angles round the circumference of the tube to the mean square pressure at $0^{o}$ (where the scattered power is theoretically zero) were theoretically calculated for the first transverse acoustic duct cut-on mode. The tube was in the same position in the duct as in the experiments. Scattering from the pressure measuring tube was taken into account, but scattering from nearest neighbours was considered to be a second order effect and hence was neglected. The relative amplitudes of the peaks in the P.S.D.'s of pressure at 425 Hz were measured as a function of angle for an entirely fixed row of tubes and with a flexible tube mounted next to the pressure measuring tube. The results compared with the theoretical curve are shown in Figure 4.19.

The acoustic pressures measured round the tube differ from the theoretically predicted pressure distribution, due simply to the scattering of the acoustic waves. It should be noted that there is a large difference in pressure variations between the case where the pressure measuring tube is mounted next to a fixed tube and when it is mounted next to a vibrating flexible tube. This would suggest that the acoustic interaction with the pressures in the boundary layer of the measuring tube is not entirely a direct linear interaction. This observation has also been made by Kacker and Hill [4.21]. The large difference in the pressure variations between the case where a fixed tube and the case where a flexible tube was mounted next to the pressure measuring tube indicates that the vibrating tube is affecting the flow round the measuring tube so as to change the degree of coupling of the acoustic pressure signal into the boundary layer of the tube. It is therefore postulated that the pressure fluctuations produced in the boundary layer of the tube due to the presence of an acoustic pressure field are not directly related to the magnitude of the acoustic field outside the boundary layer but some complex interaction mechanism is involved. The receptivity of the boundary layer to external acoustic pressure fluctuations is therefore a function of the exact nature of the flow around the tubes and the properties of the boundary layer.

Several investigators have theoretically analysed the effects of sound on a boundary layer particularly with respect to the excitation of instabilities; for a brief review see [4.4]. Very little experimental work has been carried out on the interaction of

sound with boundary layers in the regimes investigated by the author. A review on oscillating boundary layers is given in [4.14] and a general review of work carried out on unsteady boundary layers is given in [4.30].

Pressure spectra measurements were carried out round a single tube in cross-flow in [4.8]. However in the investigation there was no superimposed sound or duct resonance. Other investigations have measured pressure spectra at either one position in a tube bank, e.g. [4.17] or measured just the r.m.s. pressure as a function of angle e.g. [4.16, 4.21].

### 4.4.8 Interaction of a vibrating flexible tube with the pressure field round a neighbouring tube

Figures 4.20a-h show:-

(i) the P.S.D. of the pressure on the measuring tube,

(ii) the C.S.D. of the pressure on the measuring tube and the displacement signal of a neighbouring vibrating flexible tube,

(iii) the P.S.D. of the vibrating tube displacement signal,

(iv) the coherency function between the pressure and displacement signals.

The figures show the power spectra and coherency spectra for selected angles before separation and after separation on both sides of the tube and in the wake of the tube.

The coherency spectra have peaks at the vortex shedding frequency (360 Hz) and the first transverse duct cut-on frequency (425 Hz). The maximum values of the coherency are less than 0.5 implying that over half of the pressure excitation field on the pressure measuring tube, and also on flexible tube is uncorrelated at these frequencies.

The coherency at the maximum displacement response frequency of the flexible tube (285 Hz) is very low (<0.1) which implies that the vibration of the flexible tube has very little direct linear effect on the pressure field round a neighbouring tube. The velocity of the flexible tube at the maximum response frequency is approximately $4 \times 10^{-2}$ $ms^{-1}$ which is of the same order as the velocity fluctuations associated with the first transverse duct cut-on frequency. From the low value of the coherency at the flexible tube resonance frequency, it is postulated that the aerodynamic pressure and velocity fluctuations

created by the movement of the tube do not travel sufficiently large distances in the flow to be transmitted to the pressure measuring tube. However from Figures 4.16 and 4.18 it is apparent that the presence of a vibrating tube does change the flow field so as to change the nature of the pressure signal on a neighbouring tube. It is postulated that the interaction mechanism is affected by the mean flow field and turbulence levels in the mean flow which affect the transmission of the pressure fluctuations from the mean flow into the boundary layer.

The peak in the coherency spectra at the vortex shedding frequency is due to a partially common pressure field round the flexible and pressure measuring tubes produced by vortex shedding from the tubes.

The peak in the coherency spectra at the first transverse duct cut-on frequency is due to excitation of both the flexible and pressure measuring tubes by a common coherent acoustic field.

The coherency at the vortex shedding frequency at the front of the tube ($0^{o}$) is higher than at any other angle. This is because the vortex shedding frequency component of the pressure field is larger compared to the turbulence at the front of the tube. At angles further round the tube the turbulence levels increase so the relative contribution of the vortex shedding process to the excitation flow field is less than the turbulent contribution.

### 4.4.9 Interaction of a vibrating flexible tube with the wake of a neighbouring tube

Figures 4.21 i-iv show:-

(i) the P.S.D. of the velocity fluctuations in the wake of the pressure measuring tube,

(ii) the C.S.D. of the wake velocity fluctuations and the vibrating tube displacement signal,

(iii) the P.S.D. of the vibrating tube displacement signal,

(iv) the coherency between the displacement and wake velocity signals.

The peak in the coherency spectrum at 180 Hz corresponds to the common excitation of the flexible tube and the wake flow at half the vortex shedding frequency by a partially common flow field. Exact measurements show that the coherency at the maximum response frequency of the flexible tube is low (<0.1). This implies that the

vibration of the flexible tube has very little direct linear effect on the velocity fluctuations in the wake of a neighbouring tube.

## 4.5 P.S.D. Measurements of Pressure as a Function of Static Tube Displacement

### 4.5.1 Experimental method

The fluctuating pressure signals were measured at angles $0^{\circ}$, $90^{\circ}$, $180^{\circ}$ and $270^{\circ}$ for different static displacements of the pressure measuring tube from a uniformly spaced position next to a neighbouring flexible tube in a fixed row of tubes. The displacement signal from the flexible tube was simultaneously measured with the pressure signal and the P.S.D.'s of pressure and displacement were calculated. The C.S.D. and coherency between the displacement and pressure signals were also calculated for the maximum and minimum pressure measuring tube displacements.

### 4.5.2 Aims of the experiments

The aim of the experiments was to investigate the change in the pressure fluctuations acting on a tube as a function of static tube displacement. The experiment shows the effect of the proximity of a neighbouring vibrating tube on the exciting pressures on the measuring tube and also the effect of the proximity of a neighbouring fixed tube on the vibration characteristics of a flexible tube.

In current theoretical models for large tube vibrations, the variation of the pressure spectrum exciting a tube due to the changing fluid dynamic field as a tube is displaced is not taken into account. These experiments show the importance of the change in exciting pressure fluctuations as a tube is displaced.

### 4.5.3 Variation of P.S.D. of pressure on the measuring tube with static displacement of the measuring tube

Figures 4.22 a-d(i)-(ii) show the variation of the P.S.D. of pressure round the measuring tube with static displacement of the measuring tube from a uniformly spaced position towards a flexible moving tube at angles of $0^{\circ}$, $90^{\circ}$, $180^{\circ}$ and $270^{\circ}$ respectively. Frequencies below 80 Hz were filtered out in order to 'highlight' the vortex shedding

peaks when plotted on a linear scale.

At all angles the amplitude of the vortex shedding peak decreases and the peak is broadened in frequency as the displacement of the measuring tube is increased. In general as the measuring tube displacement is increased the amplitude of the duct acoustic modal frequency decreases. This is because as the displacement of the tube is increased the tube is moved towards the acoustic pressure node at the centre of the duct.

When the measuring tube is displaced towards the flexible tube the vortex shedding frequency varies and at some displacements two distinct vortex shedding frequencies are present. This is due to the different flow speeds and conditions at opposite sides of the tube which produces two stable vortex shedding modes.

In the wake of the tube at $180^{o}$ there are large amplitude peaks at half the vortex shedding frequency for all tube displacements. As the tube displacement is increased the fundamental vortex shedding peak reduces in amplitude and frequency but the subharmonic vortex shedding peak (i.e. a frequency of half the vortex shedding frequency) stays at approximately the same amplitude.

As the tube is moved towards the flexible tube the level of the turbulence throughout the frequency spectrum increases and at the maximum displacement of x/d=0.7 the general level of turbulence is the same amplitude as the vortex shedding peak.

At the front of the tube ($0^{o}$) there are very low levels of turbulence at all tube displacements and there is no subharmonic of the vortex shedding frequency present.

Near the laminar separation points at $90^{o}$ and $270^{o}$ there is a peak in the spectrum at a frequency between 140 Hz and 155 Hz at all tube displacements greater than x/d=0. These peaks are not simple integer subharmonics of the vortex shedding frequency peaks which lie between 350 Hz and 400 Hz. The mechanism for the generation of the pressure fluctuations between 140 Hz and 150 Hz has not been established but could be associated with vortex coalescence in the wakes of the tubes.

### 4.5.4 Variation of the amplitude probability distribution of pressure with static displacement of the measuring tube

Figures 4.23a-d show the variation of the amplitude probability

distribution of pressure with static displacement of the measuring tube at angles of $0^{o}$,$90^{o}$,$180^{o}$ and $270^{o}$.

At $0^{o}$ the probability distributions are triangular in shape with some small peaks superimposed on the general distribution curve. This corresponds to a distribution function of a process involving the superposition of several independent Gaussian processes with some superimposed narrowband processes, see [4.20]. This implies that the total pressure excitation at $0^{o}$ consists of several independent pressure excitation sources, i.e. vortex shedding and acoustic excitation by duct modes.

At $90^{o}$ the pressure fluctuations are larger which broadens the probability distribution peaks. There are several small peaks superimposed on the distribution curve which are produced by low amplitude narrowband processes corresponding to the pressure excitation by duct modes.

In the wake at $180^{o}$ the broadband turbulence increases with increasing tube displacement which broadens the pressure probability distribution curves at large displacements. At lower pressure values superimposed small peaks corresponding to duct mode pressure excitations are again present.

At $270^{o}$ in the gap nearest the flexible tube the fluctuating pressure levels at tube displacements of x/d=0 and x/d=0.1 are approximately double the values at other displacements. At x/d=0 there is little evidence of narrowband pressure excitation at low amplitudes but at high amplitudes there is a peak at one side of the probability distribution curve. This peak corresponds to a narrow band excitation process at high amplitude which can be seen as a high level duct modal frequency in Figure 4.22d(i).

### 4.5.5 Variation of the P.S.D. of the flexible tube displacement with pressure measuring tube static displacement

Figures 4.24(i)-(ii) show the variation of the P.S.D. of the flexible tube displacement with the pressure measuring tube static displacement.

The flexible tube maximum displacement response peak at the tube rigid body frequency is always a factor of 10 greater than any other response peak (neglecting very low frequency vibration). The response of the flexible tube displacement is a maximum at a pressure measuring tube displacement of x/d=0 and remains approximately constant

at higher measuring tube displacements.

Figure 4.25 shows the r.m.s. displacement of the flexible tube plotted against the static displacement of the measuring tube. The r.m.s. displacement in general decreases with increasing measuring tube displacement from the mean position. Therefore the presence of a fixed tube next to a vibrating tube does not increase the vibrating tube's amplitude.

### 4.5.6 Variation of the amplitude probability distribution of flexible tube displacement with static tube displacement

Figure 4.26 shows the amplitude probability distribution functions of the flexible tube displacement signal plotted against the static displacement of the pressure measuring tube.

The probability distribution curves are all Gaussian in shape which implies that the tube is responding to an excitation of a broad band signal. (In general when a linear system or a combination of linear systems responds to a broad band excitation process, even if it is not Gaussian, the response of the system is Gaussian.)

### 4.5.7 Interaction of a vibrating flexible tube with the pressure field round a neighbouring tube

Section 4.4.8 has shown that there is very little direct linear interaction between a vibrating tube and the pressure field round its neighbour when the tubes are separated by approximately 1.09 diameters.

Figures 4.27a-d(i)-(iv) show for angles of $0^{\circ}$, $90^{\circ}$, $180^{\circ}$ and $270^{\circ}$:

(i) the P.S.D. of the pressure on the measuring tube,

(ii) the C.S.D. between the pressure on the measuring tube and the vibrating tube displacement signal,

(iii) the P.S.D. of the tube displacement signal,

(iv) the coherency between the pressure on the measuring tube and the flexible tube displacement signal,

when the separation between the pressure measuring tube and the flexible tube is approximately 0.39 diameters.

The coherency at the frequency of the maximum response peak of the flexible tube is less than 0.1 showing that when a vibrating tube is less than half a diameter from a neighbouring tube there is very little direct linear interaction between the vibrating tube and

the pressure field round its neighbour when the tube has an r.m.s. displacement of 30 μm. At higher amplitudes of tube vibration it is expected that there will be a linear interaction but it was beyond the scope of the present experiments to investigate this.

## 4.6 P.S.D. Measurements of Pressure and Coherency along the Spanwise Axis of a Tube

### 4.6.1 Experimental method

The fluctuating pressure signals were measured simultaneously at three different stations separated by 1,3 and 4 diameters along the axis of the pressure measuring tube, when an instrumented flexible tube was mounted next to the pressure measuring tube. These measurements were carried out at angles of $0^{\circ}$,$90^{\circ}$, $180^{\circ}$ and $270^{\circ}$ with the tubes in a uniformly spaced arrangement. The P.S.D. of the pressure signals, C.S.D. of the different pressure signals and coherency between the different stations were calculated.

### 4.6.2 Aims of the experiment

The experiment was carried out to determine the levels of coherency of the fluctuating excitation pressures along the spanwise axis of the tube. The degree of coherency of the exciting pressure forces affects the total excitation force on the tube and hence the vibration amplitude of the tube.

### 4.6.3 Experimental results

Figures 4.28-4.30 show the P.S.D.'s of the pressure signals, the C.S.D. of the pressure signals and the coherency between the pressures measured at different positions along the spanwise axis of the tube. Figures 4.31a-b show the values of the coherency at the vortex shedding frequency and the first transverse duct cut on modal frequency plotted against the separation along the spanwise tube axis.

The coherency at the vortex shedding frequency is the highest at the front of the tube ($0^{\circ}$) and lowest in the wake ($180^{\circ}$). The coherency near the separation point on the side of the tube nearest the flexible tube ($270^{\circ}$) is higher than at the separation point on the opposite side of the tube ($90^{\circ}$). This suggests that the

vibrating tube does not disrupt the vortex shedding process. However it cannot be assumed that the higher coherency at 270° implies that the action of the vibrating tube directly increases the coherency of the pressure along the spanwise axis of it's neighbouring tube because it has already been shown in sections 4.4 and 4.5 that the tube vibrating does not directly influence the pressure fluctuations round a neighbouring tube. If there was a direct linear interaction between the vibration of the flexible tube and the pressure field at 270° on the measuring tube the coherency along the spanwise axis of the measuring tube would be high at the tube rigid body modal frequency. The coherency would not be expected to vary much with increasing separation between measuring stations since the whole length of the tube would be subjected to coherent pressure fluctuations created by the vibrating tube. The variation of the coherency with separation distance at 270° implies that this is not the case. The coherency between measuring stations separated by 4 tube diameters at the first duct modal frequency is greater than 0.95 at 0°. This is because the pressure fluctuations due to the duct excitation frequency are much greater than the turbulence pressure levels at the front of the tube.

In the wake of the tube the coherency between different measuring stations decreases only slightly with increasing separation. This is because the turbulent pressure fluctuations at the same frequency as the duct modal frequency are only coherent over very short spanwise distances in the wake so the only significant coherent pressure fluctuations are due to the acoustic duct mode, which has a coherency unity in the spanwise direction. The total contribution to the wake signal is therefore a random turbulent pressure fluctuation with low spanwise coherency and a highly coherent duct acoustic pressure fluctuation.

At angles near separation (90° and 270°) the coherency at axial spacings of one diameter is greater than twice the value at 3 tube diameters. This implies that the turbulent pressure fluctuations at the same frequency as the duct modal frequency have a high spanwise coherency at spacings of 1 diameter but at larger spacings the coherency of the turbulent pressure fluctuations decrease.

The correlation lengths of the pressure fluctuations at different angles were obtained by extrapolating the curves of coherency plotted against spanwise spacing and integrating. At the vortex shedding frequency the correlation lengths at angles of 0°,90°180° and 270° are 3.7, 2.6, 1.3 and 3.2 respectively. At the first transverse duct cut-on frequency the correlation length is very large (>20) at

$0^{o}$,$90^{o}$ and $180^{o}$ and at $270^{o}$ lies between 3 and 4 diameters.

Figure 4.32 shows the broadband correlation coefficient at zero time delay plotted against the spanwise spacing. The correlation length is the greatest at $0^{o}$ and the smallest in the wake of the tube. The correlation lengths, at $0^{o}$,$90^{o}$,$180^{o}$ and $270^{o}$ are 2.9,1.7,2.6 and 1.2 diameters respectively.

### 4.6.4 Comparison with previous results

Several investigators have measured broadband correlation lengths along single cylinders in a low turbulence flow. A summary of the results at $90^{o}$ round the tube from the stagnation point is given in [4.8]. The results of Bruun and Davies [4.8] and Toebes [4.31] are shown plotted in Figure 4.32 with the results of the present investigation. Previous investigators measured the broadband correlation coefficients along the spanwise axis of a single tube in crossflow. The results cannot be compared directly since the Reynolds numbers were not exactly the same. However the correlation length measured by Bruun and Davies at a Reynolds number of $2.4 \times 10^{5}$ is very similar to the present investigations. The correlation coefficients obtained in the present investigation are lower at one diameter spacing and higher at three diameters spacing.

## 4.7 P.S.D. Measurements of Pressure and Displacement as a Function of Flow Velocity

### 4.7.1 Experimental method

The pressure signal at an angle of $0^{o}$ on the pressure measuring tube was measured simultaneously with the displacement signal from a flexible tube which was mounted next to the pressure measuring tube in a uniformly spaced fixed tube row. The P.S.D.'s of the pressure and displacement signals were calculated, as well as the amplitude probability distributions of pressure and displacement. The coherency between the pressure and displacement signals was calculated for the conditions where the vortex shedding frequency was below resonance, near resonance and above the resonance frequency of the flexible tube rigid body mode.

### 4.7.2 Aims of the experiment

The experiment was carried out to investigate the effect of different flow velocities on the pressures produced by vortex shedding, and the effect of varying the flow velocity on the flexible tube vibration amplitudes.

### 4.7.3 Variation in the pressure fluctuations with flow velocity

Figures 4.33(i)-(ii) show the P.S.D. of the pressure fluctuations at the stagnation point on the measuring tube ($0^{o}$) plotted against the free stream flow velocity. Figure 4.34 shows the frequency of the vortex shedding peak plotted against the free stream flow velocity.

At low flow velocities the excitation pressure is very small compared to the pressure at the maximum flow velocity and has a peak at the vortex shedding frequency corresponding to a Strouhal number of 0.168 based on minimum gap velocity. At 23 $ms^{-1}$ a large peak at a frequency of half the vortex shedding frequency is present in the spectrum and corresponds to a Strouhal number excitation at 0.083 based on minimum gap velocity. When the flow velocity is increased the pressure fluctuations at the fundamental vortex shedding frequency increase in amplitude and frequency until there is sufficient energy at the frequency of the first transverse duct cut-on mode to excite the mode. This occurs at approximately 32 $ms^{-1}$. As the flow velocity is further increased the vortex shedding energy (i.e. pressure fluctuations at the vortex shedding frequency) at the frequency of the duct mode increases and so the amplitude of the excited mode increases.

At some point the feedback of energy from the transverse duct acoustic pressure fluctuations enhances the exciting pressure fluctuations in the boundary layer of the tube so that the amplitude of the duct mode becomes very large and dominates the excitation pressures at all other frequencies in the spectrum. At flow velocities above 30 $ms^{-1}$ a second higher frequency duct mode is excited.

It is postulated that the peak in the exciting pressure spectrum at the vortex shedding frequency does not have to be coincident with the frequency of the duct mode to obtain positive feedback into the boundary layer. The only requirement to excite a very strong duct mode is to have sufficiently large pressure fluctuations at the duct mode

frequency to excite a strong enough mode to overcome the losses in transferring the acoustic pressure fluctuations into the tube boundary layer to establish a positive feedback path with a gain greater than unity. Hence this effect is different from the vortex duct mode 'lock in' phenomena as described by many investigators, e.g. Hill [4.19]. In the 'lock in' phenomena the frequency of the vortex shedding peak shifts to the duct mode frequency when the vortex shedding frequency is sufficiently close to the duct mode frequency. This effect produces a high amplitude duct mode by a positive feedback mechanism. In the present investigation there was no evidence of the 'lock in' phenomena since the vortex shedding frequency occurred at a constant Strouhal number of 0.168 throughout the flow velocity range investigated. However, if the duct mode became sufficiently strong the 'lock in' phenomenom would probably occur.

Figure 4.35 shows the variation of the amplitude probability distribution of pressure at $0^{o}$ on the measuring tube with flow velocity. The probability distribution curve is Gaussian in shape showing that the pressure excitation is broadband in nature.

### 4.7.4 Variation in the flexible tube displacement with flow velocity

Figures 4.36(i)-(iii) show the P.S.D. of the flexible tube displacement signal plotted against the free stream flow velocity.

The maximum peak in the displacement spectrum is at the constant frequency of the tube rigid body mode at flow speeds above 18 $ms^{-1}$. Below 18 $ms^{-1}$ there is very little pressure excitation energy at the resonance frequency of the tube (i.e. rigid body mode) and the off resonance excitation at the vortex shedding frequency is the dominant excitation pressure exerted on the tube. The peak displacement response of the tube is therefore at the vortex shedding frequency. As the vortex shedding frequency approaches the tube resonance frequency the tube displacement increases until it reaches a maximum at the vortex shedding frequency. Above the vortex shedding frequency the tube displacement decreases.

Figures 4.37 and 4.38 show the amplitude probability distribution and the peak probability distribution of the flexible tube displacement signal.

At the same flow velocities the peak probability distribution function has two peaks which implies that the displacement signal is

modulated by a narrowband signal. This occurs when the pressure excitation to the measuring tube contains large pressure fluctuations at half the vortex shedding frequency. It is postulated that some form of beating phenomena is being observed.

### 4.7.5 Variation of r.m.s. pressure and r.m.s. displacement with flow velocity

Figure 4.39 shows the r.m.s. pressure fluctuations exerted on the measuring tube at $0^{o}$ and the r.m.s. displacement of the flexible tube plotted against flow velocity.

The r.m.s. pressure exerted on the tube increases from 0 $ms^{-1}$ to 20 $ms^{-1}$ in proportion to the free stream dynamic pressure. (i.e. in proportion to the square of the flow velocity) when the subharmonic of the vortex shedding frequency appears in the spectrum the r.m.s. pressure increases very rapidly to a peak at approximately 23 $ms^{-1}$. As the subharmonic decreases in amplitude with increasing flow velocity the r.m.s. pressure decreases. At 26 $ms^{-1}$ the r.m.s. pressure again increases in proportion to the free stream dynamic pressure.

The flexible tube r.m.s. displacement remains below 20 μm up to flow velocities of 18 $ms^{-1}$. The displacement of the flexible tube then increases rapidly as the vortex shedding frequency approaches the frequency of the flexible tube rigid body modal frequency. Above the tube resonance frequency the r.m.s. displacement decreases with increasing flow velocity. The maximum tube r.m.s. response was below 300 μm which is less than 0.01 of a tube diameter.

### 4.7.6 Comparison with other investigations

Other investigators have measured r.m.s. tube displacement as a function of flow velocity during the course of investigations, mainly into the onset of large amplitude fluid elastic instabilities in tube banks, e.g. [4.7, 4.10, 4.11, 4.12, 4.25, 4.28, 4.29, 4.32, 4.33, 4.34, and 4.35]. However because there are so many variables in the tube dynamic parameters, flow parameters and geometric parameters there are no results available to the author for exact comparison. However the general form of the results is in agreement with the results of much of the previous work.

A thorough investigation into the pressure spectra and tube vibration spectra at different flow speeds has not been carried out

previously, to the author's knowledge.

The present investigation has been carried out for one special case but has shown the effects of broadband turbulence and vortex shedding on the spectrum of the displacement of a tube vibrating in a single tube row.

## 4.8 Measurement of the Effect of Sound on the Pressure Round a Tube and on the Vibration Response of a Flexible Tube

### 4.8.1 Experimental method

The static and r.m.s. pressure distributions were measured round a tube in a uniformly spaced arrangement of fixed tubes when the measuring tube was next to a flexible tube. This was carried out without superimposed sound and with sound superimposed at a frequency of 425 Hz and average SPL of 138 dB, and at a frequency of 360 Hz and average SPL of 136 dB. i.e. the first transverse duct cut-on frequency and the vortex shedding frequency respectively.

The fluctuating pressure signals at an angle of $0^{o}$ on the pressure measuring tube and the displacement signals of the flexible tube were measured without sound excitation and when the sound excitation frequencies and levels were;

(i) 285 Hz (the flexible tube resonant frequency) at 130 dB,

(ii) 360 Hz (the vortex shedding frequency) at 136 dB,

(iii) 425 Hz (the first transverse duct cut-on frequency) at 138 dB.

The P.S.D.'s of the pressure and displacement signals and the C.S.D.'s and coherencies between the pressure and displacement signals were calculated. The amplitude probability distributions of the fluctuating pressure and the flexible tube displacement signals were also calculated.

### 4.8.2 Aims of the experiment

The static and r.m.s. pressure distributions were measured round the tube with and without superimposed sound to see if sound has any effect on the mean flow round the tube and on the amplitude of the fluctuating pressures round the tube.

The P.S.D.'s, C.S.D.'s and coherencies of the pressure and displacement signals were calculated to investigate the effect of superimposed sound on the mean flow which could change the pressure

excitation levels on the tubes and hence change their displacement levels. The effect of sound on the interaction of a vibrating tube with the pressure field on a neighbouring tube was also to be investigated using the calculated coherency spectra. The amplitude probability distribution functions of pressure and displacement were calculated to investigate the effect of sound on the statistics of the exciting pressure signal and on the statistics of the flexible vibrating tube response.

### 4.8.3 Variation of the static and r.m.s. pressure distribution round a tube with superimposed sound

Figures 4.40(i)-(iii) show the static and r.m.s. pressure distributions measured round a tube in an uniformly spaced row when the pressure measuring tube is next to a flexible tube for the cases:

(i) without sound,

(ii) with superimposed sound at 425 Hz and a SPL of 138 dB,

(iii) with superimposed sound at 360 Hz and a SPL of 136 dB

respectively.

The static pressure distributions for all three cases investigated are all very similar and the lift and drag are the same within experimental error. The r.m.s. pressure coefficient distributions are very similar for all the cases investigated except near the front of the tube where levels are higher when the sound is present. The effect of sound is therefore to increase the r.m.s. pressure fluctuations on the tubes. However, this does not have any noticeable effect on the static pressure distributions, position of separation points, lift and drag, so it can be deduced that sound at the frequencies and levels investigated does not significantly affect the tube boundary layer so as to change the mean flow.

### 4.8.4 The effect of sound on the fluctuating pressure and displacement signals

Figures 4.41a-d(i)-(iv) show;

(i) the P.S.D. of the fluctuating pressure on the pressure measuring tube at the stagnation point,

(ii) the C.S.D. of the vibrating tube, displacement and the pressure on the pressure measuring tube at stagnation,

(iii) the P.S.D. of the fluctuating displacement of the vibrating

tube,

(iv) the coherency between the pressure and displacement signals for: (a) no sound,

(b) sound at 285 Hz and a SPL of 130 dB,

(c) sound at 360 Hz and a SPL of 134 dB,

(d) sound at 425 Hz and a SPL of 138 dB.

The imposition of sound significantly increases the vibration amplitude of the flexible tube at the rigid body modal frequency (285 Hz). There is negligible effect on the tube vibration amplitude at the frequency of the imposed sound (except when the imposed sound is at 285 Hz). It is postulated that the effect of the superimposed sound is to increase the general level of broadband pressure fluctuations in the boundary layers of the tubes by a non-linear interaction. The increased pressure fluctuations then produce an increased displacement response of the tube which is only noticeable near the resonance frequency of the tube.

Through a non-linear mechanism, the imposition of sound causes high order duct modes to be excited, some of which have amplitudes greater than the first transverse duct mode. The fluctuating pressures due to the duct modes increases the displacement of the flexible tube at the frequency of the acoustic mode and high values of coherency between the pressure and displacement signals at the duct modal frequencies imply this is a linear interaction. It is postulated that the sound interacts with the boundary layer flow of the tubes by a non-linear mechanism to increase the broadband pressure fluctuations. The increased pressure fluctuations at the frequencies of the duct modes then excite the modes to produce the peaks in Figures 4.41b-d. Figures 4.42a-d and 4.43a-d show the probability distribution of the flexible tube displacement signal and the probability distribution of the pressure signal respectively measured at $0^{o}$ on the pressure measuring tube for:

(a) no sound,

(b) sound at 285 Hz and a SPL of 130 dB,

(c) sound at 360 Hz and a SPL of 134 dB,

(d) sound at 425 Hz and a SPL of 138 dB.

The amplitude probability distributions of the flexible tube displacement signals are all gaussian in shape. The effect of sound on the distribution of displacement amplitude can be clearly seen as an increase in the standard deviation of the distribution functions.

The amplitude probability distributions of the pressure signals

at $0^{o}$ on the pressure measuring tube are flat topped with many small peaks superimposed on them when the superimposed sound is present. This suggests that the pressure fluctuations consist of the superposition of several independent Gaussian pressure excitation processes with superimposed narrowband pressure excitation processes, i.e. broadband turbulence, vortex shedding processes and duct modal excitation frequencies.

### 4.8.5 Comparison with other investigations

Kacker and Hill [4.21] investigated the effect of sound on vortex shedding from a single cylinder in a duct at Reynolds numbers of $8.2 \times 10^{4}$. In the investigation the locking of the vortex shedding frequency on to the frequency of the exciting sound field was found to occur at levels greater than approximately 135 dB. They found that the effect of the sound field could not be totally accounted for by a direct acoustic interaction which is in agreement with the results of section 4.8.4.

Kacker and Hill found that sound excitation at a level of 145.7 db SPL and a frequency of 2.6% lower than the vortex shedding frequency increased the static wake pressure coefficient by approximately 0.2. This increased the drag on the tube by approximately 30%. In the present investigation the levels of sound used in the experiments were lower than those used by Kacker and Hill and there was no evidence of the sound interacting with the boundary layer of the tube so as to change the position of separation which affects the mean flow, wake pressure and drag on the tube.

Okamoto et al [4.24] investigated the effects of sound on vortex shedding from a cylinder at Reynolds numbers of up to 4500. However, the major part of the investigation was into the laminar-turbulent transition wave excitation, in the boundary layer of the tube by the imposition of an external sound field. The frequency of the laminar-turbulent transition wave in the boundary layer of the tube in the present investigation is well above the frequency range of interest. Both Kacker and Hill and Okamato et al found that the static wake pressure was decreased by the imposition of sound at levels greater than 140 dB. In the present investigation the vortex shedding duct mode 'lock in' phenomenon was not investigated since current design methods in heat exchanges avoid using ducts with modal frequencies

near the vortex shedding frequency of the tubes or use baffles to reduce the acoustic resonances in the heat exchanger duct.

## 4.9 Measurement of the Relative Phase of the Vortex Shedding Mode as a Function of Angle round the Tube

### 4.9.1 Experimental method

The cross-correlation function between the fluctuating pressure measured round the tube and a hot wire anemometer velocity signal from a probe in a fixed wake position was calculated using a Hewlett Packard correlator type 3721A.

The periodicity in the cross-correlation function corresponded to the period of vortex shedding so that peaks in the cross-correlation function corresponded to the maximum correlation at the vortex shedding frequency. The relative phases of the signals at different angles were calculated from measurements of the delay times of the peaks in the cross-correlation function from the zero time axis. The phases relative to zero phase at the stagnation point on the tube were then calculated as a function of angle round the pressure measuring tube.

### 4.9.2 Aims of the experiment

The total pressure excitation force on a tube at a dominant excitation frequency is dependent on the phase relationship of the force round a tube. These experiments were therefore carried out to investigate the phase relationship of the vortex shedding frequency (i.e. the dominant excitation) round the tube which could give some indication of the total force likely to be experienced by a tube from which vortex shedding was taking place.

### 4.9.3 Experimental results and discussion

Figures 4.44(i)-(iii) show the variation of phase of the vortex shedding pressure fluctuations round the pressure measuring tube in:

(i) a uniformly spaced arrangement of fixed tubes,

(ii) a fixed row of tubes with pressure measuring tube displaced by 0.1 diameter,

(iii) a uniformly spaced arrangement of a fixed row of tubes with a flexible tube mounted next to the pressure measuring

The variation of phase of the vortex shedding frequency with angle round the tube varies considerably between the different configurations investigated. The phase at small angles changes slowly with angle for the uniformly spaced arrangement of tubes but when the tube is displaced by 0.1 diameter there is a rapid phase variation with angle at small angles.

It is postulated that the phase of the pressure fluctuations at the vortex shedding frequency depends on the mechanism by which the pressure fluctuations are transmitted through the boundary layer and the parameters of the boundary layer on the tube. The results imply that the exact flow configuration outside the boundary layer must influence the phase of the pressure variations at the vortex shedding frequency inside the boundary layer, since the replacement of a fixed tube by a flexible tube only indirectly effects the boundary layer on the pressure measuring tube by interaction with the mean flow. The results of the investigation imply that it is difficult to predict the phase of the pressure fluctuations at the vortex shedding frequency since the phase is sensitive to the exact flow configuration. This seems to be a reasonable conclusion since it is expected that aerodynamic pressure fluctuations in the gaps and wakes of the tubes produced by vortex shedding are transmitted through the boundary layer. Therefore if the flow outside the boundary layer changes (e.g. the gap flow velocity and hence connection velocity of the vortices changes) then it is expected that the phase of the pressure fluctuations transmitted through the boundary layer would change also.

### 4.9.4 Comparison with other investigations

Ferguson and Parkinson [4.16] measured the relative phases of the pressure round a single cylinder in a flow for Reynolds numbers between $1.5\times10^4$ and $4.1\times10^4$. They found that there was a phase shift of $180^\circ$ between angles of $150^\circ$ and $210^\circ$. Time history measurements of the velocity fluctuations round a cylinder at Reynolds numbers of $6.8\times10^4$ were made by Toebes [4.31]. The phase of the signals was very difficult to estimate reliably because the waveforms of the signals at different angles were very different and correlation techniques were not used. Bublitz [4.9] carried out cross-correlation measurements of pressure round a cylinder at Reynolds numbers of $1.53\times10^5$. He found that between angles of $30^\circ$ and $120^\circ$ there was

a zero time delay of the vortex induced pressure fluctuations. However, it is estimated that the accuracy of the time delay measurements was only sufficient to resolve the phase of the vortex shedding frequency to within $90^{o}$. The detailed phase variation with angle were therefore not resolved.

## 4.10 Measurement of the Velocity and Turbulence Intensity in the Wake of a Row of Tubes

### 4.10.1 Experimental method

The velocities and turbulence intensities were measured using a hot wire anemometer at 5 mm intervals down the vertical centre line of the working section, two tube diameters downstream of the row of tubes. This was carried out for a uniformly spaced arrangement of fixed tubes and for an evenly spaced arrangement of tubes where one tube was displaced by 0.1 tube diameter.

### 4.10.2 Aims of the experiment

The aim of the experiment was to investigate the effect of displacing a tube on the wake structure behind a tube row. The similarity of the wakes of nominally similar tubes was also to be investigated at critical Reynolds numbers where the separation position is very sensitive to the flow conditions and surface roughness of the tubes.

### 4.10.3 Experimental results and discussion

Figures 4.45 and 4.46 show the velocities and turbulence intensities measured two diameters downstream of a row of uniformly spaced fixed tubes and of a row of fixed tubes with one tube displaced by 0.1 diameter.

The velocity profile in the wake of the tubes varies considerably for different tubes. In particular, the pressure measuring tube (although precautions were taken in its manufacture) has a rougher surface which causes earlier separation. The wake velocity profile is therefore considerably different from the non instrumented fixed tubes. When the measuring tube is displaced by 0.1 diameter the maximum velocity in the larger gap becomes greater than the maximum velocity in the smaller gap, producing an asymmetric velocity profile.

The turbulence intensity in the wakes of the tubes varies considerably between the different tubes and when the pressure measuring tube is displaced by 0.1 diameter the turbulence levels in the smaller gap increase. The turbulence intensity levels in the gaps of the instrumented tube are lower than in the gaps of the other tubes. This implies that the recirculation wake structure of the instrumented tube is different from the other fixed tubes, but the wake structures of the other tubes also varies considerably.

These experiments show that the exact flow configuration and turbulence intensity through a single row of tubes and in their wakes at Reynolds numbers of approximately $1.2 \times 10^5$ is very sensitive to surface roughness of the tubes and their position in the tube row. This implies that the assumption that separation occurs in the minimum gap for all the tubes in a row is invalid in this flow regime and hence, theories which predict the onset of the fluid elastic instabilities in tube rows using this assumption, e.g. [4.6] need to be modified for use at the Reynolds numbers studied in the present investigation.

### 4.10.4 Comparison with other investigations

Pridden [4.26] carried out velocity and turbulence intensity measurements just behind rows 1 to 11 in a 12 row staggered tube bank.

The velocity and turbulence intensity profiles behind each row after the first row were very similar and turbulence intensity levels of up to 60% were observed, as compared with 50% in the present investigation. The velocity profiles behind each tube in the same row were very similar in the measurements made by Pridden. This is accounted for by the fact that his measurements were carried out at sub-critical Reynolds numbers where flow separation on all the tubes in a row occurred at approximately the same point. The levels of turbulence intensity in the gaps between the tubes was found to be similar to the levels in the present investigation and turbulence intensity was a minimum at the maximum flow velocity in the tube gap which agrees with the results of the present investigation.

## 4.11 Measurement of the Time History of the Displacement of a Vibrating Tube

### 4.11.1 Experimental method

The displacement signal from the vibrating flexible tube mounted in a single row of uniformly spaced fixed tubes was acquired on the D.A.C. computer. The length of the time history acquired was 15 seconds and the values were scaled to produce graphs of the instantaneous tube displacement in μm plotted against time in ms, which are given in Figure 4.47.

### 4.11.2 Aims of the experiment

The r.m.s. displacement of a vibrating tube gives an indication of the tube vibration levels in heat exchangers. However, if a tube is responding to a pressure field with an r.m.s. value which varies with time (i.e. a non-stationary pressure field) the characteristics of the response of the tube may vary for different time periods. The r.m.s. response of a tube integrated over a large period of time does not give any indication of the peak values of the tube response which can be expected to occur . Peak values, which are required for the calculation of the time when tube fatigue failures are likely to occur, can only be obtained by referring to amplitude probability distributions or time histories of the tubes' displacement responses.

### 4.11.3 Results and discussion

The displacement response of the tube is non-stationary which implies that the pressure field round the tube is non-stationary. For some time periods the tube peak displacement is lower than the average r.m.s. value by a factor of up to 3 and at other time periods the tube peak displacement is greater than the average r.m.s. value by factors of up to 7. Hence when assessing the probable time for fatigue failures of tubes in a heat exchanger a knowledge of average r.m.s. values of tube vibration is insufficient. The amplitude probability distribution of the tube displacement measured over a long averaging time (at least 15 seconds) must be used to assess the proportion of the time the tube displacement is above the acceptable level so that fatigue failures can be predicted reliably.

## 4.12 Conclusions

### 4.12.1 Conclusions from section 4.3

(i) The flow configuration round a tube in a row of tubes depends on the static displacement of the tube, from a uniformly spaced arrangement, in the direction transverse to the mean flow.

(ii) As a tube is statically displaced from its mean position in a tube row the stagnation and separation points move round the tube which produces an asymmetry in both the average and fluctuating pressure distribution round the tube.

(iii) The average and r.m.s. pressure distributions round a tube are affected by the presence of a neighbouring vibrating tube.

(iv) The lift and drag on a tube varies with tube displacement in the transverse flow direction and does not vary as a linear function of displacement. The presence of a vibrating tube changes the lift and drag on a neighbouring tube.

(v) The flow round tubes in a single row at Reynolds numbers of approximately $1.2 \times 10^5$ is three dimensional and there can be a considerable difference in the position of the separation points along the spanwise tube axis.

(vi) Current theories which predict the lift and drag forces on a tube in a single row do not agree with the experimental results of the present investigation. It has been shown that the assumption that separation always occurs in the minimum gap is not true. The assumption that tube displacements only affect the forces on the tube in a direction perpendicular to the tube displacement has been shown to be not generally true.

### 4.12.2 Conclusions from section 4.4

(i) The presence of a neighbouring vibrating tube does not affect the amplitude of the vortex shedding pressure fluctuations measured on a tube. However the vortex shedding peak is broadened on a tube with a neighbouring vibrating tube.

(ii) The presence of a vibrating tube in a fixed tube row changes the receptivity of the boundary layer round a neighbouring tube to acoustic excitations from an acoustic duct mode. This produces a larger variation of the amplitude of the acoustic mode, in the tube boundary layer, with angle round the

tube. Hence a vibrating tube changes the flow field round a neighbouring tube.

(iii) Tubes are excited by pressure fluctuations at subharmonics of the vortex shedding frequency. The subharmonic has a higher amplitude when the tube is displaced from a uniformly spaced position between its two neighbouring tubes in the row.

(iv) The vibration of a tube has very little direct linear effect on the pressure fluctuations measured round a neighbouring tube when the tube r.m.s. displacement amplitude is approximately $2 \times 10^{-3}$ diameters. Hence there is very little direct linear interaction between tubes which are executing small amplitude vibrations.

(v) There is a degree of coherency in the pressure fluctuations acting on neighbouring tubes in a single tube row at the vortex shedding frequency.

(vi) The vibration of a tube has very little direct linear effect on the velocity fluctuations in the wake of a neighbouring tube in a single row of tubes.

4.12.3 Conclusions from section 4.5

(i) As a tube is statically displaced from a uniformly spaced arrangement between its two neighbouring tubes the amplitude of the vortex shedding mode measured on the tube decreases and the vortex shedding peak broadens in frequency as the displacement is increased.

(ii) The turbulence level round a fixed tube increases with increasing displacement of a fixed tube towards a vibrating tube. At high displacements of 0.7 diameters from the uniformly spaced arrangement the level of the turbulent pressure fluctuations is greater than the level of the vortex shedding pressure fluctuations.

(iii) Near the laminar separation points on the tube there are peaks in the pressure excitation forces at frequencies below the vortex shedding frequency which are not related to the vortex shedding frequency by simple integers. It is postulated that these fluctuations are produced in the wake region, possibly by eddy coalescence.

(iv) The displacement response of a vibrating tube decreases as a fixed tube is displaced from a uniformly spaced position

between two tubes towards the vibrating tube.

(v) There is little direct linear interaction between a vibrating tube and the pressure field round a neighbouring tube which is separated by 0.4 diameters from the vibrating tube. Hence with tubes which are closely spaced there is no significant linear interaction between them when they are vibrating with small amplitudes.

(vi) The amplitude probability of the displacement of the vibrating tube is Gaussian in shape.

Note - the response of a linear system to a general excitation force is Gaussian.

4.12.4 Conclusions from section 4.6

(i) The presence of a vibrating tube does not decrease the coherency of the vortex shedding mode along the spanwise axis of the tube. Hence a vibrating tube does not disrupt vortex shedding on a neighbouring tube.

(ii) The axial correlation length of the vortex shedding mode round a tube is a function of angle and is highest at the stagnation point and lowest in the wake.

(iii) The level of coherency along a fixed tube at the rigid body modal frequency of a neighbouring vibrating tube is low. This implies that there is no direct interaction of the vibrating tube with the pressure field round a neighbouring tube.

(iv) The broadband correlation lengths are a maximum at the stagnation point and in the wake of the tube. Near the separation points the correlation coefficients are lower than in the wake which implies that broadband turbulent pressure fluctuations are less correlated along the spanwise tube axis near the separation points.

(v) Along the tube spanwise axis, the correlation of broadband pressure fluctuations is a factor of 1.7 smaller for a tube in a row of tubes than for a single tube in a low turbulence free stream. This implies that the presence of neighbouring tubes decreases the correlation of turbulent pressure fluctuations along the spanwise tube axis.

4.12.5 Conclusions from section 4.7

(i) The level to which an acoustic duct mode is excited is dependent on the level of the pressure fluctuations generated by the presence of the tubes in the duct. The pressure fluctuations created by the tubes in general increase with increasing flow velocity. Hence the level to which duct modes are excited in general increases with flow velocity.

(ii) When the vortex shedding frequency is near the frequency of a duct mode the mode is excited to high amplitude because there are large pressure fluctuations at the frequency of the duct mode.

(iii) At some flow velocities there is a strong vortex shedding sub-harmonic pressure fluctuation round the tubes.

(iv) The r.m.s. response of the vibrating tube increases in proportion to the free stream dynamic pressure when there are no strong peaks in the pressure excitation spectrum near the resonance frequency of the tube. When the pressure excitation on the tube has a peak due to vortex shedding or an acoustic duct mode near the tube resonance frequency there is a very large increase in the response of the tube.

(v) The increase in the tube r.m.s. displacement due to off resonance forced response of the tube by acoustic duct modes or vortex shedding modes is negligible.

4.12.6 Conclusions from section 4.8

(i) Superimposed sound coincident with the vortex shedding frequency at a SPL of up to 136 dB and coincident with an acoustic duct modal frequency at a SPL of up to 138 dB does not effect the static pressure distributions, and hence the average lift and drag on a tube. The r.m.s. pressure distributions are very similar to those obtained without the presence of superimposed sound except that they are higher in amplitude due to the increased pressure fluctuations produced in the boundary layer by the superimposed sound.

(ii) The superimposed sound excites higher order duct modes at frequencies not related to the frequency of the exciting sound. This implies that there is a non-linear interaction of the

sound with the pressure fluctuations in the tube boundary layer to produce pressure fluctuations at the frequency of the duct modal frequencies. The increased pressure fluctuations then excite the duct modes.

(iii) Superimposed sound increases the vibration of the tube significantly at the frequency of the tube rigid body mode. This implies that there is a non-linear interaction of the sound with the pressure fluctuations in the tube boundary layer which increases the pressure excitation on the tube and hence increases its vibration level.

4.12.7 Conclusions from section 4.9

(i) The static displacement of a tube by 0.1 diameter and the presence of a flexible vibrating tube greatly affect the phase of the vortex shedding pressure fluctuations round the boundary layer of a tube. It is postulated that the variation of phase of the pressure fluctuations, at the vortex shedding frequency, in the boundary layer of the tube is highly sensitive to the flow situation round the tube.

4.12.8 Conclusions from section 4.10

(i) The flow at Reynolds numbers of $1.2 \times 10^5$ is very sensitive to the surface roughness of the tubes. The separation points and wake structure between different tubes are different for tubes which are manufactured to be nominally the same. Hence the lift and drag forces on the tubes in a row at Reynolds numbers of $1.2 \times 10^5$ vary considerably.

(ii) The turbulence intensities in the wake of a tube row can be as high as 50% and are generally higher where the mean flow velocity is low.

4.12.9 Conclusions from section 4.11

(i) The displacement response of a tube in a single tube row at a Reynolds number of $1.2 \times 10^5$ is non-stationary which implies that the exciting pressure field round the tube is non-stationary.

(ii) When predicting fatigue failures of tubes it is necessary not

only to have a measure of the r.m.s. tube vibration levels but the amplitude probability distributions of the tubes' displacements measured over a long averaging time (at least 15 seconds) is required.

## 4.13 References


4.1 E. ACHENBACH 1969 Wärme und Stoffübertragung Bo.2 pp 47-52. "Investigations on the Flow through a Staggered Tube Bundle at Reynolds Numbers up to $Re=10^7$".

4.2 E. ACHENBACH 1971 Wärme und Stoffübertragung Bo.4 pp 120-126. "Influence of Surface Roughness on the Flow through a Staggered Tube Bank".

4.3 E. ACHENBACH 1971 Wärme und Stoffübertragung Bo.4 pp 152-155. "On the Cross Flow through In-Line Tube Banks with Regard to the Effect of Surface Rougness".

4.4 K.K. AHUJA and C.K.W. TAM 1982 J.S.V. 83(3) pp 433-439. Letters to the Editor. "A Note on the Coupling between Flow Instabilities and Incident Sound".

4.5 R.D. BLEVINS 1974 Journal of Pressure Vessel Technology. Transaction of A.S.M.E. series J, Vol. 96 pp 263-267. "Fluid Elastic Whirling of a Tube Row".

4.6 R.D. BLEVINS 1977 Journal of Fluids Engineering. Transactions of A.S.M.E. series I, Vol. 99 pp 457-460. "Fluid Elastic Whirling of Tube Rows and Tube Arrays".

4.7 R.D. BLEVINS 1978 Proceedings of the B.N.E.S. International Conference on Vibration in Nuclear Plant, held at Keswick, U.K. 9-12 May 1978. Paper 3:4. "Buffeting of heat exchanger tube arrays in a cross flow".

4.8 H.H. BRUUN and P.O.A.L. DAVIES 1975 J.S.V. 40(4) pp 535-559. "An experimental investigation of the unsteady pressure forces on a circular cylinder in a turbulent cross-flow".

4.9 P. BUBLITZ 1972 Proceedings of the IUTAM/IAHR Symposium on Flow-Induced Structural Vibrations, held at Karlsruhe, Germany, 14-16 August 1972. Paper E2. "Measurements of the unsteady pressure and forces acting upon an oscillating circular cylinder in transverse flow".

4.10 S.S. CHEN and J.A. JENDRZEJCZYK 1981 J.S.V. 78(3) pp 355-382. "Experiments on fluid elastic instability in tube banks subjected to liquid cross-flow".

4.11 Y.N. CHEN 1972 Jornal of Engineering for Industry. Transactions of A.S.M.E. series B, Vol. 94 pp 623-628. "Fluctuating Lift Forces of the Karman Vortex Streets on Single Circular Cylinders and in Tube Bundles. Part 3 - Lift forces in Tube Bundles".

4.12 Y.N. CHEN 1978 Proceedings of the B.N.E.S. International Conference on Vibration in Nuclear Plant, held at Keswick, U.K. 9-12 May 1978. Paper 2:6. "Criteria for the cross-flow-induced tube vibrations in tube bank heat exchangers".

4.13 H.J. CONNORS, Jr. 1970 Proceedings of A.S.M.E. Winter Annual meeting held in New York, U.S.A. 1 December 1970. Flow-Induced Vibrations in Heat Exchangers. pp 42-56. "Fluidelastic Vibrations of Tube Arrays Excited by Cross Flow".

4.14 T. COUSTEIX 1979 N.A.S.A. Technical Memorandum TM-75806. "Outline of Research on Oscillating Boundary Layers".

4.15 D.A.C. 1980 University of Southampton, ISVR. Data Analysis Centre manual sections 1-4. "Description of Available Programs".

4.16 N. FERGUSON and G.V. PARKINSON 1967 Journal of Engineering for Industry. Transaction of A.S.M.E. series B, Vol. 89 pp 831-838. "Surface and Wake Flow Phenomena of the Vortex Excited Oscillation of a Circular Cylinder".

4.17 J.A. FITZPATRICK and I.S. DONALDSON 1980 J.S.V. 73(2) pp pp 225-237. "Row Depth Effects on Turbulence Spectra and Acoustic Vibrations in Tube Banks".

4.18 J.A. FITZPATRICK, I.S. DONALDSON and W. McKNIGHT. 1978. Proceedings of the B.N.E.S. International Conference on Vibration in Nuclear Plant, held at Keswick, U.K. 9-12 May 1978. Paper 3:6. "Some observations of the pressure distribution in a tube bank for conditions of self generated acoustic resonance".

4.19 R.S. HILL 1976 North East Coast Institution of Engineers and Shipbuilders Transactions 92 pp 91-100. "Tube Vibration in Boiler and other Heat Exchangers".

4.20 N.L. JOHNSON and S. KOTZ 1970 "Distributions in Statistics. Continuous univariate distributions - 2". New York: John Wiley and Sons.

4.21 S.C. KACKER and R.S. HILL 1974 University of Newcastle-upon-Tyne, Department of Mechanical Engineering Report No.Tb30A Nov. 74. "Flow over a circular cylinder in the presence of standing sound waves".

4.22 M.G. MORSY 1975 Proceedings of Institute of Mechanical Engineers, Vol. 189 pp 519-532. "Skin Friction and Form Pressure Loss in Tube Bank Condensers".

4.23 J.E. NAMORK 1977 University of Salford M.Sc. Thesis. "Flow-Induced Vibrations in a Tube Bank".

4.24 S. OKAMOTO, T. HIROSE and T. ADACHI 1981 Bulletin of J.S.M.E. Vol. 24 No. 187 pp 45-53. "The Effect of Sound on the Vortex-Shedding from a Circular Cylinder. (Acoustical Vibrations Directed along Axis of Cylinder)".

4.25 M.J. PETTIGREW and D.J. GORMAN 1978 Proceedings of the B.N.E.S. International Conference on Vibration in Nuclear Plant, held at Keswick, U.K. 9-12 May 1978. Paper 2:3. "Vibration of Heat Exchange Components in Liquid and Two-Phase Cross-Flow".

4.26 D.L. PRIDDEN 1976 University of Salford M.Sc. Thesis. "An investigation into Cross-Flow-Induced Vibrations in a Closely Packed Staggered Tube Bank".

4.27 B.W. ROBERTS 1966 Mechanical Engineering Science Monograph No. 4 Sept. 1966. "Low frequency, Aeroelastic Vibrations in a Cascase of Circular Cylinders".

4.28 P.J. SOUTHWORTH 1973 University of Salford M.Sc. Thesis. "An investigation into Cross-Flow-Induced Vibration in in-line tube banks".

4.29 H. TANAKA and S. TAKAHARA 1977 J.S.V. 77(1) pp 19-37. "Fluid Elastic Vibration of Tube Arrays in Cross Flow".

4.30 D.P. TELIONIS 1979 Journal of Fluids Engineering. Transactions of A.S.M.E. series I, Vol. 101 pp 24-43. "Review - Unsteady boundary layers, separated and attached".

4.31 G.H. TOEBES 1969 Journal of Basic Engineering. Transactions of A.S.M.E. series D, Vol. 91 pp 493-505. "The unsteady flow and wake near an oscillating cylinder".

4.32 D.S. WEAVER and M. EL-KASHLAN 1981 J.S.V. 75(2) pp 265-273. "On the number of tube rows required to study cross-flow induced vibrations in tube banks".

4.33 D.S. WEAVER and M. EL-KASHLAN 1981 J.S.V. 76(2) pp 283-294. "The effect of dmping and mass ratio on the stability of a tube bank".

4.34 D.S. WEAVER and L.K. GROVER 1978 J.S.V. 59(2) pp 277-294. "Cross-Flow Induced Vibrations in a Tube Bank - Turbulent Buffeting and Fluid Elastic Instability".

4.35 M.S. WELBOURNE 1978 Proceedings of the B.N.E.S. International Conference on Vibration in Nuclear Plant, held at Keswick, U.K. 9-12 May 1978. Paper 3:2. "Flow Induced Vibration of A.G.R. Heat Exchanger Tubes".

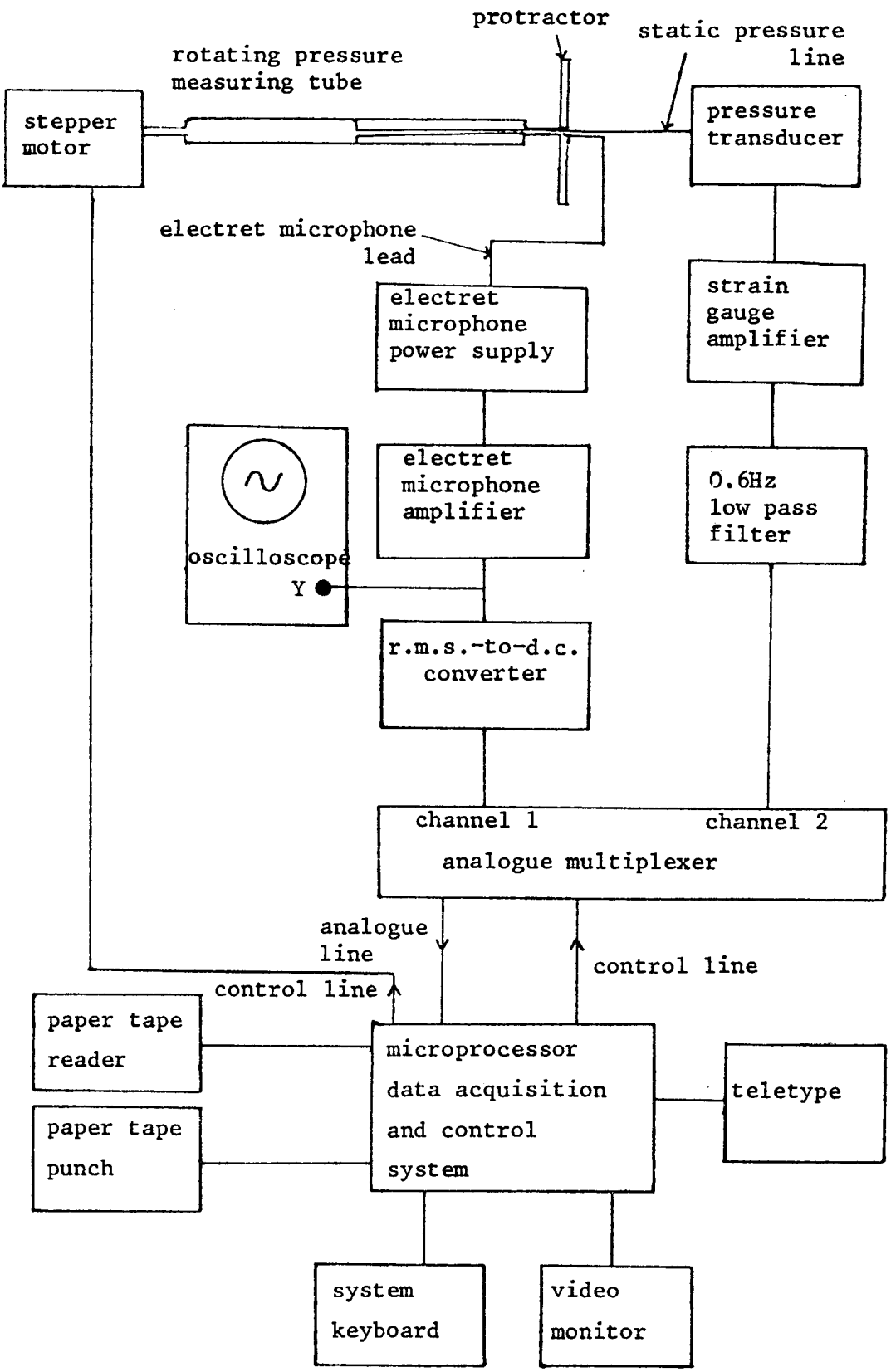


FIGURE 4.1a. Block diagram showing configuration of apparatus for measuring static and fluctuating pressure distributions round a tube.

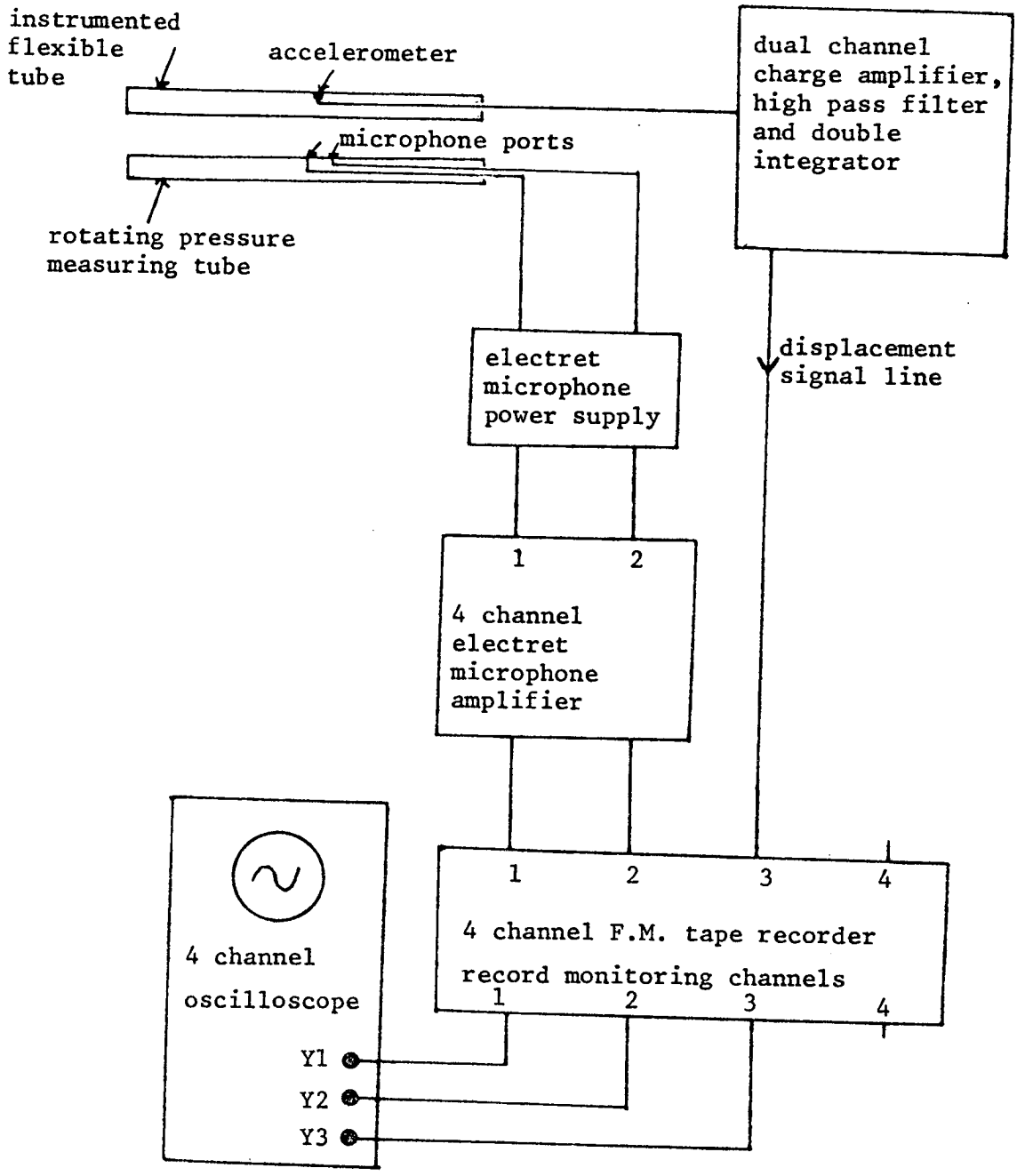


FIGURE 4.1b. Block diagram showing configuration of apparatus for measuring the vibration of a flexibly mounted tube and for measuring the P.S.D. of pressure fluctuations on a fixed tube.

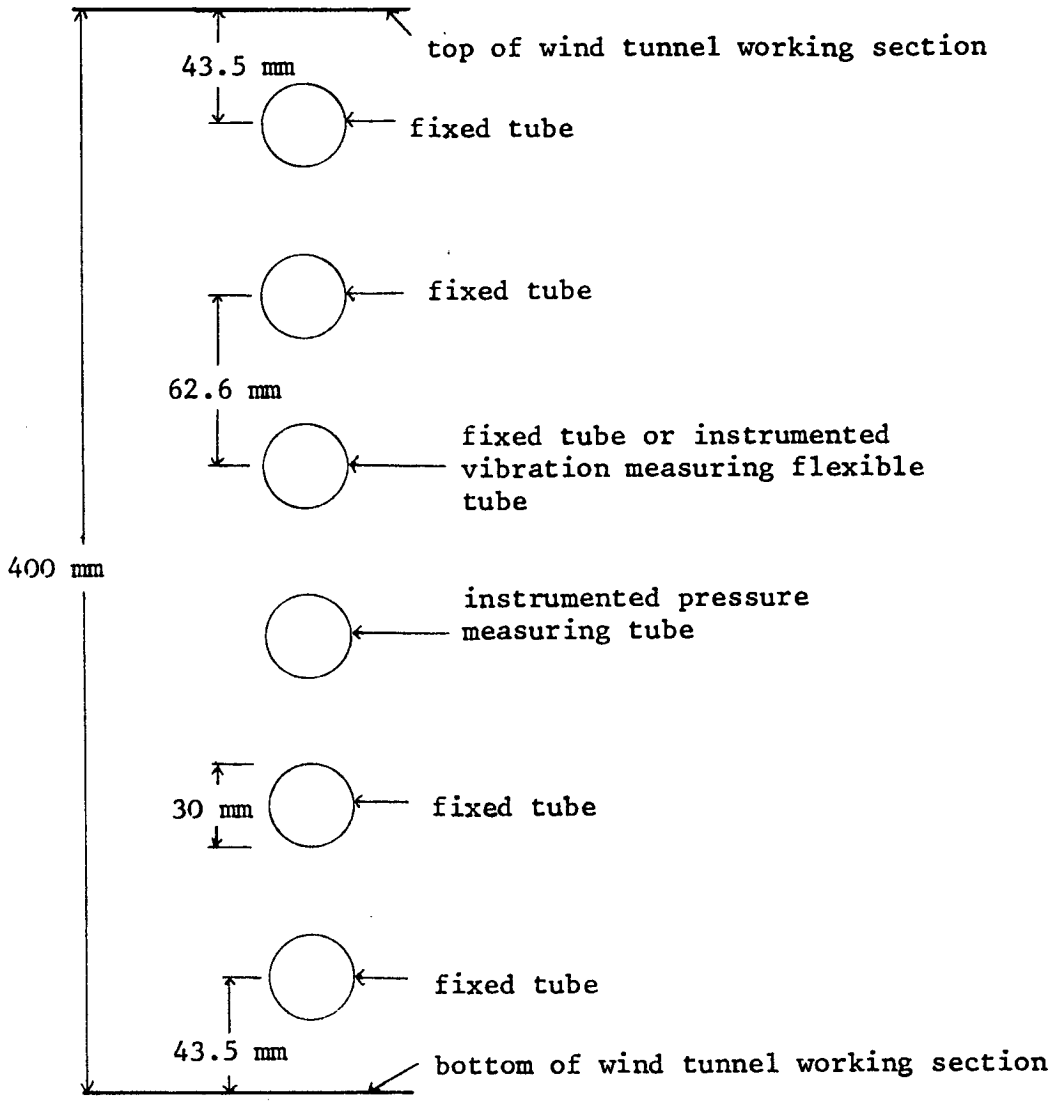


FIGURE 4.2. Arrangement of the single row of uniformly spaced tubes in the wind tunnel working section.

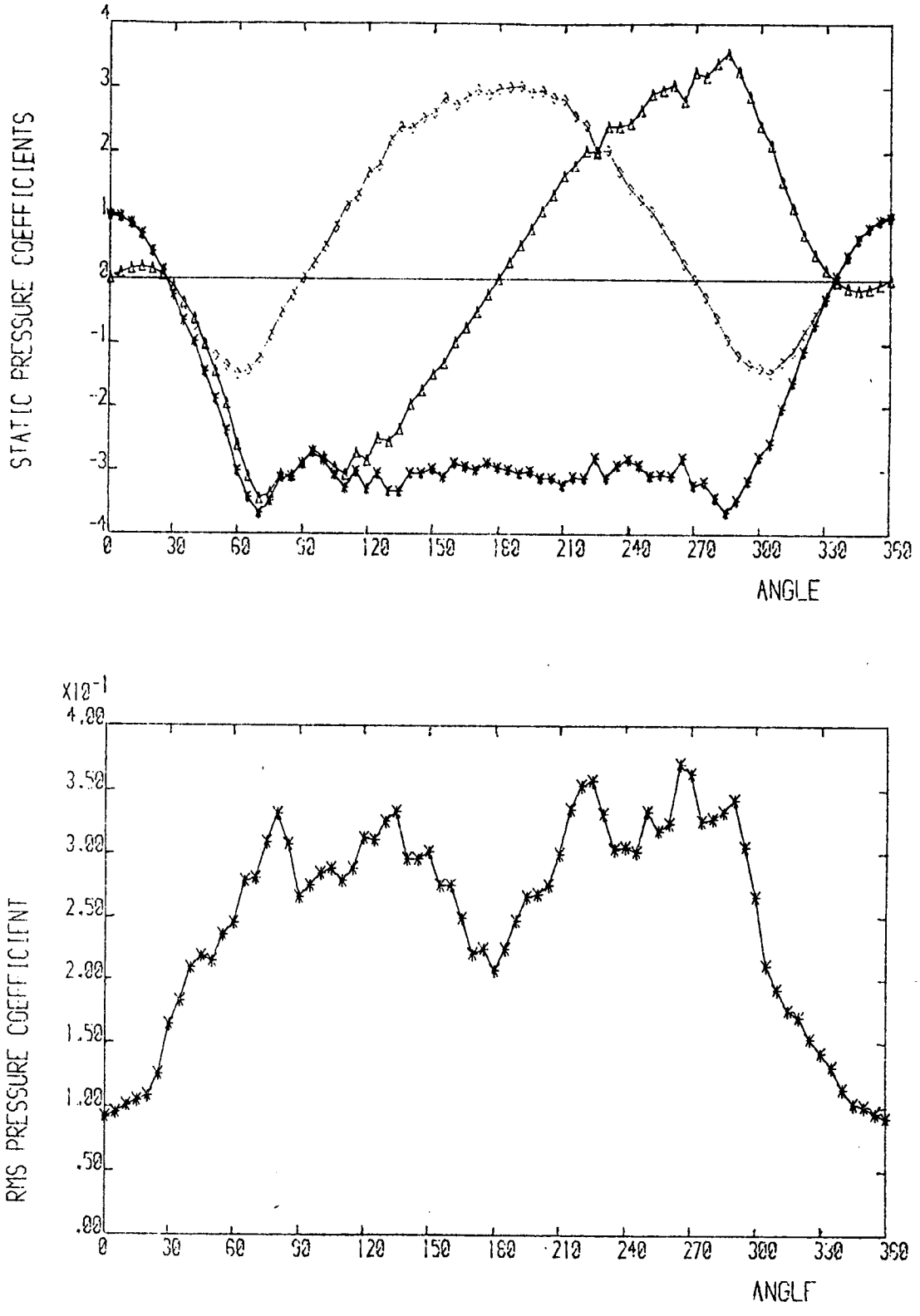


FIGURE 4.3a. Variation of static and r.m.s. pressure coefficients round a fixed tube mounted in a fixed tube row. x/d = 0.0.

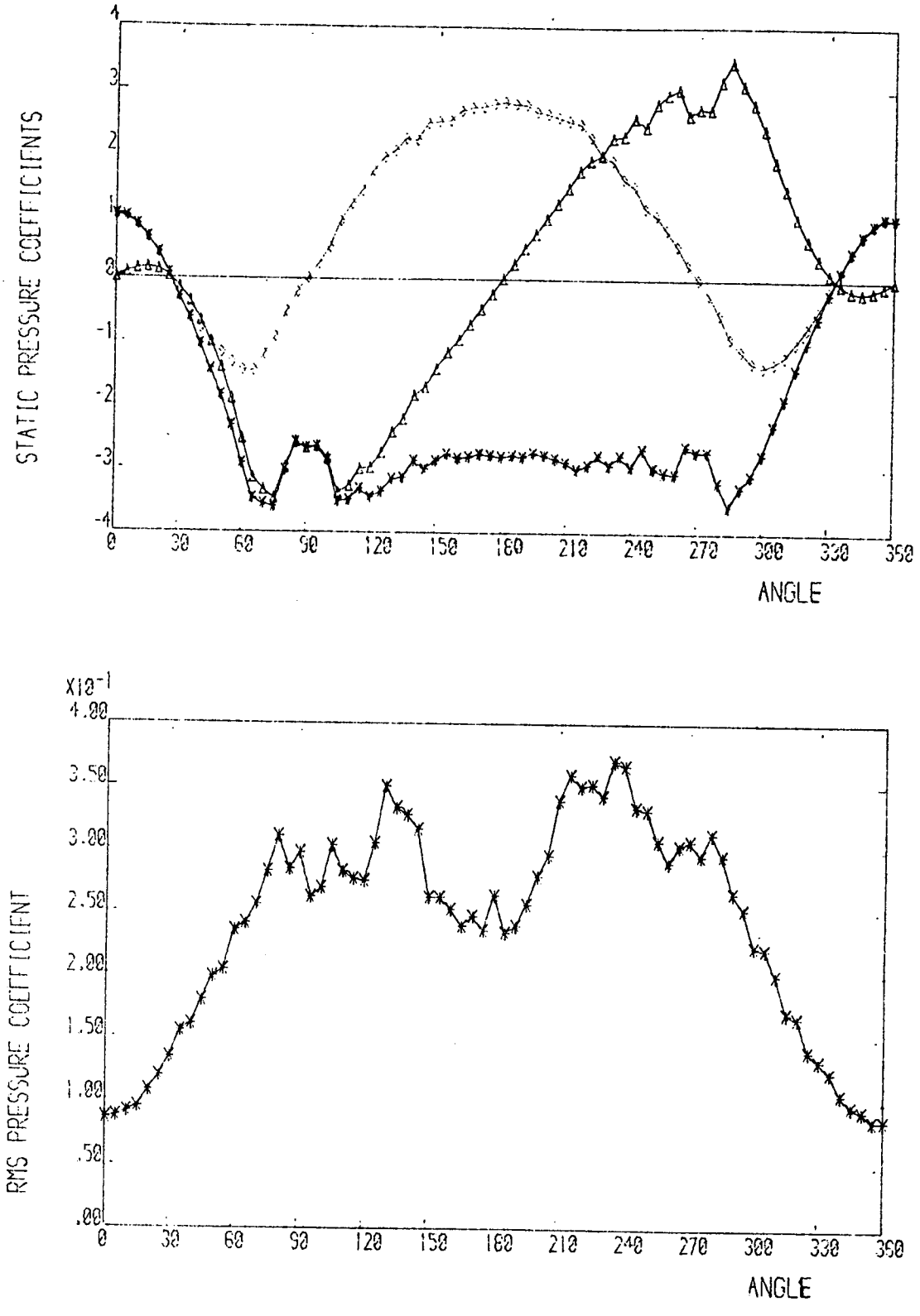


FIGURE 4.3b. Variation of static and r.m.s. pressure coefficients round a fixed tube mounted in a fixed tube row. x/d = 0.05.

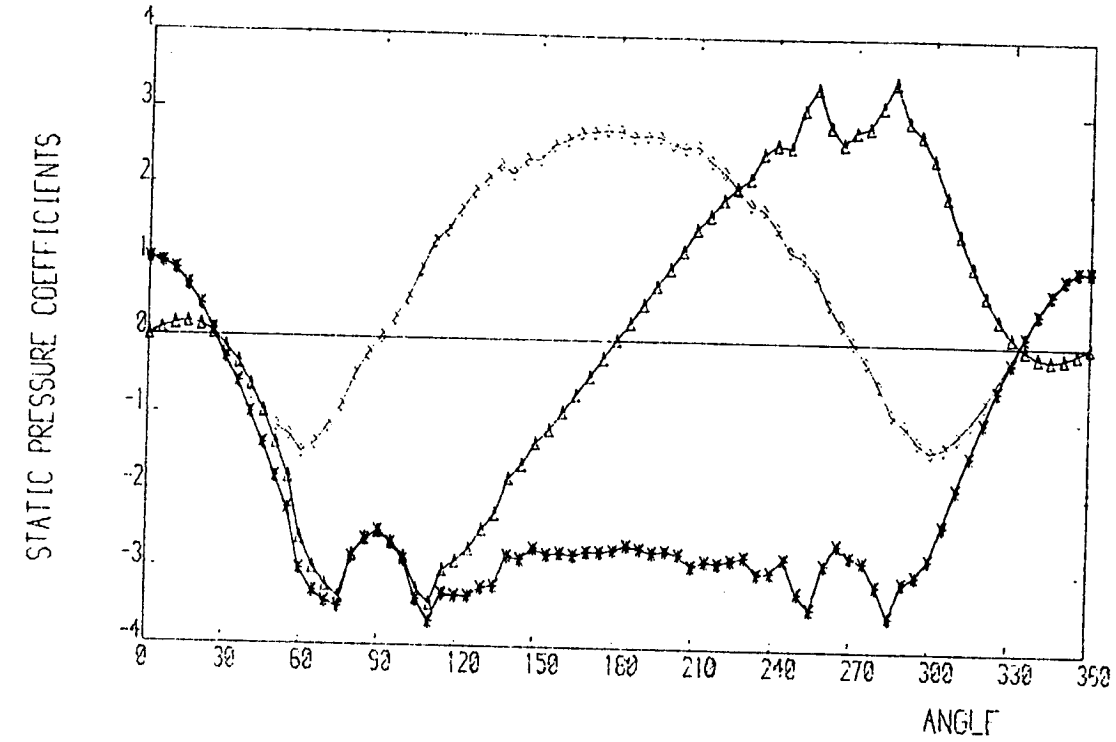


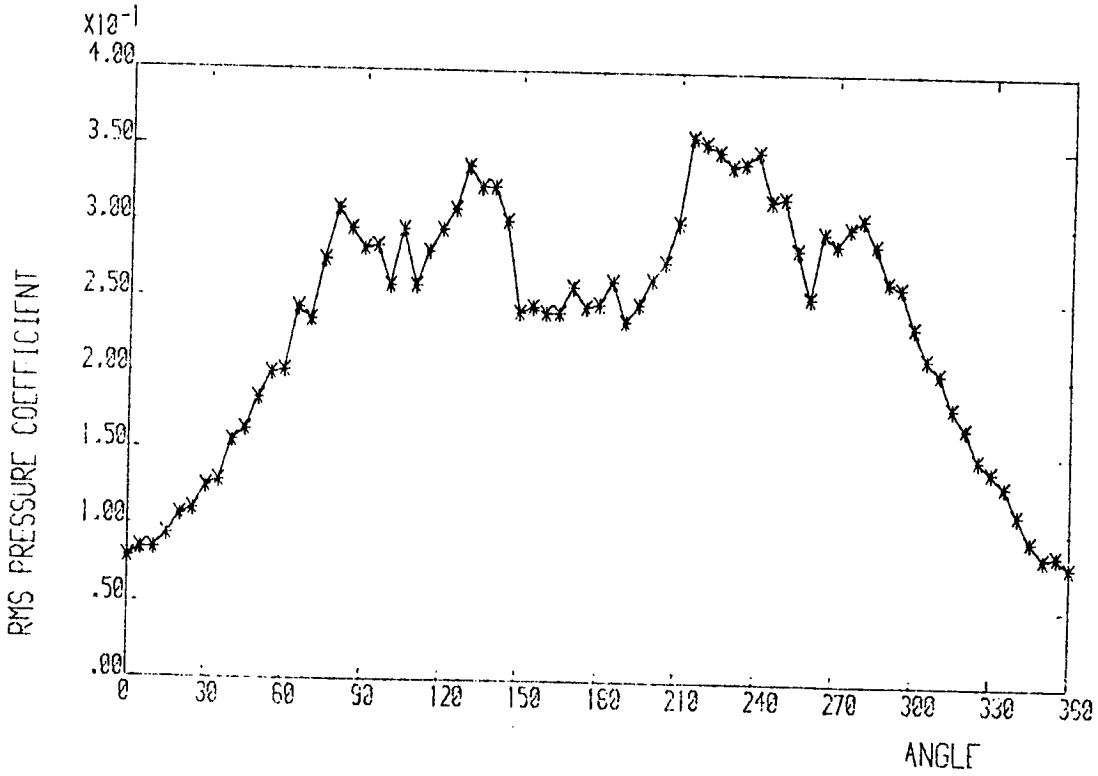


FIGURE 4.3c. Variation of static and r.m.s. pressure coefficients round a fixed tube mounted in a fixed tube row. x/d = 0.10.

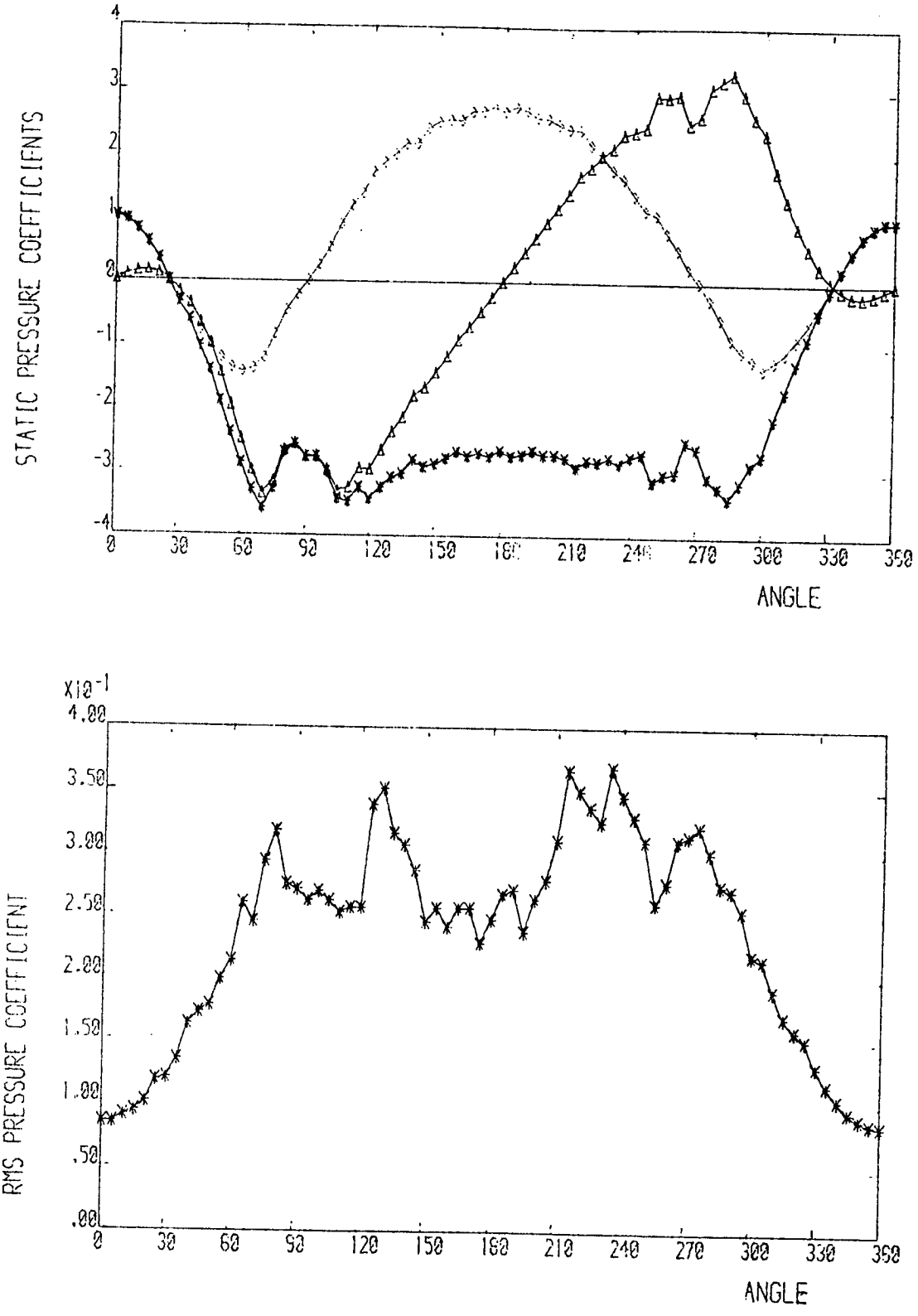


FIGURE 4.3d. Variation of static and r.m.s. pressure coefficients round a fixed tube mounted in a fixed tube row. x/d = 0.15.

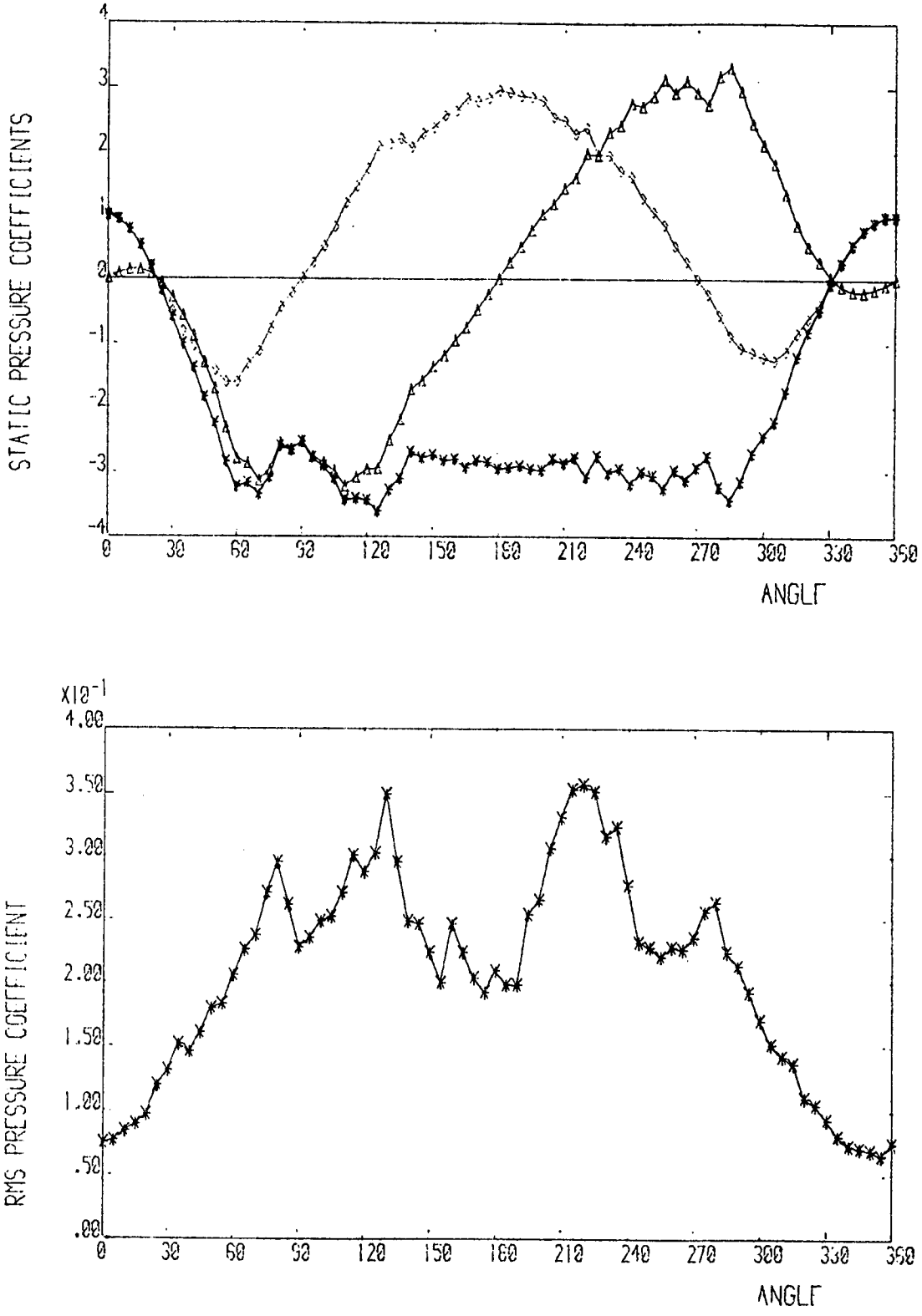


FIGURE 4.3e. Variation of static and r.m.s. pressure coefficients round a fixed tube mounted in a fixed tube row. x/d = 0.20.

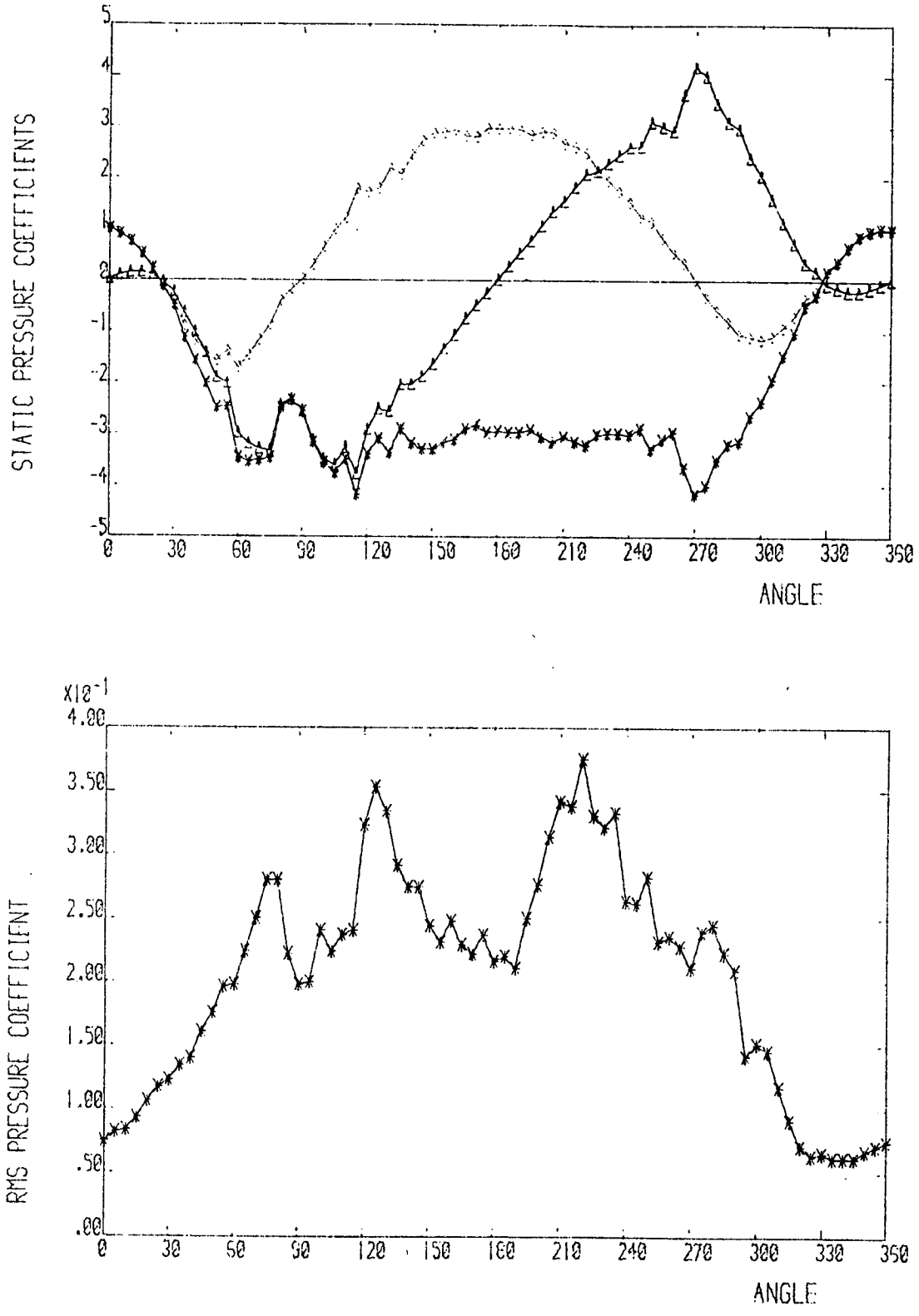


FIGURE 4.3f. Variation of static and r.m.s. pressure coefficients round a fixed tube mounted in a fixed tube row. x/d = 0.25.

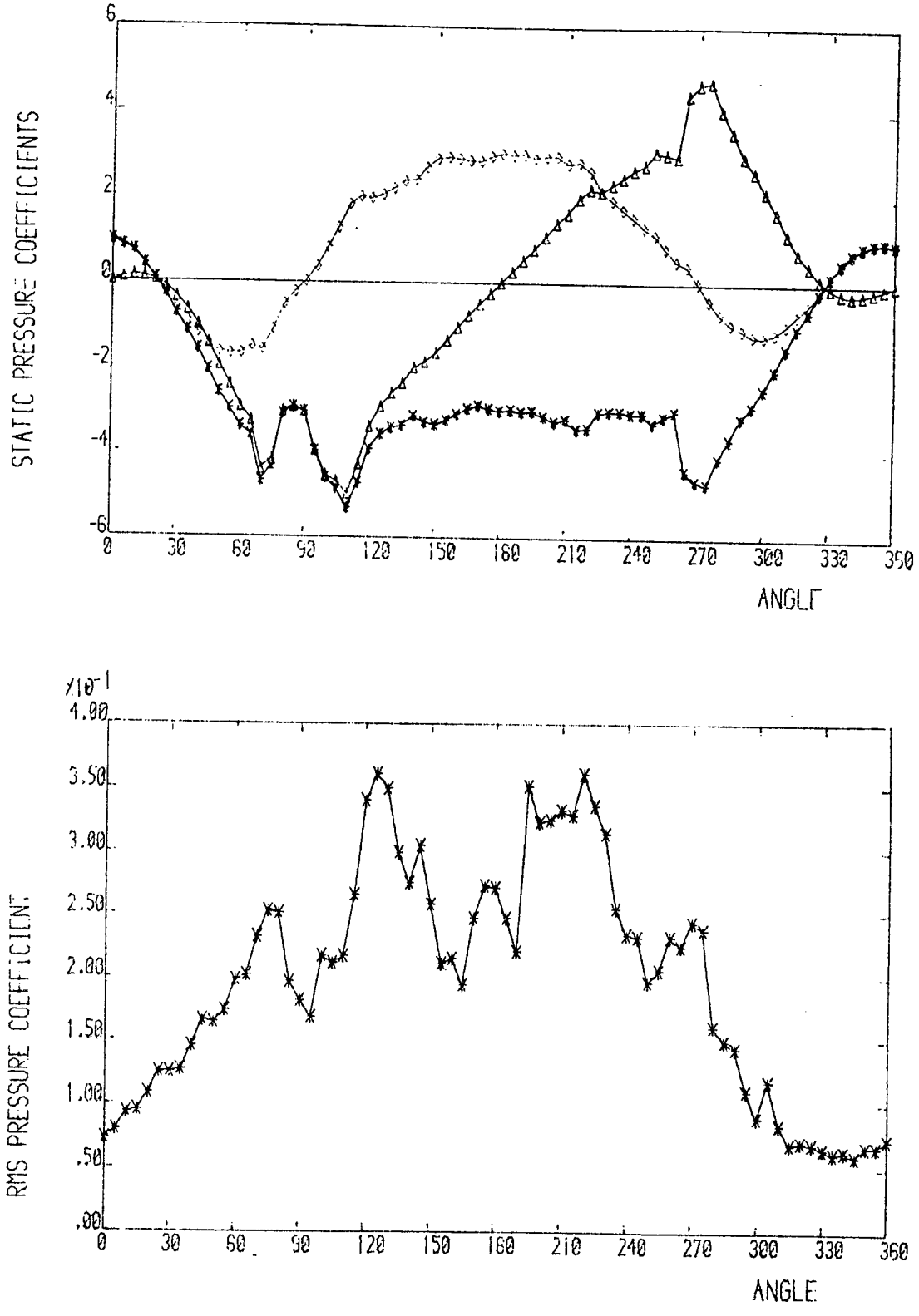


FIGURE 4.3g. Variation of static and r.m.s. pressure coefficients round a fixed tube mounted in a fixed tube row. x/d = 0.3.

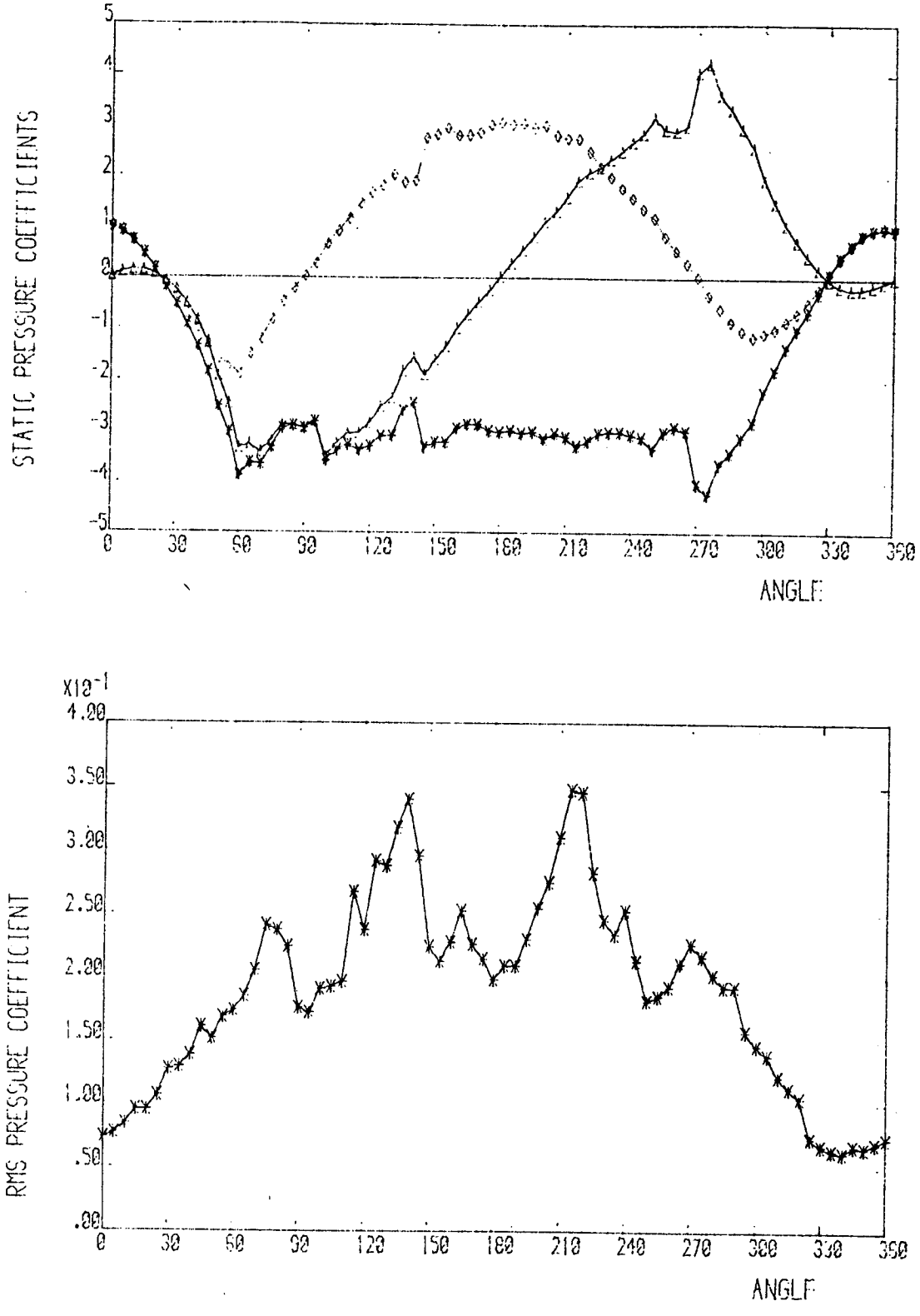


FIGURE 4.3h. Variation of static and r.m.s. pressure coefficients round a fixed tube mounted in a fixed tube row. x/d = 0.4.

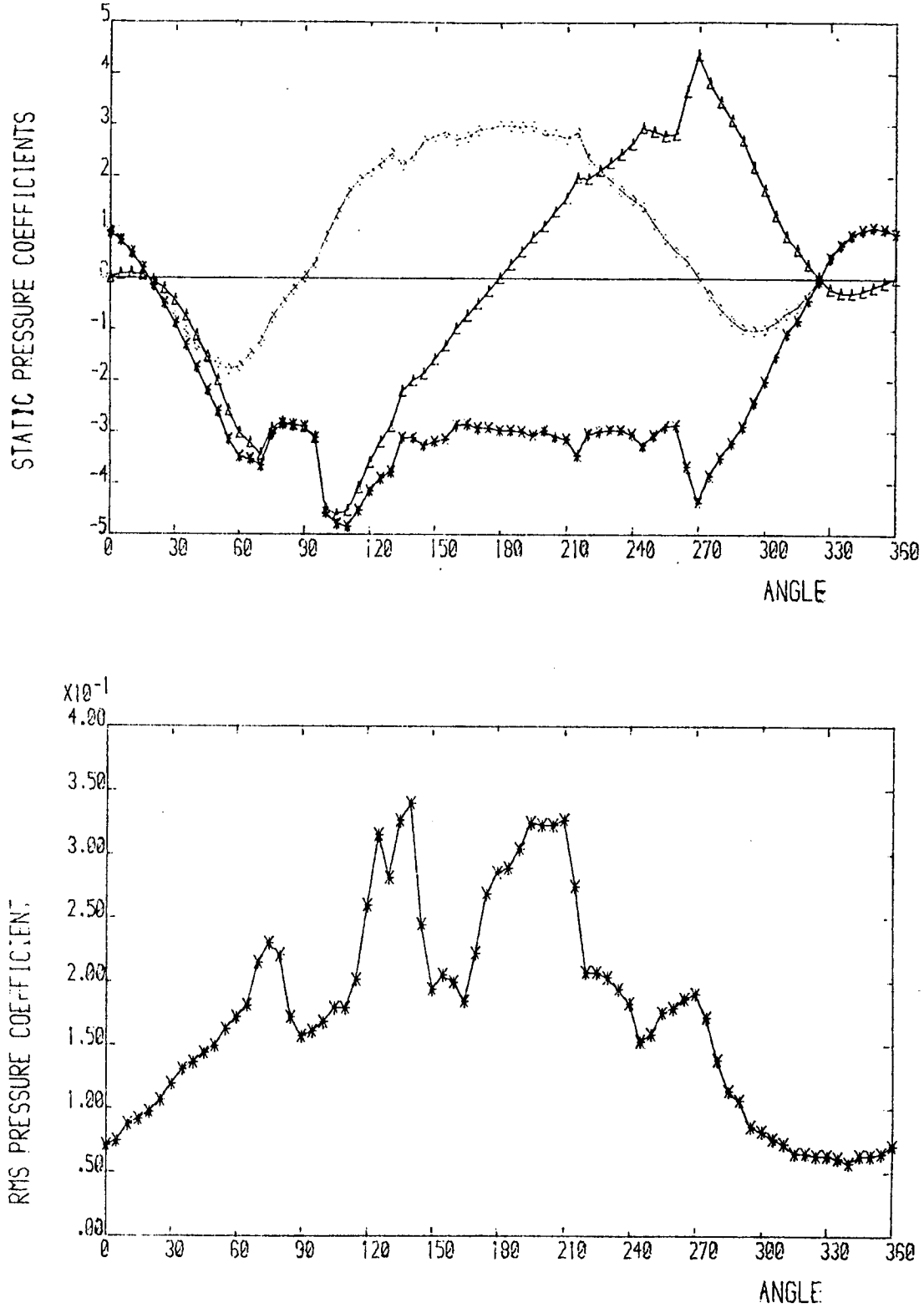


FIGURE 4.3i. Variation of static and r.m.s. pressure coefficients round a fixed tube mounted in a fixed tube row. x/d = 0.5.

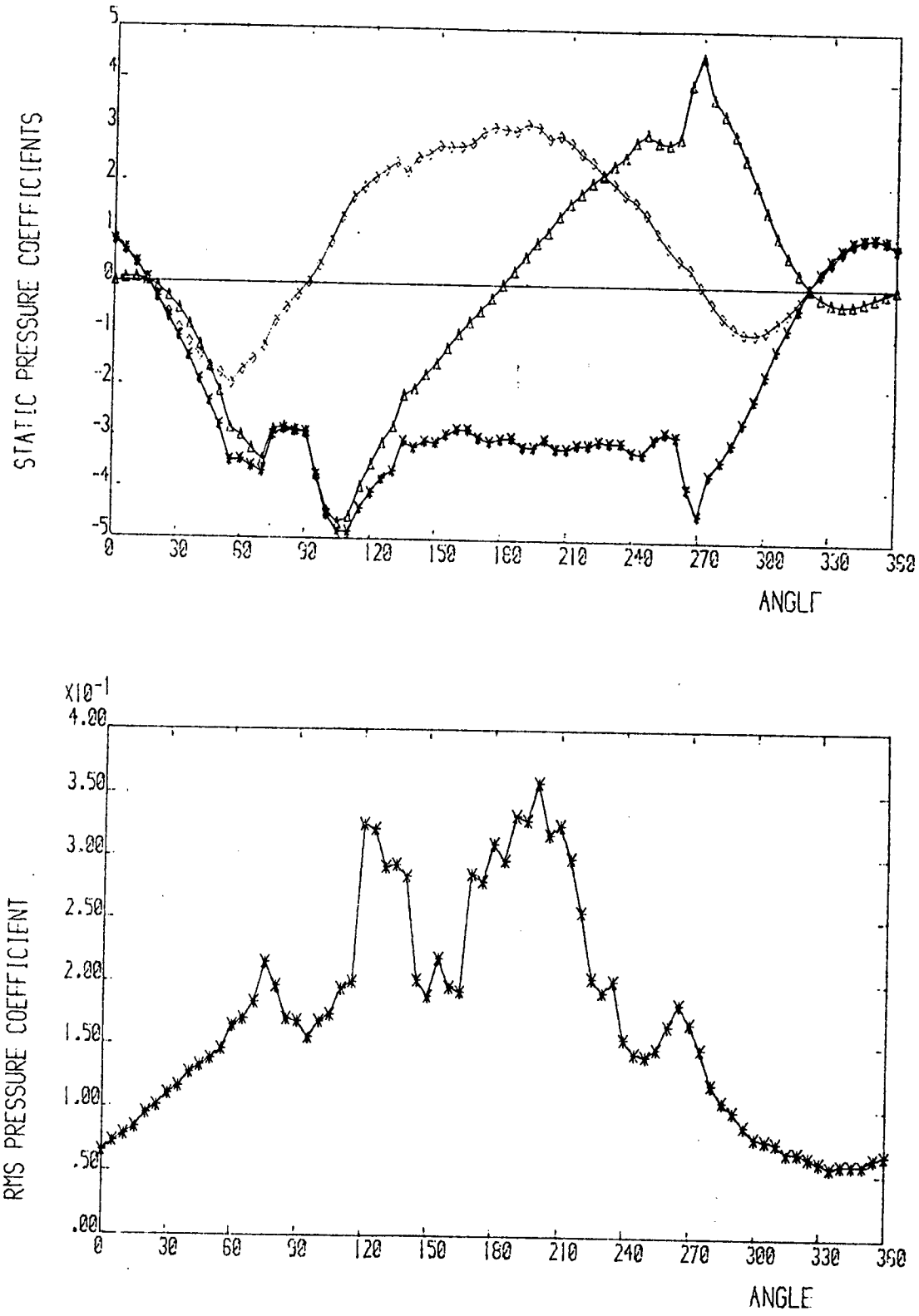


FIGURE 4.3j. Variation of static and r.m.s. pressure coefficients round a fixed tube mounted in a fixed tube row. x/d = 0.6.

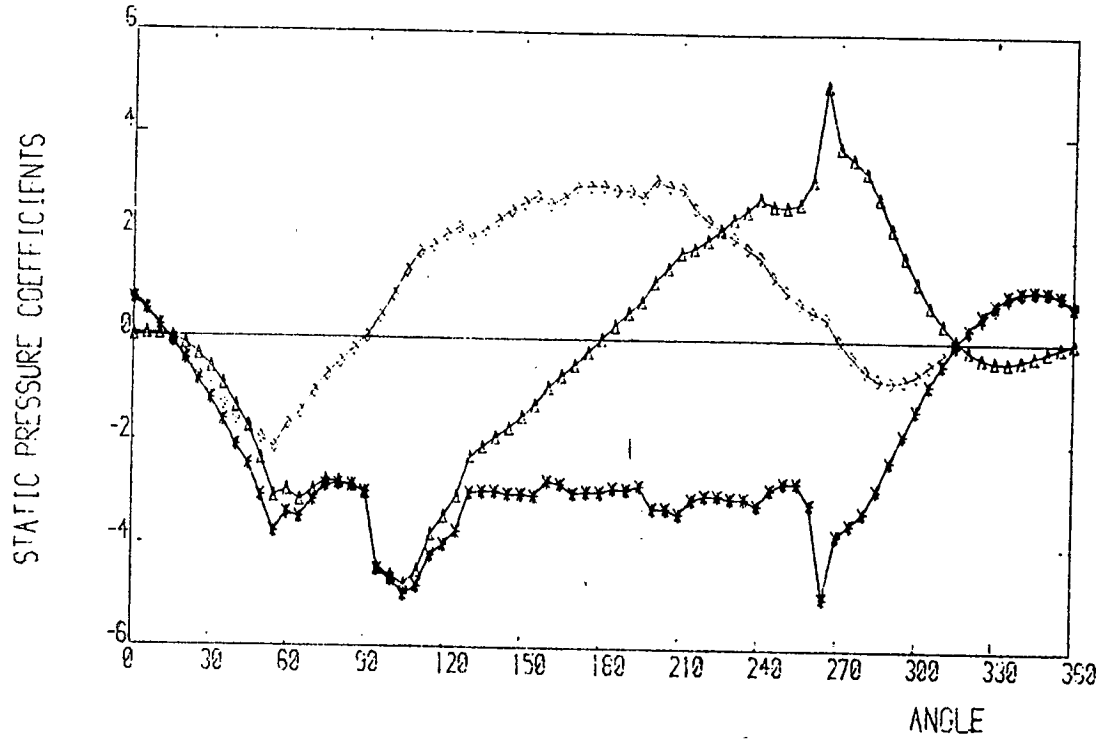


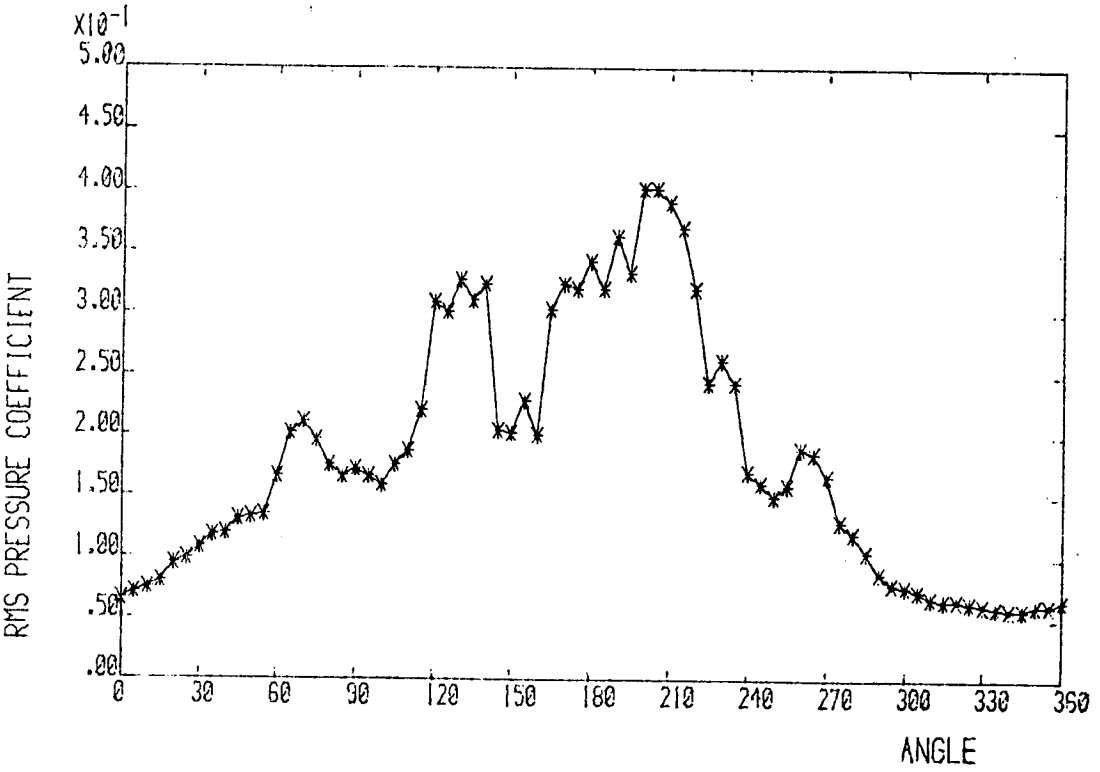


FIGURE 4.3k. Variation of static and r.m.s. pressure coefficients round a fixed tube mounted in a fixed tube row. x/d = 0.7.

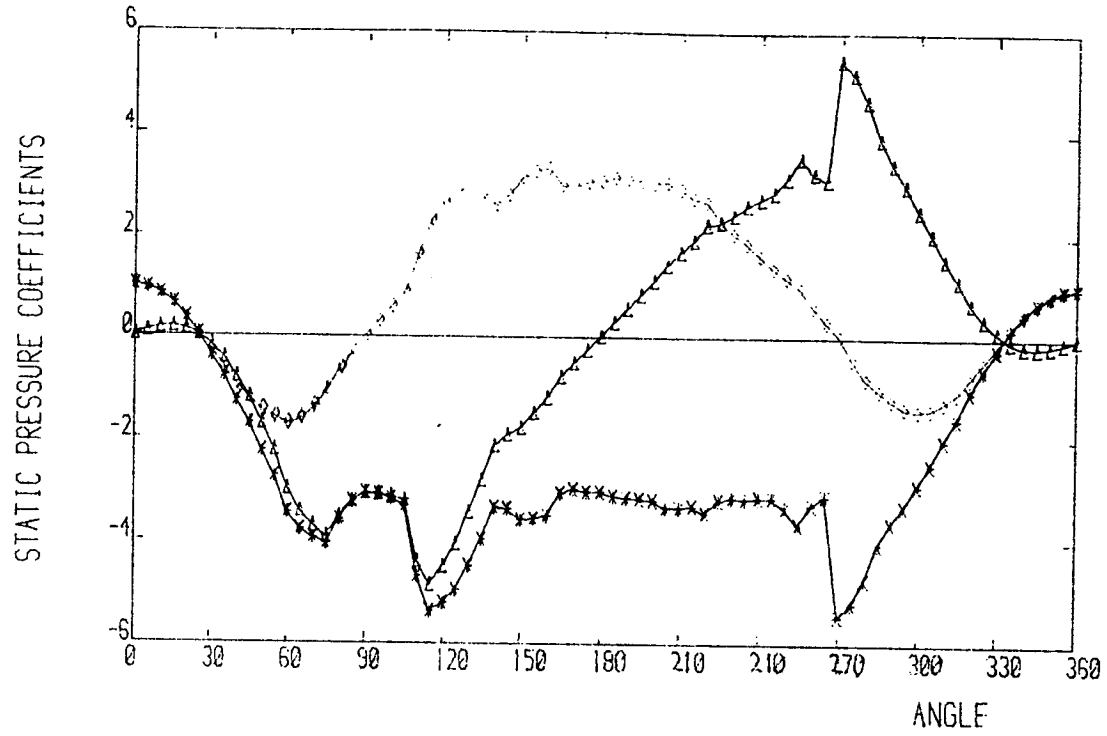


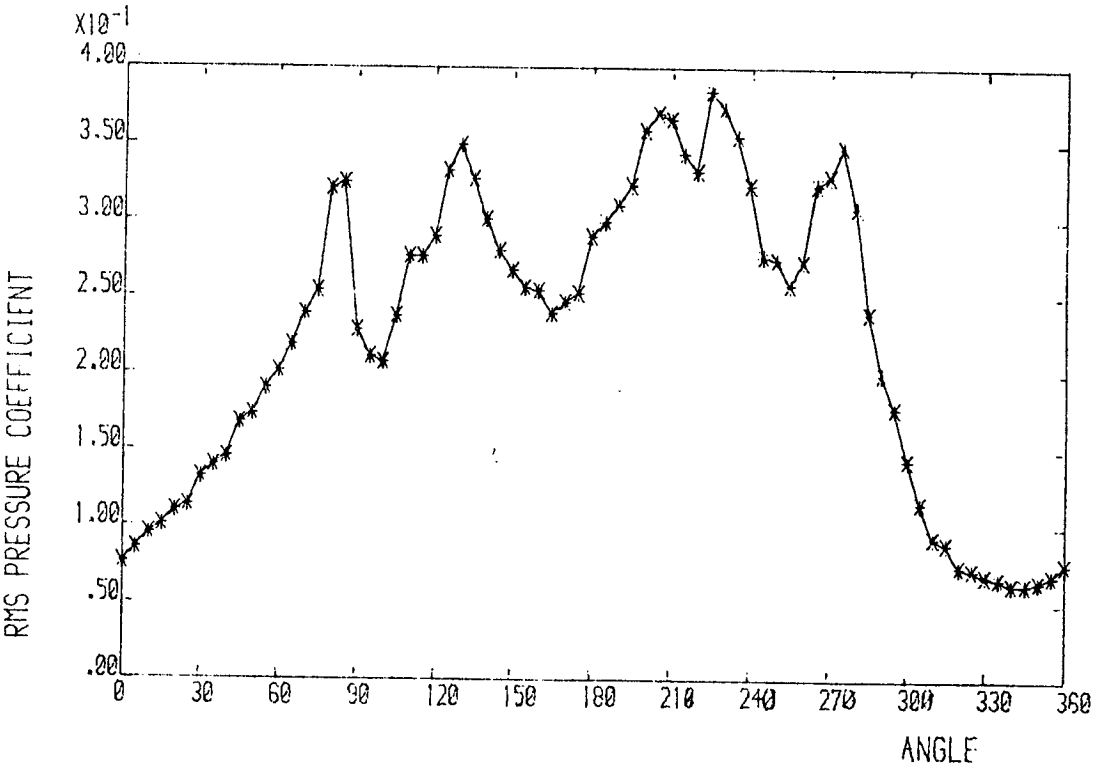


FIGURE 4.4a. Variation of static and r.m.s. pressure coefficients round a fixed tube mounted next to a vibrating tube in a single tube row. x/d = 0.0.

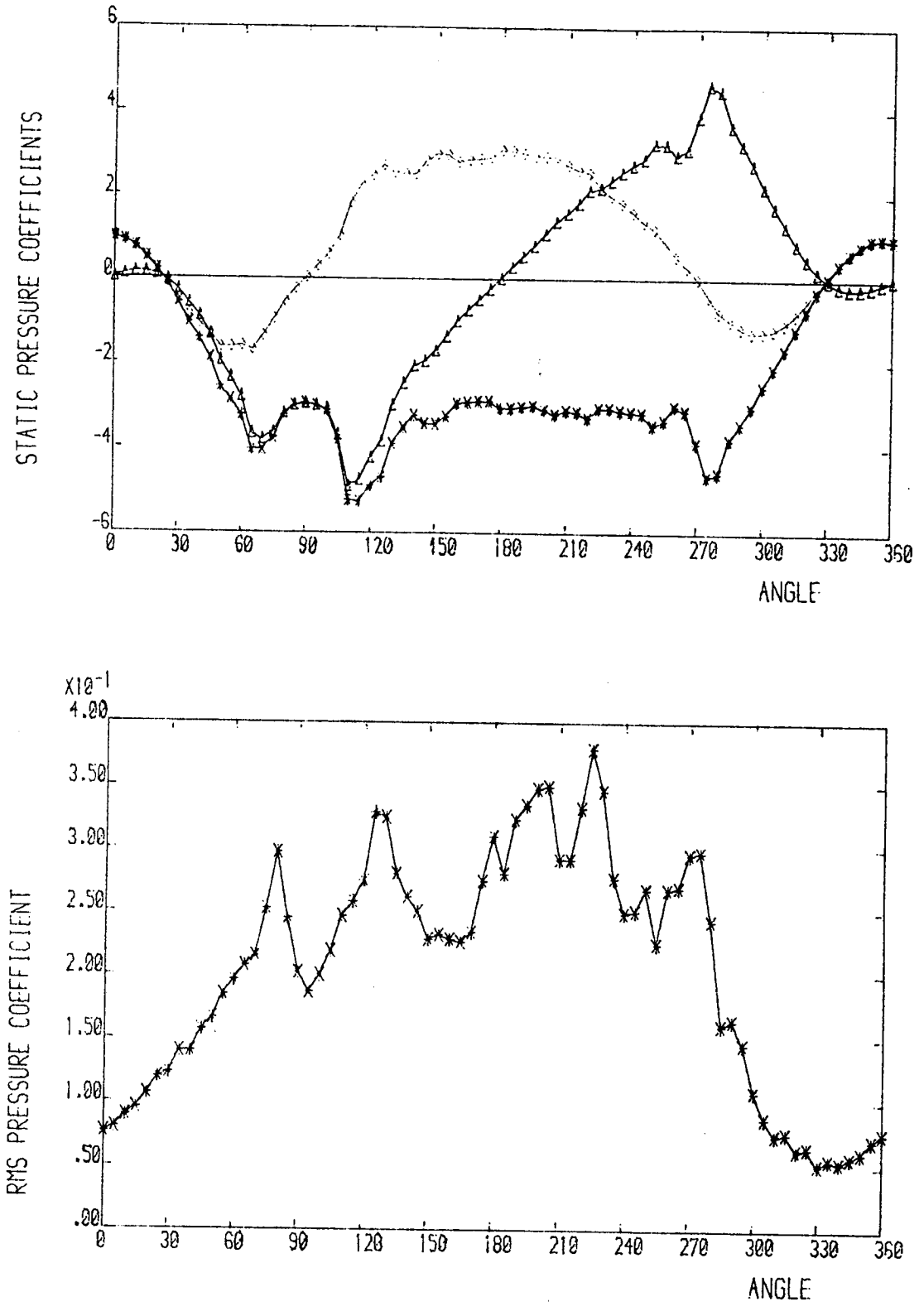


FIGURE 4.4b. Variation of static and r.m.s. pressure coefficients round a fixed tube mounted next to a vibrating tube in a single tube row. x/d = 0.1.

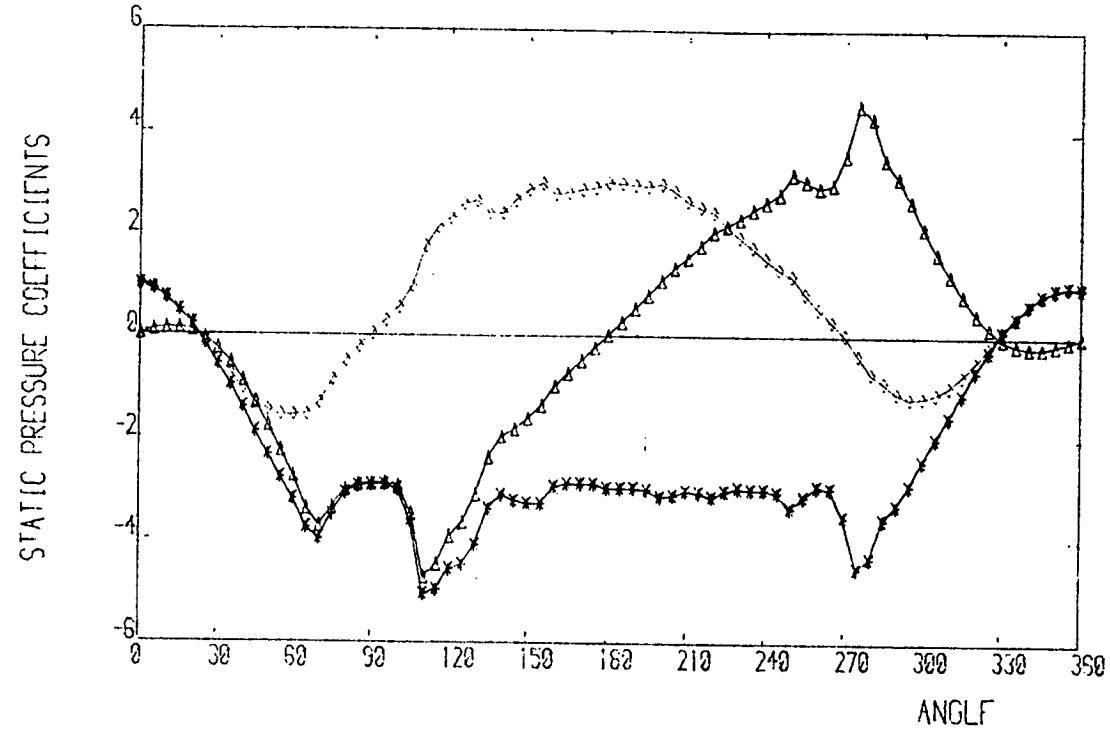


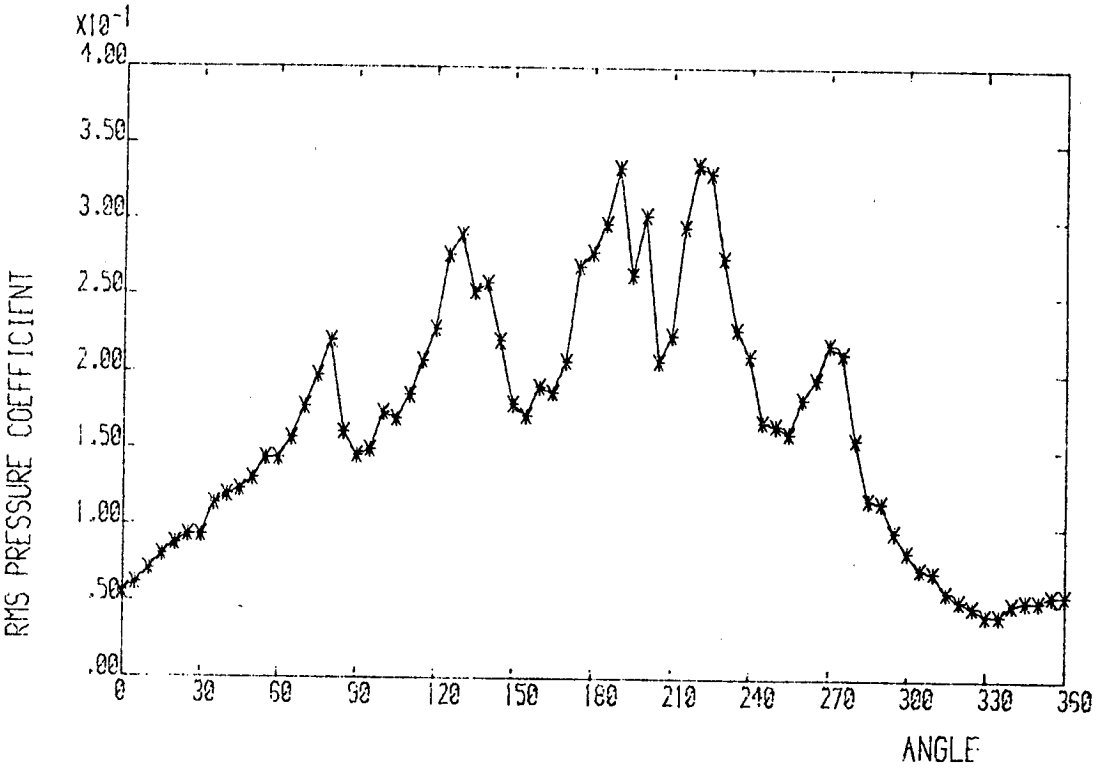


FIGURE 4.4c. Variation of static and r.m.s. pressure coefficients round a fixed tube mounted next to a vibrating tube in a single tube row. x/d = 0.2.

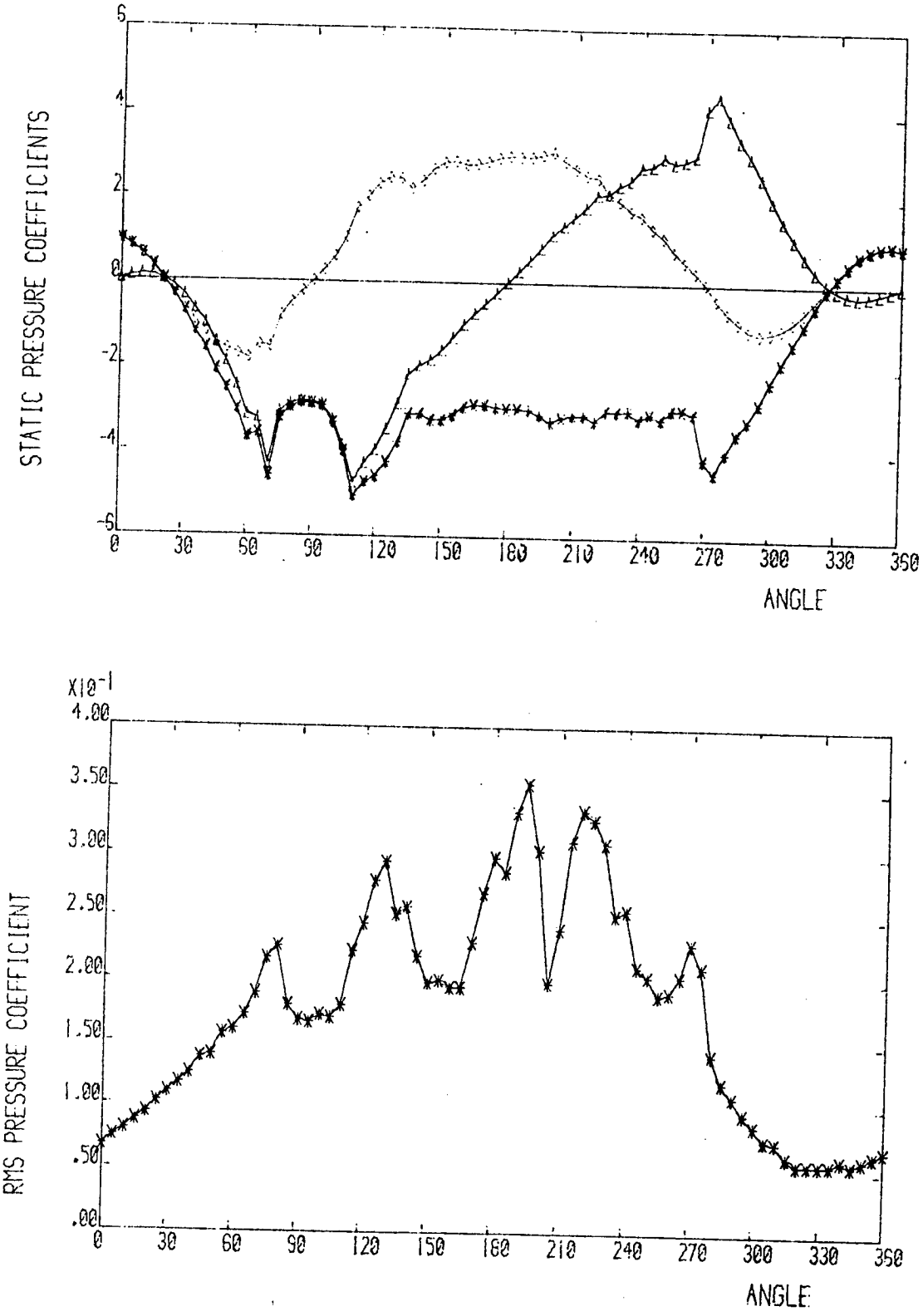


FIGURE 4.4d. Variation of static and r.m.s. pressure coefficients round a fixed tube mounted next to a vibrating tube in a single tube row. x/d = 0.3.

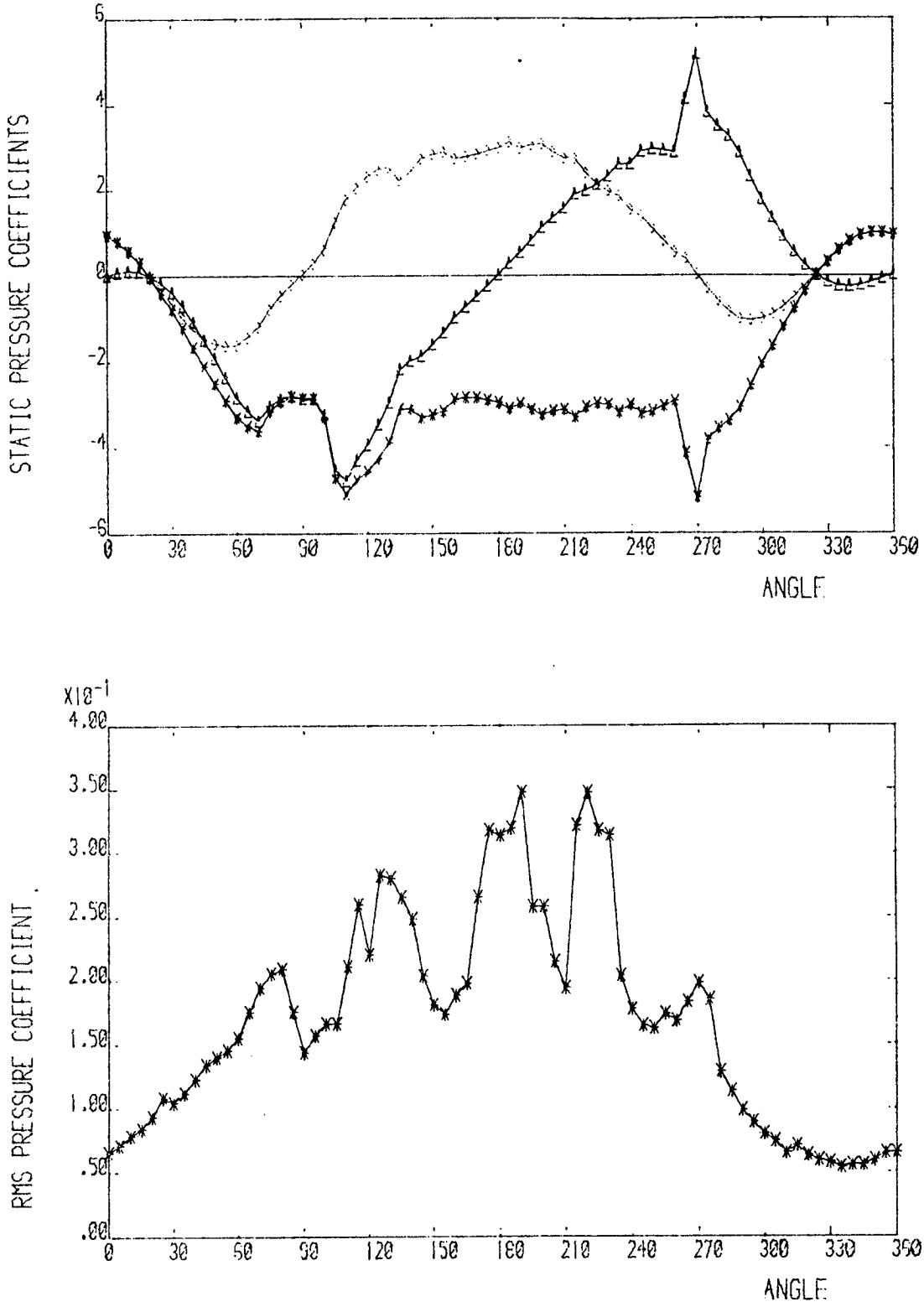


FIGURE 4.4e. Variation of static and r.m.s. pressure coefficients round a fixed tube mounted next to a vibrating tube in a single tube row. x/d = 0.4.

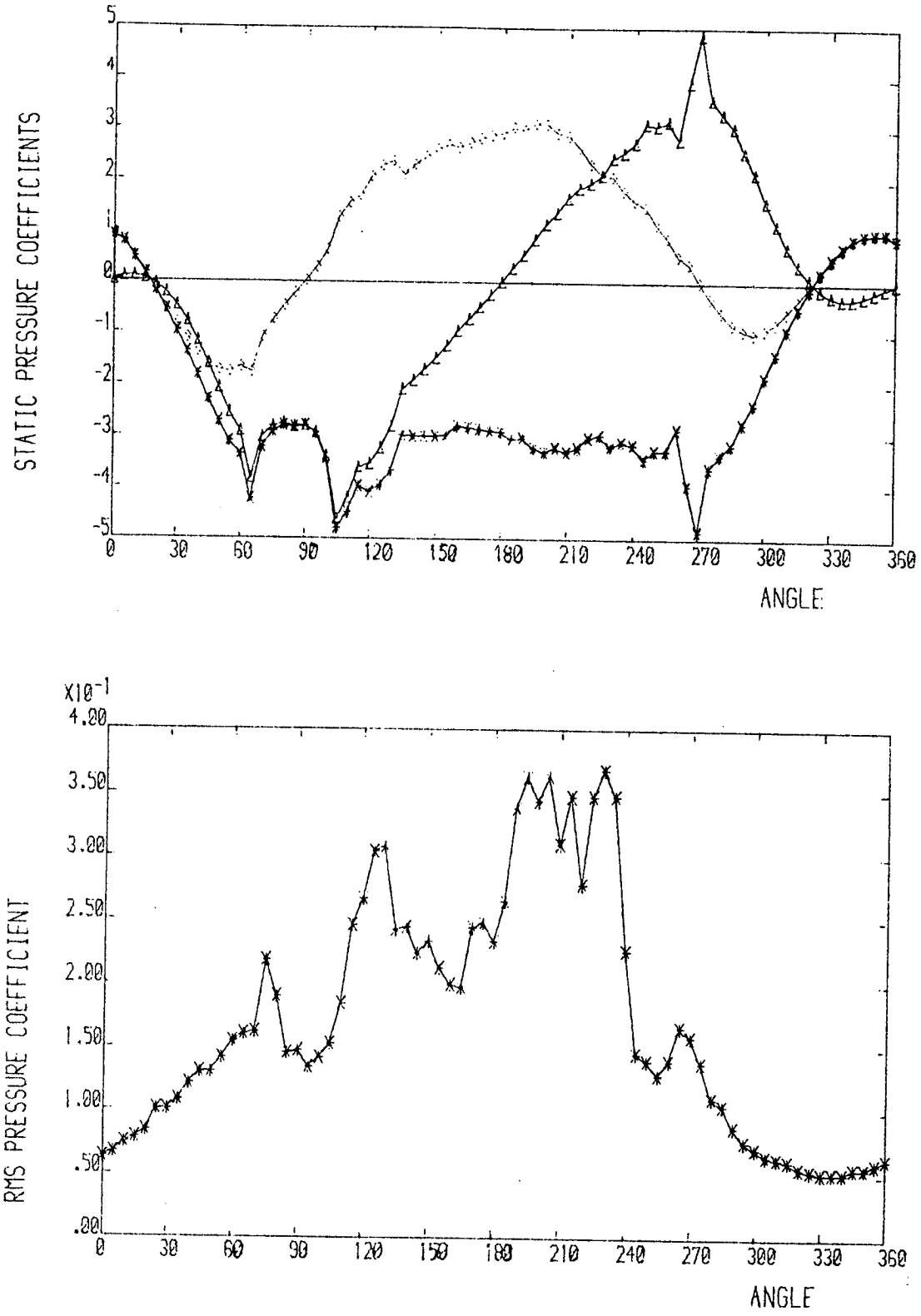


FIGURE 4.4f. Variation of static and r.m.s. pressure coefficients round a fixed tube mounted next to a vibrating tube in a single tube row. x/d = 0.5.

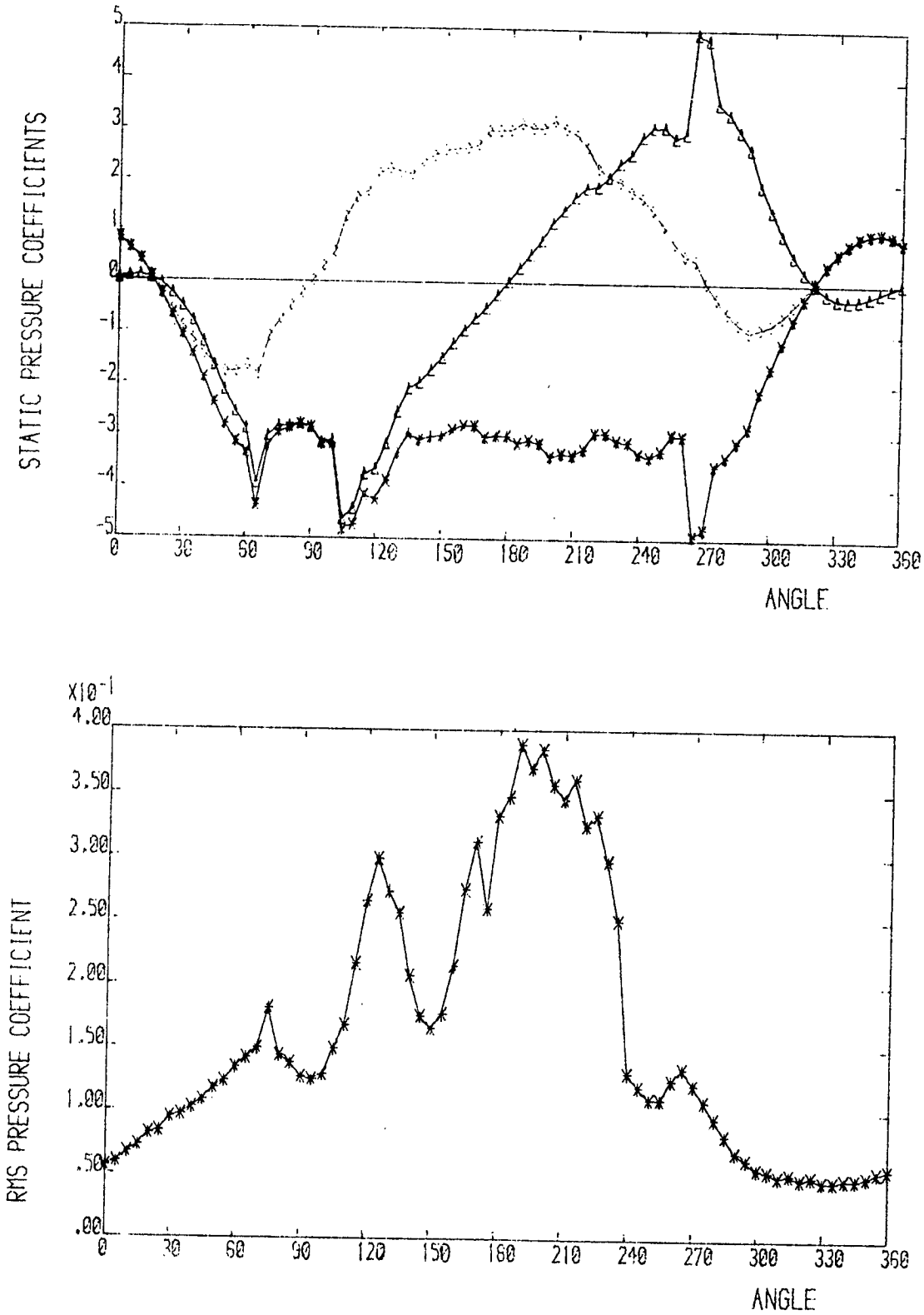


FIGURE 4.4g. Variation of static and r.m.s. pressure coefficients round a fixed tube mounted next to a vibrating tube in a single tube row. x/d = 0.6.

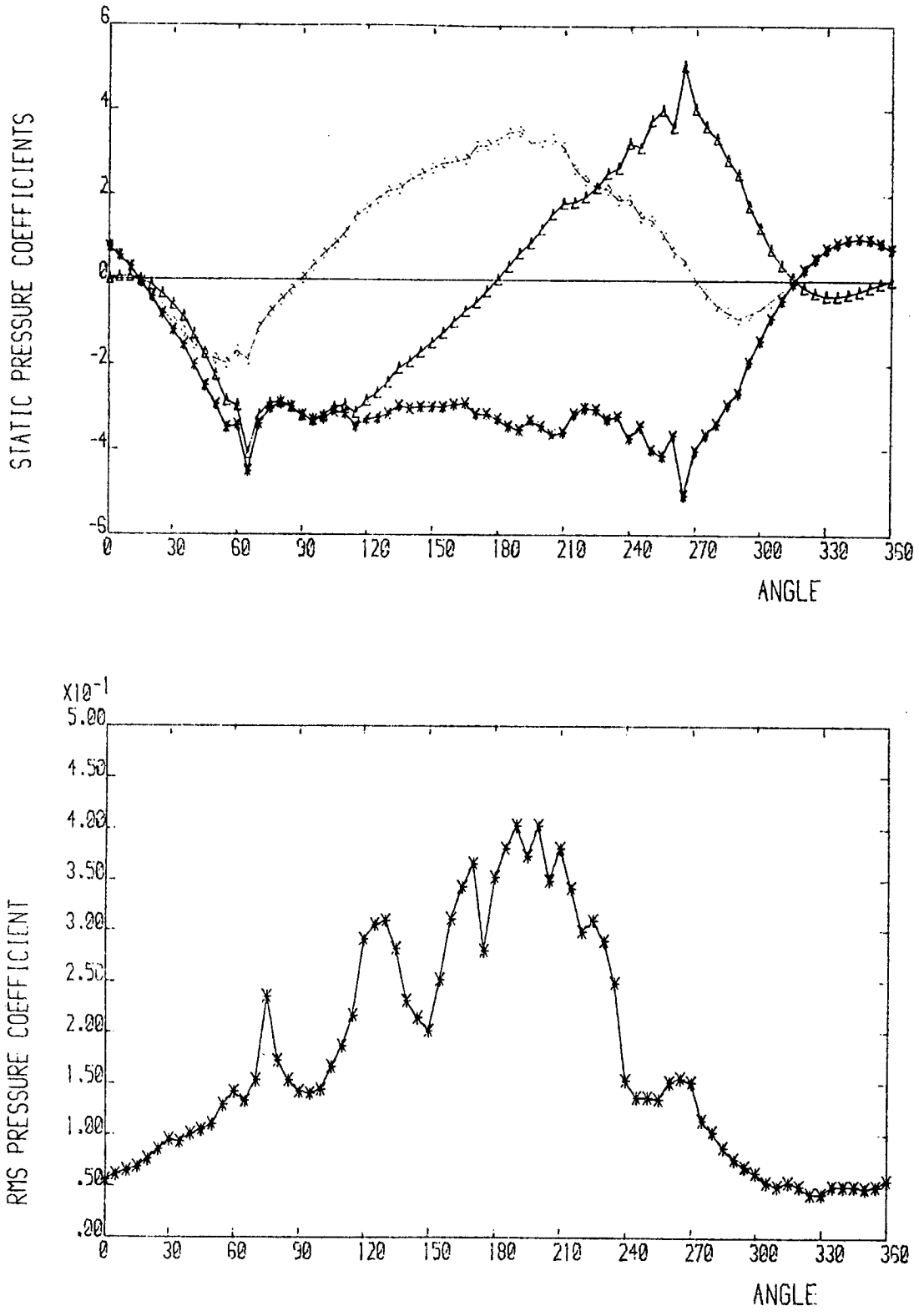


FIGURE 4.4h. Variation of static and r.m.s. pressure coefficients round a fixed tube mounted next to a vibrating tube in a single tube row. x/d = 0.7.

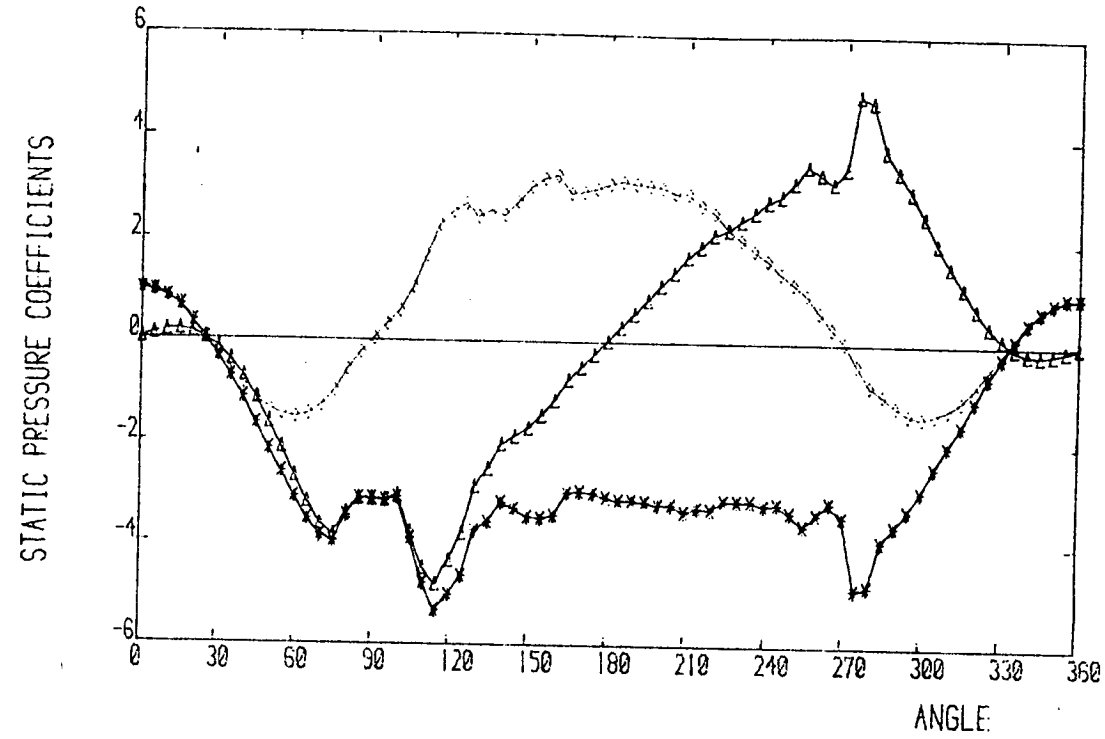


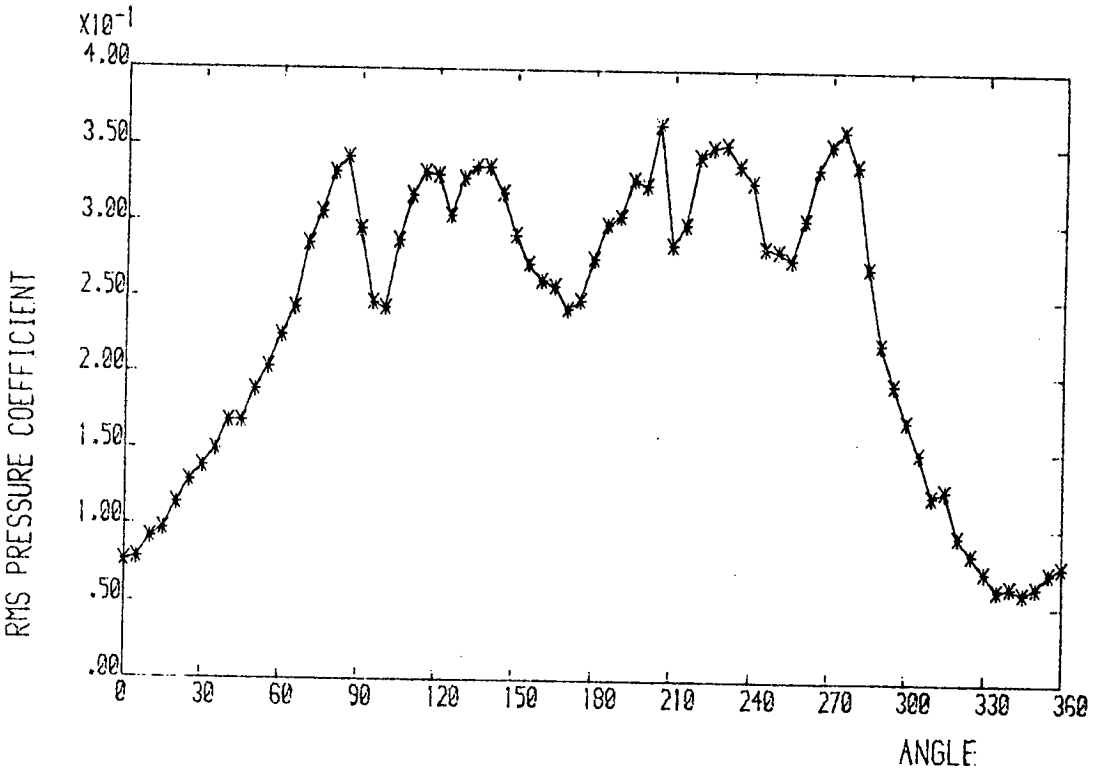


FIGURE 4.5a. Variation of static and r.m.s. pressure coefficients round a fixed tube in a single tube row at 0 diameters from the centre of the tube along the spanwise axis.

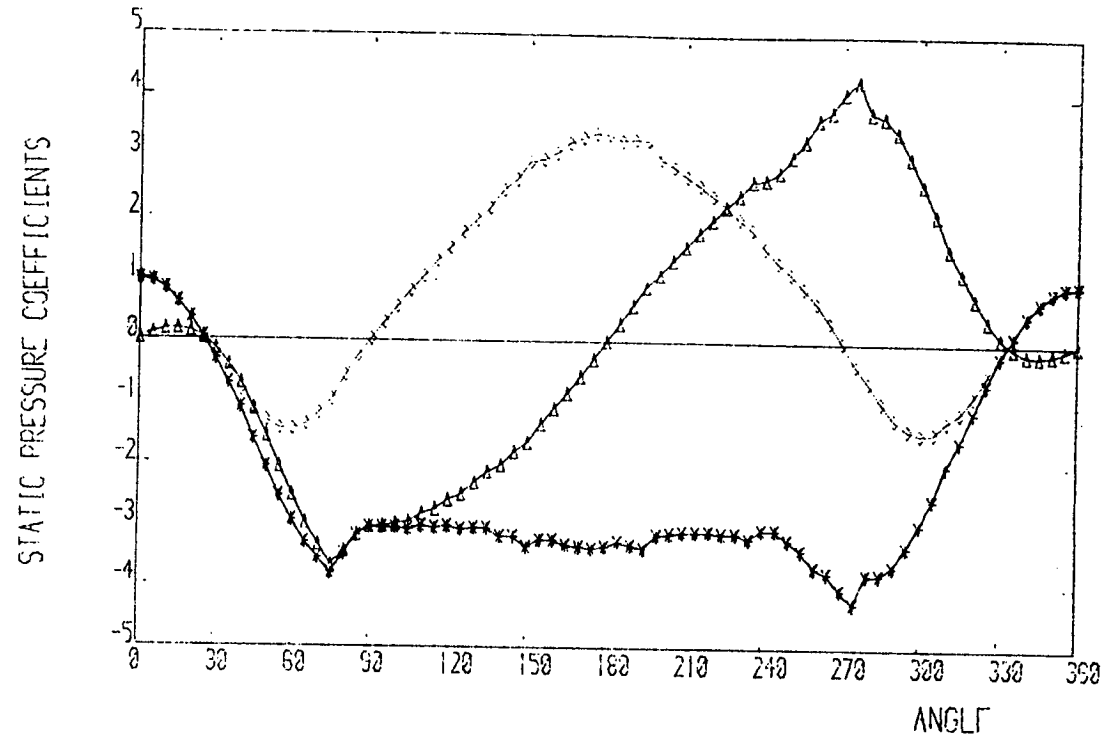


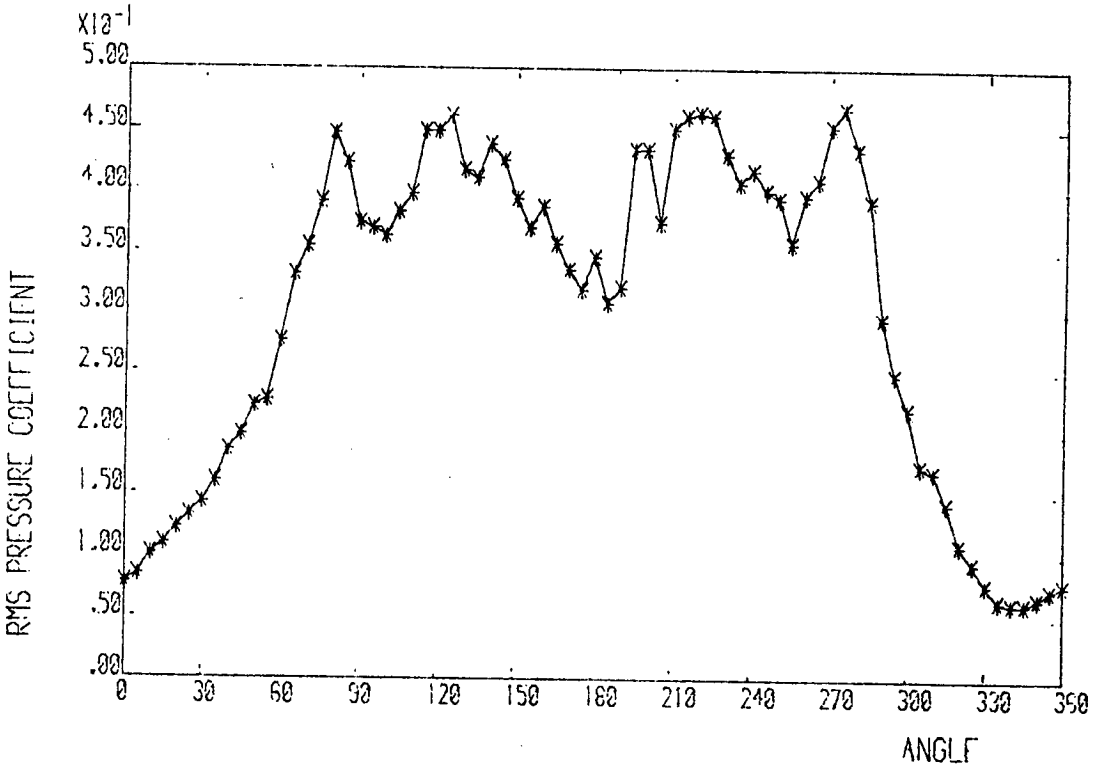


FIGURE 4.5b. Variation of static and r.m.s. pressure coefficients round a fixed tube in a single tube row at 1 diameter from the centre of the tube along the spanwise axis.

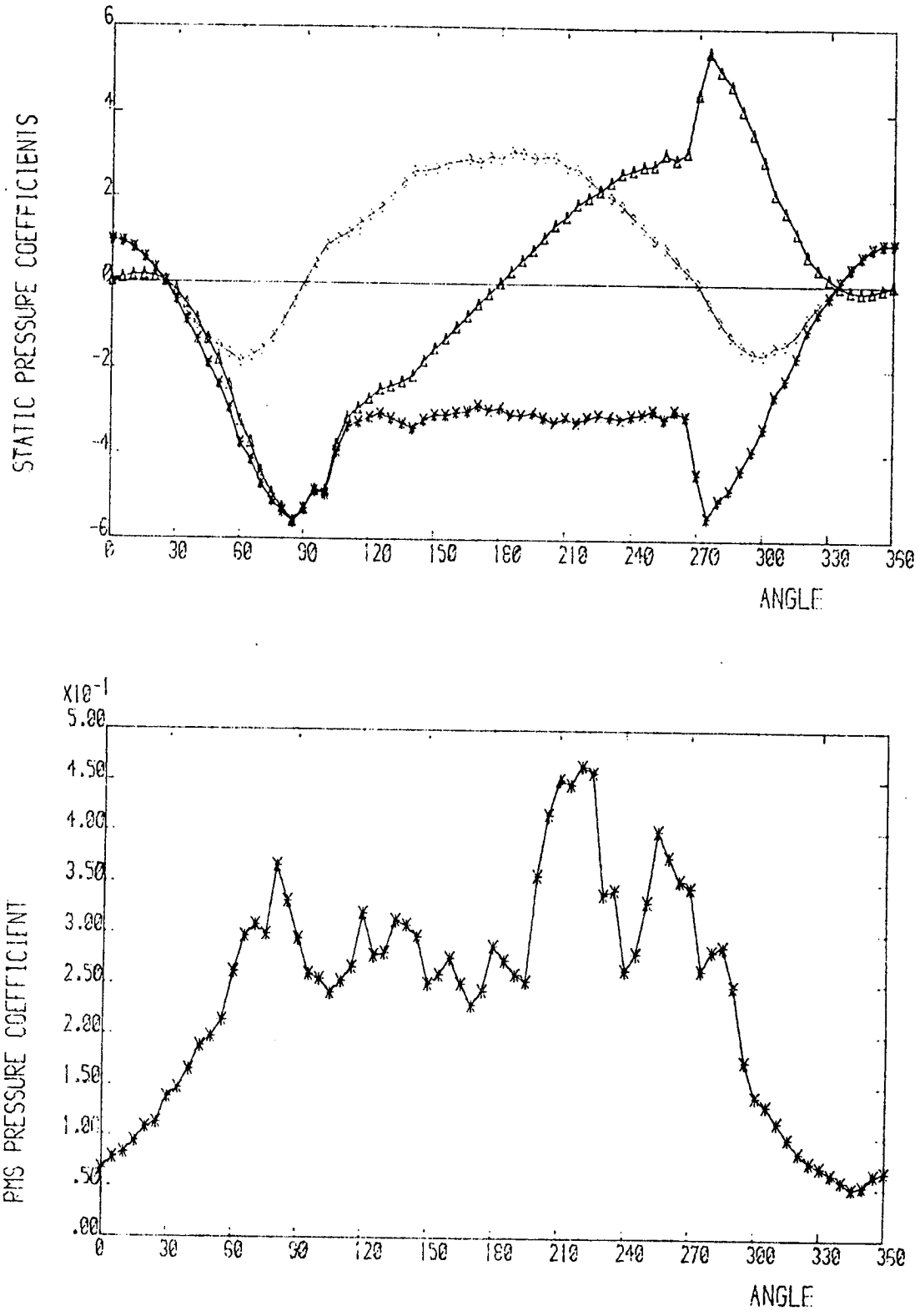


FIGURE 4.5c. Variation of static and r.m.s. pressure coefficients round a fixed tube in a single row at 4 diameters from the centre of the tube along the spanwise axis.

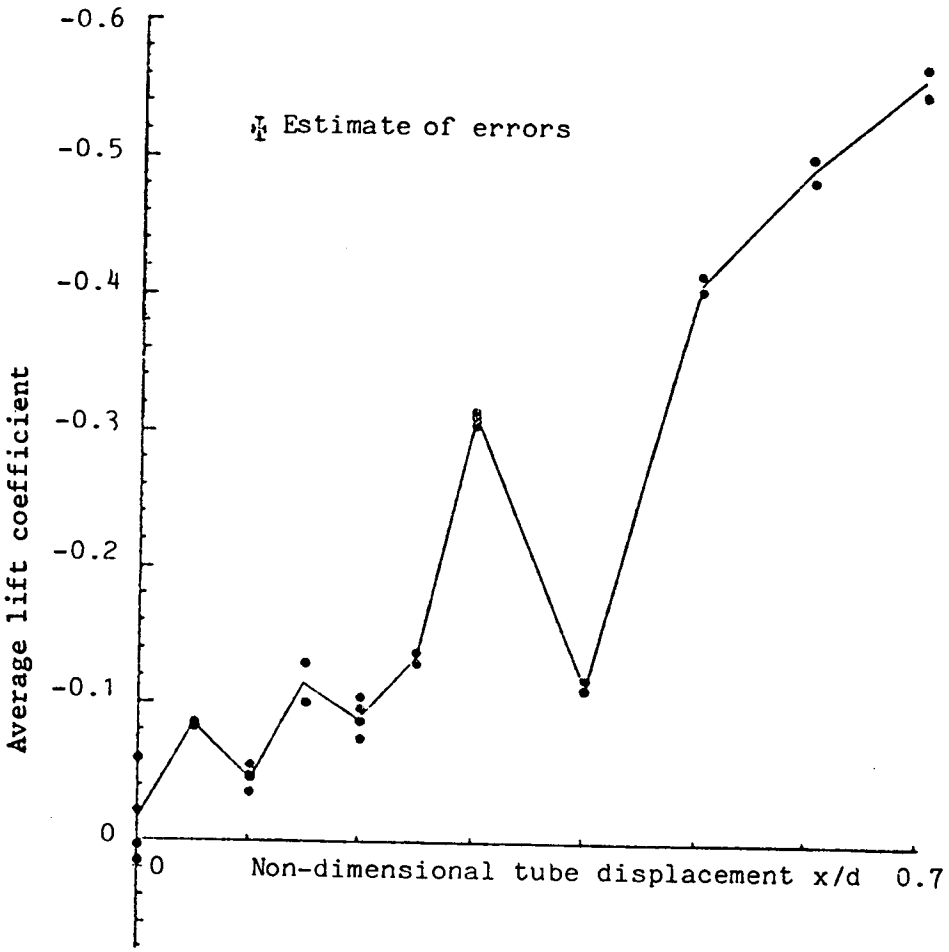


FIGURE 4.6. Average lift coefficient versus tube displacement for a tube in a fixed tube row.

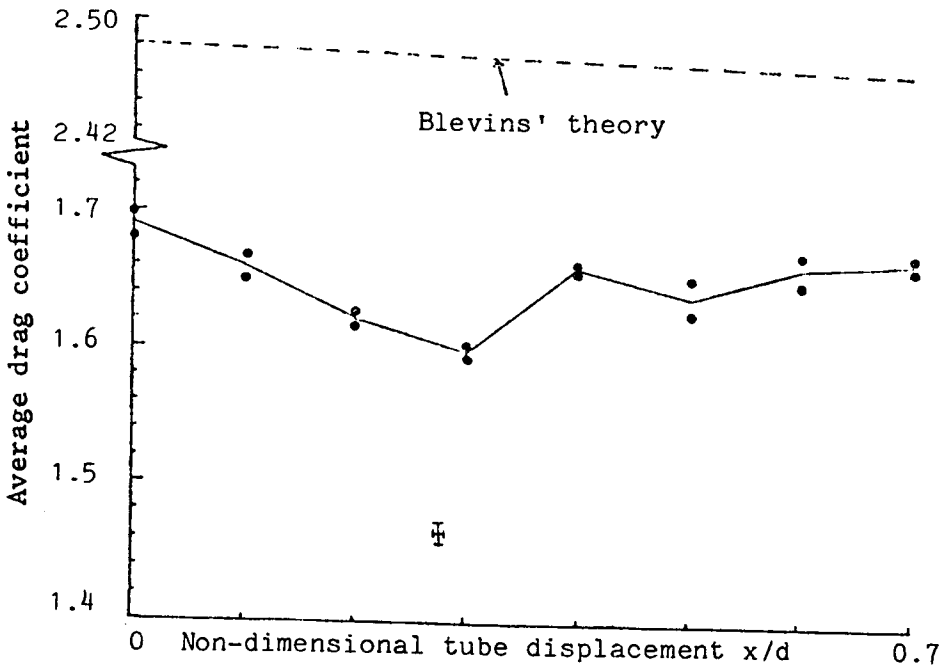


FIGURE 4.7. Average drag coefficient versus tube displacement for a tube in a fixed tube row.

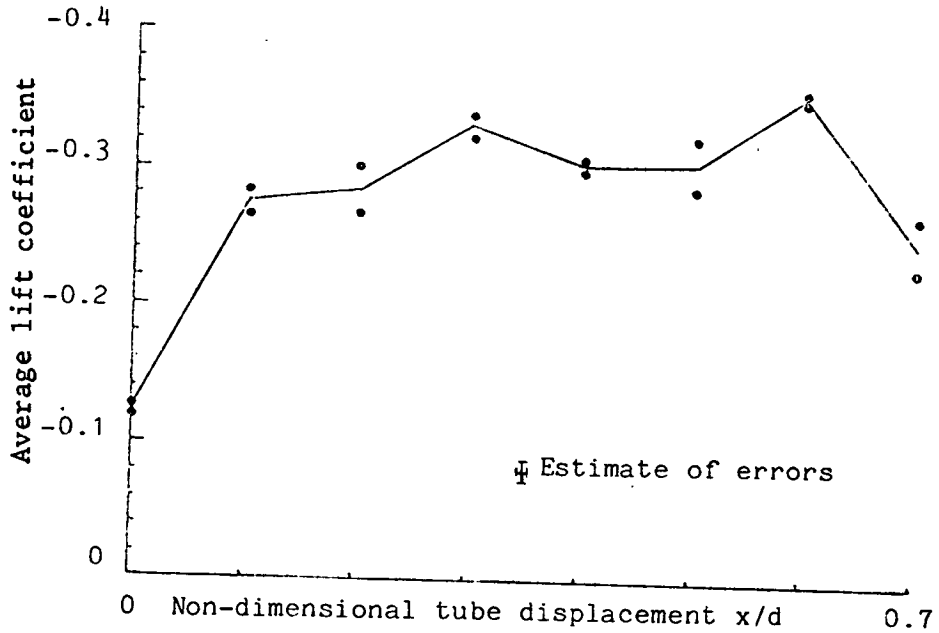


FIGURE 4.8. Average lift coefficient versus tube displacement for a tube mounted next to a vibrating tube in a fixed tube row.

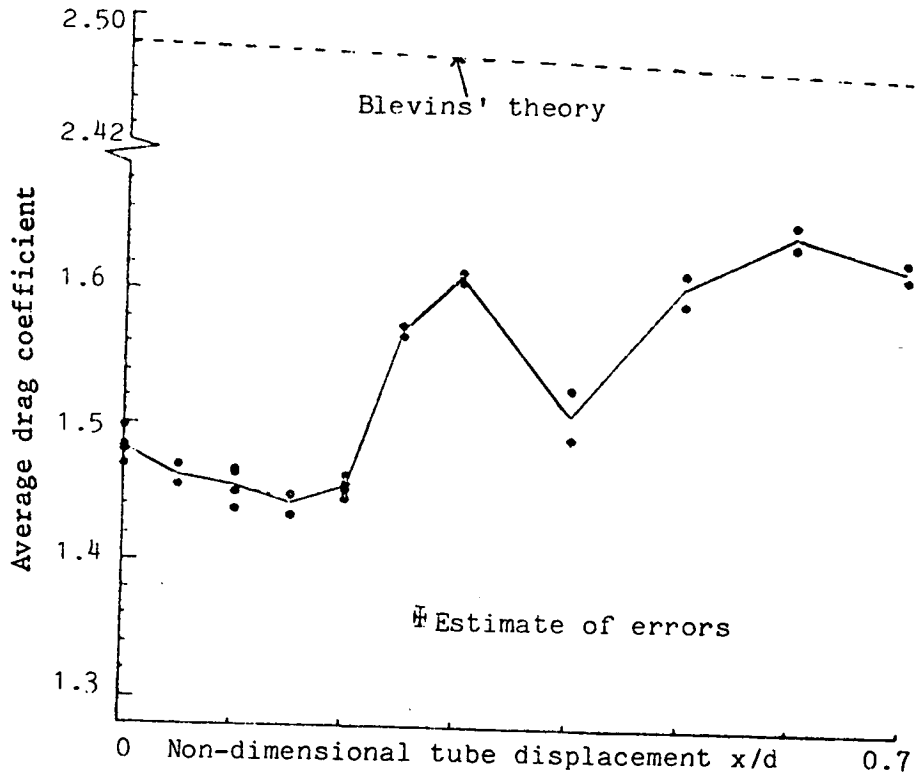


FIGURE 4.9. Average drag coefficient versus tube displacement for a tube next to a vibrating flexible tube.

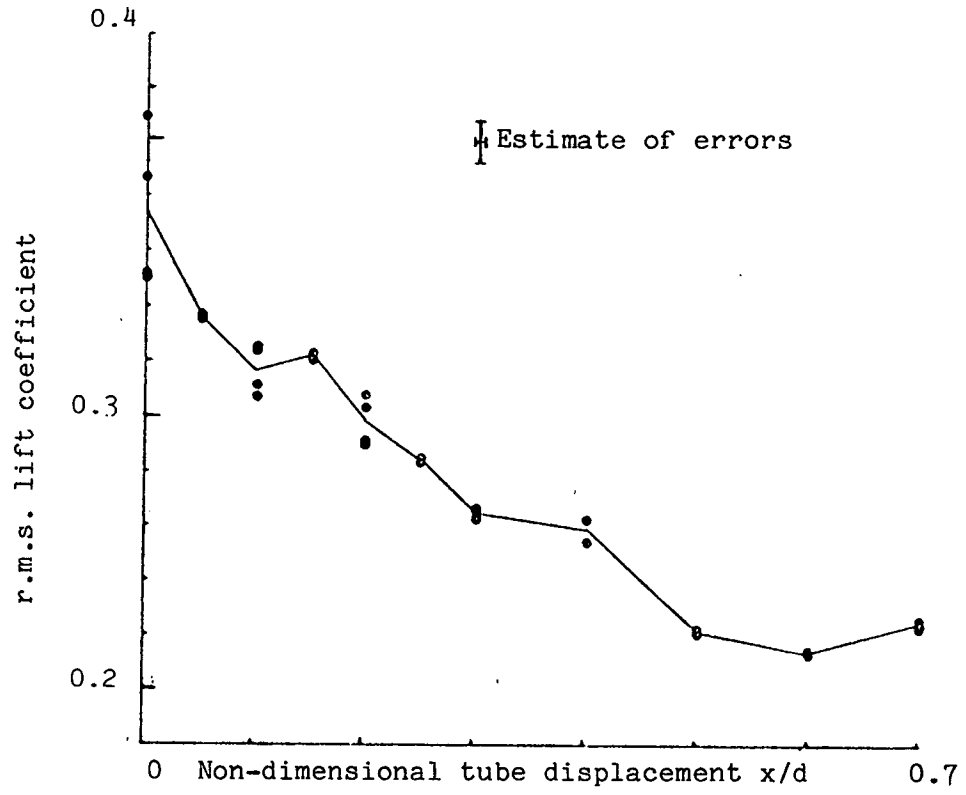


FIGURE 4.10. Fluctuating (r.m.s.) lift coefficient versus tube displacement for a tube in a fixed tube row.

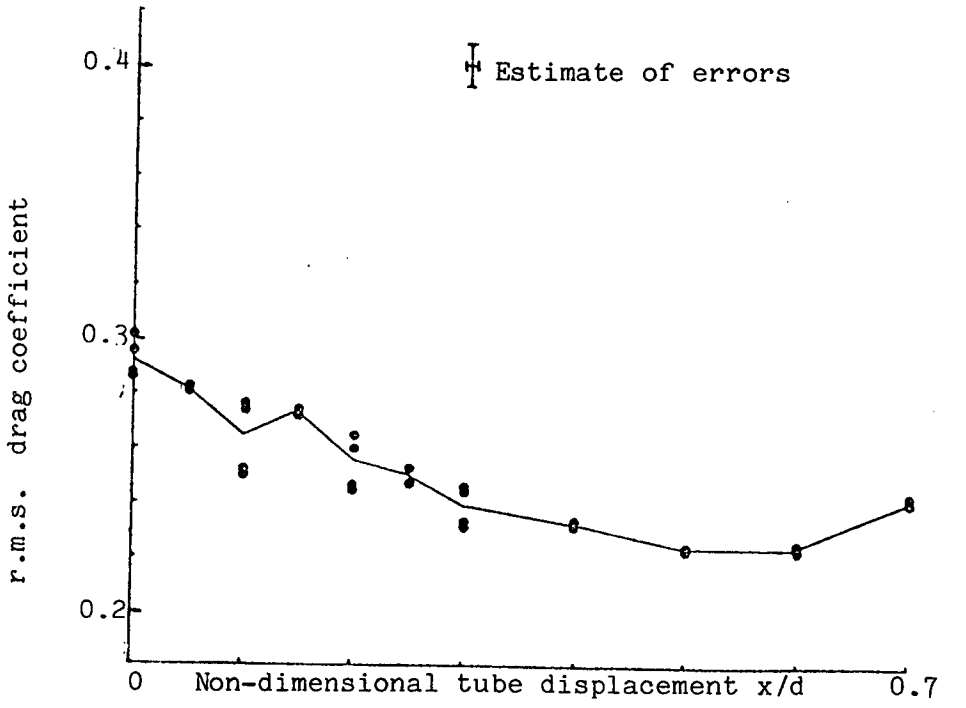


FIGURE 4.11. Fluctuating (r.m.s.)drag coefficient versus tube displacement for a tube in a fixed tube row.

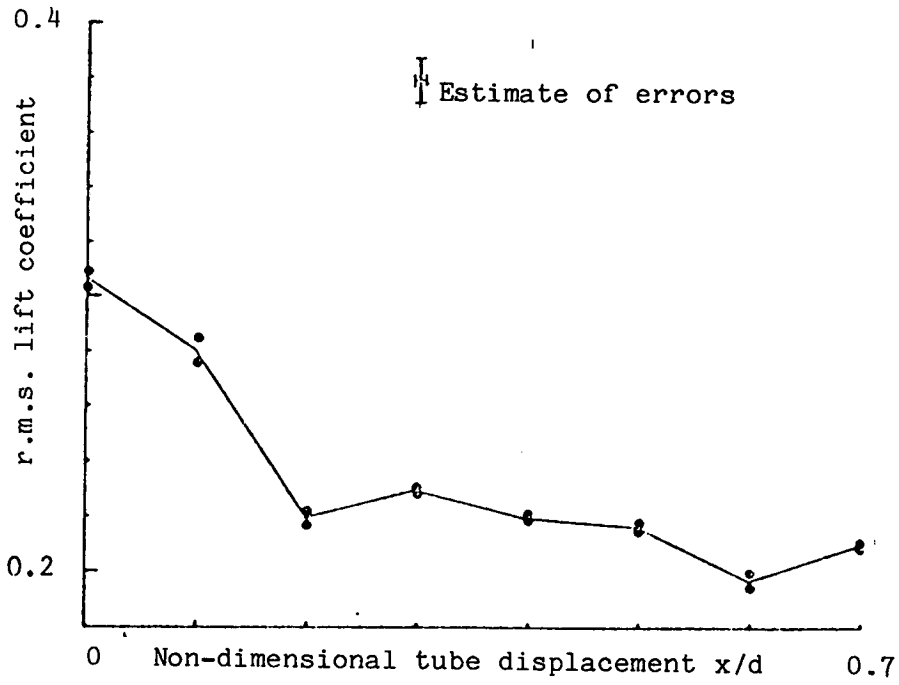


FIGURE 4.12 Fluctuating (r.m.s.) lift coefficient versus tube displacement for a tube mounted next to a vibrating tube in a fixed tube row.

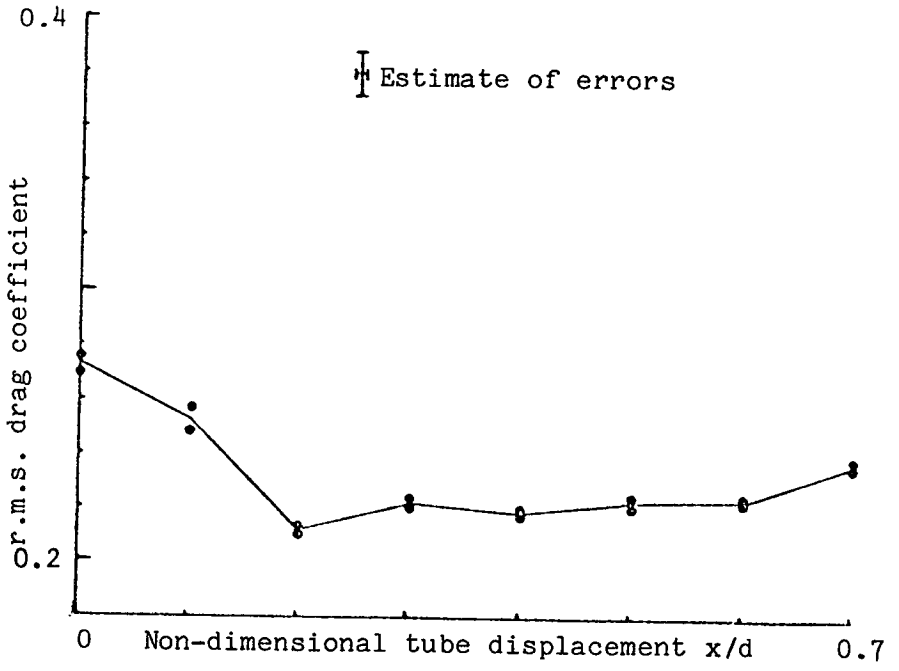


FIGURE 4.13. Fluctuating (r.m.s.) drag coefficient versus tube displacement for a tube mounted next to a vibrating tube in a fixed tube row.

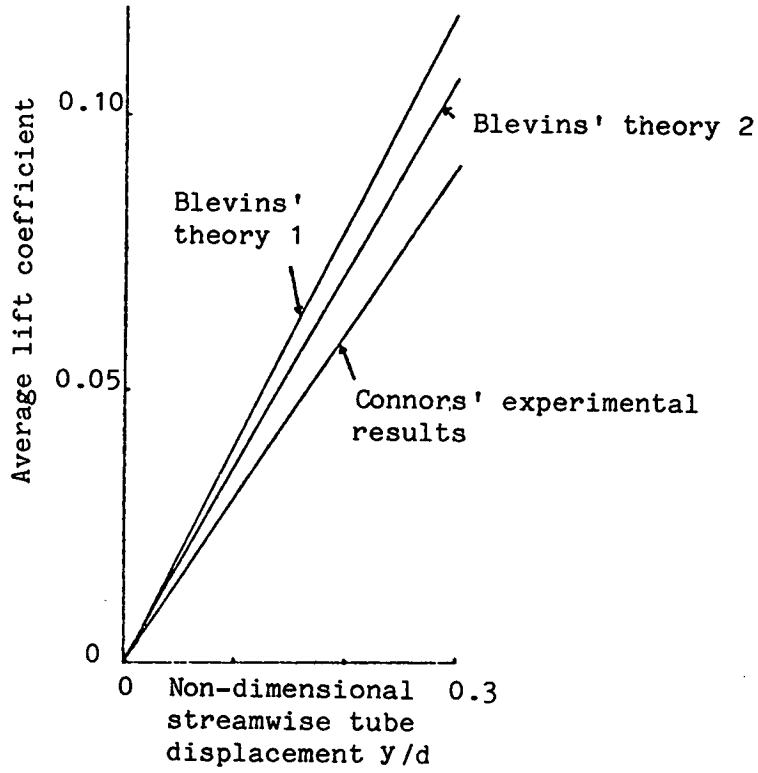


FIGURE 4.14. Comparison of average (steady) lift coefficients precicted by Blevins' theory and measured by Connors. (Based on minimum gap velocity.)

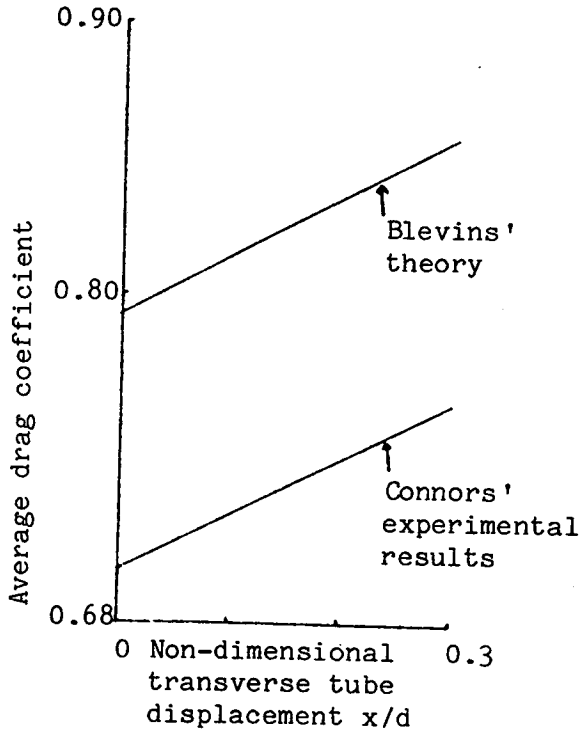


FIGURE 4.15. Comparison of average (steady) drag coefficients predicted by Blevins' theory and measured by Connors. (Based on minimum gap velocity.)

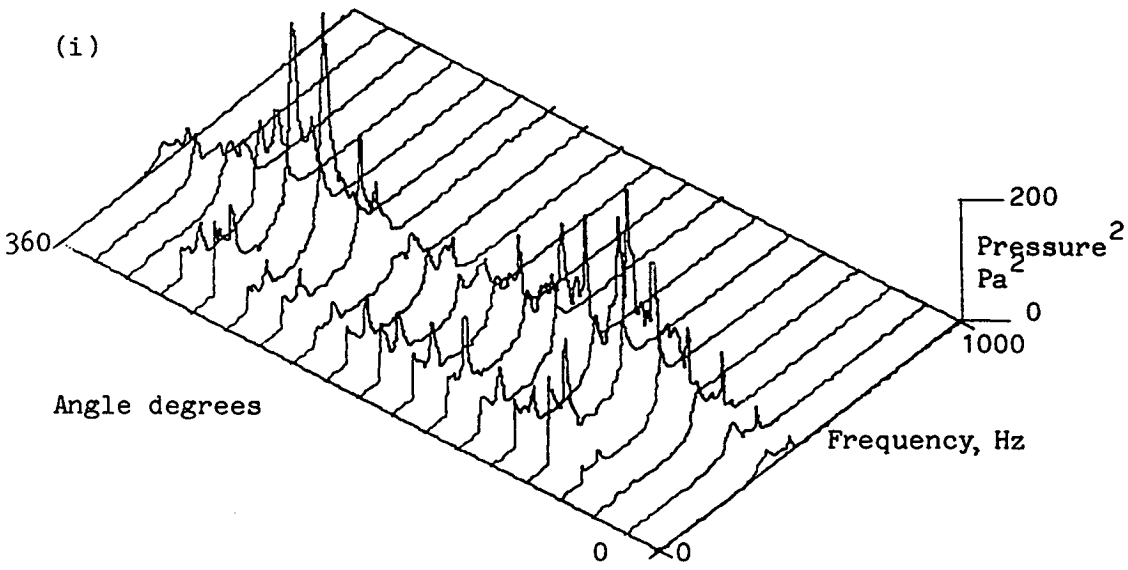


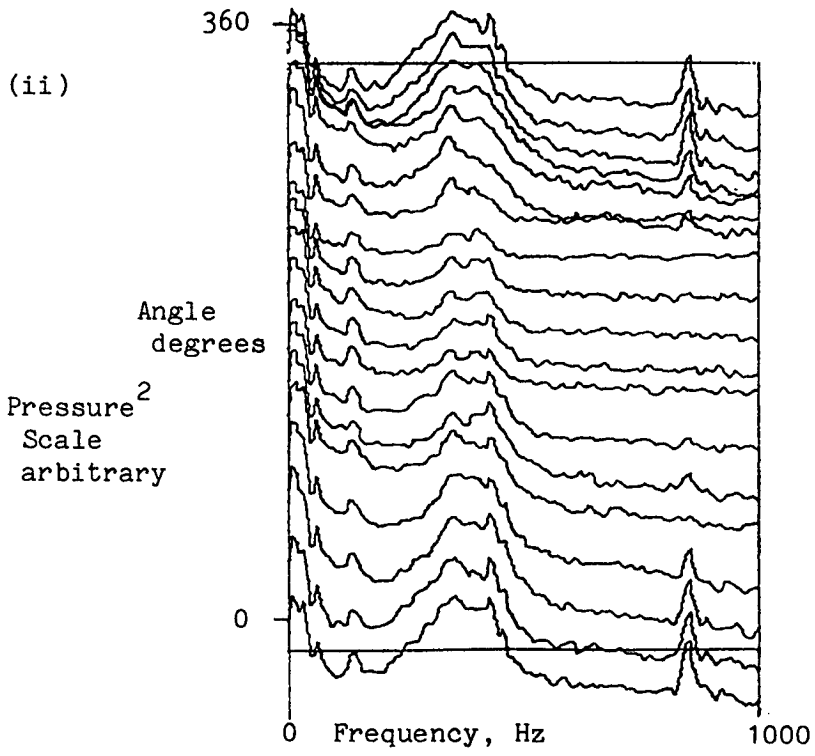


FIGURE 4.16. Variation of the P.S.D. of pressure round a fixed tube in a uniformly spaced fixed row of tubes. (i) Linear (ii) Logarithmic.

(i)

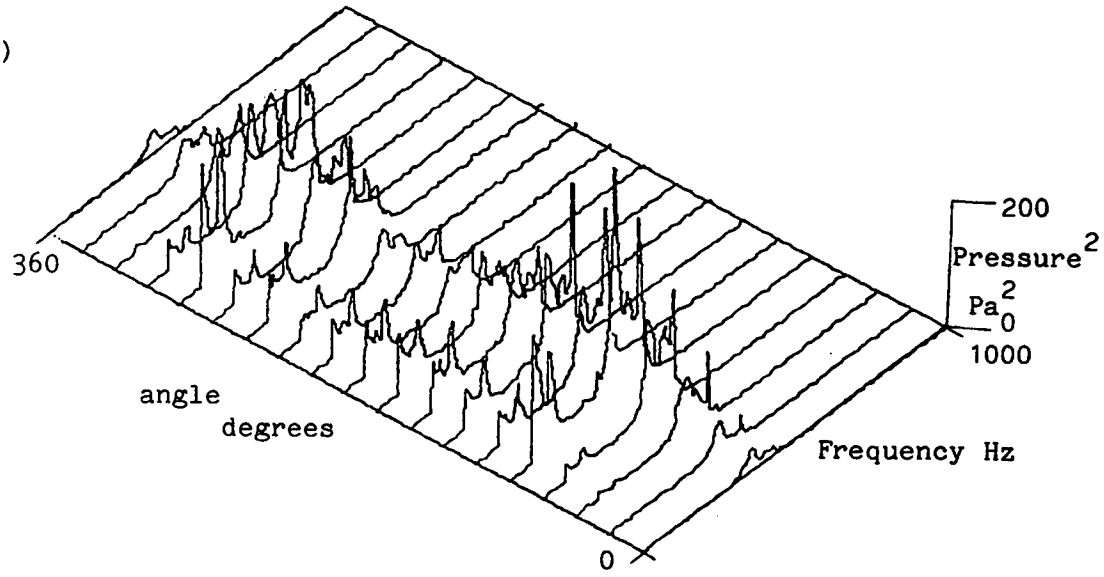


(ii)

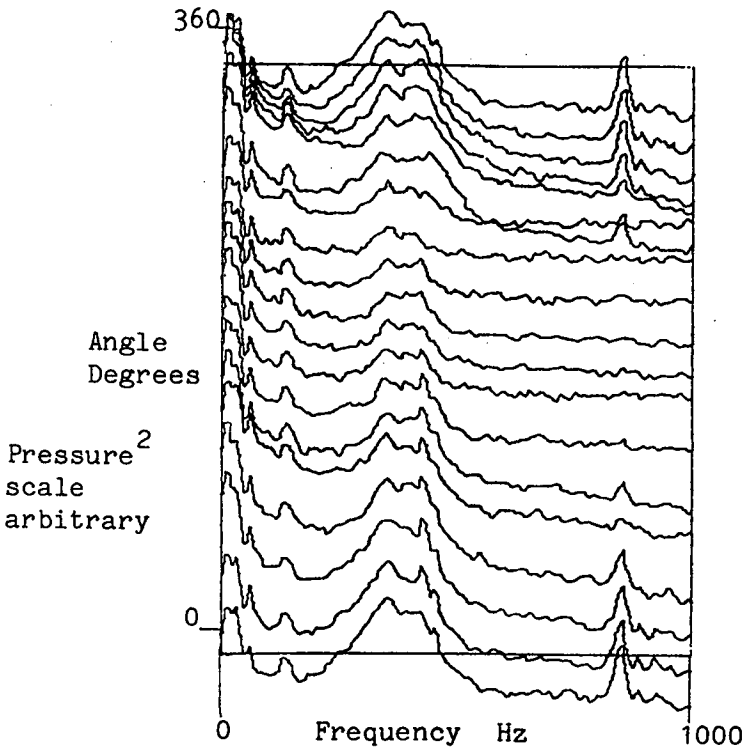


FIGURE 4.17. Variation of P.S.D. of pressure round a fixed tube displaced by 0.1 diameter in a uniformly spaced row of fixed tubes. (i) Linear (ii) Logarithmic.

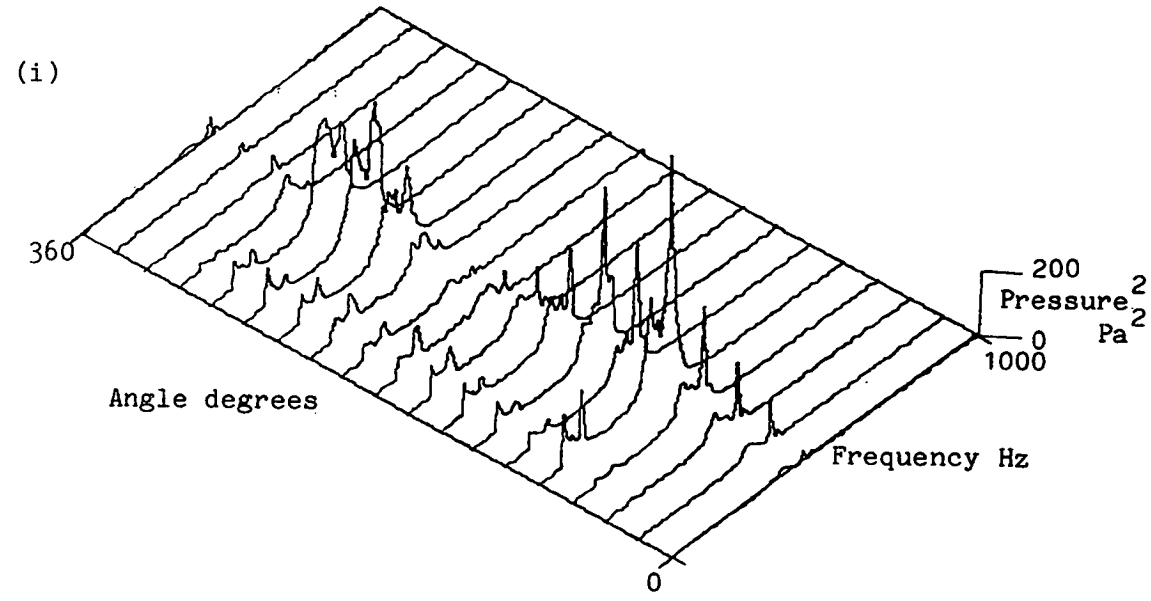


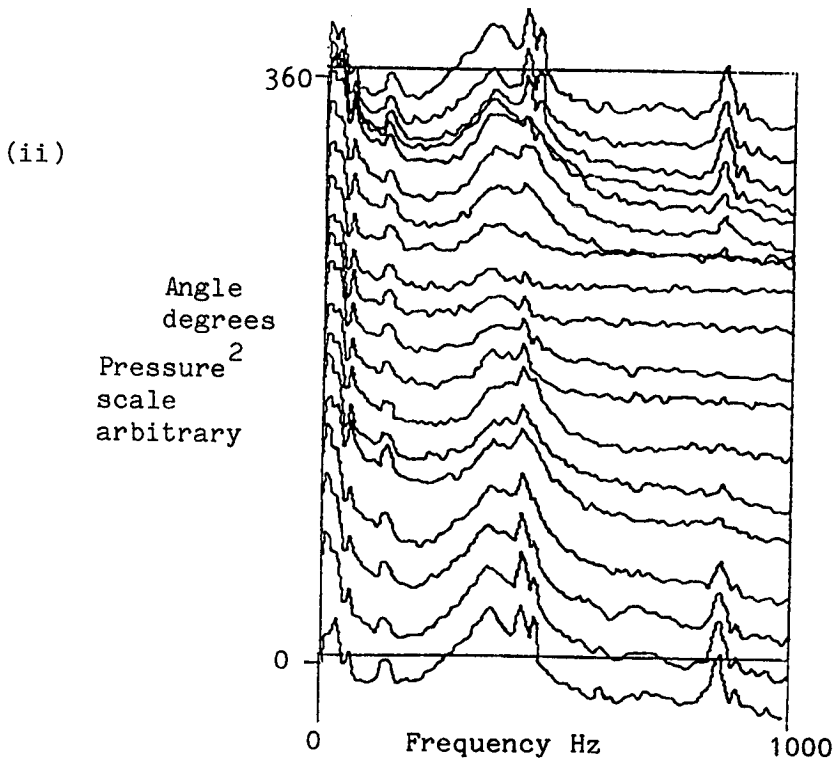


FIGURE 4.18. Variation of P.S.D. of pressure round a fixed tube mounted next to a vibrating tube in a uniformly spaced fixed tube row. (i) Linear (ii) Logarithmic.

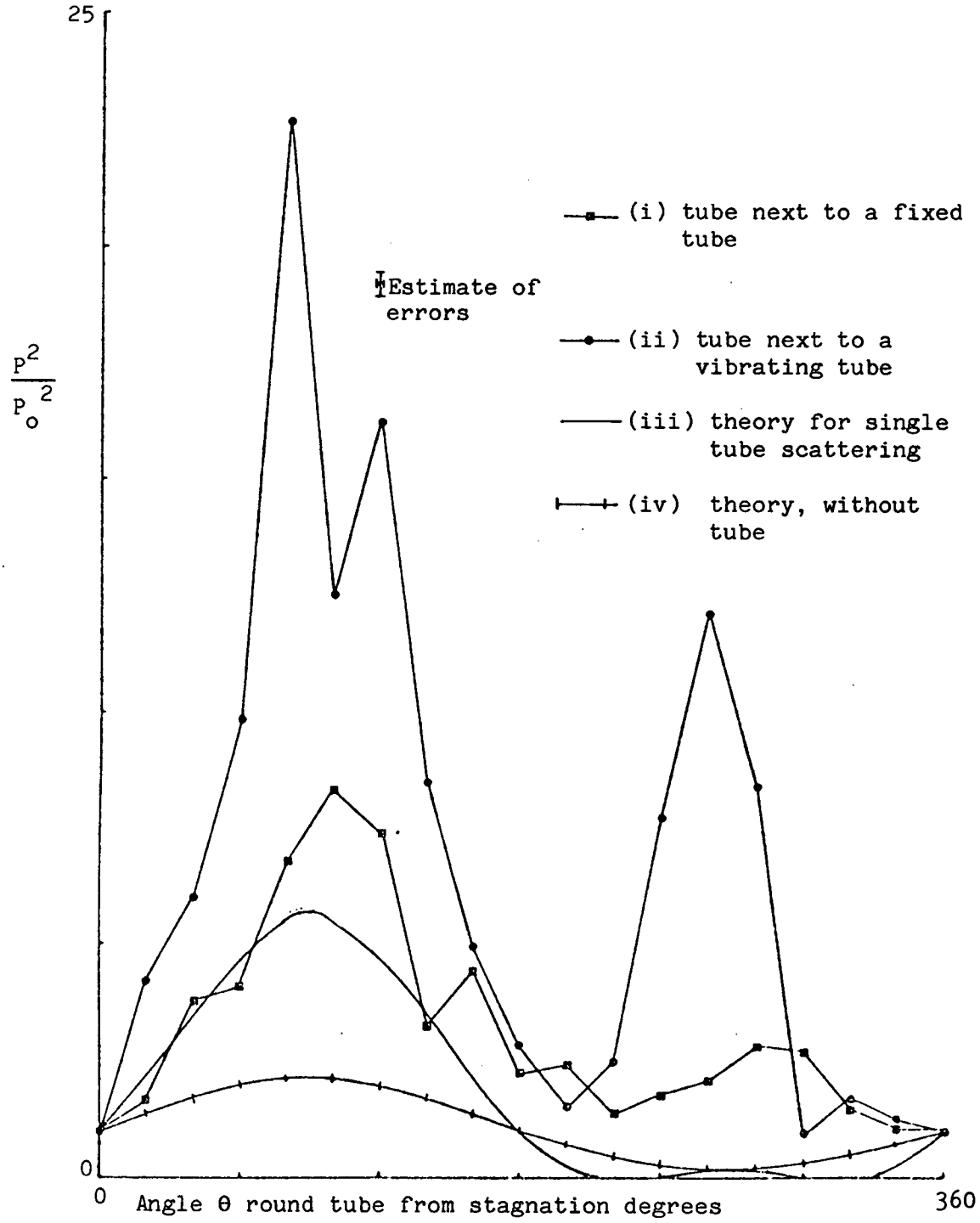


FIGURE 4.19. Variation of the ratio of pressure$^2$ at θ degrees to pressure$^2$ at 0 degrees for a tube next to a (i) fixed and (ii) vibrating tube for the first transverse acoustic duct mode. (Experimental results compared with theory)

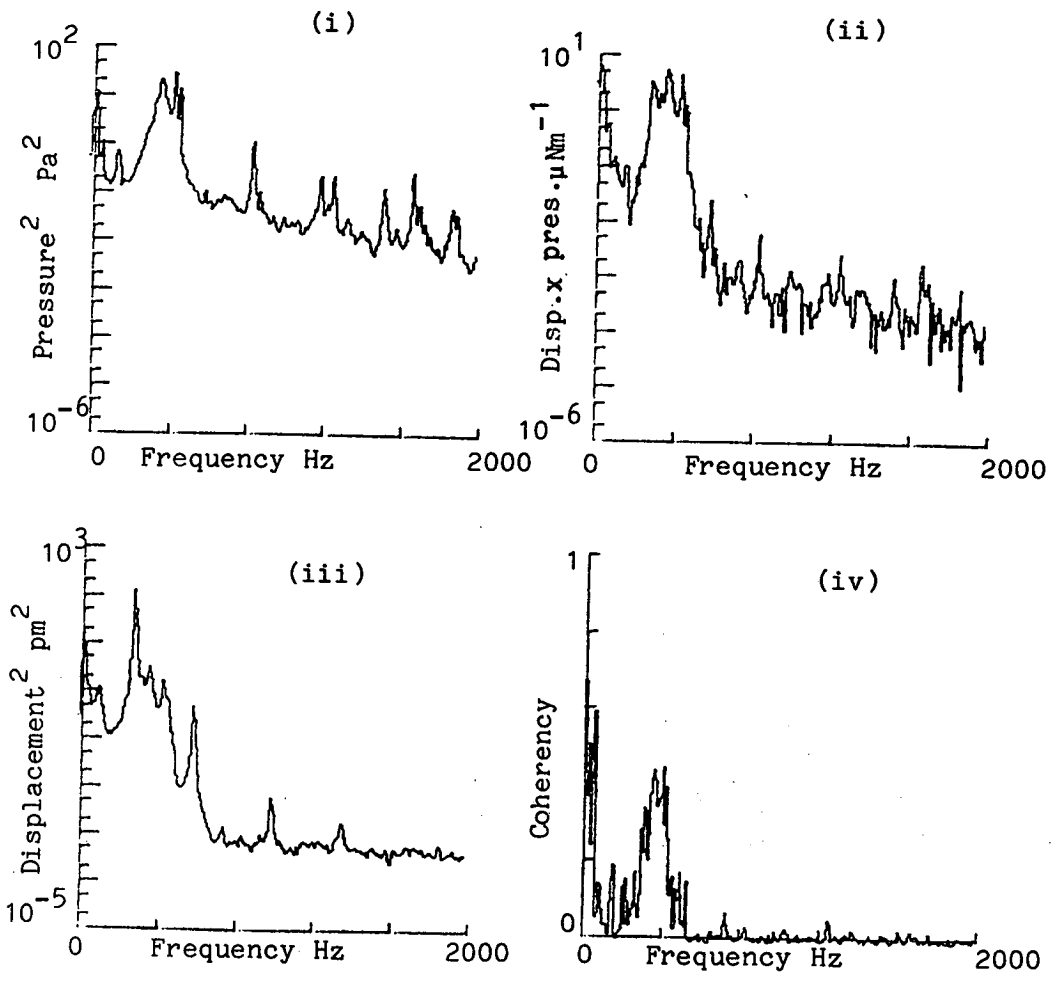


FIGURES 4.20 a-h. Variation of;

(i) P.S.D. of pressure on the fixed measuring tube, (scale logarithmic),
(ii) C.S.D. of pressure on the measuring tube and the displacement of a neighbouring vibrating tube, (scale logarithmic),
(iii) P.S.D. of the vibrating tube displacement, (scale logarithmic),
(iv) Coherency between pressure and displacement, (scale linear),

for selected angles round the tube from stagnation.

FIGURE 4.20a. Angle from Stagnation = $0^{\circ}$.

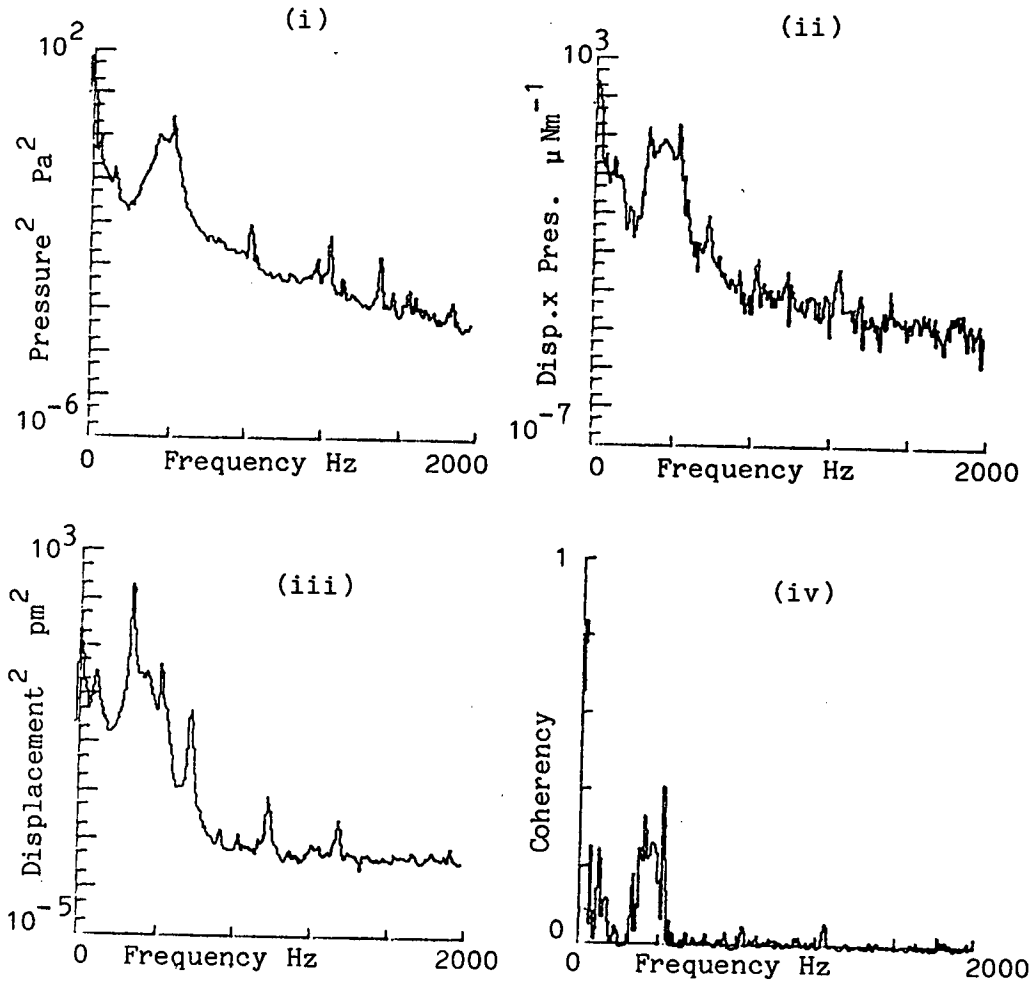


FIGURE 4.20b. Angle from stagnation = $60^{o}$.

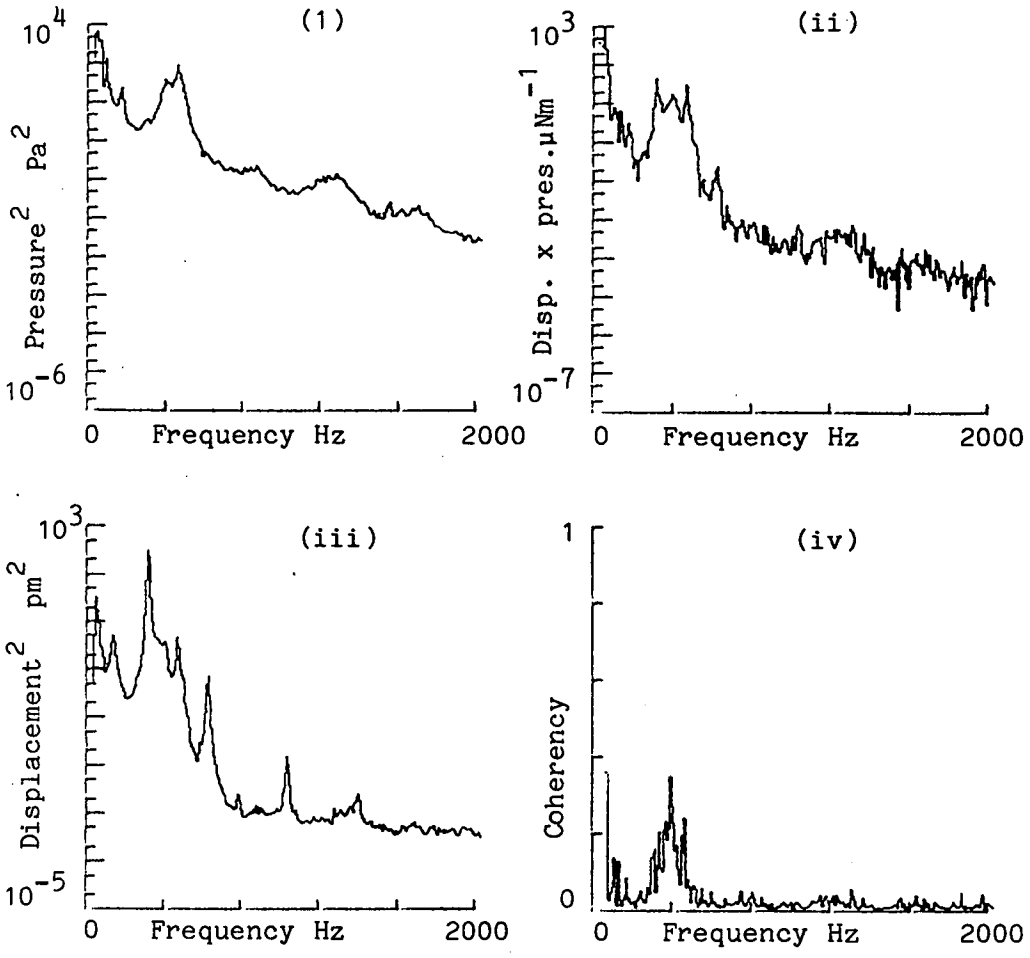


FIGURE 4.20c. Angle for stagnation = 80°.

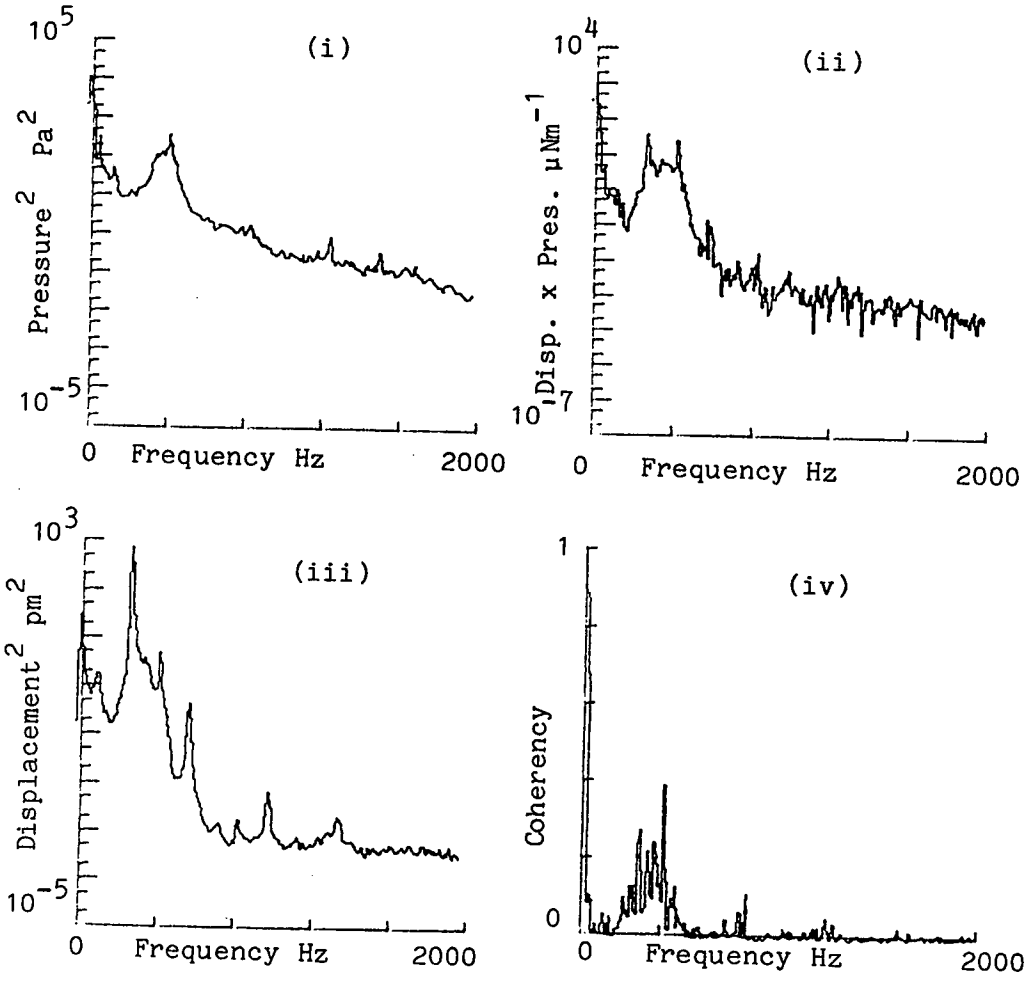


FIGURE 4.20d. Angle for stagnation = 100°.

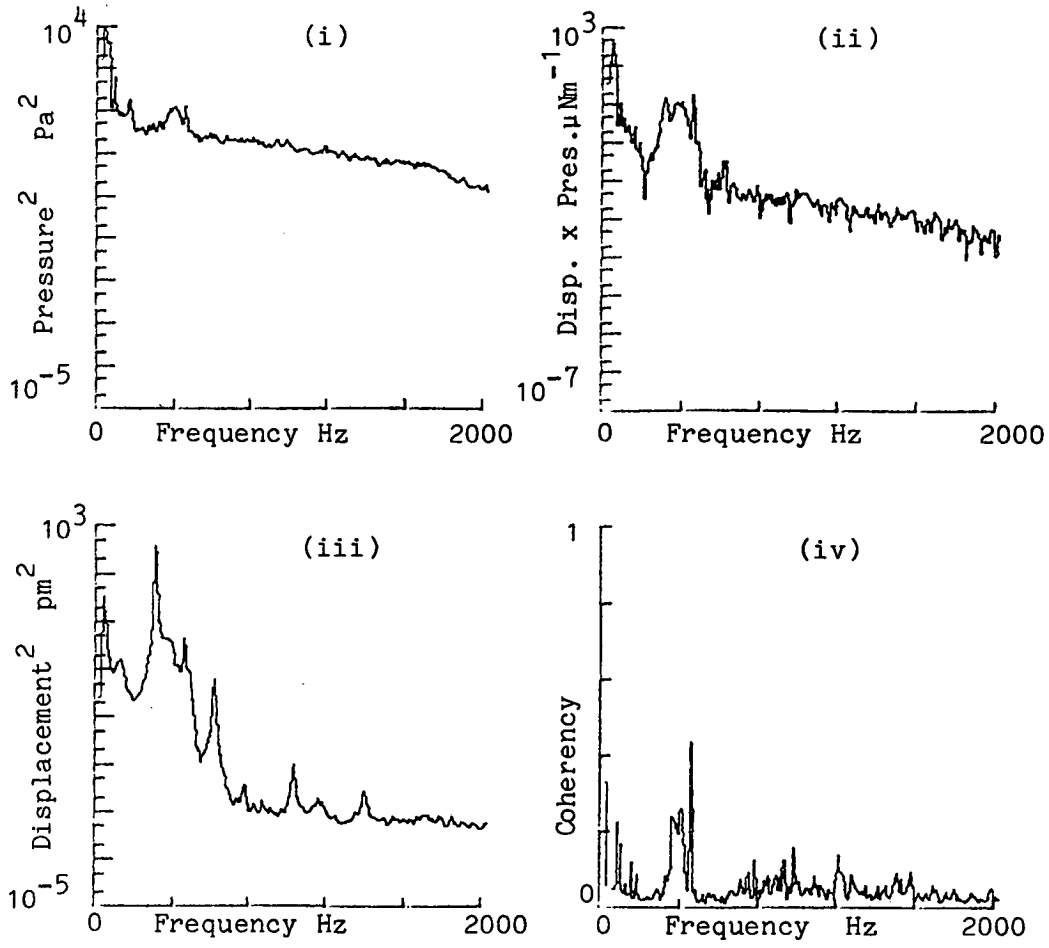


FIGURE 4.20e. Angle from stagnation = 180°.

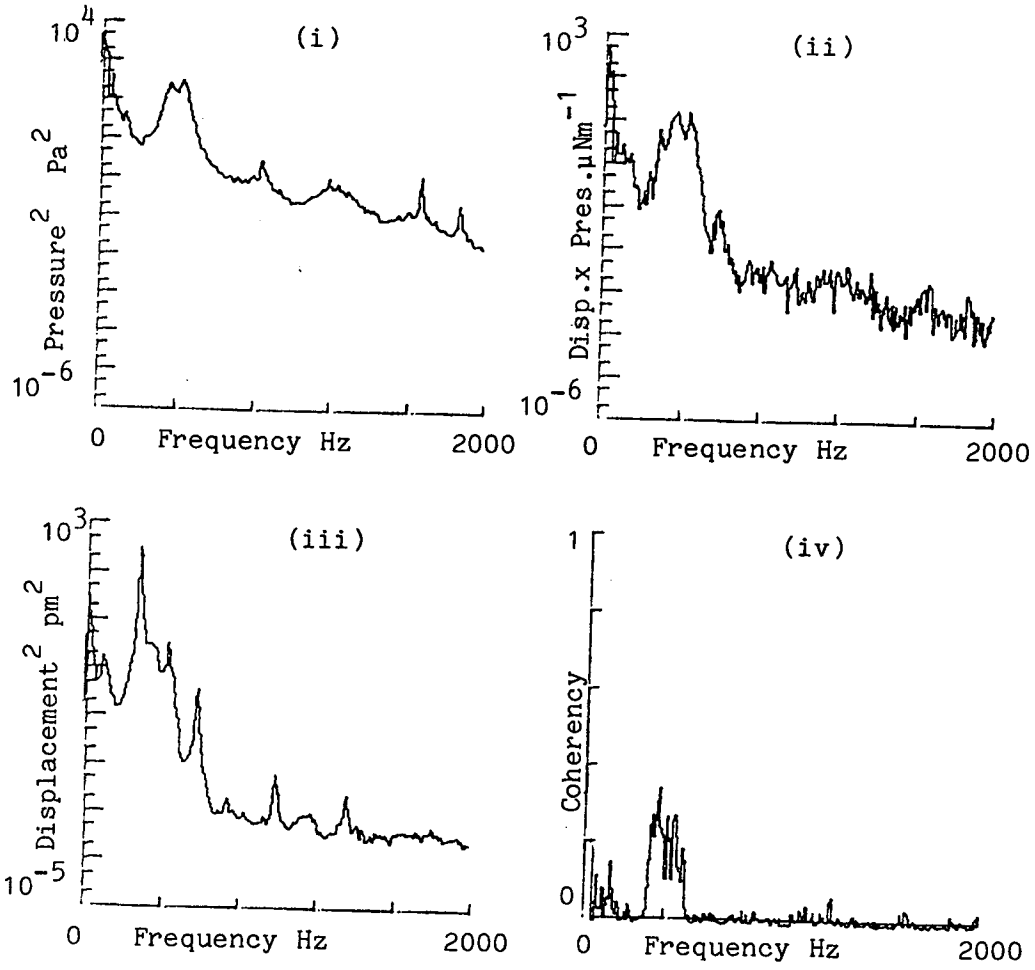


FIGURE 4.20f. Angle from stagnation = 260°

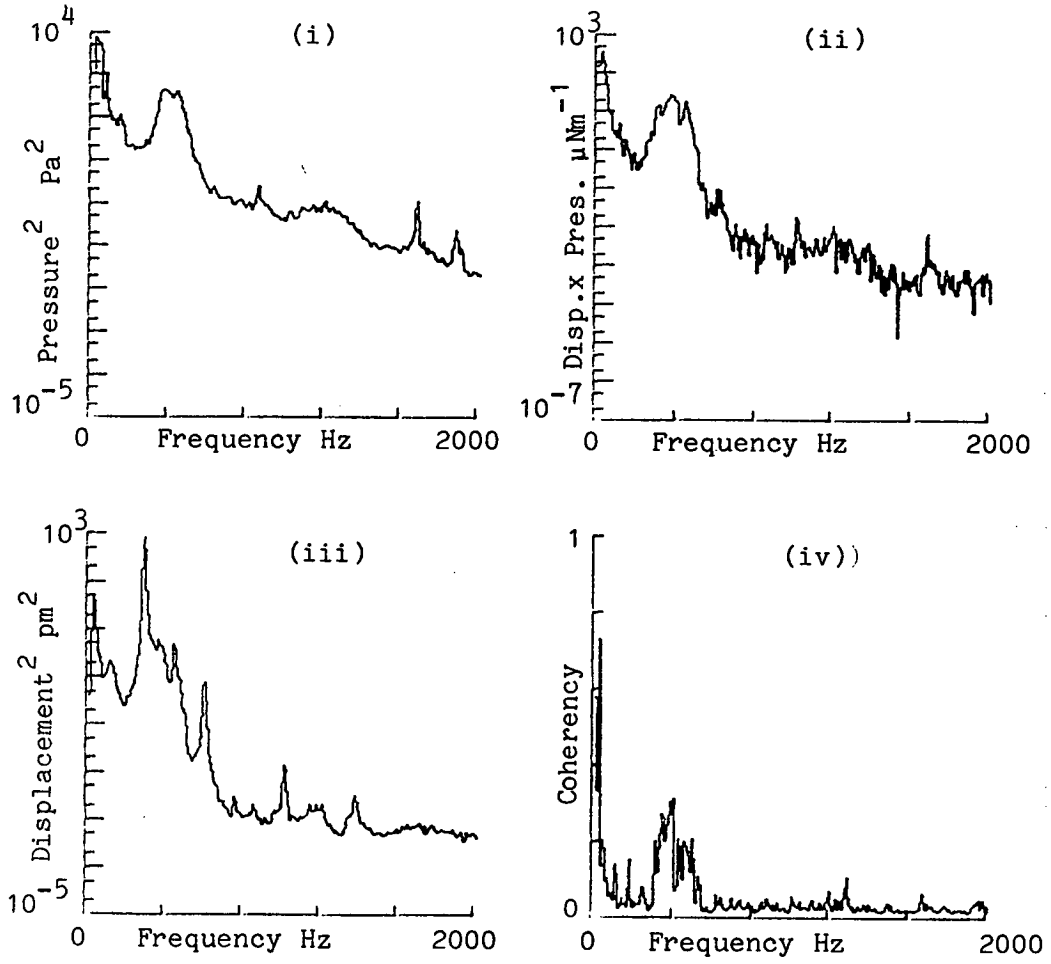


FIGURE 4.20g. Angle from stagnation = 280°

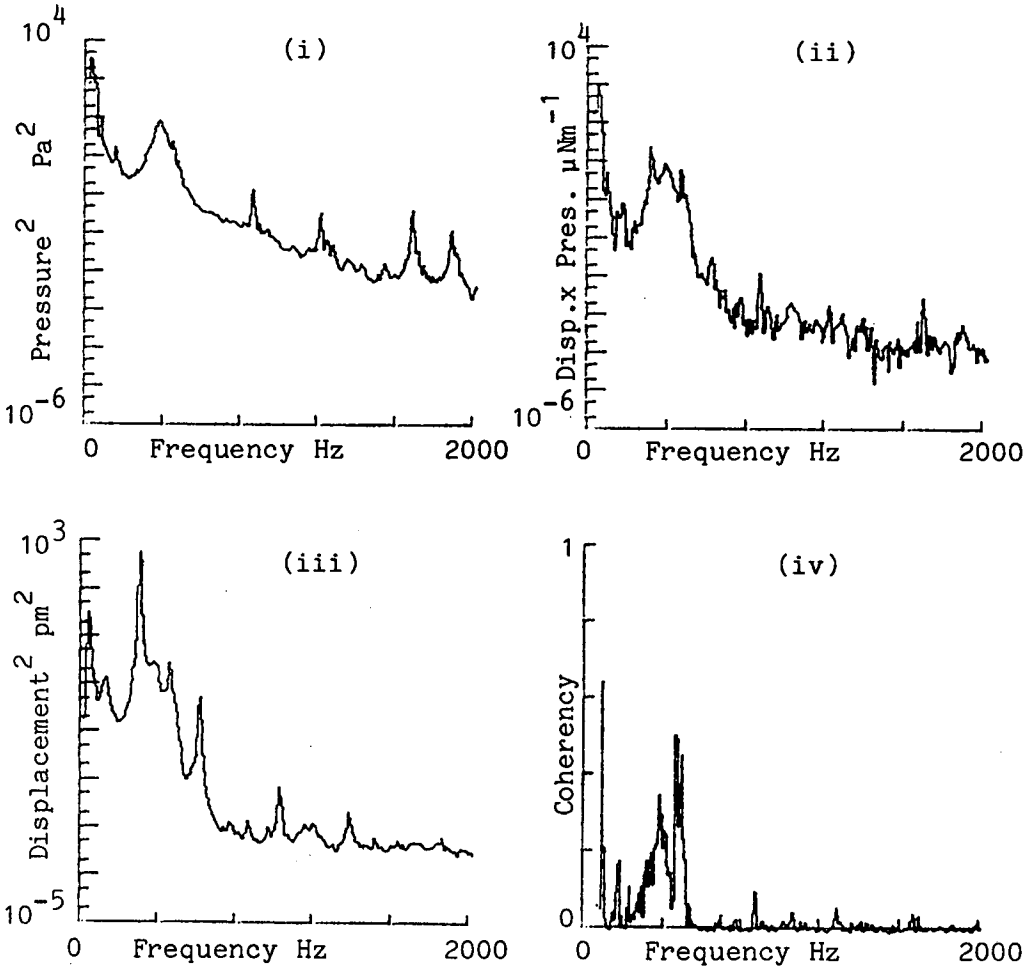


FIGURE 4.20h. Angle from stagnation = 300°.

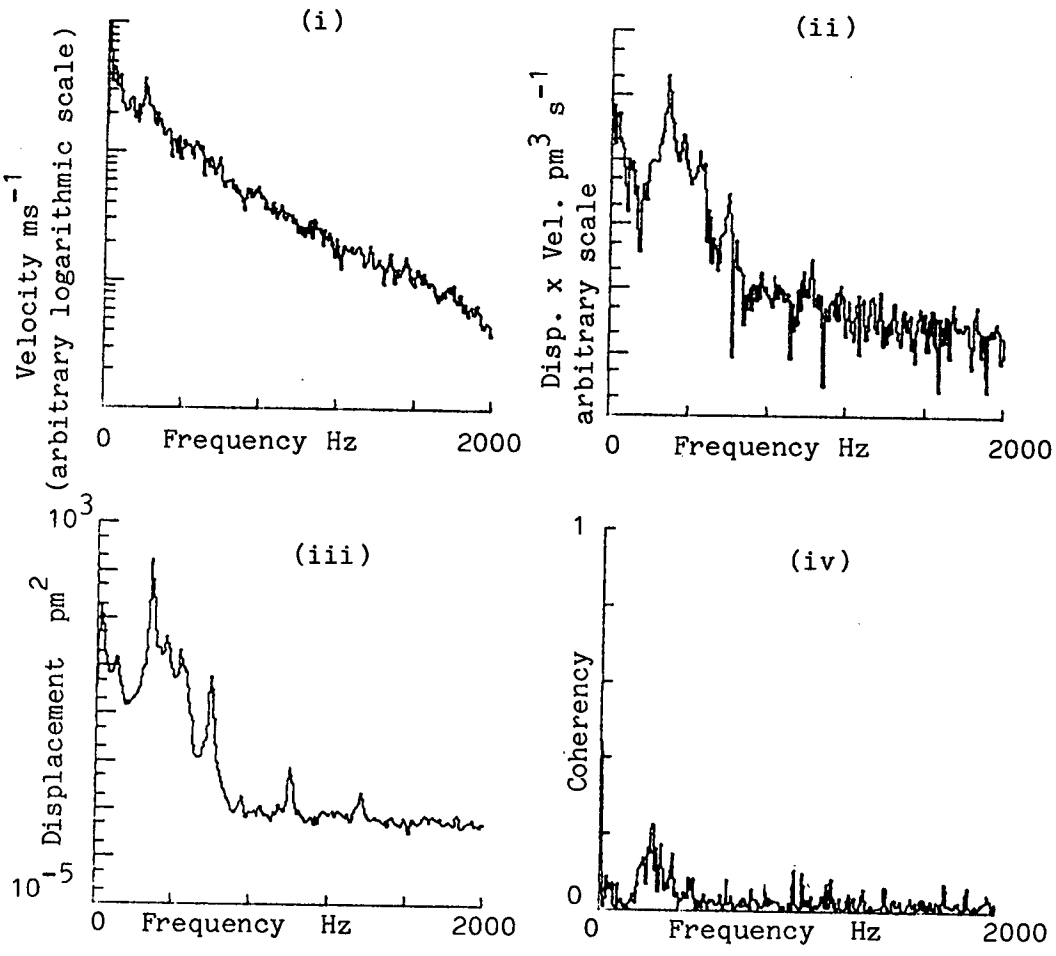


FIGURE 4.21. (i) P.S.D. of velocity in the wake of the fixed pressure measuring tube,
(ii) C.S.D. of wake velocity fluctuations and the vibrating tube displacement,
(iii) P.S.D. of vibrating tube displacement,
(iv) coherency between displacement and wake velocity.

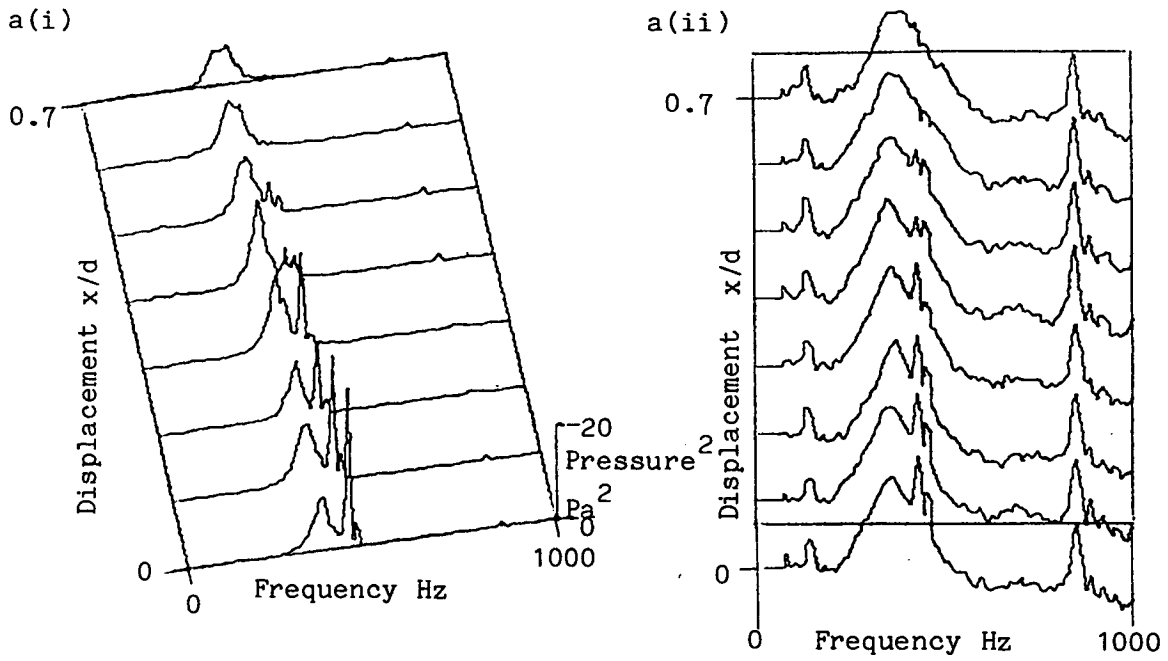


FIGURE 4.22. Variation of P.S.D. of pressure on fixed measuring tube with static displacement from a uniformly spaced arrangement.
(i) Linear scale. (ii) Arbitrary logarithmic scale.

FIGURE 4.22a. Angle from stagnation = $0^{o}$.

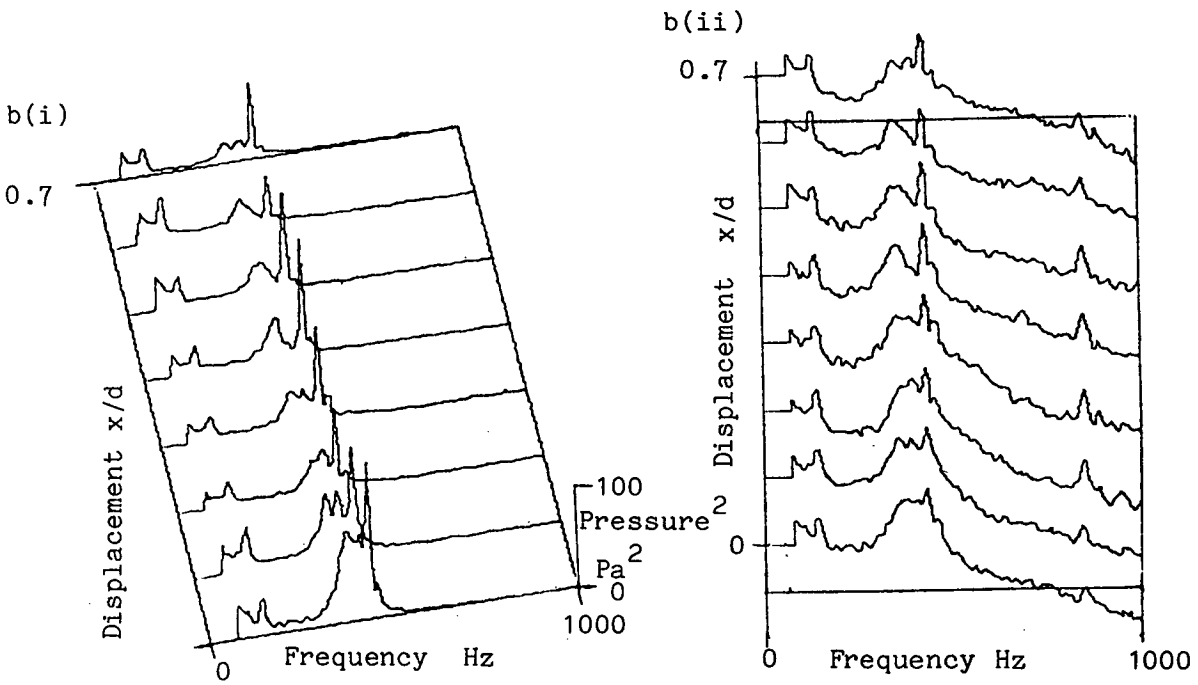


FIGURE 4.22b. Angle from stagnation = $90^{o}$.

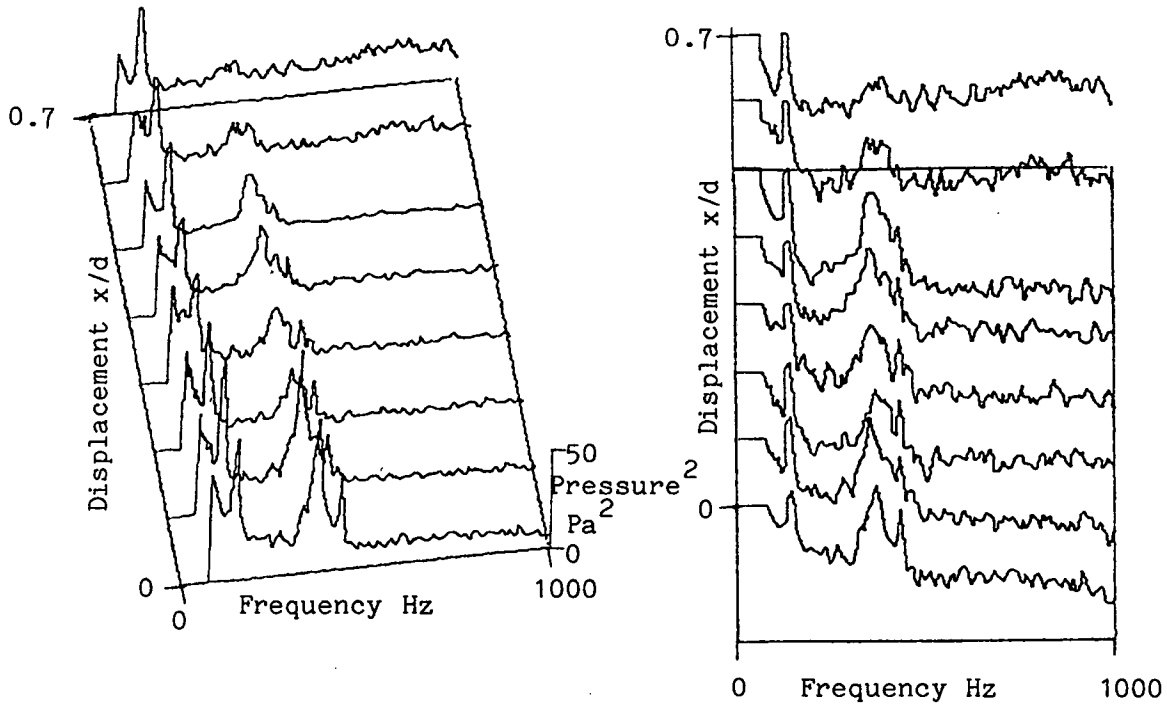


FIGURE 4.22c. Angle from stagnation = 180°.

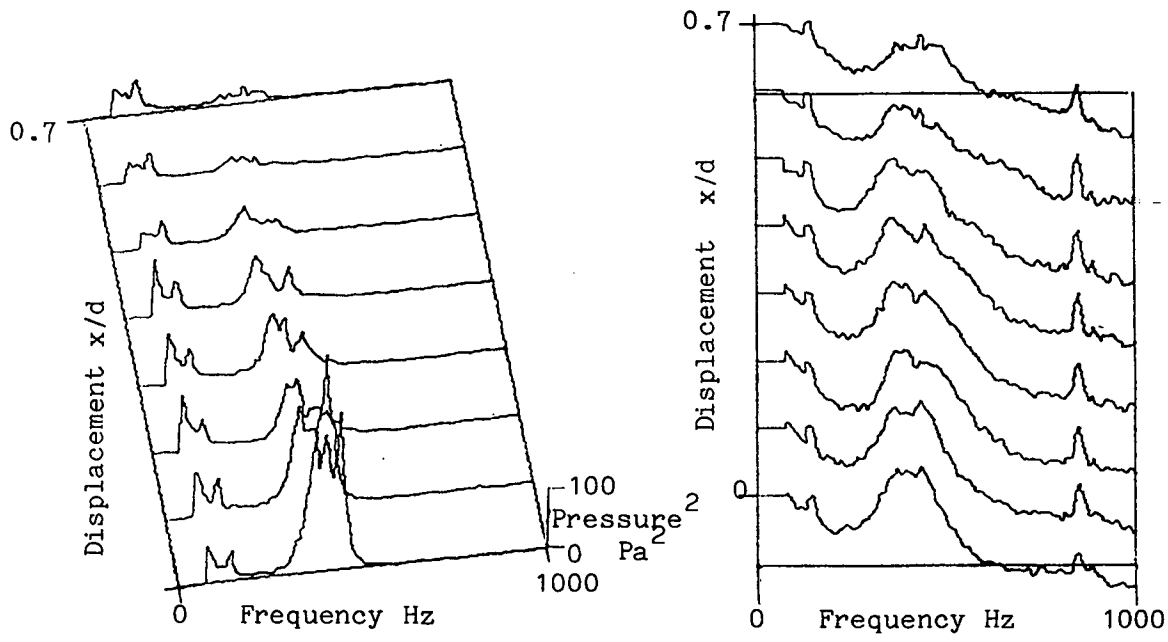


FIGURE 4.22d. Angle from stagnation = 270°.

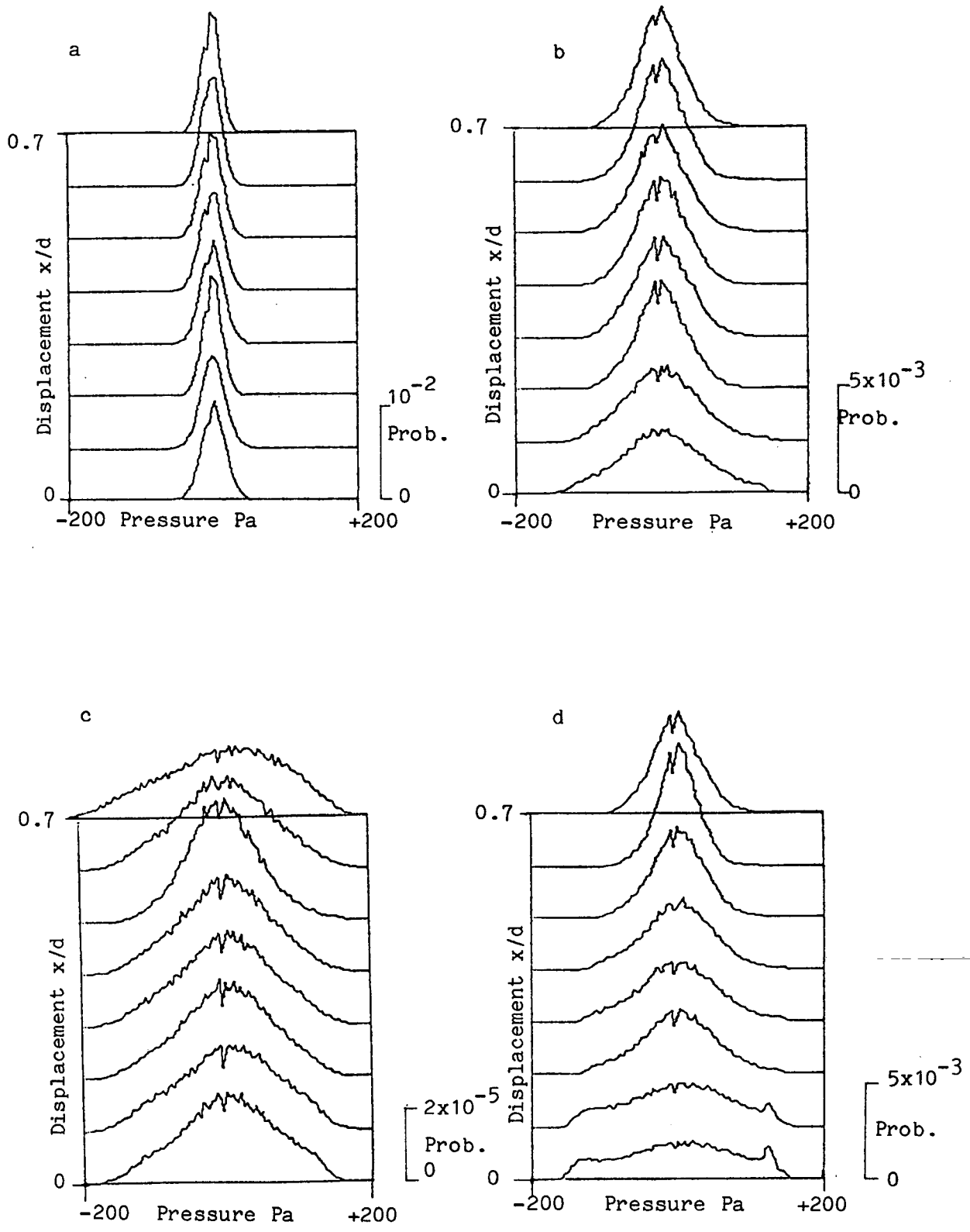


FIGURE 4.23. Variation of amplitude probability distribution of pressure on a fixed tube with displacement from a uniformly spaced position towards a vibrating tube.
Angle from stagnation = (a) $0^{o}$, (b) $90^{o}$, (c) $180^{o}$, and (d) $270^{o}$.

(i)

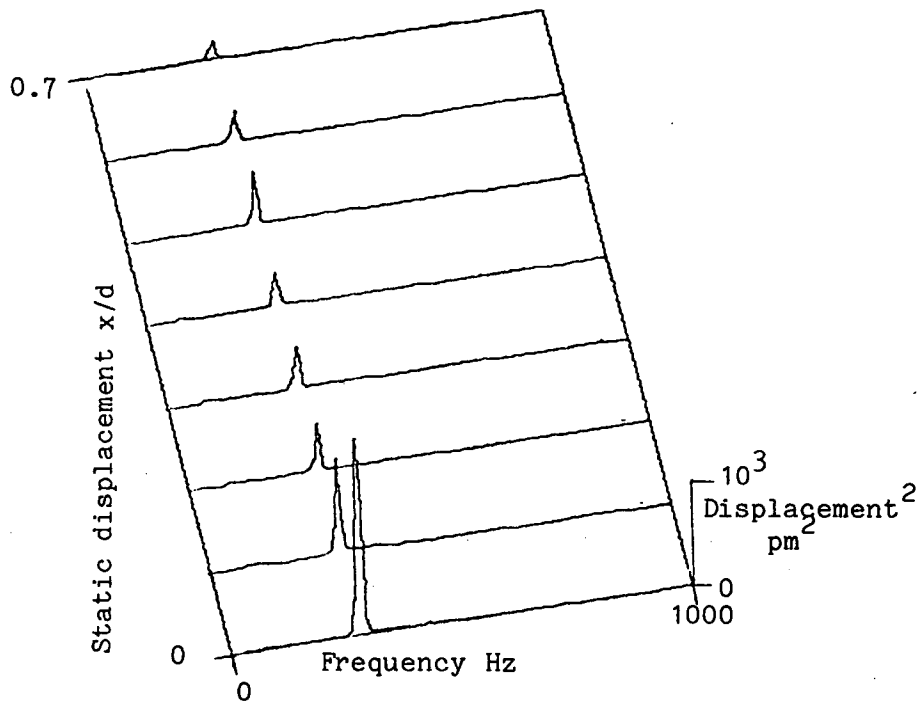


(ii)

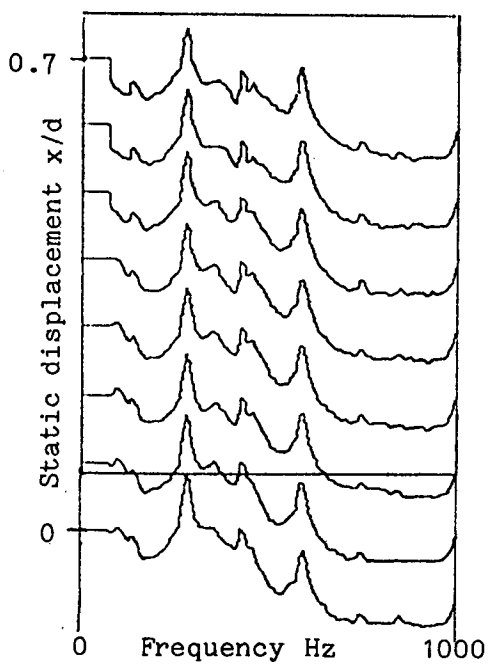


FIGURE 4.24. Variation of P.S.D. of vibrating tube displacement with distance of pressure measuring tube from a uniformly spaced position in a fixed tube row. (i) Linear (ii) Arbitrary logarithmic scale.

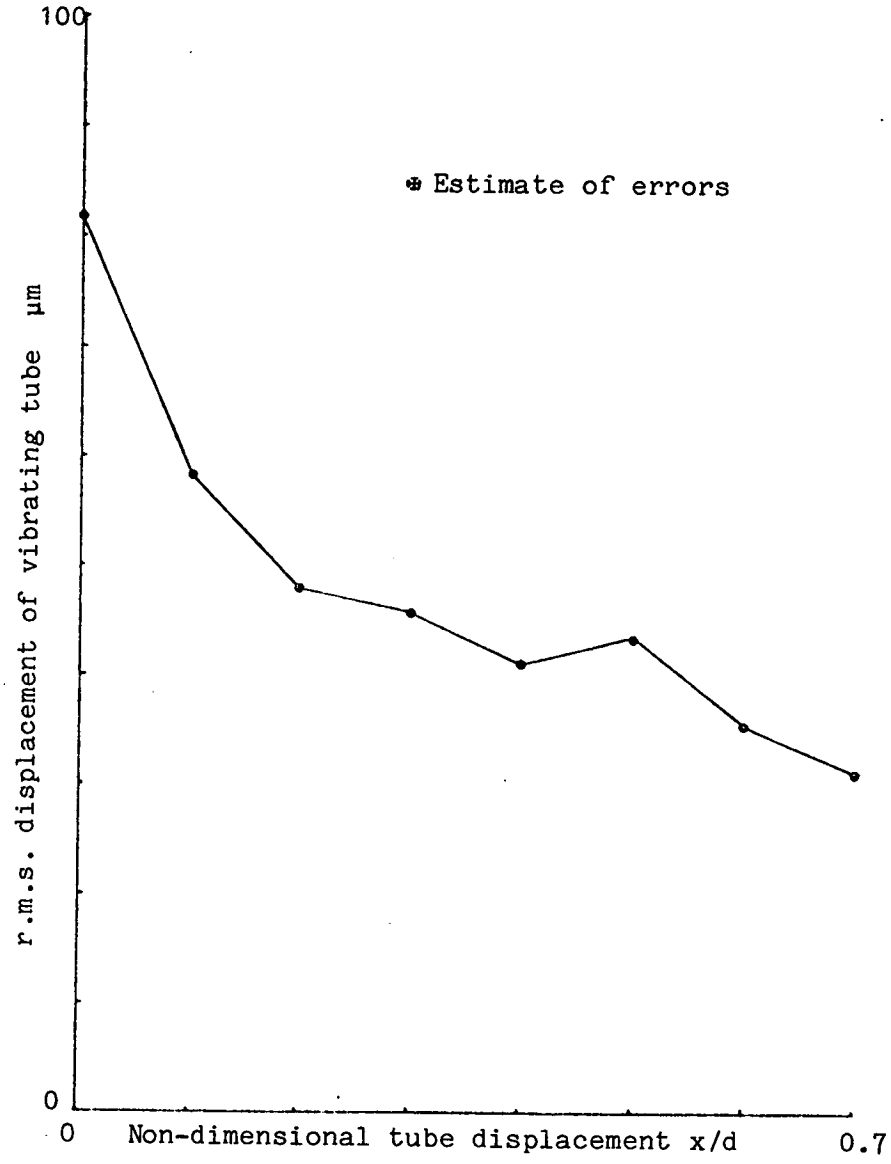


FIGURE 4.25. Variation of r.m.s. displacement of vibrating tube with pressure measuring tube static displacement towards the vibrating tube.

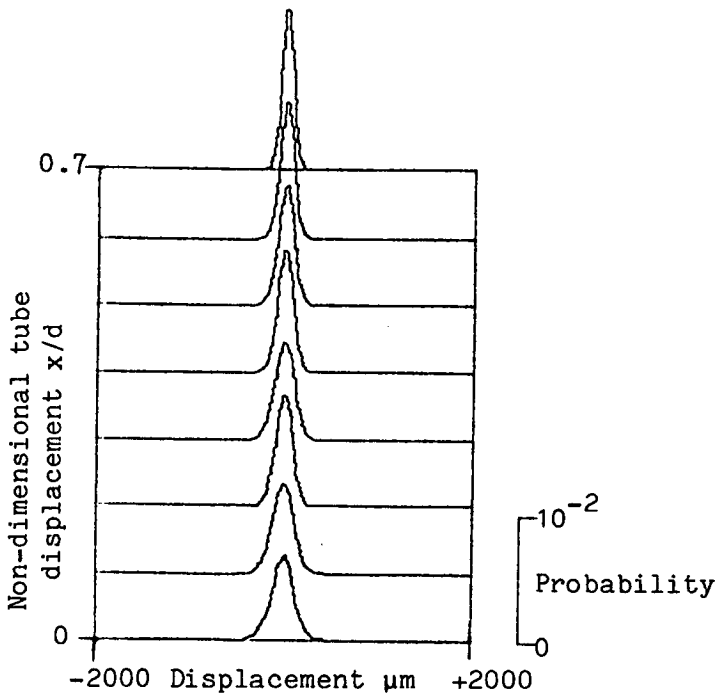


FIGURE 4.26. Variation of amplitude probability distribution of vibrating tube displacement with displacement of pressure measuring tube towards the vibrating tube.

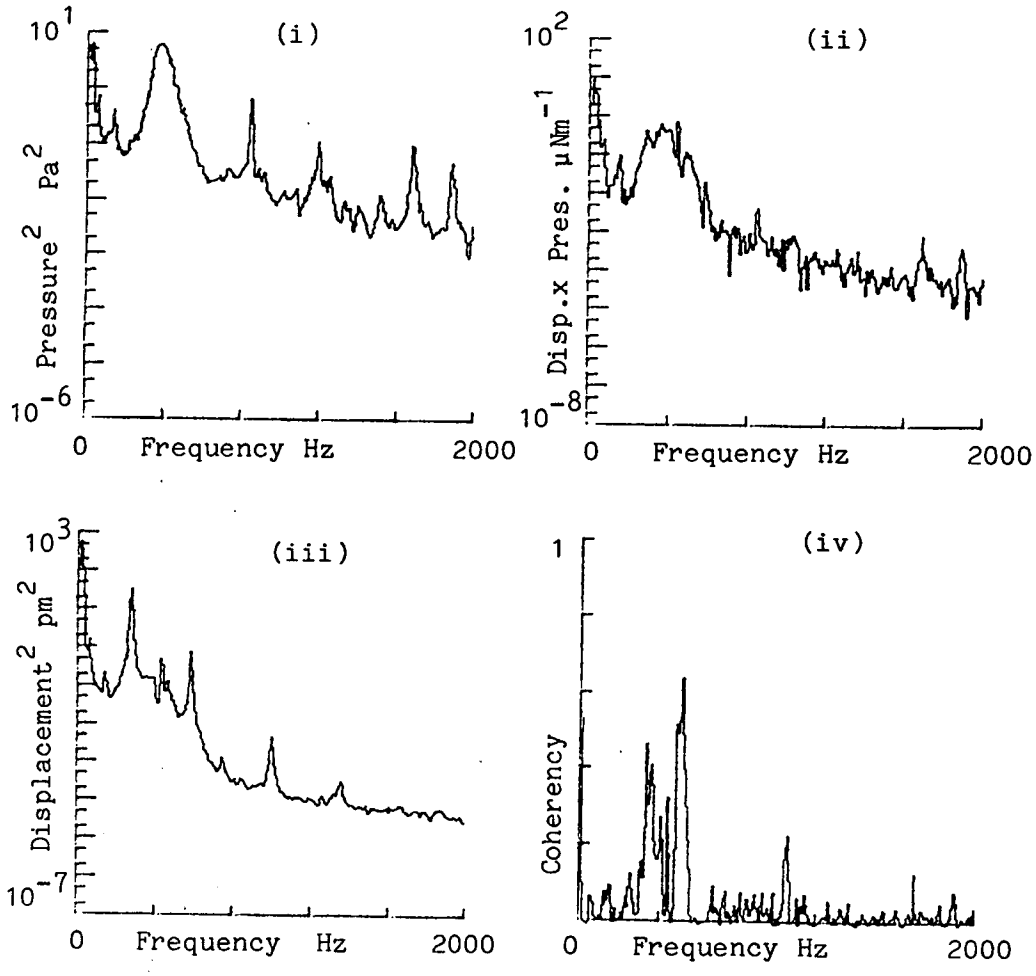


FIGURES 4.27 a-d. (i) P.S.D. of pressure on measuring tube (logarithmic scale)
(ii) C.S.P. of pressure on measuring tube and displacement of vibrating tube (logarithmic scale)
(iii) P.S.D. of displacement of vibrating tube (logarithmic scale)
(iv) Coherency of displacement and pressure (linear scale)
when the pressure measuring tube and vibrating tube are separated by 1.09 diameters.

FIGURE 4.27a. Angle from stagnation = $0^{o}$.

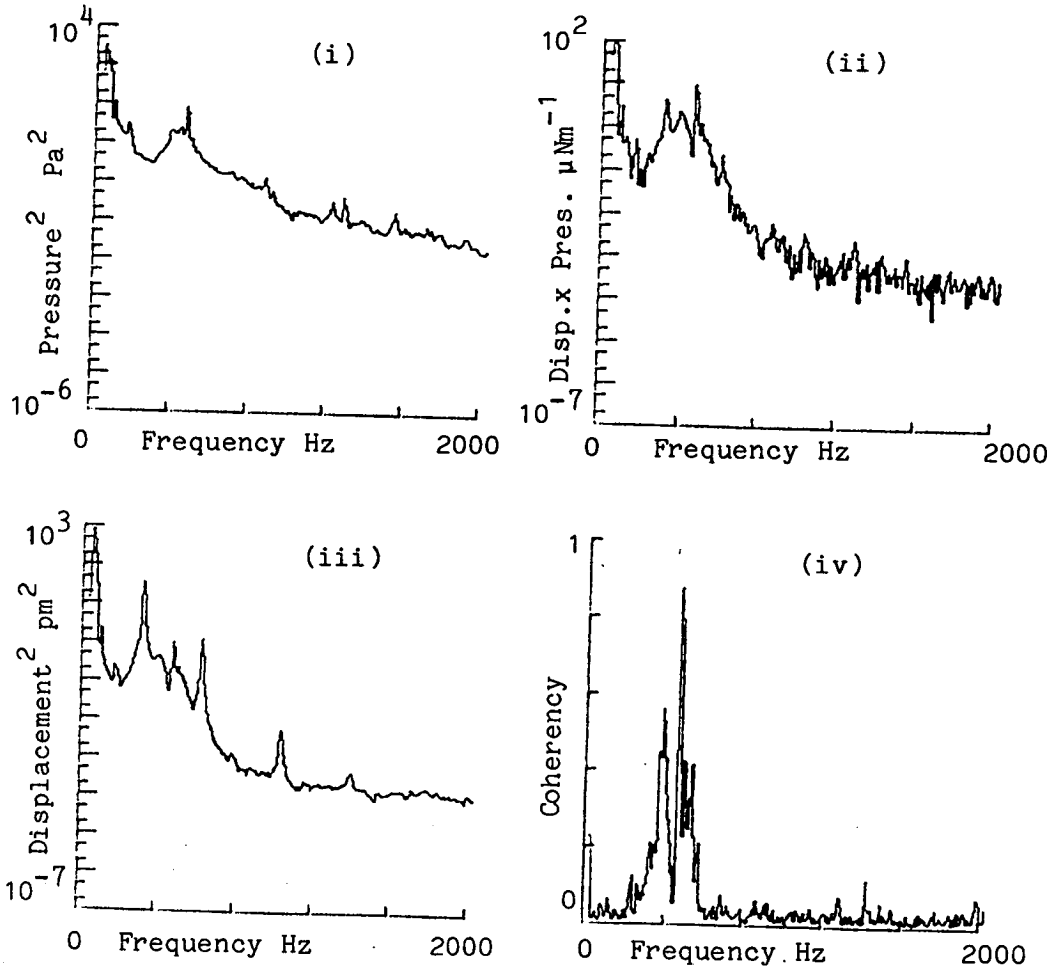


FIGURE 4.27b. Angle from stagnation = 90°.

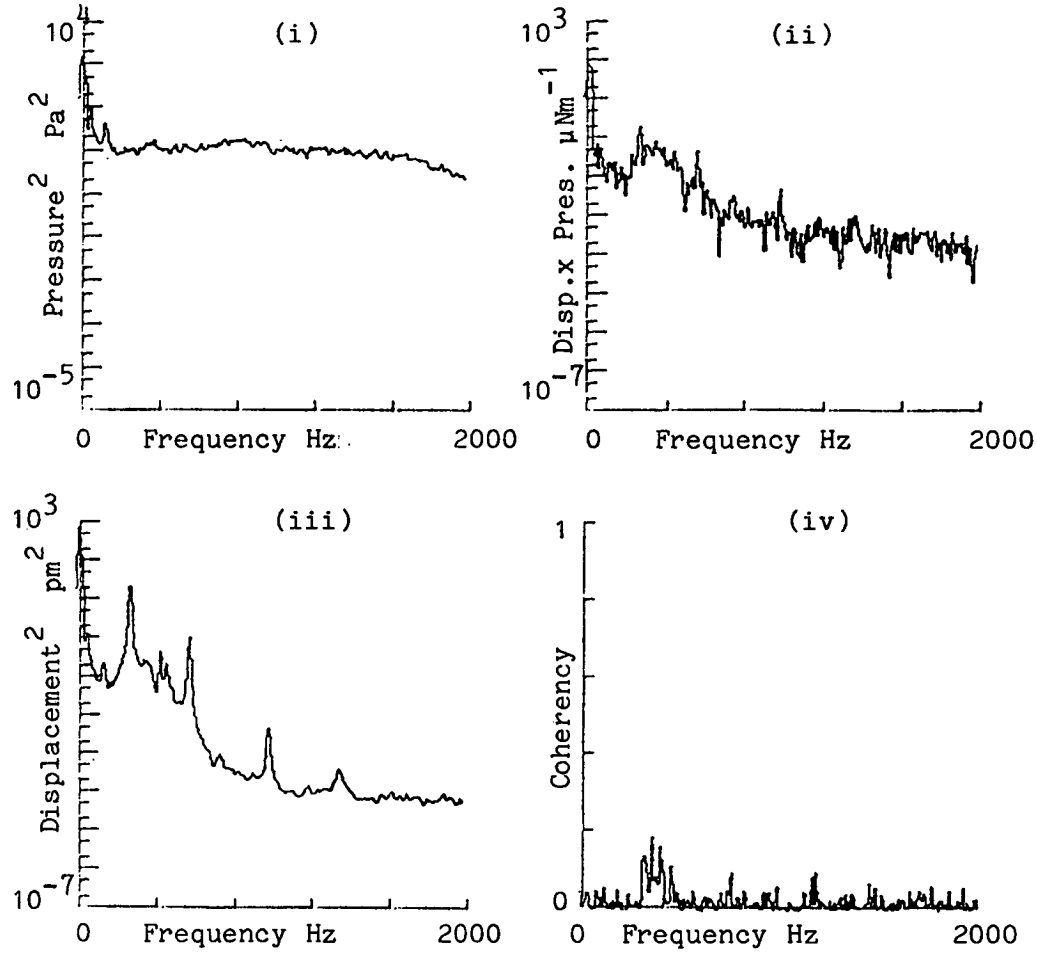


FIGURE 4.27c. Angle from stagnation = 180°.

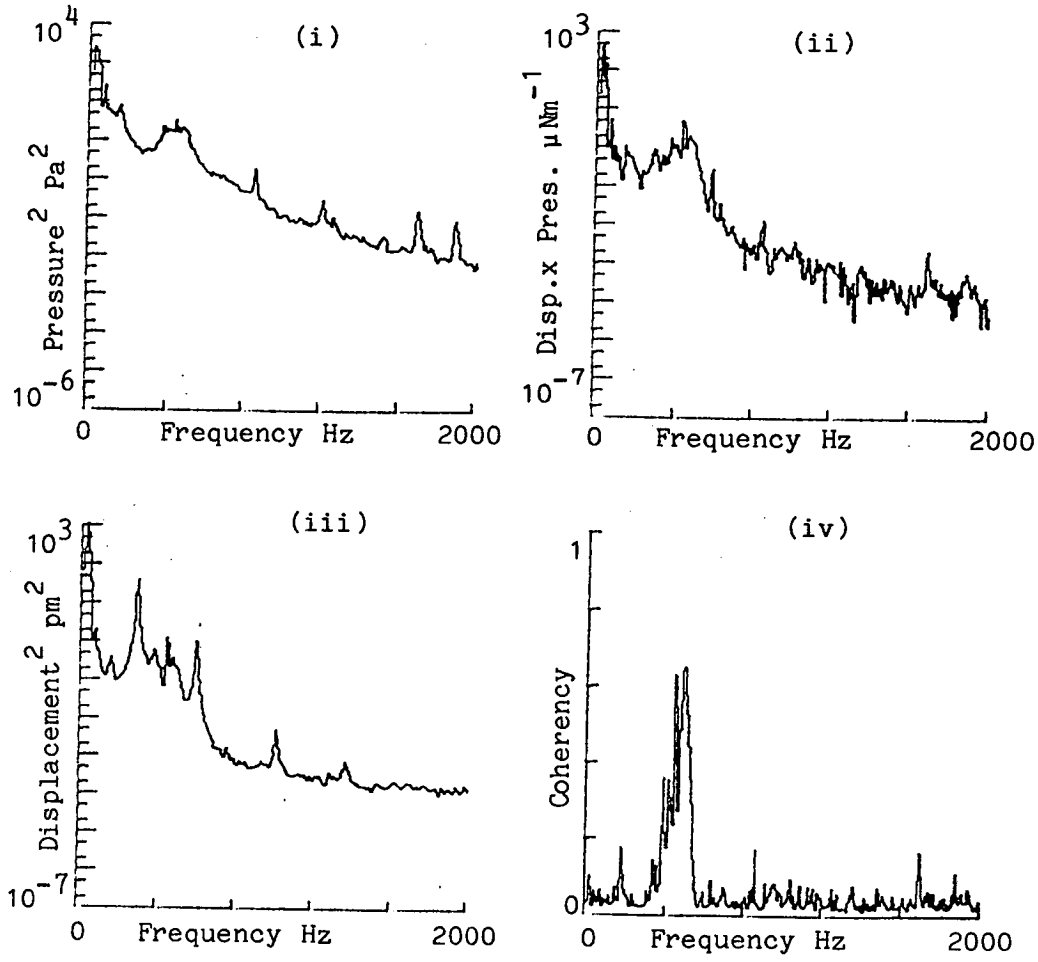


FIGURE 4.27d. Angle from stagnation = 270°.

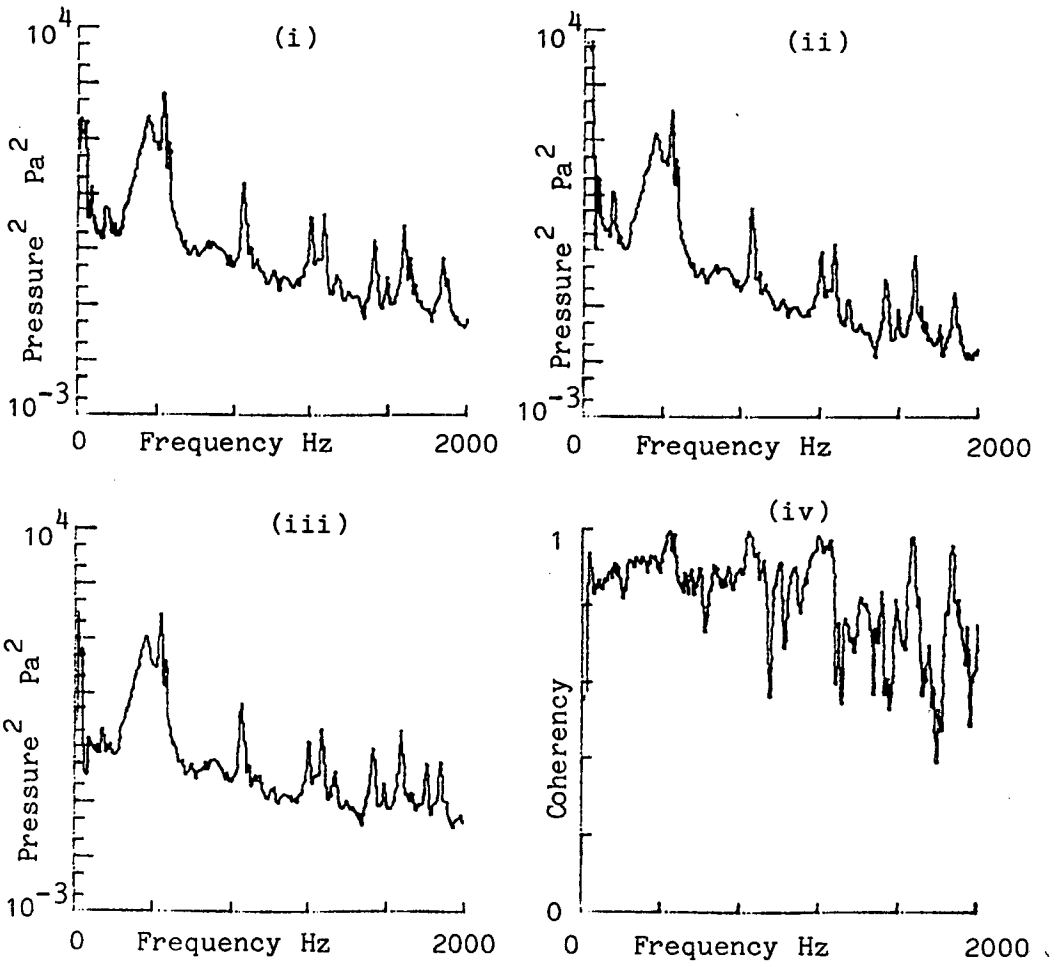


FIGURE 4.28 a-d. (i) P.S.D. of pressure at station 1, (logarithmic scale)
(ii) C.S.D. of pressure betweens stations 1 & 2, (logarithmic scale)
(iii) P.S.D. of pressure at station 2, (logarithmic scale)
(iv) Coherency between pressure signals, (linear scale)
for a tube spanwise separation of 1 diameter.

FIGURE 4.28a. Angle from stagnation = $0^o$.

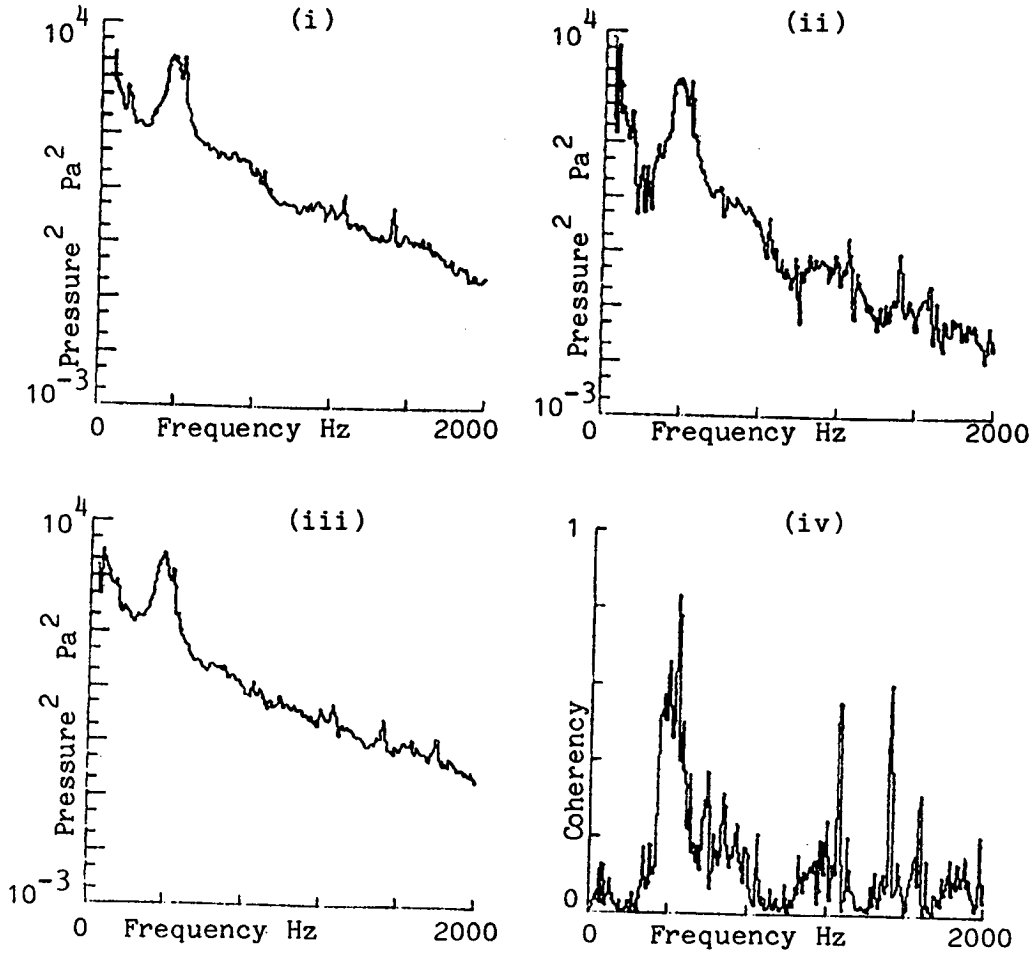


FIGURE 4.28b. Angle from stagnation = 90°.

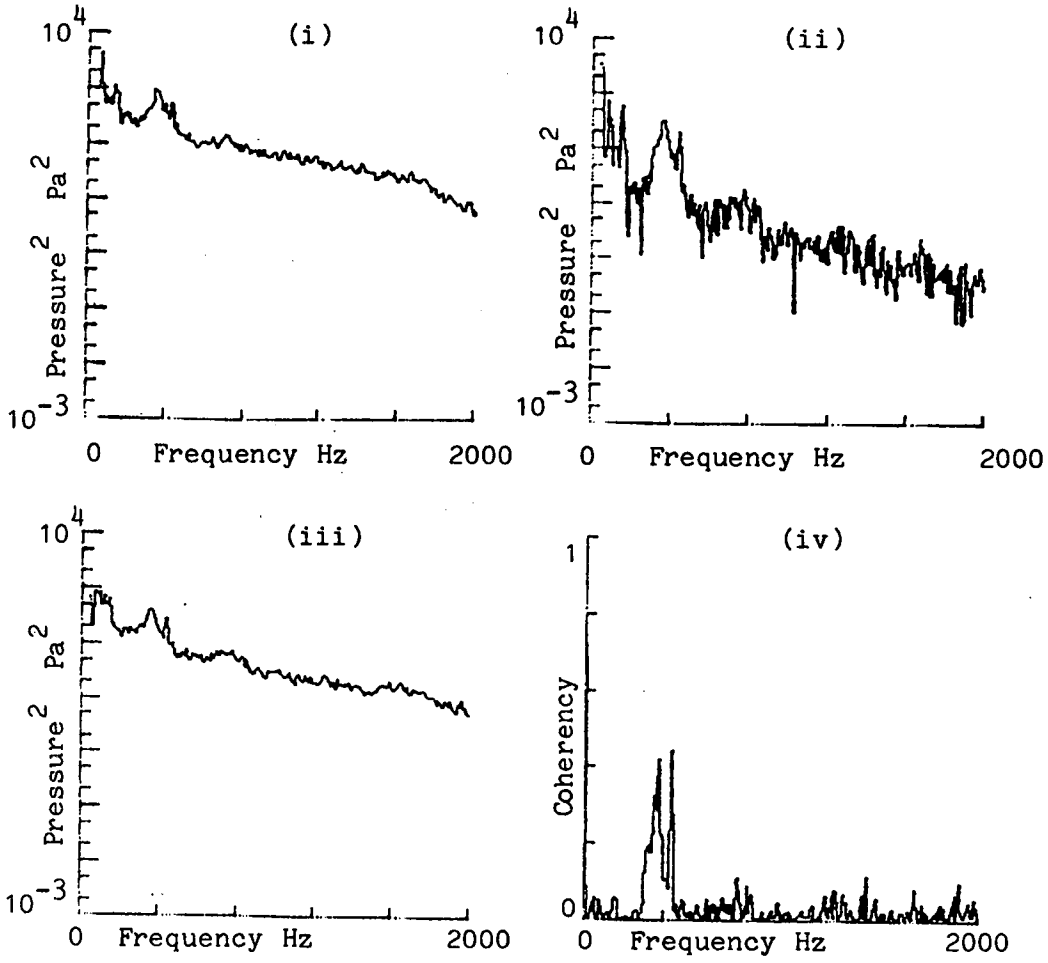


FIGURE 4.28c. Angle from stagnation = 180°.

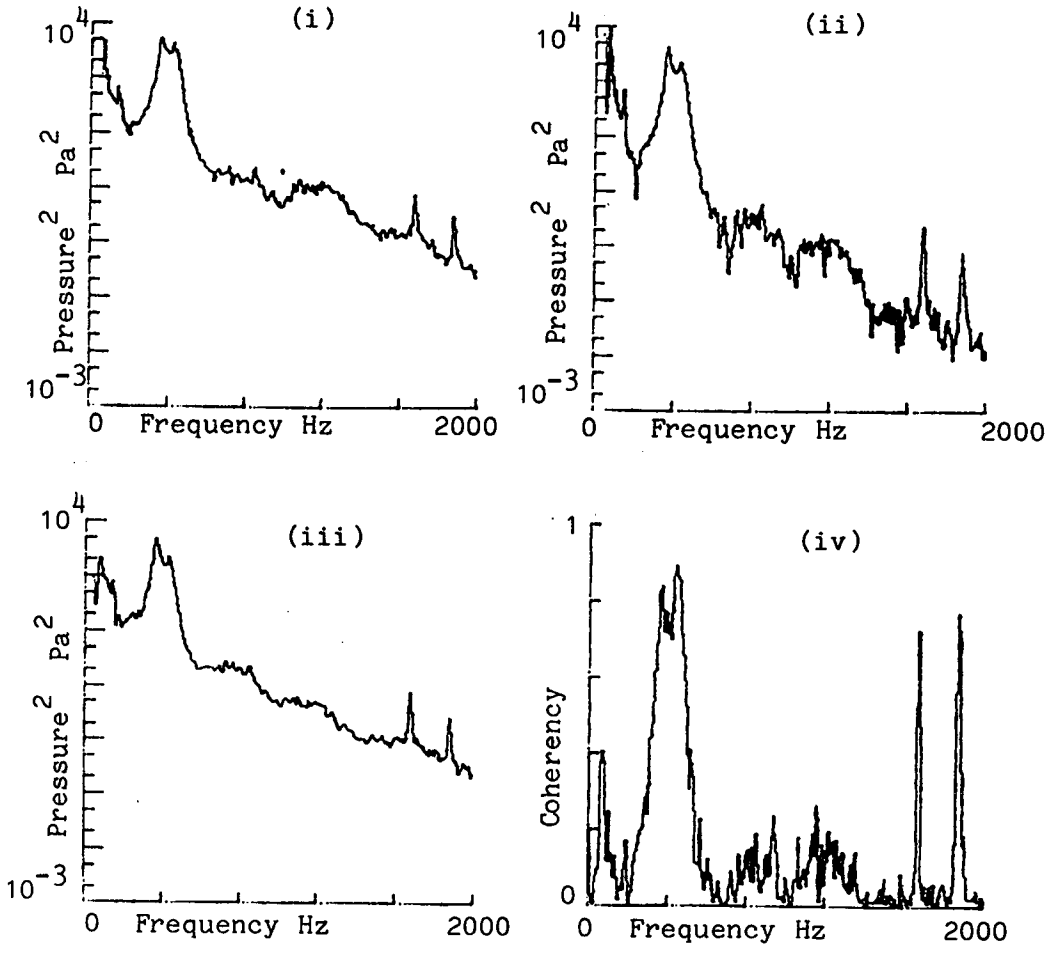


FIGURE 4.28d. Angle from stagnation = 270°.

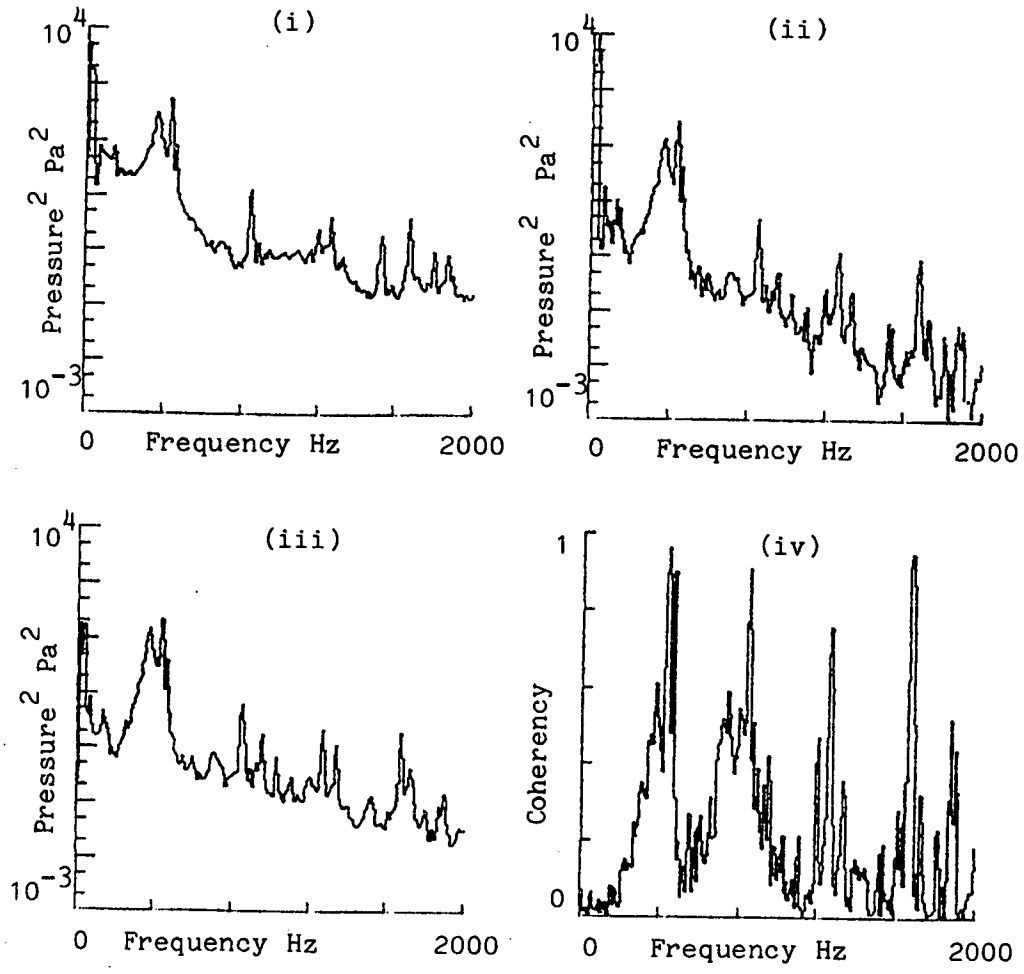


FIGURES 4.29 a-d. (i) P.S.D. of pressure at station 2, (logarithmic scale)
(ii) C.S.D. of pressure between stations, 2 & 3 (logarithmic scale)
(iii) P.S.D. of pressure at station 3, (logarithmic scale)
(iv) Coherency between pressure signals, (linear scale)
for a tube spanwise separation of 3 diameters.

FIGURE 4.29a. Angle from stagnation = $0^{\circ}$.

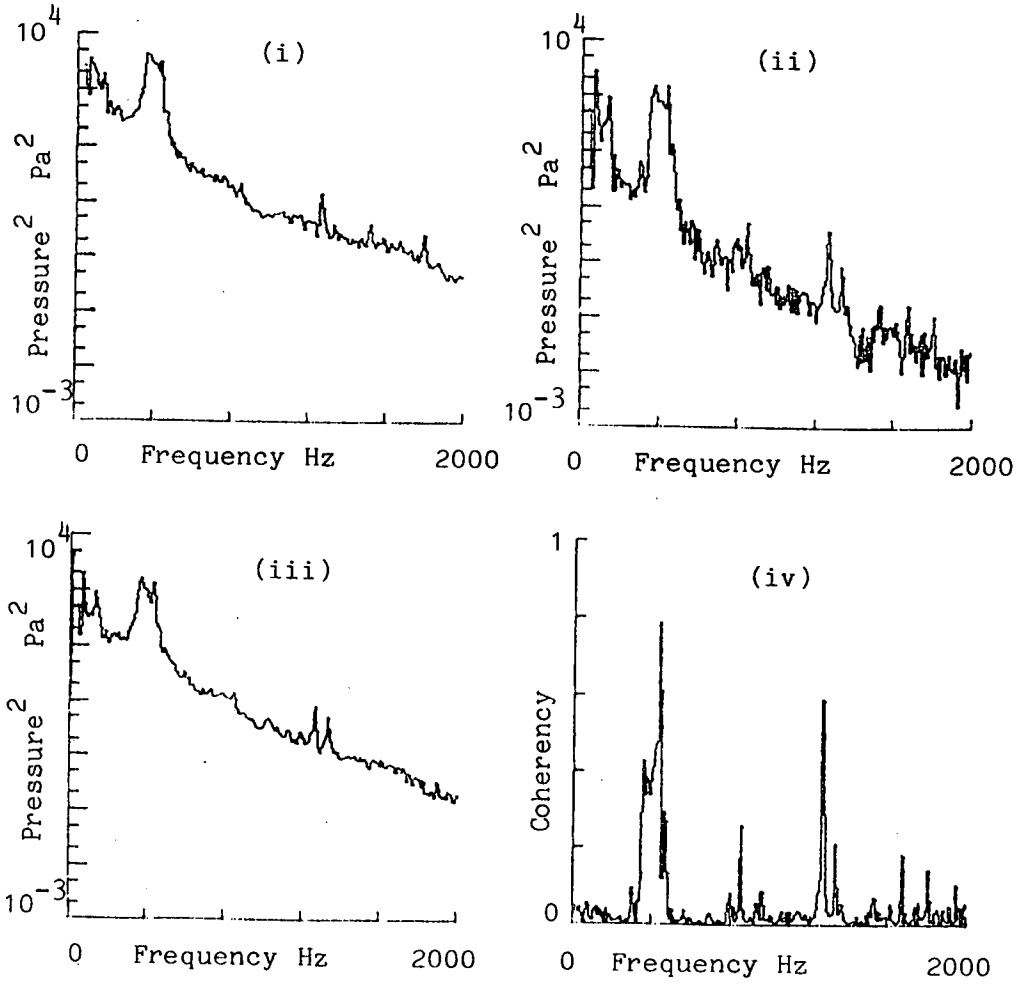


FIGURE 4.29b. Angle from stagnation = 90°.

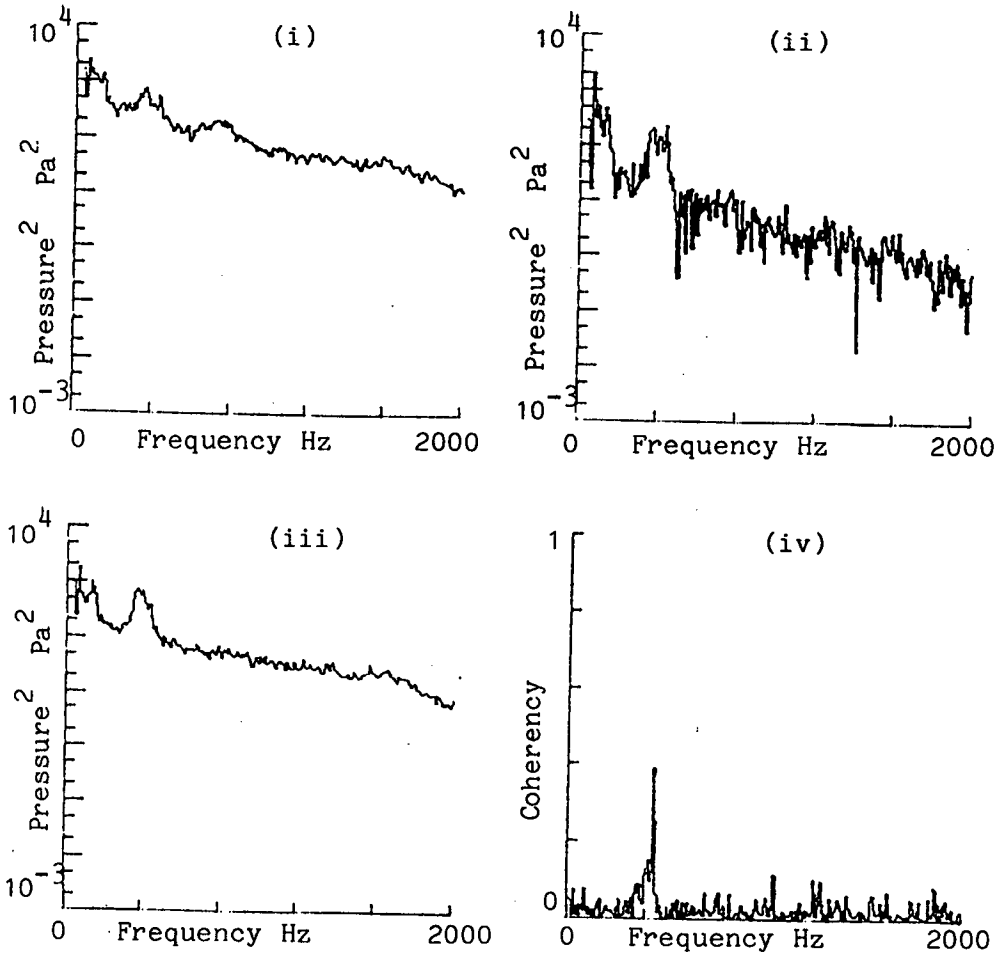


FIGURE 4.29c. Angle from stagnation = 180°.

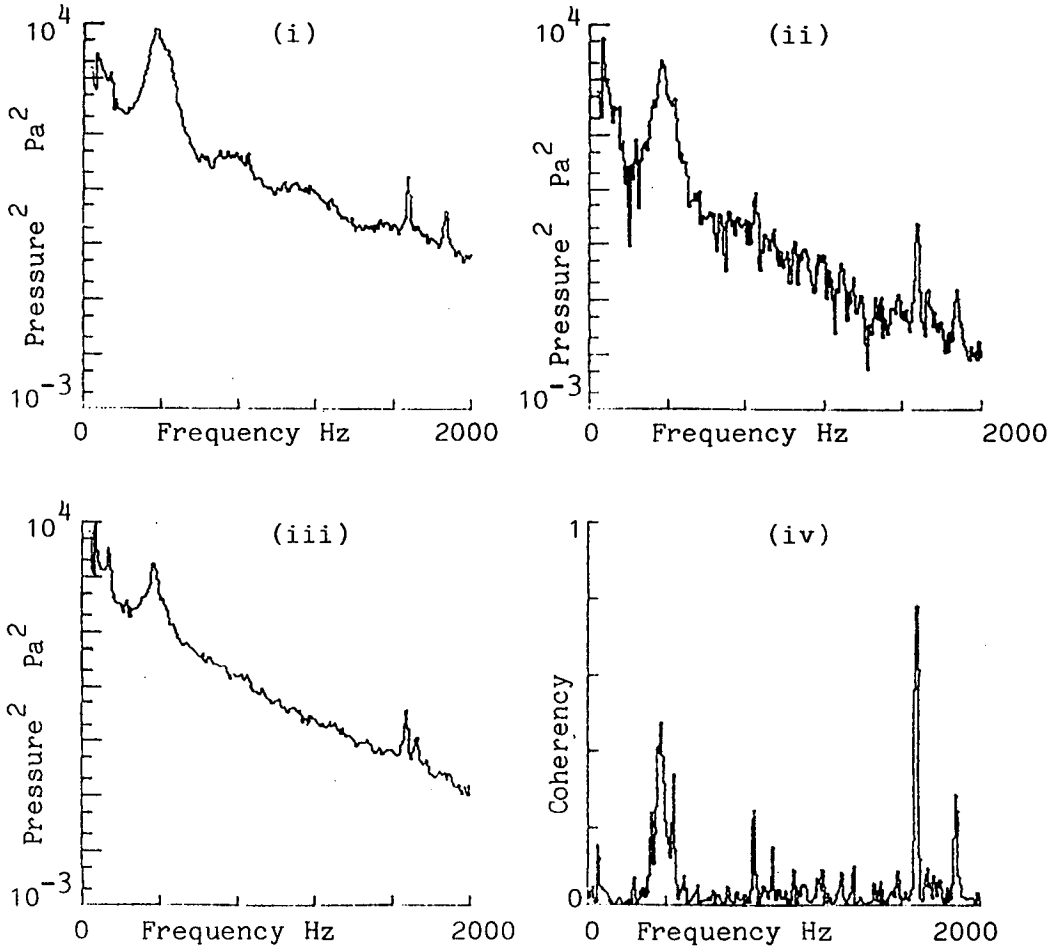


FIGURE 4.29d. Angle from stagnation = 270°.

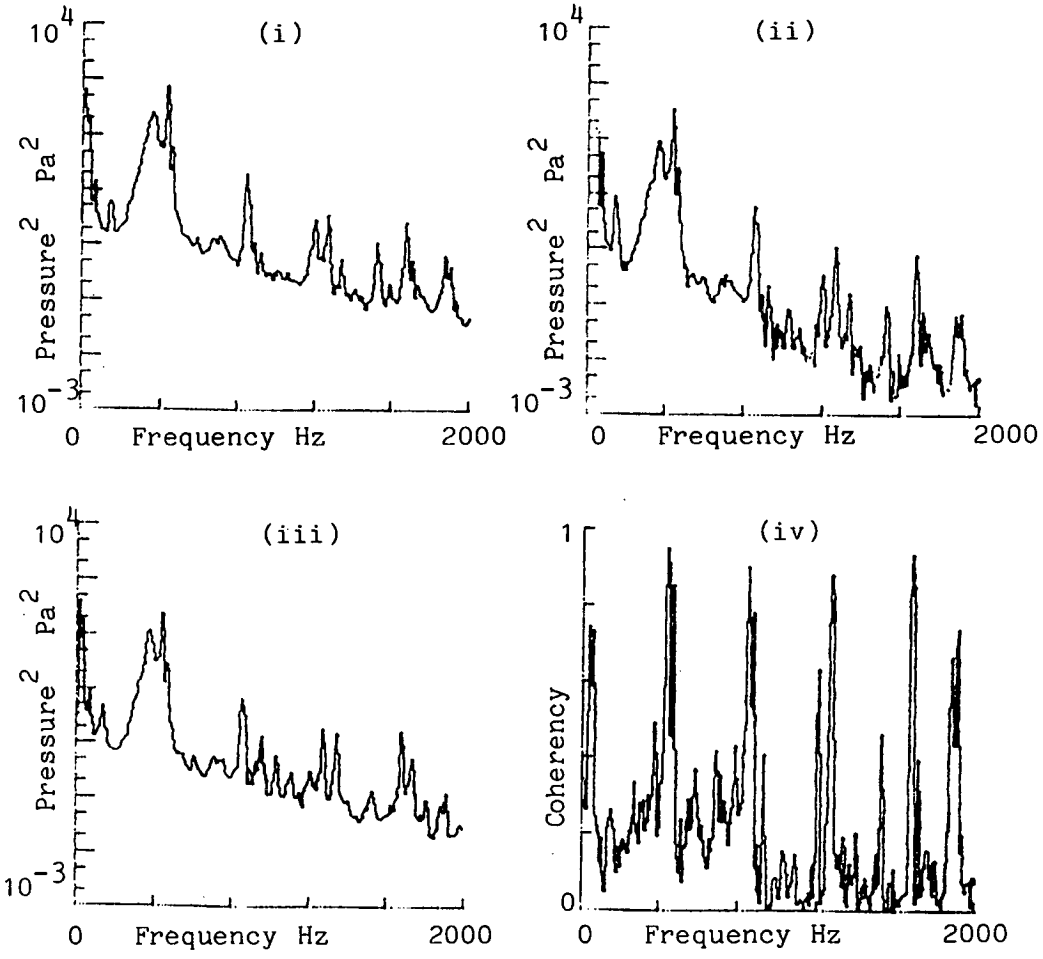


FIGURES 4.30a-d. (i) P.S.D. of pressure at station 1, (logarithmic scale)
(ii) C.S.D. of pressure between stations 1 & 3, (logarithmic scale)
(iii) P.S.D. of pressure at station 3, (logarithmic scale)
(iv) Coherency between pressure signals, (linear scale)
for a tube spanwise separation of 4 diameters.

FIGURE 4.30a. Angle from stagnation = $0^{\circ}$.

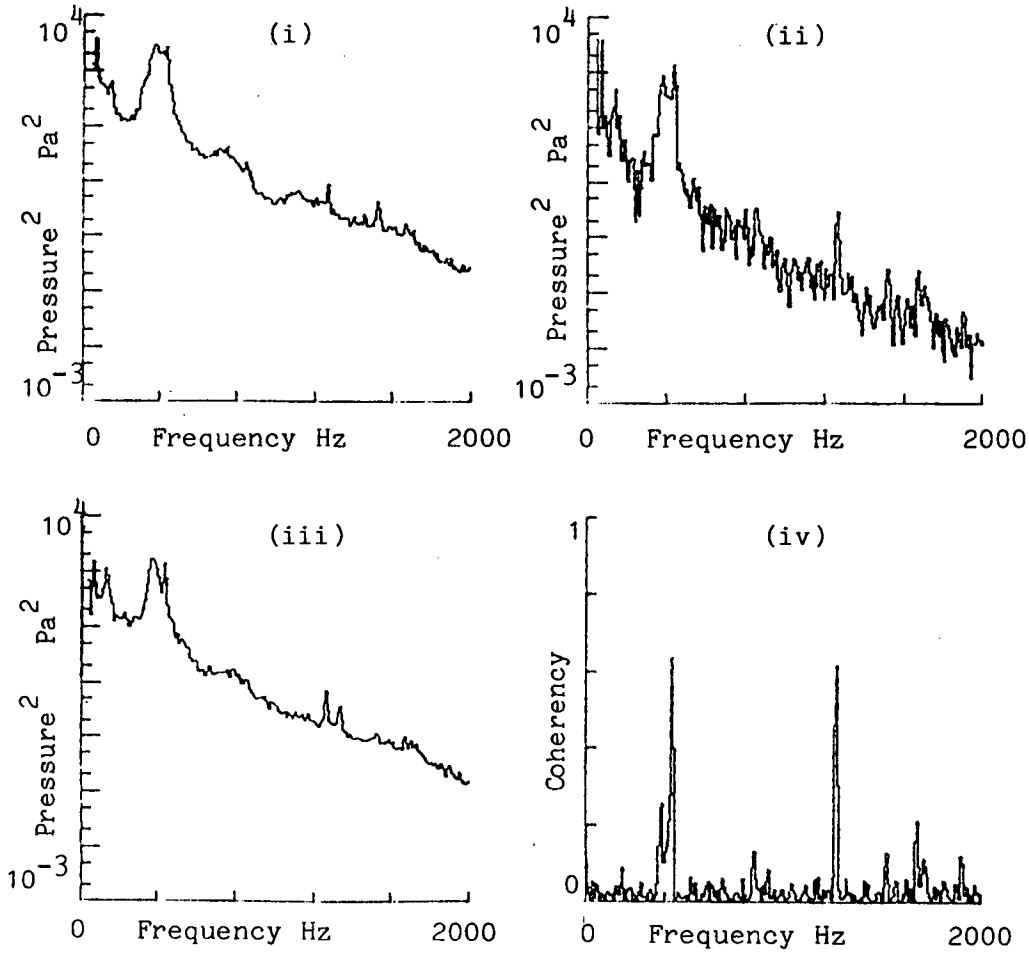


FIGURE 4.30b. Angle from stagnation = 90°.

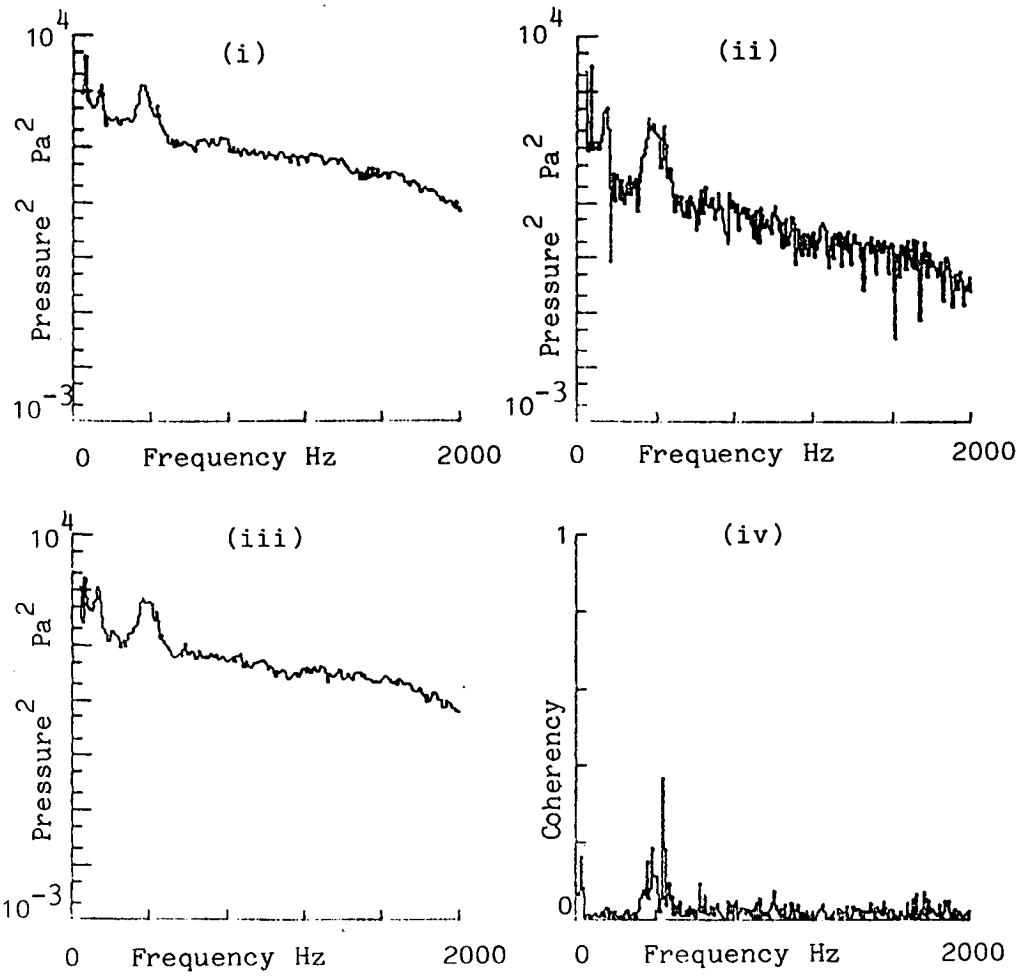


FIGURE 4.30c. Angle from stagnation = $180^{o}$.

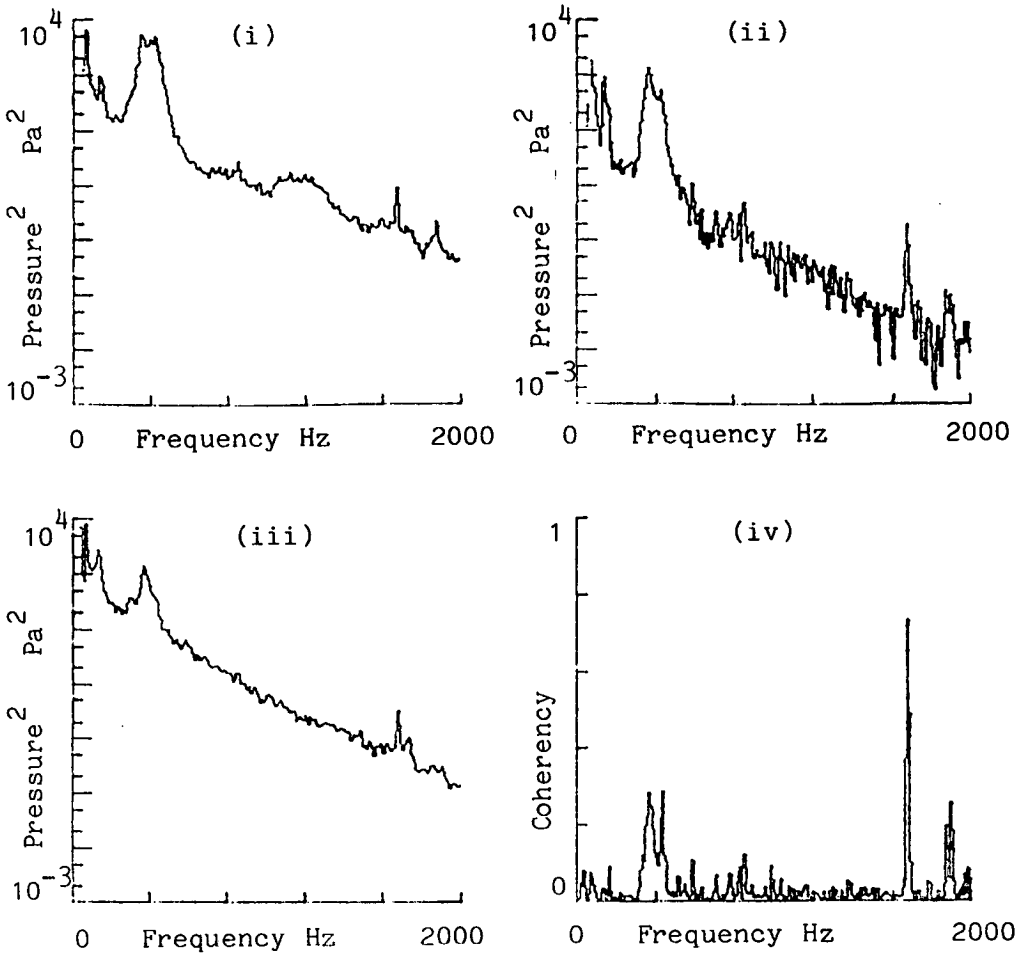


FIGURE 4.30d. Angle from stagnation = 270°.

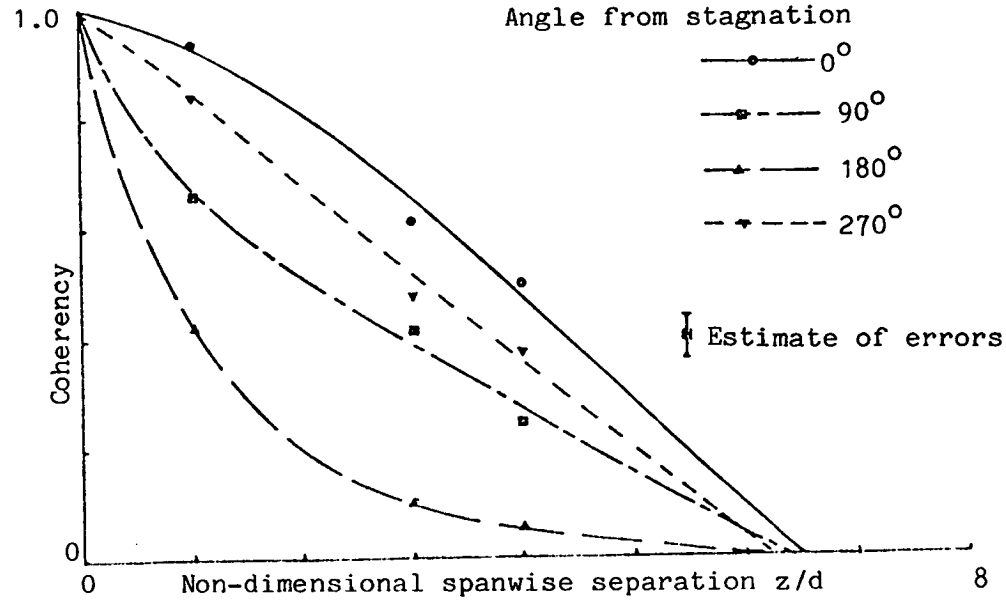


FIGURE 4.31a. Variation of coherency of pressure fluctuations at the vortex shedding frequency with spanwise separation along tube axis.

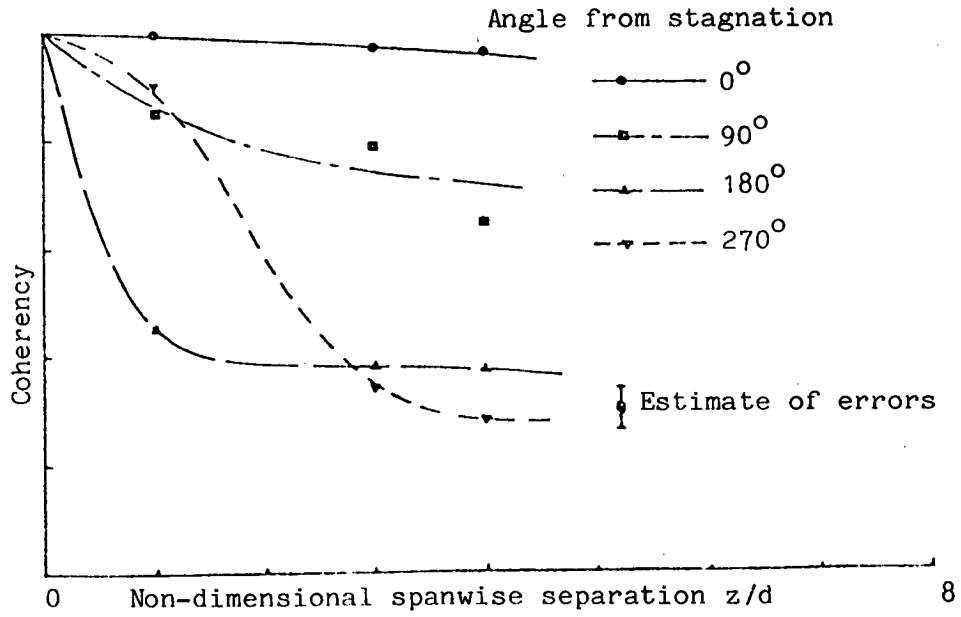


FIGURE 4.31b. Variation of coherency of pressure fluctuations at the first transverse duct cut-on frequency with spanwise separation along tube axis.

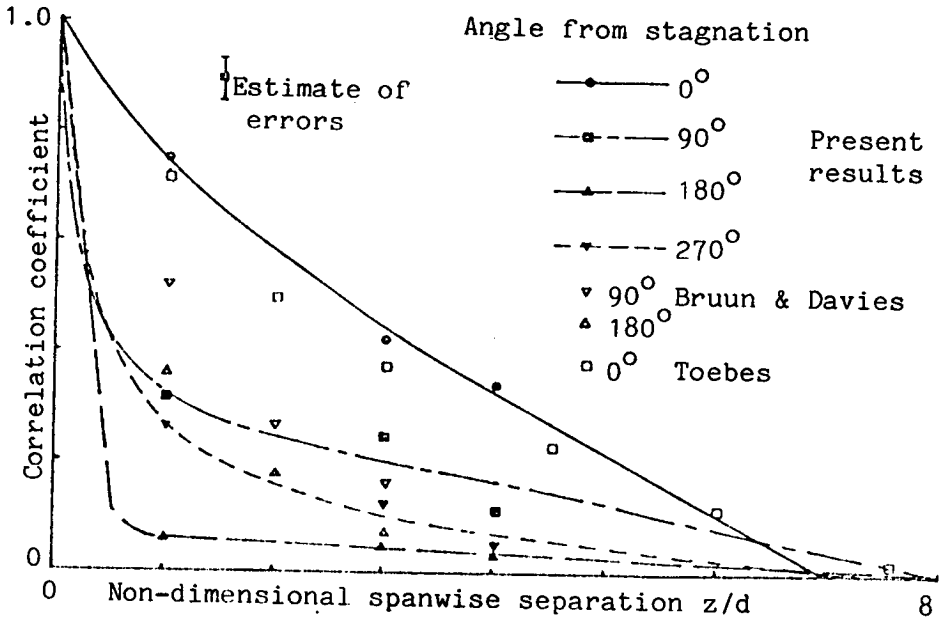


FIGURE 4.32. Variation of broad band correlation coefficient of pressure fluctuations with spanwise separation along tube axis. (Present results and previous results compared)

(i)

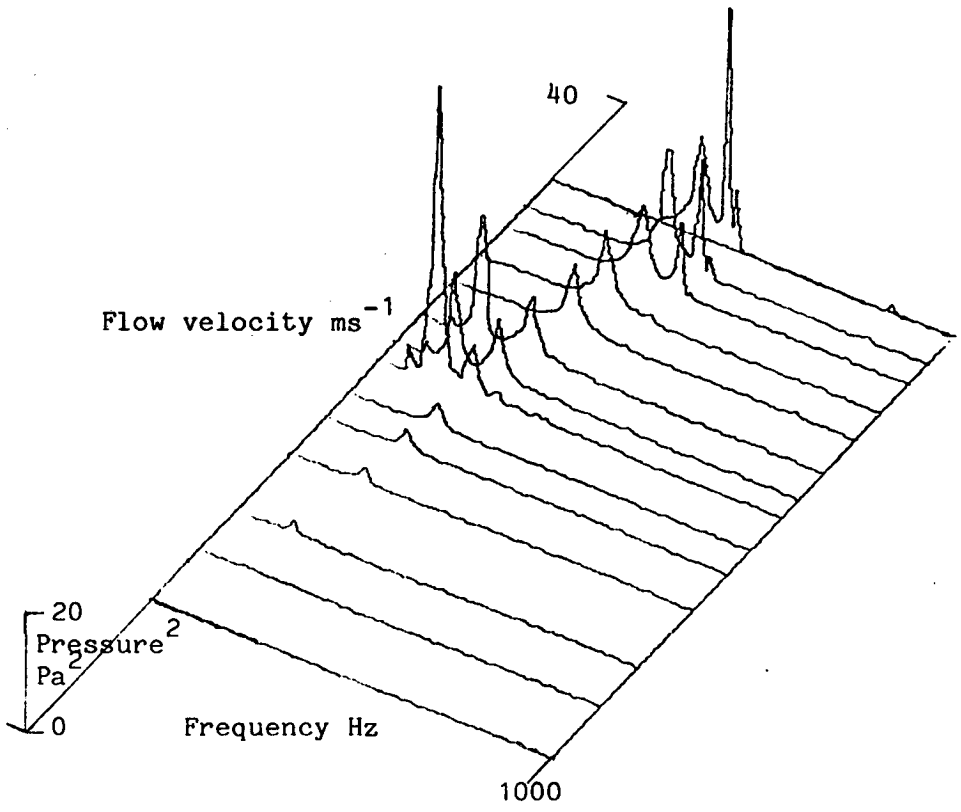


(ii)

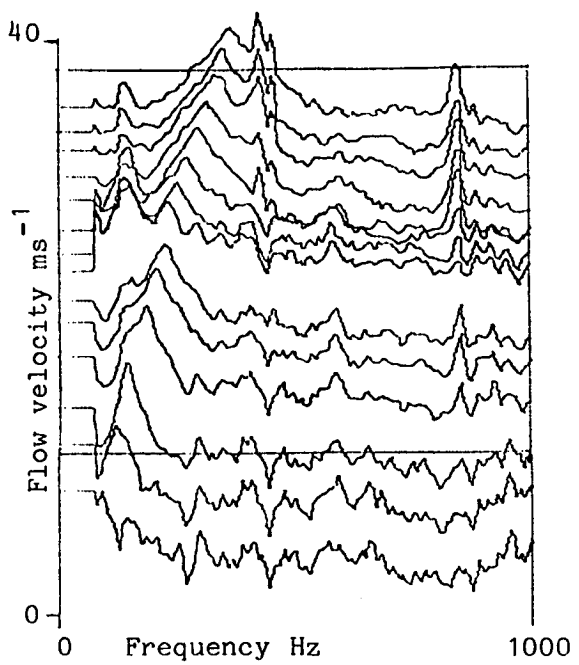


FIGURE 4.33 i-ii P.S.D. of pressure fluctuations at stagnation point versus free stream flow velocity. (i) Linear scale. (ii) Arbitrary logarithmic scale.

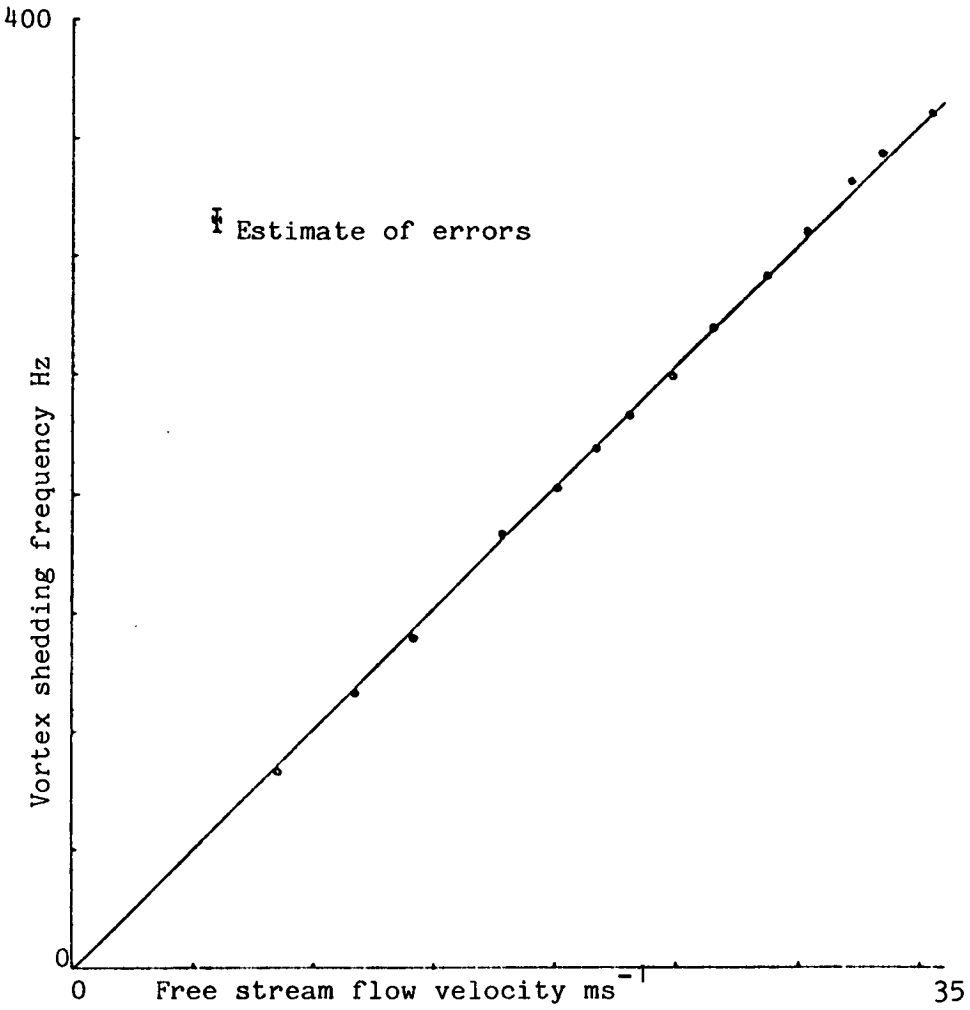


FIGURE 4.34. Vortex shedding frequency plotted against free stream flow velocity.

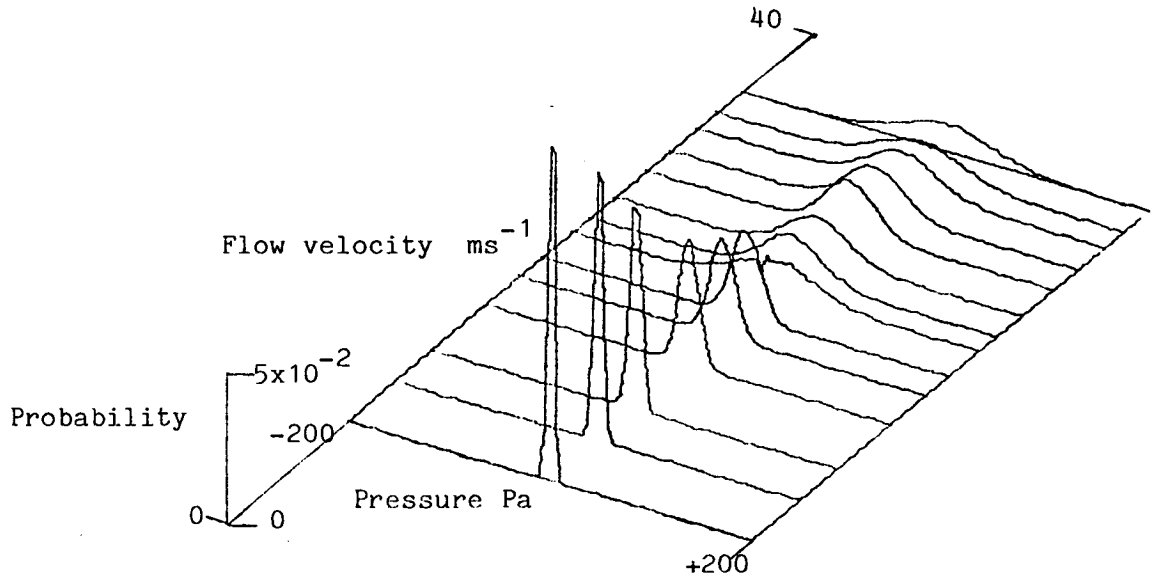


FIGURE 4.35. Amplitude probability distribution of pressure fluctuations at stagnation point versus free stream flow velocity.

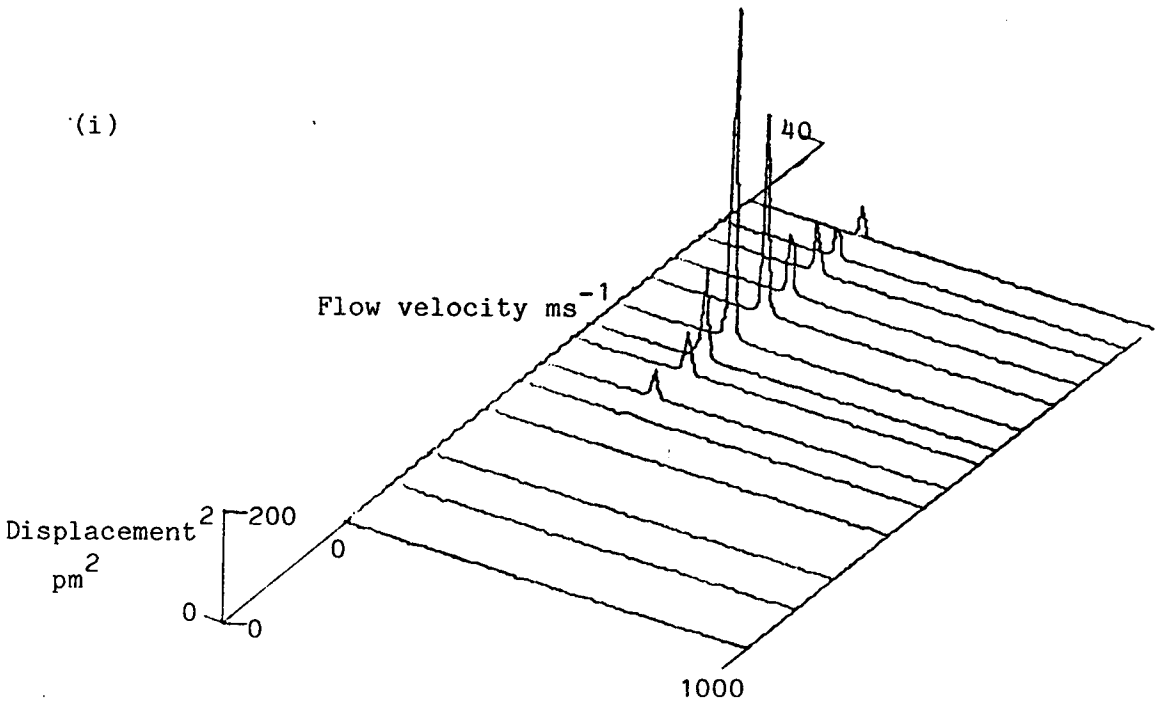


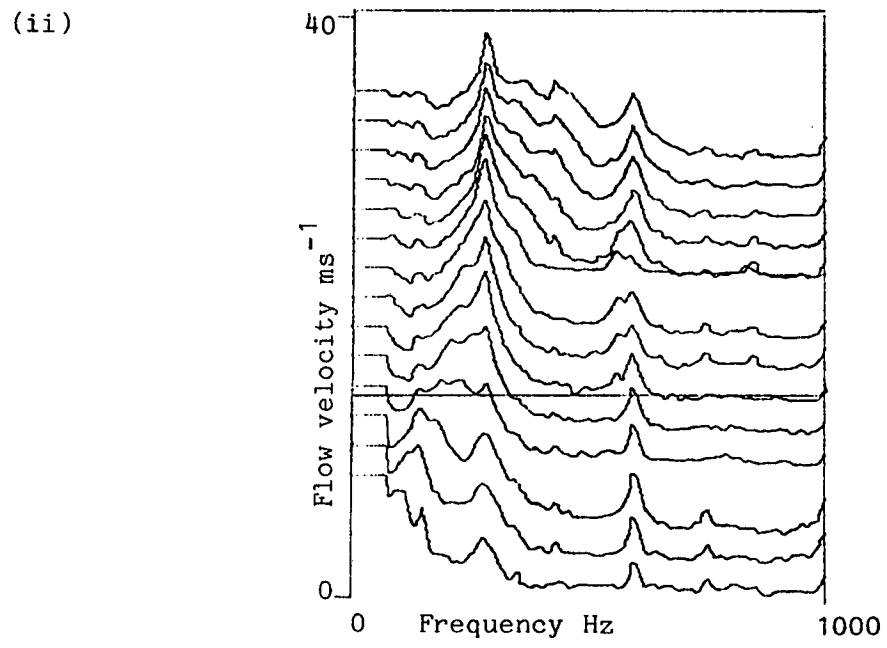


FIGURE 4.36 i-ii. P.S.D. of vibrating tube displacement versus free stream flow velocity. (i) Linear scale. (ii) Arbitrary logarithmic scale.

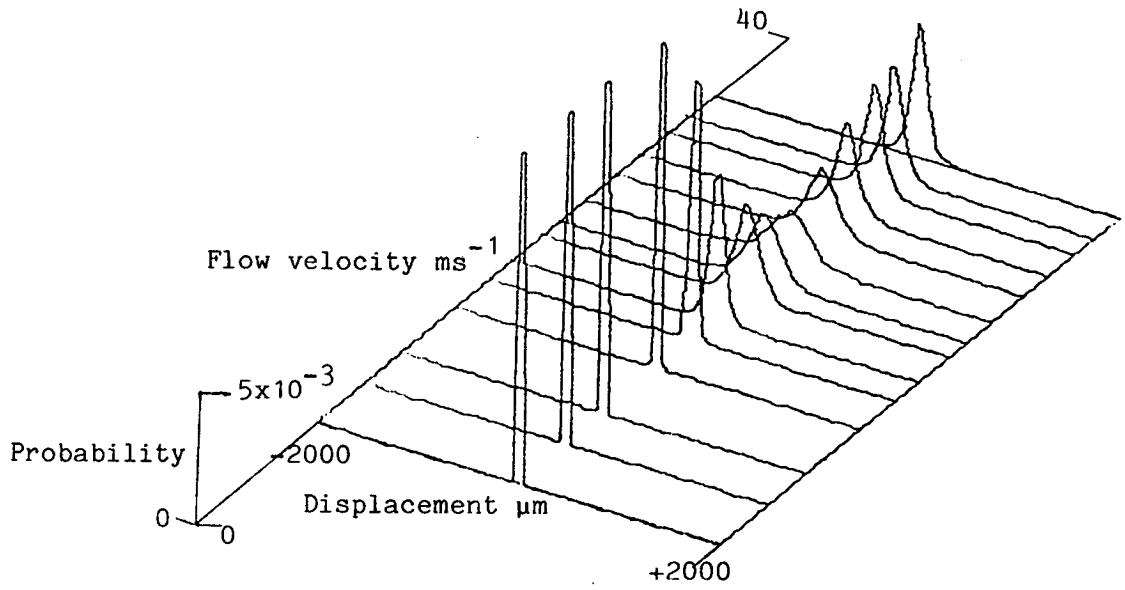


FIGURE 4.37. Amplitude probability distribution of the vibrating flexible tube displacement versus free stream flow velocity.

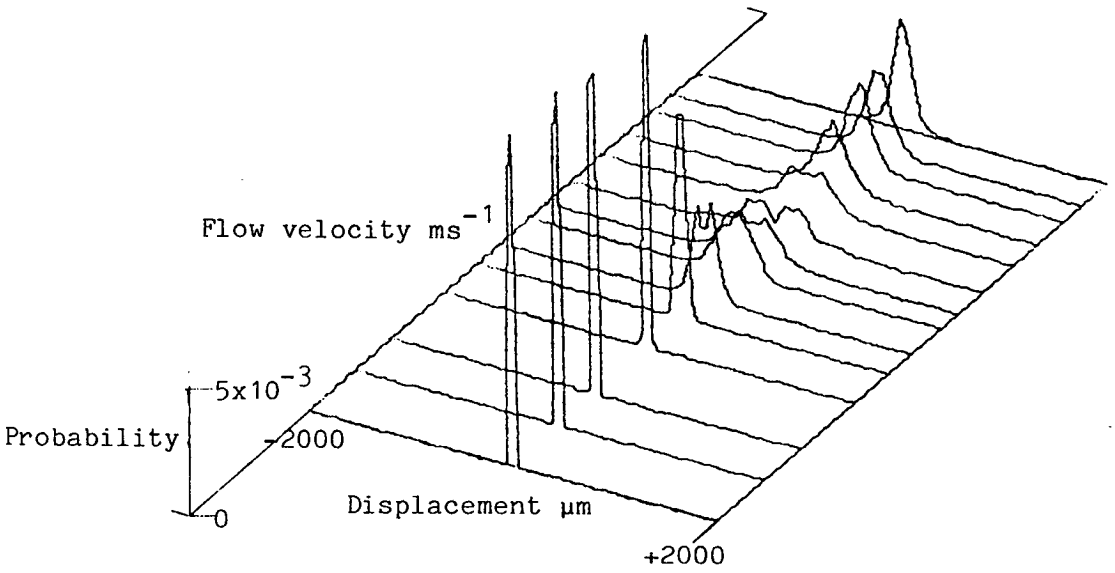


FIGURE 4.38. Peak amplitude probability distribution of the vibrating flexible tube displacement versus free stream flow velocity.

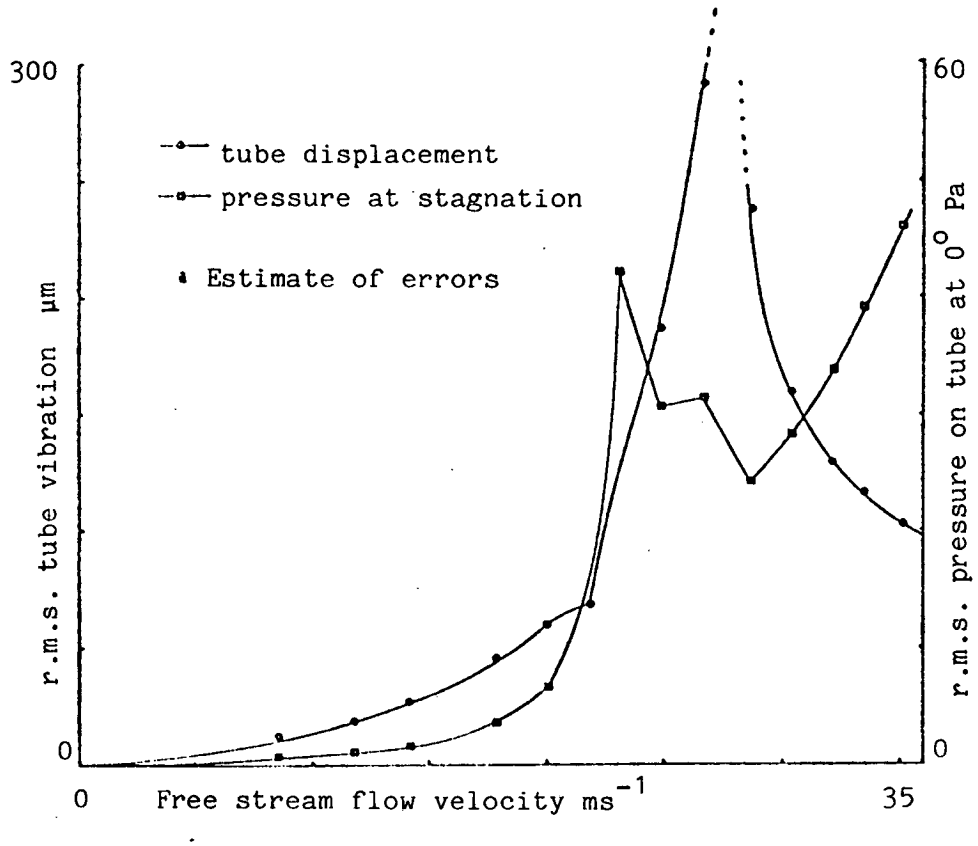


FIGURE 4.39. R.m.s. pressure fluctuations at stagnation point on the fixed pressure measuring tube and r.m.s. displacement of a neighbouring vibrating tube versus free stream flow velocity.

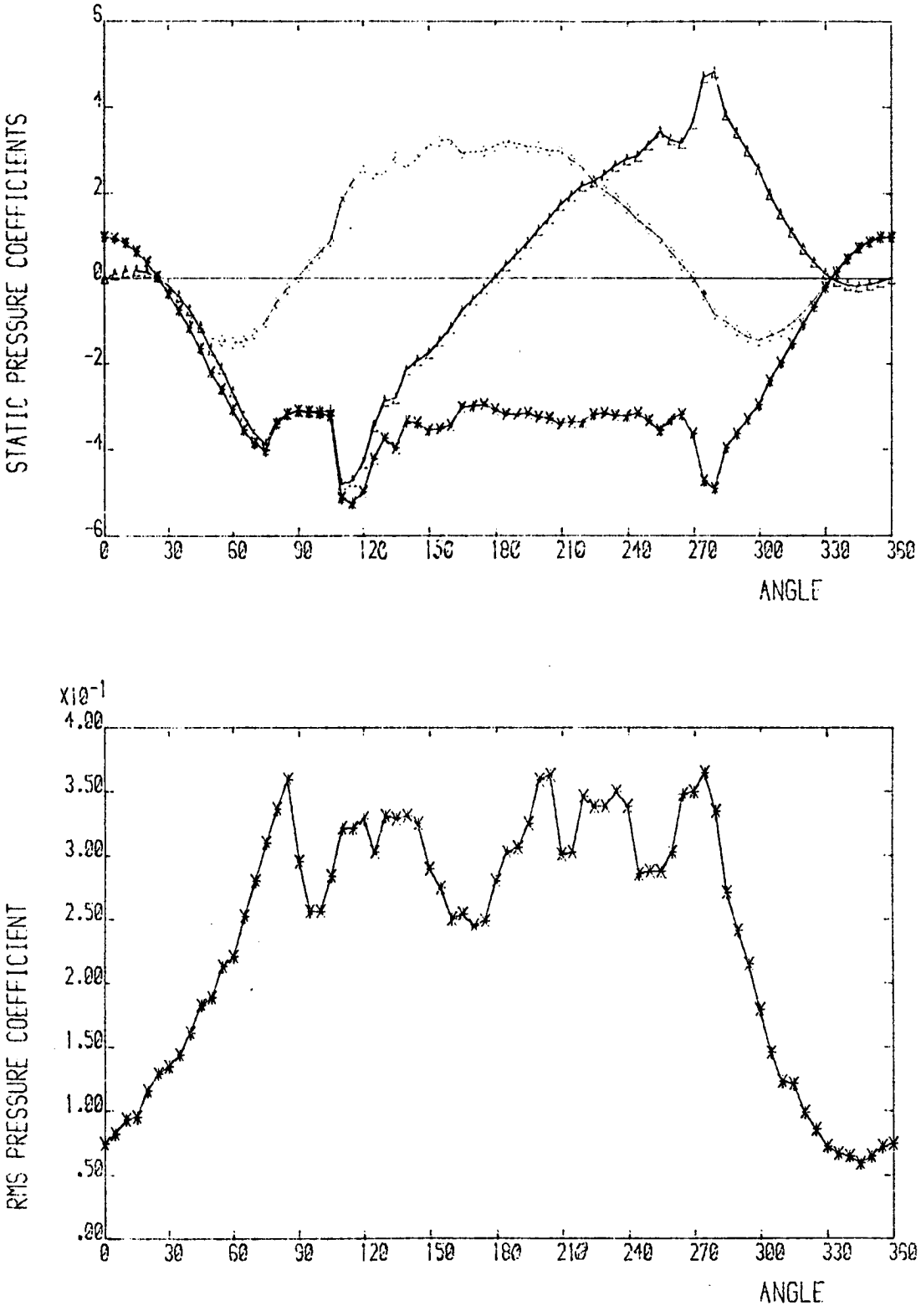


FIGURE 4.40(i) Variation of static and r.m.s. pressure coefficients round a fixed tube in a single tube row without superimposed sound.

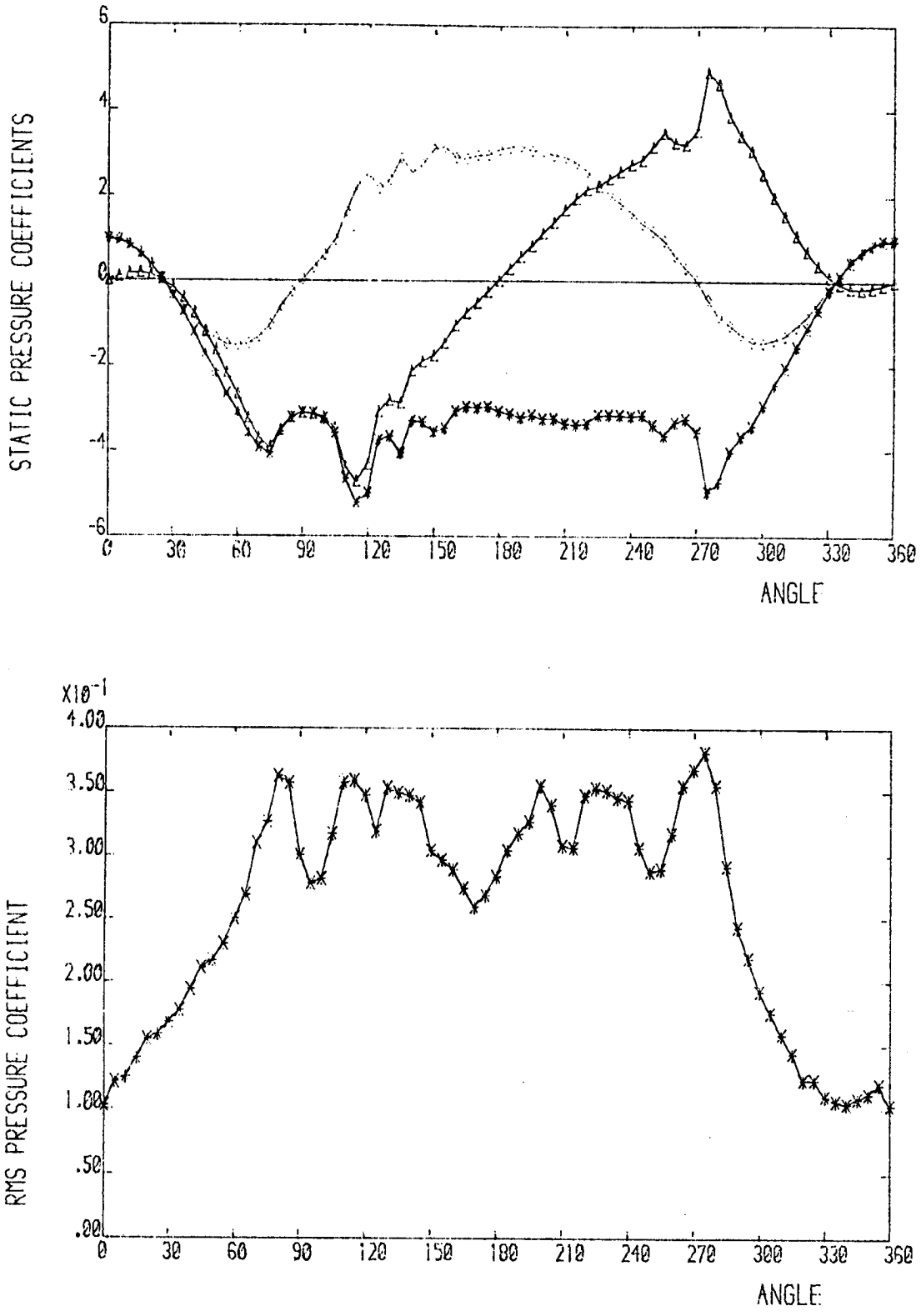


FIGURE 4.40(ii) Variation of static and r.m.s. pressure coefficients round a fixed tube in a single tube row with superimposed sound at 425 Hz at a SPL of 138 dB.

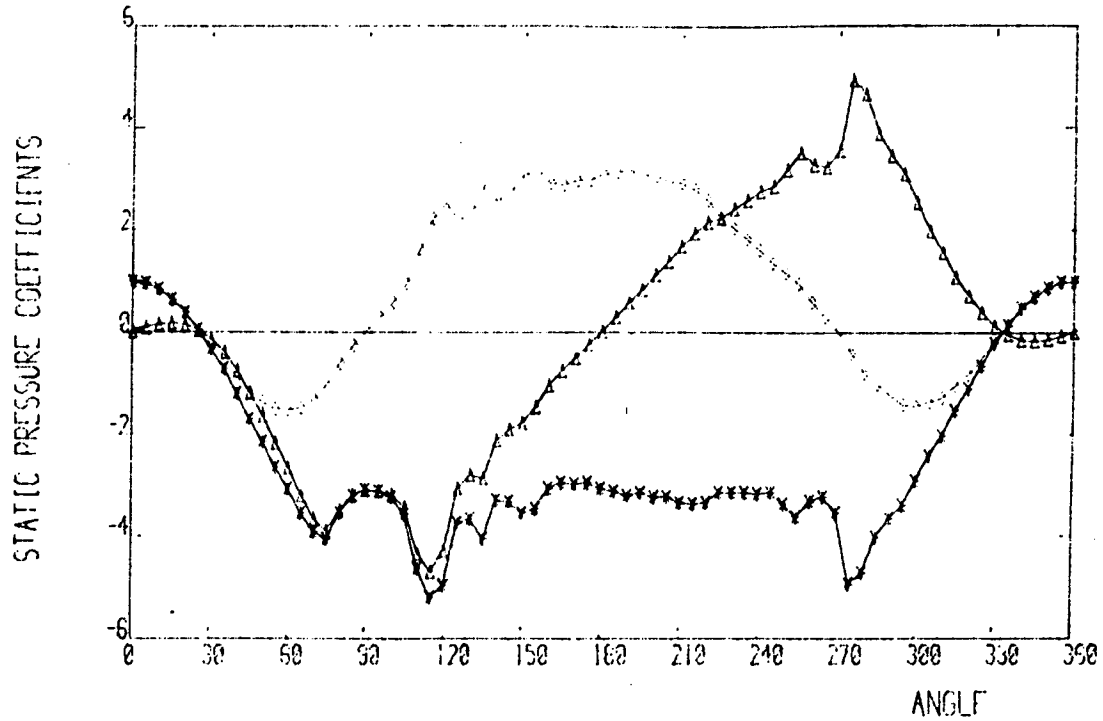


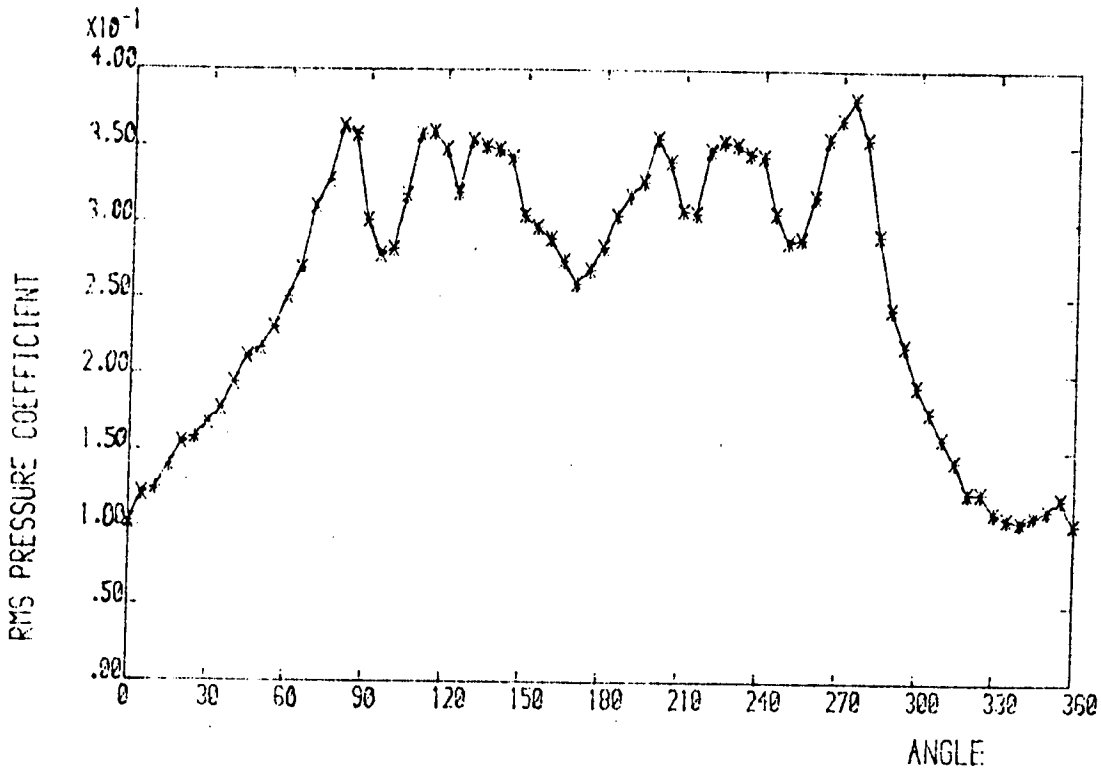


FIGURE 4.40(iii) Variation of static and r.m.s. pressure coefficients round a fixed tube in a tube row with superimposed sound at 360 Hz at a SPL of 136 dB.

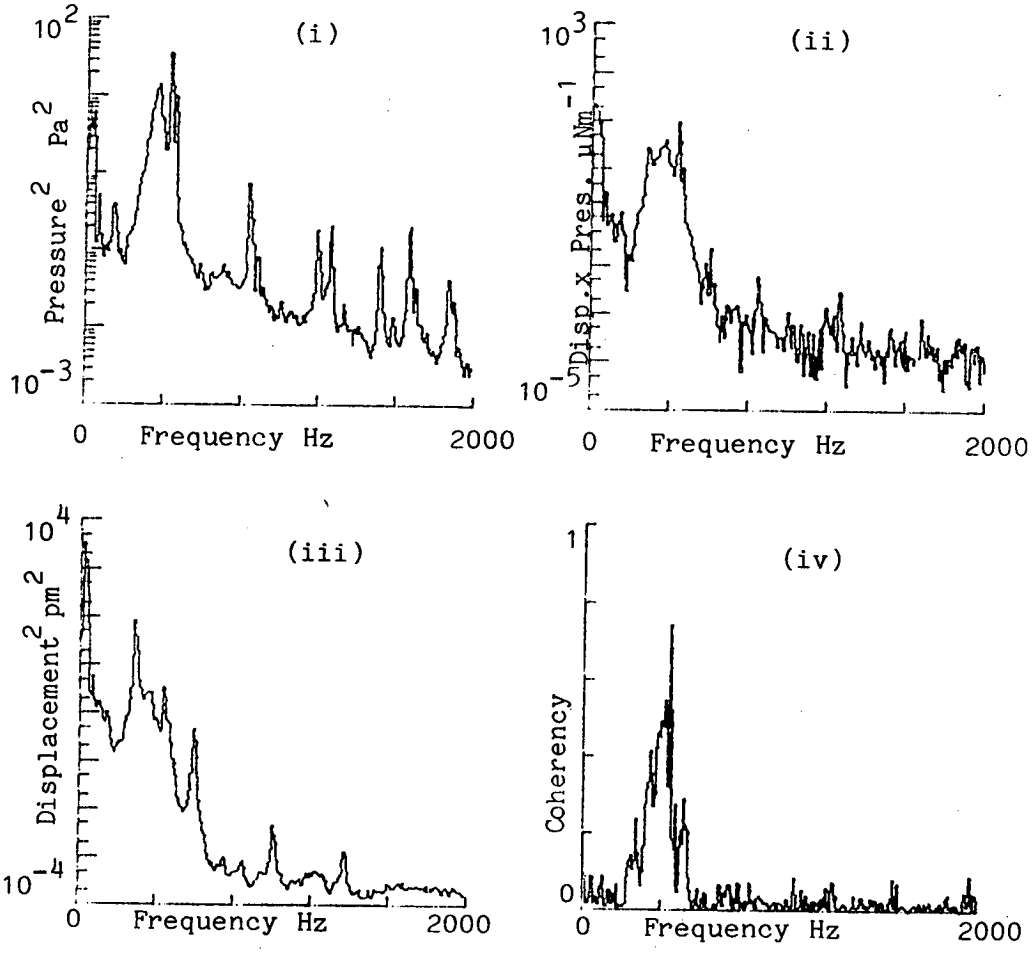


FIGURES 4.41 a-d.
(i) P.S.D. of fluctuating pressure on pressure measuring tube at stagnation point (logarithmic scale)
(ii) C.S.D. of vibrating tube displacement and the pressure at stagnation on the measuring tube (logarithmic scale)
(iii) P.S.D. of the vibrating tube displacement (logarithmic scale)
(iv) Coherency between pressure and displacement (linear scale)

FIGURE 4.41a. No sound.

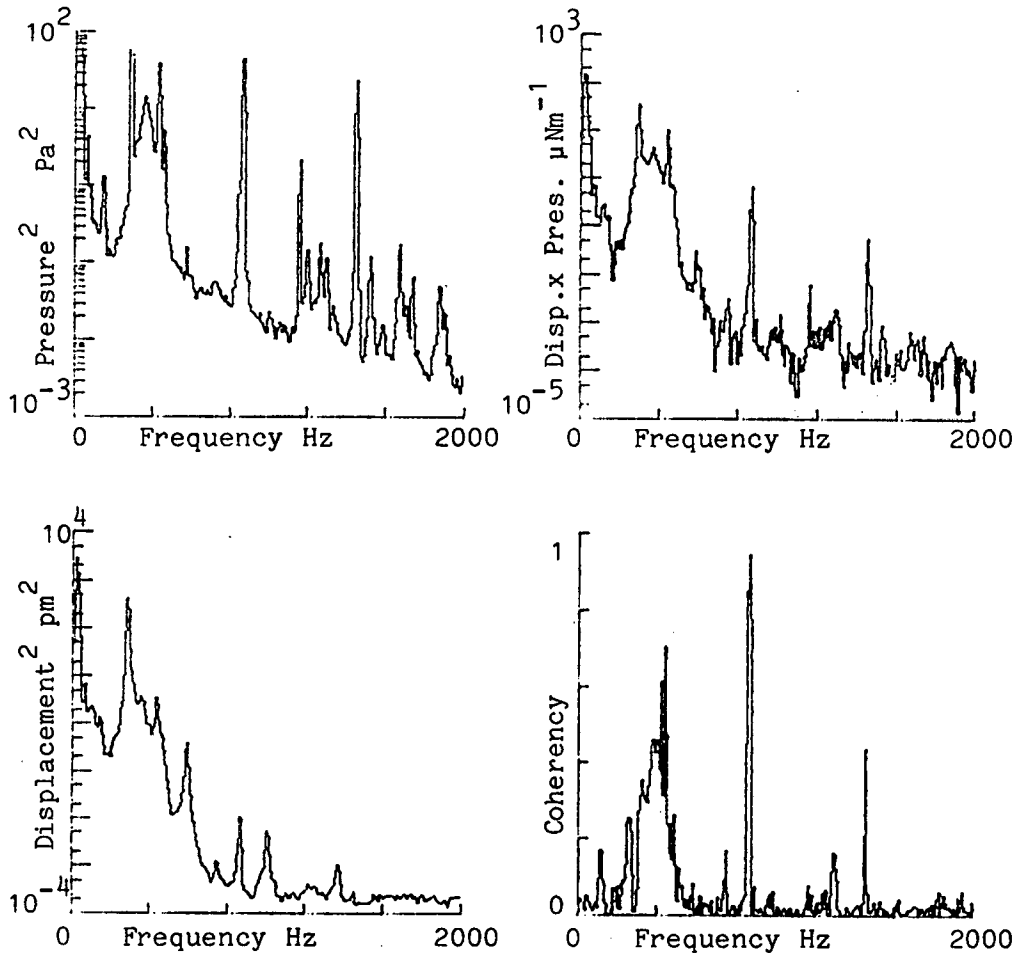


FIGURE 4.41b. Sound at 285 Hz and a SPL of 130 dB.

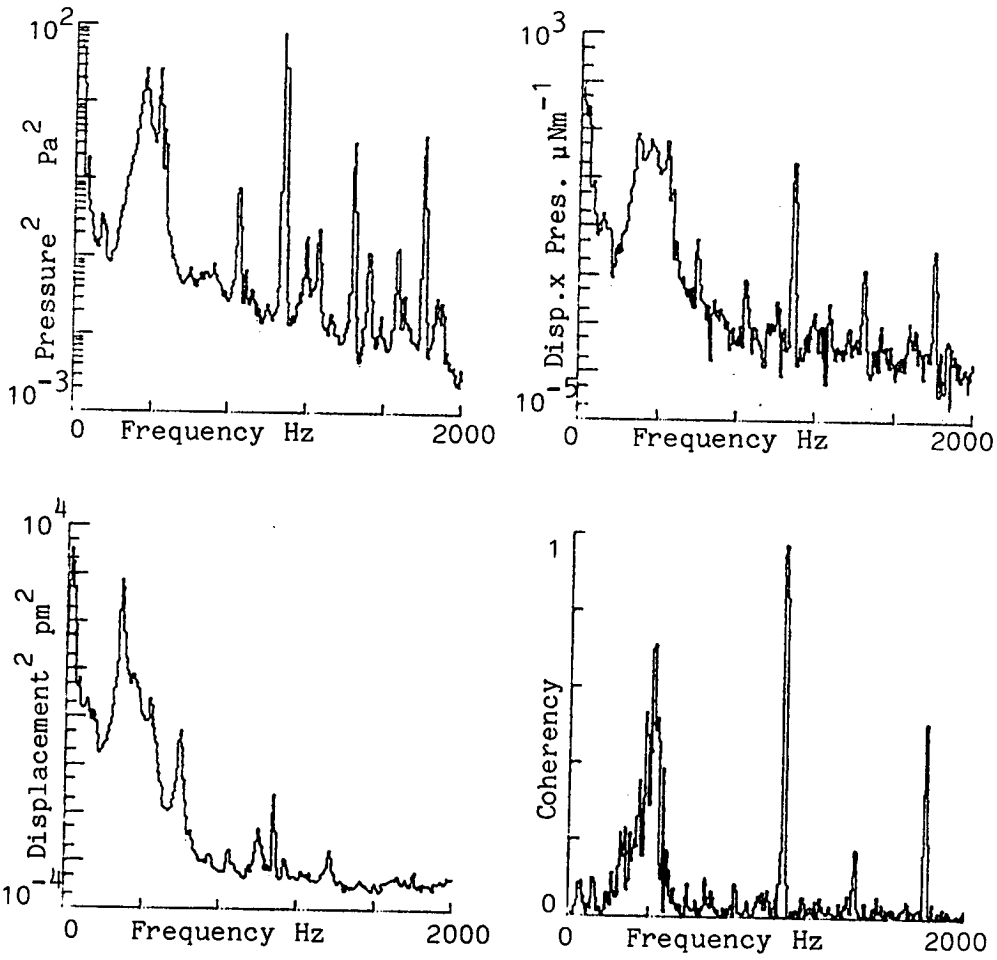


FIGURE 4.41c. Sound at 360 Hz on a SPL of 134 dB.

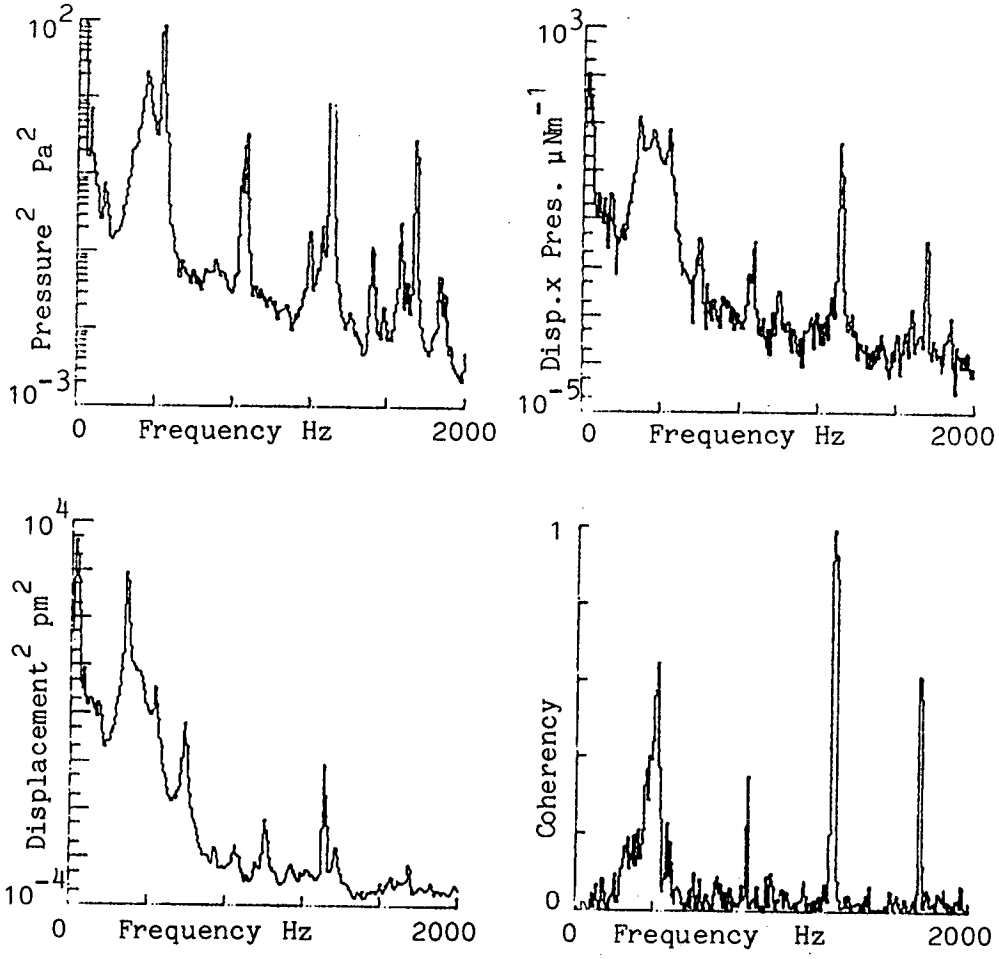


FIGURE 4.41d. Sound at 425 Hz and a SPL of 138 dB.

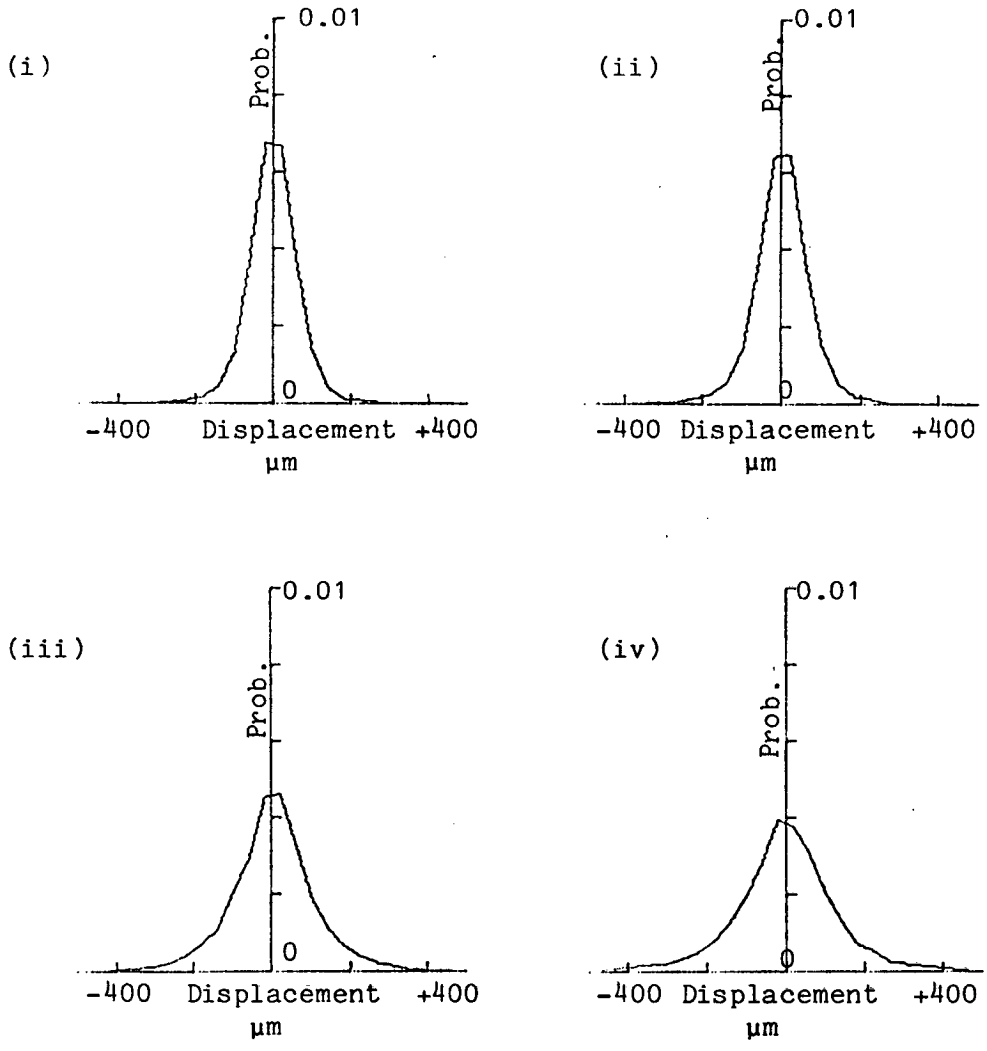


FIGURE 4.42. Amplitude probability distributions of displacement of vibrating flexible tube for;
(i) no sound,
(ii) superimposed sound at 285 Hz, SPL of 130 dB,
(iii) superimposed sound at 360 Hz. SPL of 134 dB,
(iv) superimposed sound at 425 Hz, SPL of 138 dB.

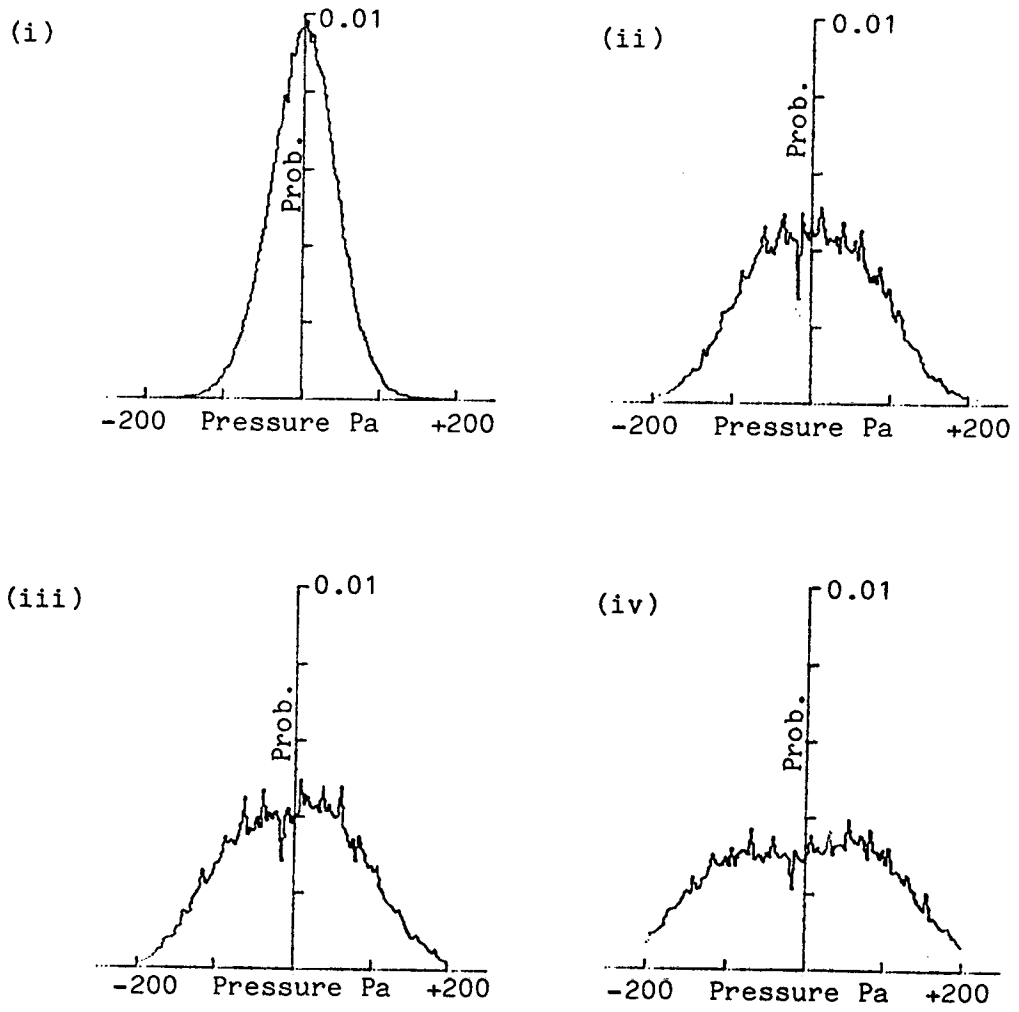


FIGURE 4.43. Amplitude probability distributions of pressure on the measuring tube at the stagnation point for;
(i) no sound,
(ii) superimposed sound at 285 Hz, SPL of 130 dB,
(iii) superimposed sound at 360 Hz, SPL of 134 dB,
(iv) superimposed sound at 425 Hz, SPL of 138 dB.

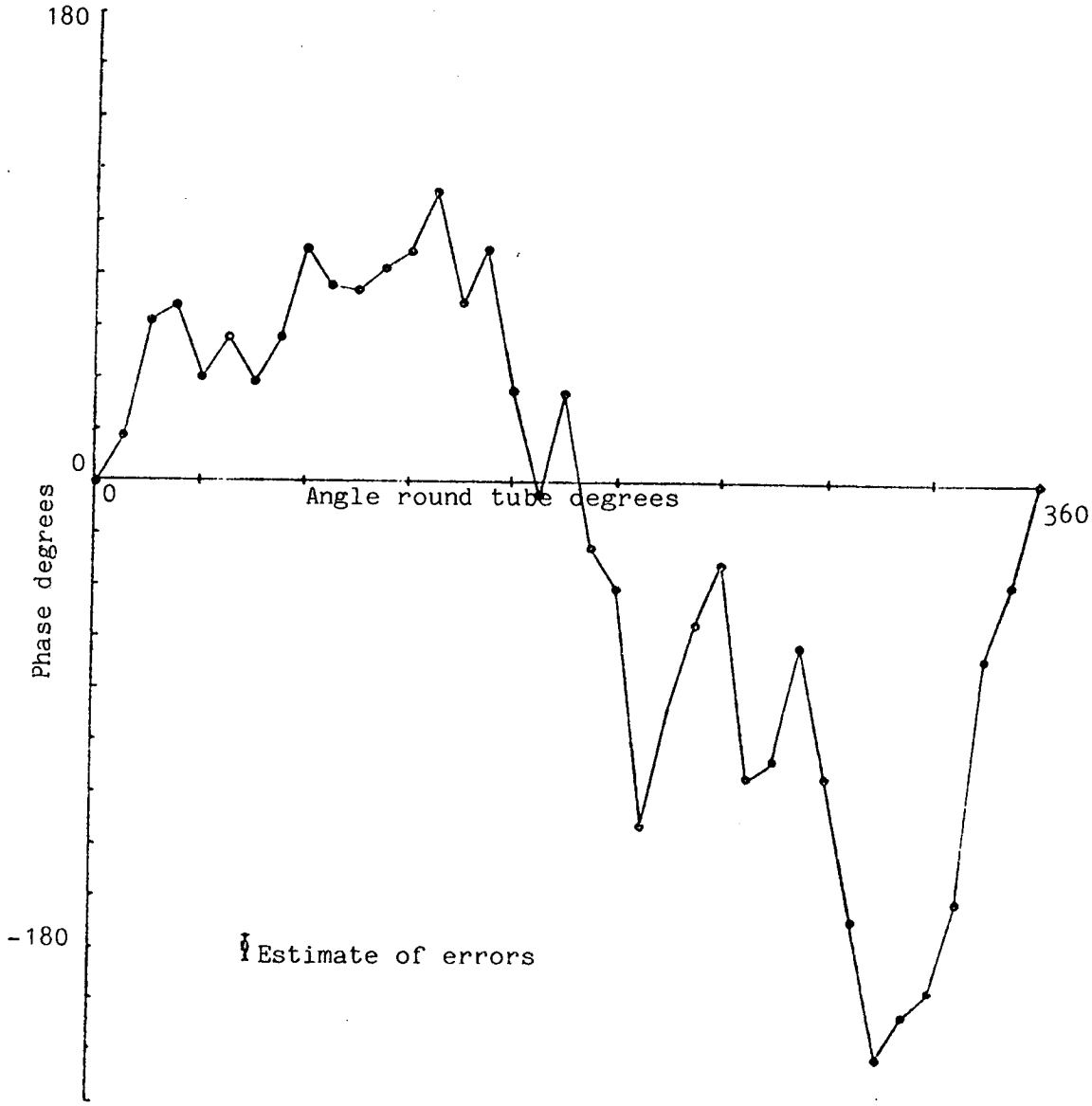


FIGURE 4.44 i-iii. Variation of phase of vortex shedding pressure fluctuations with angle round the measuring tube.

FIGURE 4.44i. Uniformly spaced arrangement of fixed tubes.

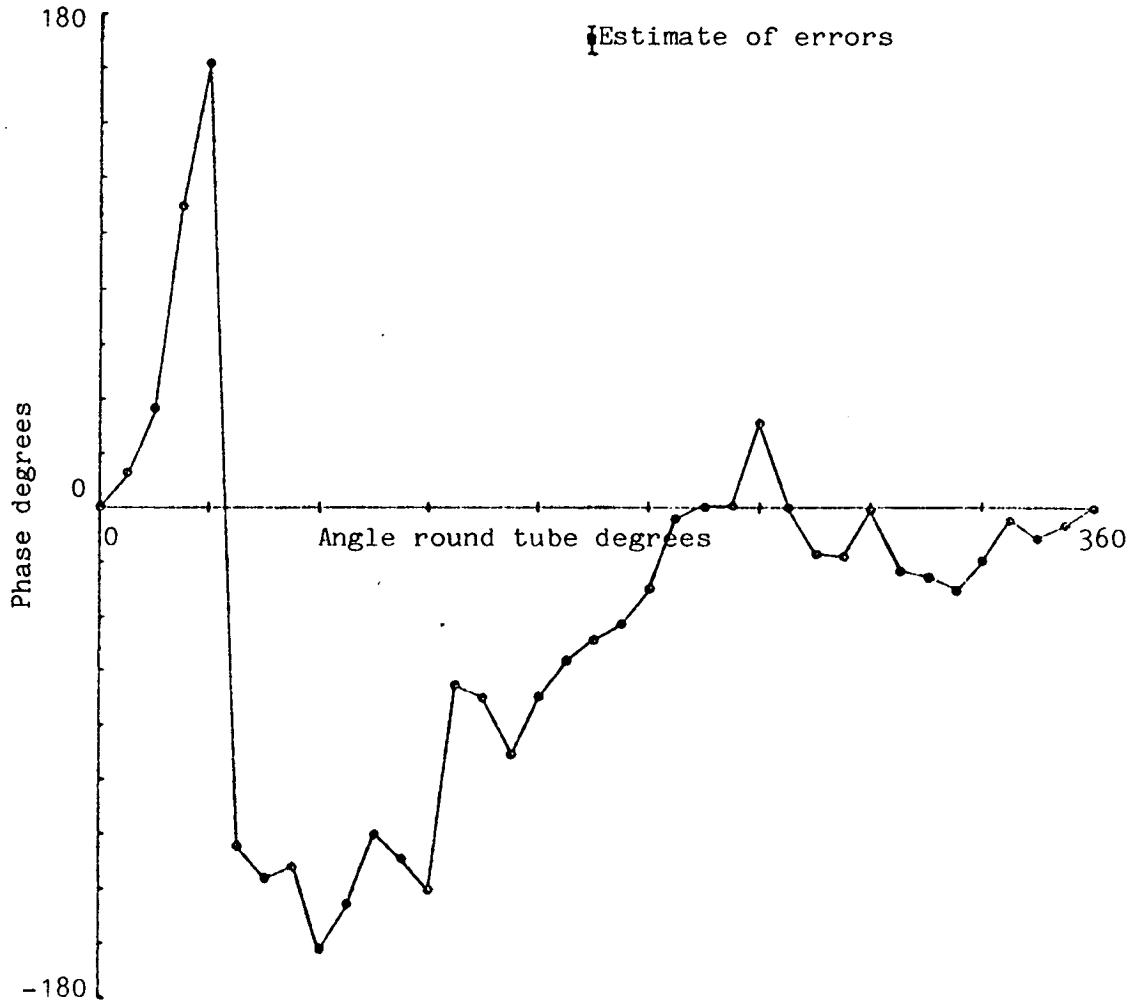


FIGURE 4.44ii. Fixed row of tubes with the pressure measuring tube statically displaced by 0.1 diameter.

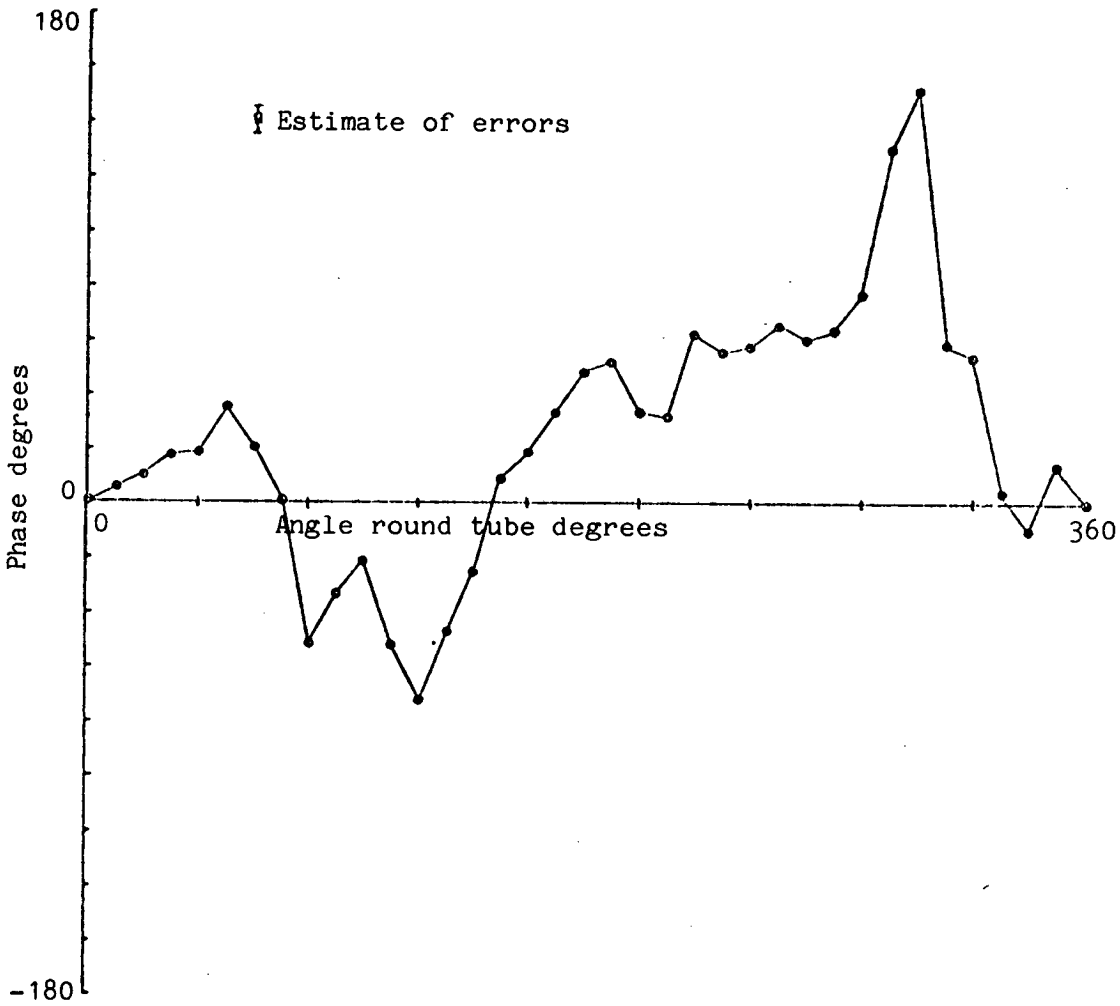


FIGURE 4.44iii. Uniformly spaced row of fixed tubes with the pressure measuring tube mounted next to a vibrating flexible tube.

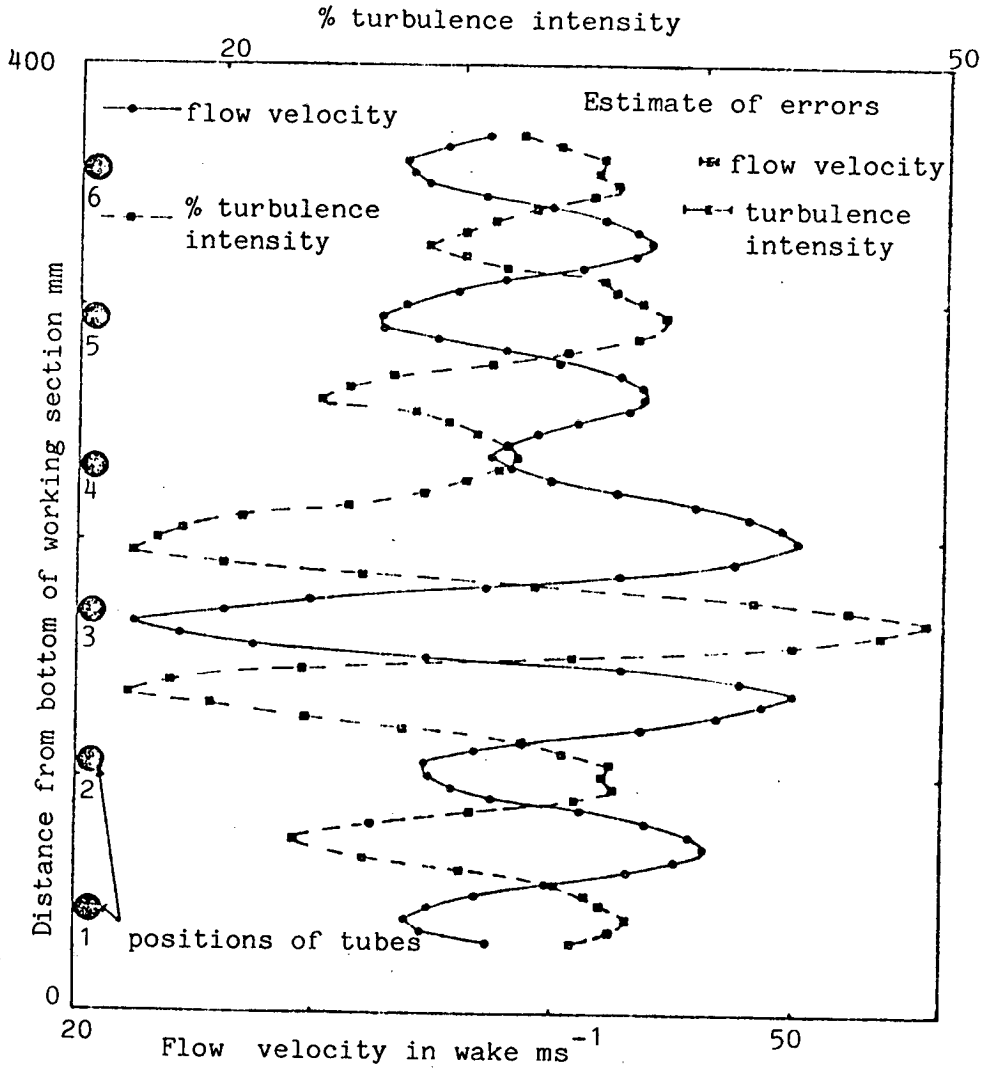


FIGURE 4.45. Flow velocity and turbulence intensity 2 diameters downstream of a row of uniformly spaced fixed tubes.

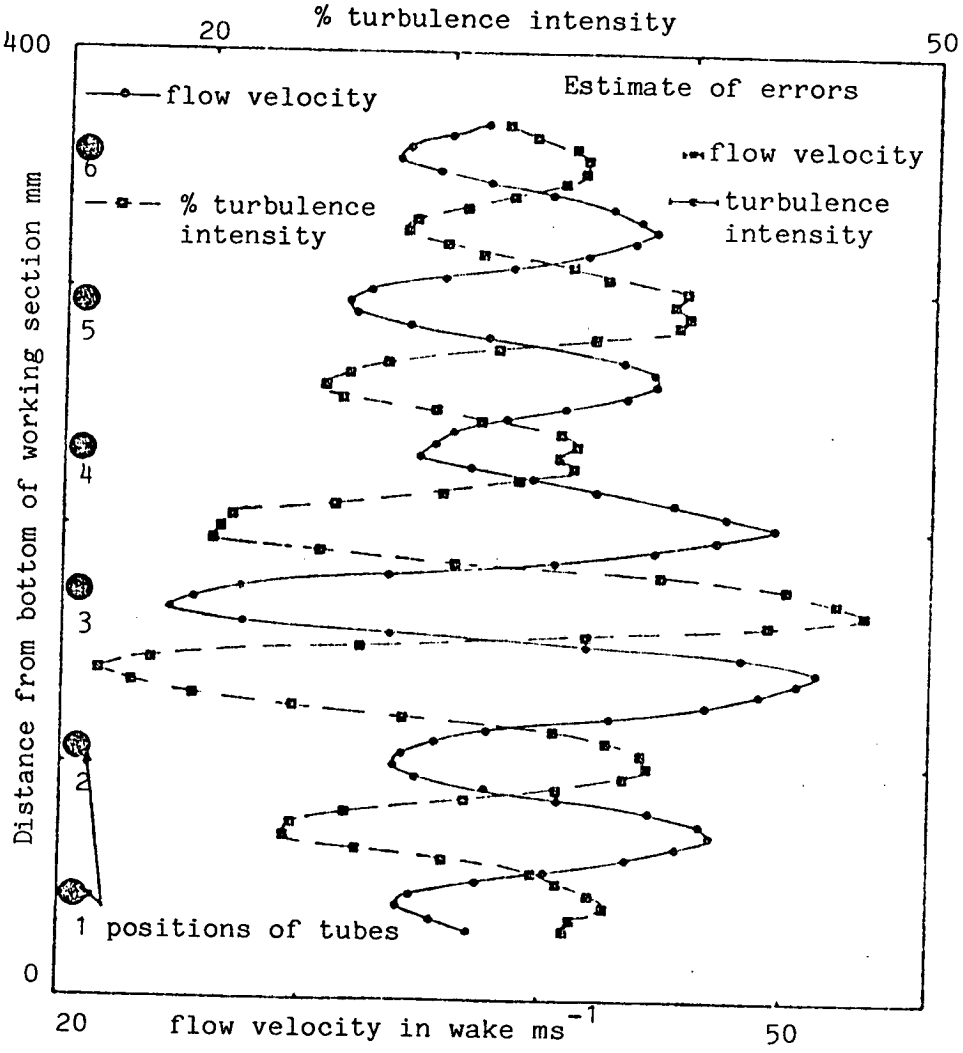


FIGURE 4.46. Flow velocity and turbulence intensity 2 diameters downstream of a row of fixed tubes with tube 3 displaced 0.1 diameter towards tube 4.

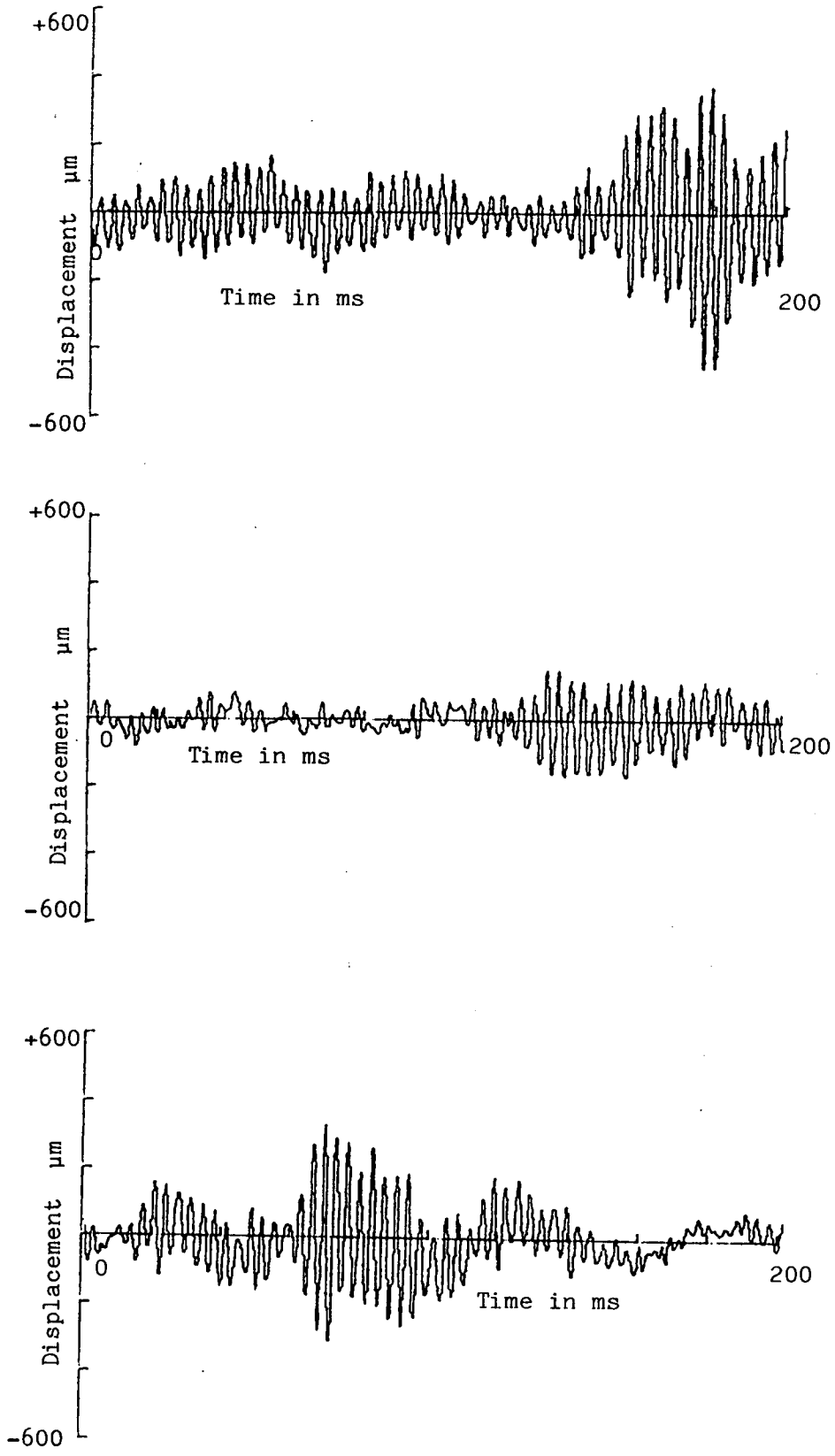


FIGURE 4.47. Typical time histories of the vibrating tube displacement when mounted in a single uniformly spaced tube row.

# CHAPTER 5

# INVESTIGATION INTO THE VIBRATION OF A DYNAMICALLY MODELLED TUBE BANK

## 5.1 Introduction

A series of experiments was carried out on a dynamically modelled tube bank (as described in Chapter 3) in order to investigate the interaction of a vibrating tube, in a tube bank, with its nearest neighbour, and the effect of externally imposed sound on the vibration responses of the tubes.

The experiments carried out were not designed to investigate the effects on the tube vibration of varying a large range of tube vibration, flow and sound parameters, but were designed to be representative of the conditions within a typical A.G.R. heat exchanger.

## 5.2 General Experimental Technique

The dynamically modelled tube bank was assembled in the working section using the purpose designed support plates and tube support rods. As each flexible tube was mounted in position it was tuned to a frequency within 2% of the desired resonant frequency of 260 Hz. This was achieved by irradiating the flexible tube with sound at a frequency of 260 Hz from a small loudspeaker and tightening the nuts on both sides of the support plates to produce a maximum in the amplitude of the displacement signal from a small accelerometer which was temporarily mounted on the tube. After each tube was tuned plasticine was used to seal the small gaps between the tube support rods and the mounting holes in the perspex windows of the working section so that atmospheric air did not leak into the working section. The damping at the resonance frequency of each tube was measured by exciting the tube with sound at its resonance frequency and then switching off the sound whilst recording the decaying tube displacement signal on a 50 dB logarithmic range B & K level recorder type 2305. The tube damping ratio at its rigid body mode resonance frequency was then estimated from the slope of the displacement decay curve.

Figure 5.1 shows the arrangement of the tubes mounted in the working section for the different measurements which were carried out, and Figure 5.2 shows the damping ratios plotted against the resonance frequencies for the various tubes. Two different arrangements of the instrumented pressure and displacement measuring tubes were used in the experiments. The first arrangement was where the two displacement measuring flexible tubes were next to each other in the same row and the pressure measuring tube was next to one of the displacement measuring tubes and also in the same row. This arrangement was used to investigate the interaction between two vibrating tubes in the same row in a staggered tube bank. The second arrannge-ment was where one displacement measuring flexible tube was mounted in the staggered row behind the other displacement measuring tube next to the first displacement measuring tube. This arrangement was used to investigate the interaction between vibrating tubes and their neighbours in the staggered position in a row in front, or a row behind. The pressure signal from a microphone mounted flush in the wall of the working section in the same plane as the instrumented tubes was used to monitor the acoustic duct modal frequencies, superimposed sound and the aerodynamic pressure fluctuations present in the vicinity of the vibrating flexible tubes.

The fluctuating pressure signal from the flush mounted wall microphone was amplified using a B & K frequency analyser type 2107. The signals from the accelerometers mounted in the flexible tubes were amplified and integrated by a dual channel charge amplifier, high pass filter and double integrating system. The amplified fluctuating pressure and displacement signals were acquired and processed on a dual channel Hewlett Packard signal analyser type 5420, and the graphs were plotted on a Hewlett Packard digital graph plotter type 7225A. In order to produce statistically reliable results the estimated spectra were averaged at least 100 times for the estimations of P.S.D's and C.S.D's and 1000 times for the estimation of the coherency spectra and amplitude histograms. The static pressure distributions were measured round the rotating pressure measuring tube using the equipment and method described in Chapter 3.

The Reynolds number at which the investigations were carried out was approximately $1.2 \times 10^5$ based on tube gap velocity, except in Section 5.5 where the effect of the variation of flow velocity on

tube vibrations was investigated and the Reynolds numbers varied over the range $3.9 \times 10^4$ to $1.2 \times 10^5$.

## 5.3 Interaction of Two Vibrating Flexible Tubes in the Same Row

### 5.3.1 Experimental measurements

The displacement signals from two instrumented flexible tubes mounted in the same row as explained in Section 5.2 were processed on the signal analyser. The displacement signal from instrumented tube 1 (see Figure 5.1) and the pressure signal from the wall microphone, were also acquired and processed on the signal analyser. The acquired signals were then processed to produce the figures described below.

Figures 5.3 i-iv show:-

(i) P.S.D. of the displacement of instrumented tube 1,

(ii) P.S.D. of the displacement of instrumented tube 2,

(iii) C.S.D. of the displacement signals,

(iv) coherency spectrum of the displacement signals.

Figures 5.4 i-iv show:-

(i) P.S.D. of the displacement of instrumented tube 1,

(ii) P.S.D. of the wall microphone pressure signal,

(iii) C.S.D. of the displacement and pressure signals,

(iv) coherency spectrum of the displacement and pressure signals.

Figures 5.5 i-iv show:-

(i) amplitude histogram of the displacement of instrumented tube 1,

(ii) amplitude histogram of the displacement of instrumented tube 2,

(iii) amplitude histogram of the wall microphone pressure signal.

### 5.3.2 Results and discussion

The two instrumented flexible tubes are observed to have vibration amplitudes which are different by a factor of 1.36 at their rigid body modal frequencies. This cannot be explained by the differences in the damping ratios of the flexible tubes which are in the ratio 1.12:1. The amplitude responses of the tubes at their rigid body modal frequencies should be approximately in the inverse ratio of their damping ratios (if it is assumed that their resonance frequencies are almost the same and the pressure excitation forces on the tubes are the same). It is therefore suggested that

the pressure excitation forces on the tubes in the different positions in the tube bank were different. This could be due to the tube with the lower amplitude response being next to the fixed pressure measuring tube which may produce a different flow field (round the instrumented tube) from the flow field produced when the flexible instrumented tube is only next to vibrating flexible tubes.

There are several peaks in the tube displacement power spectra some of which are due to the response of the tube at the other non-rigid body modal frequencies. The sharp peaks at 850 Hz correspond to the forced response of the tubes at the (2,0) transverse duct cut-on modal frequency, which can be seen as a peak in the wall microphone pressure power spectrum (Figure 5.4(ii)). The sharp peaks in the displacement coherency spectrum (Figure 5.3(iv)) correspond to the two tubes being coherently excited by acoustic duct modes which can be seen as peaks in the wall microphone pressure power spectrum. The displacement coherency spectrum has a low value at the tube rigid body modal frequency which implies that there is no direct linear interaction between the tubes at the frequency of their maximum responses. (There are large amplitude, low frequency tube responses below 30 Hz which are due to the combined response of the tubes and their supporting structure which is not well isolated below 30 Hz). At frequencies of approximately 95 Hz and 190 Hz there are peaks in the displacement coherency spectrum. Peaks at these frequencies can also be seen in the wall microphone pressure power spectrum and have the characteristics of peaks due to acoustic duct modes. It is therefore postulated that these peaks are longitudinal duct modes which are produced by reflections at the edge of the tube bank and from the impedance discontinuity at the variable throat. The displacement coherency rises between frequencies of 500 Hz and 900 Hz which may correspond to partially coherent broadband turbulent pressure excitations on both tubes. There is no evidence of a well defined vortex shedding peak in the wall microphone pressure power spectrum which suggests that the vortex shedding mechanism is not the main tube excitation mechanism at Reynolds numbers of approximately $1.2 \times 10^5$ (based on gap velocity).

Figures 5.4(ii-iv) show the coherent excitation of the flexible instrumented tube 1 by acoustic duct modes which are the dominant pressure excitation forces on the tubes above 850 Hz. Above 1.2 kHz there are many exciting acoustic duct modes which merge together and

coherently excite both flexible instrumented tubes, which increases the displacement coherency above 1.2 kHz.

The tube amplitude displacement histograms are Gaussian in shape showing that the tube exhibits a response similar to that of a linear system responding to a random excitation. The amplitude histogram of the wall microphone pressure signal appears to correspond to a superposition of two independent Gaussian pressure fields with different means. The small peaks on the distribution curve correspond to narrowband pressure signals (i.e. transverse acoustic duct modes). It is postulated that the double Gaussian distribution curve is due to the combination of the turbulent pressure field, which is convected downstream in the working section boundary layer, and the pressure fluctuations due to the combination of many narrowband acoustic modes which pass through the working section boundary layer to the wall microphone.

Further discussions on the interaction of two neighbouring tubes and the comparison with other work carried out are given in Section 5.4.

## 5.4 Interaction of Two Vibrating Flexible Tubes in a Staggered Arrangement and the Investigation of Wake Velocity and Pressure Fluctuations

### 5.4.1 Experimental measurements

The displacement signals from two tubes mounted in a staggered arrangement as explained in Section 5.2 were acquired and processed on the signal analyser. A calibrated hot wire anemometer probe was then mounted in the wake of instrumented tube 1 (see Figure 5.1) so that the combined velocity signals for the two directions perpendicular to the spanwise tube axis were obtained. The displacement signals from instrumented tube 1, and the velocity signals from the hot wire signal processing equipment were acquired and processed on the signal analyser. A calibrated $\frac{1}{4}$" B & K pressure response microphone type 4136 fitted with a B & K nose cone type UA0385 was then positioned in the wake of instrumented tube 1 in nominally the same position as the hot wire probe was previously positioned. The instrumented tube 1 displacement and the wake microphone pressure signals were then acquired and processed on the

signal analyser. (Note:- in order to mount the hot wire probe and microphone in the wake of instrumented tube 1 one of the fixed tubes as shown in Figure 5.1 was removed). The acquired signals were processed to produce the figures described below:

Figures 5.6 i-iv show:-

(i) P.S.D. of the displacement of instrumented tube 1,

(ii) P.S.D. of the displacement of instrumented tube 2,

(iii) C.S.D. of the displacement signals,

(iv) coherency spectrum of the displacement signals.

Figures 5.7 i-iv show:-

(i) P.S.D. of the displacement of instrumented tube 1,

(ii) P.S.D. of the wake velocity signal behind instrumented tube 1,

(iii) C.S.D. of the displacement and velocity signals,

(iv) coherency spectrum of the displacement and velocity signals.

Figures 5.8 i-iv show:-

(i) P.S.D. of the displacement of instrumented tube 1,

(ii) P.S.D. of the wake pressure signal behind instrumented tube 1,

(iii) C.S.D. of the displacement and pressure signals,

(iv) coherency spectrum of the displacement and velocity signals.

### 5.4.2 Results and discussion

The two instrumented flexible tubes have vibration amplitudes which are different by a factor of 1.06 at their rigid body modal frequencies. This cannot be explained by the differences in the damping ratios of the flexible tubes which are in the ratio of 1.20:1. for the staggered arrangement. The displacement amplitude of instrumented tube 1 is lower than when it was mounted next to a flexible tube in the same row in Section 5.3. It is therefore suggested that the pressure excitation forces on the two instrumented tubes are different because instrumented tube 1 is mounted next to the fixed pressure measuring tube in the same row whereas instrumented tube 2 is mounted next to flexible tubes in the same row. The amplitude response of instrumented tube 2 is greater in the staggered arrangement than in the arrangement in Section 5.3 where it was next to the fixed pressure measuring tube. (Note - the damping is slightly higher for instrumented tube 2 in the staggered arrangement). These observations further strengthen the postulate in Section 5.3.2 which suggests that the presence of a

fixed tube changes the flow field round the neighbouring tubes in the same row and hence changes the forces exciting them. The tube displacement responses at the frequency of the non-rigid body modes are similar to the responses discussed in Section 5.3 but the tubes' responses at the 850 Hz acoustic duct mode are lower because the mode was not strongly excited during this experiment. (It was found that for slightly different flow velocities, which were set up on different days during the experimental test runs, the levels to which the different duct modes were excited were different). The level of the displacement coherency spectrum at the tube rigid body modal frequency is very small which implies that there is no direct linear interaction between two vibrating neighbouring tubes at their maximum amplitude response frequencies when the tubes are in a staggered arrangement relative to each other. The sharp peaks in the displacement coherency spectrum at acoustic duct modal frequencies show that the tubes are both coherently excited at duct modal frequencies. The level of the displacement coherency spectrum rises between approximately 200 Hz to 700 Hz and is higher than the arrangement in Section 5.3 where the instrumented flexible tubes were next to each other in the same row. It is postulated that this is due to the excitation of both tubes by a partially coherent eddy structure in the turbulent flow field (see Owen [5.20] ) in the gaps between the instrumented tubes which is more coherent in the staggered arrangement than in the in-line arrangement. This is because the instrumented tubes are closer together in the staggered arrangement so experience a more highly coherent flow field than when they are next to each other in the same row.

The P.S.D. of the velocity measured in the wake of instrumented tube 1 is almost 'flat' across the entire frequency range investigated. There is a sharp peak in the velocity spectrum at 950 Hz which corresponds to an acoustic duct mode. The cross spectrum and coherency spectrum of the wake velocity and tube displacement signals show that there are other acoustic duct modes present in the wake velocity signals but they are smaller in amplitude than the overall turbulent velocity fluctuations. The wake velocity, tube displacement coherency spectrum has a low value at the tube rigid body modal frequency which implies that the vibration of a tube does not produce any significant coherent velocity fluctuations in its wake when the tube r.m.s. displacement is approximately 80 μm.

(i.e. $2.5 \times 10^{-3}$ tube diameters). The broadband velocity fluctuations have an r.m.s. value of approximately 9 $ms^{-1}$ and the mean wake velocity is 58.4 $ms^{-1}$ giving a turbulence intensity of approximately 15% at the measurement point in the wake.

The P.S.D. of the pressure signal in the wake of instrumented tube 1 is fairly 'flat' from 0 Hz to 800 Hz except for the presence of mains harmonics. Above 800 Hz there are several acoustic duct modal peaks but none of them are strong enough to produce a significant tube displacement at the duct modal frequencies. The wake pressure, tube displacement coherency has a low value at the rigid body modal frequency which implies that the vibrating tube does not produce any significant coherent pressure fluctuations in its wake at its maximum displacement response frequency.

### 5.4.3 Comparison with other work

Much work has been carried out on the measurement of r.m.s. tube vibration amplitudes in tube banks for different tube bank geometries, Reynolds numbers and tube vibrational parameters e.g. [5.6, 5.9, 5.10, 5.11, 5.16, 5.23, 5.25-5.30] . However the number and ranges of variables involved in the investigations make much of the work difficult to compare directly with the present investigations. Measurements carried out by the C.E.G.B. [5.32] indicate that the r.m.s. amplitudes of typical tubes in full scale reactor heat exchanger systems is typically between 50 μm and 100 μm for tubes of diameter 25.4 mm which is in good agreement with present investigations. (The present investigation gave r.m.s. tube vibrations between approximately 60 μm and 80 μm for tube diameters of 30 mm and frequencies above the response frequency of the tube support structure). Work has been carried out to investigate the mode shapes of neighbouring tubes in a tube bank where the tubes are executing large amplitude vibrations e.g. [5.12, 5.17, 5.24, 5.26] . Theoretical work has been carried out to attempt to predict stability boundaries for the onset of large amplitude fluid-elastic tube vibrations. e.g. [5.1, 5.4, 5.8] . However, little work published in the open literature is available on the interaction of neighbouring tubes when they are executing small amplitude vibrations. Whitton and Durrans [5.31] measured the acceleration spectra of tubes in a full scale heat exchangers and measured the coherence between two tubes approximately 4.3 metres apart. Their coherence spectrum has several sharp peaks some of which have values greater

than 0.9. These peaks are due to the same coherent mechanism exciting both tubes. Over the large separation distance measured it is postulated that the coherent excitation mechanism to both tubes is produced by acoustic modes present in the heat exchanger. It would not be expected that the flow structure would be coherent over the large distances measured by Whitton and Durrans, and the tube forced response due to excitation by a flow phenomena is generally more broadband than the narrowband response due to excitation by acoustic modes. Currently there is no data available to the author in the open literature on investigations into the interaction of neighbouring tubes when the vibration amplitudes are small compared to the diameter of the tubes.

Fitzpatrick and Donaldson [5.14] measured the velocity power spectrum behind different rows in a 10 row staggered tube bank using a hot wire anemometer at Reynolds numbers of $8.2 \times 10^3$. They also measured the pressure fluctuations at the wall of the wind tunnel working section using a flush mounted wall microphone. Both the velocity and pressure spectra have peaks at a clearly defined vortex shedding frequency and the characteristics of the vortex shedding peaks vary with the row number at which the measurements were taken. The results of the present investigation at Reynolds numbers of approximately $1.2 \times 10^5$ show no clear vortex shedding peak in the velocity and pressure spectra, suggesting that the vortex shedding process is not the main mechanism by which the tubes are excited, which is different from the observations made by Fitzpatrick and Donaldson at lower Reynolds numbers. Measurements of the pressure spectra at $\pm 80^\circ$ from stagnation on a tube in the middle of the second and seventh rows of a closely packed equilateral triangular tube bank in air flow are reported by Franklin [5.15]. In the second row the spectra were flat except for a sharp vortex shedding peak. However, in the seventh row at Reynolds numbers between $3.3 \times 10^4$ and $6.7 \times 10^4$ (based on gap velocity) the pressure spectra were broadband and the pressure amplitudes decreased with increasing frequency. There was no evidence of any distinct vortex shedding peaks which is in agreement with the wake velocity and pressure measurements made during the present investigation at Reynolds numbers of approximately $1.2 \times 10^5$.

Baylac, Bai and Gregoire [5.3] measured the velocity spectrum in the wake of a tube in staggered and in-line tube banks with

different transverse and longitudinal spacing ratios at Reynolds numbers of $1.0 \times 10^5$. The velocity spectra they obtained were flat from 0 Hz to the maximum measured frequency of 500 Hz. An acoustic mode was present in their working section which produced a peak in the velocity spectrum. These results are in good agreement with those obtained in the present investigation and show that there is no significant vortex shedding mode in tube banks at Reynolds numbers of approximately $10^5$. It appears that the main tube excitation mechanisms are associated with broadband turbulent velocity fluctuations and acoustic duct modes.

The velocity spectrum measured by Owen [5.20] behind the last row of a 4 row tube bank is not 'flat' but has a broadband dominant buffeting frequency. Owen's measurements do not agree with velocity measurements made inside a tube bank during the present investigation. It is suggested that the measurements behind the last row of a tube bank made by Owen are not representative of the conditions inside the tube bank in the present investigation (at Reynolds numbers of approximately $1.2 \times 10^5$) and should be treated with caution when estimating the fluctuating forces on tubes inside an arbitrary tube bank. Blevins [5.5, 5.6] has developed a theory for predicting the vibration amplitudes of tubes given the tube and flow parameters. He used his theory together with Owen's experimentally measured buffeting spectrum, to predict the tube displacements which were measured in a full scale heat exchanger and obtained an answer with a discrepancy of 350%. Blevins' theory predicts tube vibrations parallel with the mean flow and measurements carried out by Blevins on a model tube bank were in reasonable agreement for the vibration of tubes normal to the flow in the last row of the tube bank. However when the tube vibrations parallel to the mean flow were measured in the sixth tube row the errors in the theoretical prediction of the tube vibration amplitudes were as high as 1000%. It is suggested that the use of Owen's buffeting spectrum as the excitation spectrum in Blevins theory for predicting tube vibrations inside a tube bank was incorrect.

## 5.5 Variation of Tube Vibration with Flow Velocity

### 5.5.1 Experimental measurements

The displacement signal from instrumented tube 1 and the

pressure signal from the wall microphone were acquired and processed on the signal analyser at different measured free stream flow velocities. The signals were processed to produce the figures described below:

Figures 5.9 a-g,i-iii show:-

(i) P.S.D. of the displacement signal of instrumented tube 1,

(ii) P.S.D. of the wall microphone pressure signal,

(iii) amplitude histogram of displacement of instrumented tube 1, for various flow velocities.

Figures 5.10 a-b, i-ii show:-

(i) C.S.D. of the displacement of instrumented tube 1 and the wall microphone pressure signal,

(ii) coherency spectrum of the displacement and pressure signals for a a) flow velocity of $18.9ms^{-1}$,
b) flow velocity of $10.7ms^{-1}$.

Figure 5.11 shows the r.m.s. displacement of instrumented tube 1 plotted against the free stream flow velocity for the frequency bands (i) 0 Hz to 1600 Hz, (ii) 100 Hz to 1600 Hz, and (iii) 200 Hz to 300 Hz.

### 5.5.2 Results and discussion

The wall microphone pressure power spectra are fairly 'flat' over the frequency ranges investigated for flow velocities between $25.5\ ms^{-1}$ and $33.5ms^{-1}$ except for the presence of sharp peaked acoustic duct modes which have different amplitudes depending on the flow velocities. At flow velocities between $10.7ms^{-1}$ and $22.8ms^{-1}$ the amplitude of the pressure power spectra increases with increasing frequency until it reaches a maximum at a frequency which is dependent on the flow velocity. This is clearly a vortex shedding phenomenon which is not observed above flow velocities of $22.8ms^{-1}$. The vortex shedding peaks in the pressure power spectra can be clearly seen at the three lowest flow velocities investigated and at the two lowest velocities two vortex shedding peaks are present in the spectra. At a flow velocity of $13.5\ ms^{-1}$ the higher frequency vortex shedding peak is nearly coincident with the first transverse acoustic duct cut-on frequency and hence excites the acoustic mode to a high amplitude. Table 5.1 gives the frequencies of the vortex shedding peaks and their Strouhal numbers based on estimated tube gap velocity for different flow velocities. The estimated

Strouhal numbers are not constant with varying flow velocity suggesting that either the nature of the vortex shedding process changes with flow velocity or the calculated gap velocity is not correct, because the separation points change and the flow pattern round the tubes changes when the free stream flow velocity is varied.

The tube displacement power spectra show that at higher flow velocities higher order tube vibrational modes are excited. At the two lowest flow velocities tested the only significant tube displacement response is at the frequency of the tube rigid body mode. At higher flow velocities the tube response below 50 Hz increases which is due to increased low frequency response of the tube supporting structure which is not isolated below 30 Hz. The overall trend in the r.m.s. displacement of the tubes from 0 Hz to 1600 Hz is to increase with increasing flow velocity except at the lowest flow velocity where the lower frequency vortex shedding peak is approaching the frequency of the tube rigid body mode, giving an increased response. The tube r.m.s. displacement responses neglecting low frequencies (i.e. the responses from 100 Hz to 1600 Hz and 200 Hz to 300 Hz) generally increase with increasing flow velocity except at the lowest flow velocity where the vortex shedding excitation is near the frequency of the tube rigid body mode. At the highest flow velocity the r.m.s. displacement response above 100 Hz is lower than 28.5 $ms^{-1}$ which suggests that there is a reduction in the exciting pressure fluctuations round the tube, possibly due to a changing flow pattern. The amplitude histograms of the displacement of the vibrating tube are all Gaussian in shape and hence it is postulated that the tube is responding as an almost linear system to an arbitrary random excitation.

The coherency spectra of the tube displacement and wall microphone pressure signals reach peak values at the vortex shedding frequencies with other narrower peaks at acoustic duct modal frequencies. This suggests that when a clearly definable vortex shedding peak is present in the pressure power spectrum there is a degree of coherency throughout the tube row since the wall microphone has two tubes between it and the instrumented tube and therefore cannot be receiving the pressure fluctuations generated directly from the vibrating tube, at the vortex shedding frequency. Measurements of coherency between the tube displacement and wall microphone pressure signals in Section 5.3, when there was no clearly definable

vortex shedding frequency present, show that the coherency in a tube row at flow velocities near 30 $ms^{-1}$ is low except at the frequencies of acoustic duct modes.

### 5.5.3 Comparison with other work

Much work has been carried out into the measurement of r.m.s. tube displacement responses as a function of flow velocity, mainly as investigations into the threshold at which large amplitude fluid-elastic instabilities occur in tube banks e.g. [5.9, 5.10, 5.11, 5.16, 5.23, 5.25-5.30]. A review paper which contains many references concerned with the measurement of tube vibrations was written by Paidoussis [5.21]. No work is available in the open literature on the variation of the spectral responses of tubes with flow velocity. However some of the measurements of the variation of the r.m.s. displacement responses of tubes with flow velocity made by Pettigrew and Gorman [5.23] show similar trends to the results obtained in the present investigation. Their results show that tube vibration levels do not always increase as the flow velocity is increased and peaks occur in the displacement versus flow velocity curves when the vortex shedding frequency is near the resonance frequency of the tubes, which agrees with the results of the present investigation. The magnitude of the tube vibration levels measured in other investigations cannot be compared directly with the present investigation since the flow and tube parameters used were different in all cases. The r.m.s. tube displacement of 50 μm to 84 μm observed in the present investigation for 30 mm diameter tubes was within the range of values measured in full scale operating heat exchangers [5.32] (50 μm to 100 μm for 25.4 mm diameter tubes).

The observation of two vortex shedding peaks within an in-line tube bank was made by Dye [5.13] at Reynolds numbers in the range where two vortex shedding peaks were observed in the present investigation. Pearce [5.22] observed two vortex shedding frequencies in fixed tube banks at Reynolds numbers of $3.4 \times 10^4$ and investigations by Borges [5.7] revealed two vortex shedding frequencies generated by a single fixed tube row at Reynolds numbers up to $7.8 \times 10^4$. These observations together with the author's imply that several different vortex shedding frequencies can be generated in a tube bank.

## 5.6 Variation of Static Pressure Distributions with Tube Spanwise Axial Position and Tube Position in the Tube Bank

### 5.6.1 Experimental measurements

The static pressure distributions round the pressure measuring tube were measured at three different spanwise axial stations which were positioned 0, 1 and 4 diameters from the middle of the tube. The static pressure distributions were also measured for two different positions of the pressure measuring tube as shown in Figure 5.1.

Figures 5.12 i-iv show the variation of the static pressure distribution with angle round the measurement tube for position of (i) 0, (ii) 1 and (iii) 4 diameters from the centre along the spanwise axis of the pressure measuring tube when the tube was in measurement position 2. Figures 5.13 shows the static pressure distribution round the centre of the pressure measuring tube in position 1.

### 5.6.2 Results and discussion

The static pressure distribution curves show that there appears to be no laminar separation in contrast to the observations made in Section 4.3. Turbulent separation occurs between 140° and 150°, and between 220° and 210°, almost symmetrically round both sides of the tube. The static pressure distribution does not significantly vary between different measurement stations which are separated by up to 4 tube diameters along the spanwise axis of the tube. This suggests that the mean flow can be assumed to be two dimensional in a tube bank under the flow conditions in the present investigation. When the pressure measuring tube is near the top of the working section in position 1 the troughs in the static pressure distribution curves are lower than in measurement position 2. The wake pressure is also lower by approximately 3% in position 1. The static pressure distribution is more asymmetrical for position 1 which increases the lift coefficient from 0.048 to 0.312 between positions 2 and 1 respectively. The lower values of pressure coefficient at angles between 90° and 270° decrease the drag from 1.144 in position 2 to 0.924 in position 1. The

asymmetry in the pressure distribution round the tube in position implies that the flow near the edges of the tube bank becomes less symmetrical which tends to increase the magnitude of the lift forces on the tubes.

### 5.6.3 Comparison with other work

Measurements of static pressure distributions in staggered tube banks at similar Reynolds numbers to the present investigation have been carried out by Namork [5.19] and Morsey [5.18]. The general form of the distribution curves are very similar to the results obtained in the present investigation but, since the tube bank geometries and flow parameters were not the same, no direct comparison of results can be made.

Batham [5.2] measured the variation of the static pressure distribution as a function of distance along the tube spanwise axis for the seventh row of a ten row 1.25:1 pitch ratio in-line tube bank at a Reynolds number of $7 \times 10^4$. He found that the flow was three dimensional i.e. the pressure distribution varied with spanwise distance along the tube axis. He also found that small movements of upstream tubes of the order of $5 \times 10^{-3}$ tube diameters affected the static pressure distributions round tubes downstream of the displaced tube. In the present investigation for staggered tube banks the flow at Reynolds numbers of $1.2 \times 10^5$ was found to be approximately two dimensional. Evidence in Sections 5.3 and 5.4 suggest that small movements of a tube does effect the flow field round neighbouring tubes which agrees with the investigations carried out by Batham.

There is no data available to the author on investigations of the variation of static pressure distributions along the spanwise axis of tubes in staggered tube banks. Investigations into the variation of static pressure distributions round a tube with position in a tube bank were carried out by Namork [5.19] and Morsey [5.18] but no measurements were made near the edges of the tube bank and hence no comparison with the present investigations can be made.

## 5.7 The Effects of Sound on Tube Vibration and Static Pressure Distribution Round a Tube

### 5.7.1 Experimental measurements

The displacement signal from the flexible instrumented tube 1 and the pressure signal from the wall microphone were acquired and processed on the signal analyser with and without a superimposed sound field in the working section. The static pressure distributions round a tube were also measured as described in Chapter 3 with and without a superimposed sound field. The results were processed to produce the figures described below:

Figures 5.14 a-d i-iv show:-

(i) P.S.D. of the displacement of instrumented flexible tube 1,

(ii) P.S.D. of the wall microphone pressure signal,

(iii) C.S.D. of the displacement and pressure signals,

(iv) coherency spectrum of the displacement and pressure signals,

for a) no superimposed sound,

b) superimposed sound at a frequency of 333 Hz and SPL of 130 dB,

c) superimposed sound at a frequency of 256 Hz and SPL of 134 dB,

d) superimposed sound at a frequency of 293 Hz and SPL of 139 dB.

Figures 5.15 a-d show the amplitude histograms of the displacement of instrumented flexible tube 1 when there is:

a) no superimposed sound,

b) superimposed sound at a frequency of 333 Hz and SPL of 130 dB,

c) superimposed sound at a frequency of 256 Hz and SPL of 134 dB,

d) superimposed sound at a frequency of 293 Hz and SPL of 139 dB.

Figures 5.16 a-b show the static pressure distribution when the pressure measuring tube is in position 2 and there is

a) no superimposed sound

b) superimposed sound at a frequency of 293 Hz and SPL of 139 dB.

Table 5.2 gives the variation of the r.m.s. displacement response of the flexible instrumented tube 1 in different frequency ranges and for different levels of superimposed sound.

### 5.7.2 Results and discussion for 333 Hz sound excitation

The level of the superimposed sound is approximately 2 dB above the general level of the turbulent pressure fluctuations as measured by the wall microphone. The sound has no noticeable

effect on the vibration amplitude of the tube at 333 Hz and the low level of the displacement, pressure coherency spectrum at 333 Hz implies that the contribution of the superimposed sound to the excitation pressures round the vibrating flexible tube is small compared to the overall random excitation pressures at 333 Hz. The r.m.s. vibration amplitude of the tube in all the frequency bands measured is greater with sound excitation than without, which implies that the sound affects the flow so as to produce a larger broadband pressure excitation on the vibrating tube. The interaction of the sound is probably with the boundary layers round the tubes which increases the excitation amplitude of the tubes by 2.6% in the band 200 Hz to 300 Hz (i.e. at the tube response frequencies near the tube rigid body modal frequency). The amplitude histogram of the tube displacement signal is Gaussian in shape and is very similar to the histogram when there is no superimposed sound.

### 5.7.3 Results and discussion for 256 Hz sound excitation

The level of the superimposed sound is approximately 5 dB above the general level of the turbulent pressure fluctuations measured by the wall microphone. The response of the tube at the frequency of the tube rigid body mode is increased by approximately 4.8% of the response when there is no superimposed sound for the frequency band 200 Hz to 300 Hz. The value of the displacement, pressure coherency spectrum is low near the sound excitation frequency which implies that the pressure fluctuations on the tube due to the superimposed sound are small compared to the random pressure fluctuations round the tube produced by the turbulent pressure field in the tube bank and the pressure field created by the vibration of the tube. The amplitude histogram of the vibrating tube displacement signal has a general Gaussian shape with small peaks superimposed on the peak of the Gaussian distribution. This implies that the tube is responding to a low level narrowband excitation process which could be the acoustic duct mode at 850 Hz. However there is little evidence of this narrowband process superimposed on the tube displacement amplitude histogram when no sound is superimposed and the 850 Hz acoustic mode is present in the tube displacement power spectrum.

### 5.7.4 Results and discussion for 293 Hz sound excitation

The level of sound is approximately 12 dB above the general level of the turbulent pressure fluctuations measured by the wall microphone. The sound has no noticeable effect on the tube displacement response at 293 Hz but the small peak in the displacement, pressure coherency spectrum at this frequency implies that there is a direct linear interaction of the sound with the tube so as to produce a partially coherent response at the frequency of the superimposed sound. The level of the superimposed sound and the coherency at the sound driving frequency is small compared with the levels of sound and coherency levels at some of the acoustic duct modal frequencies. The r.m.s. vibration amplitude of the tube in the frequency band 200 Hz to 300 Hz (i.e. at frequencies near the tube rigid body modal frequency) is 5.7% greater than the response when there is no superimposed sound. The amplitude histogram of the tube displacement is Gaussian in shape and has two small superimposed side peaks which imply that the tube is responding to a narrowband excitation process at low amplitudes which is verified by the presence of several small amplitude sharp peaks in the displacement, pressure coherency spectrum.

The effect of superimposed sound on the static pressure distribution measured round a fixed tube is negligible. However it must be noted that strong acoustic modes which are up to 30 dB greater in amplitude than the superimposed sound for the cases when there was no superimposed sound and when there was superimposed sound at an SPL of 139 dB. Hence the presence of stronger acoustic modal frequencies may dominate any effect by the superimposed sound on the static pressure distribution round a tube.

### 5.7.5 General discussion of the effects of superimposed sound and comparison with other results

The effect of superimposed sound on the flexible tube r.m.s. displacement is to increase the amplitude response in the frequency band near the tube rigid body modal frequency and also by a lesser extent to increase the r.m.s. amplitude response in the whole frequency range 100 Hz to 1600 Hz. The increase in tube amplitude response per unit bandwidth in the frequency range near the rigid

body modal frequency (200 Hz to 300 Hz) is in general at least a factor of 20 greater than the increase in response per unit bandwidth for the frequency range 100 Hz to 1600 Hz (excluding 200 Hz to 300 Hz) when sound is superimposed. However it must be noted that the frequency of the sound was in or near the 200 Hz to 300 Hz band so if the effect of sound is linear the increase in tube response would only occur at the driving frequency of the sound. The effects of sound on the tube response at the driving frequency of the sound appear to be negligible for SPL's at least up to 134 dB and only start to become significant at SPL's near 140 dB. However sound does increase the tube vibration response in all the frequency bands investigated, which suggests that there is a non-linear interaction of sound with the flow. It is postulated that the non-linear interaction occurs in the boundary layers of the tubes so as to produce an increase in the boundary layer pressure fluctuations which drive the tubes and increase their displacement responses. The sound only seems to have a noticeable direct linear effect on the amplitude of the tube vibrations when the pressure fluctuations due to the sound are considerably greater than the general turbulent pressure fluctuations in the tube bank at the same frequency as the superimposed sound.

The effects of superimposed sound on single cylinders in a cross-flow is discussed in Section 4.8.5. No work carried out on the effects of superimposed sound on vibrations of tubes in tube banks is available in the open literature so a comparison of the present results with any previous work is not possible.

## 5.8 Conclusions

### 5.8.1 Conclusions from Sections 5.3 and 5.4

(i) The presence of a fixed tube in a flexible tube bank reduces magnitude of the pressure forces on a neighbouring tube. Hence there are differences in the forces on tubes in a tube bank when the tubes are (i) fixed and (ii) flexible and vibrating with small amplitudes (less than $3 \times 10^{-3}$ diameters r.m.s.).

(ii) There is no significant linear interaction between two neighbouring vibrating tubes at their maximum response frequencies when the tubes are vibrating with r.m.s. amplitudes of less than $3 \times 10^{-3}$ diameters.

(iii) Tubes which are excited by acoustic modes respond coherently to the acoustic excitation.

(iv) A vibrating tube does not produce any significant coherent pressure or velocity fluctuations in its wake when the tube r.m.s. displacement response is less than $3 \times 10^{-3}$ diameters.

(v) There is no detectable vortex shedding mode in either the wake velocity or wake pressure fluctuations behind tubes in a staggered tube bank at Reynolds numbers of $1.2 \times 10^{5}$.

(vi) At Reynolds numbers of $1.2 \times 10^{5}$ there is a degree of coherence between neighbouring vibrating tubes in the same row and in the same upstream and downstream staggered row. The coherency increases over a broad frequency band from 200 Hz to 800 Hz which corresponds to Stouhal numbers of 0.1 to 0.4 . This broadband coherency is probably not due to a common vortex shedding excitation which is a narrower band phenomena than the one observed. The increase in coherency between the tube's displacement is probably due to excitation of both tubes by some form of coherent turbulent flow passing through the tube gaps.

(vii) Current theories which try to predict the vibration levels in tube banks give large errors when compared with experimentally measured tube vibration levels in full scale and model scale heat exchangers.

5.8.2 Conclusions from section 5.5

(i) At Reynolds numbers above $8.5 \times 10^{4}$ there is no evidence of a well defined vortex shedding mode in staggered tube banks. Below Reynolds numbers of $8.5 \times 10^{4}$ clearly defined vortex shedding modes are present in the tube bank which are partially coherent in a cross-flow row. At Reynolds numbers between $3.4 \times 10^{4}$ and $5.0 \times 10^{4}$ two clearly definable vortex shedding modes are present in the staggered tube bank.

(ii) The r.m.s. displacement of the vibrating tubes varies with flow velocity and in general increases with flow velocity. The exceptions to this trend are when the vortex shedding frequency is near the tube resonance frequency which increases the tube response and at the maximum flow velocity investigated where there is a decrease in tube vibration produced by a change in the flow field round the tubes.

(iii) The r.m.s. displacements of the vibrating tubes in the scale model tube bank are in the approximate range of $2 \times 10^{-3}$ to $3 \times 10^{-3}$ diameters for Reynolds numbers of $8.4 \times 10^{4}$ to $1.2 \times 10^{5}$ which is in agreement with the measured levels of $2 \times 10^{-3}$ to $4 \times 10^{-3}$ diameters obtained from operating heat exchangers.

5.8.3 Conclusions from section 5.6

(i) The mean flow is two dimensional along the spanwise tube axis of a fixed tube in a staggered tube bank containing vibrating tubes with r.m.s. displacements of less than $3 \times 10^{-3}$ diameters at Reynolds numbers of $1.2 \times 10^{5}$.

(ii) The static pressure distributions round tubes in the middle of a staggered tube bank are symmetrical but near the edges of a tube bank become asymmetrical which increases the magnitude of the lift forces on the tubes.

5.8.4 Conclusions from section 5.7

(i) The effect of pure tone superimposed sound at levels between 130 dB and 140 dB is to increase the vibration response of tubes over a broad band of frequencies. This implies that there is a non-linear interaction of sound with the tube boundary layers so as to produce greater pressure excitation forces on the tubes.

(ii) The linear interaction of sound with the tubes only becomes significant relative to the general turbulent excitation at the same frequency as the superimposed sound when the level of sound is considerably greater than the level of the turbulent pressure fluctuations in the tube bank.

(iii) Superimposed sound does not effect the static pressure distribution round a tube in a tube bank when there are strong acoustic duct modes present in the vicinity of the tubes.

## 5.9 REFERENCES


5.1 T.F. BALSA 1977 J.S.V. 50(2) pp 285-303 "Potential Flow Interaction in an Array of Cylinders in Cross-Flow."

5.2 J.P. BATHAM 1973 J.F.M. vol. 57(2) pp 209-228. "Pressure distributions on circular cylinders at critical Reynolds numbers."

5.3 G. BAYLAC, D. BAI and J.P. GREGOIRE 1973 Proceedings of the International Symposium on Vibration Problems in Industry held at Keswick, U.K. 10-12 April 1973. Paper 219. "Study of flow and acoustic phenomena in a tube bank."

5.4 R.D. BLEVINS 1974 Journal of Pressure Vessel Technology. Transaction of A.S.M.E. Series J, vol.96. pp 263-267. "Fluid Elastic Whirling of a Tube Row."

5.5 R.D. BLEVINS 1977 "Flow-Induced Vibration." London: Van Nostrand Reinhold.

5.6 R.D. BLEVINS 1978 Proceedings of the B.N.E.S. International Conference on Vibration in Nuclear Plant held at Keswick, U.K. 9-12 May 1978. Paper 3:4. "Buffeting of heat exchanger tube arrays in a cross flow."

5.7 A.R.J. BORGES 1969 Journal of Mechanical Engineering Science vol.11 no.5 pp 498-502 "Vortex shedding frequencies of the flow through two-row banks of tubes."

5.8 S.S. CHEN 1977 Journal of Fluids Engineering. Transactions A.S.M.E. Series I, vol.99 pp 462-467. "Dynamics of heat exchanger tube banks."

5.9 S.S. CHEN and J.A. JENDRZEJCZYK 1981 J.S.V. 78(3) pp 355-382. "Experiments on fluid elastic instability in tube banks subjected to liquid cross-flow."

5.10 Y.N. CHEN 1972 Journal of Engineering for Industry. Transactions A.S.M.E. Series B, vol.94 pp 623-628. "Fluctuating Lift Forces of the Karman Vortex Streets on Single Circular Cylinders and in tube bundles. Part 3 - Lift Forces in Tube Bundles."

5.11 Y.N. CHEN 1978 Proceedings of the B.N.E.S. International Conference on Vibration in Nuclear Plant held at Keswick, U.K. 9-12 May 1978. Paper 2:6. "Criteria for the cross-flow-induced tube vibrations in tube bank heat exchangers.

5.12 H.J. CONNORS, Jr. 1970 Proceedings of the A.S.M.E. Winter Annual Meeting held in New York 1 Dec. 1970. Flow-Induced Vibration in Heat Exchangers. pp 42-56 "Fluidelastic Vibrations of Tube Arrays Excited by Cross Flow."

5.13 R.C.F. DYE 1973 Proceedings of the International Symposium on Vibration Problems in Industry held at Keswick, U.K. 10-12 April 1973. Paper 417. "Vortex excited vibration of a heat exchanger tube row in cross-flow."

5.14 J.A. FITZPATRICK and I.S. DONALDSON 1973 J.S.V. 73(2) pp 225-237."Row Depth Effects on Turbulence Spectra and Acoustic Vibrations in Tube Banks."

5.15 R.E. FRANKLIN 1974 U.K. Atomic Energy Authority. A.E.R.E. Harwell Report RS117. "Fluid dynamic forces on tubes in a typical heat exchanger array."

5.16 R.E. FRANKLIN and B.M.H. SOPER 1977 Heat Transfer and Fluid Flow Services. A.E.R.E. Harwell and National Engineering Laboratory Report no. HTFS RS192. "An investigation of fluid-elastic instabilities in tube banks subjected to fluid cross flow."

5.17 J.L. LIVERSEY and R.C.F. DYE 1962 Journal of Mechanical Engineering Science vol.4 no.4 pp 349-352. "Vortex Excited Vibration of a Heat Exchanger Tube Row."

5.18 M.G. MORSY 1975 Proceedings Institute of Mechanical Engineers vol 189 pp 519-532. "Skin Friction and Form Pressure Loss in Tube Bank Condensers."

5.19 J.E. NAMORK 1977 University of Salford M.Sc. Thesis. "Flow-Induced Vibrations in a Tube Bank."

5.20 P.R. OWEN 1965 Journal of Mechanical Engineering Science vol.7 no.4 pp 431-439. "Buffeting Excitation of Boiler Tube Vibration."

5.21 M.P. PAIDOUSSIS 1981 J.S.V. 76(3) pp 329-360 "Fluidelastic Vibrations of Cylinder Arrays in Axial and Cross Flow: State of the Art."

5.22 H.R. PEARCE 1973 University of Oxford D.Phil. Thesis. "Noise and Vibration in Heat Exchangers."

5.23 M.J. PETTIGREW and D.J. GORMAN 1978 Proceedings of the B.N.E.S. International Conference on Vibration in Nuclear Plant held at Keswick, U.K. 2-12 May 1978. Paper 2:3. "Vibration of Heat Exchange Components in Liquid and Two-Phase Cross-Flow."

5.24 D.L. PRIDDEN 1976 University of Salford M.Sc. Thesis. "An Investigation into Cross-Flow-Induced Vibrations in a Closely Packed Staggered Tube Bank."

5.25 P.J. SOUTHWORTH 1973 University of Salford M.Sc. Thesis. "An investigation into cross-flow induced vibration in in-line tube banks."

5.26 H. TANAKA and S. TAKAHARA 1977 J.S.V. 77(1) pp 19-37. "Fluid Elastic Vibration of Tube Array in Cross Flow."

5.27 D.S. WEAVER and M. EL-KASHLAN 1981 J.S.V. 75(2) pp 265-273. "On the number of tube rows required to study cross-flow induced vibrations in tube banks."

5.28 D.S. WEAVER and M. EL-KASHLAN 1981 J.S.V. 76(2) pp 283-294 "The effect of damping and mass ratio on the stability of a tube bank."

5.29 D.S. WEAVER and L.K. GROVER 1978 J.S.V. 59(2) pp 277-294. "Cross-Flow Induced Vibrations in a Tube Bank - Turbulent Buffeting and Fluid Elastic Instability."

5.30 M.C. WELBOURNE 1978 Proceedings of the B.N.E.S. International Conference on Vibration in Nuclear Plant held at Keswick, U.K. 9-12 May 1978. Paper 3:2. "Flow Induced Vibration of A.G.R. Heat Exchanger Tubes."

5.31 P.N. WHITTON and R.F. DURRANS 1978 Proceedings of the B.N.E.S. International Conference on Vibration in Nuclear Plant held at Keswick, U.K. 9-12 May 1978. Paper 7:5. "The measurement of Heat Exchanger Vibration during Reactor Operation."

5.32 D.R.W. RICHARDS C.E.R.L. Leatherhead, England, February 1982. Personal Communication.

TABLE 5.1. Variation of the vortex shedding frequencies and Strouhal numbers with flow velocity.

| Free stream flow velocity $ms^{-1} \pm 0.1ms^{-1}$ | Frequency of first vortex shedding peak Hz ± 10Hz | Strouhal number of first vortex shedding peak ± 0.01 | Frequency of second vortex shedding peak Hz ± 10Hz | Strouhal number of second vortex shedding peak ± 0.01 |
|---|---|---|---|---|
| 10.6 | 205 | 0.32 | 308 | 0.48 |
| 14.0 | 293 | 0.35 | 396 | 0.47 |
| 18.9 | 427 | 0.37 | - | - |
| 22.8 | 483 | 0.35 | 570 | 0.41 |

TABLE 5.2. Variation of the tube displacement response with superimposed sound.

| Superimposed sound frequency Hz ± 1Hz | SPL of superimposed sound dB ± 0.2dB | Response at tube rigid body frequency peak $\mu m Hz^{-1}$ ± 0.5% | r.m.s. tube response for 100Hz-1600Hz μm ± 0.5% | r.m.s. tube response for 200Hz - 300Hz μm ± 0.5% |
|---|---|---|---|---|
| - | 0 | 44.7 | 77.5 | 64.6 |
| 333 | 130 | 47.5 | 79.0 | 66.3 |
| 254 | 136 | 47.7 | 80.5 | 67.7 |
| 293 | 139 | 49.0 | 80.7 | 68.3 |

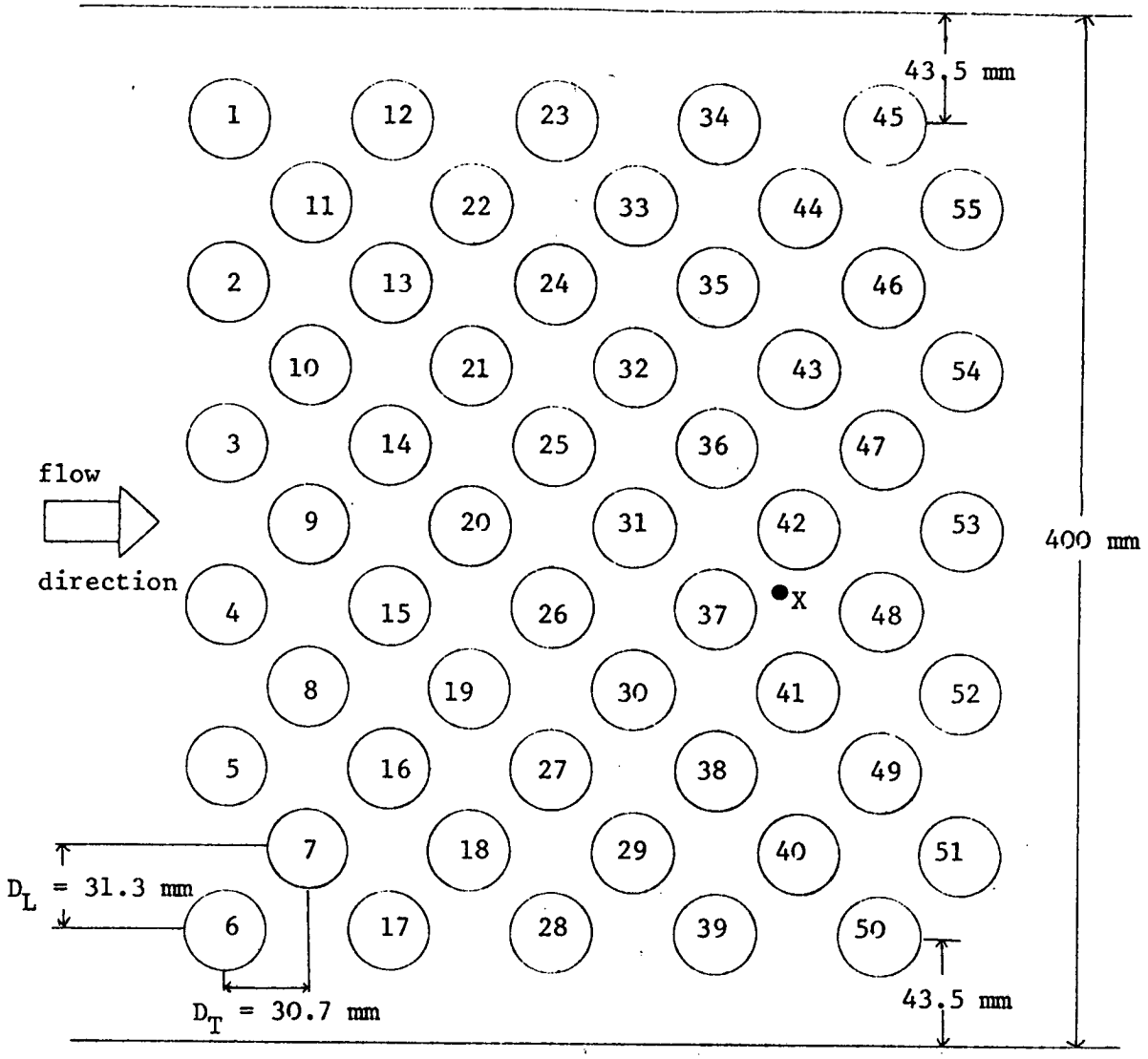


Tubes 1 to 11 and tubes 45 to 55 are fixed.
Tubes 12 to 44 are flexibly mounted tubes.

Experimental arrangement 1

Tube 35 = fixed pressure measuring tube.
Tube 36 = instrumented displacement measuring flexible tube 2.
Tube 37 = instrumented displacement measuring flexible tube 1.

Experimental arrangement 2

Tube 31 = instrumented displacement measuring flexible tube 2.
Tube 36 = fixed pressure measuring tube.
Tube 37 = instrumented displacement measuring flexible tube 1.

Wake pressure and velocity measurements

Experimental arrangement 2, but tube 48 was removed to insert microphone or hot wire anemometer probe in position X, marked by the dot.

FIGURE 5.1. Arrangement of tubes in wind tunnel working section.

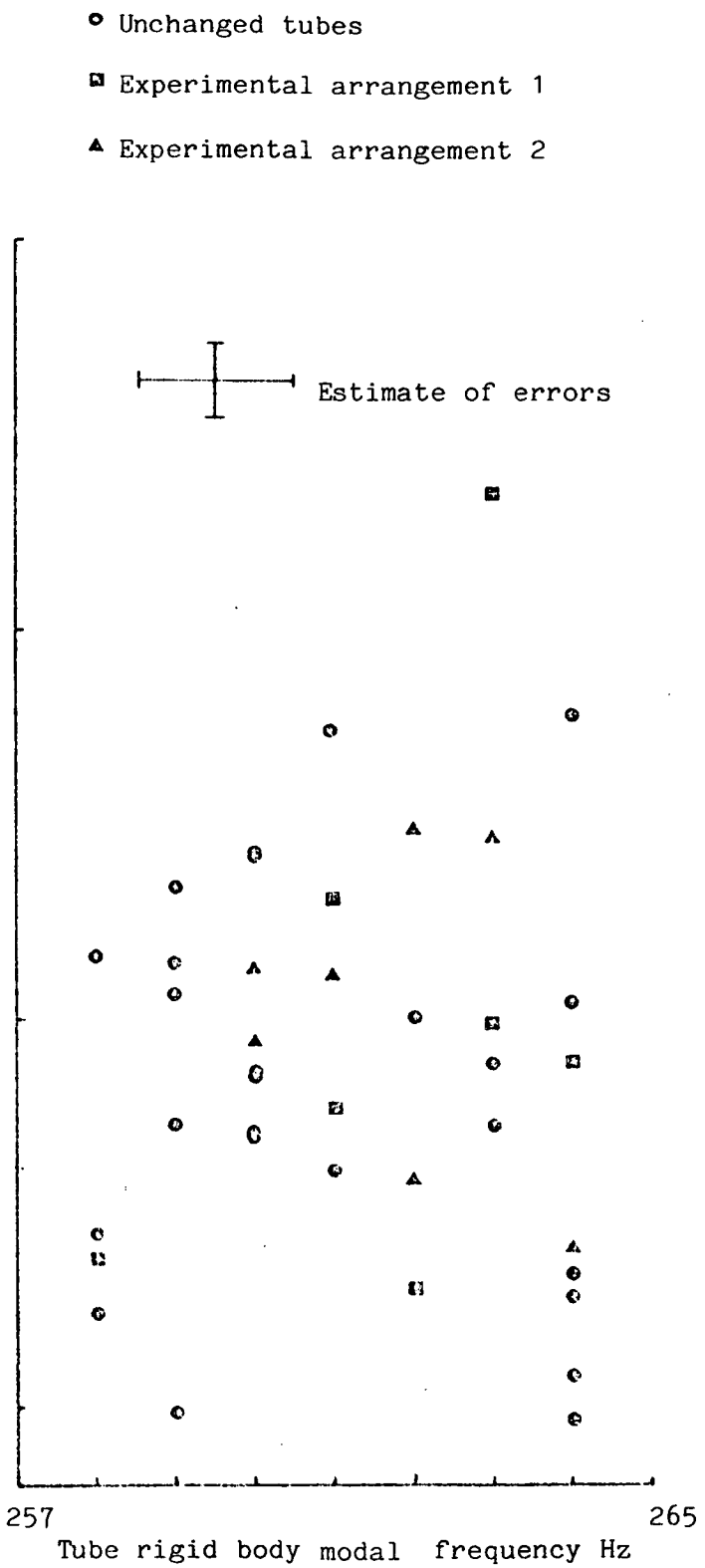


FIGURE 5.2. Tube damping ratio plotted against tube rigid body modal frequency for the different experimental arrangements.

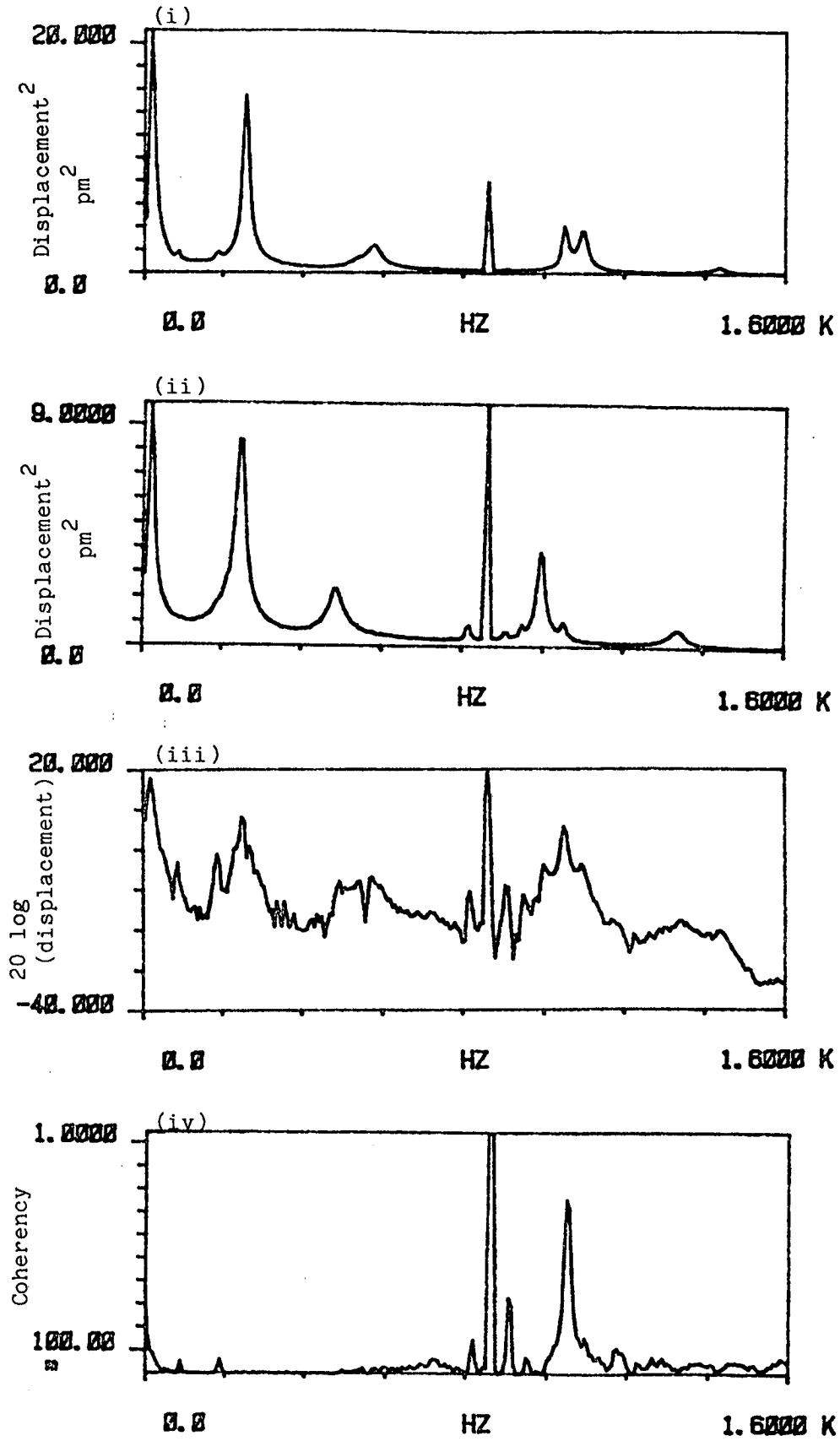


FIGURE 5.3. (i) P.S.D. of the displacement of instrumented tube 1,
(ii) P.S.D. of the displacement of instrumented tube 2,
(iii) C.S.D. of the tube displacement signals,
(iv) Coherency spectrum of tube displacement signals,
for experimental arrangement 1.

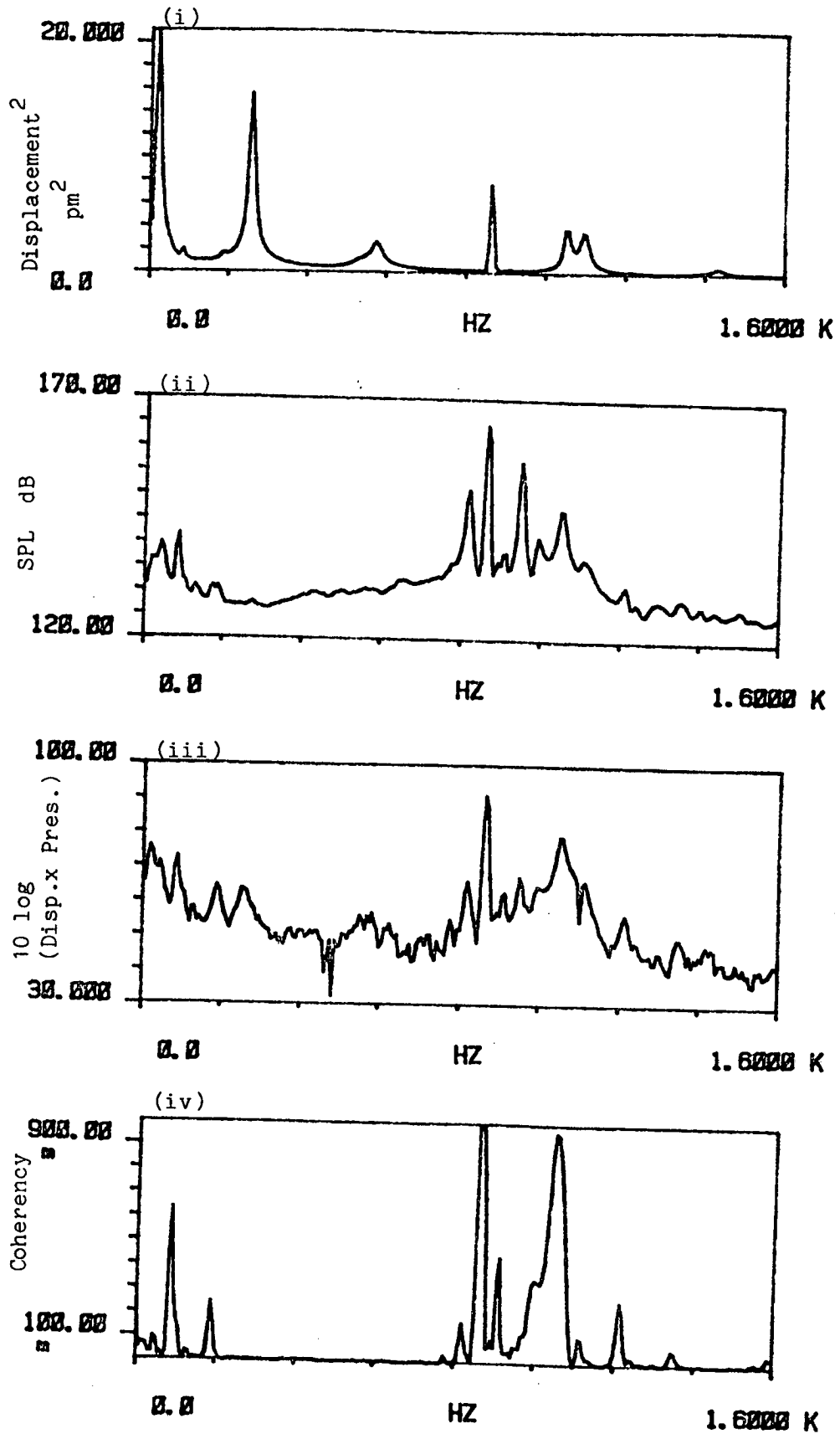


FIGURE 5.4. (i) P.S.D. of the displacement of instrumented tube 1,
(ii) P.S.D. of the wall microphone pressure signal,
(iii) C.S.D. of the displacement and pressure signals,
(iv) coherency spectrum of the displacement signals,
for experimental arrangement 1.

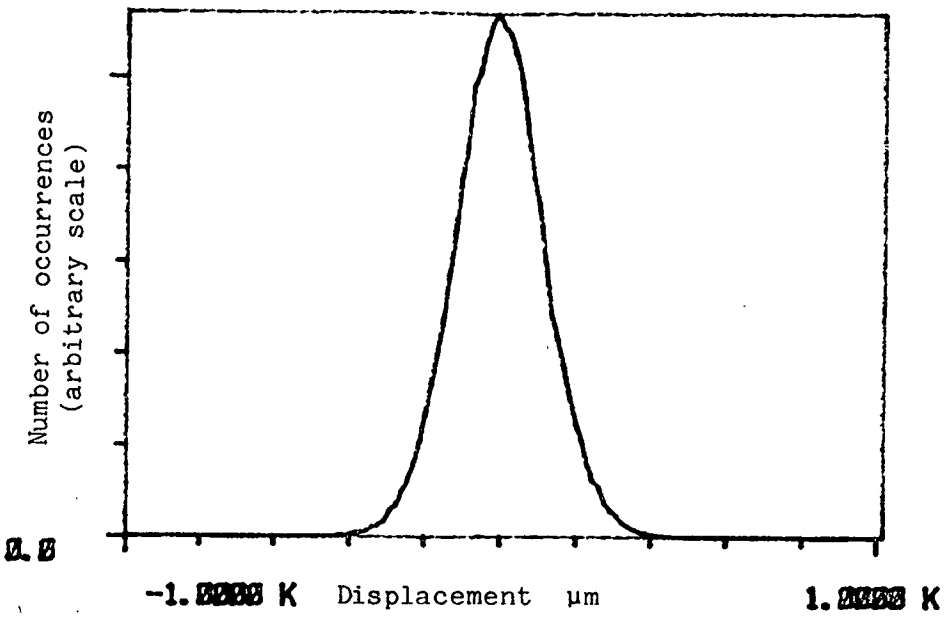


FIGURE 5.5i. Amplitude histogram of the displacement of instrumented tube 1 in experimental arrangement 1.

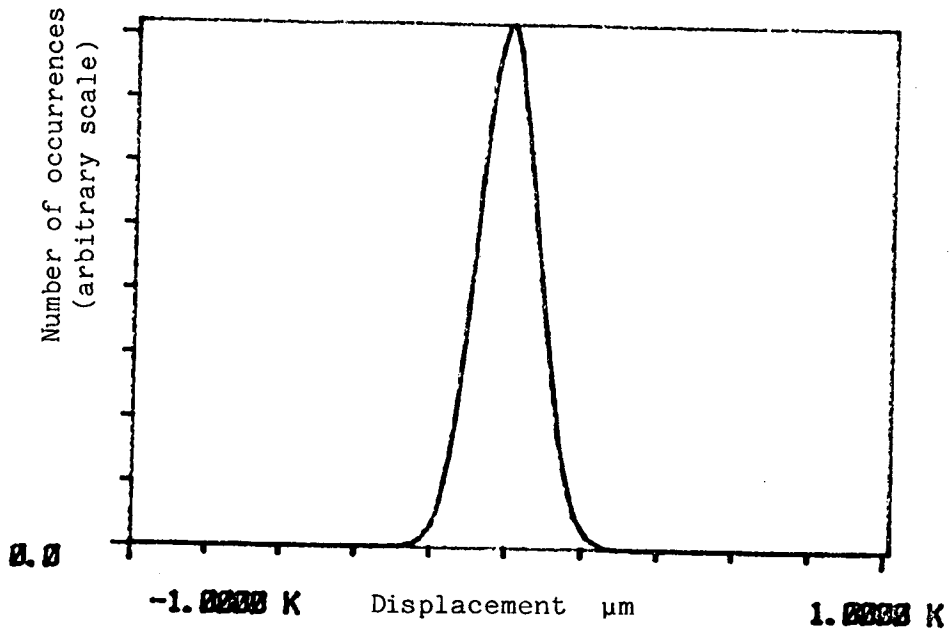


FIGURE 5.5ii. Amplitude histogram of the displacement of instrumented tube 2 in experimental arrangement 1.

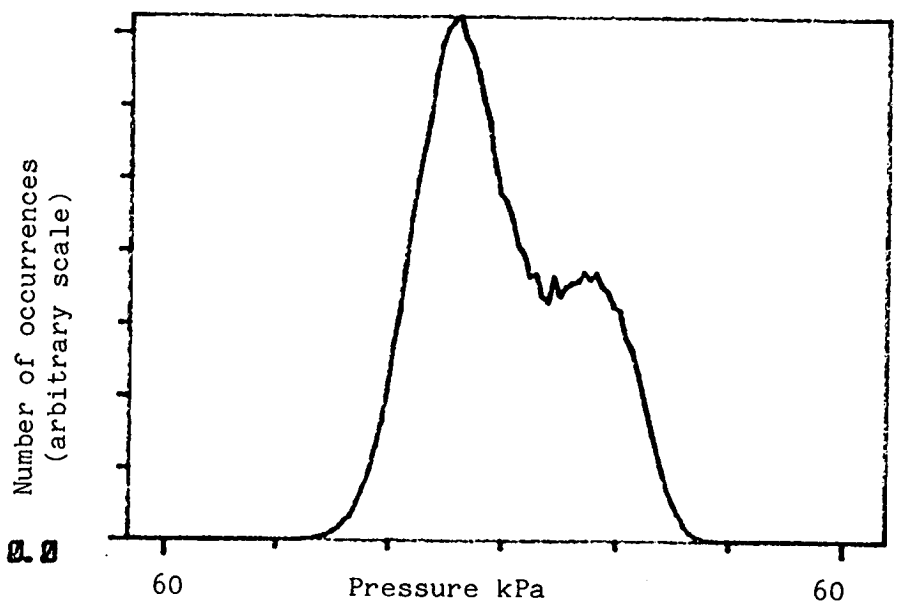


FIGURE 5.5iii. Amplitude histogram of the wall microphone pressure.

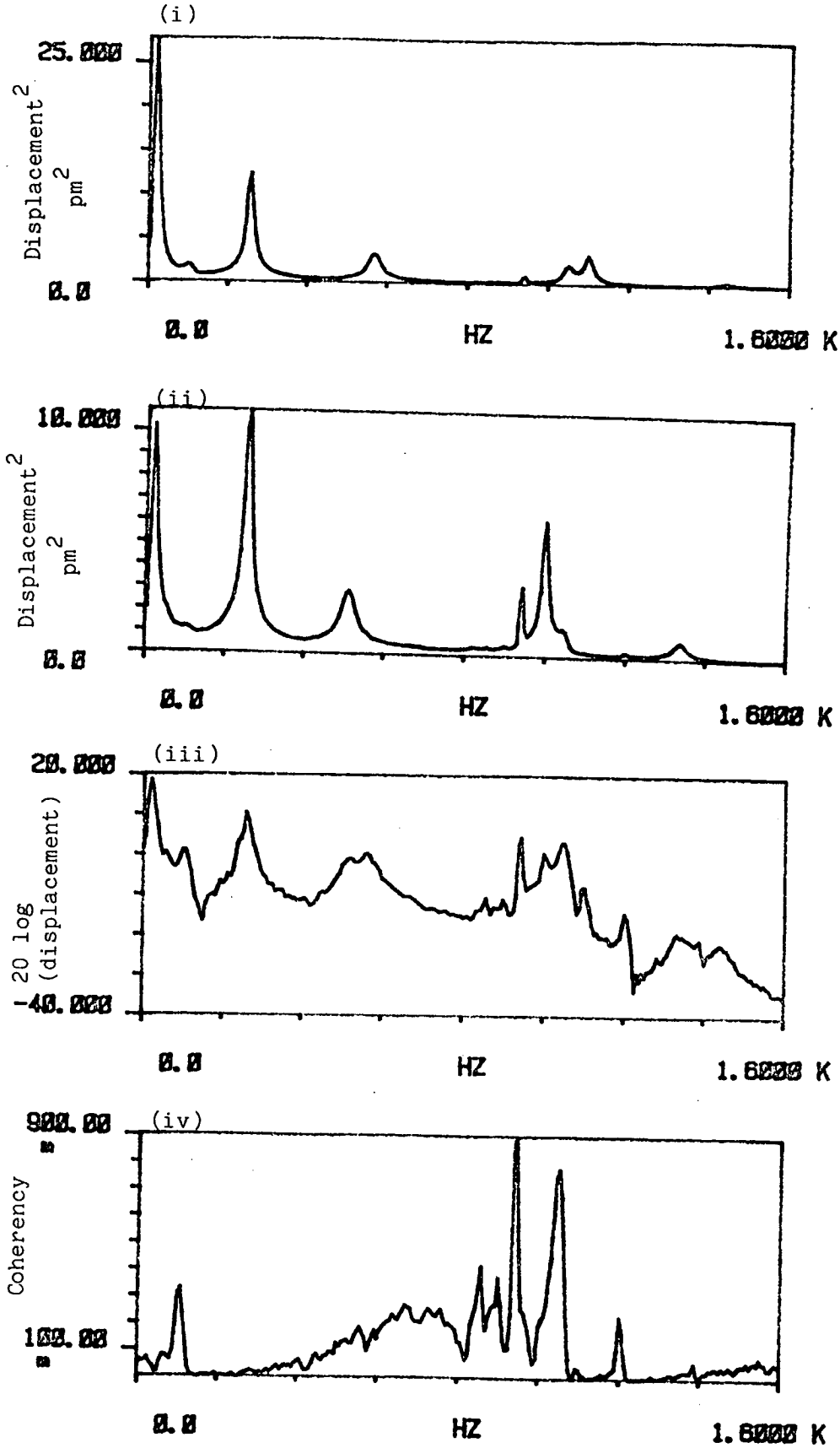


FIGURE 5.6. (i) P.S.D. of the displacement of instrumented tube 1,
(ii) P.S.D. of the displacement of instrumented tube 2,
(iii) C.S.D. of the tube displacement signals,
(iv) coherency spectrum of the displacement signals,
for experimental arrangement 2.

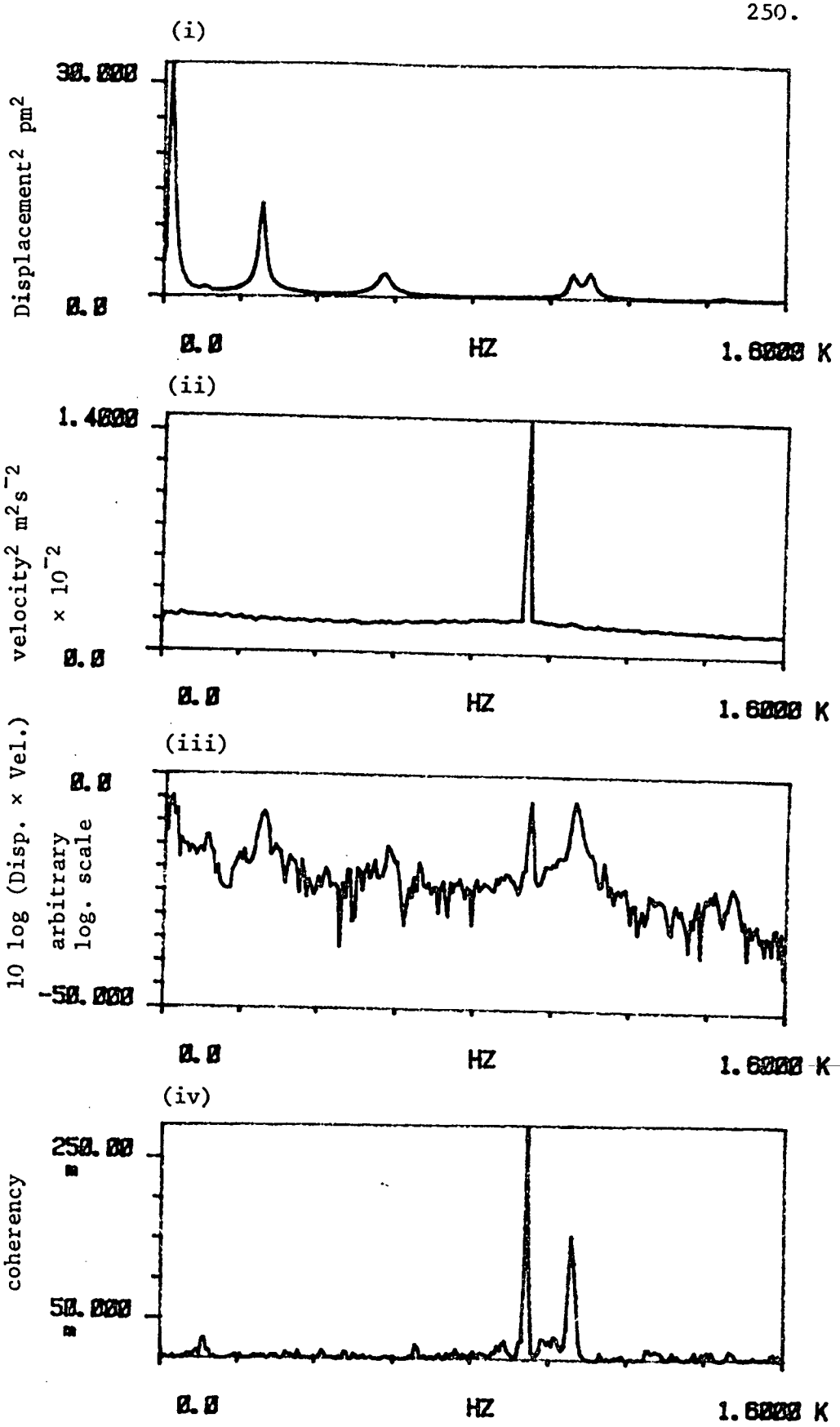


FIGURE 5.7. (i) P.S.D. of the displacement of instrumented tube 1,
(ii) P.S.D. of the wake velocity behind instrumented tube 1,
(iii) C.S.D. of the displacement and velocity signals,
(iv) coherency between displacement and wake velocity.

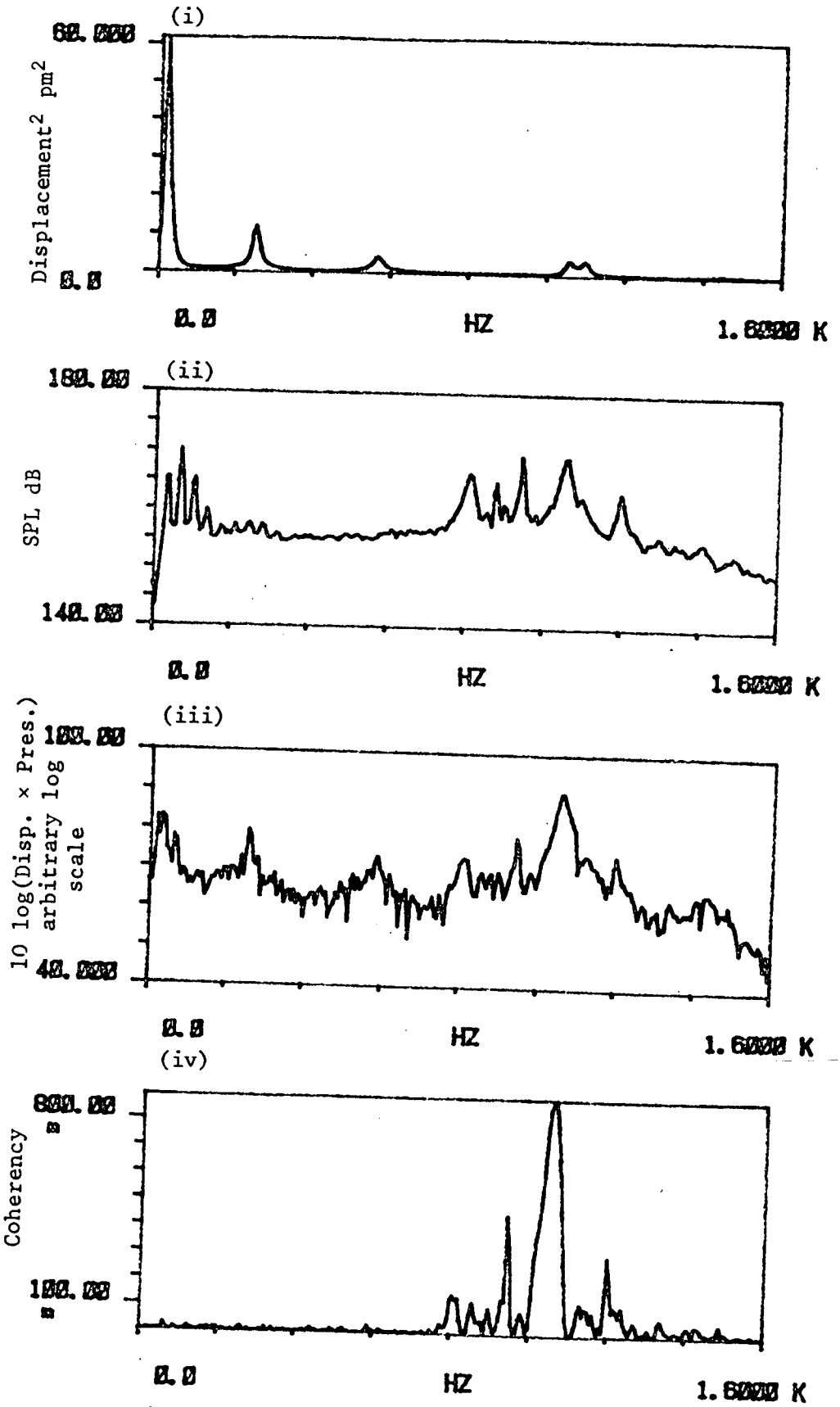


FIGURE 5.8. (i) P.S.D. of displacement of instrumented tube 1,
(ii) P.S.D. of the fluctuating pressure in the wake behind instrumented tube 1,
(iii) C.S.D. of the displacement and pressure signals,
(iv) coherency between displacement and wake pressure.

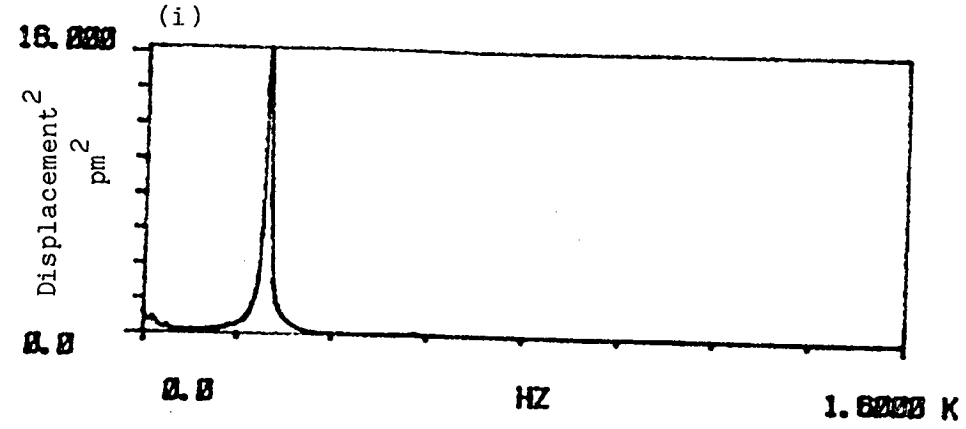



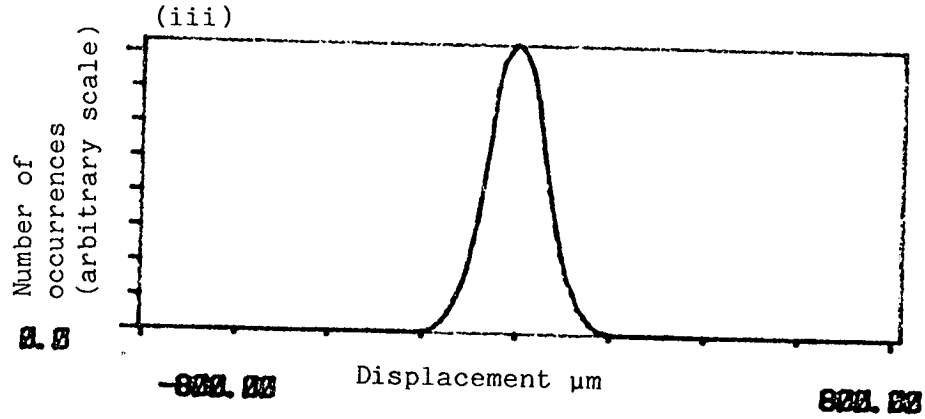


FIGURE 5.9. (i) P.S.D. of displacement of instrumented tube 1,
(ii) P.S.D. of wall microphone pressure,
(iii) Amplitude histogram of instrumented tube 1 displacement signal.

FIGURE 5.9a. Free stream flow velocity = 10.7 $ms^{-1}$

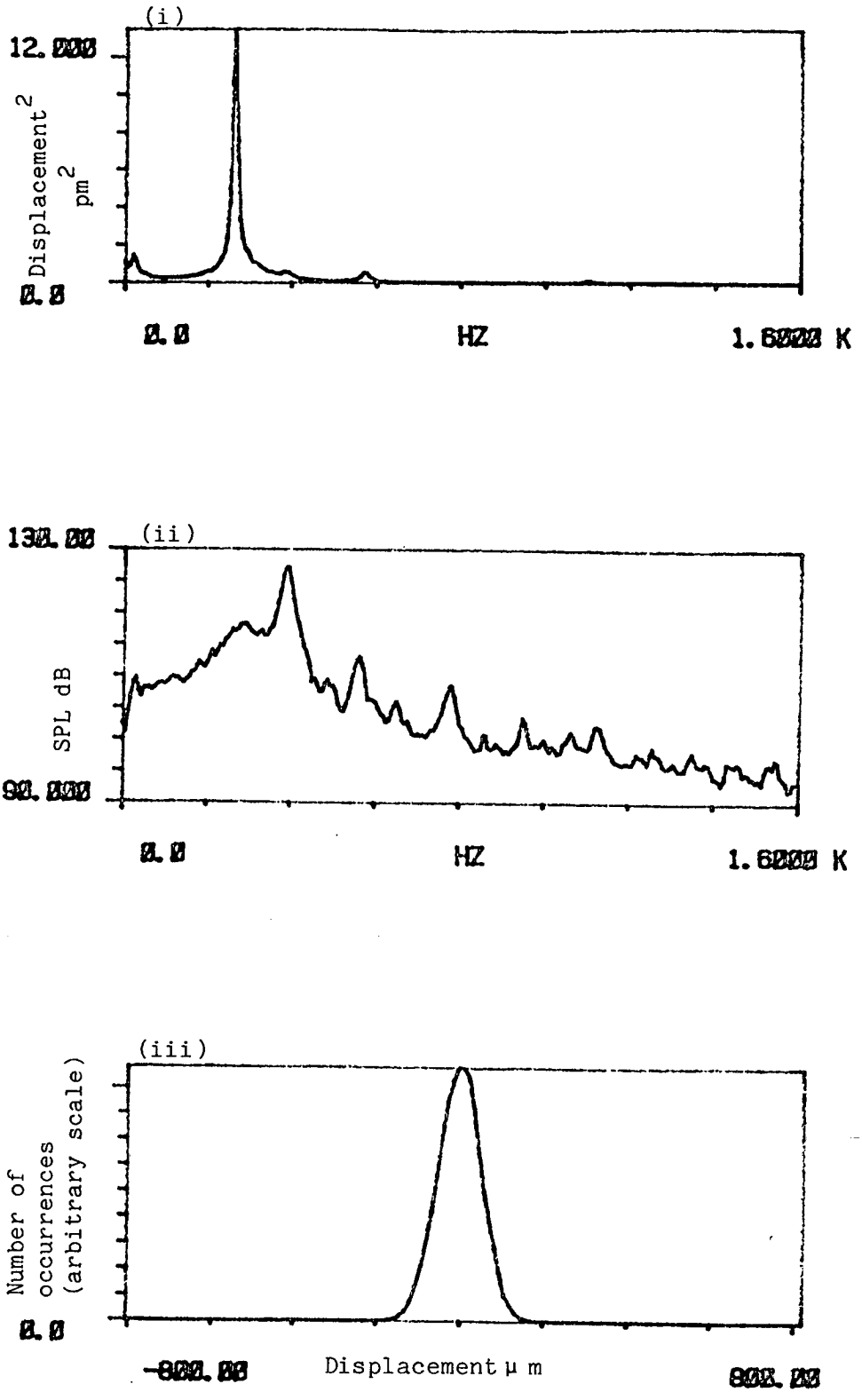


FIGURE 5.9b. Free stream flow velocity = 13.9 $ms^{-1}$

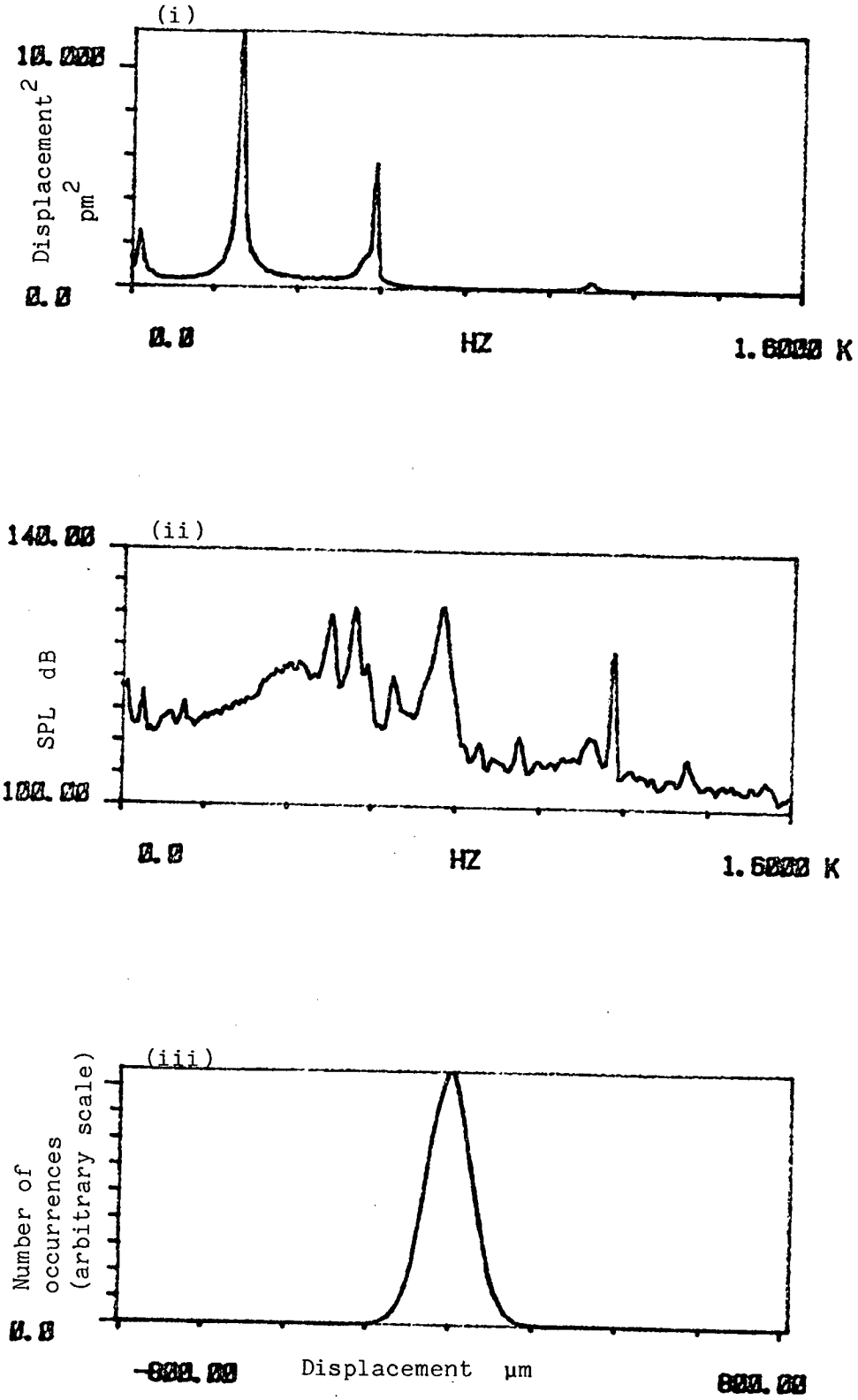


FIGURE 5.9c. Free stream flow velocity = 18.9 $ms^{-1}$

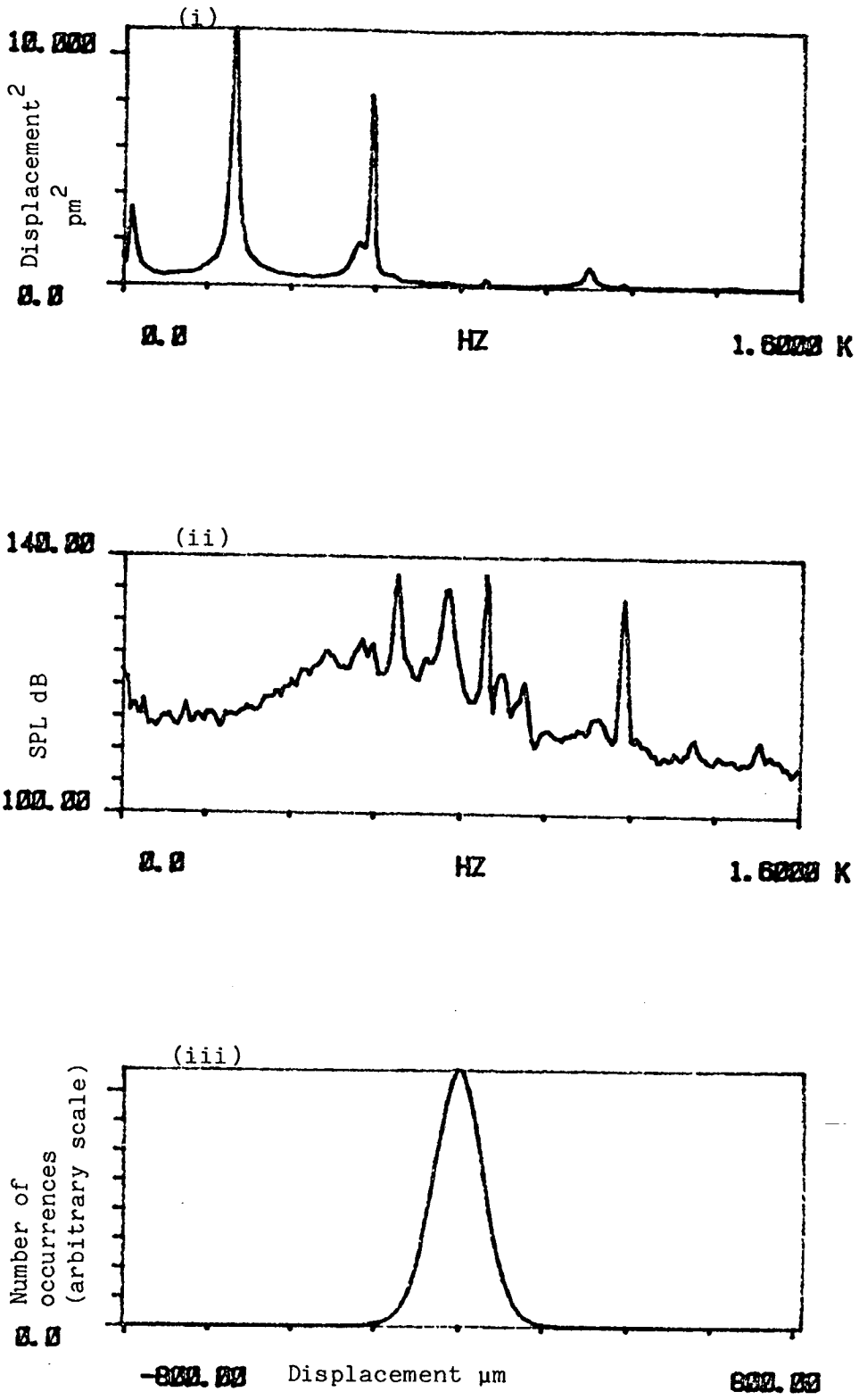


FIGURE 5.9d. Free stream flow velocity = 22.8 $ms^{-1}$

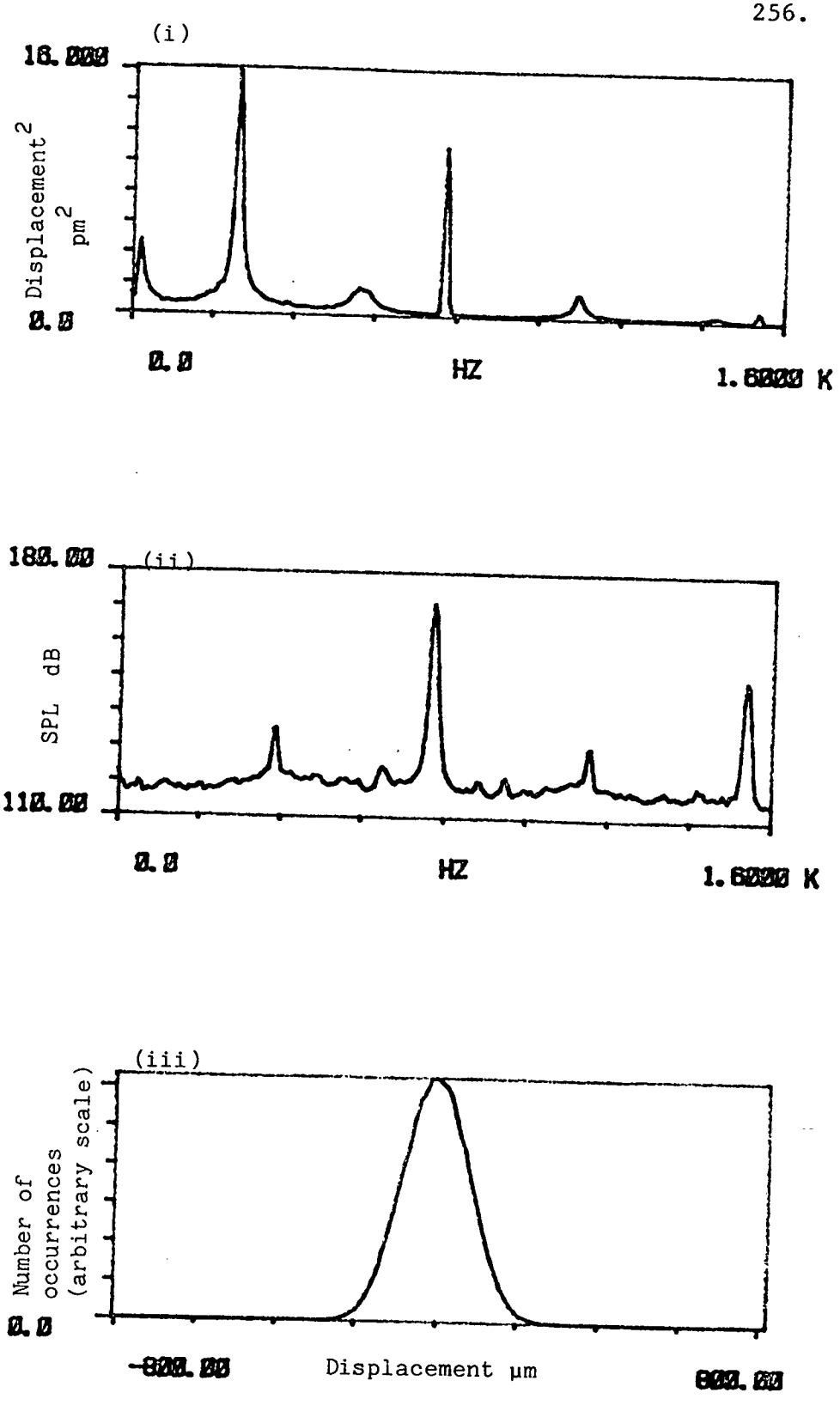


FIGURE 5.9e. Free stream flow velocity = 25.5 $ms^{-1}$

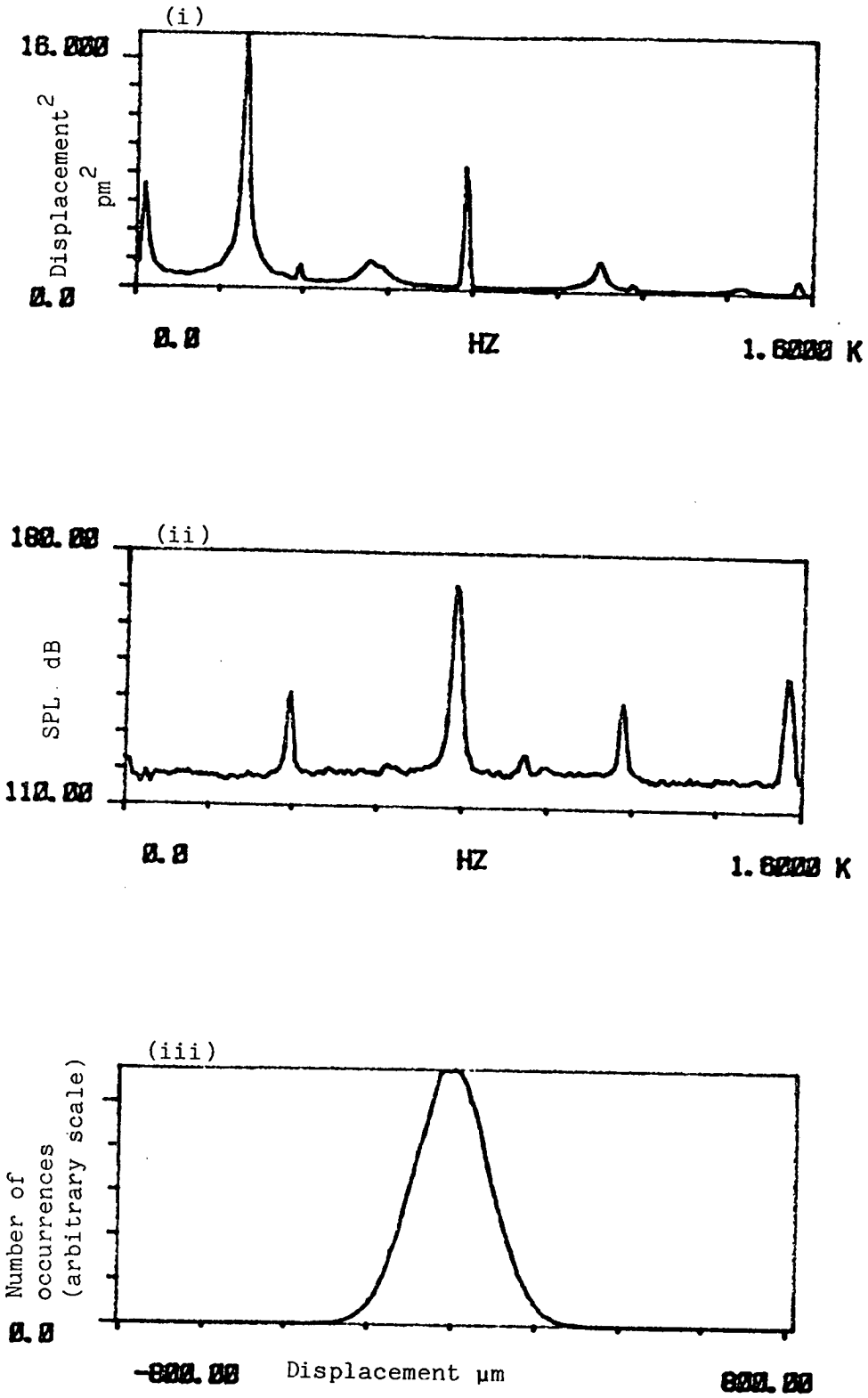


FIGURE 5.9f. Free stream flow velocity = 28.5 $ms^{-1}$

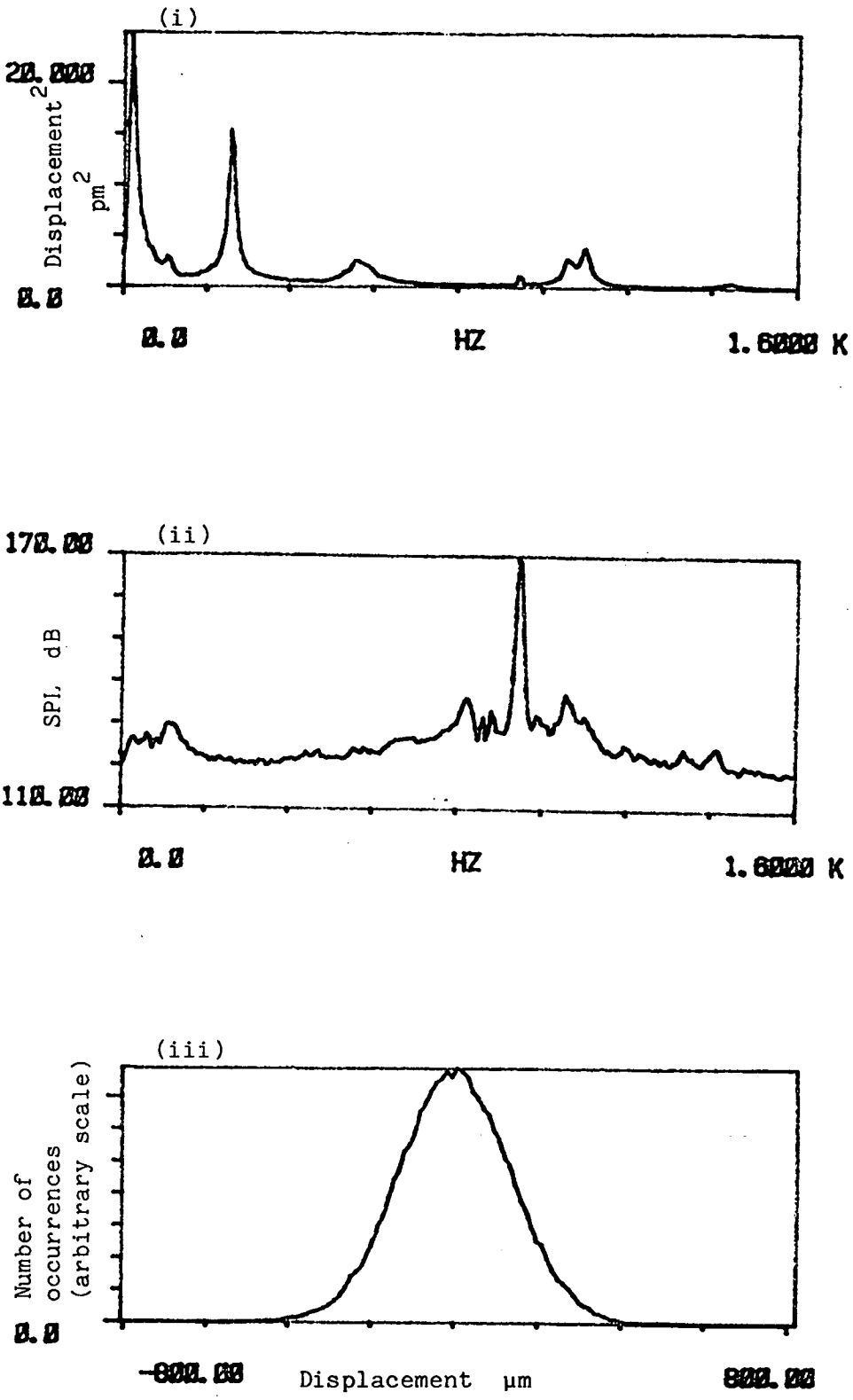


FIGURE 5.9g. Free stream flow velocity = 33.5 $ms^{-1}$

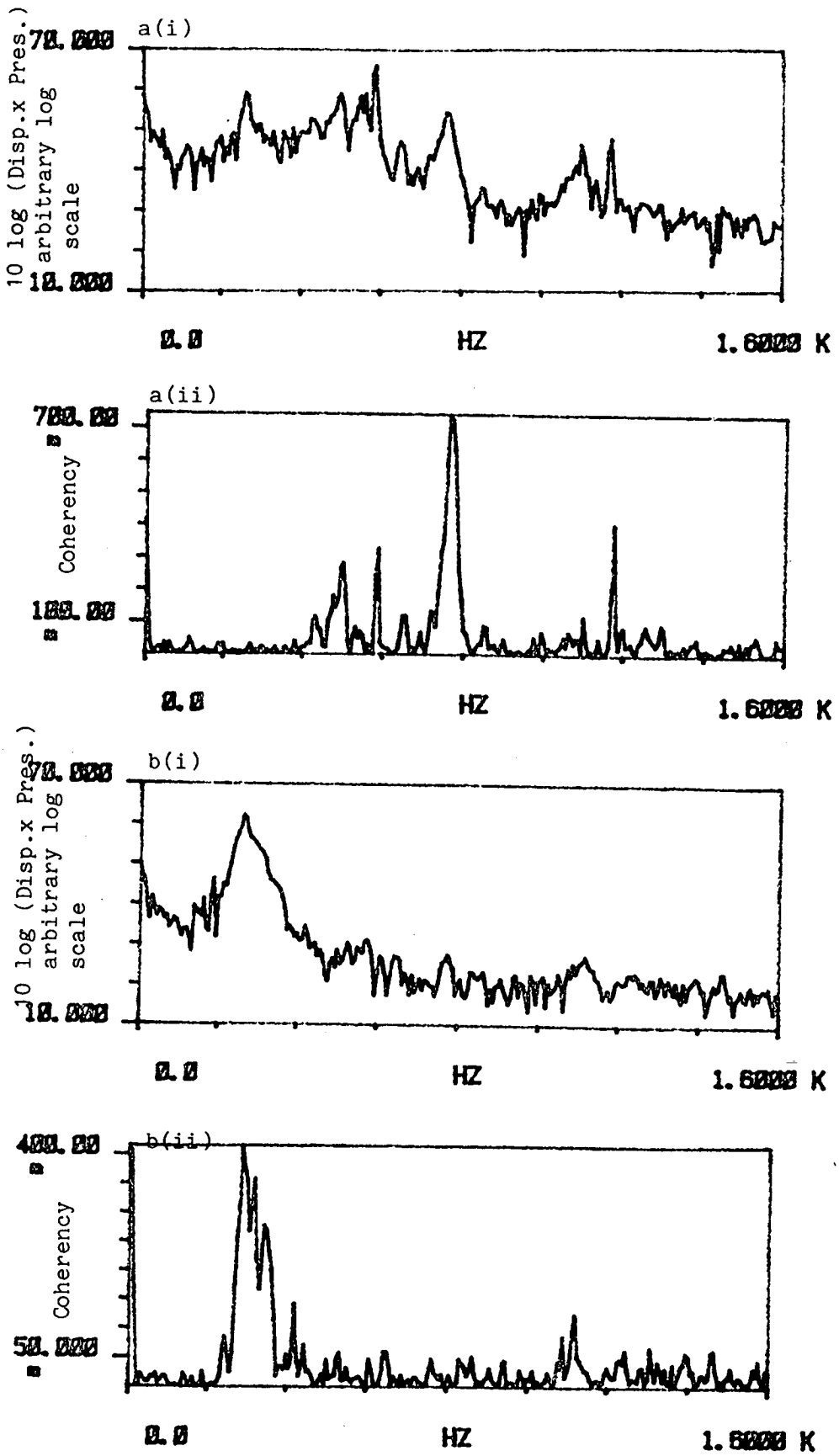


FIGURE 5.10. (i) C.S.D. of displacement of instrumented tube 1 and the wall microphone pressure signal,
(ii) Coherency spectrum of displacement and pressure for a free stream flow velocity of; (a) 18.9 $ms^{-1}$ (b) 10.7 $ms^{-1}$.

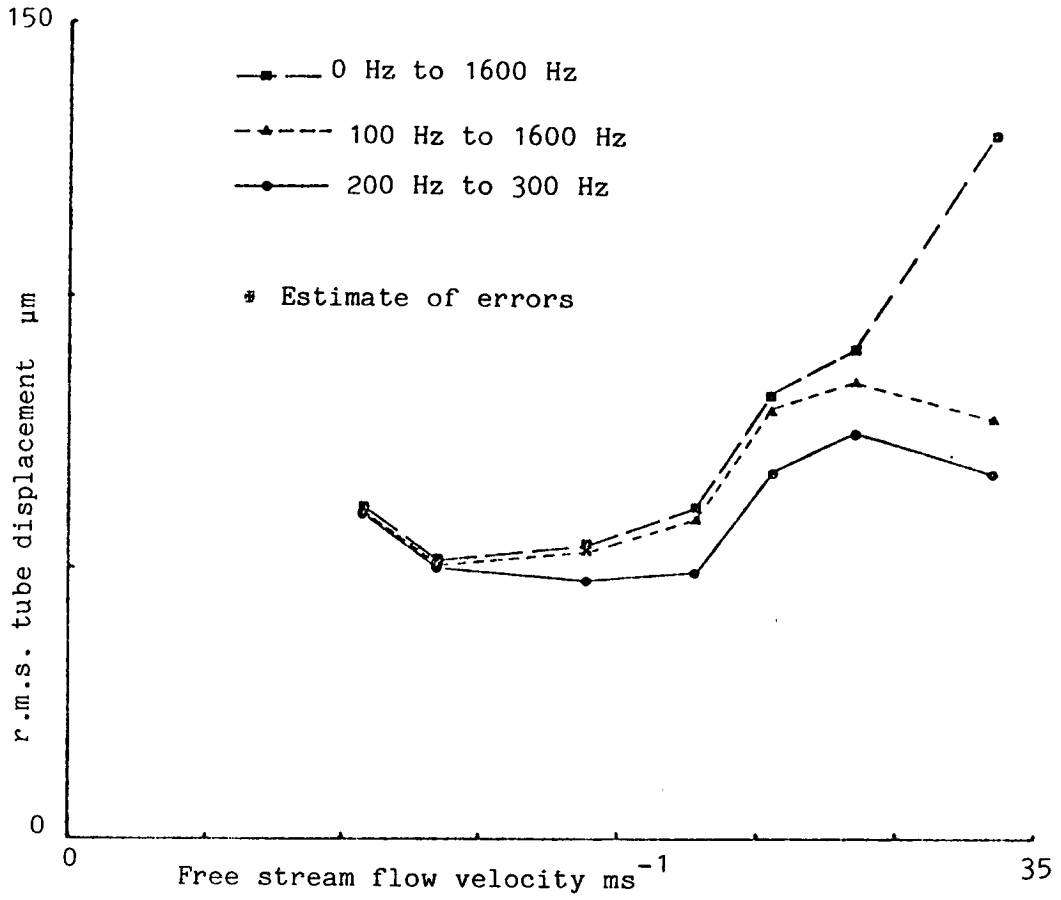


FIGURE 5.11. R.m.s. displacement of instrumented tube 1 versus free stream flow velocity for different frequency bands.

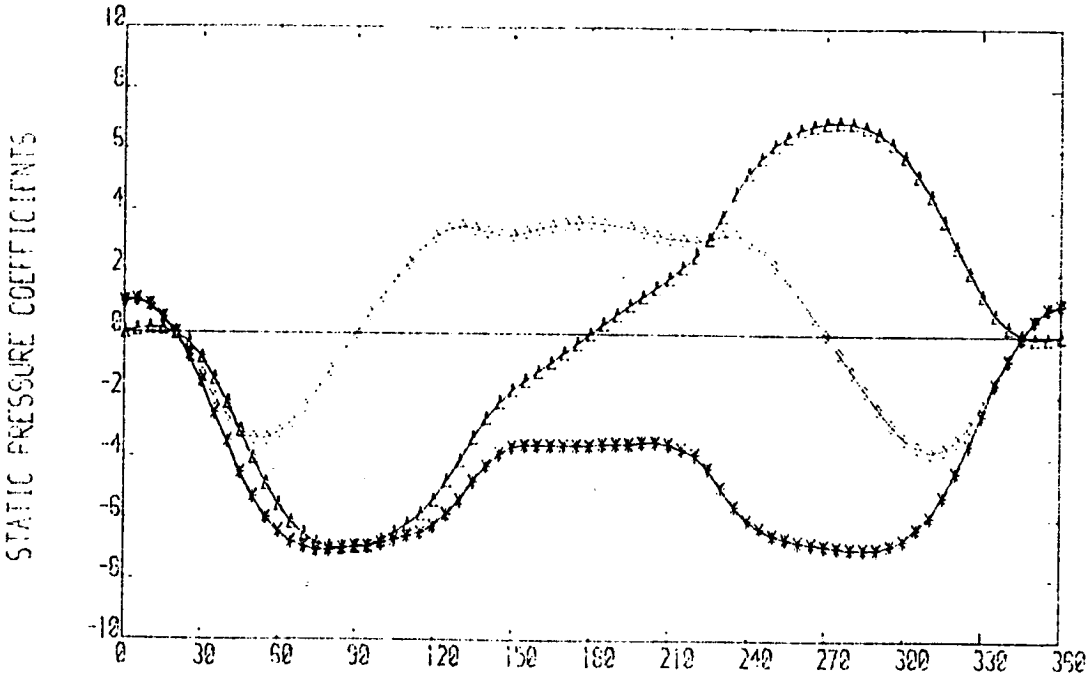


FIGURE 5.12i. Variation of static pressure coefficients with angle round the pressure measuring tube at 0 diameters from the centre along the spanwise axis of the measuring tube.

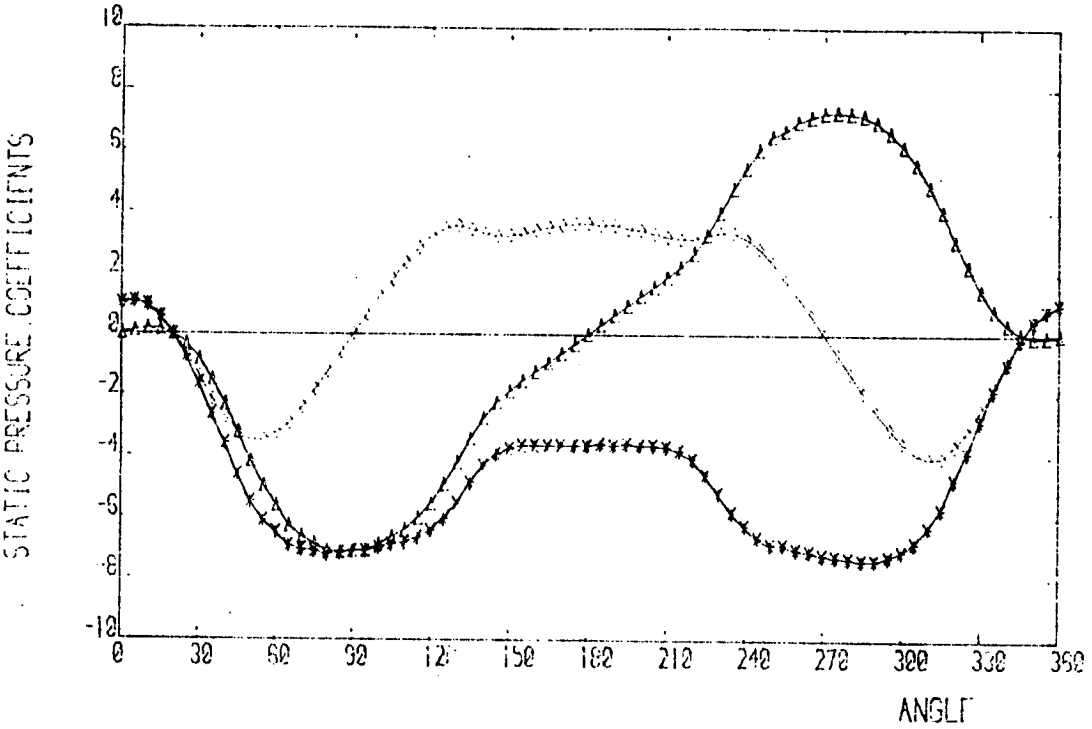


FIGURE 5.12ii. Variation of static pressure coefficients with angle round the pressure measuring tube at 3 diameters from the centre along the spanwise axis of the measuring tube.

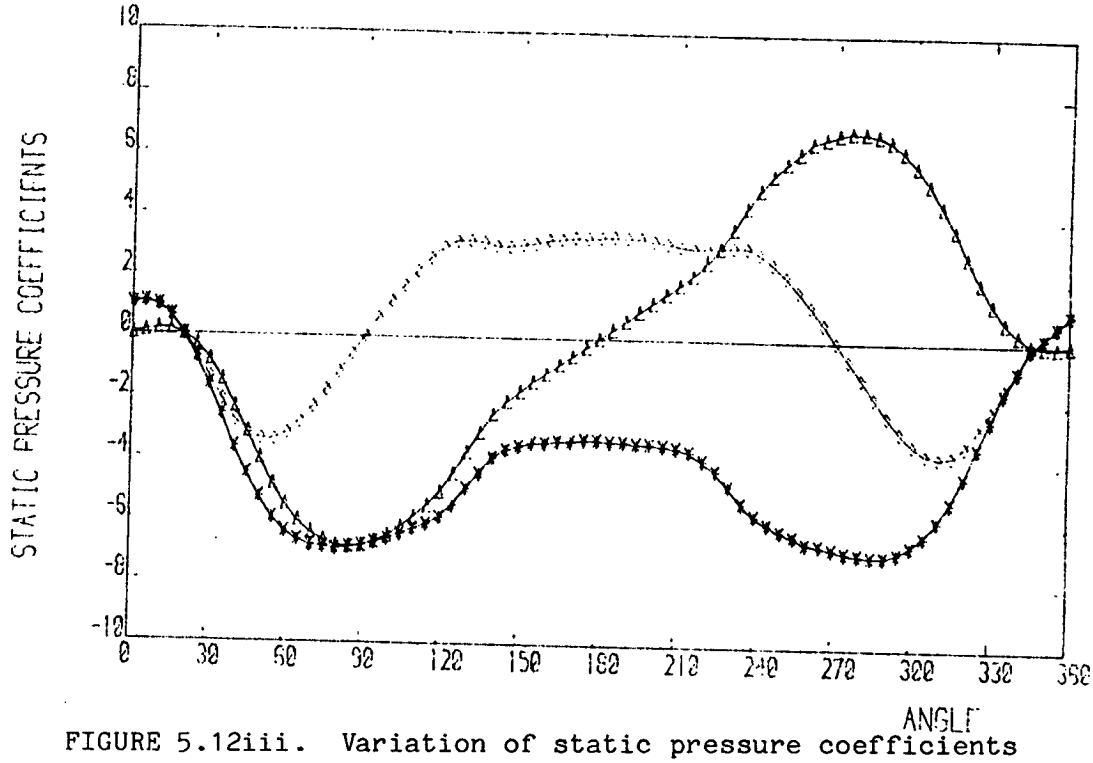


FIGURE 5.12iii. Variation of static pressure coefficients with angle round the pressure measuring tube at 4 diameters from the centre along the spanwise axis of the measuring tube.

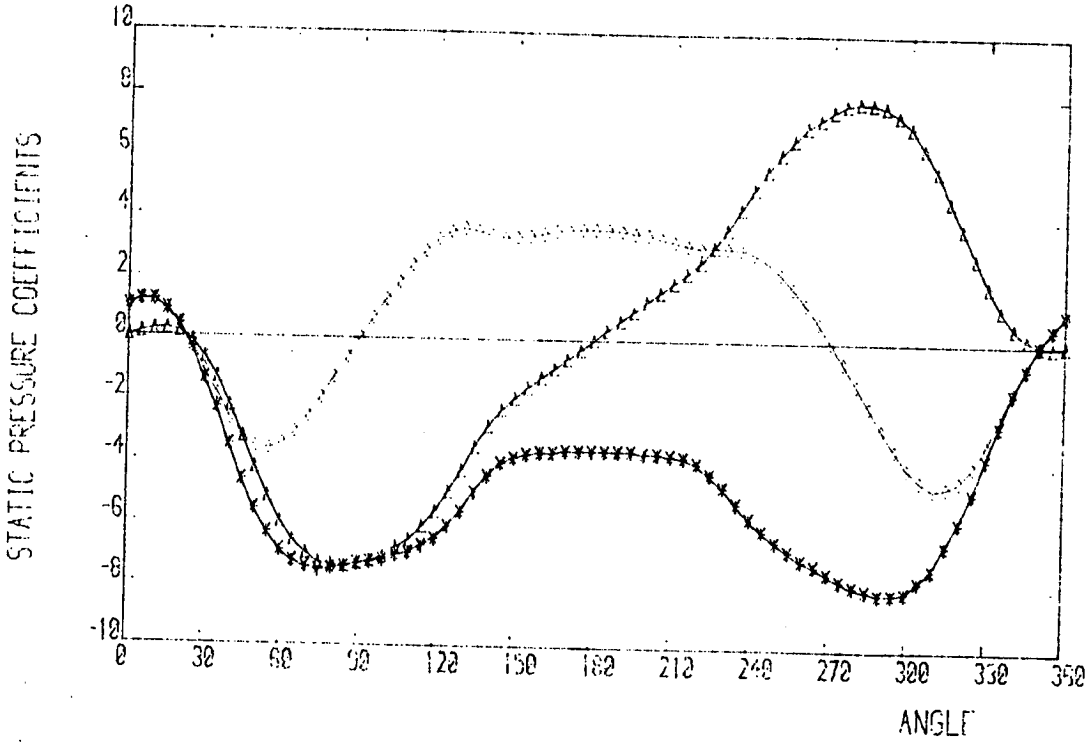


FIGURE 5.13. Variation of static pressure coefficients with angle round the pressure measuring tube when the measuring tube is near the edge of the tube bank (i.e. experimental arrangement 1).

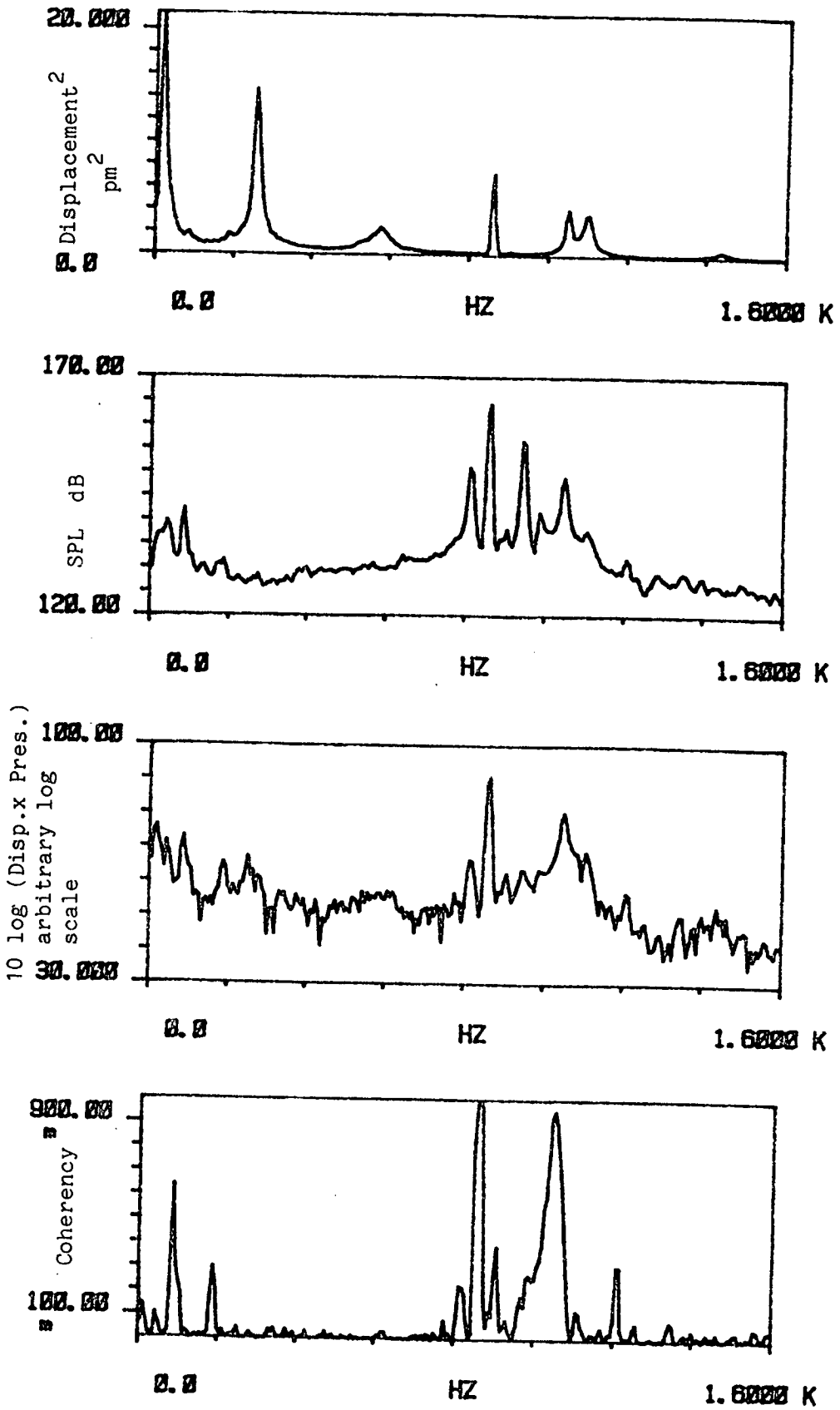


FIGURE 5.14. (i) P.S.D. of the displacement of instrumented tube 1,
(ii) P.S.D. of the wall microphone pressure,
(iii) C.S.D. of the displacement and pressure signals,
(iv) Coherency spectrum of the displacement and pressure signals.

FIGURE 5.14a. No superimposed sound.

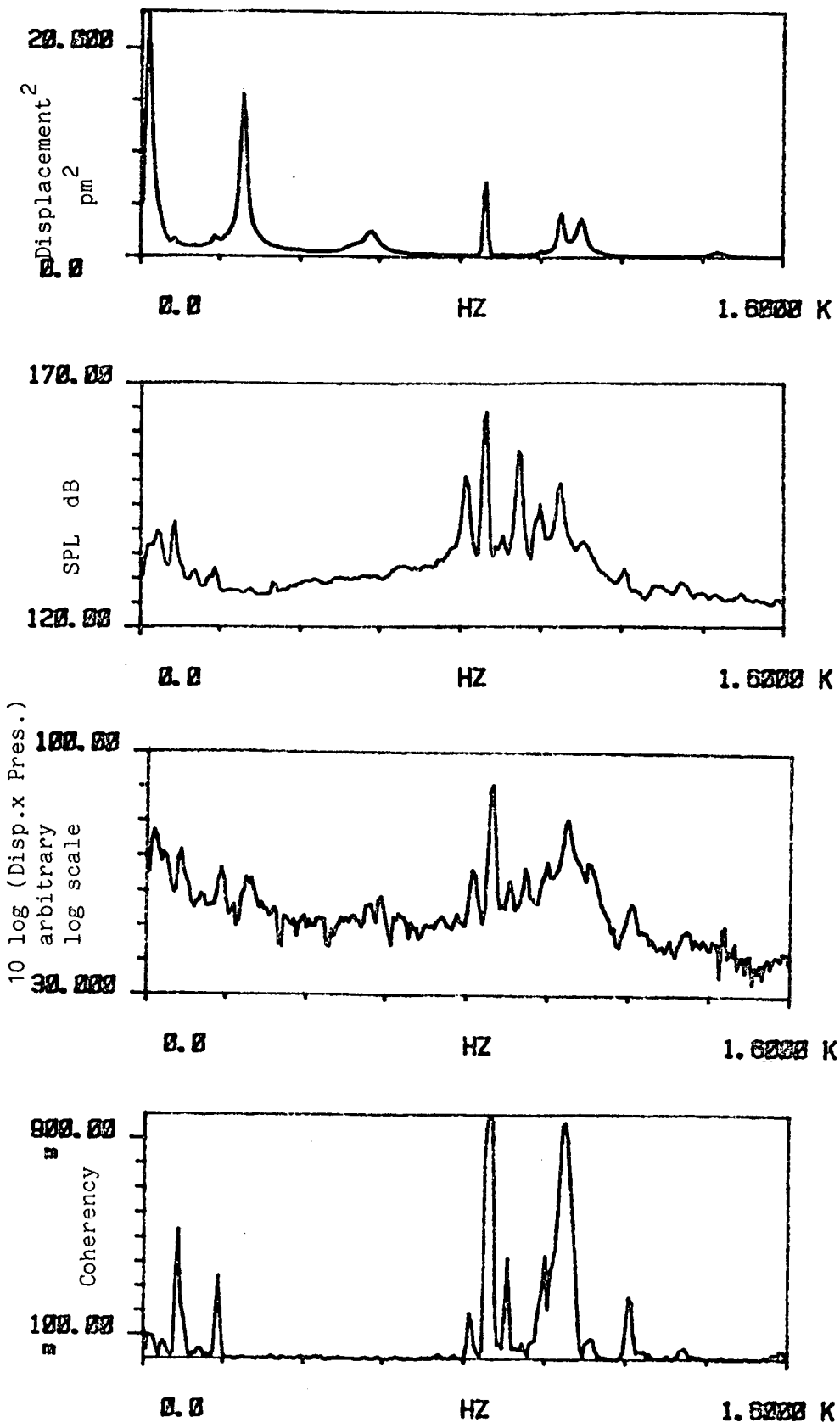


FIGURE 5.14b. Superimposed sound at 333 Hz and a SPL of 130 dB.

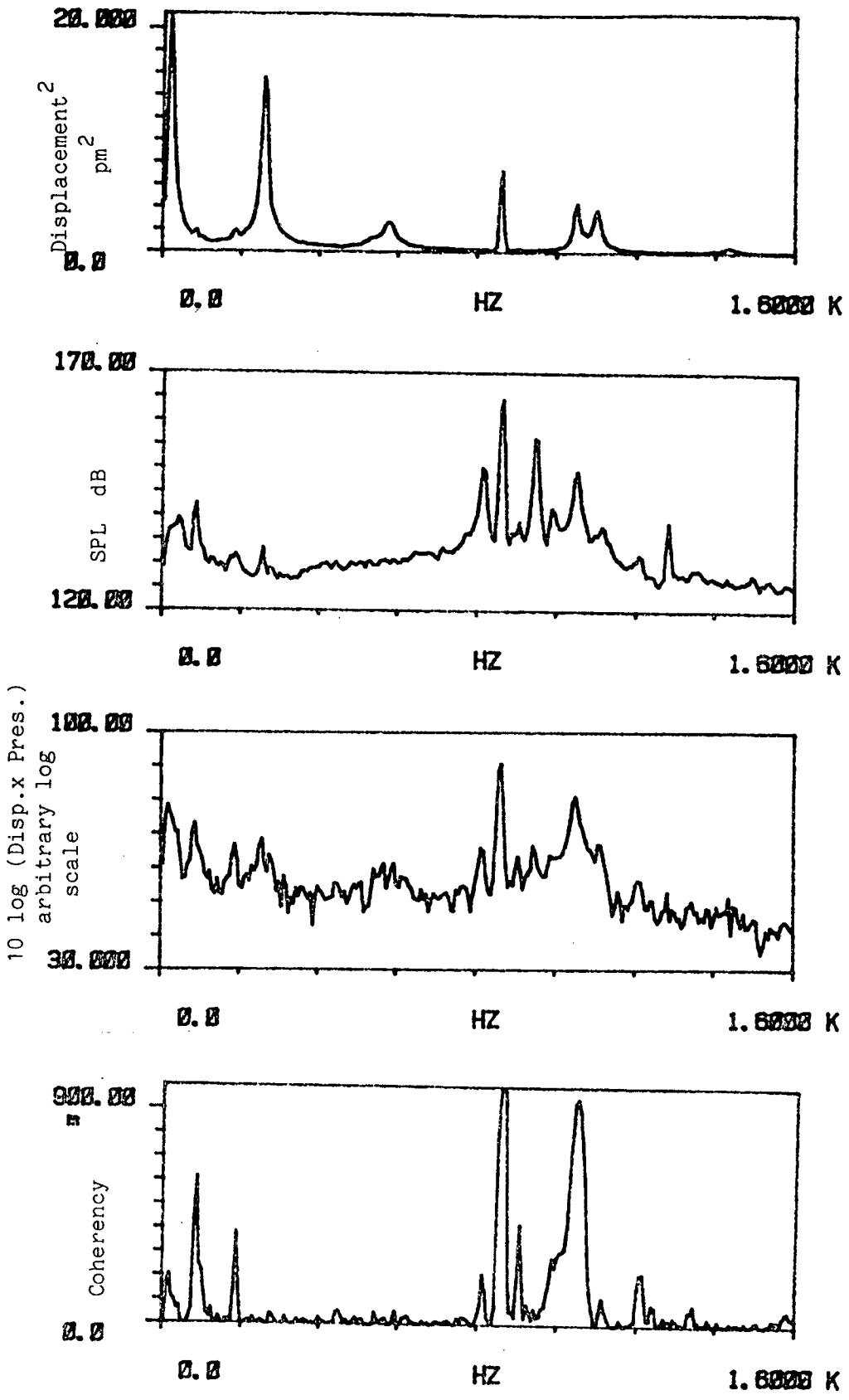


FIGURE 5.14c. Superimposed sound at 256Hz and a SPL of 134dB.

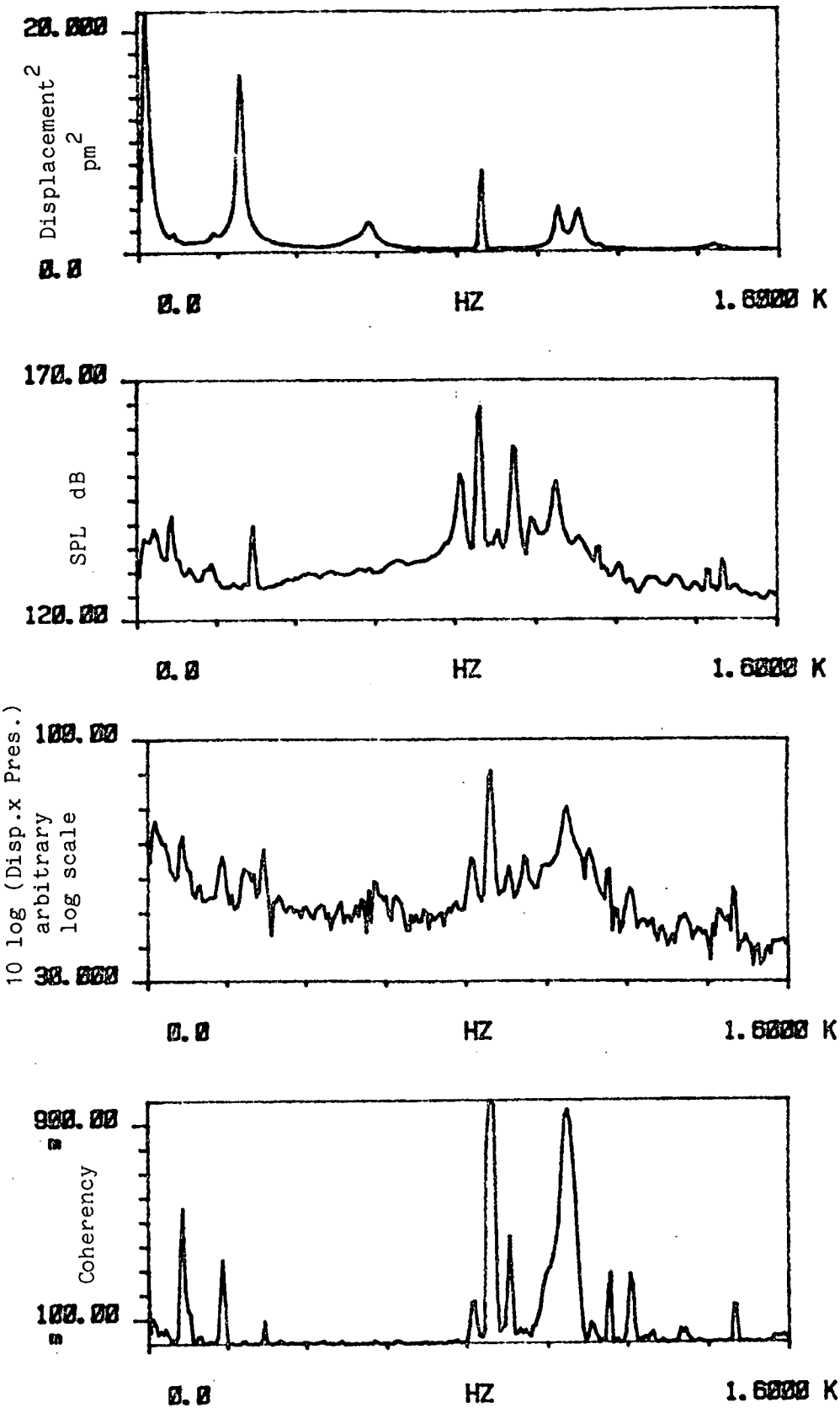


FIGURE 5.14d. Superimposed sound at 293 Hz and a SPL of 139 dB.

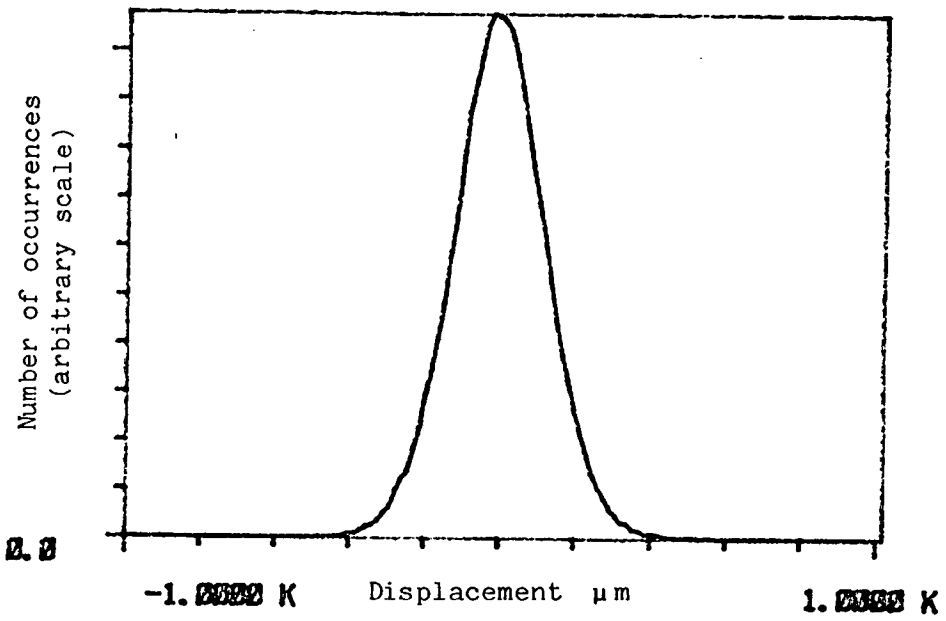


FIGURE 5.15a. Amplitude histogram of displacement of instrumented tube 1 with no superimposed sound.

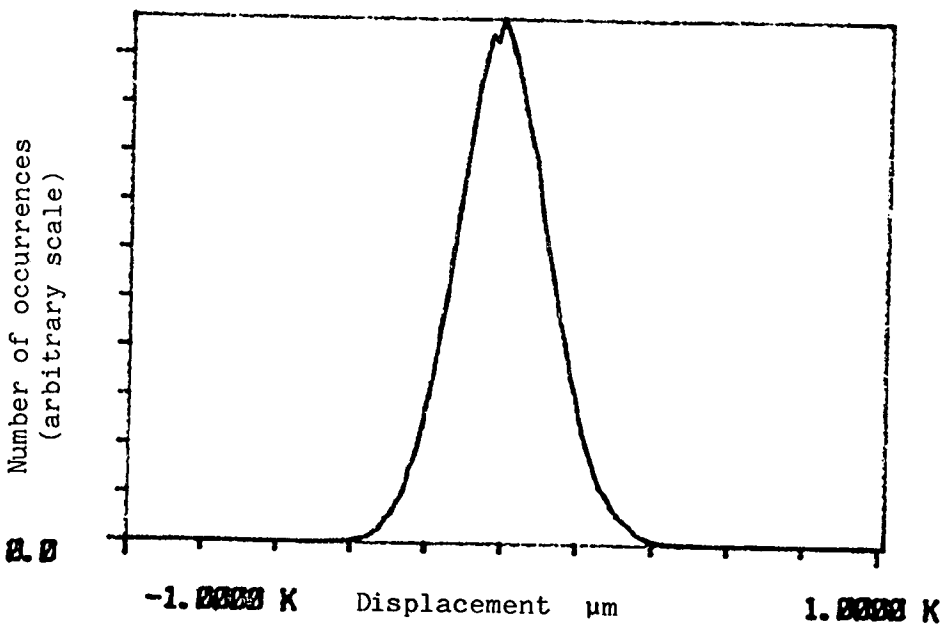


FIGURE 5.15b. Amplitude histogram of displacement of instrumented tube 1 with superimposed sound at 333 Hz and a SPL of 130 dB.

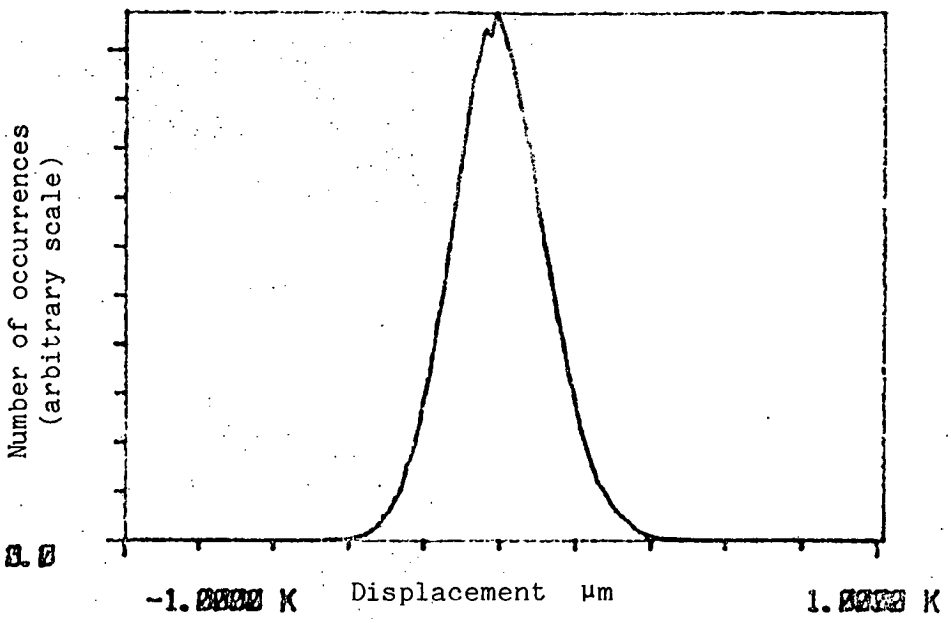


FIGURE 5.15c. Amplitude histogram of displcement of instrumented tube 1 with superimposed sound at 256 Hz and a SPL of 134 dB.

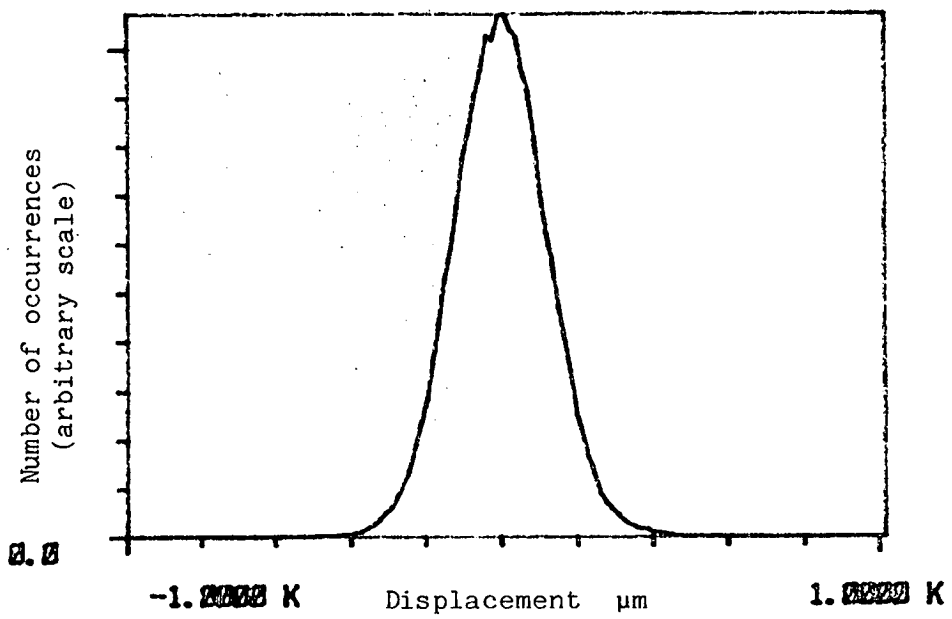


FIGURE 5.15d. Amplitude histogram of displacement of instrumented tube 1 with superimposed sound at 293 Hz and a SPL of 139 dB.

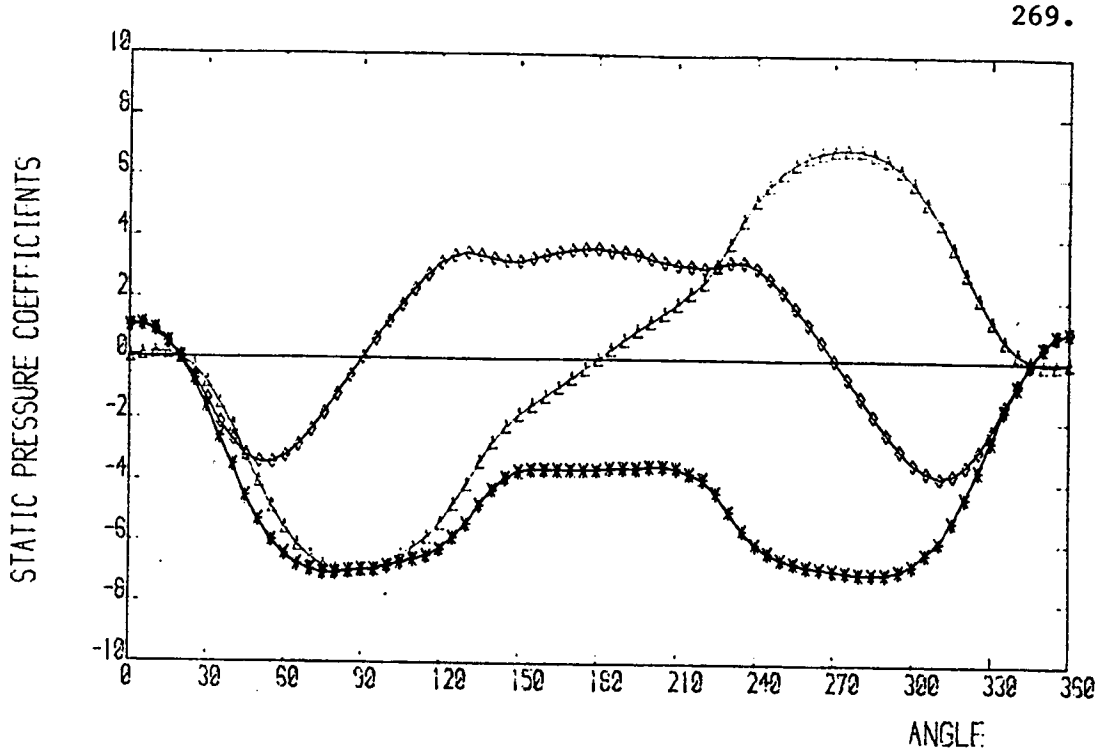


FIGURE 5.16a. Variation of static pressure coefficients with angle for experimental arrangement 2 and no superimposed sound.

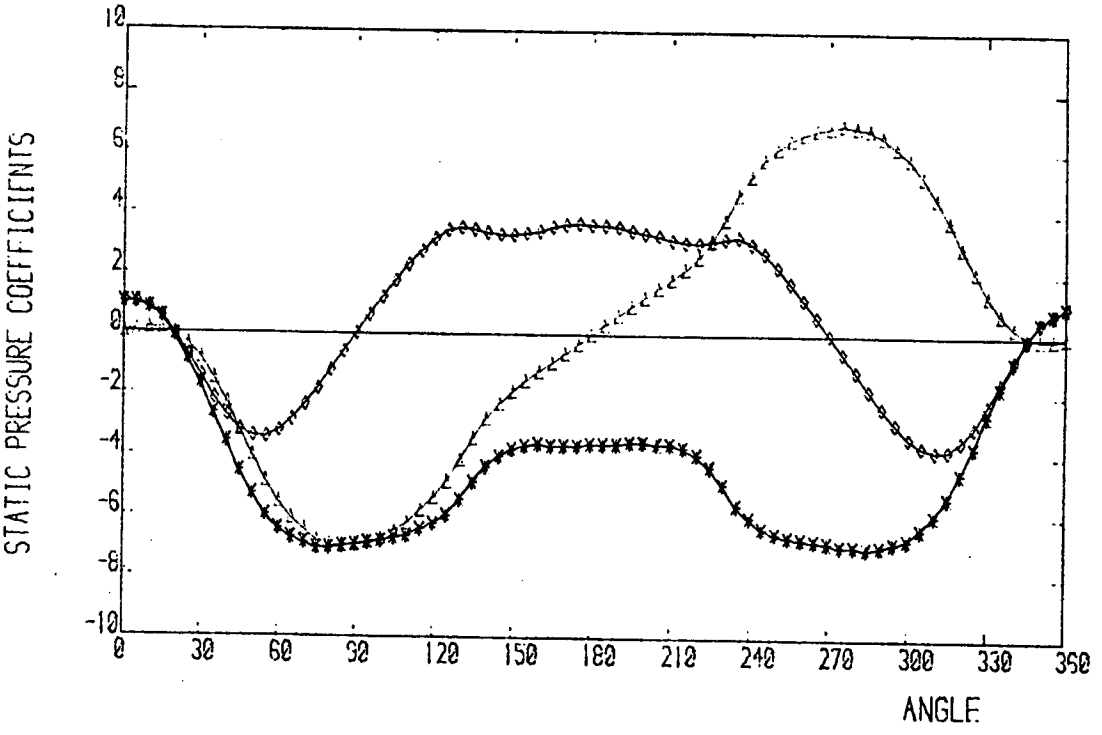


FIGURE 5.16b. Variation of static pressure coefficients with angle for experimental arrangement 2 and superimposed sound at 293 Hz and a SPL of 139 dB.

# CHAPTER 6

# MODELLING OF TUBE COUPLING VIA THE FLOW IN TUBE ROWS AND TUBE BANKS

## 6.1 Introduction

In this chapter a critical review of the current models for predicting the onset of large amplitude tube vibrations due to the coupling of neighbouring tubes via the flow in tube rows and tube banks is given.

A potential flow model for a single tube row and a small tube bank is developed using the boundary element technique, and the effects of statically displacing a single tube in a tube row, and in a tube bank, on the pressure distribution, lift and drag on the displaced tube are investigated.

## 6.2 Review of Tube Row and Tube Bank Models

### 6.2.1 Prediction of the onset of fluid-elastic instabilities in single tube rows by Connors and modification of Connors' prediction equation by other researchers

Connors [6.12] developed an equation for predicting the onset of large amplitude fluid-elastic tube vibrations in a single tube row. In his analysis he equated the energy input per cycle from the flow to a vibrating tube to the energy dissipated per cycle by the mechanical tube damping, to obtain a value of flow velocity required to produce tube fluid-elastic instabilities, known as the critical velocity. The energy input per cycle to the tube was estimated from experimental measurements of the steady lift and drag forces on a tube for a range of different displacements of the tube from a uniformly spaced position in a single tube row. Connors found that the variations of the lift and drag with tube displacement were only functions of the tube displacement in the direction parallel to (streamwise) and perpendicular to (cross-flow) the oncoming flow direction respectively. (This was not found to be the case in the present investigation where both the lift and drag were functions of tube displacement in the cross-flow direction).

The energy dissipated per cycle by damping was calculated from the experimentally measured tube damping in still air. The equation for predicting the onset of fluid-elastic instabilities obtained by Connors is given in equation (6.1), where $\beta = 9.9$ for the particular tube row which he investigated.

$$U_c = \beta f_o D \left[\frac{m_o \delta_o}{\rho D^2}\right]^{0.5} . \qquad (6.1)$$

In a subsequent publication [6.13] , Connors derived an empirical equation for predicting the constant for in-line square tube arrays but the equation is not generally applicable to arbitary tube banks and is based on limited experimental measurements.

Connors also theoretically investigated the effects of the transverse mode shape of the tube vibration on the fluid-elastic constant $\beta$ and found that for tubes with constant mass per unit length, and for constant fluid density, the constant $\beta$ was not affected by the tube transverse mode shape. A similar conclusion was reached by Franklin and Soper [6.15] . Connors [6.13] and Franklin and Soper [6.15] also theoretically investigated the effects of partical admission of flow over a tube span and found that for most cases (except when the flow was exciting only 10% of the tube's length near a clamped end) the velocity for the onset of fluid-elastic vibrations was reduced. Hence if spanwise variations in flow velocity across a tube bank exist it is necessary to determine the vibration mode shapes of the tubes in order to predict the onset of fluid-elastic instability.

Several investigators have modified the original Connors' equation given in (6.1) in order to produce better correlations with experiments see [6.10, 6.22]

Blevins [6.5] included the effect of a fluid damping component proportional to the vibration velocity of the tubes, and predicted increased values of flow velocity for the onset of fluid-elastic instability.

Connors has undoubtedly made a significant contribution to the understanding of the mechanisms causing large amplitude tube vibrations, but until a method for predicting the constant in equation (6.1) is developed, or until a sufficiently large number of experiments are carried out to measure $\beta$ for different tube bank geometrics and flow regimes, it is difficult to predict

the onset of fluid-elastic vibrations with any degree of certainty for a new tube bank design.

### 6.2.2 Blevins' model

Blevins [6.3] formally set up the equations of motion of a tube in a single tube row taking into account the force produced by the displacement of the tube relative to its neighbours. He then solved the equation and used a stability analysis to derive a general equation for predicting the critical flow velocity for the onset of fluid-elastic instability. Blevins' equation reduced to Connors' equation when the damping ratios and resonance frequencies in orthogonal tube vibration directions for neighbouring tubes were the same. In his analysis, Blevins assumed that the force coefficients for the tubes were only functions of the tube displacements in directions perpendicular to the direction of the force. Using this assumption it was found that the constant $\beta$ in Connors' equation was given by equation (6.2).

$$\beta = (C_x K_y)^{-0.25} \quad . \qquad (6.2)$$

The assumption employed is justified for the tube row investigated by Connors, but is not necessarily correct for tube rows with different tube spacings subject to different flow conditions, as shown in the present investigation. (See Section 4.3).

Blevins' analysis suggested that the critical velocity was a function of tube damping associated with motion in both orthogonal directions, and when the resonance frequencies of neighbouring tubes were different, the critical flow velocity was predicted to increase. He also investigated the effect of the number of tubes in a row on the critical velocity and found that it increased from the value predicted by Connors' equation (6.1), as the number of tubes in a row was decreased from an infinite value. Tubes next to a wall were found to have lower critical flow velocities than those in the centre of a tube row.

In the analysis discussed above Blevins assumed the amplitude of the tube displacements to be small, and the force on a tube when it was displaced from a uniformly spaced position in a tube row to be proportional to the displacement, the constants of proportionality being referred to as the fluid force coefficients.

In a more recent publication [6.4] Blevins derived formulae for the fluid force coefficients for a tube in a single tube row.

In his derivation he assumed that :

(i) the flow separates at the point of the minimum gap between the tubes and forms jets normal to the axes of the tubes and,

(ii) the pressure drop from the free stream to the near wakes of the tubes is equal to the dynamic head of the fluid in the gaps.

He then used the steady Bernoulli equation to calculate the lift and drag forces on a tube when displaced in the directions parallel and perpendicular to, the oncoming flow respectively. The variation of the lift force with tube displacement in the cross-flow direction and the variation of the drag force with tube displacement in the steamwise direction were not included in his analysis. Blevins assumed that the velocity in the gap between the tubes was given by the product of the free stream velocity and the ratio of the pitch to the gap width. Potential flow considerations show this assumption not to be valid and although the velocity does increase as the gap width is decreased it does not increase linearly with gap width. In order to determine the force on the tube the velocity field round the tubes would be required which was not calculated in Blevins' analysis. (The determination of the velocity field can be carried out using a potential flow analysis with free streamlines to represent the wake regions of the tubes). The assumption that the separation points occur in the minimum gap between the tubes is not valid for all tube spacings and flow regimes and is not valid for the case of the experimental measurements described in section 4.3.

Hence the formulae, derived by Blevins, to predict the fluid force coefficients for a tube displaced in a single tube row are not generally applicable to arbitrary tube rows subject to arbitrary flow conditions.

In a further analysis [6.4] Blevins developed a formula for the force coefficients on tubes displaced in a tube array. His argument assumed that a constant volume flowed between tubes when they were displaced by small distances in in-line tube arrays and that the flow velocity was constant in the gaps of staggered tube arrays. He then calculated the average force on a tube by assuming that the drag on a tube was equal to the ratio of

the pressure drop across a tube row divided by the number of tubes in the row. The drag force on the tubes was found to be a function of tube spacing. There is no experimental evidence available to validate any of the above assumptions made by Blevins and the formulae he derives require the knowledge of tube friction factors for the particular tube array under investigation. Friction factor data for tubes in various tube array geometries is very sparse, and hence Blevins' formula is not of general utility.

### 6.2.3 Goyder's model

Goyder [6.16] set up the equations of motion for a cylinder array in a similar manner to Blevins [6.4] and he then expressed the relationship between the cylinder vibrations and the forces acting on them in matrix form. The solution of the eigenvalue problem for N cylinders each having 2 dgrees of freedom gave 2N modes of vibration for the cylinder array. The onset of instability for a particular vibrational mode of the tube array was given by the minimum velocity to produce a negative imaginary component of theeigenvalue associated with the instability mode. Goyder then used periodic structure theory (See [6.21] ) to calculate the stability conditions for the modes of an infinite row of cylinders and found that :

$$U_c = (C_x K_y)^{-0.25} \; f_o D \left[ \frac{2\pi m_o \delta_o}{\rho D^2 \sin(2\pi/P_R)} \right]^{0.5} \quad . \qquad (6.3)$$

Using similar assumptions to Blevins, Goyder calculated the fluid force constants on a cylinder when displaced, from a uniformly spaced position in an infinite tube row, in directions both parallel and perpendicular to the plane of the tube row. Hence the force constants only apply to single rows of cylinders where separation occurs in the minimum gap between the tubes and so the critisisms applied to Blevins' work apply equally to this analysis.

### 6.2.4 Models of Whiston and Thomas

Whiston and Thomas [6.30] extended the position dependent model of Blevins (for a single tube row) to include the effects of

fluid and mechanical coupling between tubes in two dimensional tube banks. Firstly they analysed the vibrations of an infinite set of tubes in a single tube row, setting up the equations in a similar manner to Blevins [6.3, 6.4] , but included force coefficients which depend on tube displacement in the cross-stream and streamwise flow directions, and also included terms in the equation representing linear mechanical coupling between neighbouring tubes. They solved the infinite set of linear equations and found that the 'whirling constant $\beta$ in Connors equation (6.1) was a function of the mode of vibration of the tubes in the tube row. In general the constant $\beta$ was found to vary in proportion to the square root of the modal wavelength $\lambda_{TM}$ and for wavelengths shorter than $\lambda_{TM}$= 4 the constant $\beta$ increased very rapidly with $\lambda_{TM}$. They also found that mechanical coupling for short wavelength tube row vibration modes considerably decreases $\beta$, and hence the velocity for the onset of fluid-elastic instabilities is lower than in mechanically uncoupled tube rows when the tube row vibration modes are of short wavelength.

The effects of detuning the tubes were also analysed and it was found that detuning increased the critical velocity more when the damping was low; e.g. By detuning the tubes by 10% of their resonance frequencies, the critical velocity was increased by 64% when the damping ratio was $2 \times 10^{-2}$ but the critical velocity only increased by 1.5% when the damping ratio was $2 \times 10^{-1}$.

In their extension of Blevins' theory to two dimensional tube arrays, Whiston and Thomas assumed that the aerodynamic force acting on a particular tube was only influenced by the movement of its immediate nearest neighbours. They also assumed that each tube was a member of both a cross-flow inclined row and a diagonal row, and the differential aerodynamic forces which act on the tube were the vector sums of the forces due to the tube displacement in each type of row. This assumption is only valid for very small amplitude tube vibrations since when a tube in a closely spaced array is displaced the flow field round the tube is changed in a non-linear fashion. Potential flow considerations show that the influence of the different tube boundaries on the flow field is non-linear even for relatively small tube vibrations when the spacing of the tube boundaries is small.

Whiston and Thomas then set up, and solved, the equations of motion for the tubes and calculated the critical flow velocity. They found that the simple stability constant $\beta$ in Connors equation (6.1) became a complicated function of the two dimensional mode shapes of the vibratng tube array.

In order to predict the onset of instabilities in tube arrays the fluid force coefficients for the particular tube row under consideration are required, so Whiston and Thomas used modified fluid force coefficients derived by Blevins. (See section 6.2.2). They calculated the total fluid force coefficients on a tube by linearly superposing the contributions for the force coefficients, derived by Blevins for a single tube row, assuming that the tube was a member of different cross and diagonal tube rows. This assumption, in the view of the author, is invalid since when a tube is in an array of tubes the flow separation points relative to the cross and diagonal rows are different and so separation does not occur at the points of the minimum tube gaps. Blevins based his calculations of the fluid force coefficients on the assumption that separation occurred at the point of the minimum gaps in single tube rows, and so the superposition of Blevins' fluid force coefficents cannot give the force coefficients on a tube inside a tube array. The fluid force coefficents used by Whiston and Thomas are therefore thought to be incorrect, and the author can only assume that the apparent agreement with limited experimental results , claimed by Whiston and Thomas is purely coincidental. The discussions and conclusions of Whiston and Thomas concerning tube arrays can be obtained by reference to their original paper. [6.30]

### 6.2.5 Balsa's model

Balsa [6.2] used a potential flow analysis of the vibrations of cylinders in an array to predict the instability boundary for large amplitude tube vibrations. He applied the method of matched asymptotic expansions of the boundary conditions for each cylinder to obtain the complex velocity potential for each cylinder in terms of a series containing terms of powers of $\varepsilon$ where $\varepsilon$ is the ratio of the cylinder radius to cylinder spacing.

He found that retaining terms up to $\varepsilon^3$ in the expansion, gave a good approximation to the exact solution for two cylinders separated by approximately one tube radius. Hence he concluded that his results were valid for closely packed tube arrays.

Balsa examined the partial stability of a tube row and tube array and derived the following equation for predicting the onset of large amplitude tube vibrations;

$$U_c = \frac{f_o \ell^2}{a U_\infty} \left[\frac{m_o \pi}{3\sigma}\right]^{0.5} , \qquad (6.4)$$

where $\sigma = 2$ for a single tube row and $\sigma = 3$ for square, in-line tube arrays.

In his analysis, Balsa only considered the effect of inertial fluid forces on the cylinders and did not include mechanical damping, which is an important parameter affecting the onset of large amplitude tube vibrations. The potential flow model does not account for flow separation and the wakes of the tubes, which have an important effect on the fluid forces exerted on the tubes. Hence Balsa's model would have to be modified before it could be used to predict the onset of fluid-elastic vibration in full scale tube banks.

### 6.2.6 S.S. Chen's model

S.S. Chen has published several papers [6.7, 6.8, 6.9] in which he analysed the vibrations of a row, or an array of cylinders, using potential theory. However, in his analyses, he only considered the interaction between the cylinders by coupling due to inertial effects. Hence he predicted the added masses of the cylinders due to the presence of neighbouring vibrating cylinders. Chen also assumed that there was no mean flow, so his analyses only apply to cylinders vibrating in a stationary fluid, or in axial flow. No account is taken of flow separation from the cylinders in [6.7, 6.8, 6.9] , and so the models cannot be considered to be representative of the flow situations encountered in operating heat exchangers. However, Chen has contributed to the understanding of fluid inertial coupling effects in tube banks, and also has developed a method of predicting the added masses of the tubes due to flow coupling.

In liquid heat exchangers added mass effects are significant in governing tube vibration levels but in gas heat exchangers where $m/\rho d^2$ is large, added mass effects are not significant. The work of S.S. Chen therefore has little relevance to the problem of predicting the onset of large amplitude vibrations in gas heat exchangers.

### 6.2.7 Lengendre's model

Lengendre [6.20] derived a method of potential analysis for several vibrating objects in a flow. He used conformal mappings, which often gave sets of non-linear integral equations which could only be solved by an iterative process, by approximating the solutions by a series. (The series has not been proved to converge for a general case). An empirical method was used to determine the constants in the approximating series. The method developed assumed that the vibration amplitudes of the objects were small and the fluctuating potentials generated by their vibrations could be linearly superposed on the steady state solution which was obtained by solving a set of integral equations. The method involves the choice of suitable conformal mappings which for a tube with a realistic wake model in the middle of a tube bundle are difficult to derive. The method developed for vibration analysis by Lengendre is therefore very difficult to use for a realistic flow in a tube bank and hence has not been used by researchers studying tube bank vibrations.

### 6.2.8 Roberts' model

Roberts [6.24] originally discovered the jet switching phenomenon whereby the switching of the directions of jets in the wakes of the tubes in a single tube row causes large amplitude tube vibrations. He analysed the situation using a quasi-static method to approximate the unsteady drag on the tubes, and equated the flow energy exciting the tubes to the energy lost by mechanical damping to produce a criterion which has to be satisfied for the occurrence of self excited oscillations in single tube rows.

Roberts' analysis only applied to tubes in a single tube row and therefore cannot be applied directly to predict the onset of large amplitude vibration in tube banks. The occurrence of the jet switching phenomenon in closely packed tube banks has not been observed experimentally, so this mechanism is probably not responsible for the onset of large amplitude vibrations in tube banks.

### 6.2.9 Y.N. Chen's model

Y.N. Chen [6.11] used a vortex shedding model to explain the fluid coupling of tubes in tube banks. A coupled non-linear tube and wake model originally developed by Hartlen and Currie [6.17] was used to explain the relationship between the tube vibration and the lift force. Chen then explained that the lift force is generated by movement of the separation points on the vibrating tubes which leads to a strong swing of the jets between neighbouring tubes.

In the model Chen assumed that the non-dimensional vibration frequency $fd/u$ was very small so that there was sufficient time for the entrainment of the fluid to enable jet switching to occur. Chen empirically derived an equation for the onset of large amplitude tube vibrations, assuming that a high Reynolds number, low Strouhal number and low transverse tube spacing ratio were required to establish large amplitude tube vibrations. He found that his equation (6.5) had a discrepancy of up to ±40% when compared with experiments.

$$\varepsilon \left[ \frac{m_o \delta_o}{\rho d^2} \right]^{-0.6} = 0.35 \times 10^6 \qquad (6.5)$$

where $$\varepsilon = \frac{Re\ D}{St\ X_T}$$

Chen's assumption that jet switching occurs inside tube banks is not realistic since there is not sufficient room for jets to form and coalesce and the jet switching phenomenon has not been observed experimentally under these conditions. Hence it is suggested that the model of Y.N. Chen does not describe the process

by which large amplitude vibrations occur in closely packed tube banks.

### 6.2.10 Model of Tanaka and Takahara

Tanaka and Takahara [6.28] set up the equations of motion for a tube in a tube bundle, taking into account the unsteady forces exerted on the tubes by the vibrations of neighbouring tubes. They then set up a matrix equation for the vibration of 12 tubes in 3 rows of 4 columns and solved the eigenvalue problem to obtain the vibrational modes of the tube bundle. They determined the onset of fluid-elastic vibration by calculating the velocity required to change the sign of the largest eigenvalue from negative, representing a stable mode, to positive representing an unstable mode. Experiments were then conducted to measure the unsteady fluid dynamic forces exerted on the neighbours of a tube which was excited by a vibrator. The amplitude of oscillation of the tube was 0.1 diameter and the experiments were conducted in water at Reynolds numbers between $6 \times 10^3$ and $2.4 \times 10^4$.

The unsteady forces were Fourier analysed and the amplitudes and phases relative to the phase of the vibrating tube were calculated for each Fourier component. They found that the fluid dynamic forces were functions of the reduced velocity in the tube bundle, and that the phase difference between the vibrating cylinder and the fluid forces on its neighbour remained large, even at the highest reduced velocity investigated.

Experimentally measured critical velocities were compared with the theoretically predicted critical velocities, using the experimentally measured force coefficients in the solution of the eigenvalue problem. It was found that there was good agreement between experiments and theory.

Tanaka and Takahara then analysed the effect of varying $m/\rho d^2$ on the critical velocity and found that it was increased as $m/\rho d^2$ increased, and was also a function of tube damping; high dampings gave high critical velocities. The effects of detuning the tubes were examined and it was found that the critical velocity, in general, increased with increasing tube

damping, and that the ratio of the critical velocities was given by equation (6.6)

$$\frac{V_{c\ det}}{V_{c\ tun}} = \left[\frac{\delta_{tun}}{\delta_{det}}\right]^{0.5} \qquad (6.6)$$

The major drawback of using the theory of Tanaka and Takahara is that the unsteady fluid force coefficients have to be measured experimentally in order to predict the onset of large amplitude tube vibrations.

The unsteady fluid forces measured on tubes in symmetrical positions next to a central tube appear to differ at some flow velocities which implies that the coupling between tubes in nominally the same positions is different. This suggests that the vibration of a tube does not always have a direct linear effect on the flow field and hence on the forces exerted on the neighbouring tubes. Hence a linear superposition of the individual forces created by coupling between pairs of tubes via the flow field may not always be valid for all flow regimes, particularly when the tubes are executing large amplitude vibrations. (i.e. 0.1 diameter).

It is clear from the measurements carried out by Tanaka and Takahara, that the fluid force coefficients are a strong function of flow velocity, and depend on the relative positions between the different tube pairs. The fluid force coefficients are therefore probably a function of the tube bank geometry. Hence in order to use Tanaka and Takahara's prediction scheme much experimental work has to be carried out in measuring the unsteady forces on tubes for different flow regimes and different tube bank geometries. Therefore the scheme cannot be used to predict the onset of large amplitude tube vibrations in arbitrary tube banks at the present time.

## 6.3 Discussion of the Modelling of Flow in Tube Rows and Tube Banks.

In section 6.2 the shortcomings of some of the current models for predicting the onset of large tube vibrations in tube rows and tube banks were discussed.

From the experimental results discussed in Chapters 4 and 5 it is apparent that the separation points on tubes in single tube rows and tube banks does not always occur at the point of the minimum gap between neighbouring tubes. The experiments discussed in Section 4.3 showed that as a tube is statically displaced from a uniformly spaced position in a tube row the stagnation and separation points shift round the tube. Hence quasi-static models using the Bernoulli equation to calculate the lift and drag forces on tubes, assuming that separation occurs at the minimum gap, are not representative of the flow situations encountered in all tube banks.

It was therefore decided that a better approach would be to use a potential flow model with some provision included to model the tube wakes. Wake models are required because the potential flow solution round a circular cylinder is not a good approximation to the flow round a tube where separation occurs between $80^{\circ}$ and $140^{\circ}$ depending on the tube bank geometry and flow velocity.

The model developed during the present research project was not intended to be a fully developed model to predict the onset of large amplitude tube vibrations, but was intended to be used to investigate the effects of tube displacement in a tube row on the pressure distribution round the tubes. In addition the influence of the tube wakes on the lift and drag coefficients was to be investigated. The model therefore had to be sufficiently adaptable to model arbitrary tube wakes using free streamlines, so the use of conformal mapping techniques was therefore too complex to implement.

The solution of 3 dimensional potential flow problems was impractical with the computing resources available so the model which was developed could not take into account variations of the flow field along the spanwise axes of the tubes. It was therefore decided to develop a computer programme to solve 2 dimensional potential flow problems with shapes of arbitrary cross-section and with arbitrary boundary conditions.

Initially a program to solve Laplace's equation for 2 dimensional arbitrary shaped objects in a potential flow was written using finite difference techniques. It was found that the convergence times for the solution of the problems by

iteration were greater than 2000 seconds of C.P.U. time on an ICL 2970 computer when a 100 x 100 grid of points was used. Various techniques to accelerate convergence were tried, including over-relaxation and alternating - direction - implicit methods [6.14, 6.29] but convergence times for a more refined grid, required to obtain accurate solutions, were still too large to implement on the ICL 2970. The finite difference method was therefore abandoned and a feasibility study of the use of finite elements techniques to calculate the potential flow solution was carried out. It was found that finite element solutions would require the use of large numbers of elements and large matrices which would render the technique impractical for modelling a tube bank on the ICL 2970. (The use of other larger computers was not considered since funding was not available).

The boundary element technique used for the solution of 2 dimensional potential flow problems was investigated and it was found that the solution of problems with up to 10 tubes in a flow would be possible.

The boundary element technique has the following advantages over finite difference and finite element techniques used for the solution of potential problems. [6.6]

(i) A smaller amount of data is required to represent the potential field since only the boundaries have to be specified. (In finite difference and finite element methods the whole region has to be represented by nodal points and elements respectively). Hence the systems of equations generated by boundary element solutions are smaller so solution time is less than for finite element or finite difference methods.

(ii) The numerical accuracy of the boundary element technique is generally greater than that of the finite element technique.

(iii) Boundary elements can be used to solve problems in infinite domains whereas finite difference or finite element techniques can only solve problems in finite bounded regions.

A computer program was written to calculate the pressure distributions round tubes in a 2 dimensional potential flow using the boundary element technique. A description of the method of solution is given in the following section.

## 6.4 Solution of Potential Problems using the Boundary Element Technique.

### 6.4.1 Formulation of the method

The formulation of the boundary element method has been carried out by other authors [6.6, 6.18, 6.27] but it is reproduced here for completeness.

The solution of 2 dimensional potential flow problems is expressed formally as the solution of Laplace's equation (equation 6.7) in 2 dimensions with specified boundary conditions.

$$\nabla^2 \phi = \frac{\partial^2 \phi}{\partial x^2} + \frac{\partial^2 \phi}{\partial y^2} = 0 \qquad (6.7)$$

In two dimensional potential theory Green's third identity can be written in the form,

$$\int_L \phi'(\bar{q}) \log |\bar{q}-\bar{p}| \, d\bar{q} - \int_L \phi(\bar{q}) \log' |\bar{q}-\bar{p}| \, d\bar{q} = \Omega(\bar{p})\phi(\bar{p}) \qquad (6.8)$$

for a closed domain D bounded by an external boundary $L_E$ and containing closed boundaries $L_C$ which contain no cusps or cuts. (L denotes $L_C$ and $L_E$). $\bar{p}$ and $\bar{q}$ are vectors specifying points in the x - y plane and points on the boundaries. The prime denotes differentation at the point $\bar{q}$ along the normal to the boundary directed into the region exterior to the $L_C$ boundaries and into the region interior to the $L_E$ boundary. $d\bar{q}$ is the differential increment on the boundaries $L_C$ and $L_E$ at $\bar{q}$.

If $\bar{p}$ is in the closed domain D then $\Omega(\bar{p}) = 2\pi$ and if $\bar{p}$ is on the boundaries $L_E$ or $L_C$ then $\Omega(\bar{p})$ is equal to the internal angle between the tangents to the boundary $L_C$ or $L_E$ on either side of $\bar{p}$.

Equation (6.8) therefore describes a linear relationship between the boundary values and their normal derivatives which satisfy equation (6.7). Hence, if either the potentials or normal derivatives of the potentials at all the boundaries are specified then a set of linear integral equations can be solved to obtain the complementary unknown boundary conditions.

In general the integral equation (6.8) has a unique solution but when only $\phi'$ is specified on all the boundaries (an interior Neumann problem) the condition

$$\int_L \phi'(\bar{q})\, d\bar{q} = 0 \qquad (6.9)$$

must be satisfield and the solution of $\phi$ is not unique, since an arbitrary constant can be added to it and equation (6.9) is still satisfield. The arbitrary constant can be eliminated by prescribing both the potential and normal derivative of potential on just one of the boundary elements and this is done in the computer implementation used here.

Another condition where there is not a unique solution to the problem is given where

$$\int_\Gamma \lambda(\bar{q}) \log |\bar{q}-\bar{p}| d\bar{q} = 0 \qquad (6.10)$$

and $\lambda(\bar{q})$ is a non trivial function with $\bar{q}$ on the boundary $\Gamma$. When this condition occurs and $\phi$ is specified on the boundary the solution for $\phi'$ is not unique. However problems caused by this condition can be removed by changing the scale of the domain D so that the condition in equation (6.10) no longer exists.

### 6.4.2 Discretization of the equations

The equation used to obtain a solution to Laplace's equation described in section 6.4.1 is discretized by dividing the boundaries into N smooth intervals so that changes in the boundary conditions occur at the divisions between one interval and the next. $\phi$ and $\phi'$ are then approximated by constants in each interval. Equation (6.8) then becomes

$$\sum_{j=1}^{N} \phi'_j \int_j \log|\bar{q}-\bar{q}_i| d\bar{q} - \sum_{j=1}^{N} \phi_j \int_j \log'|\bar{q}-\bar{q}_i| d\bar{q} - \Omega(\bar{q}_i)\phi_i = 0 \qquad (6.11)$$

$$i = 1, 2, \ldots\ldots N.$$

where $\bar{q}_i$ are the vectors to the nodal points i and $\Omega(\bar{q}i) = \pi$ when the boundary passes smoothly through $\bar{q}_i$. $\int_j$ denotes integration over the $j^{th}$ interval of the boundaries L.

Equation (6.11) is a system of simultaneous linear algebraic equations whose solution gives an approximation for $\phi(\bar{p})$ in the domain D. The approximation for $\phi(\bar{p})$ in equation (6.8) is given by

$$\phi^N(\bar{p}) = \frac{1}{\Omega(\bar{p})} \sum_{j=1}^{N} (\phi_j' \int_j \log|\bar{q}-\bar{p}|\, d\bar{q} - \phi_j \int_j \log'|\bar{q}-\bar{p}|\, d\bar{q}) \qquad (6.12)$$

For a Neumann problem, where only the normal derivatives are specified, an additional equation is required to produce a unique solution and this is given by equation (6.13)

$$\phi_k = \text{constant} \qquad (6.13)$$

where k is any integer between 1 and N. The N + 1 discretized equations can then be solved by the method of least squares see 6.31

### 6.4.3 Evaluation of the integrals

The integrals in equation (6.11) have to be evaluated for every nodal point. The formulae given in equations (6.14) and (6.15) are used for evaluating the integrals involving the logarithmic kernel and the normal derivative of the logarithmic kernel respectively, when i=j. See | 6.18 |

$$\int_{j=1} \log|\bar{q}-\bar{q}_i| \, d\bar{q} = a \cos\gamma(\log a - \log b) + h \log(b-1) + a\psi \sin\theta, \qquad (6.14)$$

where a, b, $\gamma$ and $\psi$ are defined in Figure 6.1.

$$\int_{j=i} \log'|\bar{q}-\bar{q}_i| \, d\bar{q} = \kappa(\bar{q}_i) \qquad (6.15)$$

where $\kappa(q_i)$ is the angle through which the vector $\bar{q}-\bar{q}_i$ rotates when $\bar{q}$ describes the $j^{th}$ interval keeping the domain D on the left.

When i = j a singularity is produced in the logarithmic kernel and the formulae given in equations (6.16) and (6.17) are used to evaluate the integrals of the logarithmic kernel and its normal derivative. See |6.18|

$$\int_{j=1} \log|\bar{q}-\bar{q}_i| \, d\bar{q} = h \log(h-1), \qquad (6.16)$$

where h is defined in Figure 6.1.

$$\int_{j=1} \log'|\bar{q}-\bar{q}_i| \, d\bar{q} = \pi \qquad (6.17)$$

### 6.4.4 Representation and solution of the integral equations on the computer

Each integral over a single boundary element, when evaluated, becomes a single term in a set of algebraic linear

simultaneous equations. The linear equations can be manipulated so as to express them in the form $\hat{G}\hat{X} = \hat{B}$ where $\hat{B}$ is the column vector of the known potentials or their normal derivatives, $\hat{X}$ is the column vector of the complementary unknown potentials or their derivatives and $\hat{G}$ is a matrix containing the numerically evaluated integrals of the logarithmic kernels and their derivatives. See [6.6] . $\hat{G}$ can be thought of as a transfer matrix between the known and unknown boundary conditions and hence each element in $\hat{G}$ is effectively an element in a transfer matrix.

The solution of the matrix equation for Neumann problems can be obtained by the method of least squares. However for large problems the matrix can become ill-conditioned so it is always necessary to check the conditioning of the matrix $\hat{G}$ before the solution is assumed to be correct. When the matrix $\hat{G}$ is ill-conditioned it is sometimes possible to shuffle the rows of the matrix to reduce ill-conditioning, but for some problems the only method of solution is to increase the precision of the matrix solution routine which increases solution time, often rendering the problem insoluble when computing resources are limited.

### 6.4.5 Brief description of the programme

A Fortran programme was written to set up a system of boundary elements representing tubes in potential flow and then form and solve the discretized integral equations to obtain a potential solution from which the pressure coefficients round the tubes were calculated. Block diagrams showing the main features of the programme are given in Figures 6.2 to 6.12 and the listing of the computer programme is given in Appendix 2.

The normalized co-ordinates of the boundary elements for the different tube models are stored in a data file which is input by a subroutine which calculates the positions of the elements in the flow field when the tube centre co-ordinates are specified. Hence, each time the position of a tube is changed in the flow field only the new centre co-ordinates have to be specified. The integrals of the logarithmic kernels and their derivatives are then evaluated and the matrix equation set up.

During the solution of the matrix equation the conditioning of the matrix is calculated and output so that a degree of confidence can be given to the results. The potentials round the tubes are used to calculate the pressure coefficients and lift and drag for each tube; these are printed out and can be plotted on the line printer or on a graph plotter.

A facility for setting the normal boundary conditions of the tubes to be non-zero was included in the programme so that tube motion could be simulated. However this facility was not used in the present investigation since fluid intertial effects produced by $\phi' \neq 0$ on the tube boundaries were not to be investigated in the research project.

In all the runs of the computer programme after it was tested the X boundary lengths were 1000 units and the Y boundary lengths 400 units, for the outer boundaries of the flow field. 20 equally spaced refined elements were used on each X boundary between X = 400 and X = 600 to improve the potential approximations near the vicinity of the tube boundaries and the rest of each X boundary was divided into 20 equally spaced elements. 20 equally spaced elements were used on eachY boundary and the normal derivatives of potential on the X = 0 and X = 1000 Y boundaries were set to 1 and -1 respectively to produce a normalized flow velocity of unity. All other normal boundary conditions were zero and the number of elements representing each tube was dependent on the tube model used.

### 6.4.6 Verification and checking of the programme

There are very few analytic results for the pressure coefficient round tubes in a bounded flow field. Hence only limited comparisons of the results produced by the boundary element computer programme with analytic results can be carried out.

The pressure coefficient round a single cylinder in a confined potential flow in the centre of a channel is given by, (see [6.1, 6.19, 6.25])

$$C_p(\theta) = 1 - 4\left[1 - \frac{\pi^2 (D/W)^2}{12 - \pi^2 (D/W)^2}\right]^2 \sin^2\theta \qquad (6.18)$$

where $\theta$ is the angle from stagnation round the cylinder of diameter D in the centre of a duct width W.

The pressure coefficients round the circumference of a single cylinder of diameter 30 units with boundary elements spaced at $10^{o}$ intervals round the circumference when the cylinder was in confined flow with centre co-ordinates (i) X = 400, Y = 200; (ii) X = 450, Y = 200 and (iii) X = 500, Y = 200 were calculated using the computer and compared with the expression in equation (6.18). It was found that the r.m.s. discrepancies of the pressure coefficients were (i) 0.039, (ii) 0.042 and (iii) 0.043 respectively. The same test cases were run with 40 refined elements on the X boundaries to determine whether the use of more elements on the external boundary near the vicinity of the cylinder would improve the accuracy of the computer solution. It was found that the r.m.s. errors were (i) 0.039, (ii) 0.043 and (iii) 0.044 respectively. Hence doubling the number of refined elements on the X boundary did not improve the solution. A further check was carried out to determine whether the number of elements on the X boundary was sufficient to give an accurate solution when a tube was near the X boundary. This was achieved by calculating the pressure coefficients round two tubes next to each other in the centre of the flow field (co-ordinates X = 500, Y = 170 and X = 500, Y = 230) and comparing the solution the equivalent image solution of a single tube co-ordinates X = 500, Y = 170 next to the upper X boundary which was changed to lie along the straight line Y = 200. It was found that the r.m.s. difference in pressure coefficients between the two solutions was 0.004. Hence it was concluded that the representation of the boundaries was sufficient to obtain pressure coefficients with r.m.s. errors of approximately 0.04 for tubes with elements spaced at $10^{o}$ intervals round their circumferences. It was found that the arrangement of boundary elements on the external boundaries as described in Section 6.4.5 was the best compromise between keeping the number of elements down to a minimum (to reduce solution time), and producing accurate solutions.

The effect on the accuracy of the solution of increasing the number of elements on a single cylinder with centre

co-ordinates X = 500, Y = 200 in a confined flow was investigated. It was found that the r.m.s. error in the pressure coefficient was approximately 0.044 for cylinders with elements spaced at angular intervals of $20^{o}$, $10^{o}$ and $5^{o}$ round the cylinder. Hence increasing the number of elements on the cylinder boundaries does not increase the accuracy of the solution significantly.

Figures 6.17a, b show the pressure coefficients and components of lift and drag round a cylinder with boundary elements spaced at $10^{o}$ and $5^{o}$ intervals round the circumference when the cylinders are in the centre of the flow field.

## 6.5 The Tube Models

Several tube models were used in the investigation of the change in pressure distribution round a tube displaced in a tube row, and in a tube bank, using the boundary element method.

The co-ordinates of the tube models were partly generated automatically by special purpose computer programmes and partly by manually inputting the co-ordinates of the boundary elements in the tube models into a file. For all the models which included separation and wake models it is assumed that the wake was a region of 'dead' flow (i.e. the wake had no circulation in it). This assumption was shown to be reasonable since agreement with experiments was achieved when the wake pressure was predicted for a cylinder in confined flow using the finite element technique. [6.1]. However this assumption may not be generally true for flows in tube banks. It is also assumed that the normal derivatives of the velocity potentials along the wake model streamlines are zero which is true, since by definition, there is no flow across streamlines. Experiments show that the pressure between the separation points round the back of a circular cylinder is almost constant as a function of angle round the cylinder. In order to achieve a constant pressure between the separation points the pressures just after both separation points must be equal. The pressure round the tube on the wake region is not actually calculated directly from the potential flow solution since there are no boundary elements round the tube in the wake region between the separation points. Therefore the wake pressure can only be estimated from the calculated pressures at the points just before

separation. If the pressure distribution round the tube and its wake model is calculated and assumed to be correct, the only method of achieving a constant wake pressure is to average the pressures at the points just before separation. Hence, the wake pressure for all the tube models including separation is assumed to be the average of the pressures on the tube just before the separation points.

A brief description of the various tube models is given below:-

(i) Two circular cylinder tube models with boundary elements spaced at equal angular intervals of $20^{o}$ and $10^{o}$ were designed with no separation streamlines and no wake models, and are shown in Figures 6.13a-b.

(ii) Two tube models both with boundary elements spaced at angular intervals of $10^{o}$, but one with a courser wake model were designed with separation streamlines occurring at $80^{o}$ from the stagnation point. The shapes of the separation streamlines were obtained from the theory of Parkinson and Jandali [6.23] who assumed that the tube was in an infinite free stream. The wake was assumed to be approximately 10 tube diameters in length. (i.e. large compared to the diameter of the tube). The arrangement of boundary elements in these models is shown in Figures 6.14a-b.

(iii) Two tube models with boundary elements spaced at angular intervals of $20^{o}$ and $10^{o}$ containing wake models suggested by Whiston and Thomas [6.30] for a tube in a 1.4 diameter pitch triangular tube bundle in the supercritical flow regine, were designed. The arrangement of boundary elements in the models is given in Figures 6.15 a-b.

(iv) Two tube models were designed to represent the flow round a tube in the dynamically modelled tube bank used in the experiments of the present investigation. The models with elements spaced at angular intervals of $20^{o}$ and $10^{o}$ respectively each have separation points occurring at $140^{o}$ from the front of the tube. The positions of the wake streamlines were empirically estimated. Figures 6.16 a-b show the arrangement of the boundary elements in the tube models.

The addition of new tube models can be carried out quite simply by inputting the co-ordinates of their boundary elements into the tube model data file.

## 6.6 Single Tube Row Model (One Tube With a Wake Model)

### 6.6.1 Description of model and investigation

Figure 6.18 shows the arrangement of the six uniformly spaced tubes in the tube row model, which contains 280 boundary elements, in total. Only one tube has a wake model which is shown in Figure 6.14 b. The pressure coefficients and components of lift and drag were calculated round the tube with a wake model when it was displaced in the cross-flow and streamwise directions. The lift and drag coefficients of the displaced tube were also calculated by integrating the appropriate components of the pressure coefficient round the circumference of the tube.

### 6.6.2 Results for a tube displaced in the cross-flow direction

Figures 6.19 i-vi show the variation of the pressure coefficients with angle from the front of the tube displaced in the cross-flow direction. Figures 6.20 and 6.21 show the lift and drag on the tube as a function of its displacement in the cross-flow direction.

The pressure coefficient just before the separation point in the smaller gap (between the displaced tube and its neighbours) decreases with increasing tube displacement, and decreases more rapidly at higher displacements. In the larger gap the pressure coefficient just before the separation point increases slightly with increasing displacement. The wake pressure therefore increases with displacement causing the drag on the tube to increase. The increase in drag is more rapid at higher tube displacements and is a non-linear function of tube displacement over the entire range investigated.

The asymmetry of the pressure distribution round the tube (about a diametric line parallel to the mean flow), with a lower pressure in the smaller gap, produces an increase in lift with tube displacements which is more rapid at higher displacements. The effect of displacing a tube in the tube

row model is therefore to produce a destabilizing lift force which increases with displacement. The variation of lift with displacement is almost linear for displacements up to 0.3 diameters; the correlation coefficient for a least squares fit is 0.9997.

At high tube displacements the stagnation point moves round the tube towards the position of the smaller gap.

### 6.6.3 Results for a tube displaced in the streamwise direction

Figures 6.22 i-vi show the variation of the pressure coefficients with angle from the front of a tube displaced in the streamwise direction. Figures 6.23 and 6.24 show the lift and drag on the tube as a function of its displacement in the streamwise direction.

As the tube is displaced downstream the pressure coefficient curve becomes more asymmetrical, with a lower pressure in the gap nearer to the Y = 400 flow border. The asymmetry can be explained by the fact that the tube is not in the centre of the flow field so the influence of the different numbers of tubes on each side of the displaced tube, and the influence of the two streamwise boundaries on the velocity potential, and hence on the pressure on the tube, produces an asymmetrical pressure distribution which varies with the displacement of the tube. This produces an increase in lift with downstream displacements. As the tube is displaced upstream the pressure coefficient curve becomes more symmetrical and the lift decreases with increasing upstream displacement. The lift is almost a linear function of streamwise displacement over the entire displacement range investigated; the correlation coefficient for a least squares fit is 0.9994.

When the tube is displaced downstream the wake pressure at first decreases, producing an increase in drag. Above displacements of 0.2 diameters the wake pressure increases with displacement producing an decrease in drag with displacement. When the wake is displaced upstream the wake pressure increases with displacement throughout the range investigated and hence the drag decreases with upstream displacement.

## 6.7 Single Tube Row Model (Three Tubes With Wake Models)

### 6.7.1 Description of model and investigation

Figure 6.25 shows the arrangement of the 6 uniformly spaced tubes in the tube row model, which contains 340 boundary elements. Three of the tubes have wake models. The pressure coefficients and components of lift and drag were calculated round the displaced tube with a wake model (as shown in Figure 6.15b) positioned between the other two tubes with wake models. (As shown in Figure 6.15a). The lift and drag coefficients of the displaced tube were also calculated by integrating the appropriate components of the pressure coefficient round the circumference of the tube. Only tube displacements in the cross-flow direction were investigated using this model.

### 6.7.2 Results for a tube displaced in the cross-flow direction

Figures 6.26 i-vi show the variation of the pressure coefficients with angle from the front of the tube displaced in the cross-flow direction. Figures 6.27 and 6.28 show the lift and drag on the tube as a function of its displacement in the cross-flow direction.

The asymmetry of the pressure distribution increases with displacement. The pressure coefficient in the larger gap decreases with displacement, and in the smaller gap increases with displacement, which produces a decrease in lift force. The lift force is negative and is therefore a stabilising force and increases almost linearly with tube displacement. (The correlation coefficient for a least squares fit is 0.998).

The wake pressure increases with displacement and increases more rapidly at higher displacements. Hence the drag decreases with displacement and more rapidly at higher displacements. The drag is therefore a non-linear function of tube displacement in the cross-flow direction.

Increasing the tube displacement produces a shift in the stagnation point round the tube towards the position of the smaller gap.

## 6.8 Discussion of Results for a Single Tube Row

The two different tube row models produce different variations of the lift and drag with tube displacement. It is therefore deduced that the type of wake models used in modelling the tubes in a tube row is an important factor governing the variation of the force acting on a tube with different tube displacements. It should be noted that only the wake models of the two neighbours of the displaced tube were changed between the models discussed in Sections 6.6 and 6.7 and hence the force on a tube is significantly affected by the wakes of its neighbours.

Both models give wake pressures which are high compared to the experimental results discussed in Section 4.3 so it is concluded that the wake models used are not sufficiently realistic to produce agreement with experiments. The approximation of the wake by a 'dead' flow region is probably not a good approximation since the wake of a tube in a gas cross-flow is not a region of 'dead' flow and can have considerable velocity gradients between the separation shear layers. See [6.26]. The flow in a real tube wake can therefore considerably change the pressure acting on the downstream side of the tube.

The lift coefficient in general becomes more negative with increasing tube displacement in the cross-flow direction for the experimental results discussed in Section 4.3. The tube row model which the neighbours of the displaced tube also have wake models produces a negative lift which increases with the displacement, and hence this is a better model than the tube row model in which one tube has a wake model, which produces a positive lift which increases with tube displacement. The variation of lift and drag with tube displacement produced by both computer tube row models does not agree with experiments. The shift in separation points and the occurrence of laminar separation and turbulent reattachment observed experimentally and discussed in Section 4.3 are not modelled in the computer tube row model so agreement between experiments and the models is not expected. However, both models produce a shift in the stagnation point towards the smaller gap between the displaced tube and its neighbours which is in agreement with experiments. (See Section 4.3).

## 6.9 Equilateral Triangular Pitched Tube Bank Model

### 6.9.1 Description of model and investigation

Figure 6.29 shows the arrangement of tubes in the equilateral triangular pitched tube bank model (pitch 1.4 diameters) which contains 372 boundary elements. A tube with a wake model as shown in Figure 6.15b is surrounded by four tubes with wake models as shown in Figure 6.15a and the outer four tubes do not have wake models. (See Figure 6.13a). The tube bank model was positioned in the centre of the field and the central tube was displaced by 0 to 0.2 tube diameters from its mean position. The pressure coefficients and components of lift and drag were calculated as a function of angle for each tube displacement. The lift and drag coefficients for the displaced tube were also calculated by integrating the lift and drag components of the pressure coefficients round the circumference of the tube.

### 6.9.2 Results and discussion

Figures 6.30 i-v show the variation in pressure coefficient with angle from the front of the tube when the tube is displaced in the cross-flow direction. Figures 6.31 and 6.32 show the lift and drag on the tube as a function of tube displacement in the cross-flow direction.

At zero tube displacement the pressure distribution round the tube is symmetrical with large differences between the wake pressure and the pressure minima (which occur at $90^{o}$ and $270^{o}$ from the front of the tube); the minimum pressures and the wake pressure are a factor of approximately 5 different. As the tube displacement is increased the pressure in the larger gap increases, and in the smaller gap decreases, to produce a high degree of asymmetry in the pressure distribution round the tube. The asymmetry produces a large increase in the lift coefficient which is approximately a factor of 8 greater than that produced by the single tube row model discussed in Section 6.6 for a displacement of 0.2 diameters. The lift on the tube is a destabilizing force, is also a non-linear function of displacement, increasing

more rapidly at higher displacements.

The wake pressure decreases with tube displacement producing an increase in the drag coefficient, which is also a non-linear function of tube displacement, increasing more rapidly at higher displacements.

Hence for the equilateral triangular pitched tube bank model the lift and drag forces acting on a tube are both non-linear functions of tube displacement; therefore, in general, it seems likely that assumption of linearity between the force and displacement used in some models is not always true.

## 6.10 Staggered Tube Bank Model (Transverse Pitch Ratio, 1.043; Longitudinal Pitch Ratio, 1.023)

### 6.10.1 Description of the model

Figure 6.33 shows the arrangement of the nine tubes in the tube bank model which contains 386 boundary elements. The central tube with a wake model as shown in Figure 6.16b is surrounded by four tubes with wake models as shown in Figure 6.16a. The outer four tubes do not have wake models and have boundary elements arranged as shown in Figure 6.13a. The model has the same transverse and longitudinal pitch ratios (1.043 and 1.023 respectively) as the dynamically modelled tube bank used in the experiments discussed in Chapter 5 and is positioned in the centre of the flow field. The pressure coefficients and components of lift and drag were calculated round the tube and the lift and drag calculated when the central tube was in its mean position in the tube bank.

### 6.10.2 Results and discussion

Figure 6.34 shows the variation of the static pressure coefficients with angle from the front of the central tube The pressure distribution round the tube is symmetrical with the minimum pressures occurring at $70^{o}$ and $290^{o}$ from the front of the tube, which is in agreement with the experiments discussed in Chapter 5. (See Figure 5.12i). Results from the computer model cannot be compared directly with the experimental results

since only nine tubes were used in the model, which changes the blockage ratio in the flow field, and hence changes the magnitudes of the pressure coefficients. However, the general shape of the pressure coefficient curves are similar in the regions of the pressure minima, but the pressure coefficients and wake pressure of the tube in the model are larger than those measured experimentally. Hence, if a more realistic model is required the number of tubes in the model should be increased, and a more realistic wake model which does not assume the wake is a region of 'dead' flow should be used.

## 6.11 Conclusions for Sections 6.6 to 6.10

(i) It has been shown that the pressure distribution round a tube is significantly affected by the type of wake models used on neighbouring tubes. Hence realistic models of the flow in the wakes of tubes in tube rows and tube banks are required if the steady forces on the tubes are to be predicted successfully.

(ii) In the simple wake models used in the present investigations it is assumed that the wake is a region of 'dead' flow. The difference between experimental results and the models show this assumption not to be valid for tubes in a gas cross-flow. Hence a more sophisticated wake model is required if the forces acting on tubes in tube rows and tube banks are to be predicted.

(iii) Two different models of a single tube row gave different variations of the lift and drag forces acting on a displaced tube. A tube row model using only one tube with a wake model produced a destabilizing (positive) lift force on a displaced tube, whereas a tube row model with wake models on neighbouring tubes produced a stabilizing (negative) lift force on a displaced tube. Hence it is concluded that some wake structures in tube rows produce a stabilizing lift force as reported in Section 4.3, and others produce a destabilizing lift force as reported by Connors [6.12]. Hence the onset of fluid elastic

vibrations is dependent on the way the wake structure of a tube changes with displacement.

(iv) The lift and drag forces acting on tubes in a single tube row have been shown to vary with tube displacements in both the cross-flow and streamwise directions. In general the variation of the forces is not a linear function of tube displacement.

(v) It was found that for both single tube row models the lift force was a linear function of the tube displacement in the cross-flow direction.

(vi) The lift was a linear function and the drag a non-linear function of the tube displacement in the streamwise direction for the tube row model containing only one tube with a wake model.

(vii) The drag force on a tube is a non-linear function of its displacement in the cross-flow direction for both single tube row models.

(viii) The tube row models gave a shift in the stagnation point towards the smaller gap between a displaced tube and its neighbours. This is in agreement with experimental results.

(ix) The lift and drag forces on a displaced tube in an equilateral triangular pitched tube bank were found to be non-linear functions of the tube displacement in the cross-flow direction. This implies that in general the lift and drag forces acting on a tube in a tube bank cannot be assumed to be linear functions of tube displacement.

(x) The tube bank computer model of the dynamically modelled tube bank produced pressure coefficients which were not in agreement with experiments. However the troughs of the pressure coefficient curves were similar in shape to those measured experimentally.

## 6.12 Summary

Several investigators have developed models to predict the onset of large amplitude tube vibrations in tube rows and tube banks. Some of the models agree with limited experimental

measurements but are not generally applicable to most tube rows and tube banks. There is no successful scheme for predicting the onset of large amplitude tube vibrations in tube banks with different geometries subjected to different flow conditions.

Current models assume that the lift and drag forces acting on tubes in a tube row or tube bank are linear functions of tube displacement. This assumption has been shown not generally to be true using potential flow models with free streamlines to represent the tube wakes. Several models also assume that the displacement of a tube only affects the force acting on it in a direction perpendicular to the displacement. This assumption is not in agreement with the results from the models developed in the present investigation (and also with experimental results).

The computer models developed in the present research project are not in agreement with experiments but show that correct modelling of the wake structure is necessary if the forces acting on tubes are to be predicted successfully.

It is therefore suggested that new models which are developed to predict the onset of large amplitude tube vibrations in tube banks, should take into account the variations of the forces in both the direction perpendicular to, and in the same direction as the tube displacement (which are not necessarily linear functions of tube displacement) and should also use realistic wake models in order to predict the forces acting on the tubes.

## 6.13 References


6.1 H.B. AWBI and J.H. SWANNEL 1974 "Finite Element Methods in Flow Problems". Huntsville, Alabama, U.S.A.: University of Alabama. U.S.A. Editor J.T. ODEN et al, pp 209-224. "A finite element solution of confined flow over a circular cylinder".

6.2 T.F. BALSA 1977 Journal of Sound and Vibration 50(2) pp 285-303. "Potential flow interactions in an array of cylinders in cross-flow".

6.3 R.D. BLEVINS 1974 Journal of Pressure Vessel Technology. Transactions of A.S.M.E. Series J, Vol 96 pp 263-267. "Fluid elastic whirling of a tube row".

6.4 R.D. BLEVINS 1977 Journal of Fluids Engineering. Transactions of A.S.M.E. Series I, Vol 99, pp 457-460 "Fluid elastic whirling of tube rows and tube arrays".

6.5 R.D. BLEVINS 1979 Proceedings of Third National Congress on Pressure Vessel and Piping Technology held at San Fransisco, U.S.A. 25-29 June 1979. "Flow induced vibrations". New York: A.S.M.E. pp 35-40. "Fluid damping and the whirling instability of tube arrays".

6.6 C.A. BREBBIA 1978 "The Boundary Element Method for Engineers". London: Pentech Press.

6.7 S.S. CHEN 1975 Nuclear Engineering Design, vol 35 pp 399-422. "Vibrations of nuclear fuel bundles".

6.8 S.S. CHEN 1975 Journal of Engineering for Industry. Transactions of A.S.M.E. Series B, Vol 97, pp 1212-1218. "Vibrations of a row of circular cylinders in a liquid".

6.9 S.S. CHEN 1977 Journal of Fluids Engineering. Transactions of A.S.M.E. Series I, Vol.99, pp 462-467. "Dynamics of heat exchange tube banks".

6.10 S.S. CHEN 1980 Shock and Vibration Digest, vol 12, pp 21-34. "Cross-flow-induced instabilities of circular cylinders".

6.11 Y.N. CHEN 1974 Journal of Engineering for Industry. Transactions of A.S.M.E. Series B Vol 96, pp 1065-1071. "The orbital movement and the damping of the fluidelastic vibration of tube banks due to vortex formation. Part 2 - Criterion for the fluidelastic orbital vibration of tube arrays".

6.12 H.J. CONNORS Jnr. 1970 Proceedings of A.S.M.E. Winter Annual Meeting held in New York, U.S.A., 1 December 1970. Flow-Induced Vibrations in Heat Exchangers. pp 42-56. "Fluidelastic vibrations of tube arrays excited by cross flow".

6.13 H.J. CONNORS Jnr. 1978 Journal of Mechanical Design. Transactions of A.S.M.E. Series L, vol 100 pp 347-353. "Fluidelastic vibration of Heat Exchanger Tube Arrays".

6.14 G.E. FORSYTHE and W.R. WASOW 1967 "Finite difference methods for partial differential equations". New York: John Wiley and Sons.

6.15 R.E. FRANKLIN and B.M.H. SOPER 1977 Heat Transfer and Fluid Flow Services. A.E.R.E. Harwell and National Engineering Laboratory Report No. HTFS RS192. "An investigation of fluidelastic instabilities in tube banks subjected to fluid cross flow.

6.16 H.G.D. GOYDER 1980 Proceedings of the International Conference on Recent Advances in Structural Dynamics held at University of Southampton, U.K. 7-11 July 1980. Paper 39. "Unstable vibrations of a bundle of cylinders due to cross flow".

6.17 R.T. HARTLEN and I.G. CURRIE 1970 Journal of Engineering Mechanics Division. Proceedings of A.S.M.E., EM5 pp577-591. "Lift-oscillator of Vortex Induced Vibration".

6.18 M.A. JAWSON and G.T. SYMM 1977 "Integral equation methods in potential theory and electrostatics". London: Academic Press.

6.19 N.E. KOCHIN, I.A. KIBEL and N.V. ROZE 1962 "Theoretical hydromechanics". New York: Interscience, John Wiley.

6.20 R. LENGENRE 1980 La Recherche Aerospatiale No. 1980-1, pp1-8. "Vibrations de plusieurs obstacles au sein de c'ecoulement plan d'un fluid incompressible". (In French).

6.21 D.J. MEAD 1973 Journal of Sound and Vibration 27(2) pp235-260. "A general theory of harmonic wave progagation in linear periodic systems with multiple coupling.

6.22 M.P. PIADOUSIS 1981 Journal of Sound and Vibration 76(3), pp329-360. "Fluidelastic vibration of cylinder arrays in axial and cross flow: state of the art".

6.23 G.V. PARKINSON and T. JANDALI 1970 J.F.M. 40(3), pp577-594. "A wake source model for bluff body potential flow".

6.24 B.W. ROBERTS 1960 Mechanical Engineering Science Monograph. No. 5. "Low frequency, aeroelastic vibrations in a cascade of circular cylinders".

6.25 J.M. ROBERTSON 1965 "Hydrodynamics in theory and application". London: Prentice Hall.

6.26 L. ROSENHEAD 1930 Proceedings of the Royal Society A 127, pp590-612. "The spread of vorticity in the wake behind a cylinder".

6.27 G.T. SYMM and R.A. PITFIELD 1974 N.P.L. Report No. NAC44. "Solution of Laplace's equation in two dimensions".

6.28 H. TANAKA and S. TAKAHARA 1977 Journal of Sound and Vibration 77(1), pp19-37. "Fluid elastic vibration of tube array in cross flow".

6.29 E.L. WACHSPRESS 1966 "Iterative solution of elliptic systems and applications to the neutron diffusion equations of reactor physics. Englewood Cliffs, New Jersey, U.S.A.: Prentice Hall.

6.30 G.S. WHISTON and G.D. THOMAS 1982 Journal of Sound and Vibration 81(1), pp1-31. "Whirling instabilities in heat exchanger tube arrays".

6.31 J.H. WILKINSON and C. REINSCH 1971 "Handbook for automatic computation - linear algebra". Berlin: Springer Verlag.

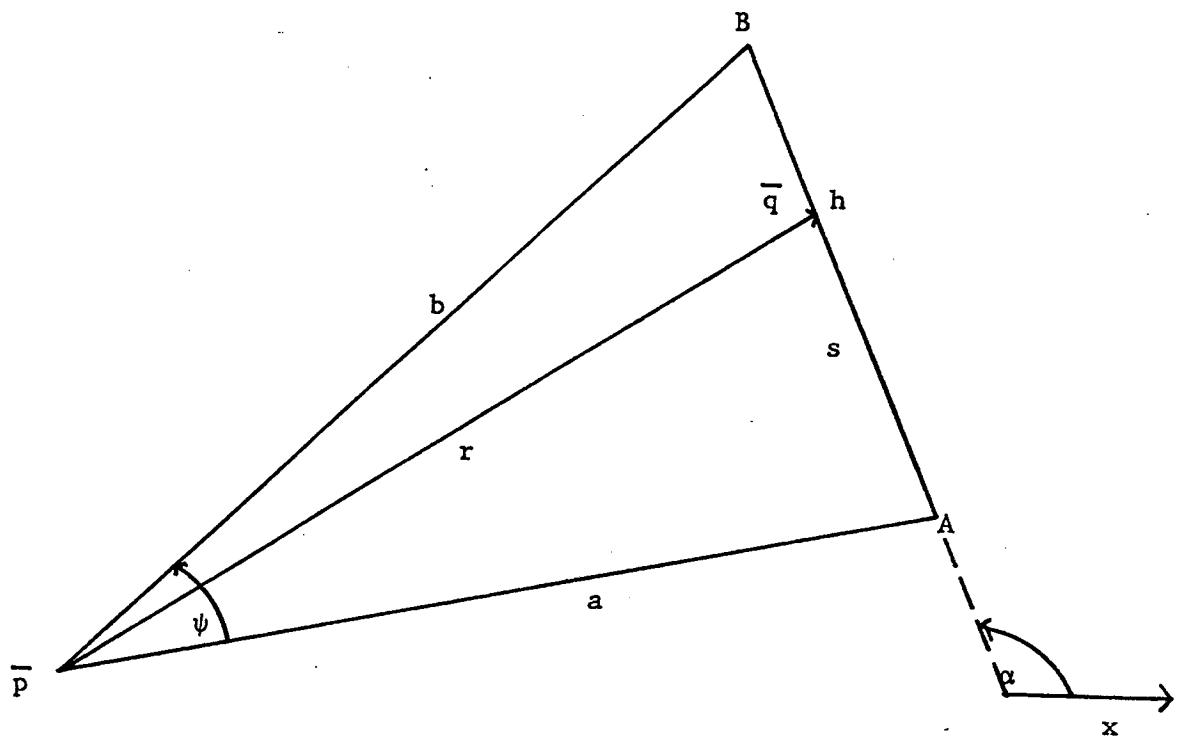


FIGURE 6.1 Diagram defining vectors and angles for the straight line integration scheme.

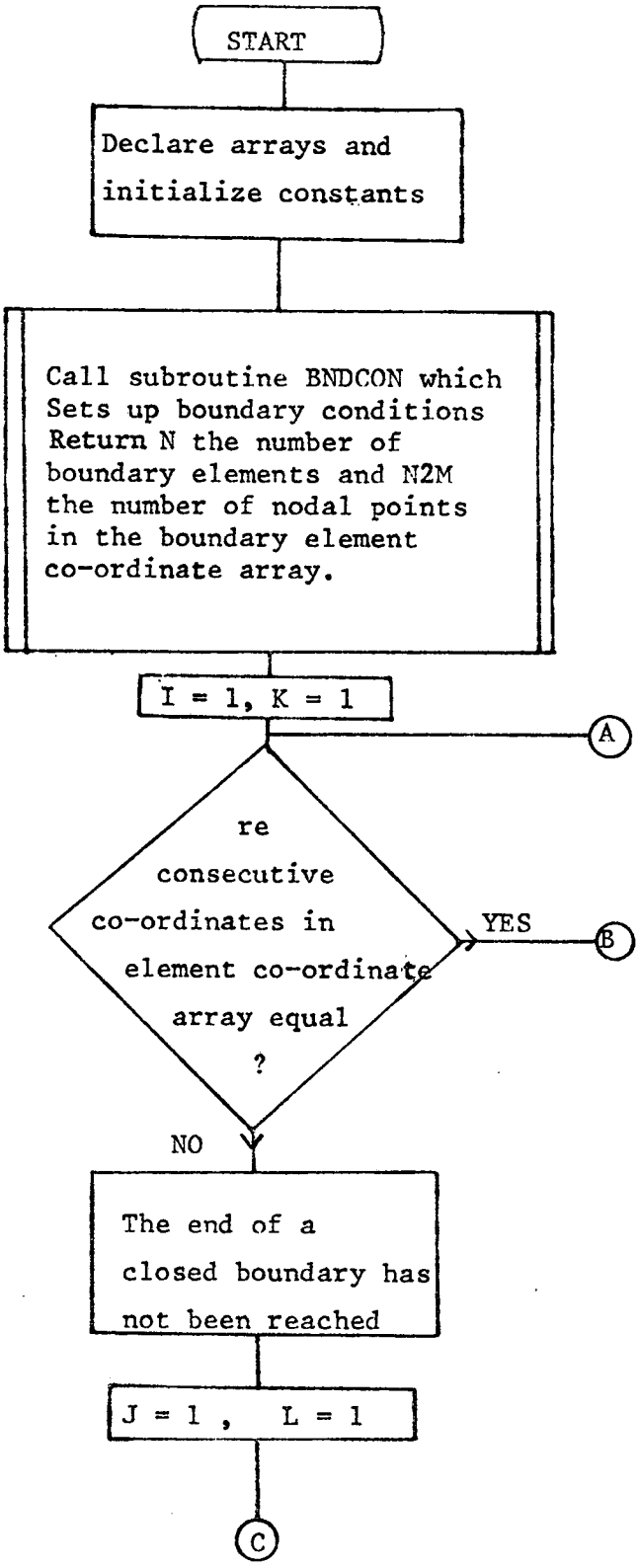


FIGURE 6.2. Flow diagram of the main programme GREEN which calculates the solution to potential flow problems using the boundary element technique.

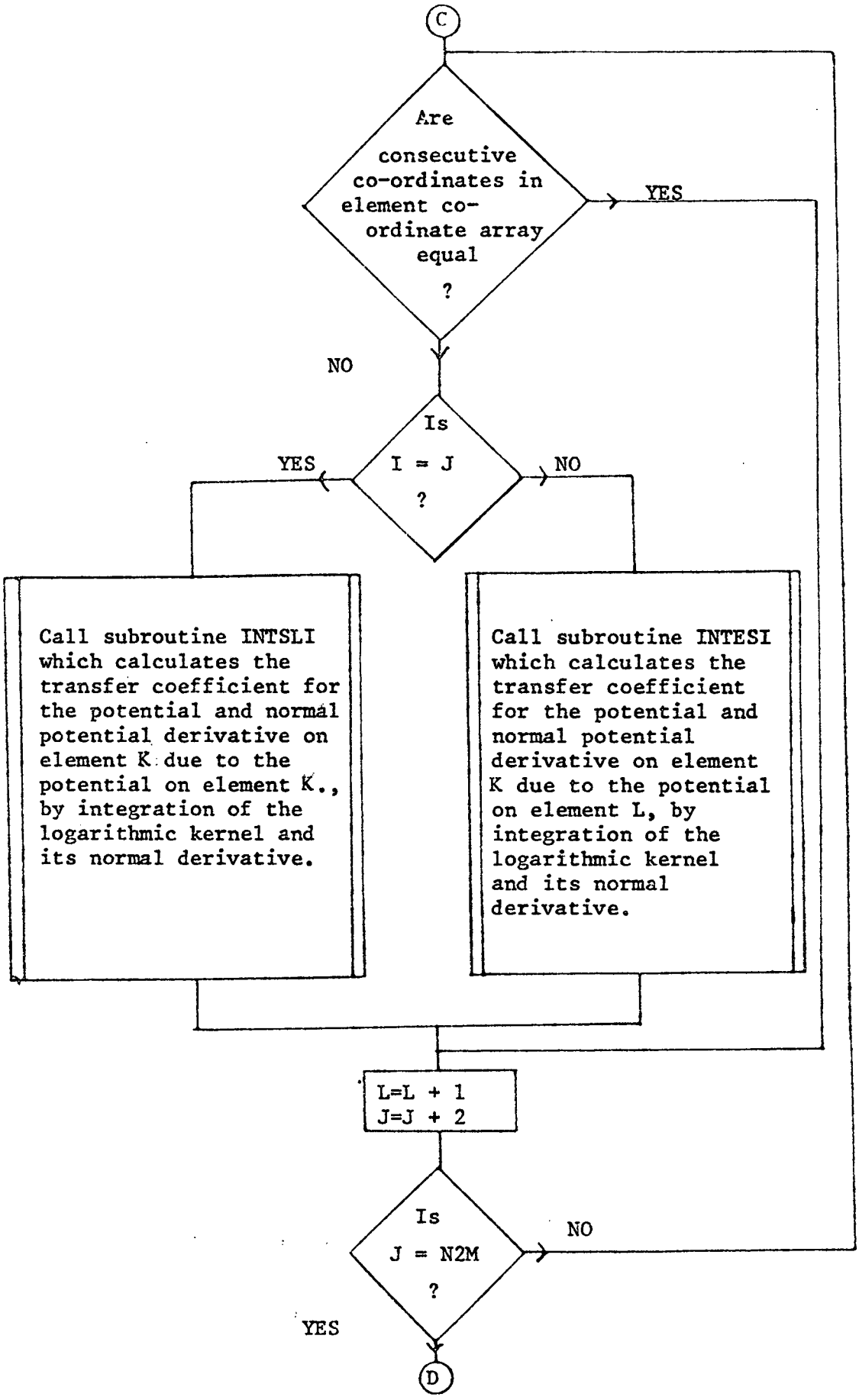


FIGURE 6.2. (continued).

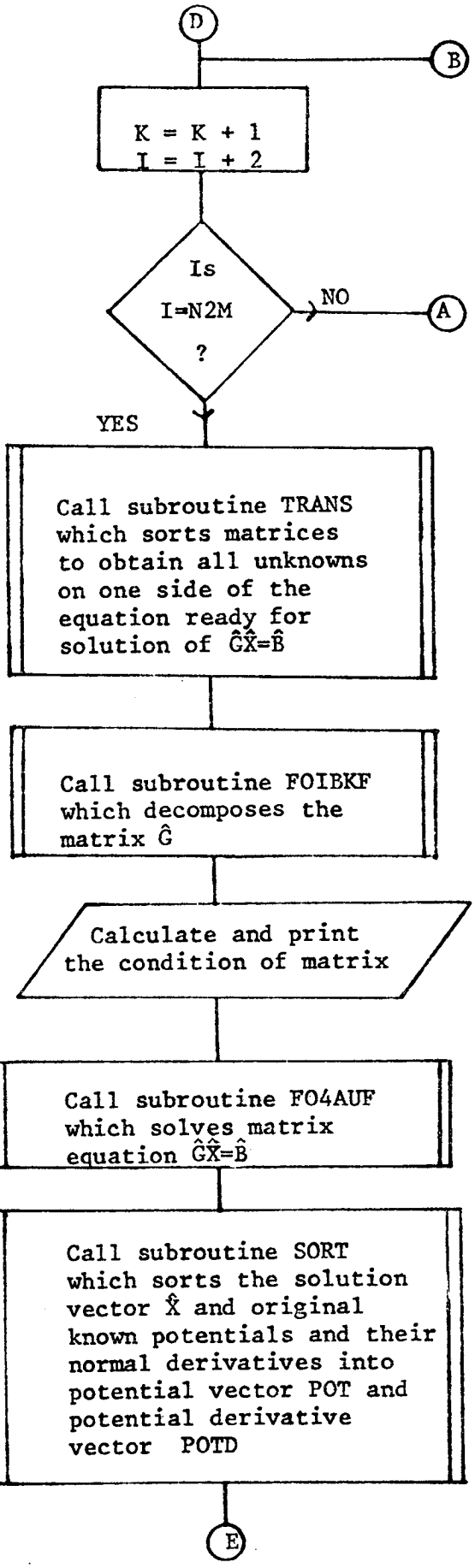


FIGURE 6.2. (continued).

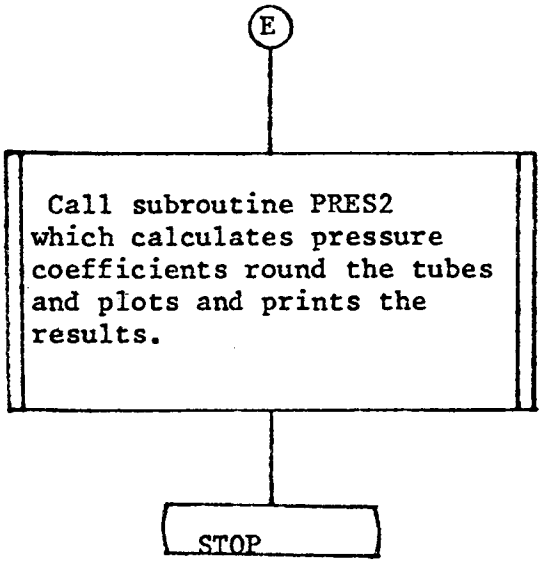


FIGURE 6.2. (continued).

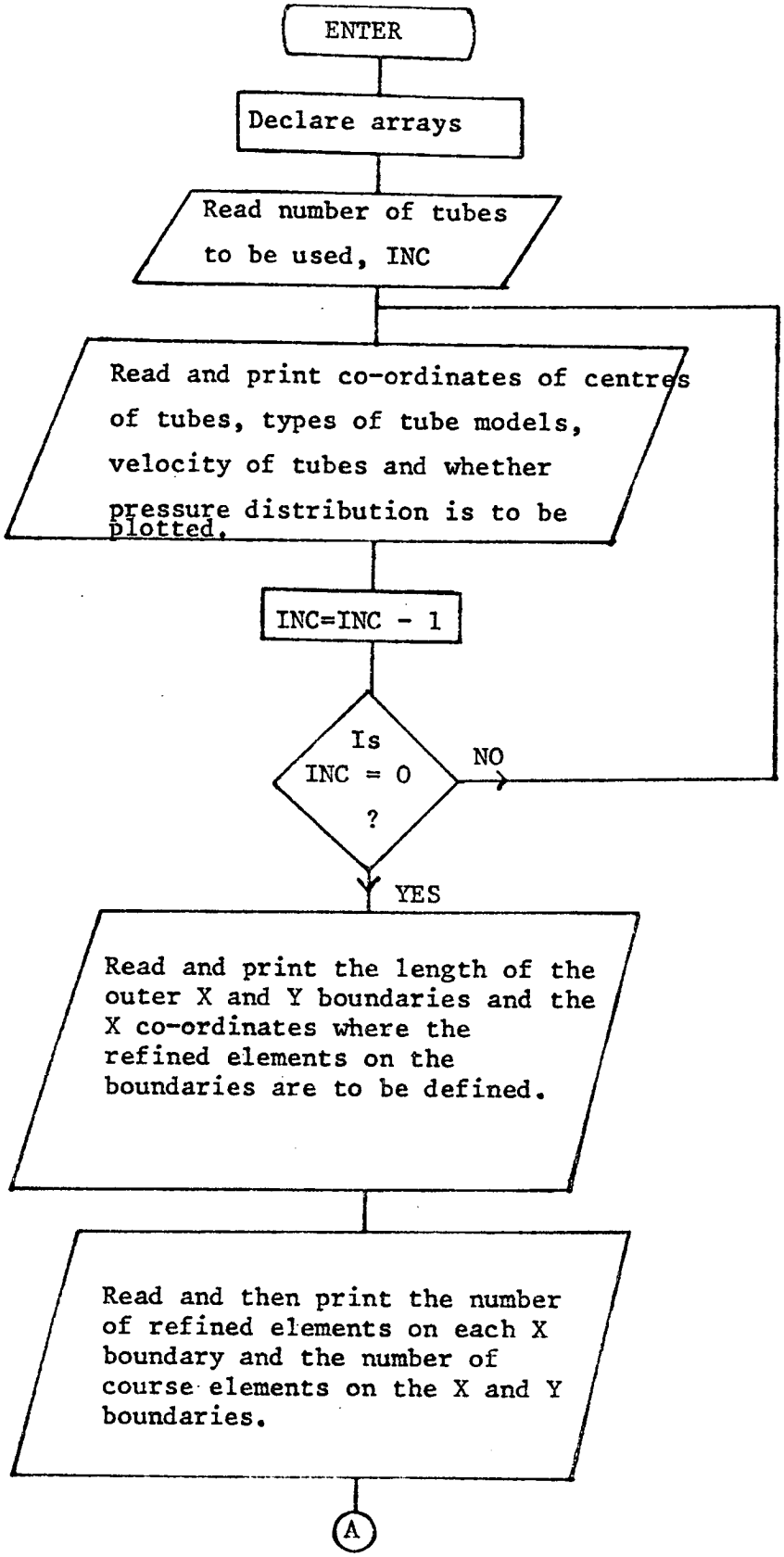


FIGURE 6.3 Flow diagram of subroutine BNDCON which sets up the boundary elements.

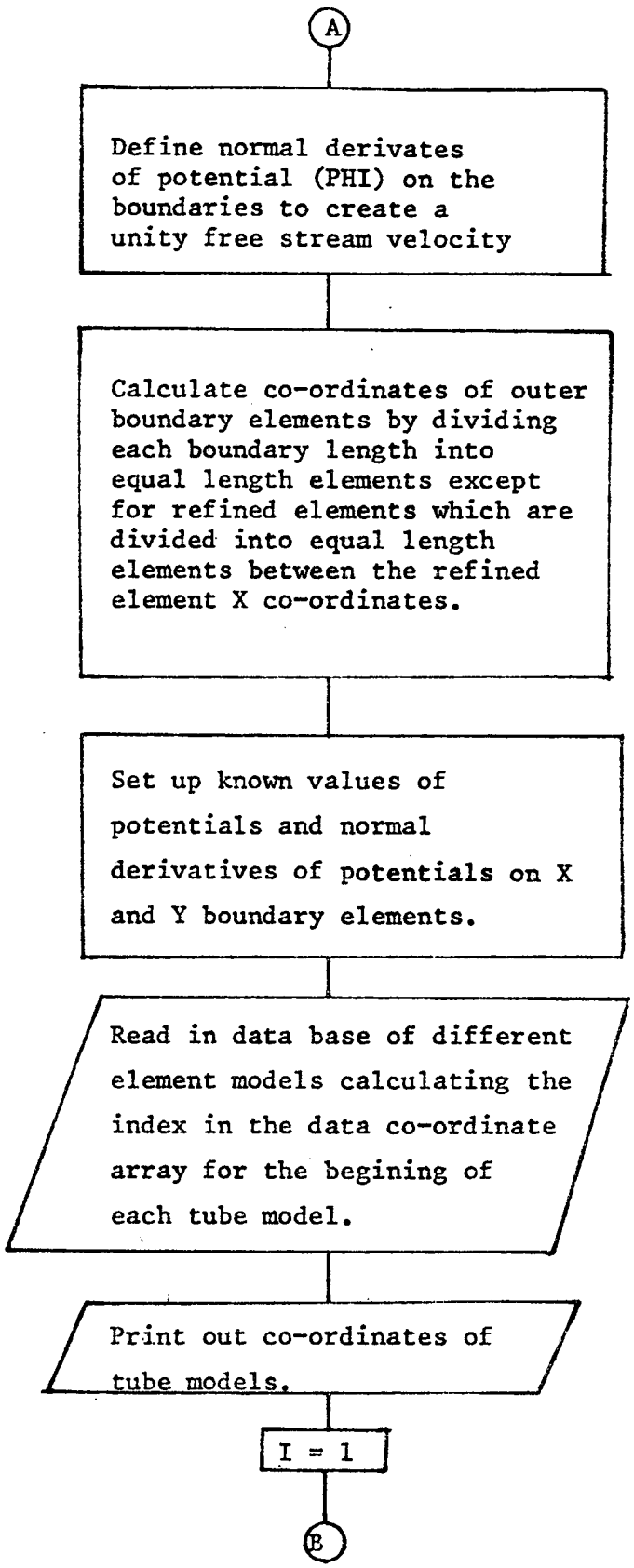


FIGURE 6.3. (continued).

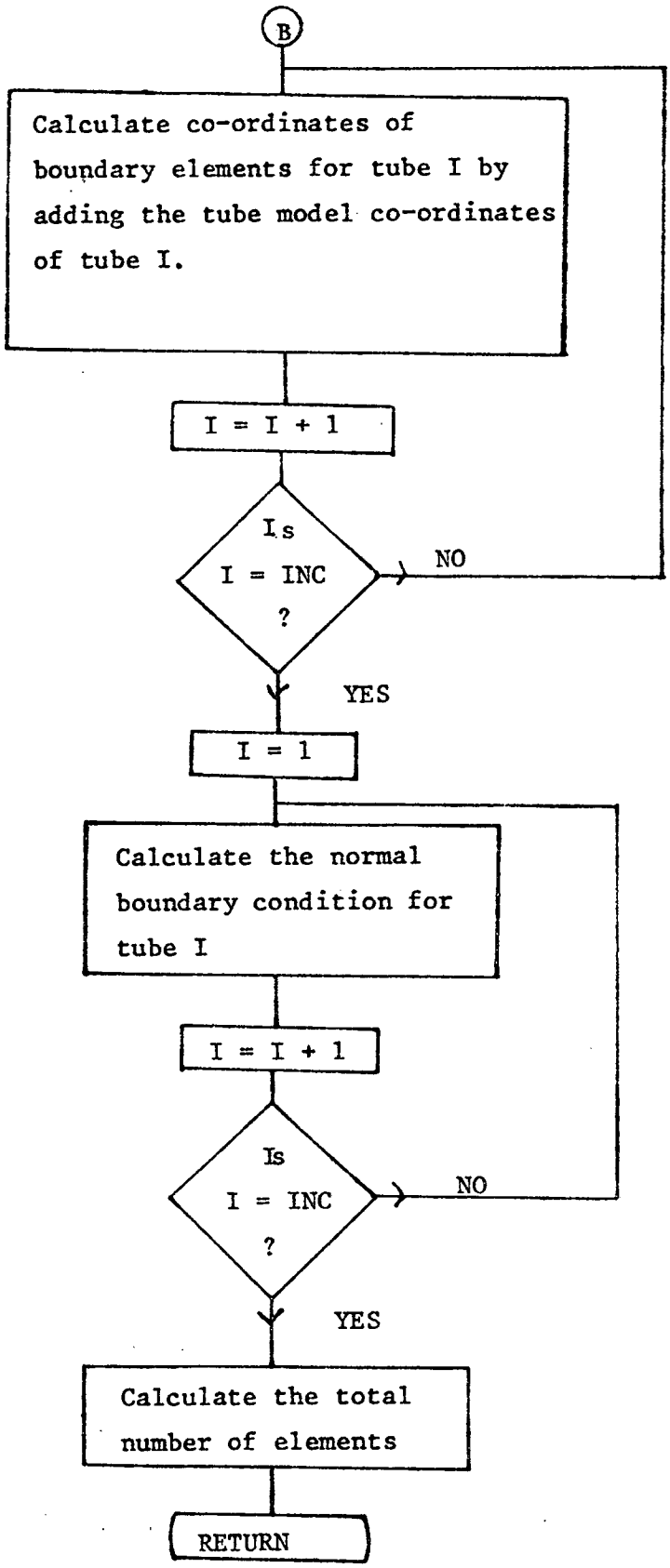


FIGURE 6.3. (continued.)

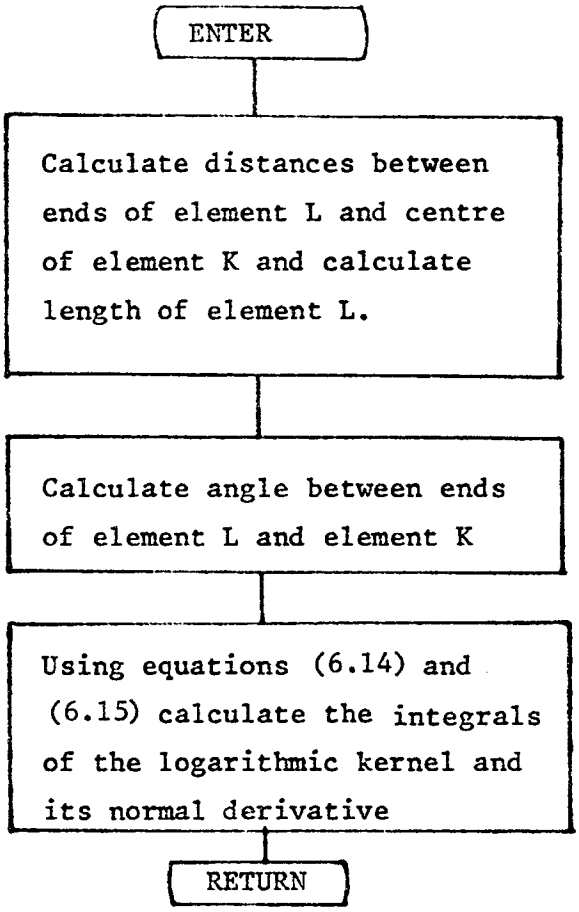


FIGURE 6.4. Flow diagram of subroutine INTES1 which integrates the logarithmic kernel and its normal derivatives when it contains no singularity.

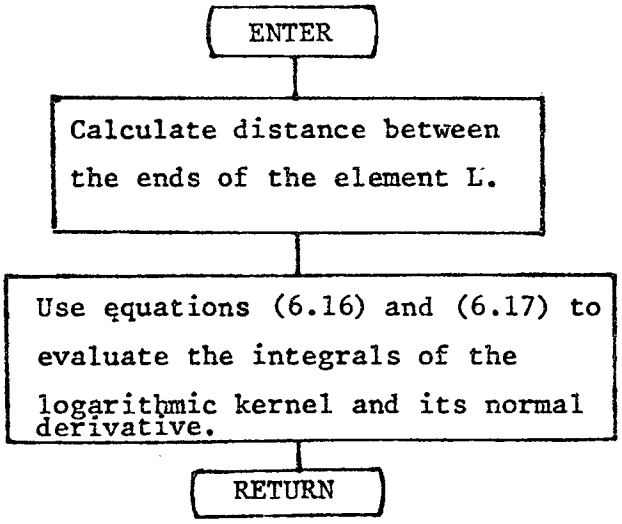


FIGURE 6.5. Flow diagram of subroutine INTSL1 which integrates the logarithmic kernel and its normal derivatives when it cotains a singularity.

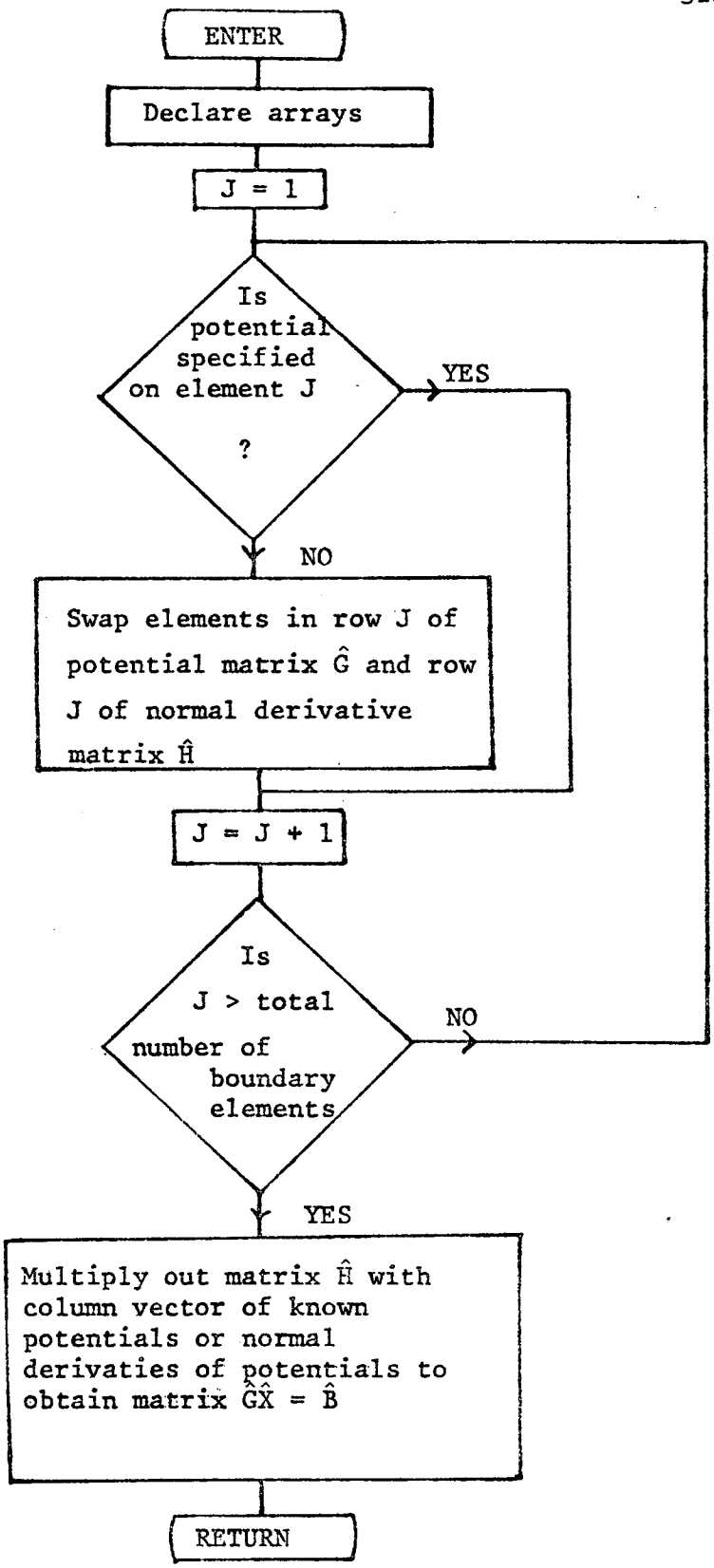


FIGURE 6.6. Flow diagram of subroutine TRANS which sorts matrices to obtain all unknowns on one side of the matrix equation $\hat{G}\hat{X} = \hat{B}$.

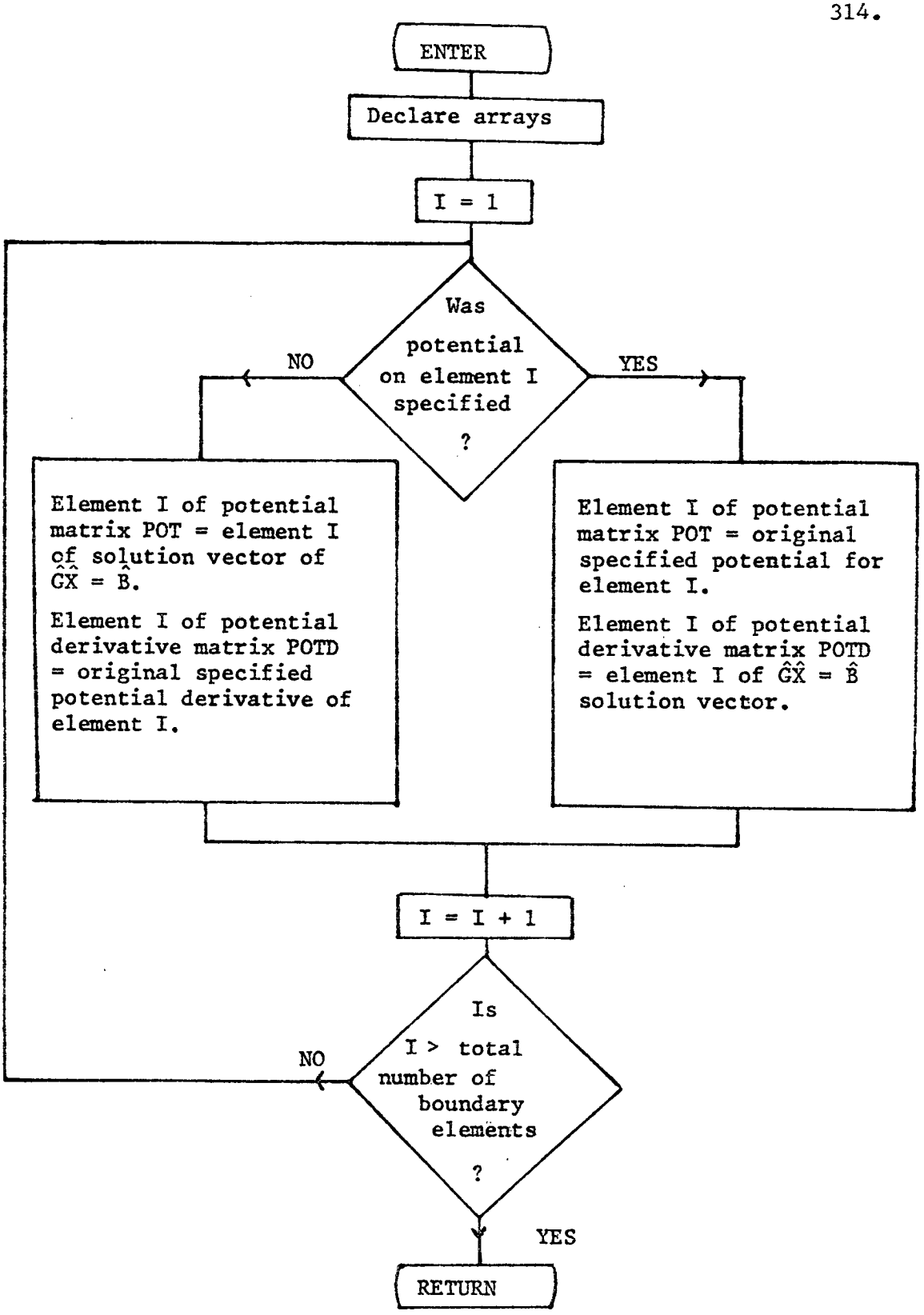


FIGURE 6.7. Flow diagram of subroutine SORT which sorts the solution vector of $\hat{G}\hat{X}=\hat{B}$ known potentials and normal derivatives into potential and potential derivative vectors.

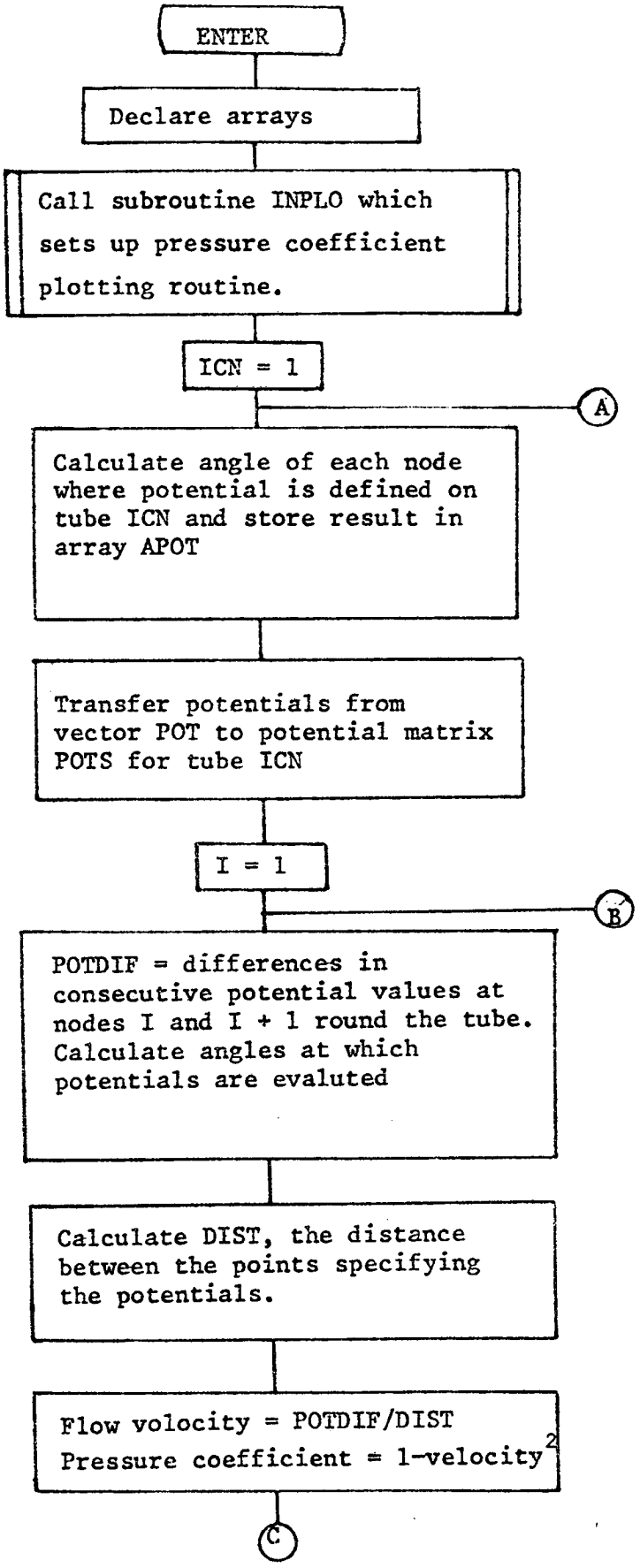


FIGURE 6.8. Flow diagram of subroutine PRES2 which calculates and plots pressure distributions round tubes.

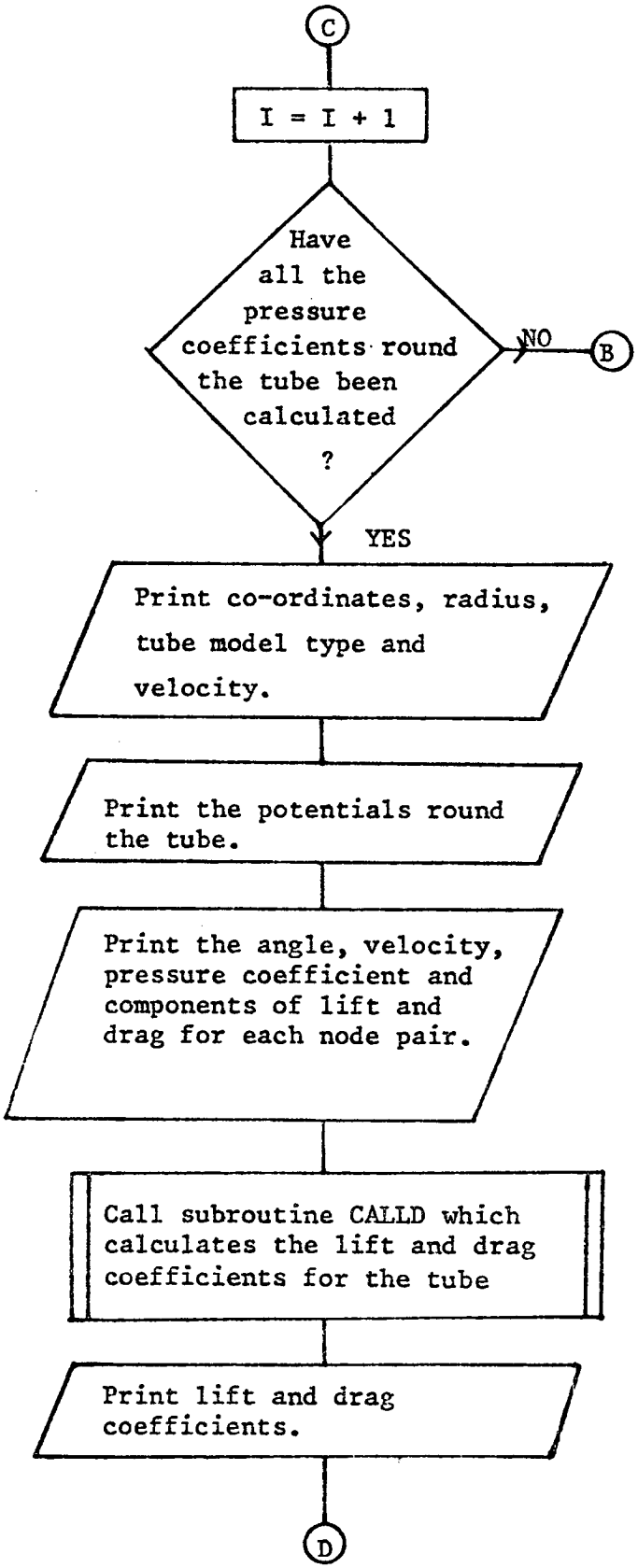


FIGURE 6.8. (continued).

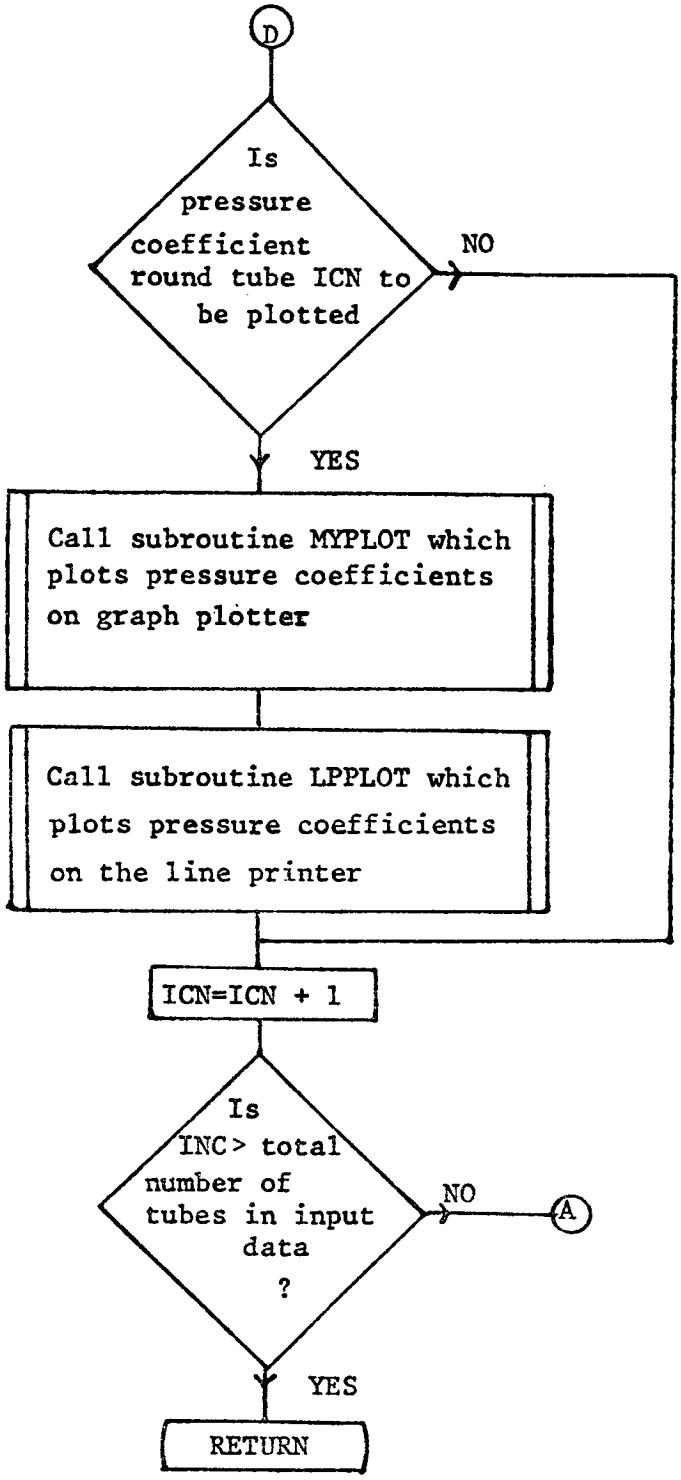


FIGURE 6.8. (continued).

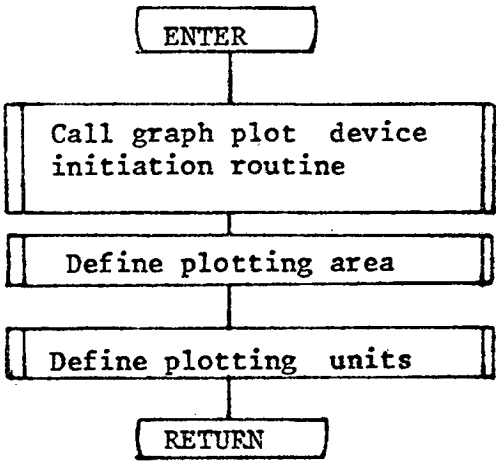


FIGURE 6.9 Flow diagram of subroutine INPLO which initiates graph plotting routine.

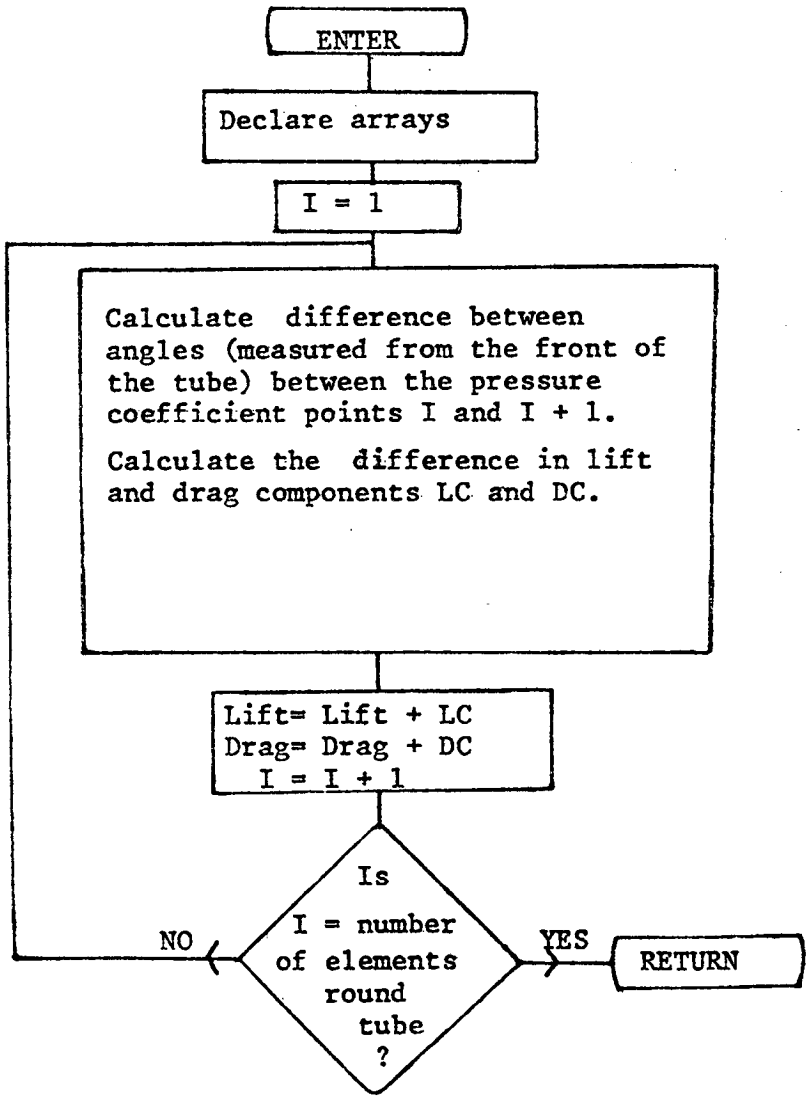


FIGURE 6.10. Flow diagram of subroutine CALLD which calculates lift and drag on a tube.

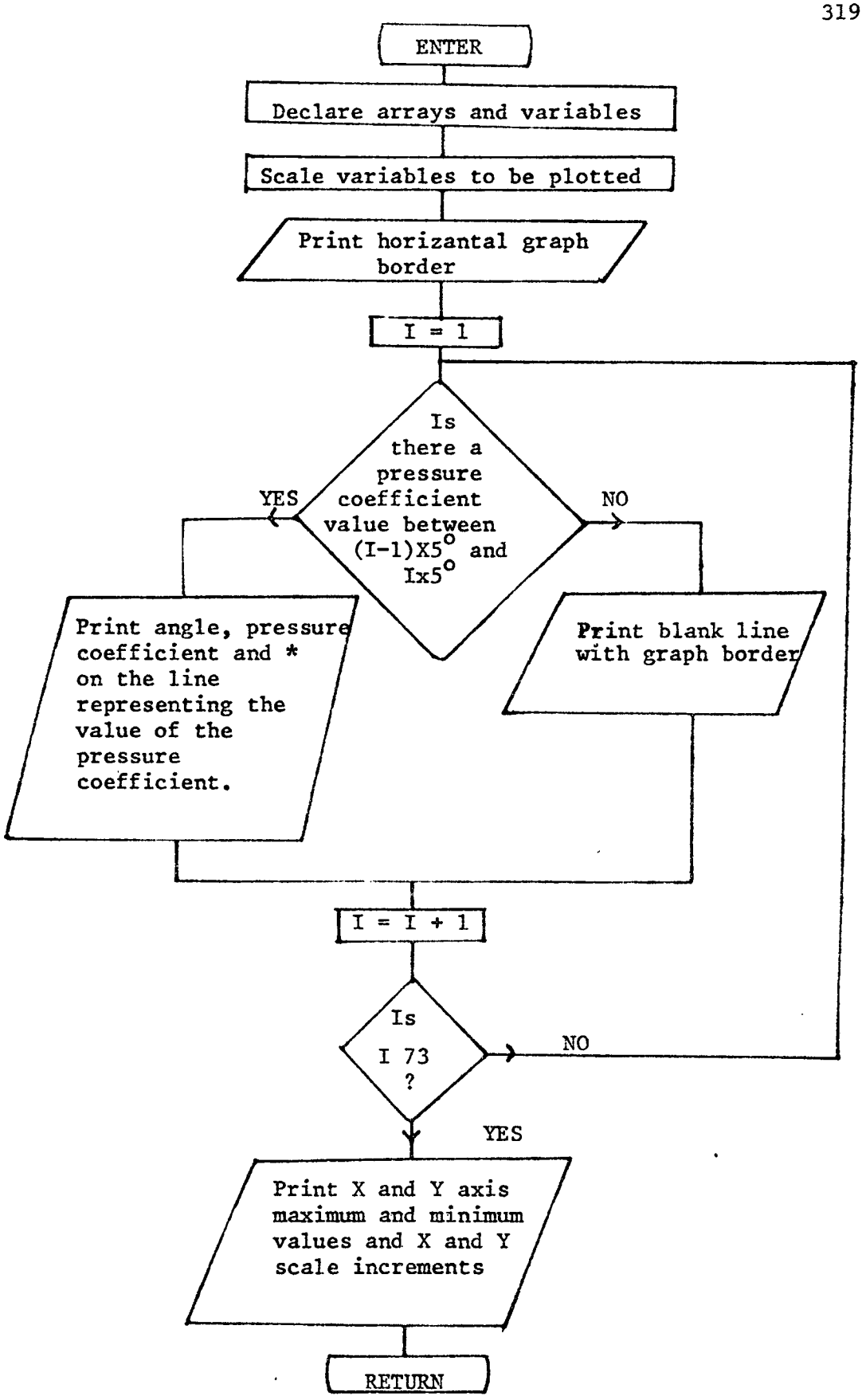


FIGURE 6.11 Flow diagram of subroutine LPPLOT which plots pressure coefficient versus angle on the line printer.

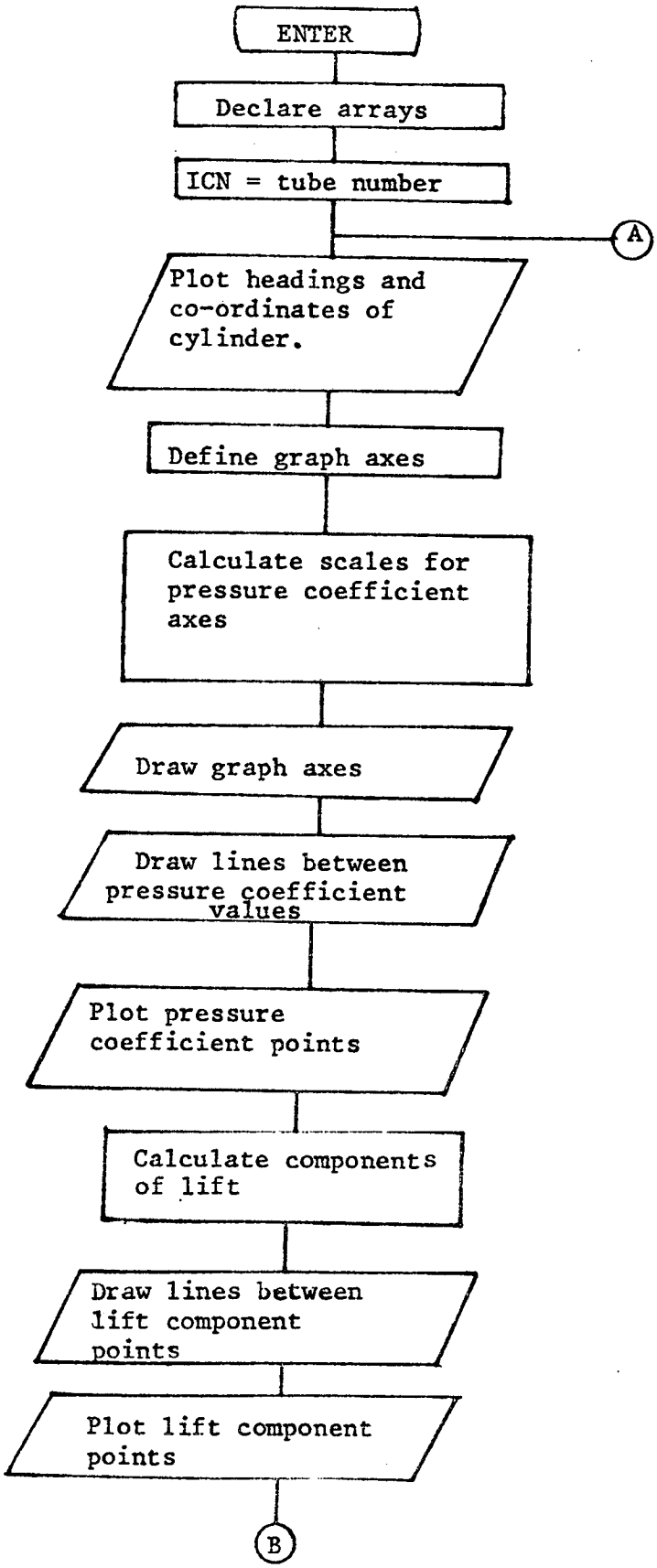


FIGURE 6.12. Flow diagram of subroutine MYPLOT which plots the pressure coefficients on the graph plotter.

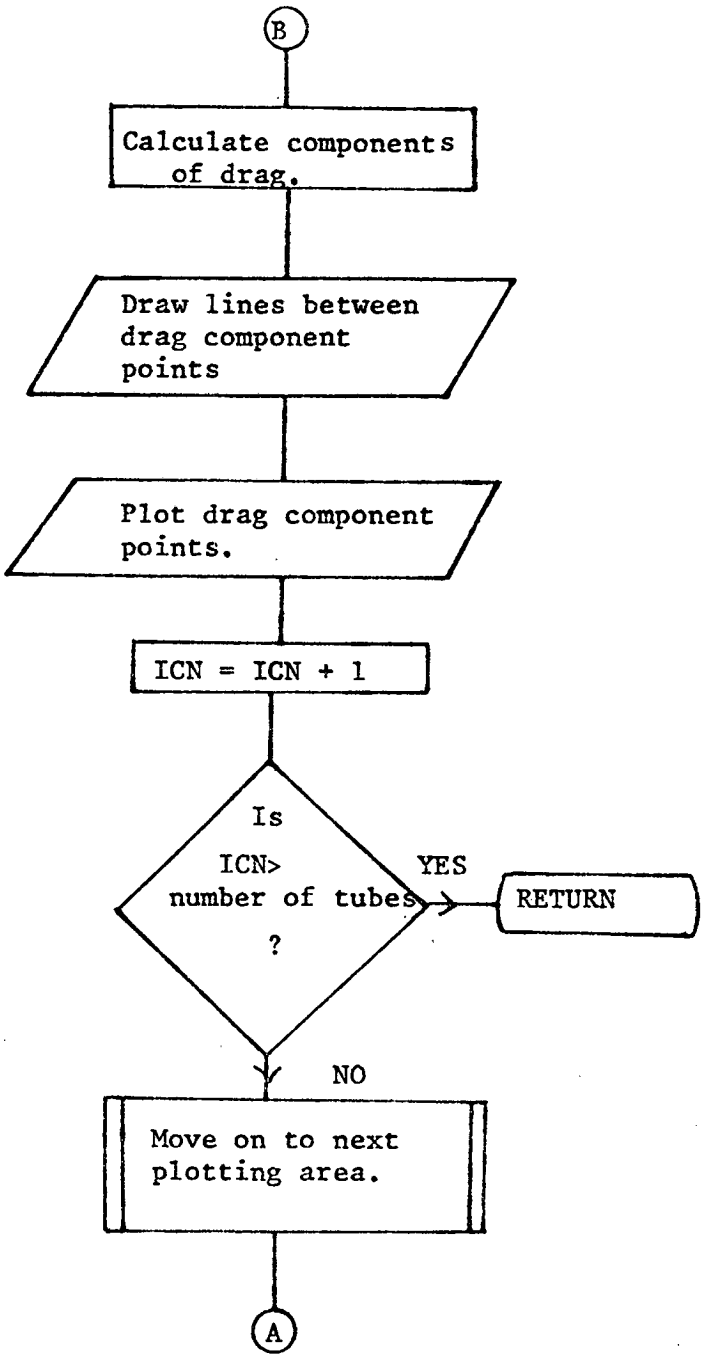


FIGURE 6.12. (continued).

(a)

Scale 1:1

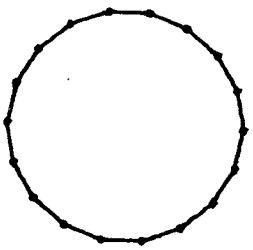

(b)

Scale 1:1

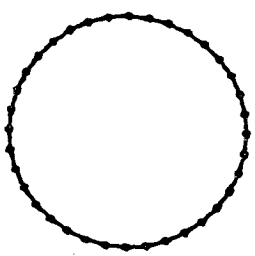

FIGURE 6.13 a-b. Arrangement of boundary elements in tube models without wakes.
(a) Elements spaced at $20^{o}$ intervals.
(b) Elements spaced at $10^{o}$ intervals.

(a) Scale 2:1

(b) Scale 2:1

FIGURE 6.14 a-b. Arrangement of boundary elements in tube model used in the single tube row.
(a) Course wake model.
(b) Refined wake model.

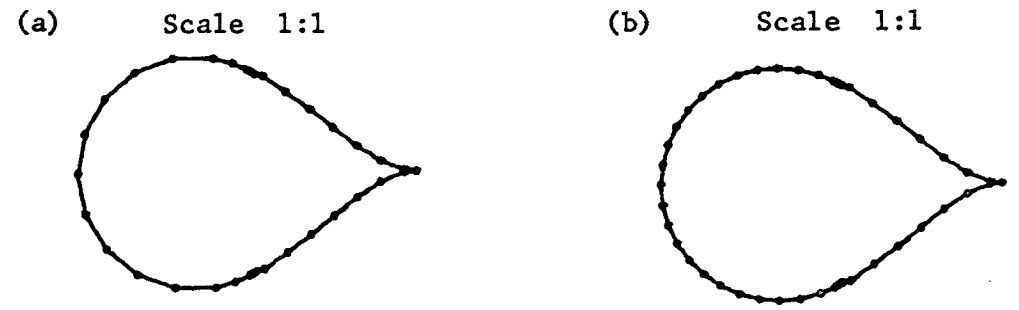


FIGURE 6.15 a-b. Arrangement of boundary elements in tube models used in the equilateral triangular pitched tube bank.
(a) Elements spaced at $20^{o}$ intervals.
(b) Elements spaced at $10^{o}$ intervals.

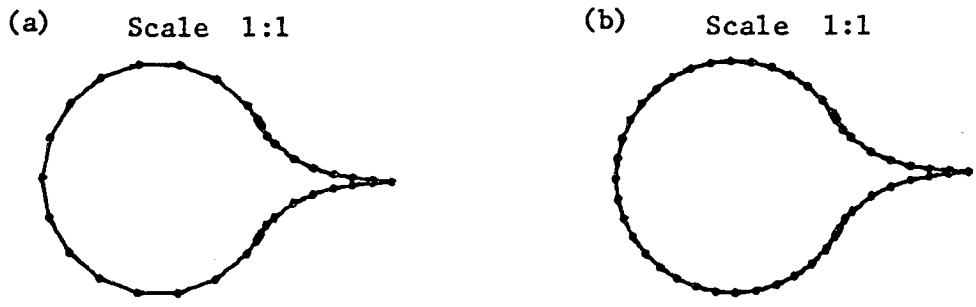


FIGURE 6.16 a-b. Arrangement of boundary elements in tube models used in the tube bank with transverse pitch ratio, 1.043; longitudinal pitch ratio, 1.023.
(a) Elements spaced at $20^{o}$ intervals.
(b) Elements spaced at $10^{o}$ intervals.

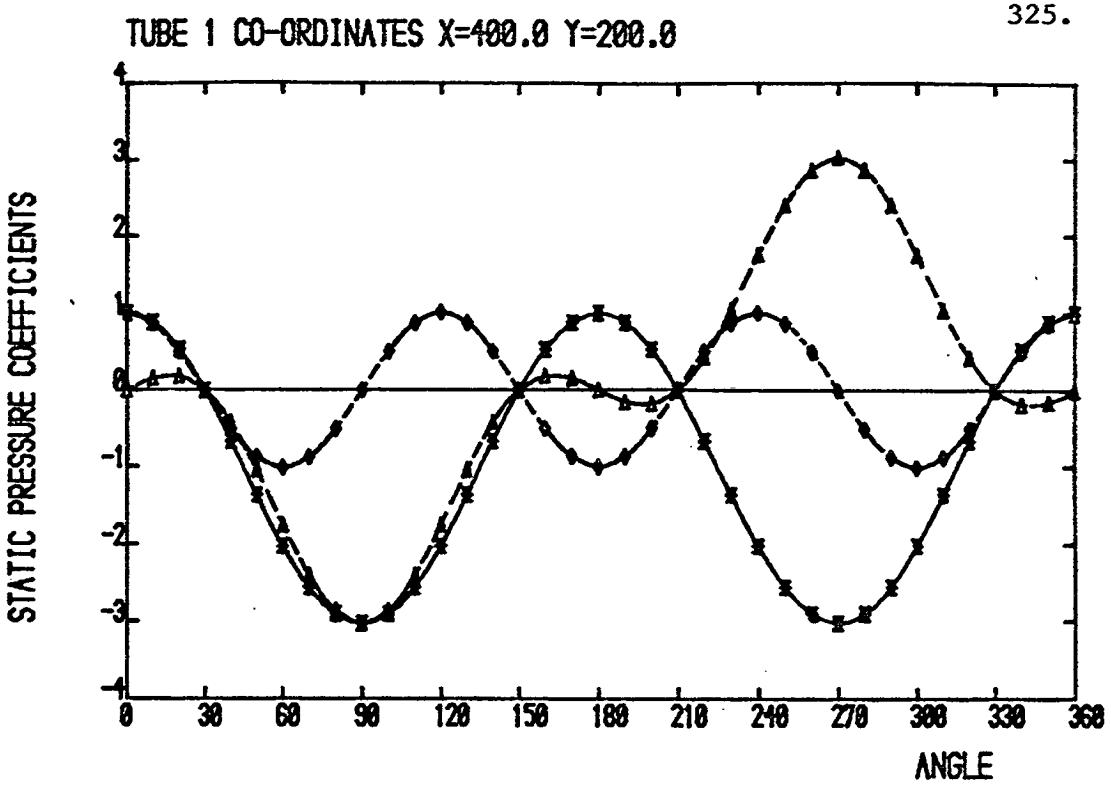


FIGURE 6.17a. Variation of static preesure coefficients round a cylinder with boundary elements spaced at $10^{o}$ intervals.

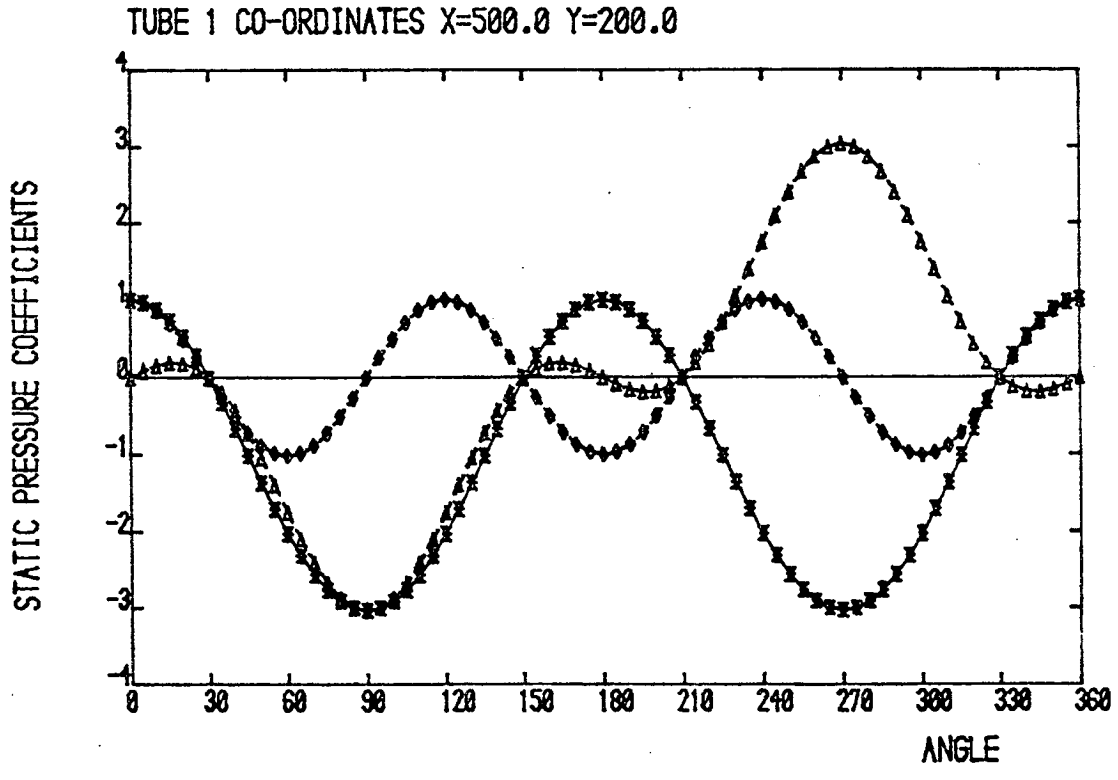


FIGURE 6.17b. Variation of static pressure coefficients round a cylinder with boundary elements spaced at $5^{o}$ intervals.

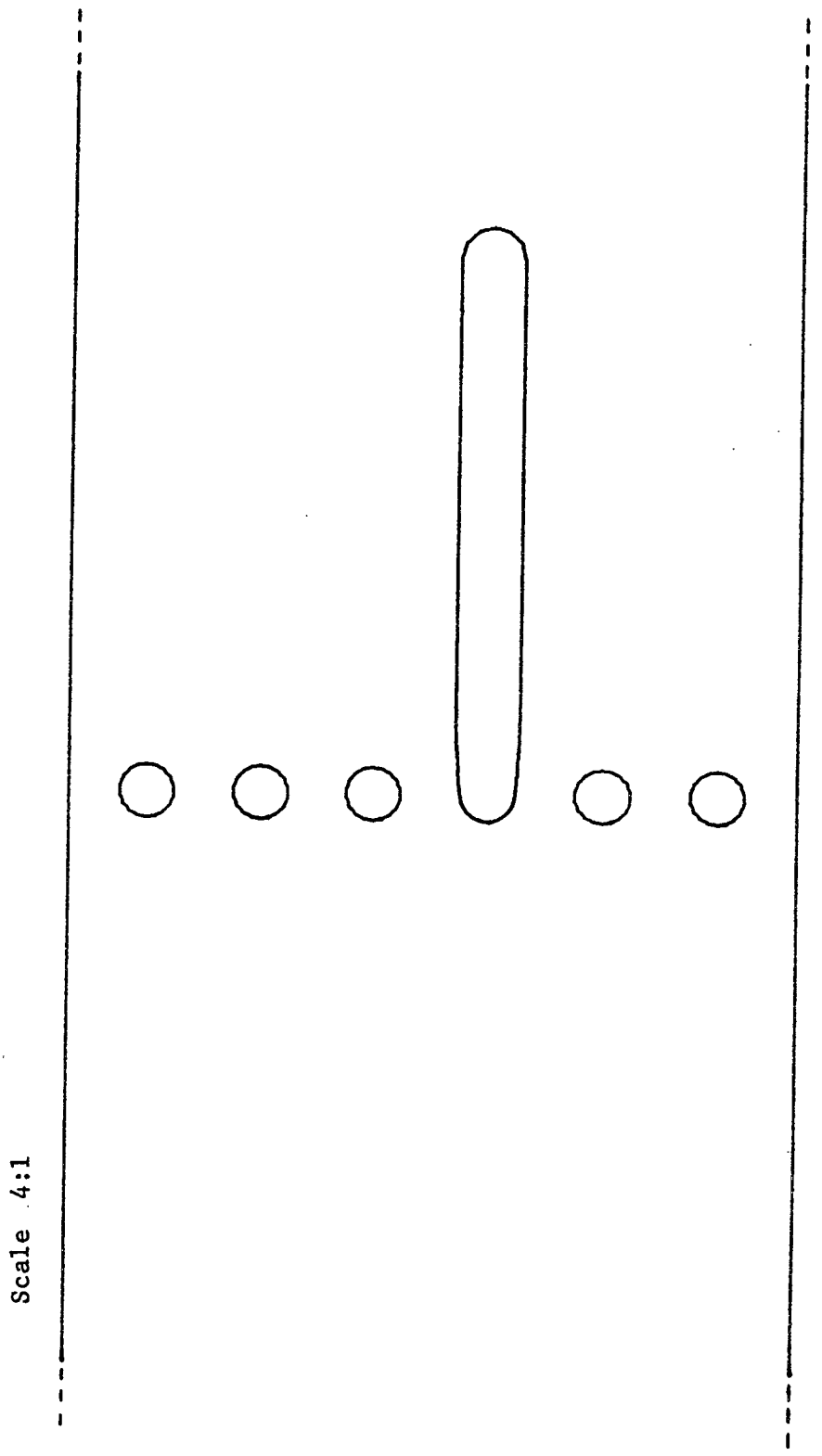


FIGURE 6.18. Arrangement of tubes in the single tube row model. (One tube with a wake model.)

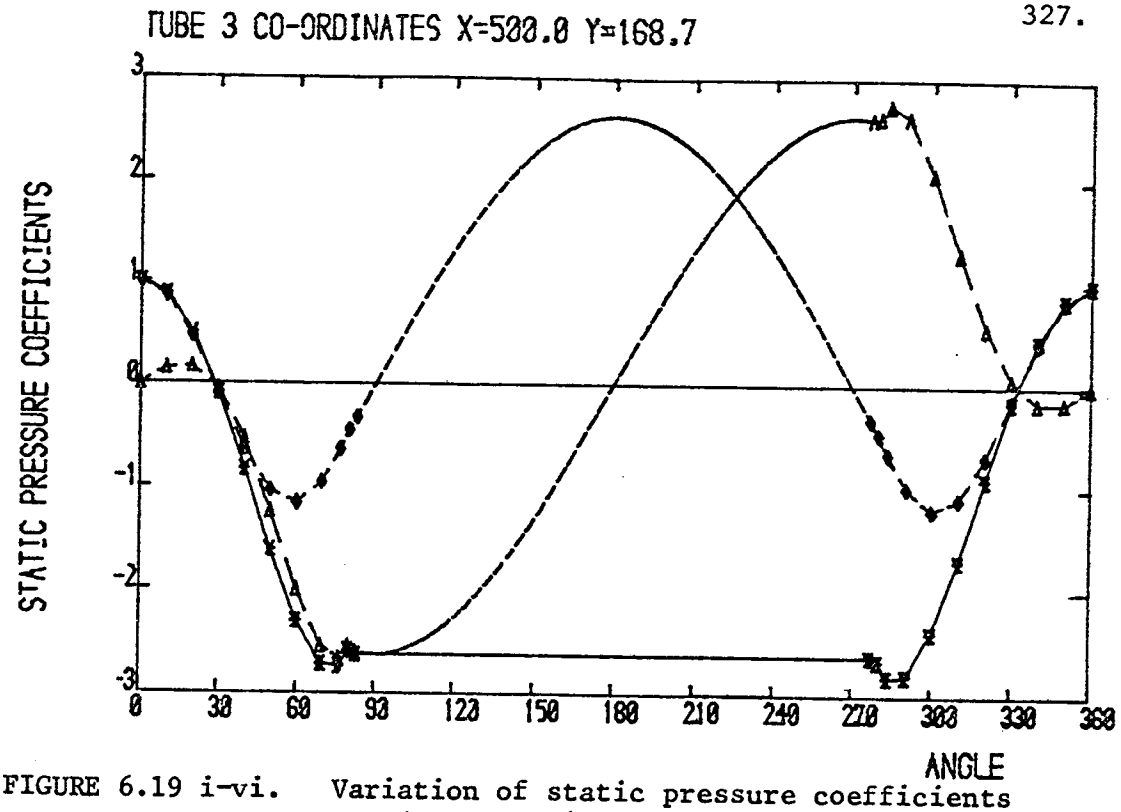


FIGURE 6.19 i-vi. Variation of static pressure coefficients round a tube displaced in the cross-flow direction in a single tube row. (One tube with a wake model.)

FIGURE 6.19i. Displacement = 0 diameters.

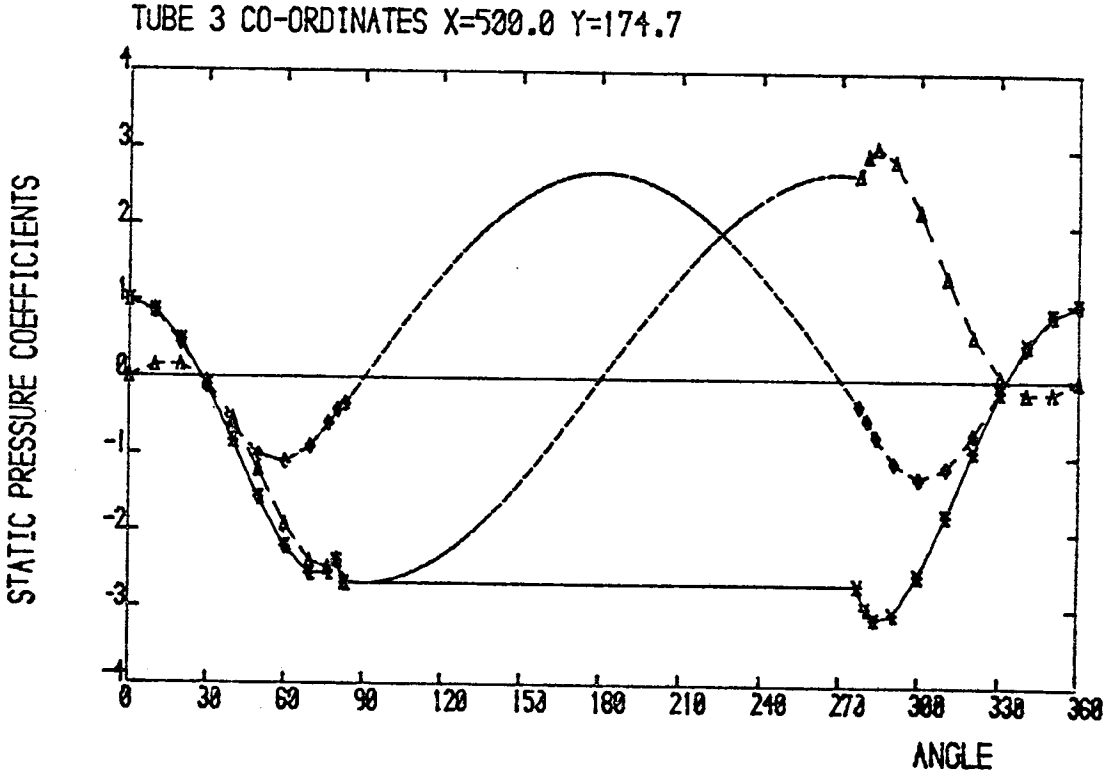


FIGURE 6.19ii. Displacement = 0.2 diameters.

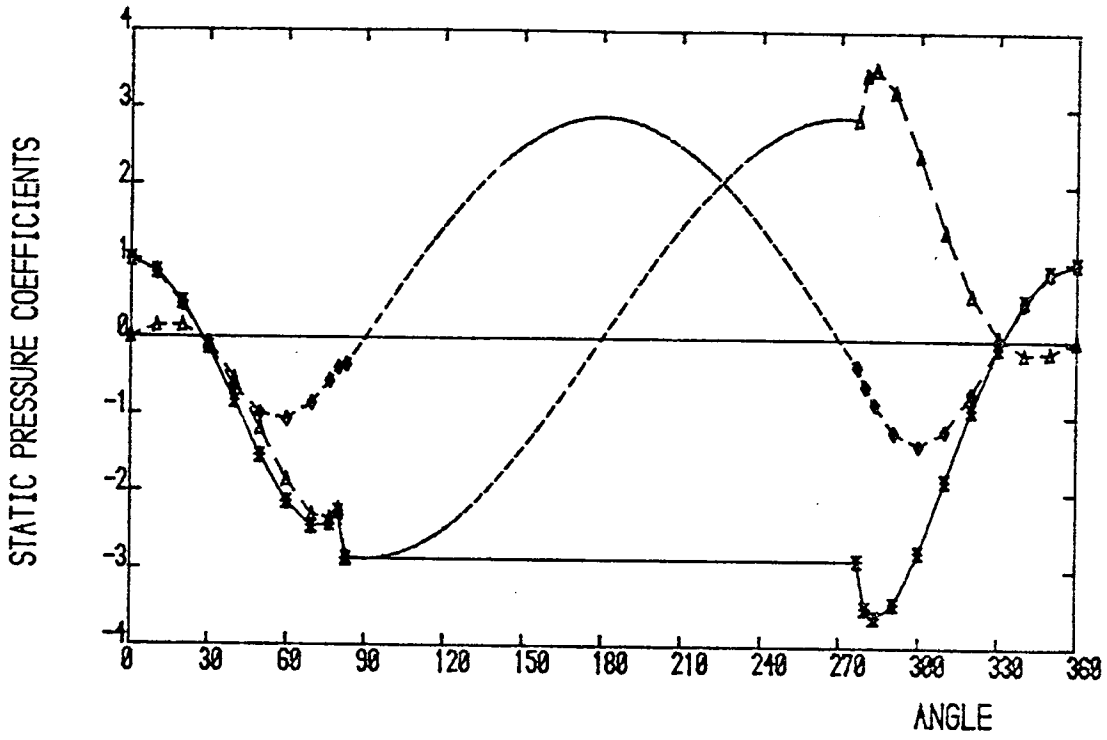


FIGURE 6.19iii. Displacement = 0.4 diameters.

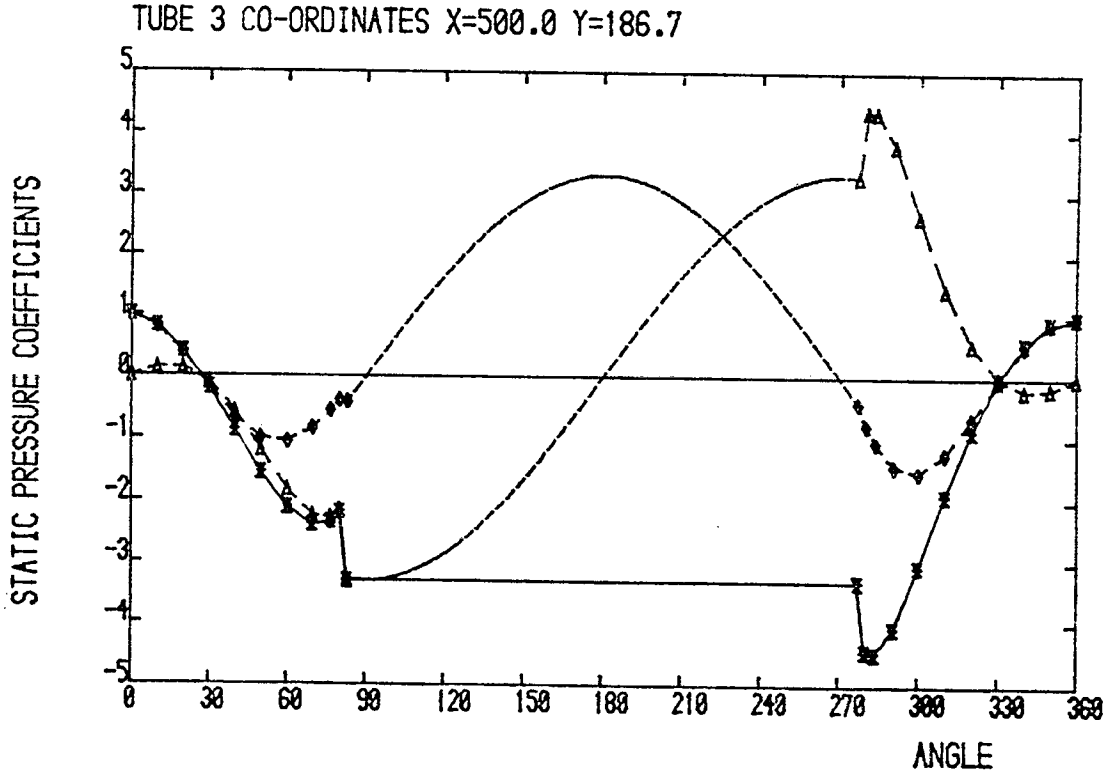


FIGURE 6.19iv. Displacement = 0.6 diameters.

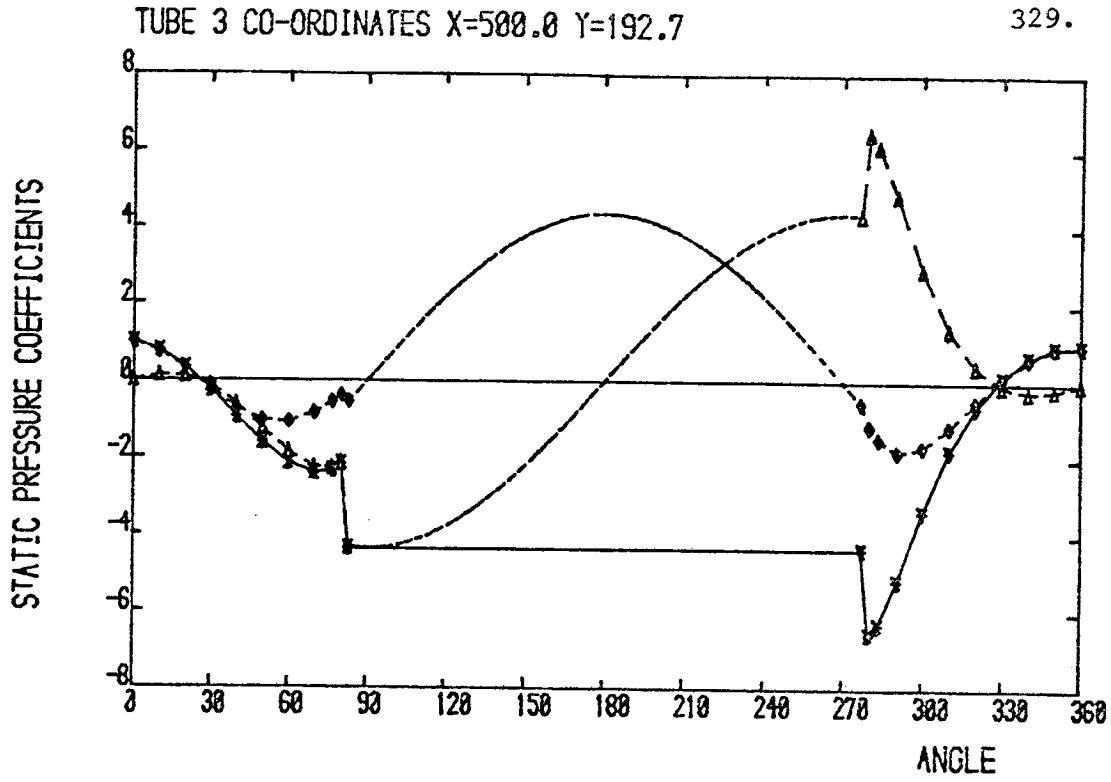


FIGURE 6.19v. Displacement = 0.8 diameters.

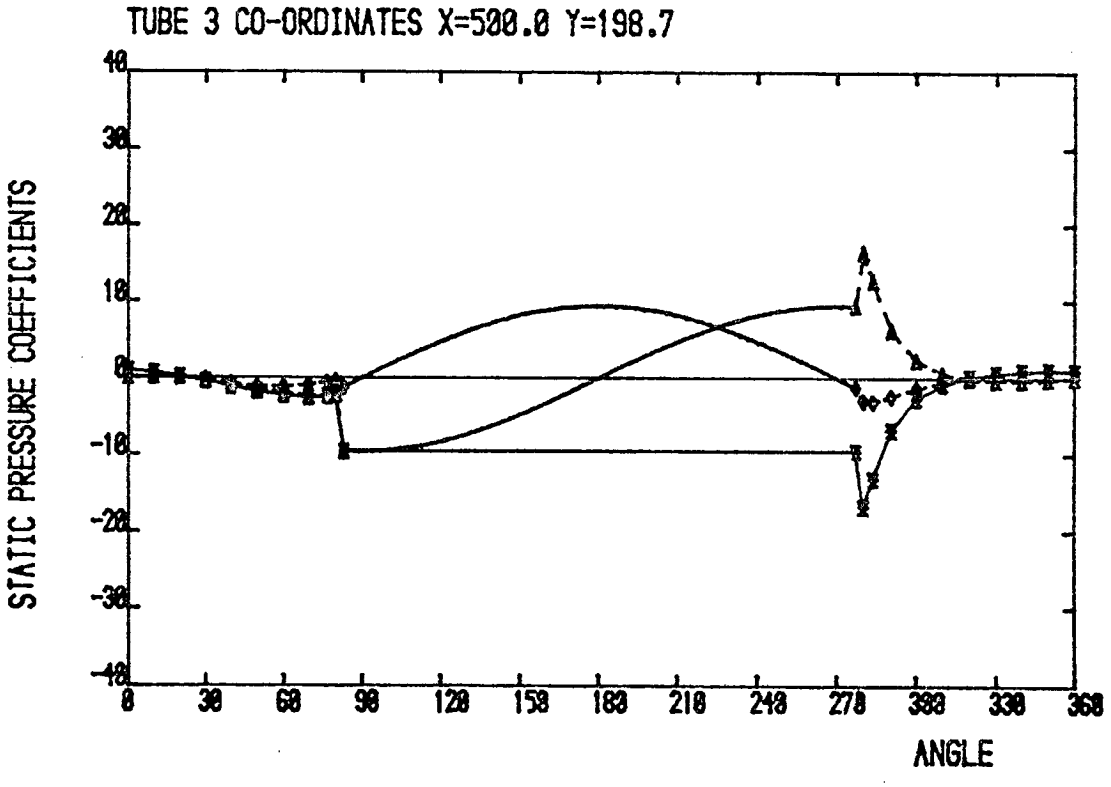


FIGURE 6.19vi. Displacement = 1.0 diameter.

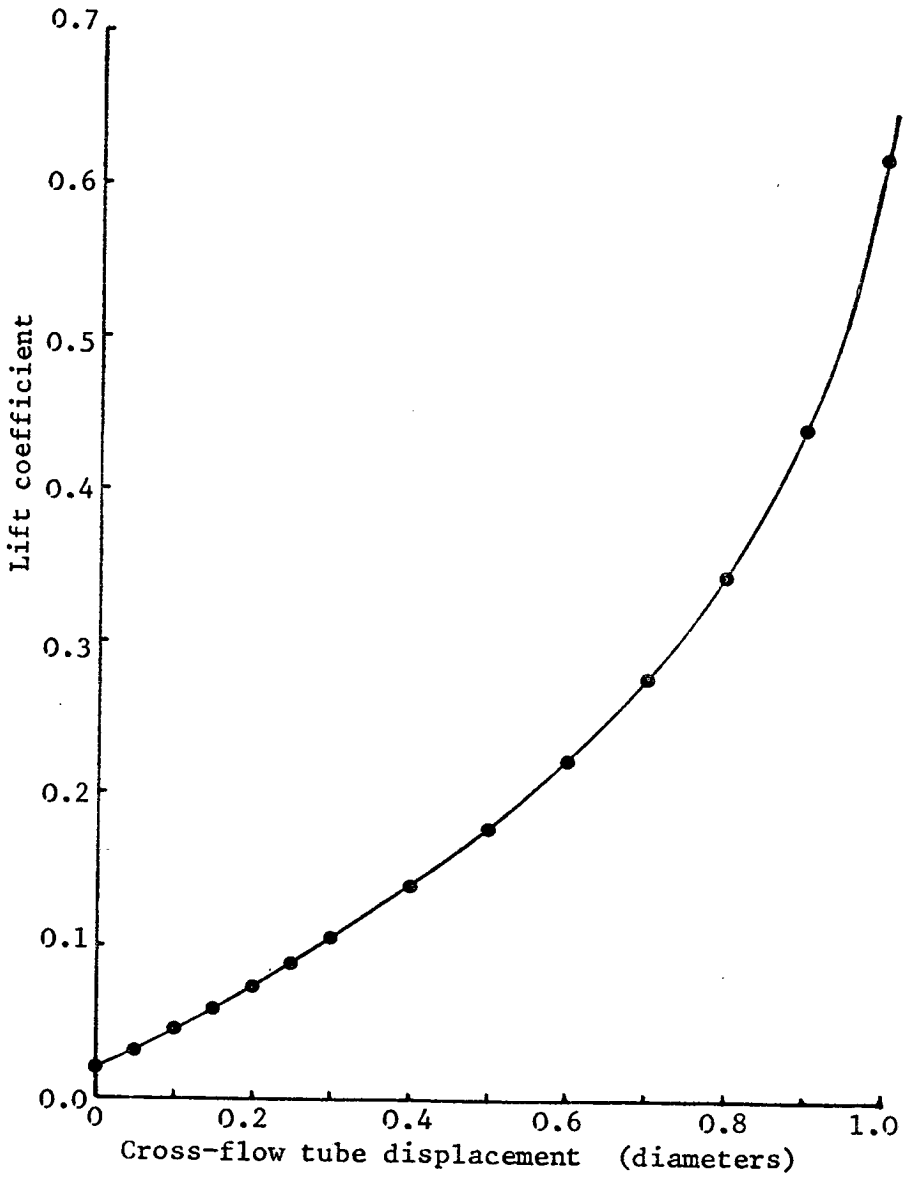


FIGURE 6.20i. Variation of lift coefficient with tube displacement in the cross-flow direction in a single tube row. (One tube with a wake model.)

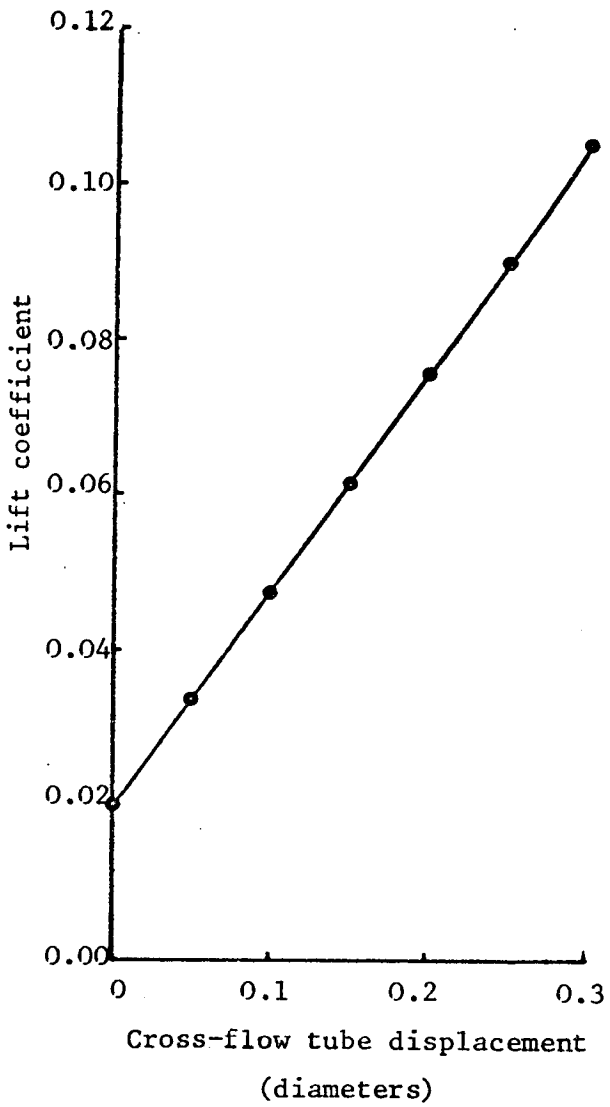


FIGURE 6.20ii. Variation of lift coefficient with tube displacement in the cross-flow direction in a single tube row. (One tube with a wake model.)

(i)

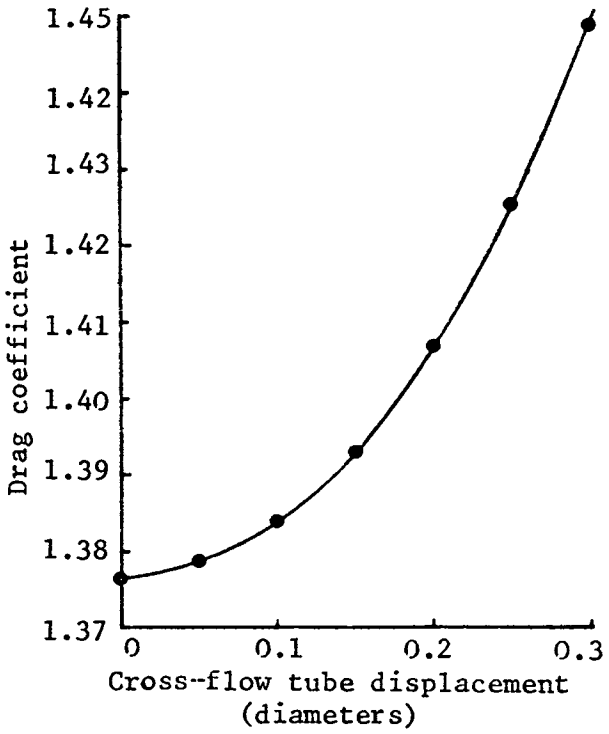


(ii)

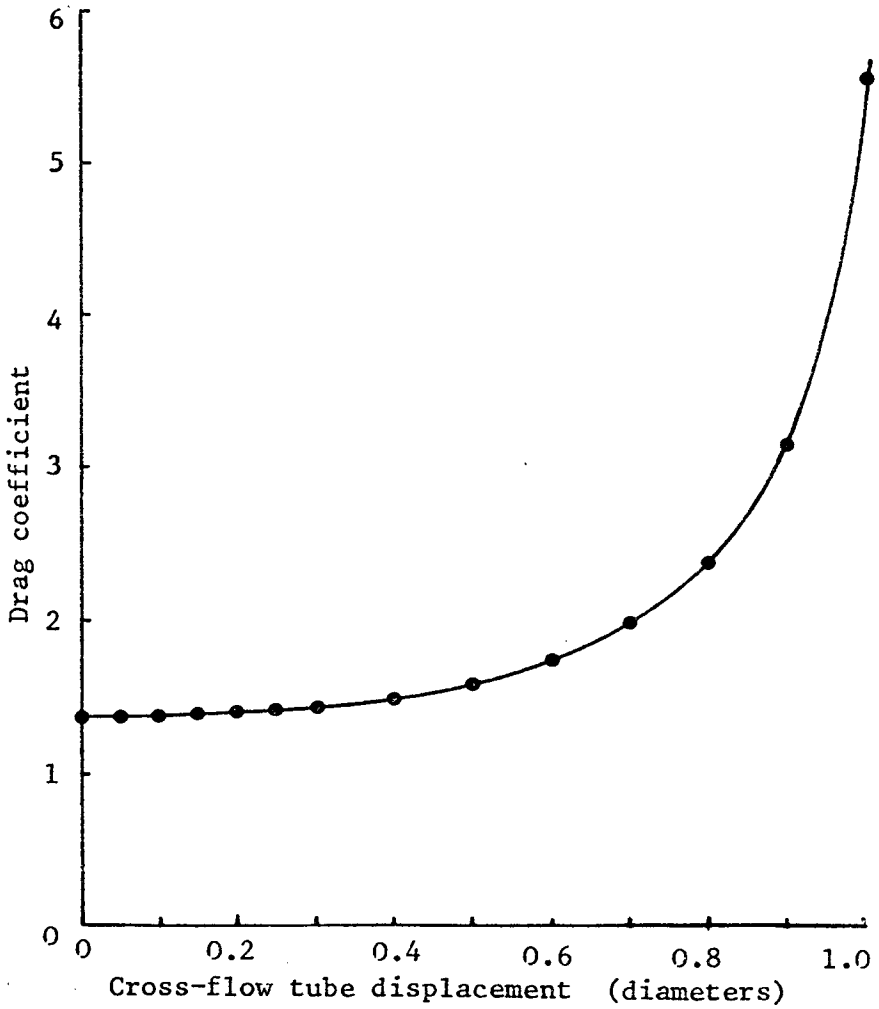


FIGURE 6.21 i-ii. Variation of drag coefficient with tube displacement in the cross-flow direction in a single tube row. (One tube with a wake model.)

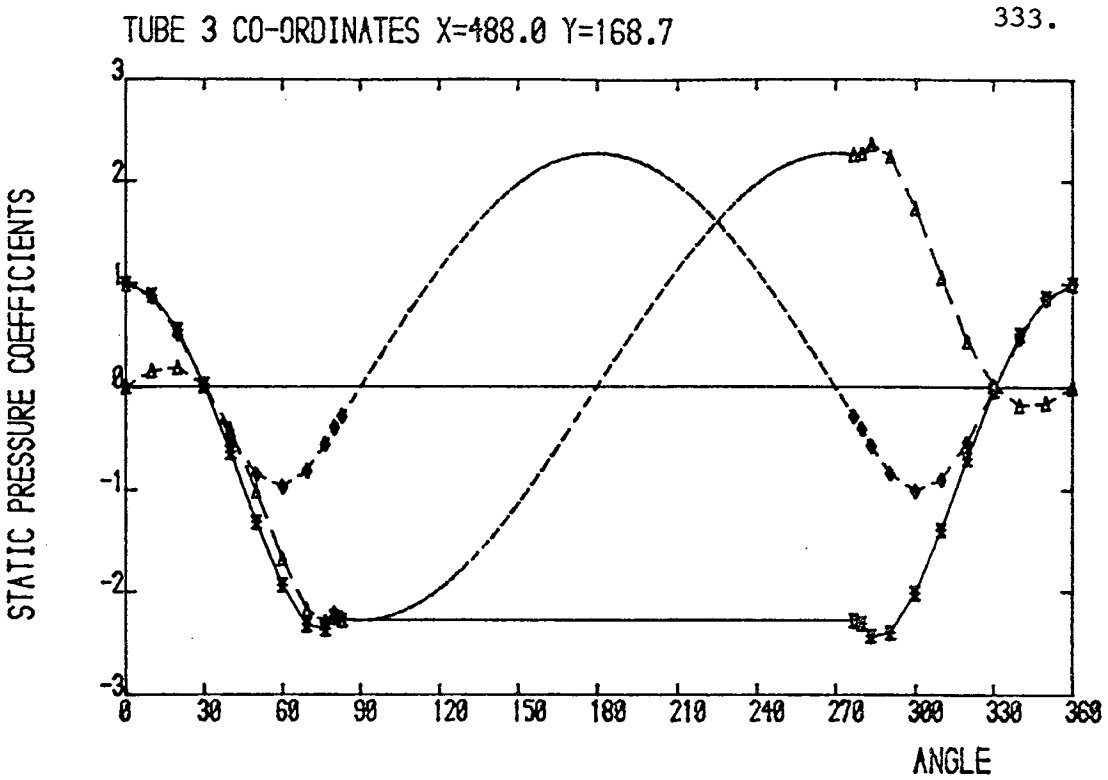


FIGURE 6.22 i-vi. Variation of static pressure coefficients round a tube displaced in the streamwise direction in a single tube row. (One tube with a wake model.)

FIGURE 6.22i. Displacement = 0.4 diameters upstream.

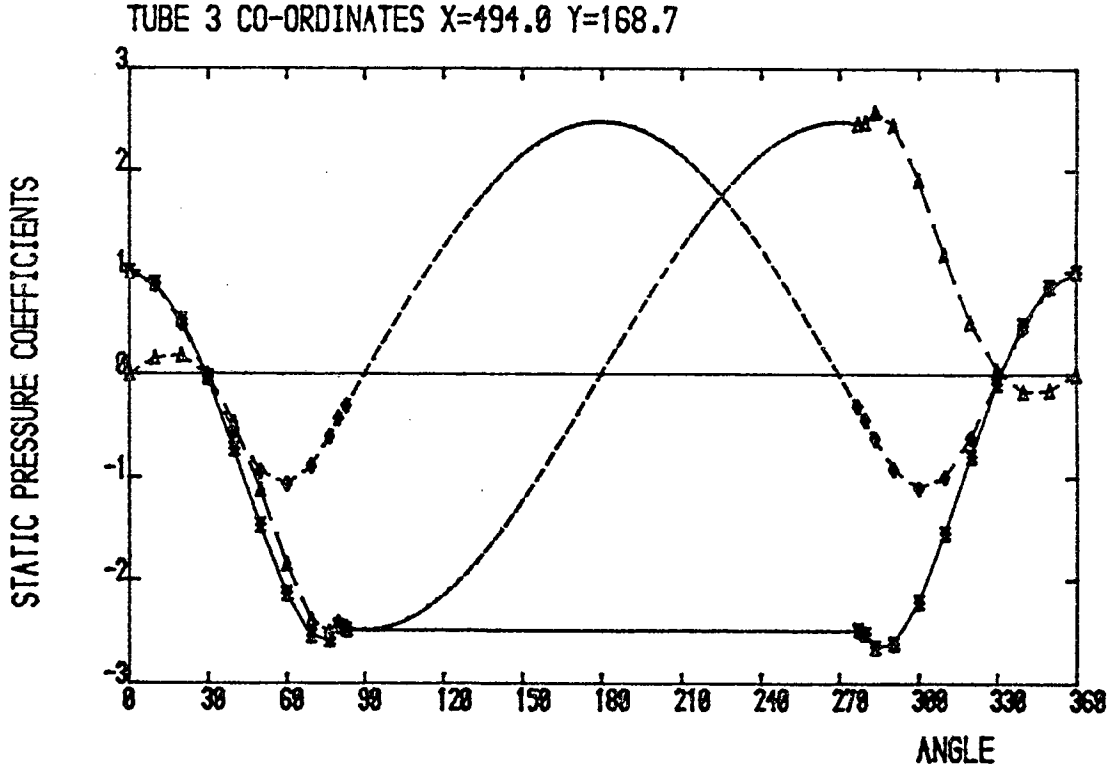


FIGURE 6.22ii. Displacement = 0.2 diameters upstream.

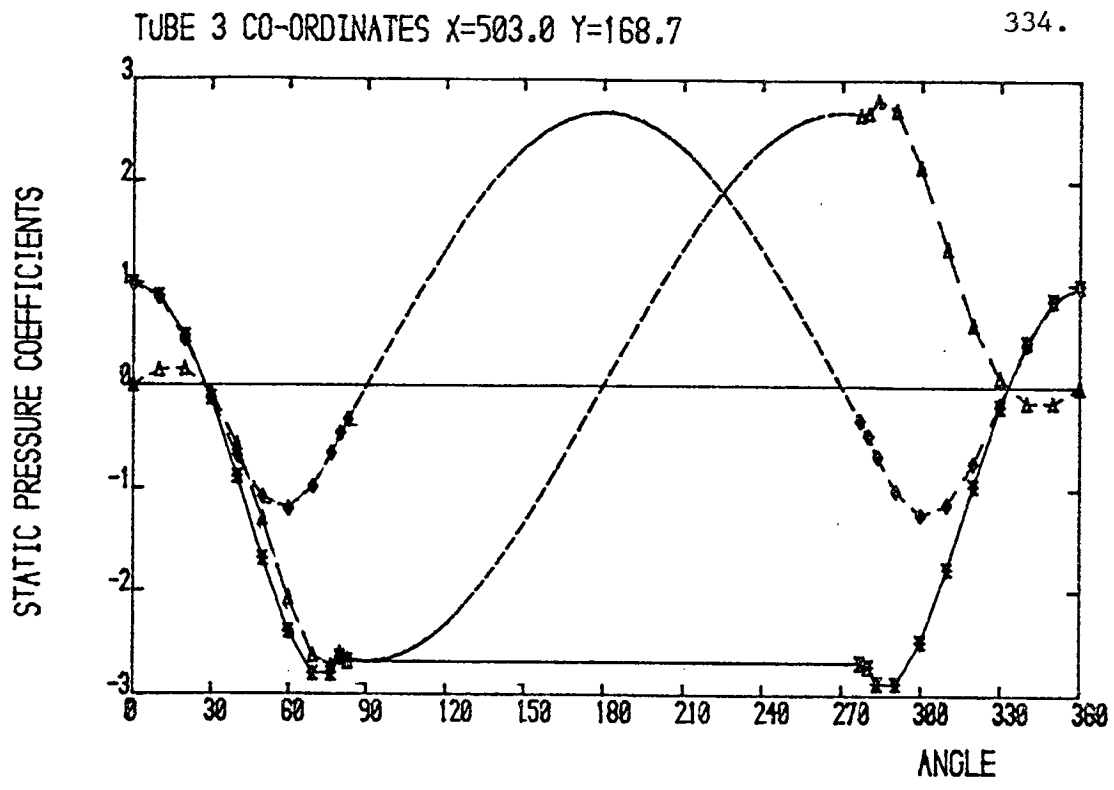


FIGURE 6.22iii. Displacement = 0.1 diameters downstream.

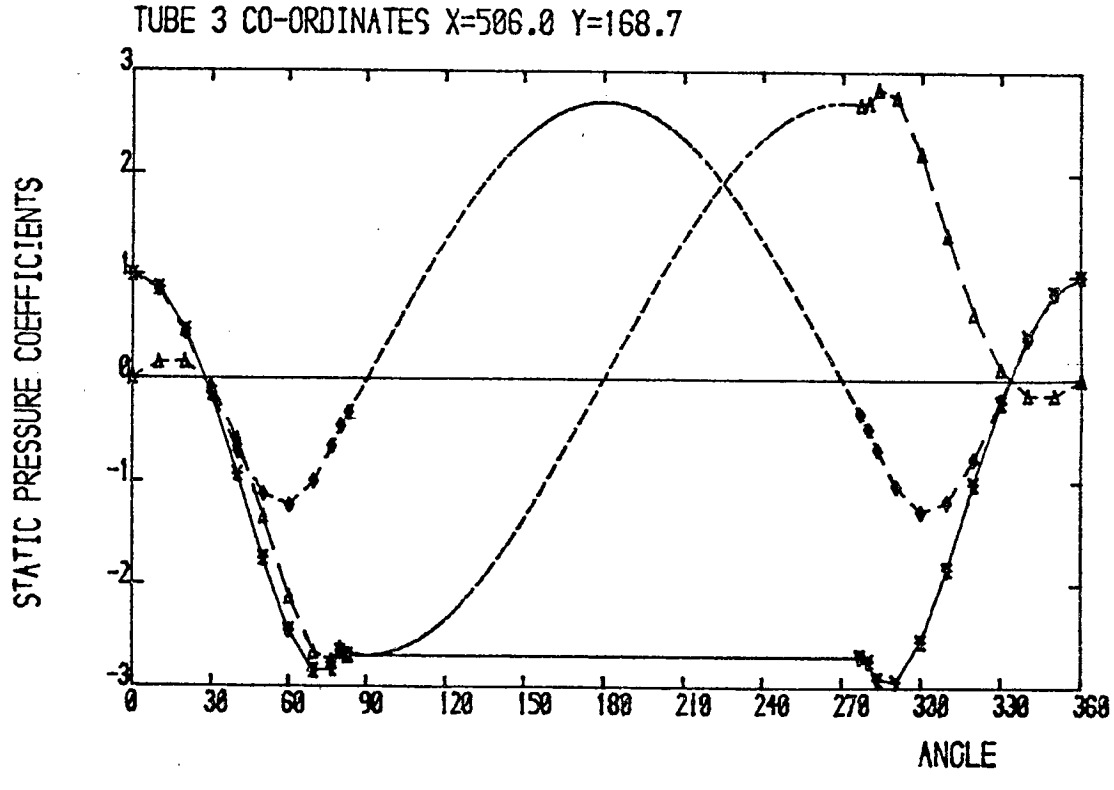


FIGURE 6.22iv. Displacement = 0.2 diameters downstream.

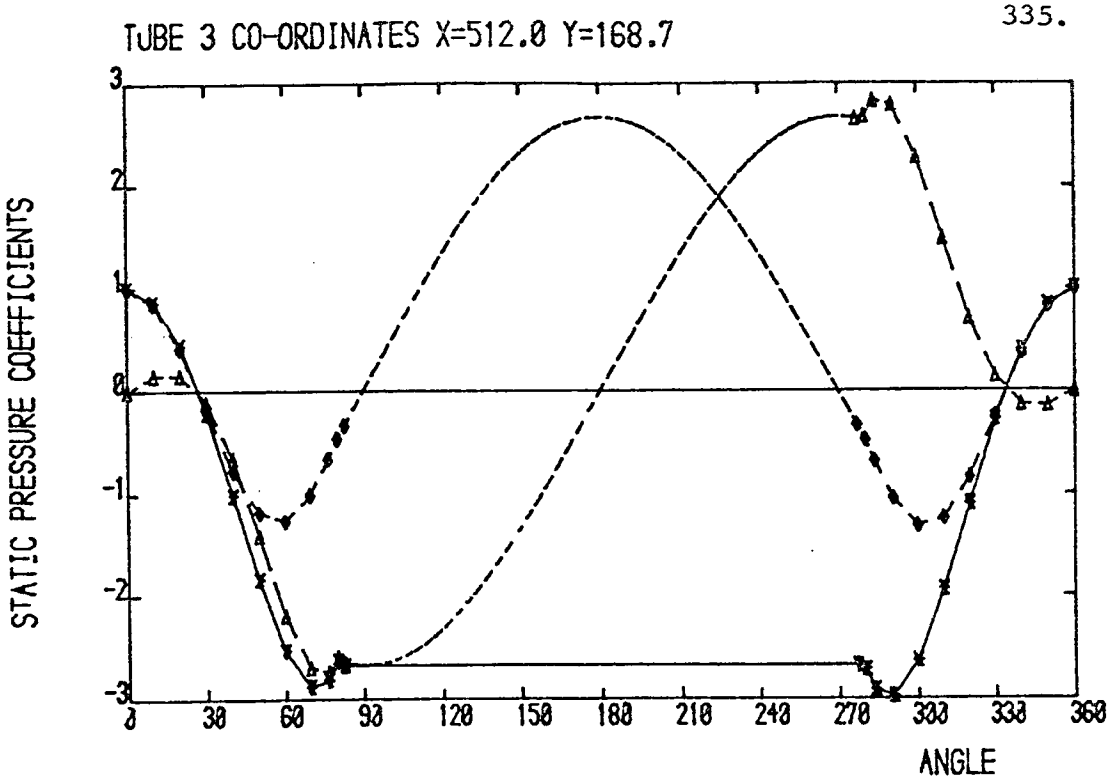


FIGURE 6.22v. Displacement = 0.4 diameters downstream.

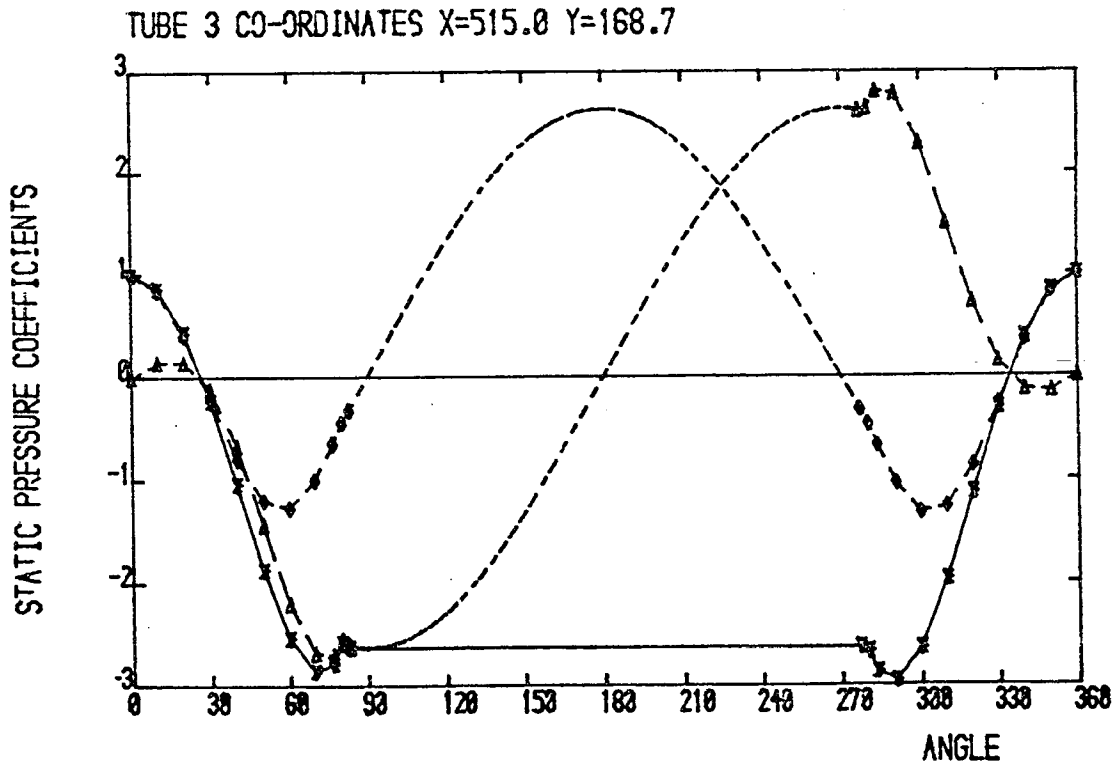


FIGURE 6.22vi. Displacement = 0.5 diameters downstream.

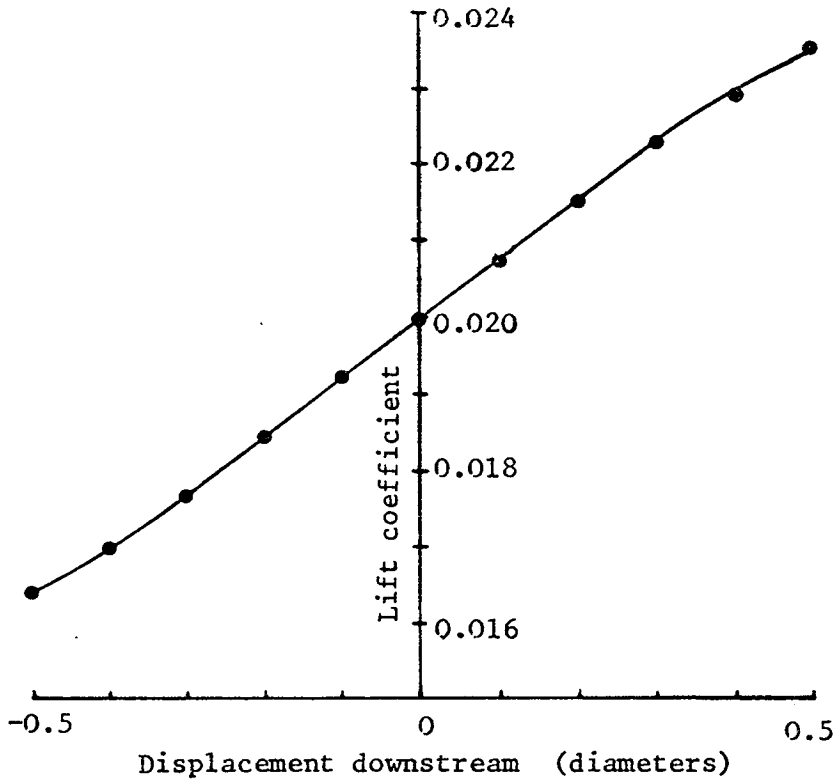


FIGURE 6.23. Variation of lift coefficient with tube displacement in the streamwise direction in a single tube row. (One tube with a wake model.)

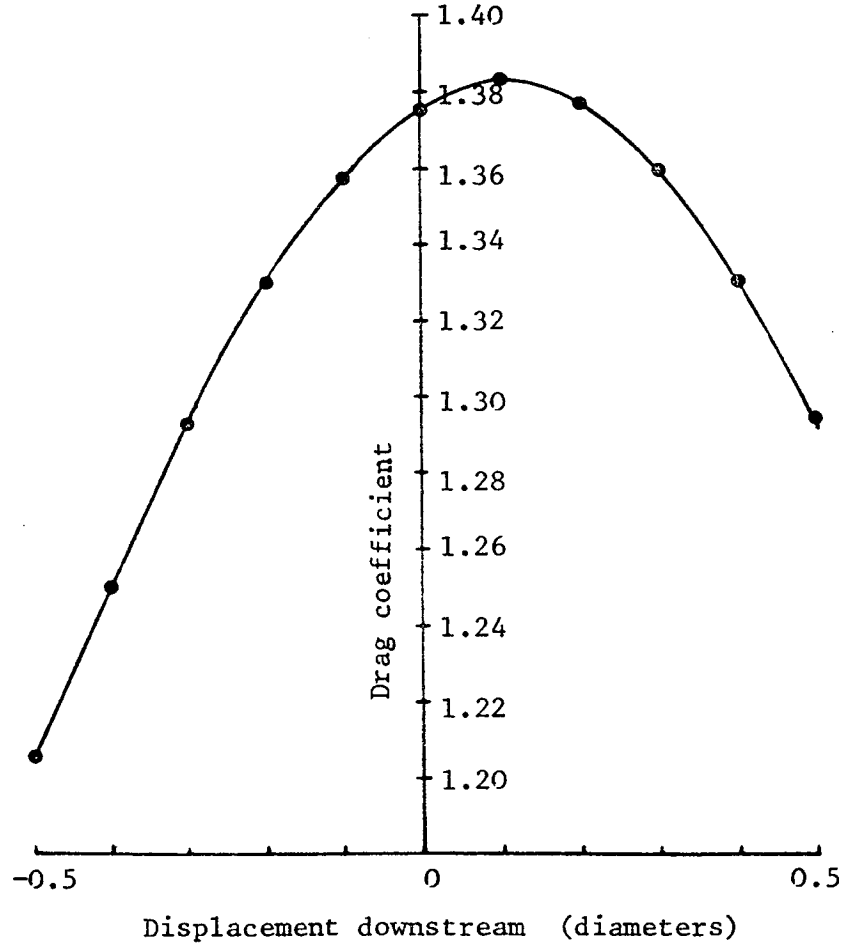


FIGURE 6.24. Variation of drag coefficient with tube displacement in the streamwise direction in a single tube row. (One tube with a wake model.)

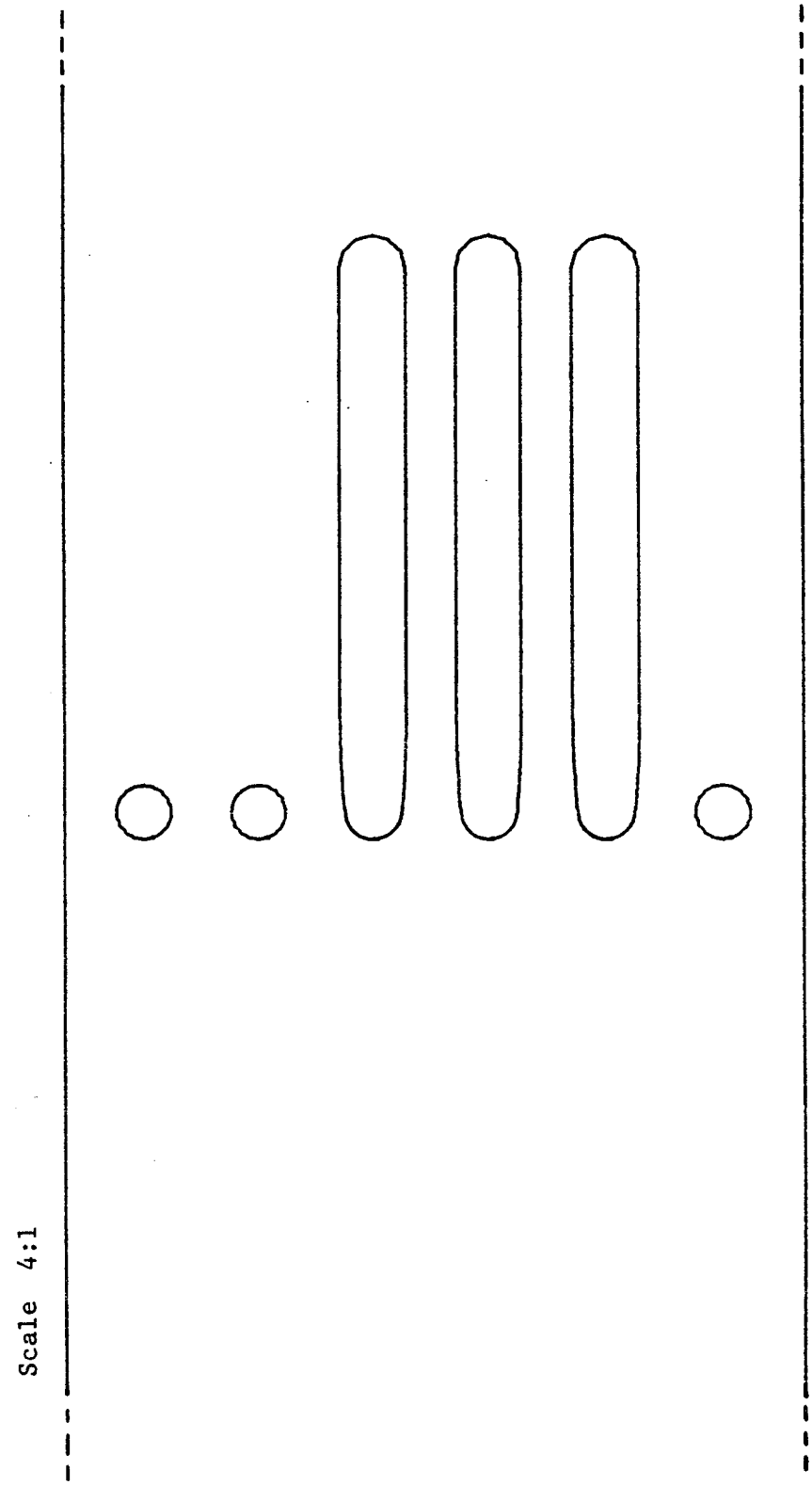


FIGURE 6.25. Arrangement of tubes in a single tube row model. (Three tubes with wake models.)

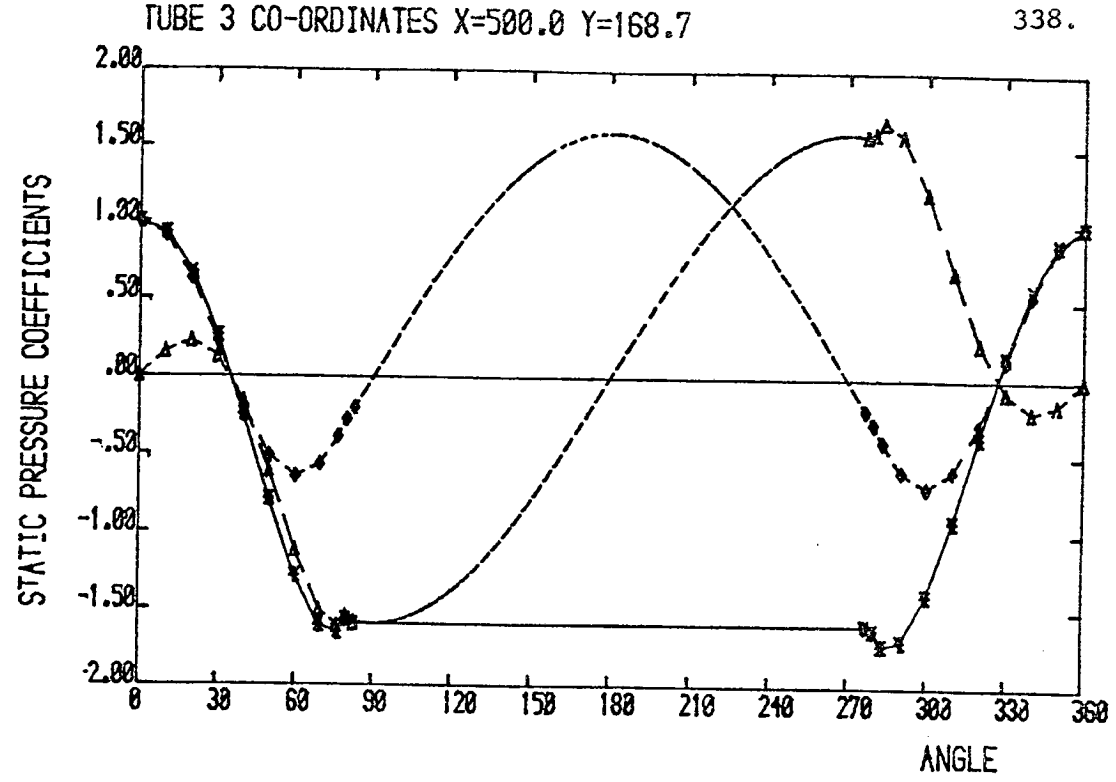


FIGURE 6.26 i-vi. Variation of static pressure coefficients round a tube displaced in the cross-flow direction in a single tube row. (Three tubes with wake models.)

FIGURE 6.26i. Displacement = 0 diameters.

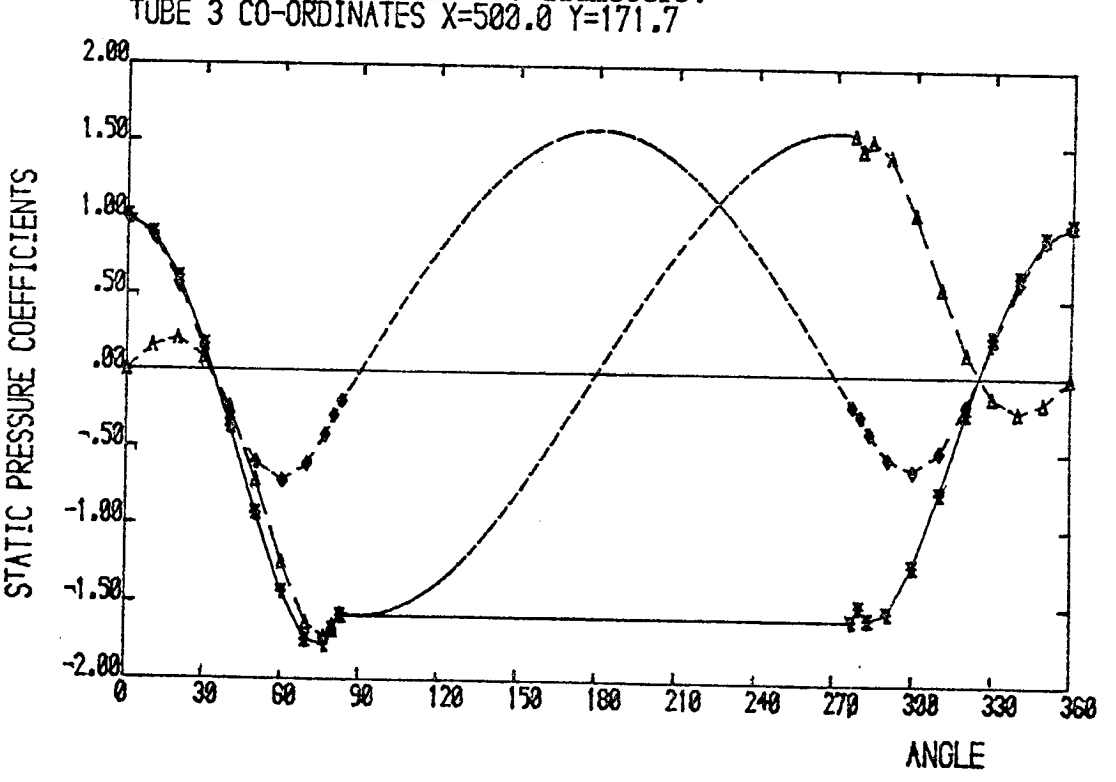


FIGURE 6.26ii. Displacement = 0.1 diameters.

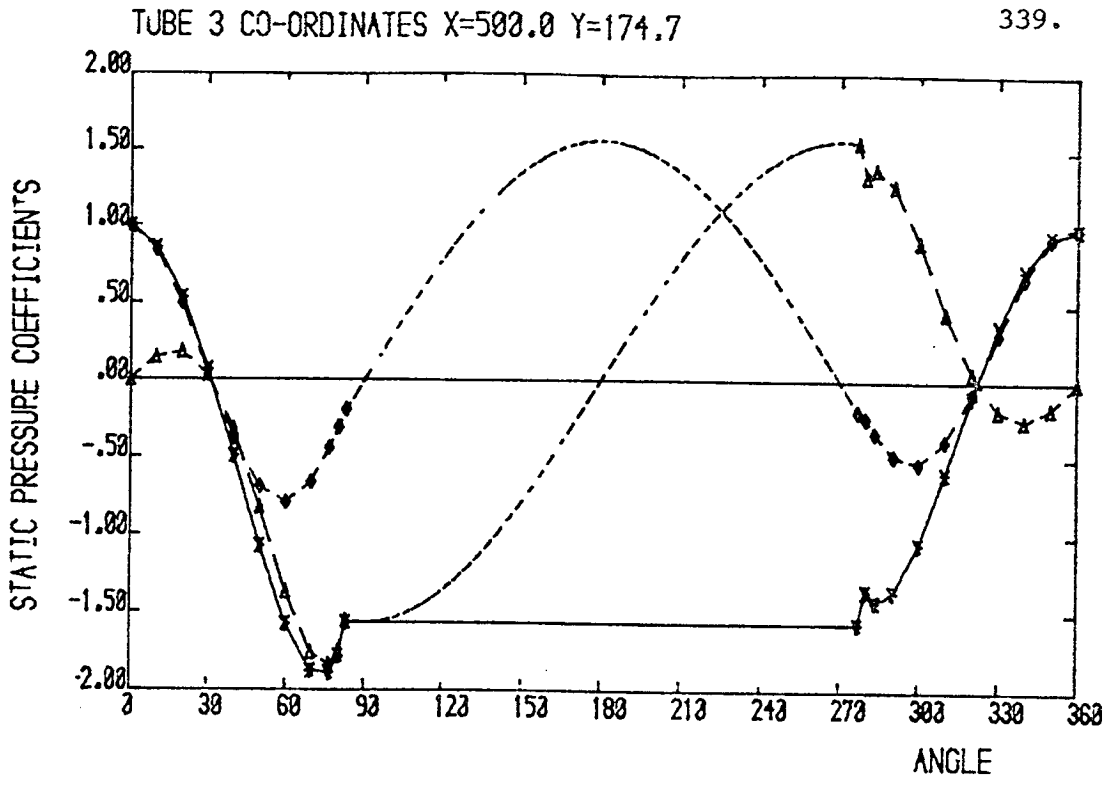


FIGURE 6.26iii. Displacement = 0.2 diameters.

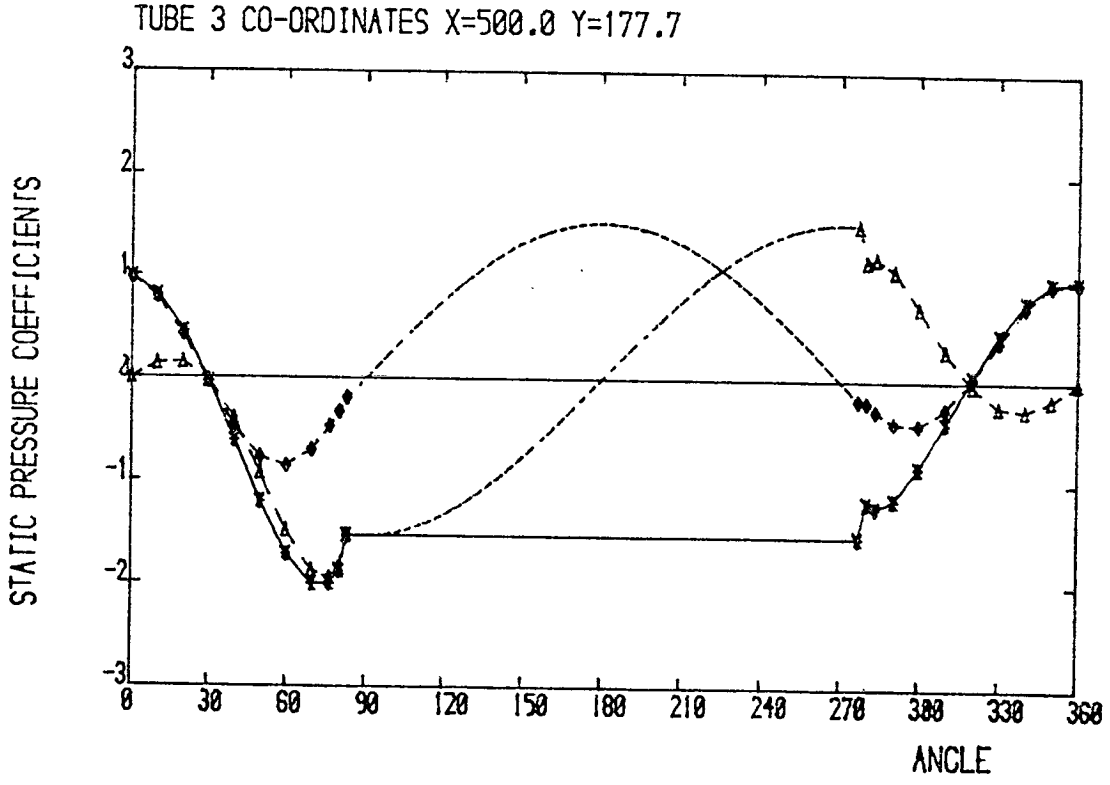


FIGURE 6.26iv. Displacement = 0.3 diameters.

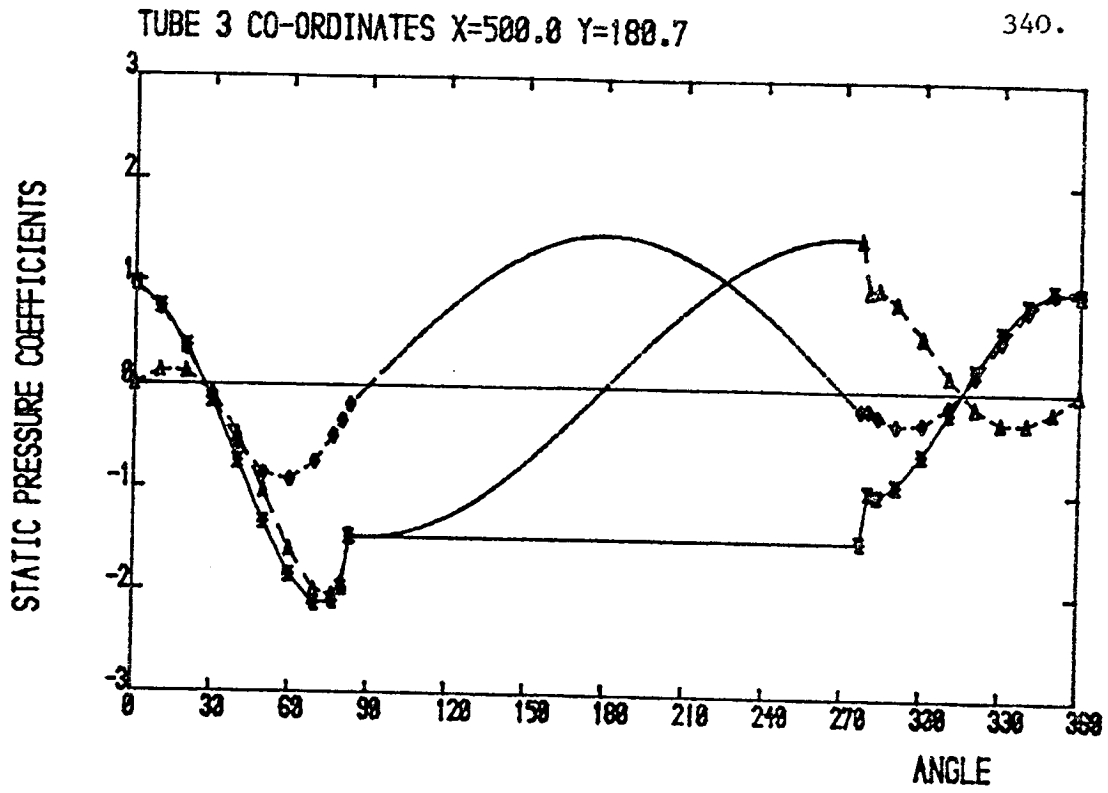


FIGURE 6.26v. Displacement = 0.4 diameters.

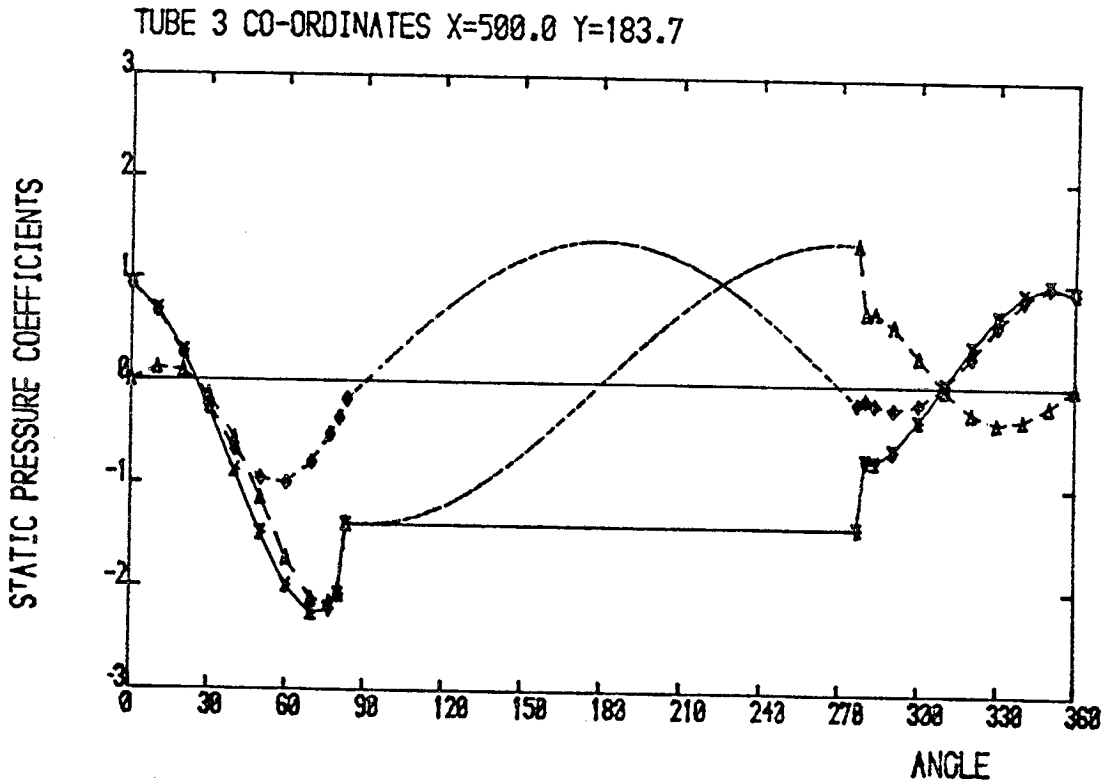


FIGURE 6.26vi. Displacement = 0.5 diameters.

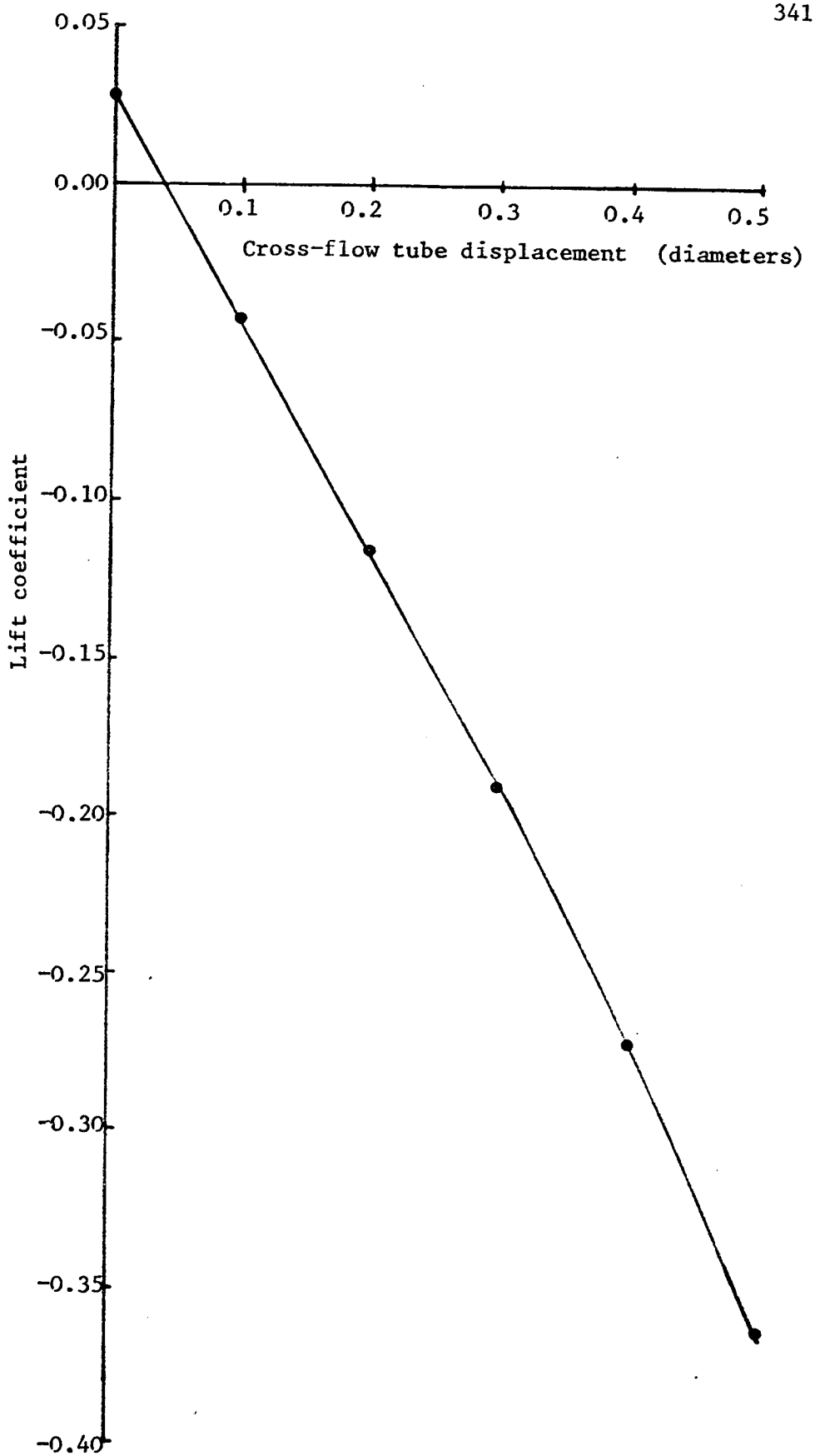


FIGURE 6.27. Variation of lift coefficient with tube displacement in the cross-flow direction in a single tube row. (Three tubes with wake models.)

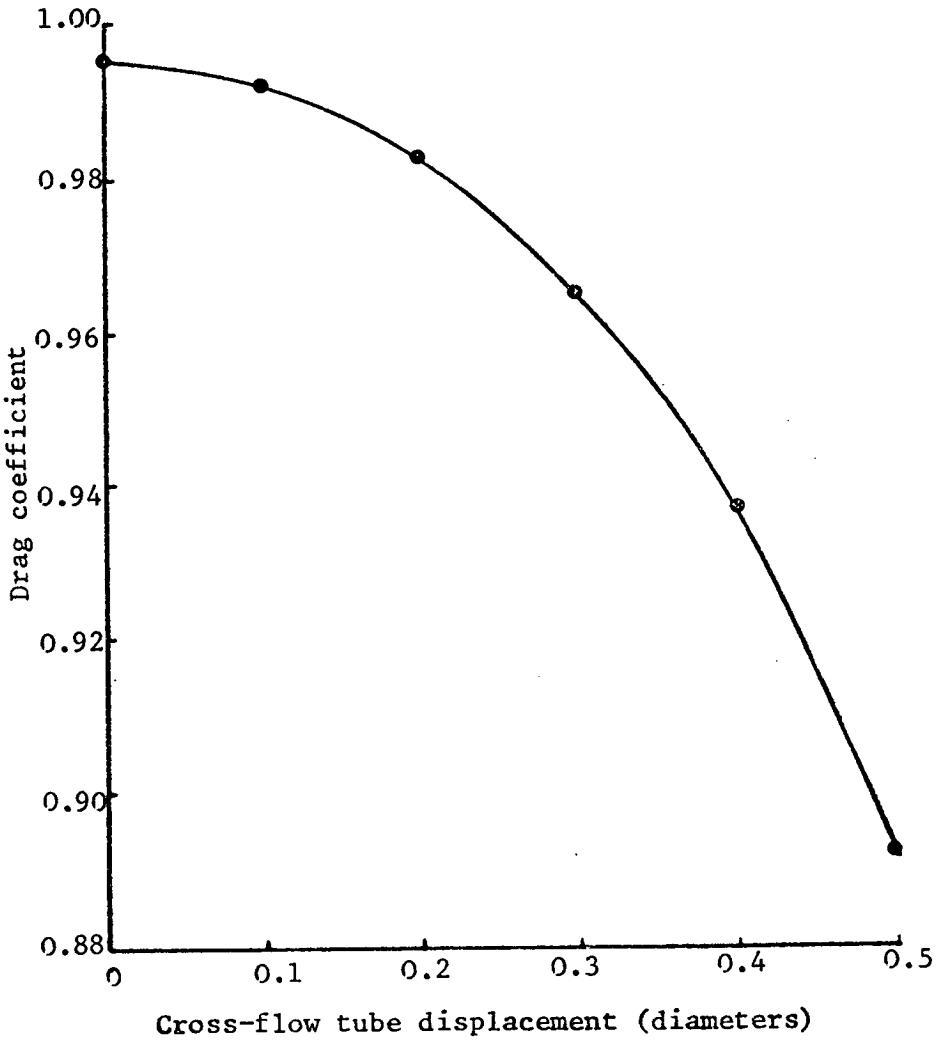


FIGURE 6.28. Variation of drag coefficient with tube displacement in the cross-flow direction in a single tube row. (Three tubes with wake models.)

Scale 4:1

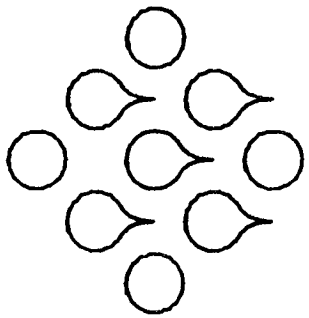

FIGURE 6.29. Arrangement of tubes in the equilateral triangular pitched tube bank model.

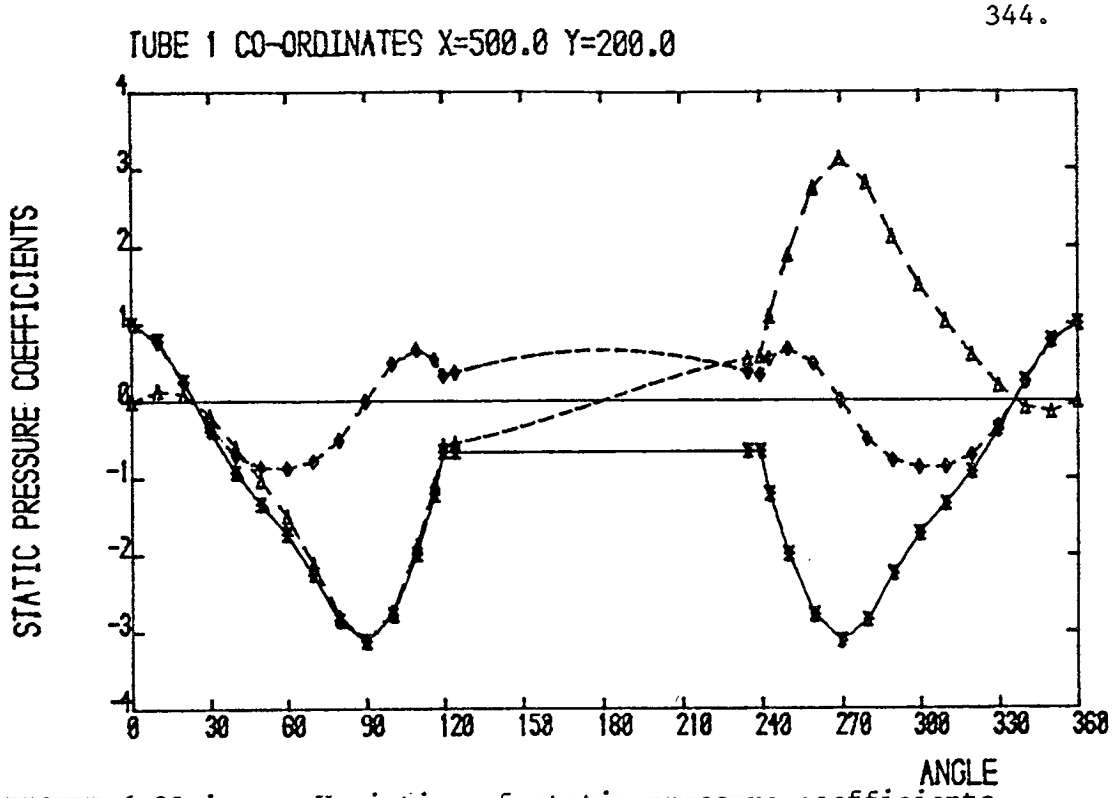


FIGURE 6.30 i-v. Variation of static pressure coefficients round a tube displaced in the cross-flow direction in the equilateral triangular pitched tube bank.

FIGURE 6.30i. Displacement = 0 diameters.

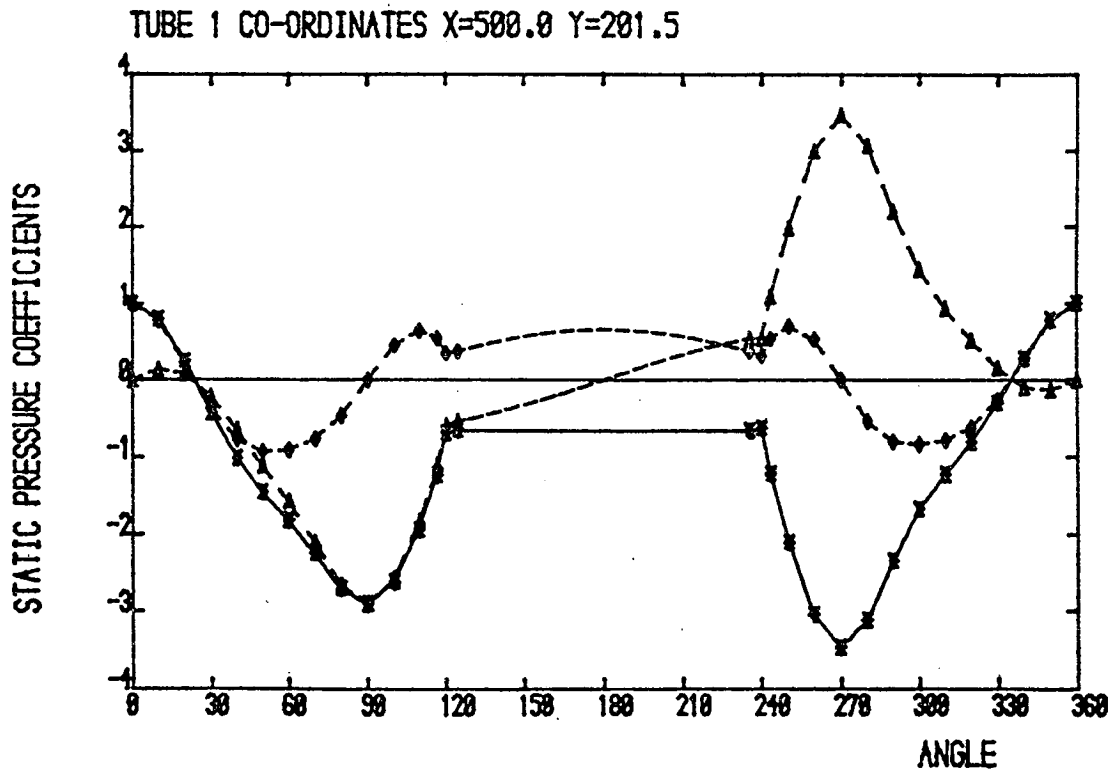


FIGURE 6.30ii. Displacement = 0.05 diameters.

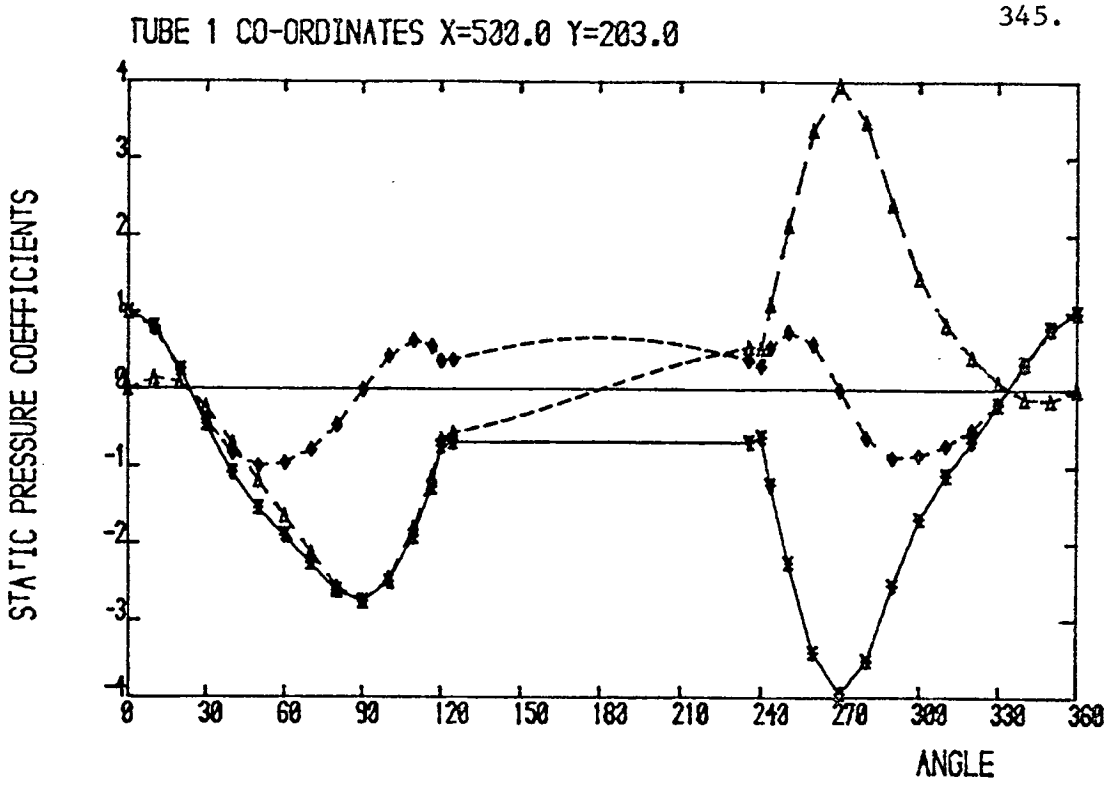


FIGURE 6.30iii. Displacement = 0.10 diameters.

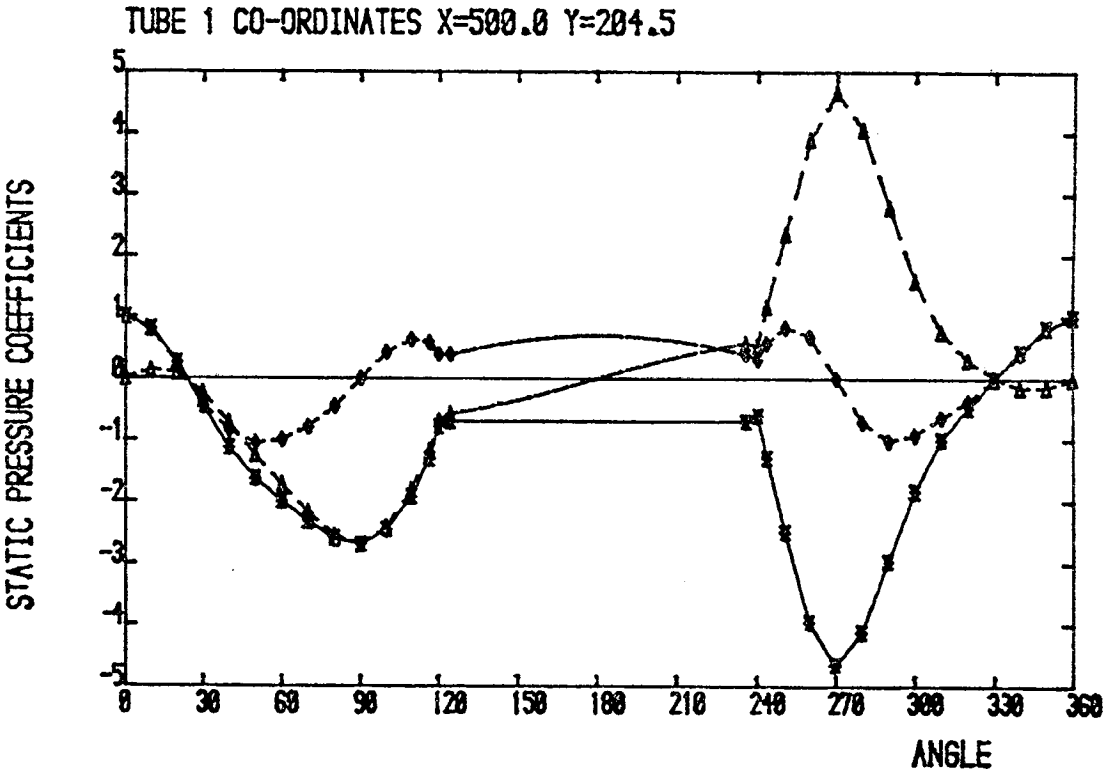


FIGURE 6.30iv. Displacement = 0.15 diameters.

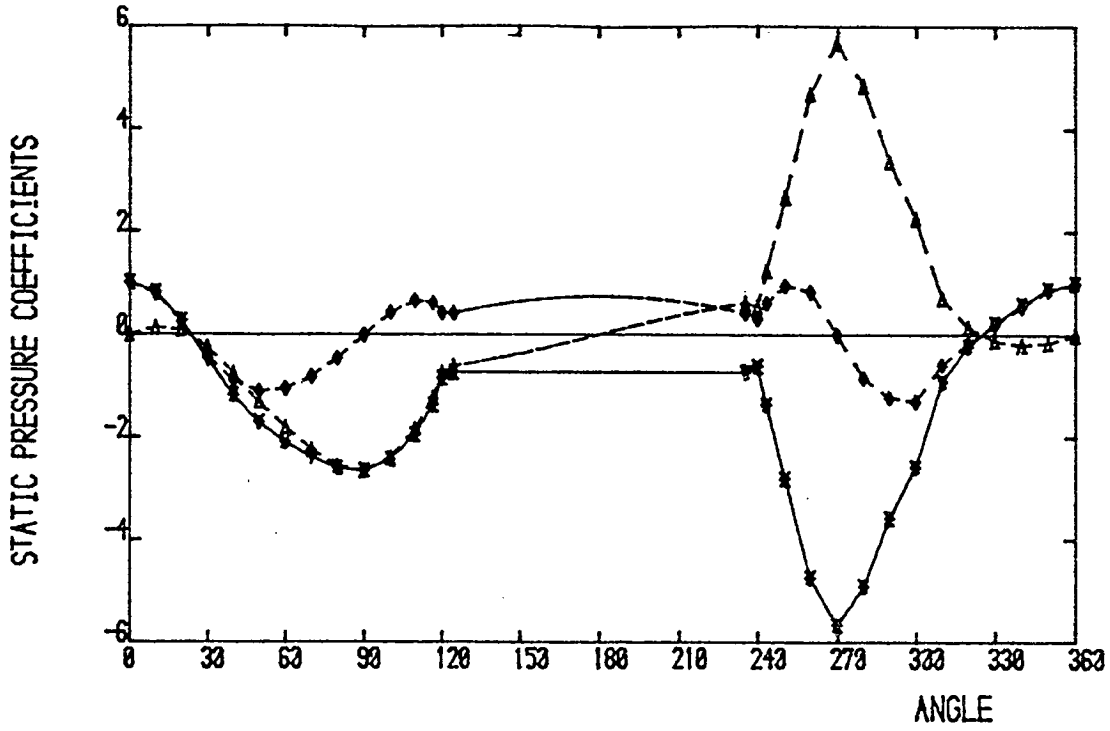


FIGURE 6.30v. Displacement = 0.20 diameters.

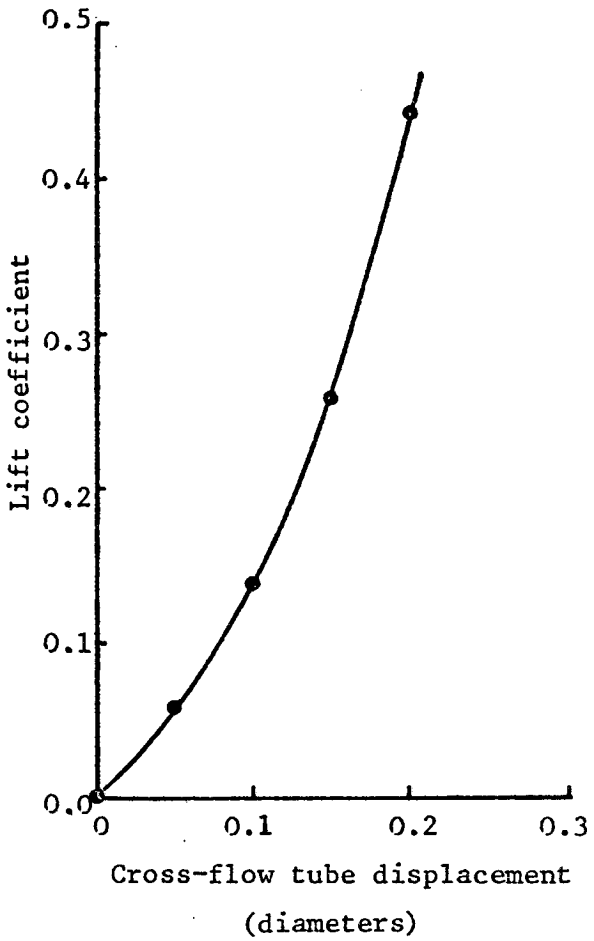


FIGURE 6.31. Variation of lift coefficient with tube displacement in the cross-flow direction in the equilateral triangular pitched tube bank.

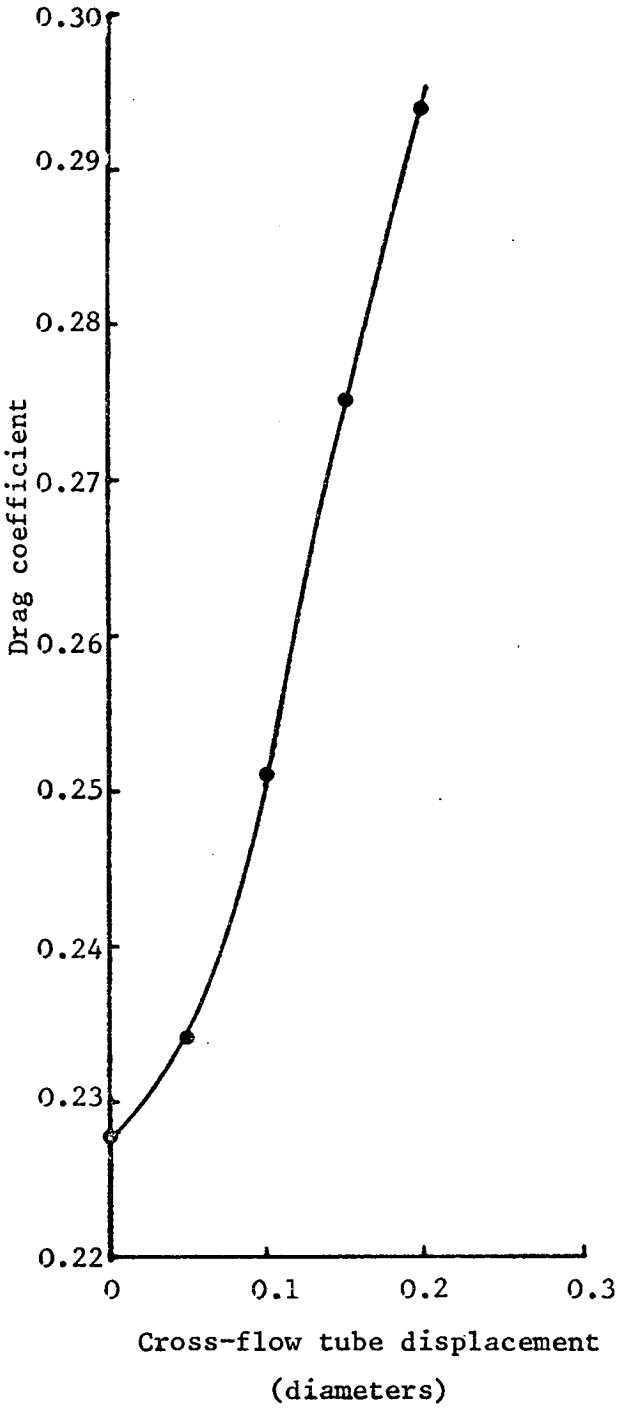


FIGURE 6.32. Variation of drag coefficient with tube displacement in the cross-flow direction in the equilateral triangular pitched tube bank.

Scale 4:1

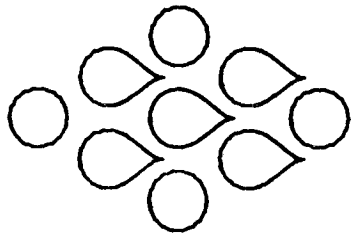

FIGURE 6.33. Arrangement of tubes in the tube bank with transverse pitch ratio, 1.043; longitudinal pitch ratio, 1.023.

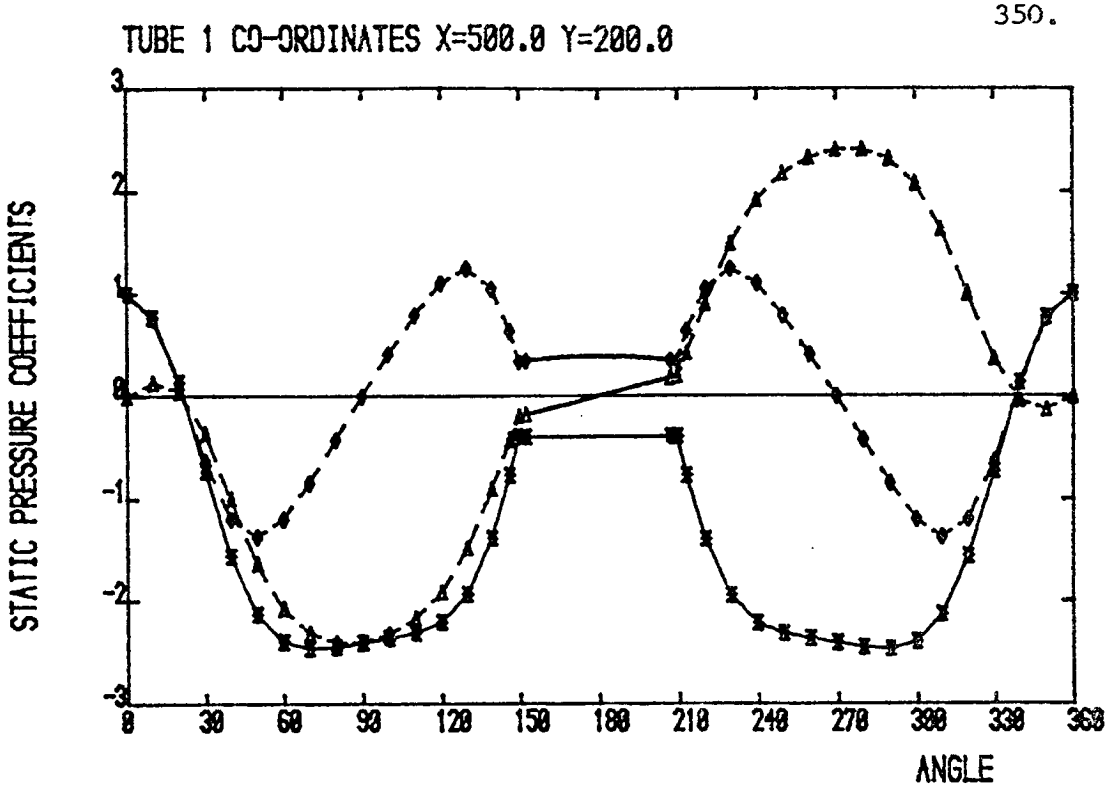


FIGURE 6.34. Variation of static pressure coefficients round a tube in the tube bank with transverse pitch ratio, 1.043; longitudinal pitch ratio, 1.023.

# CHAPTER 7

## SUMMARY AND CONCLUSIONS

Many investigations have been carried out on the various aspects of tube vibrations in heat exchanger tube banks. Particular attention has been paid to the measurement and the prediction of the onset of large amplitude tube vibrations which can lead to catastrophic failures in heat exchangers. However, the prediction schemes developed are not generally applicable to arbitrary heat exchangers subject to varying flow conditions. At present there is also no satisfactory scheme for predicting the vibration levels of tubes executing small amplitude vibrations. The occurrence of fatigue failures in heat exchanger tubes is therefore difficult to estimate.

In the present research project a wind tunnel, a dynamically modelled tube bank and the associated instrumentation were designed, constructed and tested in order to conduct experimental investigations of flow coupling between adjacent tubes and of the effect of sound on tube vibrations. Experiments were carried out on a single tube row and on a dynamically modelled staggered tube bank consisting of ten rows of tubes, six of which were free to vibrate. The detailed conclusions drawn from these experiments are given in Sections 4.12 and 5.8 respectively.

In addition potential flow models of tube rows and tube banks were developed using the boundary element technique. A computer program to solve potential flow problems was written and implemented on a digital computer. Investigations into the variation of the pressure distributions round tubes when they were statically displaced from their mean positions in a tube row and in a tube bank were conducted. The detailed conclusions drawn from these investigations are given in Section 6.11.

A summary of the main conclusions drawn from the investigations carried out during the research project is given below.

(i) The static displacement of a tube from its mean position in a tube row changes the mean and fluctuating flow field round it and its neighbouring tubes. The pressure distribution round a displaced tube becomes increasingly asymmetrical about a diameter in the streamwise direction and the

stagnation and separation points move round the tube, towards the position of the smaller gap, between the tube and its neighbours, with increasing displacement in the cross-flow direction. This changes the lift and drag forces on the tube which can either act as stabilizing or destabilizing forces, depending on the details of the tube's wake structure.

(ii) The static displacement of a tube in a tube row or tube bank does not necessarily produce lift and drag forces which vary linearly with displacement. This was shown both experimentally and theoretically, using a potential flow model and contradicts the assumption of linearity used in current schemes for predicting the forces on displaced tubes.

(iii) Displacing a tube affects the flow field round it so as to change the relative phases of pressure fluctuations in its boundary layer as a function of angle from the front of the tube.

(iv) The mean flow round tubes in a single tube row at Reynolds numbers of $1{\cdot}2 \times 10^5$ is three dimensional and in a staggered tube bank is approximately two dimensional.

(v) A tube vibrating with a small amplitude (i.e. $3 \times 10^{-3}$ diameters) has a non-linear effect on the flow field round its neighbouring tubes. There is no direct linear effect between a vibrating tube and the pressure fluctuations round and in the wake of its neighbouring tubes when the tube vibration amplitude is small. There is also no direct linear coupling via the flow between the vibrations of neighbouring tubes in a staggered tube bank.

(vi) The response of a tube in a tube row increases in proportion to the free stream dynamic pressure when there are no pressure fluctuations due to vortex shedding or acoustic duct modes near the resonance frequency of the tube and fluid-elastic coupling is negligible.

(vii) The level to which acoustic modes are excited in tube banks is dependent on the level of the pressure fluctuations at the duct modal frequencies created by the flow over the tubes.

(viii) Superimposed sound below SPL's of approximately 140 dB does not significantly affect the static pressure distributions round tubes and hence does not affect the static forces on the tubes in tube banks.

(ix) Superimposed sound affects the magnitude of the r.m.s. pressure fluctuations in tube boundary layers by means of a non-linear interaction with the flow which produces pressure fluctuations at frequencies not related to the frequency of the sound. These pressure fluctuations increase the vibration levels of the tubes over a broad band of frequencies. The increase in the pressure fluctuations at the tubes' resonance frequencies considerably increases the resonant tubes' vibrations.

(x) The linear effect of superimposed sound only becomes significant when the pressure fluctuations on the tubes, produced by the sound, are greater than the turbulent pressure fluctuations in the flow at the sound frequency.

(xi) The vibrations of a tube in a tube row are non-stationary and hence, when predicting tube fatigue failures in heat exchangers, (using measurements of tube vibrations as parameters in the calculations) it is necessary to measure the vibration responses of tubes over a long averaging time (at least 15 seconds).

(xii) The vibration responses of tubes in a tube bank are Gaussian.

(xiii) There is no evidence of vortex shedding occurring in the dynamically modelled staggered tube bank at Reynolds numbers between $8{\cdot}5 \times 10^4$ and $1{\cdot}2 \times 10^5$. Vortex shedding modes are present in the tube bank at Reynolds numbers below $8{\cdot}5 \times 10^4$ and at some flow velocities multiple vortex shedding modes are present.

(xiv) The r.m.s. tube vibration levels measured in the dynamically modelled tube bank are in agreement with the tube vibration levels measured in full scale heat exchangers, on which the model was based.

(xv) Investigations using the boundary element potential flow model of tube rows and tube banks show that realistic modelling of tube wakes is important if the forces on displaced tubes are to be predicted successfully.

(xvi) Simple tube row and tube bank models which assume separation occurs at the point of the minimum gap between tubes and which use the Bernoulli equation (applied to the jet between the tubes) to calculate the force on displaced tubes are in error. Hence, when these models are used as a basis for the prediction of the onset of large amplitude tube vibrations the results produced are not necessarily reliable.

# CHAPTER 8

## SUGGESTIONS FOR FURTHER WORK

There are many areas in which research is required before a full understanding of the mechanisms by which flow excites tube vibrations in heat exchanger tube banks can be achieved.

It is the opinion of the author that too much ad-hoc work has been previously carried out in just measuring tube vibrations in tube banks as a function of flow speed, and little attention has been paid to measuring the effect of tube vibrations on the flow field, and vice versa. It is not intended to suggest all the possible areas of research to be carried out before a full understanding of the mechanisms exciting tube vibrations in heat exchangers is obtained, but to outline a few important areas which might be fruitful in revealing more about the mechanisms of sound, flow and tube interactions in heat exchangers. The suggested areas of research are listed below.

(i) Measurement of the effect of the amplitude of vibration of a tube in a tube bank (forced to vibrate by a shaker) on the static and fluctuating pressure fields round its neighbours. This will show directly the effect of a vibrating tube (at different amplitudes) on the forces exciting its neighbouring tubes.

(ii) Measurement of the flow field round and in the wake of a stationary and vibrating tube in a tube bank using a laser Doppler velocimeter (which gives high resolution measurements and causes little interference to the flow field). This will show the effect of tube vibration on the near flow field of a tube.

(iii) Measurement of the flow field round and in the wake of a tube which is positioned near to (a) a stationary tube and (b) a vibrating tube in a tube bank. This will show directly the effect of neighbouring tube vibrations on the flow round and in the wake of a tube.

(iv) Measurement of the effect of sound at different frequencies on the amplitudes and relative phases of the pressure fluctuations at different points on the circumference of a tube in a tube bank. This might give some insight into the

effect of an external sound field on the pressure fluctuations in the boundary layer of a tube, and hence into the mechanisms by which sound excites tube vibrations.

(v) Extension of the boundary element potential flow model to include more realistic tube wake models based on experimentally measured wake velocity profiles. The shift in separation points with tube displacement could also be included in the model. If a larger and faster computer was available, a larger number of tube models could be used and the potential flow model could be coupled to a system of tube oscillator models. A dynamic simulation of the vibrating tubes excited by forces calculated from the boundary element tube bank model could then be carried out with effects due to added mass and fluid damping included.

If realistic wake models were developed, it might be possible to use the computer model as a basis for predicting the quasi-static forces on the tubes, and hence to predict the onset of fluid-elastic instabilities in heat exchanger tube banks.

# APPENDIX 1

## CIRCUIT DIAGRAMS

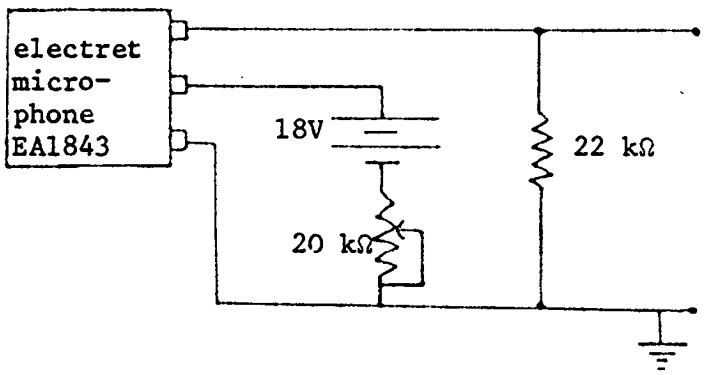


FIGURE A1.1. Electret microphone and power supply.

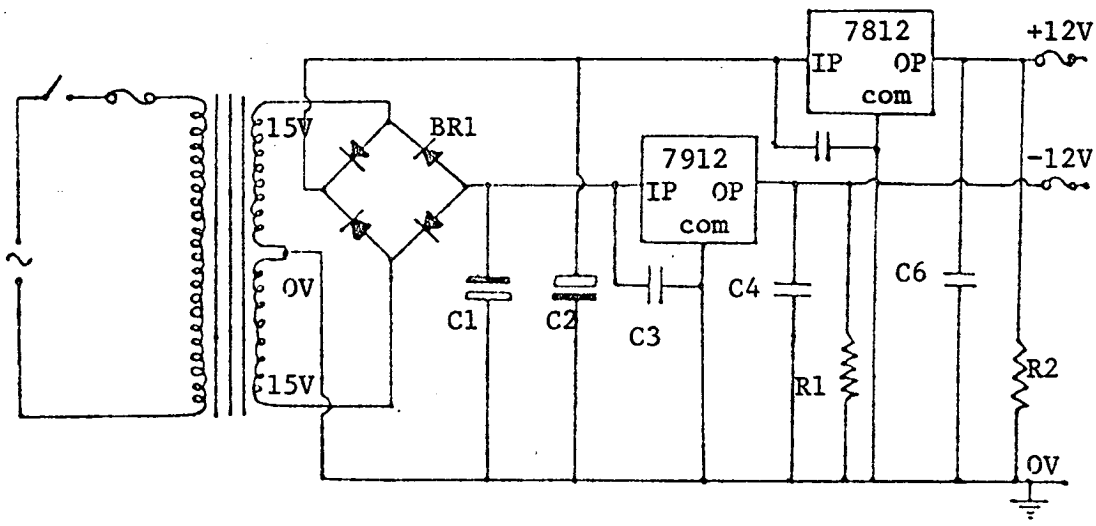


| | | | |
|---|---|---|---|
| C1 | 5000 µF | R1 | 4.7 kΩ |
| C2 | 5000 µF | R2 | 4.7 kΩ |
| C3 | 0.22 µF | BR1 | 50V 2A bridge rectifier |
| C4 | 0.47 µF | | |
| C5 | 0.22 µF | | |
| C6 | 0.47 µF | | |

FIGURE A1.2. Microphone amplifier power supply.

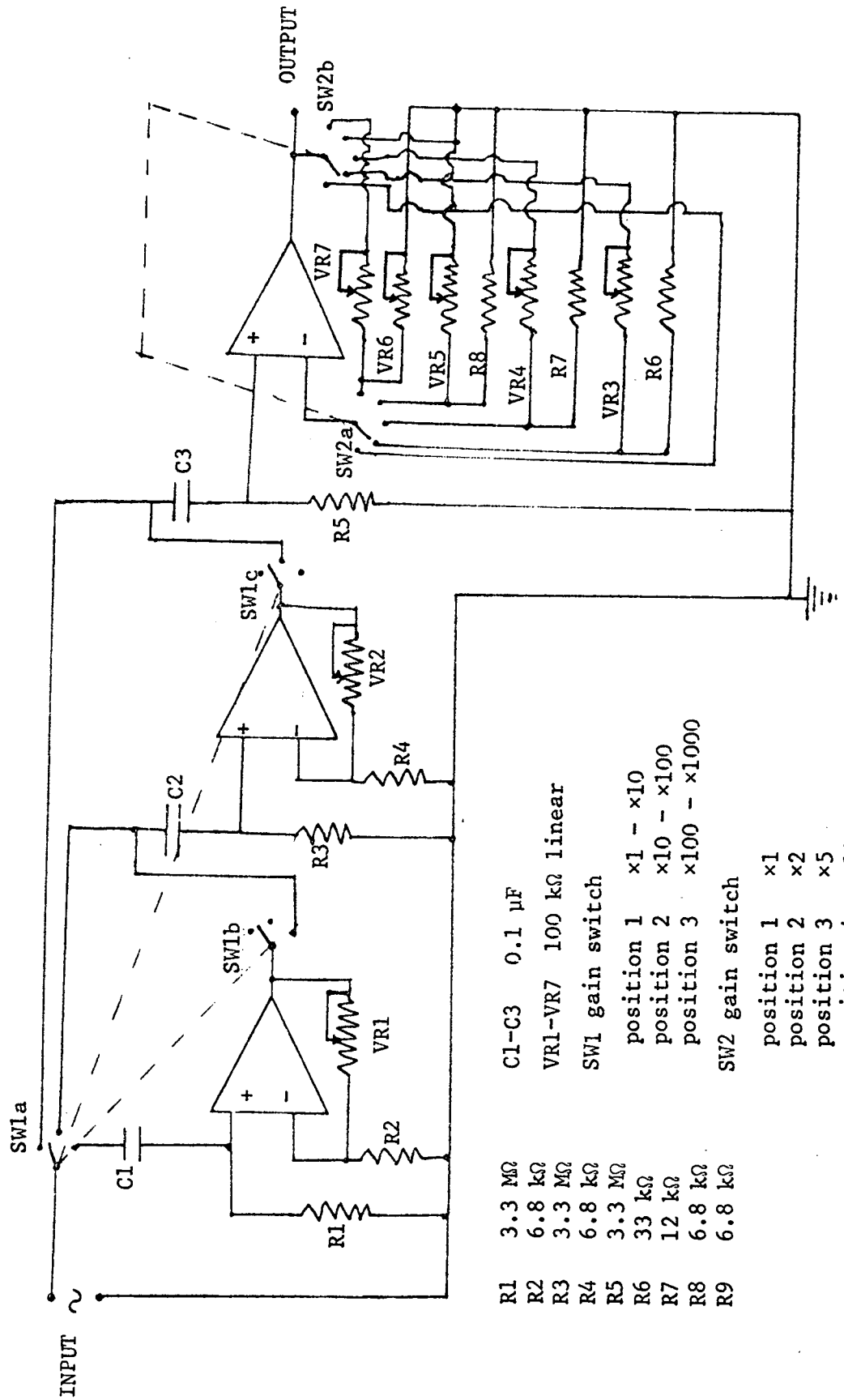


R1 3.3 MΩ
R2 6.8 kΩ
R3 3.3 MΩ
R4 6.8 kΩ
R5 3.3 MΩ
R6 33 kΩ
R7 12 kΩ
R8 6.8 kΩ
R9 6.8 kΩ

C1-C3 0.1 µF

VR1-VR7 100 kΩ linear

SW1 gain switch
position 1 ×1 - ×10
position 2 ×10 - ×100
position 3 ×100 - ×1000

SW2 gain switch
position 1 ×1
position 2 ×2
position 3 ×5
position 4 ×10
position 5 variable

FIGURE A1.3. Electret microphone amplifier (one channel shown).

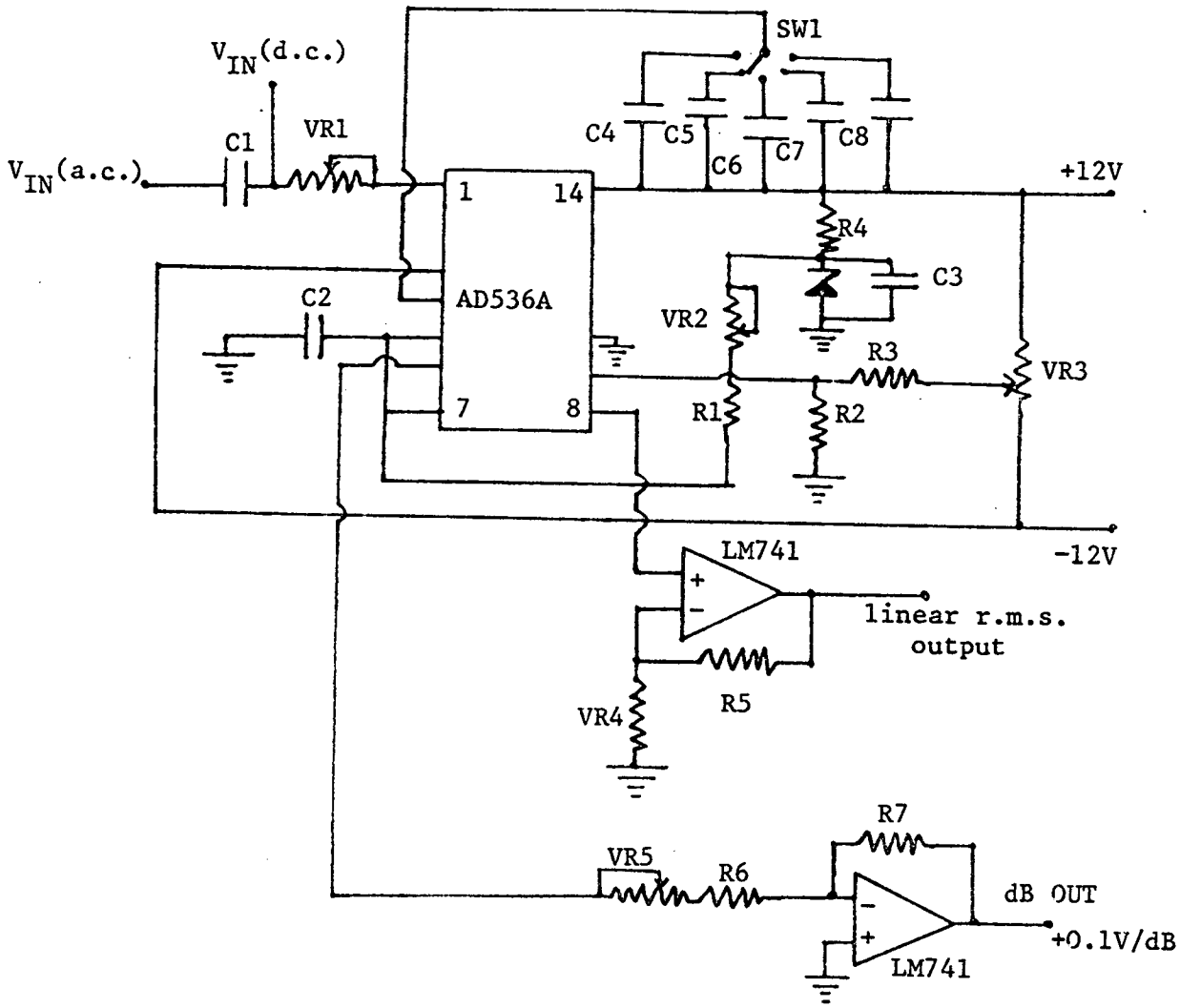


| | | | | | | | |
|---|---|---|---|---|---|---|---|
| R1 | 24 kΩ | VR1 | 500Ω | Trim Range | C1 | 4.7 µF |
| R2 | 220Ω | VR2 | 200 kΩ | dB zero | C2 | 1 nF |
| R3 | 470 kΩ | VR3 | 50 kΩ | offset | C3 | 100 nF |
| R4 | 6.8 kΩ | VR4 | 5 kΩ | dB gain | C4 | 4.7 µF |
| R5 | 22 kΩ | VR5 | 500Ω | linear gain | C5 | 10 µF |
| R6 | 1 kΩ | | | | C6 | 22 µF |
| R7 | 36 kΩ | SW1 | averaging time constant | | C7 | 47 µF |
| | | | | | C8 | 100 µF |

FIGURE A1.4. R.m.s. to d.c. converter.

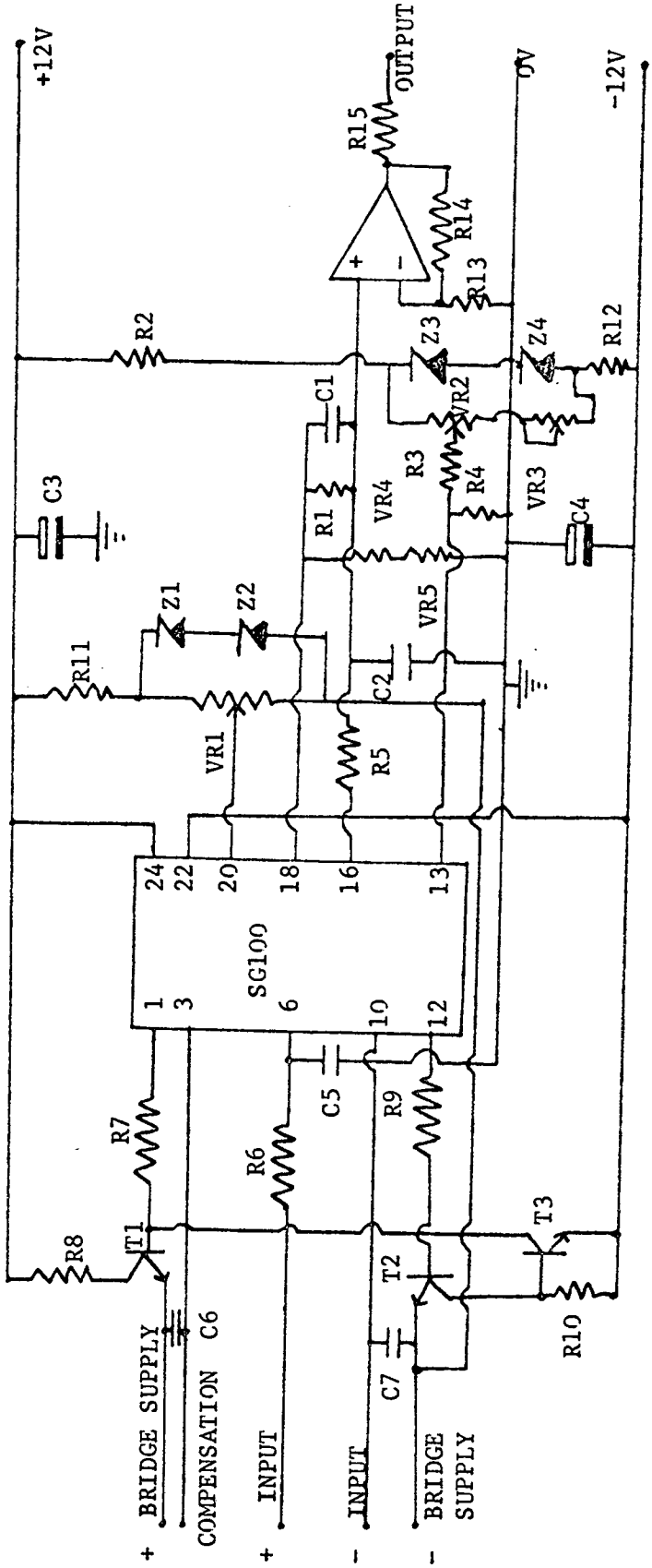


| | | | | | |
|---|---|---|---|---|---|
| R1 | 100 kΩ | R9 | 1 kΩ | C1 | 100 nF |
| R2 | 1 kΩ | R10 | 47Ω | C2 | 10 nF |
| R3 | 100 kΩ | R11 | 1 kΩ | C3 | 10 µF |
| R4 | 50Ω | R12 | 1 kΩ | C4 | 10 µF |
| R5 | 10Ω | R13 | 1 kΩ | C5 | 10 nF |
| R6 | 100Ω | R14 | 18 kΩ | C6 | 100 nF |
| R7 | 1 kΩ | R15 | 47Ω | C7 | 100 nF |
| R8 | 47Ω | | | | |

| | |
|---|---|
| T1 | BD135 |
| T2 | BD136 |
| T3 | BC108 |
| Z1-Z4 | IN827 |

| | | |
|---|---|---|
| VR1 | 10k | Set Bridge Supply |
| VR2 | 10k | Course Set Zero |
| VR3 | 2k | Fine Set Zero |
| VR4 | 5k | Course Set Gain |
| VR5 | 50Ω | Fine Set Gain |

FIGURE A1.5. Pressure transducer strain gauge amplifier.

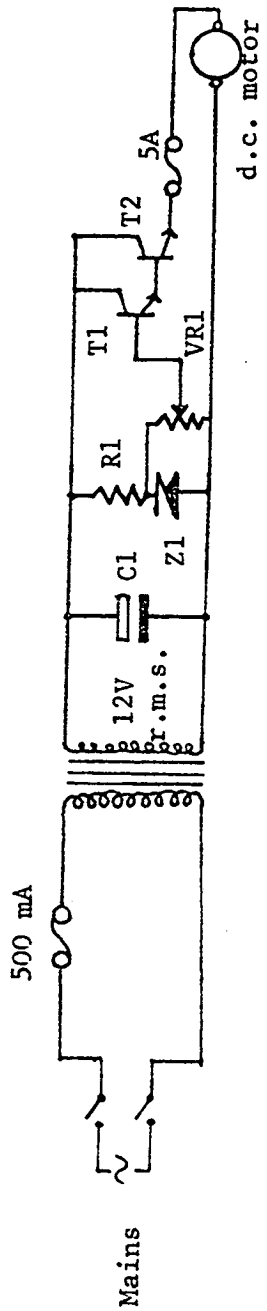


C1 5000 µF T1 TIP121

T1 470Ω T2 2N3055

VR1 10 kΩ Z1 12V zener diode

FIGURE A1.6. Power supply for rotating pressure measuring tube drive motor.

# APPENDIX 2

## LISTINGS OF COMPUTER PROGRAMMES

### LISTING 1. MICROPROCESSOR DATA ACQUISITION AND CONTROL PROGRAMME

```
1 REM MICROPROCESSOR DATA ACQUISITION
2 REM AND CONTROL PROGRAMME
9 REM
10 REM MENU AND VARIABLE DECLARATION ROUTINE
20 PRINT
30 PRINT "DATA ACQUISITION AND CONTROL SYSTEM"
40 PRINT
50 PRINT "COPYRIGHT R.G. ARAK"
60 PRINT
65 CLEAR 200
70 K=0:I=0:J=0:AV=16:A=0:B=0
75 C1=65536:C2=32768
80 DIM N(20)
85 GOSUB 1000
90 PRINT:PRINT
100 PRINT "INPUT THE NUMBER OF THE ROUTINE"
110 PRINT "YOU REQUIRE"
120 PRINT
130 PRINT "1. CALIBRATE TRANSDUCERS"
140 PRINT "2. ACQUIRE DATA AND CONTROL"
150 PRINT "3. DISPLAY DATA"
160 PRINT "4. DATA FORMATTER"
170 PRINT "5. PRINT DATA"
180 PRINT "6. PAPER TAPE PUNCH"
190 PRINT "7. PAPER TAPE READ"
195 PRINT "8. PAPER TAPE READ FORMATTER"
197 PRINT "9. CHANGE OUTPUT RATE"
198 PRINT "10. ROTATE TUBE"
200 INPUT SR
210 ON SR GOSUB 3000,5000,2000,6000,4000,7000
212 SR=SR-6
213 IF SR<0 THEN SR=0
215 ON SR GOSUB 8000,9000,1880,10000
220 PRINT:PRINT
230 PRINT "DO YOU REQUIRE ANOTHER FUNCTION?"
240 PRINT "YES OR NO?"
250 INPUT A$
260 IF LEFT$(A$,1)<>"N" GOTO 90
280 PRINT "PROGRAMME TERMINATES"
290 REM END OF EXECUTABLE PROGRAMME
300 STOP
999 REM
1000 REM MACHINE CODE SUBROUTINES
1010 DATA 205,139,233,14,5,123,211,4,6,32,237
1015 DATA 65,17,1,0,55,63,33,0,16,237,82,32,252
1020 DATA 6,176,237,65,55,63,33,0,16,237,82,32
1025 DATA 252,6,32,237,65,6,240,237,65,201
1030 DATA 62,255,211,7,62,0,211,7,211,7,62,55
1035 DATA 211,7,62,255,211,7,211,6,62,0,211,6
1040 DATA 211,6,62,55,211,6,62,255,211,6,14,4
1045 DATA 42,176,15,237,91,178,15,237,82,43,55
1050 DATA 63,0,34,180,15,17,1,0,221,42,180,15
1055 DATA 42,176,15,62,192,211,5,237,163,62
1060 DATA 2,211,5,62,0,211,5,221,25,48,242,55
1065 DATA 63,62,0,211,4,62,2,211,5,62,0,211,5
1070 DATA 223,98,48,213,201
1075 DATA 207,71,62,0,42,13,224,233
1080 DATA 245,50,58,194,234,41,194,238,128,223
1085 DATA 111,58,58,194,254,13,202,53,194,241
1090 DATA 201,62,10,195,33,194
1498 REM STORE MACHINE CODE SUBROUTINES
1499 REM IN PROGRAMME MEMORY
1500 Z1=49152
1510 IF Z1>C2 THEN Z1=Z1-C1
```

LISTING 1. (continued)

```
1520 FOR I=1 TO 46
1530 READ A
1540 POKE Z1,A
1550 Z1=Z1+1
1560 NEXT I
1570 Z1=49200
1580 IF Z1>C2 THEN Z1=Z1-C1
1590 FOR I=1 TO 99
1600 READ A
1610 POKE Z1,A
1620 Z1=Z1+1
1630 NEXT I
1640 Z1=49312
1650 IF Z1>C2 THEN Z1=Z1-C1
1660 FOR I=1 TO 8
1670 READ A
1680 POKE Z1,A
1690 Z1=Z1+1
1700 NEXT I
1710 Z1=49696
1720 IF Z1>C2 THEN Z1=Z1-C1
1730 FOR I=1 TO 26
1740 READ A
1750 POKE Z1,A
1760 Z1=Z1+1
1770 NEXT I
1780 Z1=49696
1790 IF Z1>C2 THEN Z1=Z1-C1
1800 DOKE 3192,Z1
1810 DOKE 3195,1769
1820 DOKE 4100,1848
1830 I=USR(0)
1860 NULL 5
1870 RETURN
1875 REM
1880 REM CHANGE OUTPUT SPEED ROUTINE
1885 PRINT "DO YOU WANT FAST OR SLOW OUTPUT?"
1890 PRINT "1. FAST"
1895 INPUT "2. SLOW";I
1900 IF I=1 GOTO 1935
1905 Z1=49696-C1
1910 DOKE 3192,Z1
1915 DOKE 3195,1769
1920 DOKE 4100,1754
1925 I=USR(0)
1927 DOKE 4100,1743
1928 I=USR(0)
1930 RETURN
1935 DOKE 4100,1848
1940 I=USR(0)
1950 RETURN
1999 REM
2000 REM SCOPE DISPLAY ROUTINE
2010 PRINT:PRINT "DATA DISPLAY ROUTINE"
2020 PRINT
2030 PRINT "DO YOU REQUIRE DEFAULT LOCATIONS?"
2040 DOKE 4100,-16336
2050 INPUT "Y OR N";A$
2060 IF LEFT$(A$,1)="Y" THEN GOSUB 2210
2070 IF LEFT$(A$,1)="Y" GOTO 2170
2080 PRINT "INPUT MEMORY LOCATIONS"
2090 INPUT "START OF DATA";DS
2100 PRINT "HOW MANY POINTS DO YOU WISH"
2110 INPUT "TO DISPLAY";PD
2120 DF=DS+PD
2130 IF DS>C2 THEN DS=DS-C1
2140 IF DF>C2 THEN DF=DF-C1
2150 DOKE 4016,DS
2160 DOKE 4018,DF
2170 PRINT:PRINT "HIT ANY KEY TO KILL DISPLAY"
2180 PRINT
2190 I=USR(J)
2200 RETURN
2210 PRINT
2220 PRINT "WHICH DATA DO YOU WISH TO DISPLAY?"
2230 PRINT:PRINT "1. PRESSURE TRANSDUCER"
```

## LISTING 1. (continued)

```
2240 PRINT "2. MICROPHONE"
2250 Z1=L1:Z2=F1:Z3=L2:Z4=F2
2260 INPUT I
2270 IF I=2 GOTO 2330
2280 PRINT
2290 PRINT "PRESSURE TRANSDUCER DATA"
2293 IF Z1>C2 THEN Z1=Z1-C1
2294 IF Z2>C2 THEN Z2=Z2-C1
2300 DOKE 4016,Z1
2310 DOKE 4018,Z2
2320 RETURN
2330 PRINT:PRINT "MICROPHONE DATA"
2340 IF Z3>C2 THEN Z3=Z3-C1
2345 IF Z4>C2 THEN Z4=Z4-C1
2350 DOKE 4016,Z3
2360 DOKE 4018,Z4
2370 RETURN
2999 REM
3000 REM INSTRUMENTATION CALIBRATION ROUTINE
3010 PRINT
3015 PRINT"INSTRUMENTATION CALIBRATION ROUTINE"
3020 PRINT
3030 OUT 7,255:OUT 7,4:OUT 7,0:OUT 7,55
3040 OUT 7,251:OUT 6,255:OUT 6,255:OUT 6,0
3050 OUT 6,55:OUT 6,255
3060 OUT 5,0:OUT 5,241
3070 PRINT "WHICH CHANNEL DO YOU WISH"
3080 PRINT "TO CALIBRATE?"
3090 PRINT:PRINT "1. PRESSURE TRANSDUCER"
3100 PRINT "2. MICROPHONE"
3110 INPUT I
3120 IF I=2 THEN OUT 5,96
3125 IF I=2 GOTO 3140
3130 PRINT:PRINT "1. ZERO=1 FULL SCALE=254"
3135 GOTO 3150
3140 PRINT "2. ZERO=0 FULL SCALE=254"
3150 PRINT:PRINT "TO EXIT HIT E"
3160 PRINT
3170 DOKE 4100,-16224
3200 J=USR(J)
3210 IF J=69 GOTO 3270
3215 OUT 5,208:OUT 5,240
3220 OUT 5,209
3230 R=INP(4)
3240 PRINT TAB(5);R
3250 OUT 5,241
3260 GOTO 3200
3270 OUT 5,240
3280 PRINT "CALIBRATE ROUTINE ENDS":PRINT
3290 RETURN
3999 REM
4000 REM RESULTS PRINTING SUBROUTINE
4001 Z1=49696-C1:DOKE 3192,Z1
4002 DOKE 3195,1769:DOKE 4100,1754
4003 I=USR(0):DOKE 4100,1743
4004 I=USR(0)
4005 WIDTH 72:PRINT:PRINT:PRINT
4010 PRINT:PRINT TAB(20);"RESULTS"
4020 PRINT:PRINT
4030 PRINT "DATE=";N(0);".";N(1);".";N(2)
4040 PRINT
4050 PRINT "RUN NUMBER=";N(3)
4055 DEF FNQ(DW)=9.807*(0.9982+(20-DW)*0.0002)
4057 TE=N(9)
4060 PRINT
4065 PRINT "NUMBER OF COLUMNS IN BANK=";N(4)
4070 PRINT "NUMBER OF ROWS IN BANK=";N(5)
4080 PRINT "ROW NUMBER=";N(6)
4090 PRINT "COLUMN NUMBER=";N(7)
4095 TP=N(10)*FNQ(TE):SP=N(11)*FNQ(TE)
4096 AP=N(8)*9.807*(13.595-TE*0.005)
4097 PRINT "ATMOSPHERIC PRESSURE=";AP;"PA"
4098 PRINT "TEMPERATURE=";TE;"C"
4100 PRINT "WIND TUNNEL TOTAL PRESSURE=";TP;
4105 PRINT "PA"
4110 PRINT "WIND TUNNEL STATIC PRESSURE=";SP;
4115 PRINT "PA"
4120 WD=SP-TP
4130 DE=1.21*((AP-SP)/AP)^(1/1.4)
```

LISTING 1. (continued)

```
4135 DE=DE*293.16/(273.16+TEMP)
4140 VS=1.8192E-5+0.536E-7*(TE-20)
4150 VEL=(2*WD/DE)^0.5
4160 BF=400/(400-30*N(4))
4170 RY=DE*3.0E-2*VEL*BF/VS
4180 PRINT "FREE STREAM VELOCITY=";VEL;"M/S"
4185 PRINT "TUBE GAP VELOCITY=";VEL*BF;"M/S"
4190 PRINT "BLOCKED REYNOLDS NUMBER=";RY
4200 PRINT "SPL IN TEST SECTION=";N(14);"DB"
4210 PRINT "FREQUENCY OF EXCITING SOUND=";
4215 PRINT N(15);"HZ"
4220 FOR I=1 TO 6
4230 PRINT
4240 NEXT I
4250 PRINT "ANGLE";TAB(6);"CP";TAB(20);
4251 PRINT "CL";TAB(33);"CD";TAB(46);
4252 PRINT "SPL";TAB(56);"CPRMS"
4260 PRINT "DEG";TAB(46);"DB"
4270 PRINT
4280 Z1=L1
4290 Z2=L2
4300 IF Z1>C2 THEN Z1=Z1-C1
4310 IF Z2>C2 THEN Z2=Z2-C1
4320 K=0
4325 LC=0:DC=0
4330 FOR I=1 TO D2
4340 T1=PEEK(Z1)-1
4350 T2=PEEK(Z2)
4360 T1=T1*N(12)*FNQ(TE)/(N(13)-1)
4370 T1=SP-T1
4380 V1=(2*ABS(T1)/DE)^0.5
4385 RA=K*3.1415926/180
4390 CP=T1/WD
4395 CL=CP*SIN(RA):CD=CP*COS(RA)
4397 LC=LC+CL:DC=DC+CD
4400 J=1/LOG(10)
4401 IF ABS(CP)<0.000001 THEN CP=0
4402 IF ABS(CL)<0.000001 THEN CL=0
4403 IF ABS(CD)<0.000001 THEN CD=0
4405 IF T2<=0 THEN T2=1
4410 SL=N(16)-20*J*LOG(N(17)/T2)
4412 T3=N(16)/20
4413 CF=2E-5*(10^T3)*T2/(N(17)*WD)
4420 PRINT K;TAB(5);CP;TAB(19);CL;TAB(32);
4421 PRINT CD;TAB(45);SL;TAB(55);CF
4430 K=K+D1
4440 Z1=Z1+1
4450 IF Z1>C2 THEN Z1=Z1-C1
4460 Z2=Z2+1
4470 IF Z2>C2 THEN Z2=Z2-C1
4480 NEXT I
4482 LC=LC*2/D2:DC=DC*2/D2
4485 FOR I=1 TO 4:PRINT:NEXTI
4486 PRINT "LIFT COEFFICIENT=";LC
4487 PRINT "DRAG COEFFICIENT=";DC
4490 FOR I=1 TO 10
4500 PRINT:NEXT I
4510 PRINT TAB(20);"RAW DATA"
4520 SP=IPT:EP=FPT
4530 IF SP>C2 THEN SP=SP-C1
4540 IF EP>C2 THEN EP=EP-C1
4545 S$=""
4550 FOR I=SP TO EP
4560 J=PEEK(I)
4570 IF J=13 THEN J=32
4580 IF J=10 THEN J=32
4590 S$=S$+CHR$(J)
4600 IF LEN(S$)>60 THEN GOSUB 4800
4610 NEXT I
4620 PRINT S$
4630 FOR I=1 TO 10:PRINT:NEXT I
4640 WIDTH 47
4650 DOKE 4100,1848
4660 I=USR(0)
4670 RETURN
4800 IF J=32 THEN PRINT S$
4810 IF J=32 THEN S$=""
4820 RETURN
```

LISTING 1. (continued)

```
4999 REM
5000 REM AUTOMATIC ACQUIRE AND CONTROL SEQUENCE
5010 PRINT "AUTOMATIC DATA ACQUISITION ROUTINE"
5020 PRINT
5030 OUT 7,255:OUT 7,4:OUT 7,0:OUT 7,55
5040 OUT 7,251:OUT 6,255:OUT 6,255:OUT 6,0
5050 OUT 6,55:OUT 6,255
5060 OUT 5,0
5070 PRINT "INPUT ANGULAR INCREMENT OF";
5080 PRINT " MEASUREMENTS IN DEGREES"
5090 INPUT D1
5100 D2=360/D1
5110 D3=D1/1
5120 IF INT(D3)<>D3 GOTO 5070
5130 PRINT "INPUT THE FIRST MEMORY LOCATION";
5140 PRINT " WHERE DATA IS TO BE STORED"
5150 INPUT L1
5151 IF L1<16384 GOTO 5130
5153 PRINT "INPUT DELAY BETWEEN READINGS"
5154 INPUT "IN SECONDS  DEFAULT=0";DL
5155 DL=INT(DL*900)
5156 IF DL=0 THEN DL=900
5160 L2=L1+D2
5170 OUT 5,240
5172 OUT 5,80
5174 FOR K=1 TO 100:NEXT K
5185 PRINT "PRESS RETURN TO ACQUIRE"
5186 INPUT A$
5187 PRINT "ACQUIRE SEQUENCE STARTS"
5190 Z1=L1
5200 IF Z1>C2 THEN Z1=Z1-C1
5210 Z2=L2
5220 IF Z2>C2 THEN Z2=Z2-C1
5230 FOR I=1 TO D2
5232 A=0
5234 OUT 5,208:OUT 5,240
5235 FOR K=1 TO AV
5240 OUT 5,240:OUT 5,209
5242 A=A+INP(4):NEXT K
5245 A=A/AV:B=A-INT(A)
5247 IF B>=0.5 THEN A=A+1
5248 A=INT(A)
5250 IF A>=255 THEN PRINT "OVERRANGE ON 1"
5260 OUT 5,96
5270 POKE Z1,A
5280 IF I=1 THEN FD=A
5290 A=0
5291 OUT 5,208:OUT 5,240
5292 FOR K=1 TO AV
5294 OUT 5,240:OUT 5,209
5295 A=A+INP(4):NEXT K
5298 A=A/AV:B=A-INT(A)
5300 IF B>=0.5 THEN A=A+1
5305 A=INT(A)
5307 IF A>=255 THEN PRINT "OVERRANGE ON 2"
5310 POKE Z2,A
5320 OUT 5,96
5330 OUT 5,240
5335 OUT 5,64
5338 FOR K=1 TO 100:NEXT K
5340 Z1=Z1+1
5350 IF Z1>C2 THEN Z1=Z1-C1
5360 Z2=Z2+1
5370 IF Z2>C2 THEN Z2=Z2-C1
5380 FOR J=1 TO D3
5390 OUT 5,240:OUT 5,224
5395 FOR K=1 TO 40:NEXT K
5400 OUT 5,240:OUT 5,224
5410 FOR K=1 TO 200:NEXT K
5420 NEXT J
5425 OUT 5,240:OUT 5,64
5430 FOR K=1 TO DL:NEXT K
5440 NEXT I
5450 OUT 5,64
5460 Z1=Z1-1
5470 IF Z1<-C2+1 THEN Z1=Z1+C1
```

LISTING 1. (continued)

```
5480 Z2=Z2-1
5490 IF Z2<C2+1 THEN Z2=Z2+C1
5760 FOR K=1 TO 100:NEXT K
5770 OUT 5,0
5780 PRINT
5790 PRINT "ACQUIRE SEQUENCE COMPLETED"
5800 PRINT
5810 F1=L1+D2-1
5820 F2=L2+D2-1
5830 PRINT "CHANNEL 1 FIRST LOCATION=";L1
5840 PRINT "CHANNEL 1 LAST LOCATION=";F1
5850 PRINT "CHANNEL 2 FIRST LOCATION=";L2
5860 PRINT "CHANNEL 2 LAST LOCATION=";F2
5870 PRINT:PRINT
5872 F3=F2:IF F3>C2 THEN F3=F3-C1
5874 Z1=L2:Z2=L2+(F2-L2+1)/2:A=D2/2
5876 FOR I=1 TO A
5878 IF Z1>C2 THEN Z1=Z1-C1
5880 IF Z2>C2 THEN Z2=Z2-C1
5882 T1=PEEK(Z2):T2=PEEK(Z1)
5884 POKE Z1,T1:POKE Z2,T2
5886 Z1=Z1+1:Z2=Z2+1:IF Z2>C2 THEN Z2=Z2-C1
5888 IF Z2>F3 THEN Z2=L2
5890 NEXT I
5900 RETURN
5999 REM
6000 REM DATA FORMATTING ROUTINE
6010 PRINT "DATA FORMATTING ROUTINE"
6015 REM DATA FOR PAPER TAPE HEADERS
6016 REM AND TERMINATORS
6020 DATA ":ISF002/D?"
6030 DATA "$$$$"
6080 PRINT
6090 PRINT
6120 PRINT "INPUT DATE"
6130 INPUT "DAY=";N(0)
6140 INPUT "MONTH=";N(1)
6150 INPUT "YEAR=";N(2)
6160 INPUT "RUN NUMBER";N(3)
6165 INPUT "NUMBER OF COLUMNS IN BANK";N(4)
6170 INPUT "NUMBER OF ROWS IN BANK";N(5)
6180 INPUT "ROW NUMBER";N(6)
6190 INPUT "COLUMN NUMBER";N(7)
6195 INPUT "ATMOSPHERIC PRESSURE MMHG";N(8)
6196 INPUT "TEMPERATURE C";N(9)
6200 INPUT "WT TOTAL PRESSURE MMH2O";N(10)
6210 INPUT "WT STATIC PRESSURE MMH2O";N(11)
6220 INPUT "FS PRESSURE FOR A TO D";N(12)
6225 INPUT "FS A TO D PRESSURE READING";N(13)
6230 INPUT "SPL IN TEST SECTION";N(14)
6240 INPUT "FREQUENCY OF SOUND";N(15)
6250 INPUT "FS SPL FOR A TO D";N(16)
6255 INPUT "FS A TO D SPL READING";N(17)
6260 PRINT "INPUT FIRST MEMORY LOCATION WHERE"
6270 INPUT "PSEUDO-TAPE IS STORED";PT
6271 IF PT<16384 GOTO 6260
6275 PRINT "FORMATTING STARTS"
6280 AD=PT
6290 IF AD>C2 THEN AD=AD-C1
6300 IPT=AD
6400 READ S$
6410 GOSUB 6915
6420 IF AS=37 GOTO 6400
6430 POKE AD,10
6440 GOSUB 6900
6470 FOR I=0 TO 17
6480 S$=STR$(N(I))
6490 GOSUB 6915
6500 IF INT(N(I))=N(I) THEN GOSUB 6950
6510 GOSUB 6965
6520 NEXT I
6530 D4=D2*2
6540 S$=STR$(D4)
6550 GOSUB 6915
6560 GOSUB 6950
```

LISTING 1. (continued)

```
6570 GOSUB 6965
6580 Z1=L1
6590 IF Z1>C2 THEN Z1=Z1-C1
6600 FOR I=1 TO D4
6610 S$=STR$(PEEK(Z1))
6620 GOSUB 6915
6630 GOSUB 6950
6640 GOSUB 6965
6650 Z1=Z1+1
6660 IF Z1>C2 THEN Z1=Z1-C1
6670 NEXT I
6690 READ S$
6700 GOSUB 6915
6710 IF AS=37 GOTO 6690
6720 POKE AD,10
6750 FPT=AD
6760 IF FPT<0 THEN FPT=FPT+C1
6781 RESTORE
6782 FOR I=1 TO 179
6783 READ A:NEXT I
6784 PRINT "DATA FORMATTING COMPLETE"
6800 RETURN
6810 P$=STR$(N(3))
6812 ST=LEN(P$)
6814 FOR K=1 TO ST
6816 AS=ASC(MID$(P$,K,1))
6818 IF AS=32 GOTO 6830
6820 IF K=ST GOTO 6830
6822 POKE AD,AS
6824 GOSUB 6900
6830 NEXT K
6832 RETURN
6900 AD=AD+1
6905 IF AD>C2 THEN AD=AD-C1
6910 RETURN
6915 SL=LEN(S$)
6920 FOR J=1 TO SL
6925 AS=ASC(MID$(S$,J,1))
6927 IF AS=37 THEN RETURN
6928 IF AS=63 THEN GOSUB 6810
6930 POKE AD,AS
6935 GOSUB 6900
6940 NEXT J
6945 RETURN
6950 POKE AD,46
6955 GOSUB 6900
6960 RETURN
6965 POKE AD,13
6970 GOSUB 6900
6975 POKE AD,10
6980 GOSUB 6900
6985 RETURN
6999 REM
7000 REM PAPER TAPE OUTPUT ROUTINE
7010 PRINT:PRINT "PAPER TAPE OUTPUT ROUTINE"
7020 PRINT
7030 OUT 7,255
7040 OUT 7,4
7050 OUT 7,0
7060 OUT 7,55
7070 OUT 7,251
7080 OUT 6,255
7090 OUT 6,0
7100 OUT 6,0
7110 OUT 6,55
7120 OUT 6,255
7130 OUT 5,0
7140 OUT 5,240
7150 OUT 5,48
7155 FOR I=1 TO 200:NEXT I
7160 I=49152
7170 I=I-C1
7180 DOKE 4100,I
7181 PRINT "DO YOU REQUIRE DEFAULT LOCATIONS?"
7182 INPUT "Y OR N";A$
```

LISTING 1. (continued)

```
7183 IF LEFT$(A$,1)="Y" GOTO 7190
7184 INPUT "START LOCATION=";SP
7185 INPUT "FINISH LOCATION=";EP
7186 GOTO 7197
7187 IF SP>C2 THEN SP=SP-C1
7188 IF EP>C2 THEN EP=EP-C1
7190 SP=IPT:EP=FPT
7197 IF SP>C2 THEN SP=SP-C1
7198 IF EP>C2 THEN EP=EP-C1
7199 PRINT "PRESS RETURN TO START"
7200 INPUT A$
7205 GOSUB 7300
7210 FOR I=SP TO EP
7215 IF I>C2 THEN I=I-C1
7220 J=PEEK(I)
7230 K=USR(J)
7240 NEXT I
7250 GOSUB 7300
7260 OUT 5,0
7265 PRINT "PUNCH COMPLETED"
7270 RETURN
7300 NN=500
7310 FOR I=1 TO NN
7320 K=USR(0)
7330 NEXT I
7340 RETURN
7999 REM
8000 REM PAPER TAPE INPUT ROUTINE
8010 PRINT
8020 PRINT "PAPER TAPE INPUT ROUTINE"
8040 OUT 7,251:OUT 6,255:OUT 6,255:OUT 6,0
8050 OUT 6,55:OUT 6,255
8060 OUT 5,0:OUT 5,240:OUT 5,16
8061 C1=65536:C2=32768
8070 PRINT "INPUT MEMORY LOCATION WHERE FIRST"
8080 PRINT "CHARACTER IS TO BE STORED"
8090 INPUT IT
8091 IF IT<16384 GOTO 8070
8095 PRINT "PRESS RETURN TO READ TAPE"
8096 INPUT A$
8100 Z1=IT
8110 IF Z1>C2 THEN Z1=Z1-C1
8120 OUT 5,160
8130 FOR K=1 TO 30:NEXT K
8140 OUT 5,240
8150 FOR K=1 TO 5:NEXT K
8160 A=INP(4)
8170 IF A=0 GOTO 8110
8180 POKE Z1,A
8190 J=0
8200 OUT 5,160
8210 FOR K=1 TO 30:NEXT K
8220 Z1=Z1+1
8230 IF Z1>C2 THEN Z1=Z1-C1
8240 OUT 5,240
8250 FOR K=1 TO 5:NEXT K
8260 A=INP(4)
8270 POKE Z1,A
8280 IF A<>0 GOTO 8190
8290 J=J+1
8300 IF J<20 GOTO 8200
8310 FT=Z1
8320 IF FT<0 THEN FT=FT+C1
8330 PRINT "PAPER TAPE READ COMPLETED"
8340 PRINT
8350 PRINT "FIRST CHARACTER LOCATION=";IT
8360 PRINT "LAST CHARACTER LOCATION=";FT
8370 PRINT
8380 RETURN
8999 REM
9000 REM PAPER TAPE READER FORMATTER
9010 PRINT
9020 PRINT "PAPER TAPE READER FORMATTER"
9030 INPUT "FIRST MEMORY LOCATION FOR DATA=";PR
```

LISTING 1. (continued)

```
9031 IF PR<16384 GOTO 9030
9040 Z2=IT
9050 IF Z2>C2 THEN Z2=Z2-C1
9070 A=PEEK(Z2)
9080 Z2=Z2+1
9090 IF Z2>C2 THEN Z2=Z2-C1
9100 IF A<>13 GOTO 9070
9130 FOR I=0 TO 18
9140 S$=""
9150 A=PEEK(Z2)
9160 Z2=Z2+1
9170 IF Z2>C2 THEN Z2=Z2-C1
9180 IF A=13 GOTO 9150
9190 IF A=10 GOTO 9220
9200 S$=S$+CHR$(A)
9210 GOTO 9150
9220 N(I)=VAL(S$)
9230 NEXT I
9240 Z1=PR
9250 IF Z1>C2 THEN Z1=Z1-C1
9255 D4=N(16)
9257 D2=D4/2
9260 FOR I=1 TO D4
9270 S$=""
9280 A=PEEK(Z2)
9290 Z2=Z2+1
9300 IF Z2>C2 THEN Z2=Z2-C1
9310 IF A=13 GOTO 9280
9320 IF A=10 GOTO 9350
9330 S$=S$+CHR$(A)
9340 GOTO 9280
9350 Z3=VAL(S$)
9355 D4=N(18)
9360 POKE Z1,Z3
9370 Z1=Z1+1
9380 IF Z1>C2 THEN Z1=Z1-C1
9390 NEXT I
9400 PRINT:PRINT "FORMATTING COMPLETE"
9410 L1=PR
9420 F1=PR+D2-1
9430 L2=PR+D2
9440 F2=L2+D2-1
9450 PRINT:PRINT
9460 RETURN
9999 REM
10000 REM TUBE ROTATION ROUTINE
10010 PRINT:PRINT "TUBE ROTATION ROUTINE"
10020 PRINT:PRINT
10022 PRINT "WHICH CHANNEL DO YOU WISH"
10023 PRINT "TO MONITOR; 1 OR 2?"
10025 INPUT I
10030 OUT 7,255:OUT 7,4:OUT 7,0:OUT 7,55
10040 OUT 7,251:OUT 5,0:OUT 5,240
10042 OUT 6,255:OUT 6,255:OUT 6,0
10043 OUT 6,55:OUT 6,255
10044 IF I=2 THEN OUT 5,96
10045 OUT 5,241
10050 PRINT "PRESS RETURN TO START OR STOP"
10060 PRINT "ROTATION, E TO EXIT"
10065 PRINT "PRESS R TO ACQUIRE OR E TO EXIT"
10066 PRINT "FROM ACQUIRE"
10070 PRINT "WHICH DIRECTION DO YOU REQUIRE?"
10080 PRINT "1. CLOCKWISE"
10090 PRINT "2. ANTICLOCKWISE"
10100 PRINT "3. EXIT FROM ROUTINE"
10110 INPUT R0
10120 IF R0=2 THEN OUT 5,80
10130 IF R0>2 THEN RETURN
10140 IF R0=1 THEN PRINT "CLOCKWISE"
10150 IF R0=2 THEN PRINT "ANTICLOCKWISE"
10160 A$=""
10170 INPUT A$
10180 IF A$="E" GOTO 10030
10185 IF A$="R" THEN GOSUB 3170
10186 IF A$="R" GOTO 10160
```

LISTING 1. (continued)

```
10190 OUT 5,224
10192 FOR J=1 TO 200:NEXT J
10195 OUT 5,64
10200 INPUT A$
10210 OUT 5,240
10212 OUT 5,224
10214 FOR J=1 TO 200:NEXT J
10216 OUT 5,64
10220 GOTO 10160
19999 REM END OF SUBROUTINES
```

# LISTING 2. EXPERIMENTAL RESULTS ANALYSIS AND PLOTTING PROGRAMME

```
      PROGRAM ANLYS
C
C THIS PROGRAM ANALYSES EXPERIMENTAL RESULTS
C AND PRINTS OUT TABLES OF RESULTS AND PLOTS GRAPHS
      COMMON /LARGE/ FDATA(20000)
      COMMON /WORKS/ W(6000)
      COMMON /RES4/ A(20)
      COMMON /RES5/ RES(1000)
      COMMON /SP1/ SPACE(200)
      DIMENSION FCALC(200)
C READ IN DATA FILE CONTAINING ALL THE EXPERIMENTAL
C RESULTS
      DO 25 I=1,20000
      READ(1,20) FDATA(I)
   20 FORMAT(F10.3)
      IF (FDATA(I).GE.99998.) GOTO 30
   25 CONTINUE
   30 IMAX=I-1
C READ IN WHICH EXPERIMENTAL SET OF DATA IS TO BE
C ANALYSED AND THE DISPLACEMENT OF EACH TUBE FROM
C ITS MEAN POSITION
      DO 70 I=1,200
      READ(5,40) FCALC(I),SPACE(I)
   40 FORMAT(2F10.4)
      IF (FCALC(I).GE.1000.) GOTO 80
   70 CONTINUE
   80 ICAL=I-1
C INITIALIZE GRAPH PLOTTER
      CALL CC036N
      CALL DEVPAP(200.,280.,0)
      CALL UNITS(1.0)
C CALL SUBROUTINES WHICH CALCULATE AND PLOT THE
C RESULTS FOR EACH SPECIFIED DATA SET
      DO 200 J=1,ICAL
      IKO=0
      DO 150 IM=1,200
      NP=19+INT(FDATA(19+IKO))
      IF (FDATA(4+IKO).NE.FCALC(J)) GOTO 110
      DO 100 IJ=1,19
  100 A(IJ)=FDATA(IJ+IKO)
      NP1=NP-IKO
      DO 105 IJ=1,NP
      IZ=IJ+19+IKO
  105 RES(IJ)=FDATA(IZ)
C CALL CALCULATIONS SUBROUTINE
      CALL RAWANL(J,ND1)
      GOTO 200
  110 IKO=IKO+NP
      IF (IKO.GE.IMAX) GOTO 200
  150 CONTINUE
  200 CONTINUE
      CALL DEVEND
      STOP
      END
C
C
      SUBROUTINE RAWANL(ISPACE,ND1)
C THIS SUBROUTINE ANALYSES THE RAW DATA TO CALCULATE
C PRESSURE COEFFICIENTS AND LIFT AND DRAG COEFFICIENTS
      COMMON /RES1/ CPRES(200)
      COMMON /RES2/ SPLRES(200)
      COMMON /RES3/ CPF(200)
      COMMON /XPO/ XPOS(200)
      COMMON /CON1/ PI
      COMMON /RES4/ A(20)
      COMMON /RES5/ RES(1000)
      COMMON /SP1/ SPACE(200)
      INTEGER RUN,ROWS,ROWN,COLS,COLN
      REAL LFORCE
      PI=3.1415926
      NP=INT(A(19))
      WRITE(6,45)
   45 FORMAT(1H1)
      WRITE(6,50)
   50 FORMAT(30X,'RESULTS')
      WRITE(6,60)
```

LISTING 2. (continued)

```
   60 FORMAT(1HO)
C CALCULATE THE AERODYNAMIC AND TUBE BANK PARAMETERS
      IDAY=INT(A(1))
      MONTH=INT(A(2))
      IYEAR=INT(A(3))
      WRITE(6,70) IDAY,MONTH,IYEAR
   70 FORMAT(1HO,'DATE=',I2,'.',I2,'.',I4)
      RUN=INT(A(4))
      WRITE(6,80) RUN
   80 FORMAT(1HO,'RUN NUMBER=',I5)
      COLS=INT(A(5))
      WRITE(6,90) COLS
   90 FORMAT(1H ,'NUMBER OF COLUMNS IN TUBE BANK=',I2)
      ROWS=INT(A(6))
      WRITE(6,100) ROWS
  100 FORMAT(1H ,'NUMBER OF ROWS IN TUBE BANK=',I2)
      ROWN=INT(A(7))
      WRITE(6,110) ROWN
  110 FORMAT(1H ,'ROW NUMBER',I2)
      COLN=INT(A(8))
      WRITE(6,115) COLN
  115 FORMAT(1H ,'COLUMN NUMBER=',I2)
      TEMP=A(10)
      TP=A(11)*9.807*DENW(TEMP)
      SP=A(12)*9.807*DENW(TEMP)
      WD=SP-TP
      AP=A(9)*9.807*(13.595-TEMP*0.005)
      WRITE(6,120) AP
  120 FORMAT(1H ,'ATMOSPHERIC PRESSURE=',F8.1,' PA')
      WRITE(6,130) TEMP
  130 FORMAT(1H ,'TEMPERATURE=',F6.1,' C')
      WRITE(6,140) TP
  140 FORMAT(1H ,'WIND TUNNEL TOTAL PRESSURE=',F10.2,' PA')
      WRITE(6,150) SP
  150 FORMAT(1H ,'WIND TUNNEL STATIC PRESSURE=',F10.2,' PA')
      WRITE(6,160) WD
  160 FORMAT(1H ,'WIND TUNNEL DYNAMIC PRESSURE=',F10.2,' PA')
      DEN=1.21*((AP-SP)/AP)**(1/1.4)*293.16/(273.16+TEMP)
      VIS=1.8192E-5+0.536E-7*(TEMP-20.)
      VEL=SQRT(2.*WD/DEN)
      IF (COLS.GT.6.) COLS=FLOAT(INT((COLS+0.0001)/2.))
      BF=400./(400.-30.*COLS)
      RY=DEN*3.0E-2*VEL*BF/VIS
      WRITE(6,170) VEL
  170 FORMAT(1H ,'FREE STREAM VELOCITY=',F8.2,' M/S')
      BVEL=BF*VEL
      WRITE(6,180) BVEL
  180 FORMAT(1H ,'TUBE GAP VELOCITY=',F8.2,' M/S')
      WRITE(6,190) RY
  190 FORMAT(1H ,'BLOCKED REYNOLDS NUMBER=',F10.2)
      WRITE(6,200) A(15)
  200 FORMAT(1H ,'SPL IN TEST SECTION=',F8.1,' DB')
      WRITE(6,210) A(16)
  210 FORMAT(1H ,'FREQUENCY OF EXCITING SOUND=',F8.1,' HZ')
      SPN=SPACE(ISPACE)/30.
      WRITE(6,215) SPN
  215 FORMAT(1HO,'NORMALIZED TUBE SPACING FROM MEAN POSITION=',F10.4)
      WRITE(6,220)
      WRITE(6,220)
      WRITE(6,220)
  220 FORMAT(1HO)
      WRITE(6,230)
  230 FORMAT(1HO,'ANGLE',5X,'CP',8X,'CL',8X,'CD',10X,'SPL',5X,
     *'CPRMS')
      WRITE(6,240)
  240 FORMAT(1H ,'DEGREES',35X,'DB')
      ND1=NP/2
      ANG=0.0
      ANGINC=360./FLOAT(ND1)
      ND2=ND1+1
      DO 242 I=1,ND2+1
  242 XPOS(I)=FLOAT(I-1)*ANGINC
      J=ND1+1
C CALCULATE PRESSURE COEFFICIENTS ROUND THE TUBE
      DO 300 I=1,ND1
      T1=RES(I)
      T1=T1-1
      T1=T1*A(13)*9.807*DENW(TEMP)/A(14)
      T1=SP-T1
```

LISTING 2. (continued)

```
156         V1=SQRT(2*ABS(T1)/DEN)
157         CPRES(I)=T1/WD
158         CP=T1/WD
159         RANG=ANG*PI/180.
160         CL=CP*SIN(RANG)
161         CD=CP*COS(RANG)
162         SPLRES(I)=A(17)-20.*LOG(A(18)/1.)/LOG(10.)
163         IF (RES(J).LE.0.0) GOTO 245
164         SPLRES(I)=A(17)-20.*LOG(A(18)/RES(J))/LOG(10.)
165     245 T3=SPLRES(I)/20.
166         CPF(I)=2.E-5*(10.**T3)/WD
167         WRITE(6,250) ANG,CPRES(I),CL,CD,SPLRES(I),CPF(I)
168     250 FORMAT(1H ,F5.0,3F10.4,F10.2,F10.4)
169         ANG=ANG+ANGINC
170         J=J+1
171     300 CONTINUE
172         CPRES(ND1+1)=CPRES(1)
173         SPLRES(ND1+1)=SPLRES(1)
174         CPF(ND1+1)=CPF(1)
175         WRITE(6,400)
176         WRITE(6,400)
177         WRITE(6,400)
178     400 FORMAT(1HO)
179         CALL MYPLOT(ND1,ANGINC,RUN)
180         WRITE(6,440)
181     440 FORMAT(1HO,'LINEAR APPROXIMATION OF LIFT AND DRAG COEFFICIENT')
182   C CALL SUBROUTINE WHICH CALCULATES THE AVERAGE LIFT AND DRAG
183   C ON THE TUBE USING A LINEAR APPROXIMATION OF THE
184   C LIFT AND DRAG COEFFICIENTS
185         CALL CALLD2(ND1,ANGINC,CL,CD)
186         WRITE(6,450) CL
187     450 FORMAT(1HO,'LIFT COEFFICIENT=',F10.4)
188         WRITE(6,460) CD
189     460 FORMAT(1H ,'DRAG COEFFICIENT=',F10.4)
190         LFORCE=CL*0.5*DEN*(VEL**2)*3.0E-2
191         DFORCE=CD*0.5*DEN*(VEL**2)*3.0E-2
192         WRITE(6,470) LFORCE
193     470 FORMAT(1HO,'LIFT FORCE PER UNIT LENGTH ON TUBE=',
194        *E15.4,' PA')
195         WRITE(6,480) DFORCE
196     480 FORMAT(1H ,'DRAG FORCE PER UNIT LENGTH ON TUBE=',
197        *E15.4,' PA')
198         WRITE(6,490)
199     490 FORMAT(1HO,'LINEAR APPROXIMATION OF PRESSURE COEFFICIENT')
200   C CALL SUBROUTINE WHICH CALCULATES THE AVERAGE LIFT AND DRAG
201   C ON THE TUBE USING A LINEAR APPROXIMATION OF THE
202   C PRESSURE COEFFICIENTS
203         CALL CALLD(ND1,CL,CD)
204         WRITE(6,450) CL
205         WRITE(6,460) CD
206         LFORCE=CL*0.5*DEN*(VEL**2)*3.0E-2
207         DFORCE=CD*0.5*DEN*(VEL**2)*3.0E-2
208         WRITE(6,470) LFORCE
209         WRITE(6,480) DFORCE
210   C CALL SUBROUTINE WHICH CALCULATES THE R.M.S. LIFT
211   C AND DRAG COEFFICIENTS ON THE TUBE ASSUMMING THAT
212   C THE PRESSURE FLUCTUATIONS ROUND THE TUBE ARE
213   C UNCORRELATED
214         CALL CALFLD(ND1,ANGINC,CFL,CFD)
215         WRITE(6,400)
216         WRITE(6,510) CFL
217     510 FORMAT(1H ,'RMS LIFT COEFFICIENT= ',F10.5)
218         WRITE(6,520) CFD
219     520 FORMAT(1H ,'RMS DRAG COEFFICIENT= ',F10.5)
220         RETURN
221         END
222   C
223   C
224         FUNCTION DENW(TEMP)
225   C THIS FUNCTION CALCULATES THE DENSITY OF WATER
226   C AT ANY SPECIFIED TEMPERATURE
227         DENW=0.9982+(20.-TEMP)*0.0002
228         RETURN
229         END
230   C
231   C
```

LISTING 2. (continued)

```
232         SUBROUTINE CALLD2(ND1,ANGINC,CL,CD)
233   C THIS SUBROUTINE CALCULATES THE AVERAGE LIFT AND DRAG
234   C COEFFICIENTS OF THE TUBE IN THE TUBE BANK
235   C USING A LINEAR INTERPOLATION OF THE LIFT
236   C AND DRAG COEFFICIENTS
237         COMMON /RES1/ CPRES(200)
238         COMMON /CON1/ PI
239         ANG=0.0
240         CL=0.0
241         CD=0.0
242         CPRES(ND1+1)=CPRES(1)
243         DO 20 I=1,ND1
244         RANG=ANG*PI/180.
245         CL=CL+SIN(RANG)*CPRES(I)
246         CD=CD+COS(RANG)*CPRES(I)
247         ANG=ANG+ANGINC
248      20 CONTINUE
249         CL=CL*ANGINC/180.
250         CD=CD*ANGINC/180.
251         RETURN
252         END
253   C
254   C
255         SUBROUTINE CALLD(ND1,CL,CD)
256   C THIS SUBROUTINE CALCULATES THE AVERAGE LIFT AND DRAG COEFFICIENTS
257   C USING A LINEAR APPROXIMATION FOR THE PRESSURE COEFFICIENT
258         COMMON /RES1/ CPRES(200)
259         COMMON /XP0/ XPOS(200)
260         COMMON /CON1/ PI
261         DIMENSION RESA(200)
262         DO 10 I=1,ND1+1
263      10 RESA(I)=XPOS(I)*PI/180.
264         CL=0.0
265         CD=0.0
266         DO 100 I=1,ND1
267         S1=0.0
268         S2=0.0
269         T1=(CPRES(I+1)-CPRES(I))/(RESA(I+1)-RESA(I))
270         DO 50 J=1,2
271         K=I+J-1
272         S1=S1+((-1.)**J)*(-CPRES(I)*COS(RESA(K))+T1*(SIN(RESA(K))
273        *-RESA(K)*COS(RESA(K)))+T1*RESA(I)*COS(RESA(K)))
274         S2=S2+((-1.)**J)*(CPRES(I)*SIN(RESA(K))+T1*(RESA(K)*SIN(RESA(K))
275        *+COS(RESA(K)))-T1*RESA(I)*SIN(RESA(K)))
276      50 CONTINUE
277         CL=CL+S1/PI
278         CD=CD+S2/PI
279     100 CONTINUE
280         RETURN
281         END
282   C
283   C
284         SUBROUTINE CALFLD(ND1,ANGINC,CFL,CFD)
285   C THIS SUBROUTINE CALCULATES THE R.M.S. LIFT
286   C AND DRAG COEFFICIENTS ASSUMING THAT THE PRESSURE
287   C FLUCTUATIONS ARE UNCORRELATED ROUND THE
288   C CIRCUMFERENCE OF THE TUBE
289         COMMON /RES3/ CPF(200)
290         COMMON /CON1/ PI
291         ANG=0.0
292         CFL=0.0
293         CFD=0.0
294         CPF(ND1+1)=CPF(1)
295         DO 20 I=1,ND1
296         RANG=ANG*PI/180.
297         T1=SIN(RANG)*CPF(I)
298         T2=COS(RANG)*CPF(I)
299         CFL=CFL+T1**2
300         CFD=CFD+T2**2
301         ANG=ANG+ANGINC
302      20 CONTINUE
303         CFL=CFL*ANGINC/360.
304         CFD=CFD*ANGINC/360.
305         CFL=SQRT(CFL)
306         CFD=SQRT(CFD)
307         RETURN
308         END
309   C
310   C
```

LISTING 2. (continued)

```
      SUBROUTINE MYPLOT(ND1,ANGINC,RUN)
C THIS SUBROUTINE PLOTS GRAPHS OF THE EXPERIMENTALLY
C MEASURED PRESSURE,LIFT AND DRAG COEFFICIENTS
      COMMON /RES1/ CPRES(200)
      COMMON /RES2/ SPLRES(200)
      COMMON /RES3/ CPF(200)
      COMMON /XPO/ XPOS(200)
      COMMON /CON1/ PI
      DIMENSION YPOS(200)
      INTEGER RUN
      ND2=ND1+1
      DO 20 I=1,ND2+1
   20 XPOS(I)=FLOAT(I-1)*ANGINC
      CALL CHASIZ(3.,5.)
      CALL MOVTO2(10.,250.)
      CALL CHAHOL(22HEXPERIMENTAL RESULTS*.)
      CALL CHAHOL(14H RUN NUMBER *.)
      CALL CHAINT(RUN,-4)
      CALL CHASIZ(1.5,2.5)
      CALL AXIPOS(1,30.,170.,120.,1)
      CALL AXIPOS(1,30.,130.,80.,2)
      CALL AXISCA(3,12,0.,360.,1)
      CPL=0.
C CALCULATE GRAPH SCALES FOR THE STATIC
C PRESSURE COEFFICIENTS
      DO 30 I=1,ND1
   30 IF (ABS(CPRES(I)).GT.CPL) CPL=ABS(CPRES(I))
      NMAX=INT(CPL)+1
      NINT=4
      IF (NMAX.EQ.1) NINT=8
      IF (NMAX.EQ.2) NINT=8
      IF (NMAX.EQ.3) NINT=6
      IF (NMAX.EQ.4) NINT=8
      IF (NMAX.EQ.5) NINT=10
      IF (NMAX.EQ.6) NINT=6
      IF (NMAX.EQ.7) NMAX=8
      IF (NMAX.EQ.8) NINT=8
      IF (NMAX.GT.10.AND.NMAX.LT.15) NMAX=15
      IF (NMAX.GT.10.AND.NMAX.LT.15) NINT=6
      FNM=FLOAT(NMAX)
C DRAW GRAPH AXES,HEADINGS AND SCALES
      CALL AXISCA(3,NINT,-FNM,FNM,2)
      CALL GRID(2,1,1)
      CALL CHASIZ(2.,3.)
      CALL MOVTO2(130.,120.)
      CALL CHAHOL(7HANGLE*.)
      CALL CHAANG(90.)
      CALL MOVTO2(18.,140.)
      CALL CHAHOL(30HSTATIC PRESSURE COEFFICIENTS*.)
      CALL CHAANG(0.)
      CALL CHASIZ(1.5,2.5)
      CPRES(ND2)=CPRES(1)
C PLOT STATIC PRESSURE COEFFICIENTS
      CALL GRAPOL(XPOS,CPRES,ND2)
      CALL GRASYM(XPOS,CPRES,ND2,8,0)
      ANG=0.0
      DO 50 I=1,ND2
      RANG=ANG*PI/180.
      YPOS(I)=CPRES(I)*SIN(RANG)
   50 ANG=ANG+ANGINC
      CALL PENSEL(2,0.0,0)
C PLOT LIFT COMPONENT
      CALL GRAPOL(XPOS,YPOS,ND2)
      CALL GRASYM(XPOS,YPOS,ND2,1,0)
      ANG=0.0
      DO 60 I=1,ND2
      RANG=ANG*PI/180.
      YPOS(I)=CPRES(I)*COS(RANG)
   60 ANG=ANG+ANGINC
      CALL PENSEL(3,0.0,0)
C PLOT DRAG COMPONENT
      CALL GRAPOL(XPOS,YPOS,ND2)
      CALL GRASYM(XPOS,YPOS,ND2,6,0)
      CALL PENSEL(1,0.0,0)
      CALL AXIPOS(1,30.,20.,120.,1)
      CALL AXIPOS(1,30.,20.,80.,2)
      CALL AXISCA(3,12,0.,360.,1)
      SPM=0.
```

LISTING 2. (continued)

```
C CALCULATE SCALES FOR THE R.M.S. PRESSURE
C COEFFICIENTS
      DO 70 I=1,ND1
   70 IF (ABS(CPF(I)).GT.SPM) SPM=ABS(CPF(I))
      NINT=10
      IF (SPM.GT.1.0) SPM=FLOAT(INT(SPM)+1)
      IF (SPM.GT.1.0) GOTO 100
      IF (SPM.GT.0.5) SPM=1.0
      IF (SPM.GT.0.5) GOTO 100
      IF (SPM.GT.0.4) SPM=0.5
      IF (SPM.GT.0.4) GOTO 100
      IF (SPM.GT.0.2) SPM=0.4
      IF (SPM.GT.0.2) GOTO 100
      IF (SPM.GT.0.1) SPM=0.2
      IF (SPM.GT.0.1) GOTO 100
      IF (SPM.LT.0.1) SPM=0.1
      NINT=10
  100 IF (SPM.EQ.0.2.OR.SPM.EQ.0.4) NINT=8
C DRAW GRAPH AXES,HEADINGS AND SCALES
      CALL AXISCA(3,NINT,0.,SPM,2)
      CALL GRID(2,1,1)
      CALL CHASIZ(2.,3.)
      CALL MOVTO2(130.,10.)
      CALL CHAHOL(7HANGLE*.)
      CALL CHAANG(90.)
      CALL MOVTO2(18.,25.)
      CALL CHAHOL(26HRMS PRESSURE COEFFICIENT*.)
      CALL CHAANG(0.)
      SPLRES(ND2)=SPLRES(1)
C PLOT R.M.S. PRESSURE COEFFICIENTS
      CALL GRAPOL(XPOS,CPF,ND2)
      CALL GRASYM(XPOS,CPF,ND2,8,0)
  500 CALL PICCLE
      RETURN
      END
```

Note - The graph plotting subroutines are contained in the GINO-F and GINOGRAF general purpose graphics packages, implemented on the ICL 2970 computer.

See GINO-F users manual, version 6 (1980) and GINOGRAF user manual, issue 1 (1976); published by the Computer Aided Design Centre, Cambridge, U.K.

# LISTING 3. BOUNDARY ELEMENT POTENTIAL FLOW PROGRAMME

```
      PROGRAM GREEN
C
C THIS PROGRAM SOLVES LAPLACES EQUATION FOR
C A SYSTEM OF TUBES IN A FLOW USING
C THE BOUNDARY ELEMENT METHOD
C DECLARE ARRAYS AND CONSTANTS
      COMMON /MAT1/ G(500,500)
      COMMON /MAT2/ H(500,500)
      COMMON /MAT3/ B(500)
      COMMON /VAL1/ X(1010)
      COMMON /VAL2/ Y(1010)
      COMMON /POTS1/ PHID(500)
      COMMON /POTS2/ PHI(500)
      COMMON /POTS3/ POT(500)
      COMMON /POTS4/ POTD(500)
      COMMON /RADX/ ARCOX(500)
      COMMON /RADY/ ARCOY(500)
      COMMON /SOLU/ SOL(500)
      COMMON /CYL/ COORD(36,3)
      COMMON /CONST1/ PI
      COMMON /CON1/ INC
      COMMON /RES1/ CPRES(200)
      COMMON /XPO/ XPOS(200)
      DIMENSION DU(500)
      DIMENSION AIJMAX(500)
      DIMENSION INC1(500)
      DIMENSION D(500)
      PI=3.14159265358979
      WRITE(6,2)
    2 FORMAT(1H1,'THEORETICAL BOUNDARY ELEMENT RESULTS')
      WRITE(6,3)
      WRITE(6,3)
    3 FORMAT(1HO)
C INITIALIZE ARRAYS
      IXY=1010
      IPHI=500
      DO 5 I=1,IXY
      X(I)=0.
      Y(I)=0.
    5 CONTINUE
      DO 6 I=1,IPHI
      PHI(I)=0.
      PHID(I)=0.
      ARCOX(I)=-1.0
      ARCOY(I)=-1.0
    6 CONTINUE
C CALL SUBROUTINE WHICH CALCULATES THE POSITIONS OF
C THE BOUNDARY ELEMENTS AND BOUNDARY CONDITIONS
C ON THE ELEMENTS
      CALL BNDCON(L,BLENX,BLENY,NINTX,NINTY)
      N=L-1
      N1P1=2*(N+INC+1)-1
      N2M=N1P1-2
      WRITE(6,70)N,N1P1,N2M
   70 FORMAT(1H ,3I10)
      NSPEC=NINTX+3*NINTY/2
C CALL THE INTEGRATION SUBROUTINES AND CALCULATE
C THE COEFFICIENTS IN THE TRANSFER MATRICES
C G AND H
      K=1
      DO 510 I=1,N2M,2
      IF (X(I).EQ.X(I+1).AND.Y(I).EQ.Y(I+1)) GOTO 510
      XP=(X(I)+X(I+2))*0.5
      YP=(Y(I)+Y(I+2))*0.5
      L=1
      DO 500 J=1,N2M,2
      IF (X(J).EQ.X(J+1).AND.Y(J).EQ.Y(J+1)) GOTO 500
      XL=X(J)
      XH=X(J+2)
      YL=Y(J)
      YH=Y(J+2)
```

LISTING 3. (continued)

```
      IF (I.EQ.J) CALL INTSL1(XL,XH,YL,YH,G(K,L),H(K,L))
      IF (I.NE.J) CALL INTES1(XL,XH,YL,YH,XP,YP,G(K,L),H(K,L))
  450 L=L+1
  500 CONTINUE
      K=K+1
  510 CONTINUE
C CALL SUBROUTINE TRANS WHICH FORMS THE MATRIX
C EQUATION GX=B
      CALL TRANS(N)
      IFAIL=0
      IA=500
      IX=IA
      IB=IA
      IU=IA
      IP=1
      MR=N+1
      NR=N
      DO 520 I=1,NR
  520 G(MR,I)=0.0
      PCON=BLENX
      G(MR,NSPEC)=1.0
      B(MR)=PCON
      READ(5,562) TOL
  562 FORMAT(F30.25)
      WRITE(6,563) TOL
  563 FORMAT('   TOLERANCE=',E12.3)
C CALL MATRIX DECOMPOSITION SUBROUTINE
      CALL FO1BKF(MR,NR,TOL,G,IA,D,AIJMAX,INC1,
     *IRANK,IFAIL)
      COND=AIJMAX(1)/AIJMAX(IRANK)
      WRITE(6,577) IRANK
  577 FORMAT('   RANK OF MATRIX EQUATIONS=',I5)
C PRINT THE CONDITION OF THE MATRIX
      WRITE(6,578) COND
  578 FORMAT('   CONDITION OF MATRIX=',F15.4)
C CALL THE MATRIX SOLUTION SUBROUTINE
      CALL FO4AUF(MR,NR,G,IA,IP,D,INC1,IRANK,
     *B,IB,SOL,IX,H,IU,DU,IFAIL)
      DO 580 I=1,N
  580 B(I)=SOL(I)
C CALL THE SUBROUTINE SORT WHICH SORTS THE MATRIX
C SOLUTION INTO ARRAYS OF POTENTIALS AND POTENTIAL
C DERIVATIVES
      CALL SORTP(N)
C CALL SUBROUTINE PRES2 WHICH CALCULATES THE
C PRESSURE COEFFICIENTS ROUND THE TUBES
      CALL PRES2
      STOP
      END
C
C
      SUBROUTINE BNDCON(L,BLENX,BLENY,NINTX,NINTY)
C THIS SUBROUTINE CALCULATES THE POSITIONS OF THE
C BOUNDARY ELEMENTS IN THE FLOW FIELD AND CALCULATES
C THE BOUNDARY CONDITIONS ON THE ELEMENTS
      COMMON /RADX/ ARCOX(500)
      COMMON /RADY/ ARCOY(500)
      COMMON /POTS1/ PHID(500)
      COMMON /POTS2/ PHI(500)
      COMMON /VAL1/ X(1010)
      COMMON /VAL2/ Y(1010)
      COMMON /CYL/ COORD(36,3)
      COMMON /CON1/ INC
      COMMON /CONST1/ PI
      COMMON /CYL1/ CN(36)
      COMMON /CYL2/ IPOT(36)
      COMMON /CYL3/ ICP(36)
      COMMON /CYL4/ VVEL(36)
      COMMON /CYL5/ WPR(36)
      COMMON /SEP1/ XC(1500),YC(1500),SC(1500)
      READ(5,10) INC
   10 FORMAT(I2)
C READ THE TUBE CO-ORDINATES,TUBE TYPES,VELOCITIES
C AND WHETHER THE PRESSURE COEFFICIENT IS TO BE
C PLOTTED
      DO 20 ICN=1,INC
      READ(5,15) COORD(ICN,1),COORD(ICN,2),COORD(ICN,3),
```

LISTING 3. (continued)

```
      *CN(ICN),VVEL(ICN),WPR(ICN)
   15 FORMAT(6F10.4)
      WRITE(6,16) ICN,COORD(ICN,1),COORD(ICN,2),COORD(ICN,3)
   16 FORMAT('   CO-ORDINATES OF TUBE ',I3,' ARE X=',
     *F8.2,' Y=',F8.2,' RADIUS=',F8.2)
      WRITE(6,17) CN(ICN),VVEL(ICN)
   17 FORMAT(1H ,'TUBE TYPE=',F4.0,' VELOCITY=',F10.5)
   20 CONTINUE
C READ THE FLOW FIELD BORDER LENGTHS AND THE
C NUMBER OF ELEMENTS ON EACH BORDER
      READ(5,25) BLENX
   25 FORMAT(F10.5)
      WRITE(6,26) BLENX
   26 FORMAT('   LENGTH OF X BOUNDARY= ',F10.2)
      READ(5,30) BLENY
   30 FORMAT(F10.5)
      WRITE(6,31) BLENY
   31 FORMAT('   LENGTH OF Y BOUNDARY= ',F10.2)
      READ(5,40) XRS
   40 FORMAT(F10.4)
      WRITE(6,41)XRS
   41 FORMAT('   X CO-ORDINATE OF FIRST REFINED ELEMENT=',F10.2)
      READ(5,45) XRF
   45 FORMAT(F10.4)
      WRITE(6,46) XRF
   46 FORMAT('   X CO-ORDINATE OF LAST REFINED ELEMENT=',F10.2)
      READ(5,50) NREL
   50 FORMAT(I3)
      WRITE(6,51) NREL
   51 FORMAT('   NUMBER OF REFINED ELEMENTS=',I3)
      READ(5,55) NUREL
   55 FORMAT(I3)
      WRITE(6,56) NUREL
   56 FORMAT('   NUMBER OF NON REFINED X ELEMENTS=',I3)
      READ(5,57) NINTY
   57 FORMAT(I3)
      WRITE(6,58) NINTY
   58 FORMAT('   NUMBER OF ELEMENTS ROUND Y BOUNDARY=',I3)
      POTBX=1.0
      POTEX=-1.0
      NY=NINTY*2
      NC1=NY+1
      NX3=NREL*2
      NC3=NX3+1
      NUREL2=NUREL/2
      NX2=NUREL2*2
      NC2=NX2+1
      NINTX=NREL+NUREL
      WRITE(6,59) NINTX
   59 FORMAT('   NUMBER OF ELEMENTS ROUND X BOUNDARY=',I3)
C CALCULATE THE POSITIONS OF THE BOUNDARY ELEMENTS
C ROUND THE EXTERNAL FLOW FIELD BORDER
      I=1
      DO 60 K=1,NC1
      X(I)=BLENX
      Y(I)=FLOAT(K-1)*BLENY/FLOAT(NY)
      I=I+1
   60 CONTINUE
      I=I-1
      DO 70 K=1,NC2
      X(I)=BLENX-FLOAT(K-1)*(BLENX-XRF)/FLOAT(NX2)
      Y(I)=BLENY
      I=I+1
   70 CONTINUE
      I=I-1
      DO 75 K=1,NC3
      X(I)=XRF-FLOAT(K-1)*(XRF-XRS)/FLOAT(NX3)
      Y(I)=BLENY
      I=I+1
   75 CONTINUE
      I=I-1
      DO 80 K=1,NC2
      X(I)=XRS-FLOAT(K-1)*XRS/FLOAT(NX2)
      Y(I)=BLENY
      I=I+1
   80 CONTINUE
      I=I-1
      DO 85 K=1,NC1
```

LISTING 3. (continued)

```
      X(I)=0.0
      Y(I)=BLENY-FLOAT(K-1)*BLENY/FLOAT(NY)
      I=I+1
   85 CONTINUE
      I=I-1
      DO 90 K=1,NC2
      X(I)=FLOAT(K-1)*XRS/FLOAT(NX2)
      Y(I)=0.0
      I=I+1
   90 CONTINUE
      I=I-1
      DO 100 K=1,NC3
      X(I)=XRS+FLOAT(K-1)*(XRF-XRS)/FLOAT(NX3)
      Y(I)=0.0
      I=I+1
  100 CONTINUE
      I=I-1
      DO 105 K=1,NC2
      X(I)=XRF+FLOAT(K-1)*(BLENX-XRF)/FLOAT(NX2)
      Y(I)=0.0
      I=I+1
  105 CONTINUE
      I=I-1
      X(I)=BLENX
      Y(I)=0.0
      I=I+1
      X(I)=BLENX
      Y(I)=0.
      I=I+1
C CALCULATE THE BOUNDARY CONDITIONS ON THE
C EXTERNAL FLOW FIELD BOUNDARY ELEMENTS
      L=1
      DO 110 J=1,NINTY
      PHI(L)=POTEX
      PHID(L)=1.0
      L=L+1
  110 CONTINUE
      DO 115 J=1,NINTX
      PHI(L)=0.0
      PHID(L)=1.0
      L=L+1
  115 CONTINUE
      DO 120 J=1,NINTY
      PHI(L)=POTBX
      PHID(L)=1.0
      L=L+1
  120 CONTINUE
      DO 125 J=1,NINTX
      PHI(L)=0.0
      PHID(L)=1.0
      L=L+1
  125 CONTINUE
      IS=I
      LS=L
      IK=1
      ICP(1)=IK
      IK=2
C READ THE NORMALIZED TUBE MODEL BOUNDARY
C ELEMENT CO-ORDINATES FROM THE TUBE MODEL
C DATA FILE
      DO 350 K=1,1500
      READ(4,200) XC(K),YC(K),SC(K)
  200 FORMAT(1X,3E20.9)
      IF (XC(K).GT.10000..OR.YC(K).GT.10000.) GOTO 355
      IF (XC(K).GT.1000..OR.YC(K).GT.1000.) GOTO 300
      ICP(IK)=K+2
      GOTO 350
  300 CONTINUE
      IK=IK+1
  350 CONTINUE
  355 ICP(IK+1)=K
      ICP(IK)=K
      IK=1
      WRITE(6,380)
  380 FORMAT(1H ,'NORMALIZED CO-ORDINATES')
      WRITE(6,385) IK
```

LISTING 3. (continued)

```
      385 FORMAT(1H ,'CYLINDER TYPE ',I3)
          IK=IK+1
          WRITE(6,360)
          WRITE(6,400)
      400 FORMAT(1H ,'   N       X                 Y                 S')
          IZZ=1
C PRINT THE CO-ORDINATES OF THE BOUNDARY
C ELEMENTS IN EACH TUBE MODEL
          DO 450 K=1,1500
          IF (XC(K).GT.10000..OR.YC(K).GT.10000.) GOTO 500
          IF (XC(K).GT.1000..OR.YC(K).GT.1000.) GOTO 420
          WRITE(6,410) IZZ,XC(K),YC(K),SC(K)
      410 FORMAT(1H ,I5,3F15.6)
          IZZ=IZZ+1
          GOTO 450
      420 WRITE(6,360)
          IF (XC(K+1).LT.10000..OR.YC(K+1).LT.10000.)
         *WRITE(6,385) IK
          IF (XC(K+1).LT.10000..OR.YC(K+1).LT.10000.)
         *WRITE(6,400)
          IZZ=1
          IK=IK+1
          WRITE(6,360)
      450 CONTINUE
      500 CONTINUE
          IS1=IS
          L1=LS
          IPOT(1)=L1
C CALCULATE THE POSITIONS OF THE TUBE BOUNDARY
C ELEMENTS IN THE FLOW FIELD
          DO 600 ICN=1,INC
          IK=INT(CN(ICN))
          ISS=ICP(IK)
          IFF=ICP(IK+1)-1
          DO 550 J=ISS,IFF
          X(IS1)=XC(J)+COORD(ICN,1)
          Y(IS1)=YC(J)+COORD(ICN,2)
          IF (XC(J).GT.1000..OR.YC(J).GT.1000.) GOTO 520
          GOTO 550
      520 X(IS1)=X(IS1-1)
          Y(IS1)=Y(IS1-1)
      550 IS1=IS1+1
      600 CONTINUE
          X(IS1-1)=0.0
          Y(IS1-1)=0.0
C CALCULATE THE BOUNDARY CONDITIONS ON EACH
C TUBE BOUNDARY ELEMENT
          DO 700 ICN=1,INC
          IK=INT(CN(ICN))
          ISS=ICP(IK)
          IFF=ICP(IK+1)-3
          X1=COORD(ICN,1)
          Y1=COORD(ICN,2)
          A=COORD(ICN,3)
          DO 650 J=ISS,IFF,2
          IF (XC(J).GT.1000..OR.YC(J).GT.1000.) GOTO 660
          PHID(L1)=1.0
          IF (XC(J+2).GT.5000.) GOTO 640
          PHI(L1)=(XC(J+2)-XC(J))*VVEL(ICN)/SQRT((XC(J+2)
         *-XC(J))**2+(YC(J+2)-YC(J))**2)
          GOTO 650
      640 PHI(L1)=(XC(ISS)-XC(J))*VVEL(ICN)/SQRT((XC(ISS)
         *-XC(J))**2+(YC(ISS)-YC(J))**2)
      650 L1=L1+1
      660 IPOT(ICN+1)=L1
      700 CONTINUE
      650 L1=L1+1
      660 IPOT(ICN+1)=L1
      700 CONTINUE
          L=L1
          RETURN
          END
C
C
```

LISTING 3. (continued)

```
      SUBROUTINE PRES2
C THIS SUBROUTINE CALCULATES THE PRESSURE COEFFICIENTS
C ROUND THE TUBES
      COMMON /CONST1/ PI
      COMMON /CON1/ INC
      COMMON /CYL/ COORD(36,3)
      COMMON /POTS3/ POT(500)
      COMMON /XPO/ XPOS(200)
      COMMON /RES1/ CPRES(200)
      COMMON /SEP1/ XC(1500),YC(1500),SC(1500)
      COMMON /CYL1/ CN(36)
      COMMON /CYL2/ IPOT(36)
      COMMON /CYL3/ ICP(36)
      COMMON /CYL4/ VVEL(36)
      COMMON /CYL5/ WPR(36)
      COMMON /PL/ XRX(120),YRY(120)
      DIMENSION APOT(200)
      DIMENSION POTS(200)
C CALL SUBROUTINE INPLO WHICH INITIALIZES
C THE GRAPH PLOTTING DEVICE
      CALL INPLO
      IPL=-1
C CALCULATE THE PRESSURE COEFFICIENTS ROUND
C EACH TUBE
      DO 800 ICN=1,INC
      X1=COORD(ICN,1)
      Y1=COORD(ICN,2)
      A=COORD(ICN,3)
      TVEL=VVEL(ICN)
      ITYPE=INT(CN(ICN)+0.001)
      IK=INT(CN(ICN))
      IS=ICP(IK)+1
      IF=ICP(IK+1)-2
      J=1
      JJ=0
C CALCULATE THE ANGLE ROUND THE TUBE WHERE
C EACH BOUNDARY ELEMENT IS POSITIONED
      DO 120 I=IS,IF,2
      IF (SC(I).GT.0.) GOTO 110
      XS=XC(I)
      YS=YC(I)
      XR=ABS(XS/A)
      IF (XR.GT.1.0) XR=1.0
      ANG=ACOS(XR)
      IF (XS.GT.0.0) ANG=PI-ANG
      IF (YS.GT.0.0) ANG=2.*PI-ANG
      APOT(J)=ANG*180./PI
      GOTO 120
  110 APOT(J)=-99999.
      JJ=JJ+1
  120 J=J+1
      IS=IPOT(ICN)
      IF=IPOT(ICN+1)-1
      K=1
      DO 140 I=IS,IF
      POTS(K)=POT(I)
  140 K=K+1
      NP=IPOT(ICN+1)-IPOT(ICN)
      DO 150 I=1,NP
      IF (APOT(I).LT.-1000.) GOTO 160
  150 CONTINUE
      GOTO 168
  160 AS=APOT(I-1)
      ADIF=(APOT(I+JJ)-APOT(I-1))/(JJ+1)
      JK=1
      DO 165 K=I,(I+JJ-1)
      APOT(K)=AS+FLOAT(JK)*ADIF
      POTS(K)=-99999.
  165 JK=JK+1
  168 CONTINUE
C SORT THE PRESSURE COEFFICIENTS INTO ASCENDING
C ORDER OF ANGLE MEASURED FROM THE FRONT OF THE
C TUBE
      DO 180 K=1,(NP-1)
      DO 170 I=1,(NP-K)
      IF (APOT(I).LE.APOT(I+1)) GOTO 170
```

LISTING 3. (continued)

```
453         TEMP1=APOT(I)
454         APOT(I)=APOT(I+1)
455         APOT(I+1)=TEMP1
456         TEMP1=POTS(I)
457         POTS(I)=POTS(I+1)
458         POTS(I+1)=TEMP1
459       170 CONTINUE
460       180 CONTINUE
461         NP1=NP+1
462         POTS(NP1)=POTS(1)
463     C CALCULATE THE POTENTIAL DIFFERENCE BETWEEN
464     C ADJACENT ELEMENTS ROUND THE TUBE
465         DO 200 I=1,NP1
466         IF (I.EQ.1) POTPLS=POTS(1)
467         IF (I.EQ.1) POTMIN=POTS(NP)
468         IF (I.GT.1) POTPLS=POTS(I)
469         IF (I.GT.1) POTMIN=POTS(I-1)
470         IF (I.EQ.NP1) POTPLS=POTS(1)
471         POTDIF=POTPLS-POTMIN
472         IF (POTMIN.LT.0..OR.POTPLS.LT.0.) POTDIF=-99999.
473         IF (I.EQ.1) ANG1=APOT(NP)-360.
474         IF (I.EQ.1) ANG2=APOT(1)
475         IF (I.GT.1) ANG1=APOT(I-1)
476         IF (I.GT.1) ANG2=APOT(I)
477         IF (I.EQ.NP1) ANG2=APOT(1)+360.
478         ANGAV=(ANG2+ANG1)/2.
479         ANGDIF=(ANG2-ANG1)/2.
480     C CALCULATE THE DISTANCE BETWEEN ADJACENT ELEMENTS
481         DIST=2.*A*SIN(ANGDIF*PI/180.)
482         VEL1=POTDIF/DIST
483     C CALCULATE THE PRESSURE COEFFICIENT
484         CPRES(I)=1.-VEL1**2
485       200 XPOS(I)=ANGAV
486         WRITE(6,220) ICN,X1,Y1,A
487       220 FORMAT(1H1,'TUBE NUMBER',I4,' CO-ORDINATES X=',
488          *F8.2,' Y=',F8.2,' RADIUS=',F8.2)
489         WRITE(6,221) ITYPE,TVEL
490       221 FORMAT(1H ,' TUBE TYPE=',I2,' VELOCITY=',F15.6)
491     C PRINT THE POTENTIAL ON EACH ELEMENT ROUND THE TUBE
492         WRITE(6,230)
493       230 FORMAT(1HO,'ANGLE   POTENTIAL')
494         DO 240 I=1,NP
495         WRITE(6,235) APOT(I),POTS(I)
496       235 FORMAT(1H ,F5.0,F12.4)
497       240 CONTINUE
498         IS=1
499         DO 242 I=1,NP1
500         IF (CPRES(I).LT.-9999.) GOTO 243
501       242 IS=IS+1
502       243 CPL=CPRES(I-1)
503         DO 244 IF=IS,NP1
504         IF (CPRES(IF).GT.-9999.) GOTO 245
505       244 CONTINUE
506       245 CPH=CPRES(IF)
507         IF=IF-1
508         CPA=(CPL+CPH)/2.
509         DO 246 I=IS,IF
510       246 CPRES(I)=CPA
511         WRITE(6,220) ICN,X1,Y1,A
512         WRITE(6,250)
513       250 FORMAT(1HO,'ANGLE',2X,'VELOCITY',4X,'CP',8X,'CL',8X,'CD')
514     C PRINT THE PRESSURE COEFFICIENT AND COMPONENT
515     C OF LIFT AND DRAG FOR EACH ANGLE ROUND THE TUBE
516         DO 260 I=1,NP1
517         RANG=XPOS(I)*PI/180.
518         CP=CPRES(I)
519         VEL=SQRT(1.-CP)
520         CL=CPRES(I)*SIN(RANG)
521         CD=CPRES(I)*COS(RANG)
522         WRITE(6.255) XPOS(I),VEL,CP,CL,CD
523       255 FORMAT(1H ,F5.0,4F10.4)
524       260 CONTINUE
525         WRITE(6,620)
526       620 FORMAT(1HO)
527       640 FORMAT(1HO,'LIFT COEFFICIENT=',F10.4)
528       660 FORMAT(1H ,'DRAG COEFFICIENT=',F10.4)
```

## LISTING 3. (continued)

```
      WRITE(6,670)
  670 FORMAT(1HO,'LINEAR APPROXIMATION OF PRESSURE COEFFICIENT')
C CALL SUBROUTINE CALLD WHICH CALCULATES THE TUBE
C LIFT AND DRAG COEFFICIENTS
      CALL CALLD(NP,CL,CD)
      WRITE(6,620)
C PRINT THE LIFT AND DRAG COEFFICIENTS
      WRITE(6,640) CL
      WRITE(6,660) CD
      DO 700 I=1,NP1
      XRX(I)=XPOS(I)
      YRY(I)=CPRES(I)
  700 CONTINUE
      XRX(NP1+1)=1.E31
      IFLAG=1
      IFLAG2=1
      NC=6
      XL=0.
      XH=360.
      YL=-8.
      YH=2.
      IF (WPR(ICN).EQ.0.) GOTO 800
      IFL=IFL+1
      IF (IFL.GT.1) IFL=0
C CALL THE GRAPH PLOTTING SUBROUTINE
      CALL MYPLOT(NP,ICN,X1,Y1,IFL,INC)
C CALL THE LINE PRINTER PLOTTING SUBROUTINE
      CALL LPPLOT(NC,XL,XH,YL,YH,IFLAG,IFLAG2)
  800 CONTINUE
      CALL DEVEND
      RETURN
      END
C
C
      SUBROUTINE INTES1(XL,XH,YL,YH,XP,YP,G,H)
C THIS SUBROUTINE INTEGRATES THE KERNEL WHEN IT CONTAINS NO
C SINGULARITIES ABOUT THE POINT OF INTEGRATION ALONG
C A STRAIGHT LINE
      ASQ=(XL-XP)**2+(YL-YP)**2
      BSQ=(XH-XP)**2+(YH-YP)**2
      CSQ=(XH-XL)**2+(YH-YL)**2
      A=SQRT(ASQ)
      B=SQRT(BSQ)
      C=SQRT(CSQ)
      ANG=(ASQ+BSQ-CSQ)/(2.*A*B)
      IF (ANG.LT.-1.0) ANG=-1.0
      IF (ANG.GT.1.0) ANG=1.0
      CHI=ACOS(ANG)
      ARG=(ASQ+CSQ-BSQ)/(2.*A*C)
      IF (ARG.LT.-1.0) ARG=-1.0
      IF (ARG.GT.1.0) ARG=1.0
      THETA=ACOS(ARG)
      G=-(A*COS(THETA)*(LOG(A)-LOG(B))+C*(LOG(B)-1.)
     *+A*CHI*SIN(THETA))
      H=CHI
      SIG=(XL-XP)*(YH-YP)-(XH-XP)*(YL-YP)
      IF (SIG.GT.0.0) H=-H
      RETURN
      END
C
C
      SUBROUTINE INTSL1(XL,XH,YL,YH,G,H)
C THIS SUBROUTINE INTEGRATES THE KERNEL ALONG
C A STRAIGHT LINE ABOUT A WEAK SINGULARITY
      COMMON /CONST1/ PI
      XDIF=(XH-XL)/2.
      YDIF=(YH-YL)/2.
      DIST=SQRT(XDIF**2+YDIF**2)
      G=2.*DIST*(1.-LOG(DIST))
      H=PI
      RETURN
      END
C
C
      SUBROUTINE TRANS(N)
C THIS SUBROUTINE TRANSFERS THE ROWS OF THE MATRICES
C TO GET ALL UNKNOWNS ON ONE SIDE THEN MULTIPLIES OUT
```

LISTING 3. (continued)

```
C THE R.H.S. TO GET THE EQUATION GX=B
      COMMON /MAT1/ G(500,500)
      COMMON /MAT2/ H(500,500)
      COMMON /MAT3/ B(500)
      COMMON /POTS1/ PHID(500)
      COMMON /POTS2/ PHI(500)
C THIS SECTION SWAPS THE ELEMENTS IN THE
C COLUMN VECTORS TO OBTAIN ALL THE
C UNKNOWNS ON ONE SIDE
      DO 50 J=1,N
      IF (PHID(J).EQ.0.0) GOTO 50
      DO 40 I=1,N
      TEMP=G(I,J)
      G(I,J)=-H(I,J)
      H(I,J)=-TEMP
   40 CONTINUE
   50 CONTINUE
C THIS SECTION MULTIPLIES OUT THE MATRIX
C TO GIVE THE EQUATION GX=B
      DO 100 I=1,N
      B(I)=0.
      DO 90 J=1,N
      B(I)=B(I)+H(I,J)*PHI(J)
   90 CONTINUE
  100 CONTINUE
      RETURN
      END
C
C
      SUBROUTINE SORTP(N)
C THIS SUBROUTINE SORTS THE POTENTIALS AND POTENTIAL
C DERIVATIVES INTO SEPARATE ARRAYS
      COMMON /SOLU/ SOL(500)
      COMMON /POTS1/ PHID(500)
      COMMON /POTS2/ PHI(500)
      COMMON /POTS3/ POT(500)
      COMMON /POTS4/ POTD(500)
      COMMON /MAT3/ B(500)
      DO 50 I=1,N
      IF (PHID(I).EQ.0.0) GOTO 10
      POT(I)=B(I)
      POTD(I)=PHI(I)
      GOTO 50
   10 POT(I)=PHI(I)
      POTD(I)=B(I)
   50 CONTINUE
      RETURN
      END
C
C
      SUBROUTINE CALLD(ND1,CL,CD)
C THIS SUBROUTINE CALCULATES THE LIFT AND DRAG COEFFICIENTS
C USING A LINEAR APPROXIMATION FOR THE PRESSURE COEFFICIENT
      COMMON /RES1/ CPRES(200)
      COMMON /XPO/ XPOS(200)
      COMMON /CONST1/ PI
      DIMENSION RESA(200)
      DO 10 I=1,ND1+1
   10 RESA(I)=XPOS(I)*PI/180.
      CL=0.0
      CD=0.0
      DO 100 I=1,ND1
      S1=0.0
      S2=0.0
      T1=(CPRES(I+1)-CPRES(I))/(RESA(I+1)-RESA(I))
      DO 50 J=1,2
      K=I+J-1
      S1=S1+((-1.)**J)*(-CPRES(I)*COS(RESA(K))+T1*(SIN(RESA(K))
     *-RESA(K)*COS(RESA(K)))+T1*RESA(I)*COS(RESA(K)))
      S2=S2+((-1.)**J)*(CPRES(I)*SIN(RESA(K))+T1*(RESA(K)*SIN(RESA(K))
     *+COS(RESA(K)))-T1*RESA(I)*SIN(RESA(K)))
   50 CONTINUE
      CL=CL+S1/(2.*PI)
      CD=CD+S2/(2.*PI)
  100 CONTINUE
```

LISTING 3. (continued)

```
      CL=CL*2.
      CD=CD*2.
      RETURN
      END
C
C
      SUBROUTINE INPLO
C THIS SUBROUTINE INITIALIZES THE GRAPH PLOTTER
      CALL CCO36N
      CALL DEVPAP(200.,280.,0)
      CALL UNITS(1.0)
      RETURN
      END
C
C
      SUBROUTINE MYPLOT(NP,ICN,X1,Y1,IFL,INC)
C THIS SUBROUTINE PLOTS THE PRESSURE COEFFICIENTS
C ROUND THE TUBE AS A FUNCTION OF ANGLE
      COMMON /RES1/ CPRES(200)
      COMMON /XPO/ XPOS(200)
      DIMENSION YPOS(200)
      DIMENSION XRES(200)
      COMMON /CONST1/ PI
      IF (IFL.EQ.0) YD=110.
      IF (IFL.EQ.1) YD=0.0
      CALL CHASIZ(3.,5.)
      CALL MOVTO2(10.,250.)
C DEFINE AXES AND PLOT SCALES AND HEADINGS
      IF (IFL.EQ.0)
     *CALL CHAHOL(21HTHEORETICAL RESULTS*.)
      CALL CHASIZ(2.,3.)
      CALL MOVTO2(30.,105.+YD)
      CALL CHAHOL(7HTUBE *.)
      CALL CHAINT(ICN,-3)
      CALL CHAHOL(18H CO-ORDINATES X=*.)
      CALL CHAFIX(X1,5,1)
      CALL CHAHOL(5H Y=*.)
      CALL CHAFIX(Y1,5,1)
      CALL MOVTO2(18.,30.+YD)
      CALL CHAANG(90.)
      CALL CHAHOL(30HSTATIC PRESSURE COEFFICIENTS*.)
      CALL CHAANG(0.)
      CALL MOVTO2(130.,10.+YD)
      CALL CHAHOL(7HANGLE*.)
      CALL CHASIZ(1.5,2.5)
      CALL AXIPOS(1,30.,60.+YD,120.,1)
      CALL AXIPOS(1,30.,20.+YD,80.,2)
      NP1=NP+1
      CPRES(NP1)=CPRES(1)
      CPRES(NP1+1)=CPRES(2)
      CPL=0.
C SCALE THE PRESSURE COEFFICIENTS
      DO 10 I=1,NP
      IF (ABS(CPRES(I)).GT.CPL) CPL=ABS(CPRES(I))
   10 CONTINUE
      NMAX=INT(CPL)+1
      IF (NMAX.EQ.1) NINT=8
      IF (NMAX.EQ.2) NINT=8
      IF (NMAX.EQ.3) NINT=6
      IF (NMAX.EQ.4) NINT=8
      IF (NMAX.EQ.5) NINT=10
      IF (NMAX.EQ.6) NINT=6
      IF (NMAX.EQ.7) NMAX=8
      IF (NMAX.EQ.8) NINT=8
      IF (NMAX.EQ.9) NMAX=10
      IF (NMAX.EQ.10) NINT=10
      IF (NMAX.LT.11) GOTO 15
      IF (NMAX.LT.20) NMAX=20
      IF (NMAX.EQ.20) NINT=10
      IF (NMAX.LT.40) NMAX=40
      IF (NMAX.EQ.40) NINT=8
      IF (NMAX.LT.41) GOTO 15
      NMAX=(NMAX/10+1)*10
      NINT=NMAX/5
   15 CONTINUE
      FNM=FLOAT(NMAX)
      NPH=NP1/2
```

LISTING 3. (continued)

```
      CALL AXISCA(3,12,0.,360.,1)
      CALL AXISCA(3,NINT,-FNM,FNM,2)
      CALL GRID(2,1,1)
      DO 20 I=1,NP1
   20 YPOS(I)=CPRES(I)
C DRAW LINES BETWEEN PRESSURE COEFFICIENT POINTS
      CALL GRAPOL(XPOS,YPOS,NP1)
      II=0
      DO 23 I=1,NP1
      IF (I.EQ.1) GOTO 22
      IF (CPRES(I-1).EQ.CPRES(I).AND.I.LE.NPH) GOTO 23
      IF (CPRES(I).EQ.CPRES(I+1).AND.I.GE.NPH) GOTO 23
   22 II=II+1
      YPOS(II)=CPRES(I)
      XRES(II)=XPOS(I)
   23 CONTINUE
C PLOT PRESSURE COEFFICIENT POINTS
      CALL GRASYM(XRES,YPOS,II,8,0)
      RADA=0.
      DO 30 I=1,NP1
      RADA=XPOS(I)*PI/180.
   30 YPOS(I)=CPRES(I)*SIN(RADA)
      CALL BROKEN(1)
C DRAW LINES BETWEEN LIFT COEFFICIENT POINTS
      CALL GRAPOL(XPOS,YPOS,NP1)
      II=0
      DO 33 I=1,NP1
      IF (I.EQ.1) GOTO 32
      IF (CPRES(I-1).EQ.CPRES(I).AND.I.LE.NPH) GOTO 33
      IF (CPRES(I).EQ.CPRES(I+1).AND.I.GE.NPH) GOTO 33
   32 II=II+1
      TEMP=YPOS(I)
      YPOS(II)=TEMP
      XRES(II)=XPOS(I)
   33 CONTINUE
C PLOT LIFT COEFFICIENT POINTS
      CALL GRASYM(XRES,YPOS,II,1,0)
      RADA=0.
      DO 40 I=1,NP1
      RADA=XPOS(I)*PI/180.
   40 YPOS(I)=CPRES(I)*COS(RADA)
      CALL BROKEN(4)
C DRAW LINES BETWEEN DRAG COEFFICIENT POINTS
      CALL GRAPOL(XPOS,YPOS,NP1)
      II=0
      DO 43 I=1,NP1
      IF (I.EQ.1) GOTO 42
      IF (CPRES(I-1).EQ.CPRES(I).AND.I.LE.NPH) GOTO 43
      IF (CPRES(I).EQ.CPRES(I+1).AND.I.GE.NPH) GOTO 43
   42 II=II+1
      TEMP=YPOS(I)
      YPOS(II)=TEMP
      XRES(II)=XPOS(I)
   43 CONTINUE
C PLOT DRAG COEFFICIENT POINTS
      CALL GRASYM(XRES,YPOS,II,6,0)
      CALL BROKEN(0)
      IF (IFL.EQ.1.AND.ICN.NE.INC) CALL PICCLE
      RETURN
      END
C
C
      SUBROUTINE LPPLOT(NC,XL,XH,YL,YH,IFLAG,IFLAG2)
C THIS SUBROUTINE PLOTS A GRAPH OF X AGAINST Y ON
C THE LINE PRINTER ASSIGNED TO CHANNEL NC
      COMMON /PL/ XRX(120),YRY(120)
      INTEGER BLANK,AST,VBORD,HBORD
      DIMENSION LINE(101)
      DATA AST/1H*/,BLANK/1H /
      DATA VBORD/1H[/,HBORD/1H_/
      NXL=73
      NYL=101
      WRITE(NC,10)
   10 FORMAT(1H1)
      DO 20 I=1,120
```

LISTING 3. (continued)

```
      IF (XRX(I).GT.1.E30) GOTO 30
   20 CONTINUE
   30 NVAL=I-1
C SORT X AND Y VALUES INTO ASCENDING ORDER
C OF X
      DO 50 I=1,(NVAL-1)
      DO 40 J=1,(NVAL-I)
      IF (XRX(J).LT.XRX(J+1)) GOTO 40
      TEMP=XRX(J)
      XRX(J)=XRX(J+1)
      XRX(J+1)=TEMP
      TEMP=YRY(J)
      YRY(J)=YRY(J+1)
      YRY(J+1)=TEMP
   40 CONTINUE
   50 CONTINUE
C CALCULATE X AND Y MAXIMUM AND MINIMUM VALUES
      XMAX=-1.E30
      XMIN=1.E30
      YMAX=-1.E30
      YMIN=1.E30
      DO 60 I=1,NVAL
      IF (XRX(I).GT.XMAX) XMAX=XRX(I)
      IF (XRX(I).LT.XMIN) XMIN=XRX(I)
      IF (YRY(I).GT.YMAX) YMAX=YRY(I)
      IF (YRY(I).LT.YMIN) YMIN=YRY(I)
   60 CONTINUE
      IF (IFLAG.EQ.0) GOTO 70
      XMAX=XH
      XMIN=XL
      YMAX=YH
      YMIN=YL
C CALCULATE SCALING FACTORS
   70 XINC=(XMAX-XMIN)/(NXL-1)
      YINC=(YMAX-YMIN)/(NYL-1)
      DO 80 I=1,101
   80 LINE(I)=HBORD
C PRINT THE HORIZONTAL GRAPH BORDER
      IF (IFLAG2.EQ.0) WRITE(NC,100) LINE
      IF (IFLAG2.NE.0) WRITE(NC,107) LINE
  100 FORMAT(5X,101A1)
  105 FORMAT(1H ,F8.0,1X,F11.5,1X,101A1)
  106 FORMAT(1H ,21X,A1)
  107 FORMAT(1H ,21X,101A1)
      K=1
C CALCULATE THE POSITION OF THE SCALED
C POINTS ON THE GRAPH AND PRINT THEM
      DO 200 J=1,NXL
      DO 110 I=2,101
  110 LINE(I)=BLANK
      LINE(1)=VBORD
  115 XRXOS=XMIN+XINC*FLOAT(J-1)
      XRXOF=XRXOS+XINC
      XRXSE=XRXOS-0.001
      XRXFE=XRXOF-0.001
  116 IF (XRX(K).GT.XRXSE) GOTO 117
      K=K+1
      GOTO 116
  117 IF (XRX(K).GT.XRXFE) GOTO 120
      IY=IFIX((YRY(K)-YMIN)/YINC)+2
      IF (IY.GT.100) IY=100
      IF (IY.LT.1) IY=1
      LINE(IY)=AST
      IF (IFLAG2.EQ.0) WRITE(NC,100) LINE
      IF (IFLAG2.NE.0) WRITE(NC,105) XRX(K),YRY(K),LINE
      K=K+1
      GOTO 200
  120 WRITE(NC,106) VBORD
      IF (XRX(K).GT.XRXFE) GOTO 200
      K=K+1
      GOTO 115
  200 CONTINUE
      WRITE(NC,220)
  220 FORMAT(1H )
```

LISTING 3. (continued)

```
C PRINT THE X AND Y MAXIMUM AND MINIMUM
C VALUES AND INCREMENTS
      WRITE(NC,230) XMIN,XMAX,XINC
  230 FORMAT(10X,15HX AXIS MINIMUM=,G10.4,9H MAXIMUM=,G10.4
     *,11H INCREMENT=,G10.4)
      WRITE(NC,240) YMIN,YMAX,YINC
  240 FORMAT(10X,15HY AXIS MINIMUM=,G10.4,9H MAXIMUM=,G10.4
     *,11H INCREMENT=,G10.4)
      WRITE(NC,220)
      RETURN
      END
```

Note - The graph plotting suroutines are contained in the GINO-F and GINOGRAF general purpose graphics packages, implemented on the ICL 2970 computer.

See GINO-F users manual, version 6 (1980) and GINOGRAF user manual, issue 1 (1976); published by the Computer Aided Design Centre, Cambridge, U.K.

Note - Subroutines F01BKF and F04AUF are contained in the FORTRAN NAG library, implemented on the ICL 2970 computer.

See NAG FORTRAN Library Manual, mark 8, volumes 4 and 5; published by the Numerical Algorithms Group, Oxford, U.K.

## APPENDIX 3

### CALIBRATION OF THE PRESSURE MEASURING TUBE ELECTRET MICROPHONES

Let the gain of the B & K 2107 frequency analyser be $G_1$
Let the gain of the electret microphone amplifier be $G_2$
Let the 124 dB B & K 4220 pistonphone calibration signal give an output of x volts from the B & K 2107 frequency analyser when set to gain $G_3$.

The calibration factor for the B & K microphone and frequency analyser when on gain range $G_1$ is given by $C_1$ where :

$$C_1 = 2 \times 10^{-5} \times 10^{(124/20)} \times \frac{xG_3}{G_1} \quad VPa.^{-1}$$

$$\therefore C_1 \simeq 31.7x \frac{G_3}{G_1} \quad VPa.^{-1}$$

The calibration factor for the electret microphone and amplifier when on gain range $G_2$ is given by $C_2$ where :

$$C_2 = G_2.$$

Let $P_{xy}(f)$ be the cross-spectral power density of the amplified signals from the B & K microphone and the electret microphone.
Let $P_{xx}(f)$ be the auto-power spectral density of the amplified signal from the B & K microphone.
The transfer function $H_{xy}(f)$ between the B & K microphone and electret microphone is given by

$$H_{xy}(f) = \frac{P_{xy}(f)\ C_1}{P_{xx}(f)\ C_2} .$$

The amplitude and phase calibration curves for the electret microphone are given by $C_A(f)$ and $C_p(f)$ respectively where

$$C_A(f) = (Re(H_{xy}(f))^2 + Im(H_{xy}(f))^2)^{0.5}$$

and $C_p(f) = \arctan \frac{Im(H_{xy}(f1)}{Re(H_{xy}(f1)}$ .

Re and Im represent the real and imaginary parts of a complex number respectively.

# APPENDIX 4

## TABLES OF CO-ORDINATES OF THE WIND TUNNEL SECTIONS

TABLE A4.1. Co-ordinates of bellmouth inlet section

| Control Point | x co-ordinate mm ±0.25 mm | y co-ordinate mm ±0.25 mm |
|---|---|---|
| 0 | 0.00 | 0.00 |
| 1 | 38.07 | 1.20 |
| 2 | 76.13 | 2.40 |
| 3 | 114.20 | 7.60 |
| 4 | 152.27 | 14.17 |
| 5 | 190.33 | 24.27 |
| 6 | 228.40 | 38.07 |
| 7 | 266.47 | 56.20 |
| 8 | 304.53 | 82.80 |
| 9 | 342.60 | 120.33 |
| 10 | 342.60 | 331.00 |
| 11 | 304.53 | 360.67 |
| 12 | 266.47 | 376.00 |
| 13 | 228.40 | 381.00 |
| 14 | 190.33 | 379.33 |
| 15 | 152.27 | 375.33 |
| 16 | 114.20 | 368.67 |
| 17 | 76.13 | 360.00 |
| 18 | 38.07 | 352.00 |

TABLE A4.2. Co-ordinates of inlet contraction

| Control Point | x co-ordinate mm ±0.25 mm | y and z co-ordinate mm ±0.25 mm |
|---|---|---|
| o | 0.00 | 800.00 |
| 1 | 50.00 | 797.45 |
| 2 | 100.00 | 794.70 |
| 3 | 150.00 | 791.68 |
| 4 | 200.00 | 788.36 |
| 5 | 250.00 | 784.71 |
| 6 | 300.00 | 780.70 |
| 7 | 350.00 | 776.13 |
| 8 | 400.00 | 771.45 |
| 9 | 450.00 | 766.13 |
| 10 | 500.00 | 760.28 |
| 11 | 550.00 | 753.87 |
| 12 | 600.00 | 746.84 |
| 13 | 650.00 | 739.12 |
| 14 | 700.00 | 730.67 |
| 15 | 750.00 | 721.41 |
| 16 | 800.00 | 711.29 |
| 17 | 850.00 | 700.23 |
| 18 | 900.00 | 688.18 |
| 19 | 950.00 | 675.06 |
| 20 | 1000.00 | 660.81 |
| 21 | 1050.00 | 645.39 |
| 22 | 1100.00 | 628.76 |
| 23 | 1150.00 | 610.86 |
| 24 | 1200.00 | 591.67 |
| 25 | 1250.00 | 571.12 |
| 26 | 1300.00 | 549.11 |
| 27 | 1350.00 | 525.48 |
| 28 | 1400.00 | 500.00 |

TABLE A4.2 (continued)

| Control Point | x co-ordinate mm ±0.25 mm | y and z co-ordinate mm ±0.25 mm |
|---|---|---|
| 29 | 1450.00 | 472.40 |
| 30 | 1500.00 | 442.45 |
| 31 | 1550.00 | 410.16 |
| 32 | 1600.00 | 375.99 |
| 33 | 1650.00 | 341.23 |
| 34 | 1700.00 | 308.08 |
| 35 | 1750.00 | 279.08 |
| 36 | 1800.00 | 255.89 |
| 37 | 1850.00 | 238.64 |
| 38 | 1900.00 | 226.39 |
| 39 | 1950.00 | 217.92 |
| 40 | 2000.00 | 212.13 |
| 41 | 2050.00 | 208.20 |
| 42 | 2100.00 | 205.54 |
| 43 | 2150.00 | 203.74 |
| 44 | 2200.00 | 202.00 |
| 45 | 2250.00 | 200.50 |
| 46 | 2300.00 | 200.00 |

TABLE A4.3. Co-ordinates of high speed contraction

| Control Point | x co-ordinate mm ±0.25 mm | y co-ordinate mm ±0.25 mm | z co-ordinate mm ±0.25 mm |
|---|---|---|---|
| 0 | 0.00 | 76.20 | 120.00 |
| 1 | 50.00 | 76.30 | 120.68 |
| 2 | 100.00 | 76.67 | 121.49 |
| 3 | 150.00 | 77.71 | 123.05 |
| 4 | 200.00 | 80.60 | 126.00 |
| 5 | 250.00 | 88.38 | 131.45 |
| 6 | 300.00 | 105.65 | 140.50 |
| 7 | 350.00 | 129.04 | 152.68 |
| 8 | 400.00 | 149.73 | 165.26 |
| 9 | 450.00 | 165.55 | 175.86 |
| 10 | 500.00 | 177.04 | 183.85 |
| 11 | 550.00 | 185.10 | 189.56 |
| 12 | 600.00 | 190.65 | 193.52 |
| 13 | 650.00 | 194.45 | 196.24 |
| 14 | 700.00 | 197.03 | 198.09 |
| 15 | 750.00 | 198.79 | 199.35 |
| 16 | 800.00 | 200.00 | 200.00 |